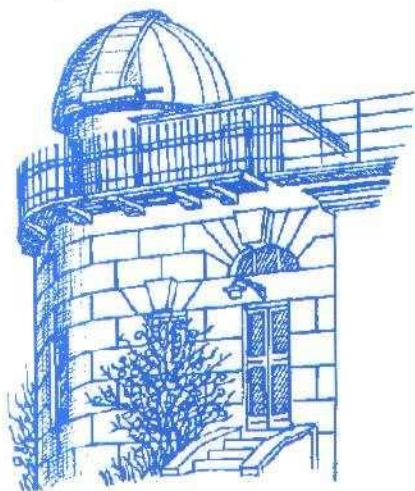


ODESSA ASTRONOMICAL PUBLICATIONS

Volume 14 (2001)



Odessa National University

ODESSA ASTRONOMICAL PUBLICATIONS

Volume 14 (2001)

(Известия Одесской астрономической обсерватории)

Special issue with the proceedings
of the international conference
“Variable Stars - 2001”

Editorial Board:

V. G. Karetnikov – *Editor-in-Chief*
G. A. Garbuzov – *Associate Editor*
I. L. Andronov – *Executive Editor*

Advisory Editors:

S. K. Aslanov, V. N. Ivanov, N. S. Komarov, T. V. Mishenina,
I. V. Poplavskiy, M. Yu. Volyanskaya, Yu. I. Zaginailo, A. I. Zhuk

Responsible for this Issue: I. L. Andronov

Technical editing: L. L. Chinarova, L. V. Korniychuk, E. A. Korobeinikova, S. L. Strakhova

Address:

Astronomical Observatory, Odessa National University
T. G. Shevchenko Park, Odessa 65014 UKRAINE
Tel., Fax: + 038 + 0482 + 22 84 42

E-mail: astro@paco.odessa.ua
<http://www.astro.od.ua> (AO)
<http://oap14.pochtamt.ru> (OAP)

Печатается по решению Ученого совета Астрономической обсерватории
Одесского национального университета им. И. И. Мечникова
от 15 октября 2001 г., протокол № 7

CONTENTS

<i>Karetnikov V.G.</i>	
Foreword	2
Contents	3
Section 1: "Interacting binary stars"	
<i>Andronov I.L.</i>	
Magnetic cataclysmic variables: 25 years of exciting performance	7
<i>Andronov I.L., Kolesnikov S.V., Niarchos P.G., Shakhovskoy N.M., Zola S.</i>	
BH Lyn: UBVR _I and CCD photometry of the eclipsing cataclysmic variable	15
<i>Andronov I.L., Yushchenko A.V., Niarchos P.G., Gazeas K.</i>	
Early superhumps in the "King of the superoutbursts" system WZ Sge	17
<i>Baklanov A.V., Pavlenko E.P.</i>	
Photometrical study of SU UMa-type binary RZ LMi during the superoutburst in 2001	21
<i>Baklanov A.V., Pavlenko E.P.</i>	
MR Ser: Photometric portrait of unusual polar	23
<i>Baklanov A.V., Pavlenko E.P., Dudka O.I.</i>	
CCD-photometry of cataclysmic variable ES Dra in 2001	24
<i>Bondarenko I.I., Perevozkina E.L.</i>	
Determination of age of low-mass close binary stars of the early spectral classes	25
<i>Chochol D., Pribulla T.</i>	
Multi-frequency study of symbiotic novae	26
<i>Kalimeris T., Rovithis-Livaniou H.</i>	
Observed properties of contact binary systems	33
<i>Kilpio A.A.</i>	
On the estimation of the lifetime of the accretion disk in the semidetached binaries ...	38
<i>Kilpio E.Y.</i>	
2D Modeling of the Gas Flow Structure in the Symbiotic Star Z Andromedae	41
<i>Kotnik-Karuza D., Friedjung M.</i>	
RR Tel: Mass loss rate of the cool component	44
<i>Miroshnichenko A.S., Bjorkman K.S., Krugov V.D., Usenko I.A.</i>	
Properties of classical Be stars from analysis of high-resolution H α profiles	47
<i>Nazarenko V.V., Glazunova L.V., Karetnikov V.G.</i>	
2D and 3D mass transfer simulation in β Lyrae system.	48
<i>Niarchos P.G.</i>	
Eclipsing binary stars: light curve models and software	53
<i>Parimucha S., Chochol D., Pribulla T.</i>	
Symbiotic nova V1016 Cyg as interacting binary	61
<i>Polubek G.</i>	
DV Aquarii Revisited.	65
<i>Pribulla T., Chochol D., Parimucha S., Rovithis P., Rovithis-Livaniou E., Tremko J.</i>	
Photoelectric monitoring of active close binaries.	69
<i>Pribulla T., Tremko J., Rovithis-Livaniou H., Rovithis P.</i>	
An active triple system 44i Bootis	74
<i>Prokhorov M.E., Postnov K.A.</i>	
Why NS and BH mass distribution is bimodal?	78

Pustynnik I.B.

- On the observed physical properties and evolutionary trends of hot subdwarfs
in binary systems 82

Pustynnik I., Pustynski V.F., Kubat J.

- Reprocessing of Lc in irradiated atmospheres of unevolved companions in
precataclysmic binaries (PCB) as a sensitive tool of measuring the
temperatures of hot subdwarf primaries 87

Rovithis-Livaniou H.

- The (O-C) diagrams of eclipsing binaries: traditional and new ways of treatment 91

Shugarov S.Yu., Ostrova N.I.

- CCD observations of the polar AM Her 97

Solheim J., Nasser M.R.

- The AM CVn systems - the final stage of binary white dwarf evolution 98

Vanko M.

- Photometric monitoring of short-period contact binaries 106

Section 2: "Pulsations: from seconds to years"

Aliev S.G., Ismailov N.Z.

- Rapid oscillations in the spectrum of roAp stars χ Psc and γ Equ 110

Andronov I.L., Chinarova L.L.

- Determination of characteristic time scales in semi-regular stars: Comparison
of different methods 113

Beletsky Yu.V., Halevin A.V., Kudashkina L.S.

- The photometric study of two faint Mira-type stars UX Cyg and AP Cyg 116

Bezdeneshnyi V.P.

- On the periods of the β Cephei stars 118

Bezdeneshnyi V.P.

- Frequency analysis of photographic observations of pulsating stars 122

Brukhanov I.S.

- BD +20°1171 - long-periodic variable star. 124

Brukhanov I.S.

- BM Eri - SR-type variable star. 125

Daszynska J., Cugier H.

- Spectroscopic non-adiabatic diagrams for multi-modal pulsating stars 126

Dorokhova T.N., Dorokhov N.I., Solheim J.E., Gonzalez Perez J.M.

- About the 21-st run of WET: PG1336-018 129

Efimov Yu.S., Kudashkina L.S.

- Photopolarimetry of some Mira-type stars 134

Egorova I.A., Kovtyukh V.V.

- Search for variability of the companion of the classical Cepheid EV Sct. 140

Falcon N., Labrador J.

- Thermal waves and unstable convection in ZZ Ceti stars. 141

Feast M.W.

- Cepheids as distance indicators: some current problems 144

Gorynya N.A., Samus N.N.

- Cepheid pulsations from radial velocity measurements 149

Marsakova V.I.

- Numerical criteria of the variability of the individual pulsating cycles in the LPVs ... 154

<i>Molenda-Zakowicz J.</i>	
False alarm probability in the multi-periodicity search	156
<i>Pena J.H., Peniche R., Garcia Cole A., Plascencia J.C., Parrao L., Pena R.</i>	
Strömrgren photometry and search for short period variables in the open clusters NGC 6910 and NGC 6913	159
<i>Pikhun A.L., Kudashkina L.S., Brukhanov I.S.</i>	
The investigation of semi-regular variable UV Boo.	162
<i>Rosenbush A., Reszelski M., Myullaert E.</i>	
FG Sge: the R Coronae Borealis - type activity and pulsations.	164
<i>Turner D.G.</i>	
A new mapping of the Cepheid instability strip	166
<i>Turner D.G., Berdnikov L.N.</i>	
The stability of Cepheid pulsations.	170
<i>Usenko I.A., Kovtyukh V.V.</i>	
Three Cepheids in galactic open clusters: chemical composition and evolution	174
<i>Vasilyeva S.V.</i>	
Frequency analysis of radial velocities variations of XZ Cyg.	178
<i>Whitelock P.</i>	
Asymptotic giant branch variables	180
Section 3: "Eruptive stars"	
<i>Bondar' N.I.</i>	
Rotation periods and activity of red dwarfs.	185
<i>Ismailov N.Z.</i>	
On the spectral and photometric activity in young stars	188
<i>Pavlenko Y.V.</i>	
Ultra fast evolution of Sakurai's object (V 4334 Sgr)	192
<i>Petrov P.P.</i>	
Magnetospheric accretion in T Tauri stars: observational test	194
Section 4: "Variable radio sources"	
<i>Galanin V.V., Derevyagin Ya.V., Derevyagin V.G.</i>	
A study of ionospheric refraction of radio waves from observations of cosmic radio sources using the radio telescope URAN-4	198
<i>Litvinenko O.A., Panishko S.K.</i>	
Variable radio sources and taking into account of ionospheric effects	200
Section 5: "Microlensing variability, exoplanets, exostars"	
<i>Bannikova E.Yu.</i>	
Radiation from vicinity of supermassive object without events horizon	202
<i>Evsukov N.N., Zakhzhaj V.A., Psaryov V.A.</i>	
Planetary systems of the Galaxy	205
<i>Miroshnichenko A.P.</i>	
Periodicity of luminosity of quasars and galaxies at cosmological scale	208
<i>Yushchenko A.V., Niarchos P.G., Terpan S., Manimanis V.</i>	
Gravitational lensing by globular clusters. Influence of microlensing	211
Section 6: "Stellar magnetism"	
<i>Monin D.N., Fabrika S.N., Valyavin G.G.</i>	
A statistical approach to the investigation of magnetic properties of main sequence stars	215

<i>Plachinda S.L., Johns-Krull C.M., Tarasova T.N.</i>	
Direct measurements of the general magnetic field on solar-like stars	219
<i>Popov S.B., Prokhorov M.E.</i>	
Magnetic fields of isolated neutron stars: Evidence for decay	224
<i>Skulsky M.Y.</i>	
The system of secondary periodicities and resonances based on β Lyrae magnetic field.	227

Section 7: "Stellar Atmospheres"

<i>Belik S.L., Komarov N.S., Dragunova A.V.</i>	
Determination of the fundamental characteristics of cold stars.	231
<i>Gorbaneva T.I., Kantzen L.E., Komarov N.S.</i>	
The abundances of nuclides of Magnesium in atmospheres of the Arcturus and the Aldebaran	235
<i>Gopka V.R., Mishenina T.V., Kovtyukh V.V., Yushchenko A.V.</i>	
About heavy element abundances in the atmospheres of stars with low metallicity ...	237
<i>Komarov N.S., Dorokhov N.I., Dorokhova T.N.</i>	
Search for TiO-band variability of cool giant	241
<i>Komarov N.S., Zgonjajko N.S., Vasilyeva S.V.</i>	
Abundances of Na, Ca, Mg and Al in the atmospheres of K supergiants of the Small Magellanic Cloud	242
<i>Lyubchik Yu.P., Martin E., Basri G., Pavlenko Ya.V.</i>	
Chemical abundances in binaries with twin components	244
<i>Mishenina T.V., Gorbaneva T.I., Kantzen L.E.</i>	
Preliminary abundance analysis of 9 subdwarfs	247
<i>Shavrina A.V., Khalack V., Polosukhina N.S., Zverko J., Žižnovský J., Gopka V.F., North P., Tsybmal V.V., Yushchenko A.V.</i>	
Lithium blend fitting for roAp star HD 101065 (Przybylski's star)	249
<i>Yakovina L., Pavlenko Ya.</i>	
Li I Line λ 460.3 nm in spectra of super lithium-rich carbon stars	253

Section 8: "Software, Instrumentation and Large Databases"

<i>Andronov I.L.</i>	
"Observations Obscurer - time series viewer, editor and processor	255
<i>Mikhailchuk V.V.</i>	
Elaboration of the batch of the programs for celestial mechanics for the computation of the astronomical ephemeris.	261
<i>Rosenbush A.E.</i>	
On the errors in the practice of observations and their reductions.	265
<i>Samus N.N., Kazarovets E.V., Durlevich O.V.</i>	
General Catalogue of Variable Stars	266
<i>Sergeev A.V., Sergeeva T.P.</i>	
The system for quick monitoring of astronomical plate archives. Main principles and purposes	270
<i>Shakhrukhanov O.Sh., Yushchenko A.V., Techuk O.</i>	
CCD detector in TV standard with small exposure time.	273
<i>Tatarnikov A.M., Shenavrin V.I., Whitelock P.A., Feast M.W., Yudin B.F.</i>	
Infrared Photometry of Sakurai's Object (V4334 Sgr) in 1996-2000.....	275
<i>Tatarnikova A.A., Kolotilov E.A., Munari U., Yudin B.F.</i>	
Photometric and spectrophotometric observations of the classical symbiotic star YY Her	277
<i>Yankiv-Vitkovska L.</i>	
Investigation of the damping constant of Fraunhofer's lines in solar atmosphere	279
<i>Author index</i>	282

FOREWORD

The present 14-th volume of the "Odessa Astronomical Publications" contains papers submitted by the participants of the international scientific conference "Variable Stars - 2001", after revising the reports and taking into account discussions. This conference is traditional and, since 1982, is organized in Odessa once per four years. This subsequential conference was held in Odessa from August 20 till August 25, 2001, and was devoted to the 130-th anniversary of the Astronomical observatory of the Odessa National University named after I.I.Mechnikov and to the memory of the director of the observatory in 1945-1983 years, the outstanding variable star researcher of the twentieth century, Professor Vladimir Platonovich Tsessevich (1907- 1983). The previous conference "Variable stars" was held in 1997 out of sequence and was devoted to the 90-th anniversary of the birthday of V.P.Tsessevich.

In the conference took part 116 participants from 16 countries of the world. 5 Plenary meetings and 9 sectional meetings in total were held, on which 143 reports were presented, from which 24 reports were plenary, 68 - sectional oral and 51 - poster presentations. During the conference, worked three basic sections and five joined sections. The themes of basic sections concerning the physics of binary, pulsating and eruptive stars. Joined sections worked on problems, close to the basic subjects: variable radiosources, microlensing, stellar magnetism and stellar atmospheres, and also on software and instrumental support and large astronomical data bases. The summer international astronomical school of the young scientists "Astronomy at the junction of sciences: Astrophysics, Astrochemistry, Astrobiology" was joined to conference.

The international scientific conference "Variable stars - 2001" was held with the financial help of the INTAS and the Ministry of Education and Science of Ukraine. It was organized by the Astronomical observatory and Department of Astronomy of the Odessa National University, Odessa radio-astronomical observatory of the Institute of a radio astronomy of the National Academy of Sciences of Ukraine and the Odessa Astronomical Society with an effective support of the Ukrainian Astronomical Association (Kiev) and Euro-Asian Astronomical Society (Moscow). The large help in fixing the topics of the conference was rendered by the members of the Scientific Organizational Committee and especially the chairman Professor N.N.Samus', and also convenors of all basic and joined sections, for whom I express the sincere thanks.

The scientific papers, published in the present volume, are located on sections, declared at the conference, in the correspondence with subjects of conference, according to an alphabetic order (in each section) of the authors. Unfortunately, before the deadline, not all the lecturers have submitted their works, probably, by deciding them to process, or to submit to other journals. Therefore, the current 14-th volume of the "Odessa Astronomical Publications" contains only a part of scientific reports from that presented at the conference. Totally, in the volume are included 82 scientific papers by 133 authors. The electronic version of the papers are available via Internet at the WWW-address: <http://oap14.pochtamt.ru>). *The editorial board of the journal hopes, that the materials published in the present volume, will discover the interested reader.*

V.G.Karetnikov

MAGNETIC CATAclySMIC VARIABLES: 25 YEARS OF EXCITING PERFORMANCE

I.L. Andronov

Department of Astronomy, Odessa National University, T.G.Shevchenko park,
Odessa 65014 Ukraine, e-mail: il-a@mail.od.ua, astro@paco.odessa.ua

ABSTRACT. Exactly 25 years ago, Santiago Tapia has detected circular and linear polarization of AM Her varying with the same period as the photometric and spectral characteristics. This had lead to a discovery of unprecedentedly exotic binary systems, in which the strength of the magnetic field is large enough to keep the white dwarf in a synchronism, dominating the accretion torque. Nowadays, about 70 representatives of this class of polars have been registered.

We review the history of study of polars, starting with a "standard model", according to which, the red dwarf fills its Roche lobe and the flow is captured and channelized by a magnetic field of the white dwarf in the vicinities of the inner Lagrangian point. The models of the "propeller", "idling", "magnetic valve", "swinging dipole", "boiling asymmetric rainbow column" are reviewed, with a special attention to the unsolved problems of this study - contradiction between the observed synchronism of spin and orbital periods of the white dwarf with a possible presence of the partially ballistic trajectory of the accretion flow and possibly important contributions of the dipole and multipole components of the magnetic fields; presence of few mechanisms of luminosity variations; various types and mechanisms of variability at different time scales from seconds to decades.

The monitoring of AM Her (and later on other objects) has started in Odessa in 1978 and was regularly continued in the Crimean Astrophysical observatory since 1989. The results will be published in the "Atlas and catalogue of the polarimetric and photometric characteristics" by N.M.Shakhovskoy, I.L.Andronov and S.V.Kolesnikov. Other papers absent in the ADS are available via <http://il-a.pochtamt.ru> or www.paco.odessa.ua/~il-a.

Despite 25 years have passed, these stars still exhibit new observational surprizes challenging theoretical models.

Key words: Stars: variable: cataclysmic: AM Her

1. Introduction

AM Her - type stars are the class of systems, which are intensely observed and modeled theoretically since

the discovery of linear and circular polarization of their emission superimposed onto synchronous variability of the X-ray, optical and infrared flux and characteristics of the emission lines. Thus these objects are often called "polars".

Despite the photometric variability of this system was detected in 1924, the real progress in understanding has begun in 1976, when the observations obtained by various groups have lead to the development of so-called "standard model" (Chanmugam and Wagner, 1977).

According to it, these objects are highly magnetic cataclysmic variables containing a red dwarf filling it's Roche lobe, and of a white dwarf, the magnetic field of which is sufficient to prevent formation of the accretion disk. The orbital periods lie within intervals 80-120 minutes, with another group of "long-period" polars from another side of the "2-3 - hour period gap".

However, AM Her itself, as well as other objects of this class discovered later, exhibit variability in a very wide range from seconds to decades. Thus it became obvious, that an intensive monitoring is needed to check variations of the characteristics of the phase curves. Nowadays, about 70 representatives of this class of polars have been registered, but only few are observed more or less regularly.

The evolution of these objects is determined by the angular momentum loss due to gravitational radiation and magnetic stellar wind (see recent monographs by Warner (1995) and Hellier (2001)).

A long-term photometric monitoring was initiated by Professor V.P.Tsessevich (1907-1983) and started in the Astronomical observatories of the Odessa (I.L.Andronov, S.V.Vasilieva, V.P.Tsessevich 1980, 1984; Andronov et al., 1983) and Kishinev (V.P.Smykov, L.I.Shakun, 1985) Universities. In 1985-1987, it continued in the Abastumani astrophysical observatory. Since 1978, the polarimetric observations of AM Her and other polars have started in the Crimean Astrophysical Observatory using 2.6m and 1.25m telescopes (Yu.S.Efimov and N.M.Shakhovskoy, 1981, 1982; V.Piirola et al., 1985). Since 1989, the monitoring has moved to CrAO completely. Altogether about 300 nights of observations have been obtained.

In this paper, we present a brief review of the properties of polars with an accent to AM Her. Currently, in the ADS are listed 605 papers corresponding to the "object search" option "AM Her", thus it is not possible to refer to all of them. We also present a self-review of the observational and theoretic results obtained by our research group.

2. Long-term variability

The long-term variations have been found by Hudec and Meinunger (1976) on the Sonneberg Sky Patrol plates with switches between high and low luminosity states. Feigelson et al. (1978) have measured the Harvard plates and noted the brightness variations by $\approx 3^m$ at the $\approx 100^d$ time scale and more rapid (0.1^d) variations by 1^m . The latter ones are caused by orbital variability, whereas the long-term luminosity variations may be a consequence of variable mass transfer. Since 1976, the patrol brightness estimates of the star are being made by various observers, the longest data set obtained by M. Verdenet (AFOEV).

These variations have been recently analyzed by Andronov et al. (1997). The switches between the high and low luminosity states are sometimes very rapid, lasting down to $\sim 3^d$. However, such variability is superimposed onto year-scale variations. Detailed study of photometric and polarimetric curves is in preparation by Shakhovskoy et al. (2001).

3. Orbital variability

The orbital variability and flickering was discovered by Berg and Duthie (1976), who first determined the orbital period of 186 minutes. The compilation of curves of phase variations of different physical characteristics was published by Friedhorsky et al. (1978b).

An excellent estimate of the period made Szkody and Brownlee (1977), who proposed an ephemeris

$$Min.HJD = 2443014.71266 + 0.128927(2) \cdot E \quad (1)$$

The initial epoch for the pulse of the linear polarization, which coincides with the zero crossing by the circular polarization is $T_{pol} = 2443014.7647(5)$ (Tapia, 1977).

The recent ephemeris for the photometric V or R minima obtained using 267 timings (1976-1999) corresponds to

$$Min.HJD = 2446637.0510(6) + 0.12892711(3) \cdot E', \quad (2)$$

where $E' = E - 28096$ (Andronov et al., 2002).

From 19 times of the minimum of the circular polarization in the R band, Shakhovskoy et al (2001) derived the ephemeris

$$Min.circ.pol.HJD = 2450304.83378(43) + 0.128927088(66)(E - 56545). \quad (3)$$

The phase of the polarizational minima, according to the photometric ephemeris, is 0.500(3), i.e. are accurately in the opposite phase.

They also note the presence of phase shifts with a typical cycle of $\approx 1100 - 1200^d$, which were explained by the "swinging dipole" model (Andronov 1987a).

Despite these variations, the value of the photometric period is in an excellent agreement with the spectral ephemeris presented by Schwarz et al. (2002) for the superior conjunction:

$$T_{sp.HJD} = 2446603.40308(35) + 0.128927103(6) \cdot E \quad (4)$$

Andronov, Vasilieva and Tsessevich (1980) have detected drastic changes of the phase curves, with an extreme case, when during two subsequent cycles, the amplitude jumped from 0.2^m to 0.16^m . The tables of observations obtained in 1988-1989 and the atlas of light curves was published by Andronov, Vasilieva and Tsessevich (1984). Based on these data, Andronov (1985) obtained statistical dependence of the phase curve on luminosity in the active and intermediate luminosity state. This dependence was continued to minor amplitude variations at the low state based on the observations obtained in Abastumani in 1985-1987.

Phenomenological classification of the characteristic types of the light curves was presented by Shakhovskoy et al. (1994). The atlas of the polarizational and UB-VRI light curves is being prepared by Shakhovskoy et al. (2001).

4. Fast variability ("red noise")

Individual light curves of AM Her exhibit strong flickering, as was first detected by Berg and Duthie (1976). Bailey et al. (1977) made an autocorrelation analysis and have shown, that the autocorrelation function is characterized by an exponential decay with a characteristic time $\tau = 90$ sec both in V and R, despite the cycle-to-cycle values are within the range from 30 to 200 sec. Kornilov and Moskalenko (1979) confirmed this result and estimated a mean flare rate of 0.5 ± 0.3 sec, their mean duration of 20-25 sec and the degree of emitted energy is 0.3 ± 0.2 . Stockman and Sargent (1979) found a large difference between the times in V and R: $\tau_V = 28$ sec and $\tau_R = 60$ sec. Subsequent observational study of the fast variability was made by Friedhorsky et al. (1978a), Szkody and Margon (1980) et al. Panek (1980) argued for transformation of initial plasma blobs into long (tidal interaction) and thin (distance between the magnetic field lines decreases when approaching the white dwarf) plasma "spaghetti".

We have observed AM Her and a group of cataclysmic variables with a time resolution from 12 sec (1.25m, UB-VRI) to 1-4 sec (2.6m, R) (Shakhovskoy et al., 1994, 2001). The periodograms show a presence of the strong "red noise", i.e. a systematic decrease of the test function with trial frequency. This could

be explained within the physical model of accreting "spaghetties" (or "shot noise"), or in a frame of mathematical model of first-order auto-regressive processes. Andronov (1994) has derived precise formulae for autocorrelation analysis, taking into account the length of the run and removal of the long-periodic trend. This method allowed to interpret minute-scale variability as the "shot noise" without quasi-periodic oscillations (as one could suggest using the formulae for infinite undetrended runs), and to detect variations of the model characteristics of the with luminosity. The values of τ ranged from 99 ± 19 sec for high state to 38 ± 6 sec in the low state.

Beardmore and Osborne (1997b) explained the hard X-ray variability from the Ginga observations by shot noise, with a time-scale of 70s, and a correlation between the hard X-ray and optical red variability. They derived a blob length-scale of $\sim 10^{10}$ cm, a blob radius of $6 \cdot 10^5 - 4 \cdot 10^6$ cm, and a mass of $\sim 10^{16}$ g.

Using the "corrected ACF analysis" (Andronov, 1994), Halevin et al. (2000) have studied phase-dependent flickering activity in magnetic cataclysmic variables BY Cam and QQ Vul and estimated the characteristic length of "spaghetties".

The scalegram analysis of the optical data has shown a power law character of the dependence of unbiased estimate of the r.m.s. deviation of the data from the fit on the filter half-width Δt , which is valid for a remarkably wide interval from 3 seconds to 10 years (7.5 orders of magnitude). This argues for a presence of variations at all time scales and a joint component acting both in fast and slow variability (Andronov et al., 1997).

The wavelet analysis (Andronov, 1998, 1999) of AM Her confirms, that irregular variability dominates over possible periodic or quasi-periodic oscillations, except at the orbital frequency and its first harmonic, as the phase curve exhibits a double-peaked behaviour.

Some methods for mathematical modelling of the "red noise" have been elaborated and originally applied to AM Her, i.e. the periodogram-, scalegram-, wavelet-, autocorrelation-, principal component- analysis, as well as the determination of the characteristics of the multicolor correlated and uncorrelated variability. They are briefly reviewed by Andronov (1999) and comparatively described by Andronov (2001).

5. Fast quasi-periodic oscillations (QPO)

Langer et al. (1992) have theoretically shown the possibility of excitation of the QPOs and thus second-scale variability of the structure of the accretion column. According to their computations, the period of QPOs is inversely proportional to the accretion rate per unit area. Imamura (1985) theoretically studied the stability properties of white dwarf radiative shocks and determined conditions needed to the excitation of

quasi-periodic oscillations.

Larsson et al. (1990) discussed the possibility of mapping the accretion flow using the QPO studies during eclipse of the column by the white dwarf. Wu et al. (1992) reviewed QPOs in magnetic cataclysmic variables.

Beardmore and Osborne (1997a) failed to detect 1-3s quasi-periodic oscillations in AM Her, EF Eri and V834 Cen in the GINGA hard X-ray observations, giving upper limits of 4, 5 and 18 per cent, respectively. However, such QPOs are possible within these limits, as, for EF Eri and V834 Cen the amplitude of QPOs in the optical bands is 1-3%.

It should be noted, that the density of the accretion column, even if to neglect blobby structure, is not constant through the cross-section. Thus one may assume oscillations of individual blobs at different frequencies, what will significantly decrease the effect. There may be additional types 3-d variations of the structure, which have been discussed by Andronov (1987b).

6. X-ray, UV, optical and IR emission

6.1. Observations

AM Her was detected as an X-ray source by Hearn et al. (1976), and since then is one of the often observed objects. X-ray properties of AM Herculis binaries have been described e.g. by Bennermann (1998).

Silber et al. (1996) made a fit for the IUE and our optical data. The temperature of the white dwarf during phases of low brightness is estimated to be of 20 000 K, whereas at phases of brighter flux, a second component is present, which may be explained as a bright spot with a temperature of $35\,000 \pm 5\,000$ K, which covers $\leq 8\%$ of the surface.

Recently, de Martino et al. (1998) detected a deep X-ray low state of AM Herculis with a flux decrease by a factor of 7 during 40 min. Usually, coronal emission from the secondary may contribute significantly during the inactive phase. The new BeppoSAX observations of AM Her (Matt et al., 2000) show that during an intermediate state, the source was in its "normal" one-pole accretion mode. In the high state it switched an atypical "two-pole" accretion mode, with significant soft and hard X-ray emission from both poles. However, the emission from the second pole is much softer than that from the primary pole, suggesting the blobs penetrating deeply in the photosphere.

Thus, the complete emission contains at least 5 components, partially separated in wavelengths:

1. Cyclotron emission from the accretion column, increasing from visual to near-IR bands;
2. Hard X-ray bremsstrahlung emission from the shock;
3. Hard UV and soft X-ray nearly blackbody

emission from irradiating the cyclotron and bremsstrahlung emission by the white dwarf and possibly from the local thermonuclear reactions;

4. Secondary emission of the accreting stream above the shock and of the irradiated atmosphere of the secondary;
5. Emission of the secondary filling its Roche lobe.

6.2. The polar cap model

Having no possibility to describe numerous models of X-ray emission, we point out two of them. The model of surface polar cap (Andronov, 1986b) used constant and variable distribution of brightness and assuming absorption in the accretion column. It was shown on the base of the X-ray curve published by Hearn and Richardson (1977), that the accretion column is optically thick. Moreover, the source of the emission is extended in height and is asymmetric owed to the inclination of the column.

Silber et al. (1996) modeled the UV spectrum within the frame of two-component model, and estimated temperatures of the white dwarf and of the heated spot.

The observed soft X-ray excess is owed to the blob - type accretion instead of the homogeneous column (Andronov, 1987b; Wu et al., 1995) Most recent models of the ionization structure of the accretion region are presented by Wu et al. (2001).

7. Polarization and magnetic field of the white dwarf

Polarization of the emission was discovered by Tapia (1977), who noted a spike of linear polarization with a few minute duration, and continuous variations of the circular polarization. He suggested a mechanism of cyclotron emission of plasma in the strong magnetic field. Polarization decreases with wavelength, disappearing at $\lambda = 4000\text{\AA}$. This allows to estimate an upper value of the magnetic field of 270 MGs (Kruszewski, 1978) assuming that the emission occurs at the cyclotron frequency $\omega_B = eB/mc$, estimated it as 230 MGs.

The penetration and polarization of emission in the cosmic medium was studied by Dolginov et al. (1979).

Assuming that the emission occurs at the cyclotron frequency, which is dependent on the height above the surface of the white dwarf, Friedhorsky et al. (1978b) have studied dependence on the wavelength of the polarization minimum. Their conclusion was that the field strength varies with height more slowly than according to the dipole $\sim r^{-3}$ law.

However, direct measurements of the magnetic field from the Zeeman absorptions in the spectrum of the white dwarf during inactive state had lead to the conclusion, that the magnetic field in AM Her itself is really much smaller, i.e. only ~ 14 MGs (Schmidt et al.,

1981).

8. Accretion column

The accretion column is the main source of emission, which exceeds the emission of stellar components by a factor of few dozens. To interpret the corresponding variations, the relativistic models of the column are needed. A brief review of the models was presented by Andronov (1990), who studied the influence of the inhomogeneity of accretion column onto polarization and spectrum of its emission. In stationary symmetric models, one should assume the temperature and density structure. The observational spectra in both polarizational modes are strongly dependent on these assumptions. E.g., for a finite-width column, the emission is not dependent on optical thickness τ , if $\tau \gg 1$. Geometrical effects of the inclination of the columns were studied by Andronov (1986a).

For the columns with gradually decreasing density, the effective radius of the column is dependent on the density distribution, wavelength, polarization mode and the angle between the column and line of sight.

Elliptic columns will produce an additional dependence on the second angle between the major axis and the projection of the line of sight onto the cross-section.

The dependence of the spectrum on the magnetic field, as well as the vertical structure of the column may cause an effect of the "rainbow" column, if the spectrum contains strong cyclotron lines. This method of determination of the magnetic field strength in the emission region was proposed by Mitrofanov (1980) and then widely used in the case of cyclotron emission at few harmonics (cf. Cropper, 1990).

Non-stationary "boiling" columns will significantly change the spectrum of the outgoing radiation (Andronov, 1987b).

Another problem arises, if the accretion column is not single. In this case, the inverse problem of parameter determination becomes much more uncertain, as the inclined asymmetric columns may correspond to magnetic poles of different strength, which are located not exactly at the opposite points of the white dwarf (Kruszewski, 1978; Piirola et al., 1985; Muslimov et al., 1995 et al.).

9. Synchronization

9.1. Dipole - sphere interaction

One of the most striking features of the polars is the synchronism between the rotation of the white dwarf and the orbital motion. This class of binary stars is the only one, where such a synchronism exists, because the angular momentum of the infalling matter should be compensated by some loss mechanism (e.g. Lipunov, 1987).

The fact of synchronization is justified by the coin-

cidence of the period of variations of polarization and X-ray flux (originated near the white dwarf) with the period of radial velocities measured using emission lines (dominating in the high state and originating in the accretion flow and heated part of the red dwarf) and using the narrow Na lines (originating in the atmosphere of the red dwarf and seen at the low luminosity state).

Despite it was obvious, that this synchronism is caused by a sufficient strength of the magnetic field, the first physical model was proposed by Joss et al. (1979). The accretion was neglected, the orbit was assumed to be circular, and the interaction between the rotating white dwarf with a conducting sphere caused excitation of the Foucault currents, the Ohm dissipation of which caused heating of the atmosphere and thus the decrease of rotation energy. However, the characteristic times for such synchronization are $\sim 10^{11}$ years ($5 \cdot 10^9$ yrs for most optimistic estimates of the magnetic field). This is too long to explain the existence of the synchronism.

Andronov (1983) extended this model to the case of elliptic orbits. This mechanism leads to the circularization of orbits, but is much less effective than the tidal circularization.

9.2. Magnetic field - plasma stream interaction

Andronov (1982, 1987a) has proposed a "propeller" model, assuming that the accretion stream is frozen into magnetic field. An additional centrifugal force ejects the matter causing deceleration of the rotation. The corresponding synchronization time is only 6-260 years, i.e. $\leq 10^3$ years. This stage is similar to the "propeller" stage in the systems (Illarionov and Sunyaev, 1976), but in the polars it differs by an absence of symmetry of the structure of infalling matter. Synchronization with such characteristic time was found in the Nova 1975 Cyg (V 1500 Cyg) (Pavlenko and Pelt, 1991) and BY Cam (an extensive observational campaign of this star was organized by Silber et al., 1997).

Other estimates of the synchronization time were larger $\sim 10^3 - 10^5$ years (Lamb et al., 1983). Recent review of the situation may be found in the monographs by Warner (1995), Campbell (1997) and Hellier (2001).

10. "Swinging dipole" model

10.1. Magnetic interaction with secondary

An important question is the further evolution of the rotation of the synchronizing white dwarf. Will it be "phase-locked", "idling" or "swinging" around some equilibrium state?

According to Joss et al. (1979), the synchronization leads to a phase-locked state. However, there may be damping oscillations of the orientation of the magnetic axis around the stable position with a characteristic period of a dozen of years, i.e. the "swingsings".

10.2. "Magnetic valve"

The model of structure of the accretion flow in the vicinities of the inner Lagrangian point in the presence of dominating magnetic field was proposed by Andronov (1982a). The flow is maximal, when the magnetic field near the inner Lagrangian point is oriented along the line of centers, and vanishes, when they are orthogonal. Thus one may call this model "the magnetic valve".

The drag force from the accretion stream is also dependent on the angle ψ between the magnetic axis and the line of centers. The equilibrium positions are $\psi = 0^\circ$ and $\psi = 90^\circ$ (Andronov, 1987a), which coincide with that of the "dipole-sphere" interaction by Joss et al. (1979). A grid of models of orientation oscillations, computed taking into account both these effects in various proportions, has shown, that the period value is dependent on the accretion rate and on the amplitude. However, the equilibrium position at $\psi = 90^\circ$ corresponds to the "magnetic valve" closed. However, the theory of evolution predicts, that the mean accretion rate should be non-zero owed to gravitational radiation and magnetic stellar wind (cf. Tutukov and Yungelson, 1979; Warner, 1995). Thus should be the auto-excited oscillations, during which the portions of plasma are accreted at a mean level corresponding to evolutionary status. The estimated value of the characteristic time P ranged from 1 to 10 years.

10.3. Dipole-dipole interaction

In this model, the potential energy is dependent on orientations of both dipoles. Andronov (1995) has computed a grid of time-dependent models. However, the red dwarf has much larger moment of inertia than the white dwarf, so the cycle of orientation variations is ~ 6 times larger than of the white dwarf. So the "free oscillations" may be described as relatively slow variations of the red dwarf, and faster cycles of the primary around slowly changing position of equilibrium. For non-planar case, both the longitude and latitude chaotically vary, with redistribution of oscillation energy between the two co-ordinates and two dipoles. Sometimes even the changing of the pole facing to the larger star occurs for few dozens cycles. A very interesting phenomenon, which should be searched in the observations!

Recent theory of the orientation changes was described by Campbell (1997).

10.4. Observational tests

The "swinging dipole" model may be tested by the presence of the statistical dependence of the orbital light curve on luminosity and characteristic time of its variability. There are some observational facts, which may give evidence on the type of changes of the accretion structure in AM Her:

- 1 Long-term variations of the luminosity;
- 2 Long-term variations of the shape of the phase curves of various physical characteristics;
- 3 Statistical luminosity dependence of the phase curves.

The systematic study of the phase characteristics has begun with the monitoring, what lead to detection of the statistical dependence of the phase curve on luminosity at high and intermediate state (Andronov 1985). The phases underwent 3-yr modulation, just in the middle of theoretically predicted range 1-10 yr (Andronov et al., 1982), what was interpreted as orientation oscillations with an amplitude of $17^\circ \pm 3^\circ$. Smykov and Shakun (1985) confirmed this result, noting an existence of the "phase-luminosity" dependence in the sense that brighter curves are more positive-shifted from the linear ephemeris. Another object showing cyclical variability of phases with variable amplitudes is QQ Vul (Andronov and Fuhrmann, 1987).

However, it is not expected that these "swingings" will be strictly periodic, as varies not only the longitude of the magnetic pole, but the latitude as well (Shakhovskoy et al., 1992). Moreover, the luminosity variations may be also modulated by the irradiation of the secondary by the hard emission from the vicinities of the white dwarf (Basko and Sunyaev, 1973; King and Lasota, 1984). Another unpredictable source of modulation of the accretion rate may be spots on the red dwarf (Hessman et al., 2000). The light curves show a strong flickering displacing the phases of minima. The joint influence of these mechanisms cause very complicated changes both in luminosity and shapes.

The model of "swinging dipole" may be challenged for some polars by a model with a ballistic part of the trajectory and the capture of the stream much closer to the white dwarf than the inner Lagrangian point (cf. Warner, 1995). However, even in this case, the orientation oscillations should exist, thus new realistic models of the emission are needed, as well as determinations of orientation from individual photometric and polarimetric chase curves.

Much more accurate are polarimetric timings, which are less affected by flickering. Detailed discussion of these results is prepared by Shakhovskoy et al. (2001).

11. The red dwarf

11.1. Effective radius of the Roche lobe and the "Period-mass" relation

An usual assumption is that the low-mass red dwarf is unevolved and thus belongs to the main sequence either in magnetic and non-magnetic systems. The classical mass-radius relations obtained for single stars must be revised by introducing an "effective" radius of the Roche lobe. So the problem is splitted into

two: dependence of the effective radius of the star filling it's Roche lobe on the mass ratio and the mass-radius relation for real stars. Assuming that the distorted star has the same volume as the spherical one, Warner (1976) obtained $M_2/M_\odot = 2.45(P/1^d)^{1/3}$; Echevarria (1983) proposed a revised approximation, $M_2/M_\odot = 0.0751(P/1^h)^{1.16}$. Recently de Loere and Doorn (1992) redetermined the mass-radius relation for low-mass main sequence stars, and thus one may obtain much stronger dependence $M_2 \propto P^{2.5}$.

For example, the mass estimates for the polar AM Her obtained by using these statistical relationships and different sets of parameters are 0.32, 0.28 and 0.061 solar masses, respectively. The last value significantly differs from that with $n \approx 1$ and does not seem to be realistic. Götz (1991) noted that the mean estimate of the spectral class of the red dwarf in AM Her (M4.5) is in a good agreement with the estimate M5.4 obtained from the "period - spectral class" relation by Echevarria (1983). It corresponds to the mass $M_2 = 0.266M_\odot$ and radius $R_2 = 0.314R_\odot$.

A comparative analysis of various models was made by Andronov (1982b) and revised by Andronov (1992b), who tabulated numerous characteristics of the Roche lobe and proposed approximating fits. It is important to note that the values of the "barotropic" radius are systematically larger by 2-4% than that of the "equi-volume" one for the same mass ratio. This leads to a $\sim 10\%$ difference in the theoretically expected volumes, mean densities and thus masses.

11.2. Is the red dwarf a main sequence star?

Current models of the red dwarfs in cataclysmic variables show that they may be slightly evolved stars (Echevarria, 1983; Warner, 1995). Bennermann et al. (1998) showed that in the short-period cataclysmic variables, the red dwarf is close to the main sequence, whereas in the long-period (> 3 hours), the majority of secondaries have later spectral types owed to the nuclear evolution prior to mass transfer and lack of thermal equilibrium due to mass transfer.

11.3. Magnetic activity of the red dwarf

The secondary in magnetic cataclysmic variables is a red dwarf, thus one may assume corresponding physical variability. Solar-type magnetic activity may cause variations of the accretion rate in cataclysmic variables (Bianchini, 1990), as well as the migrating spots (Hessman et al., 2000). The star underwent an unprecedented UV Cet - type flare (Shakhovskoy et al., 1993). Statistical study of the variability of accretion and flare nature was published by Bonnet-Bidaud et al. (2000). An additional mechanism of modulation of the accretion rate may be present, if a third body (massive planet or brown dwarf) causes minor variations of the orbital separation.

12. Conclusion

To make a statistical study of variability with characteristic times from seconds to decades, a long-term monitoring has been carried out since 1978. The phase light curve of sometimes undergoes drastic changes even from one cycle to another. Its shape statistically depends on luminosity, despite of significant physical variability. AM Her exhibits a variety of types of variability, with a cease of the fast variability and polarization in the low state. An unprecedented flare has been detected, which resembles the flares of the UV Cetype stars, and is within 5 most powerful flares. Much smaller accretion event at a low state was registered spectrally at the 6m telescope. Our low state multi-color observations and the IUE data allowed to propose a two-temperature model for the emitting region. For overlapping flares producing a "red noise" (flickering), we have used statistical methods. The most accurate photometric ephemeris (based on 279 minima timings), was determined. The 3 year variations of the phase shift of the curve have been interpreted as a result of the "swinging dipole" model - two-dimensional variations of the orientation of the white dwarf in respect to the red dwarf both in the latitude and longitude. Because of few processes involved, the variations are not strictly periodic, but show some characteristic cycle a time scale of 1-10 years. Our theoretical models were applied to a "standard model" (Chamugam and Wagner 1977), according to which, the dependence of the accretion rate on the orientation of the magnetic axis of the white dwarf exists in a case, when the magnetic field is strong enough to capture the flow near the inner Lagrangian point ("magnetic valve"); the synchronization time may not exceed 10^5 years (an excellent example of such a system is BY Cam). Following the model of the dipole-star interaction for synchronization of the white dwarf by Joss et al., (1979), we estimated characteristic times of the orbit circularization. Using a simplified column model, the soft X-ray curves were modelled showing either large optical depth of the column as well as the non-zero height of the emitting "polar cap" region. The accretion column exhibits effects of asymmetry, inclination, instability of few types. This causes changes in the polarization and spectra, as compared with stationary axis-symmetrical models.

Results of 13 recent years of polarimetric monitoring of AM Her are prepared for publication in the monograph "Atlas and catalogue of the polarimetric and photometric characteristics of the magnetic cataclysmic variable star AM Her" by Shakhovskoy, Andronov and Kolesnikov (2001).

Despite an unprecedented database of polarimetric observation already exists, the star needs further multi-wavelength monitoring, which will allow to study details of structure and evolution of these interesting objects.

Acknowledgements. I thank Drs. N.M.Shakhovskoy, S.V.Kolesnikov and other co-authors of our joint projects on AM Her for fruitful collaboration.

References:

- Andronov I.L.: 1982a, *Prepr. Ukr. Res. Inst. Sci. Tech. Inform. (UkrNIINTI)*, **5900**, 20p.; *Astrofizika*, 1984, **20**, 165.
- Andronov I.L.: 1982b, *Problemy Kosmicheskoy Fiziki*, **17**, 106.
- Andronov I.L.: 1983, *Conf. Young Sci.*, Odessa Univ. Press, 144.
- Andronov I.L.: 1985, *Pis'ma AZh*, **11**, 203.
- Andronov I.L.: 1986a, *Astron. Zh.*, **63**, 274.
- Andronov I.L.: 1986b, *Astron. Zh.*, **63**, 508.
- Andronov I.L.: 1987a, *Ap.Space Sci.*, **131**, 557.
- Andronov I.L.: 1987b, *Astron. Nachr.*, **308**, 229.
- Andronov I.L.: 1990, *Astrofizika*, **32**, 117.
- Andronov I.L.: 1992, *As.Ap.Transact.*, **2**, 341.
- Andronov I.L.: 1994, *Astron.Nachr.*, **315**, 353.
- Andronov I.L.: 1995, *Structure and evolution of magnetic close binary systems*, Odessa Univ., 396p.
- Andronov I.L.: 1997, *As. Ap. Suppl. Ser.*, **125**, 207.
- Andronov I.L.: 1998, *Kinematika i Fizika Nebesnykh Tel*, **14**, N6, 490.
- Andronov I.L.: 1999, in: "Self-Similar Systems", eds. V.B. Priezzhev, V.P. Spiridonov, Dubna, JINR, 57.
- Andronov I.L.: 2001, "Time series analysis of astronomical signals", Odessa, Astroprint, in press.
- Andronov I.L., Banny M.L., Korotin S.A., Yavorskij Yu.B.: 1982, *Astron. Tsirk.*, **1225**, 5.
- Andronov I.L., Fuhrmann B.: 1987, *IBVS*, **2976**.
- Andronov I.L., Kolesnikov S.V., Shakhovskoy N.M.: 1997, *Odessa Astron. Publ.*, **10**, 15.
- Andronov I.L., Kolesnikov S.V., Shakhovskoy N.M.: 2002, *ASP Conf. Ser.*, **261**, 129.
- Andronov I.L., Rajkov A.A., Udovichenko S.N., Tsessevich V.P., Yavorskij Yu.B.: 1983, *Problemy Kosmicheskoy Fiziki*, **98**.
- Andronov I.L., Vasilieva S.V., Tsessevich V.P.: 1980, *Astron. Tsirk.*, **1142**, 5.
- Andronov I.L., Vasilieva S.V., Tsessevich V.P.: 1984, *Preprint UkrNIINTI*, **1234**, 28p.
- Bailey J., Mason K.O., Parkes G.E.: 1977, *MNRAS*, **180**, 35.
- Basko M.M., Sunyaev R.A.: 1973, *Ap.Space Sci.*, **23**, 117.
- Beardmore A.P., Osborne J.P.: 1997a, *MNRAS*, **286**, 77.
- Beardmore A.P., Osborne J.P.: 1997b, *MNRAS*, **290**, 145.
- Berg R.A., Duthie J.G.: 1977, *ApJ*, **211**, 859.
- Bianchini A.: 1990, *AJ*, **99**, 1941.
- Bennermann K.: 1988, *Adv. Space Res.*, **8**, 283.
- Bennermann K., Baraffe I., Kolb U., Weichhold M.: 1998, *As.Ap.*, **339**, 518.

- Bonnet-Bidaud J.M., Mouchet M., Shakhovskoy N.M., Somova T.A., Somov N.N., Andronov I.L., de Martino D., Kolesnikov S.V., Kraicheva Z.: 2000, *As.Ap.*, **354**, 1003.
- Campbell C.G.: 1997, *Magnetohydrodynamics in Binary Stars*, Kluwer, 320p.
- Chanmugam G., Wagner R.L.: 1977, *ApJ*, **213**, L13
- de Loore C.W.H., Doom C.: 1992, *Structure and Evolution of Single and Binary Stars*, Kluwer.
- de Martino D., Gaensicke B.T., Matt G., Mouchet M., Belloni T., Bennermann K., Bonnet-Bidaud J.-M., Mattei J., Chiappetti L., Done C.: 1998, *As.Ap.*, **333**, L31.
- Cropper M.: 1990, *Space Sci Revs.*, **54**, 195.
- Dolginov A.Z., Fiedin Yu.N., Silant'ev N.A.: 1979, *Penetration and polarization of emission in the cosmic medium*, Moscow, Nauka, 424p.
- Echevarria J.: 1983, *Rev.Mex.As.Ap.*, **8**, 109.
- Efimov Yu.S., Shakhovskoy N.M.: 1981, *Izv.Krym. Astrophys.Obs.*, **64**, 55.
- Efimov Yu.S., Shakhovskoy N.M.: 1982, *Izv.Krym. Astrophys.Obs.*, **65**, 143.
- Feigelson E., Dexter L., Liller W.: 1978, *ApJ*, **222**, 263.
- Götz W.: 1991, *Astron. Nachr.*, **312**, 103.
- Halevin A.V., Shakhovskoy N.M., Andronov I.L., Kolesnikov S.V.: 2000, *Kinem. Phys. Celestial Bodies. Suppl. Ser.*, **3**, 402.
- Hearn D.R., Richardson J.A.: 1977, *Ap.J.*, **213**, L115.
- Hellier C.: 2001, *Cataclysmic Variable Stars: how and why they vary*, Springer-Verlag UK, 210pp.
- Hessman F.V., Gansicke B.T., Mattei J.A.: 2000, *As.Ap.*, **361**, 952.
- Hudec R., Meinunger L.: 1976, *IBVS*, **1184**.
- Joss P.S., Katz J.L., Rappaport S.A.: 1979, *Ap.J.*, **230**, 176.
- Illarionov A.F., Sunyaev R.A.: 1975, *As.Ap.*, **30**, 185.
- Imamura J.N.: 1985, *ApJ*, **296**, 128.
- King A.R.: 1989, *MNRAS*, **241**, 365
- King A.R., Lasota J.P.: 1984, *As.Ap.*, **140**, L16.
- Kornilov V.G., Moskalenko E.L.: 1979, *Pis'ma AZh.*, **4**, 456.
- Kruszewski A.: 1978, in: *Nonstationary Evolution of Close Binaries*, A.Żytkow (ed.), Warszawa, p.55.
- Lamb F.K., Aly J.J., Cook M.C., Lamb D.Q.: 1983, *Ap.J.*, **274**, L71.
- Langer S.N., Chanmugam G., Shaviv G.: 1981, *Ap.J.*, **245**, L23.
- Larsson S., Pirola V., Takalo L.: 1990, in: *Nordic-Baltic Astron. Meet.*, 173.
- Lipunov V.M.: 1987, *Astrophysics of neutron stars*, Moscow, Nauka.
- Matt G., de Martino D., Gansicke B.T., Negueruela I., Silvotti R., Bonnet-Bidaud J. M., Mouchet M., Mukai K.: 2000, *As.Ap.*, **358**, 177.
- Mitrofanov I.G.: 1980, in: *Close Binary Stars: Observations and Interpretation*, Dordrecht, 453.
- Muslimov A.G., van Horn H.M., Wood M.A.: 1995, *ApJ*, **442**, 758
- Panek R.J.: 1980, *ApJ*, **241**, 1077.
- Pavlenko E.P., Pelt J.: 1991, *Astrofizika*, **34**, 169.
- Pirola V., Vilhu O., Kyrolainen J., Shakhovskoi N., Efimov Y.: 1985, *ESA SP-236*, 245.
- Priedhorsky W.C., Krzeminsky W., Tapia S.: 1978a, *ApJ*, **225**, 542.
- Priedhorsky W., Matthews K., Neugebauer G., Werner M., Krzeminsky W.: 1978b, *ApJ*, **226**, 397.
- Schmidt G.D., Stockman H.S., Margon B.: 1981, *Ap.J.*, **243**, L151.
- Schwarz R., Hedelt P., Ran A., Stande A., Schwöpe A.D.: 2002, *ASP Conf. Ser.*, **261**, 167.
- Shakhovskoy N.M., Alexeev I.Yu., Andronov I.L., Kolesnikov S.V.: 1993, in: *Annals of the Israel Physical Society*, **10**, 237.
- Shakhovskoy N.M., Andronov I.L., Kolesnikov S.V.: 1994, *Odessa Astron. Publ.*, **7**, 40.
- Shakhovskoy N.M., Andronov I.L., Kolesnikov S.V.: 2001, "Atlas and catalogue of the polarimetric and photometric characteristics of the magnetic cataclysmic variable star AM Her" (in preparation).
- Shakhovskoy N.M., Kolesnikov S.V., Andronov I.L.: 1992, in: "Stellar Magnetism", St.Petersburg, 148.
- Silber A.D., Raymond J.C., Mason P.A., Andronov I.L., Borisov N.V., Shakhovskoy N.M.: 1996, *ApJ*, **460**, 939.
- Silber A.D., Szkody P., Hoard D.W., Hammergren M., Morgan J., Fierce E., Olsen K., Mason P.A., Rolleston R., Ruotsalainen R., Pavlenko E.P., Shakhovskoy N.M., Shugarov S., Andronov I.L., Kolesnikov S.V., Naylor T., Schmidt E.: 1997, *MNRAS*, **290**, 25.
- Smykov V.P., Shakun L.I.: 1985, *Kinem. Phys. Celestial Bodies*, **1**, N 6, 43.
- Stockman H.S., Sargent T.A.: 1979, *ApJ*, **227**, 197.
- Szkody P., Brownlee D.: 1977, *ApJ*, **212**, L 113.
- Szkody P., Margon B.: 1980, *Ap.J.*, **256**, 862.
- Tapia S.: 1977, *ApJ*, **212**, 125
- Terada Y., Ishida M., Makishima K., Imanari T., Fujimoto R., Matsuzaki K., Kaneda H.: 2001, *MNRAS*, **328**, 112.
- Tutukov A.V., Yungelson L.R.: 1979, *Acta Astr.*, **24**, 665.
- Warner B.: 1995a, *Cataclysmic Variable Stars*, Cambridge University Press, 572p.
- Warner B.: 1995b, *Ap.Sp.Sci.*, **232**, 89.
- Wu K., Chanmugam G., Shaviv G.: 1992, *ApJ*, **397**, 232.
- Wu K., Chanmugam G., Shaviv G.: 1995, *ApJ*, **455**, 260.
- Wu K., Cropper M., Ramsay G.: 2001, *MNRAS*, **327**, 208.

BH LYN: UBVRI AND CCD PHOTOMETRY OF THE ECLIPSING CATAclySMIC VARIABLE

I.L. Andronov¹, S.V. Kolesnikov¹, P.G. Niarchos², N.M. Shakhovskoy³, Zola S.^{4,5}

¹Department of Astronomy and Astronomical observatory,
Odessa National University, T.G.Shevchenko park, Odessa 65014 Ukraine,
e-mail: il-a@mail.od.ua, astro@paco.odessa.ua

²Department of Astrophysics, Astronomy and Mechanics,
University of Athens, GR 157 84 Zografos, Athens, Greece,
e-mail: pniarcho@cc.uoa.gr

³Crimean Astrophysical Observatory,
Nauchny, Crimea, 98409 Ukraine, *e-mail: shakh@crao.crimea.ua*

⁴Mt.Suhora Observatory, Pedagogical University
ul. Podchorążych 2, 30-084 Kraków, Poland
e-mail: zola@astro1.as.wsp.krakow.pl

⁵Astronomical Observatory, Jagiellonian University
ul. Orla 171, 30-244 Kraków, Poland

ABSTRACT. We report preliminary results of the UBVRI photoelectric and R CCD observations obtained in the Crimean astrophysical observatory and the Astronomical observatory of the Athens University. The light curve represents well-pronounced eclipses with a total duration of the most sharp phase of 0^m.422. At the eclipse, the color index U–B becomes smaller by 0^m.2 than outside eclipse, contrary to other colors, where the color indices become larger. This indicates a presence of uneclipsed source of ultraviolet emission, possibly the wind from the accretion disc.

Key words: Stars: variable: cataclysmic: BH Lyn

1. Introduction

PG 0818+513 (=BH Lyn) was detected as an UV - excess object ($V=15^m.58$, $B-V=0^m.15$, $U-B=0^m.77$) by Green et al. (1982, 1986), who classified it as a cataclysmic variable (CV). Andronov (1986) discovered its photometric variability and suspected that it is an eclipsing CV. Richter (1989) confirmed the eclipsing nature of the star. The 224-minute orbital period was determined by Andronov et al. (1989) using the method for determining the photometric period using moments of characteristic events (Andronov, 1991).

Thorstensen et al. (1991) confirmed the period from the emission lines, however, noting a significant ($\sim 57^\circ$) phase lag in respect to the eclipse. He classified the star as belonging to the subgroup of SW Sex-type stars,

also containing DW UMa, V1315 Aql and PX And.

Hoard and Szkody (1997) estimated the masses of the white and red dwarfs in the system as $M_{wd} = 0.7M_\odot$, $M_2 = 0.3M_\odot$ and the inclination angle $i = 79^\circ$. Hellier (2000) currently reviewed the properties and models of the SW Sex-type stars.

Our observations span a 14-year interval, and will be discussed elsewhere. In this paper, we present a sample light curve and its brief discussion.

2. Observations

The UBVRI observations have been obtained at the 1.25m telescope AZT-11 of the Crimean astrophysical observatory using the 5-color photometer-polarimeter. The time resolution in the photometric mode is 12 sec.

The CCD observations have been carried out at the 1.2m telescope at the Kryonerion observatory.

5-color photometry

One of the light curves is shown in Fig.1 in the instrumental system. One may note prominent eclipses. To smooth the observations, we have applied the method of running parabolae using the program OO described by Andronov (2001). The basic points used as the characteristics are the top of the hump at time .4105-.4151 (instrumental brightness m_0), the first and second minima and brightness m_3 at $t = .44396$ after the first minimum. Here times are expressed as time-2448245, and

magnitudes as differences from the hump value. These results are listed below:

m_0	t_1	m_1	t_2	m_2	m_3
4.693	.43489	1.249	.58997	1.446	0.260
5.531	.43480	1.441	.59040	1.545	0.188
5.884	.43421	1.349	.59055	1.498	0.169
5.898	.43421	1.080	.59041	1.051	0.203
5.759	.43344	0.746	.59055	0.640	0.192

One may note significant difference between the values of brightness in two subsequent minima which is strongly wavelet-dependent and reaches 0^m197 in U and -0^m106 in I. The hump is the largest in U (0^m26) and is in the range $0^m17..0^m20$ in other colors. For both minima, the depth is maximal in B (1^m35-1^m50) and minimal in I (0^m75-0^m64). The minima timings in different filters differ no more than for 58 seconds, i.e. within error estimates.

Despite the system becomes "redder" in red colors, the U-B color becomes smaller than at the hump by -0^m19 and 0^m10 for first and second minima, respectively. This argues for a presence of an extended region of ultraviolet emission, which is not completely eclipsed. It is interesting to note that, in addition to the ultraviolet continuum, there is a source of another emission (i.e. of the H α lines), which is less eclipsed than the underlying optical continuum (Thorstensen et al., 1991). This is a common feature of the SW Sextype stars (Dhillon et al., 1992; Hoard and Szkody, 1997).

Such behaviour may be explained by a presence of wind from the accretion disc.

Acknowledgements. This work was partially supported by the grant 02/07/451 of the Ukrainian State Fund of Fundamental Research.

References

- Andronov I.L.: 1986, *Astron. Tsirk.*, 1418, 1
 Andronov I.L.: 1991, *Kinem.Fizika Neb. Tel (Kinematics and Physics of Celestial Bodies)*, 7, N2, 78
 Andronov I.L.: 2001, *Odessa Astron. Publ.*, 14, 255
 Andronov I.L., Kimeridze G.N., Richter G.A., Smykov V.P.: 1989, *IBVS*, 3388, 1
 Dhillon V.S., Jones D.H.P., Marsh T.R., Smith R.C.: 1992, *MNRAS*, 258, 225
 Green R.F., Ferguson D.H., Liebert J., Schmidt M.: 1982, *PASP*, 94, 560
 Green R.F., Schmidt M., Liebert J.: 1986, *ApJ. Suppl. Ser.*, 61, 305
 Hellier C.: 2000, *NewAR*, 44, 131
 Hoard D.W., Szkody P.: 1997, *ApJ*, 481, 433
 Richter G.A.: 1989, *IBVS*, 3287, 1.
 Thorstensen J.R., Davis M.K., Ringwald F.A.: 1991, *AJ*, 102, 683

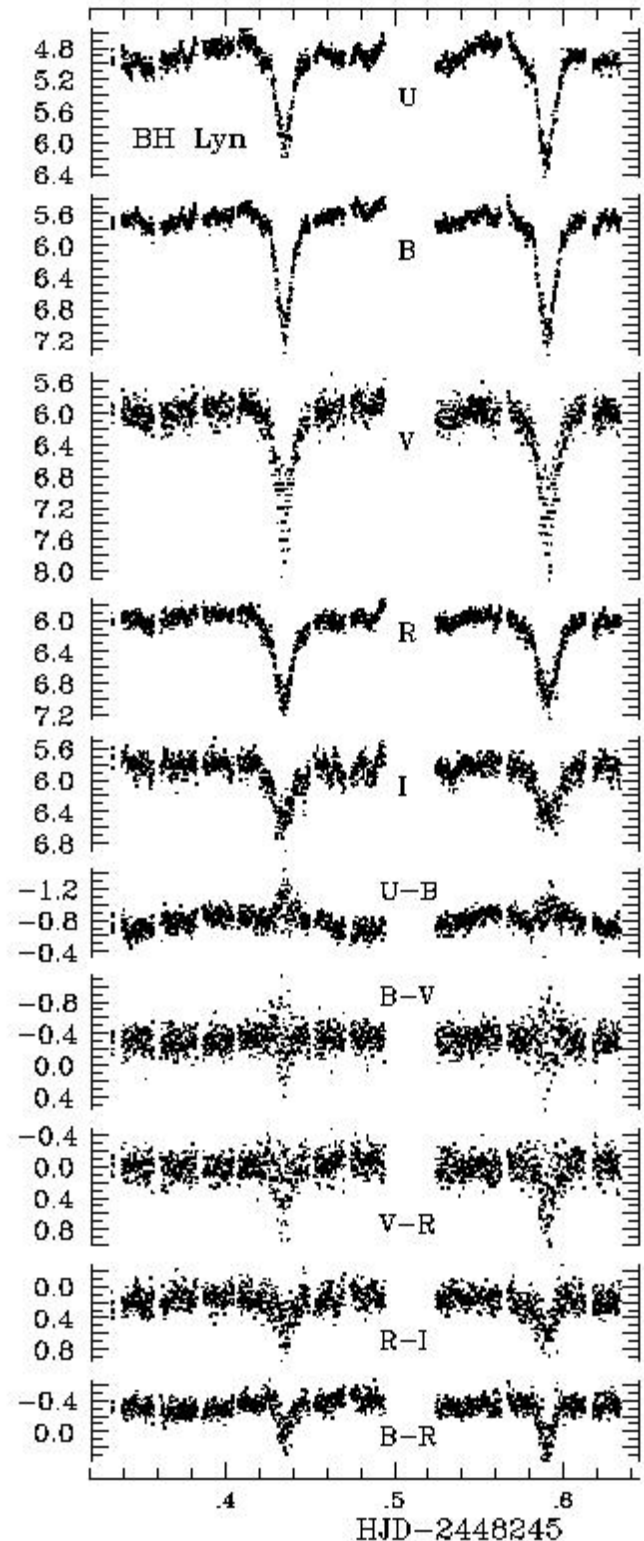


Figure 1: UBVR observations of BH Lyn in the instrumental system and instrumental colors.

EARLY SUPERHUMPS IN THE "KING OF THE SUPEROUTBURSTS" SYSTEM WZ SGE

I.L. Andronov¹, A.V. Yushchenko¹, P.G. Niarchos², K.Gazeas²

¹Department of Astronomy and Astronomical observatory,
Odessa National University, T.G.Shevchenko park, Odessa 65014 Ukraine,
e-mail: il-a@mail.od.ua, yua@lens.tenet.odessa.ua

²Department of Astrophysics, Astronomy and Mechanics,
University of Athens, GR 157 84 Zografos, Athens, Greece,
e-mail: pniarcho@cc.uoa.gr, kgaze@skiathos.physics.auth.gr

ABSTRACT. Time series analysis of 6 nights of CCD observations of WZ Sge after it's unexpected superoutburst on July 23, 2001 has shown highly asymmetric periodic variations with a period $0^d.0566513(22)$, full amplitude $0^m.218(4)$ and a very high asymmetry $M - m = 0.670(9)$, a secondary minimum $0.38P$ after the main one. The initial epochs are $T_{max} = BJD2452118.7483(3)$ and $T_{min} = BJD52118.7670(2)$. The characteristics of the phase light curve are listed. In addition, we have found superhumps with a semi-amplitude of $0^m.021(2)$ and an ephemeris $T_{max,sh} = BJD2452117.6830(8) + 0^d.057435(45) E$. Other peaks at 21 and 25 minutes possibly correspond to quasi-periodic oscillations with an effective semi-amplitude of $0^m.014$.

Key words: Stars: variable: cataclysmic: UG SU: WZ Sge

1. Introduction

WZ Sge was known as a cataclysmic variable (CV) exhibiting outbursts every 33 years. Previous ones were detected in 1913, 1946, 1978 with a recurrence time of 11876^d (Ritter and Kolb, 1998), and the next one, achieved from this short sequence, could be predicted for 2011. However, it occurred on July 23, 2001, as was reported by T.Watanabe based on observations by M.Oshima. The extending story of recent studies of this object is presented at the VSNET page www.kusastro.kyoto-u.ac.jp/vsnet/DNe/wzsge01.html. At the figure taken from this site, one may see "evolution of early superhumps". Their period is equal to the orbital one, and there is a hump at the ascending branch.

G.Masi (www.bellatrixobservatory.it) presented numerous individual light curves obtained at the Bellatrix Observatory, often revising his site to add new results.

E.Kuulkers presented an outburst light curve which is compiled from the data obtained during previous three outbursts (http://saturn.sron.nl/~erikk/wzsge/wzsge_1913.1946.1978.gif).

D.Steeghs (www.astro.soton.ac.uk/~ds/wzsge.html) presented a timetable containing dates of past and planned future observations of WZ Sge, which played an important role for coordinating research of various groups.

The object has become the CV target number one at the CBA (Center for Backyard Astrophysics) network supervised by J.Patterson (cba.phys.columbia.edu) and AAVSO (www.aavso.org, director J.Mattei). At these pages, one may find a list of runs obtained by the CBA and AAVSO members.

2. Basic information

Since the first two detected outbursts in 1913 and 1946, the star was classified as a recurrent nova, which contains a white dwarf (Greenstein, 1957). Krzeminski (1962) had found, that the star is an ultra-short period binary star with a period of 82 minutes. Krzeminski and Kraft (1964), while searching for "Binary Stars among Cataclysmic Variables", have published the paper on this star as the fifth one in these series. Thus the star was one of the key objects leading to a current paradigm, that all cataclysmic variables are close binaries.

Faulkner (1971) propose a model for ultrashort-period binaries with an example of WZ Sge, according to which, the mass transfer is powered by gravitational radiation, determining the evolution. This model was developed in detail by Tutukov and Yungelson (1979).

Warner and Nather (1972) reported on rapid variability of WZ Sge while searching for it in blue stars. The coherent 27.87s oscillations, which are often de-

tected, argue for a presence of magnetic white dwarf (Patterson et al., 1998). Sometimes the periods are slightly larger, corresponding to beat periods.

However, the nature of outbursts was believed to be similar to the Novae, i.e. the thermonuclear outburst after gaining of the critical mass of hydrogen on a white dwarf. The situation has changed drastically during the subsequent outburst in 1978, when the star was intensely observed photometrically and spectroscopically. Despite the light curve is very similar to that of Novae, the outburst is caused by a distinctly other mechanism similar to the SU UMa-type dwarf novae, and thus the subclass of WZ Sge-type stars was separated from the recurrent novae.

Gilliland and Kemper (1980) pointed out a formation of a circumbinary disk and discussed the origin of superhumps - photometric wave with a period P_{sh} slightly exceeding the orbital one P_{orb} . Patterson et al. (1981) studied the observational appearance of the superhump during the outburst in 1978. In the case of WZ Sge, the period excess $E_p = (P_{sh} - P_{orb})/P_{orb} = 0.8\%$. Current models of superhumps have been discussed by Osaki (1995), O'Donoghue (2000) and Patterson (2001).

Thus the star is still among the first few ones, which lead to the present knowledge of cataclysmic variables.

3. Observations

The object was also observed during 6 nights at the 40cm reflector of the University of Athens Observatory by using a CCD SBIG ST-8 camera by K.G., A.Y., P.N. in the Bessel R filter. The comparison star is GSC 1621:1830 (= "C") with $R=8.663$ (Hemden 2001). Altogether 1109 data points have been obtained from July 24 to July 31 (BJD 2452115.503-2452121.614). The time series analysis was made by I.L.A.

Our light curves for 6 runs show a nearly linear trend only for intermediate 4 nights from JD 2452116 to 2452119, whereas the first and last nights lie significantly above this line. This conclusion is also justified by the outburst light curve obtained during the international campaign (Fig. 1). Thus, for further analysis, we have used extracted 653 data points obtained during 4 subsequent nights on BJD 2452116.332-9.364.

The individual light curves are shown in Fig.2. They show a composite structure with two minima and two maxima during the period. This is also consistent with the "rise to the outburst" data from the VSNET (Fig.3).

The study of individual runs and of evolution of characteristics is planned to be done elsewhere.

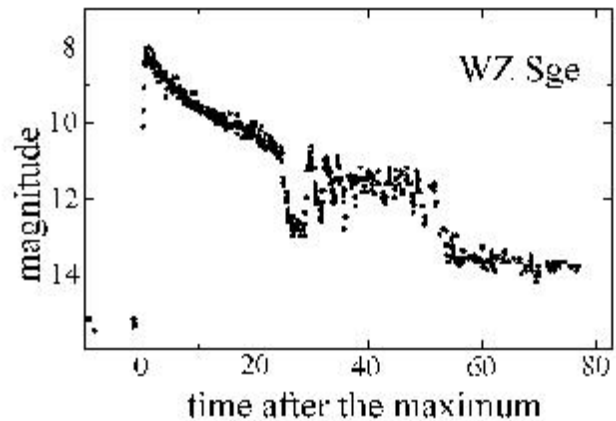


Figure 1: Long-term light curve based on the orbit-average magnitudes of WZ Sge compiled by D.Steeghs (<http://www.astro.soton.ac.uk/~ds/wzsge2001.gif>) using the VSNET and AFOEV data. Our data were obtained after 1...7 days after the maximum (complete interval shown by a horizontal line) during a stage of significant nonlinearity of the decay.

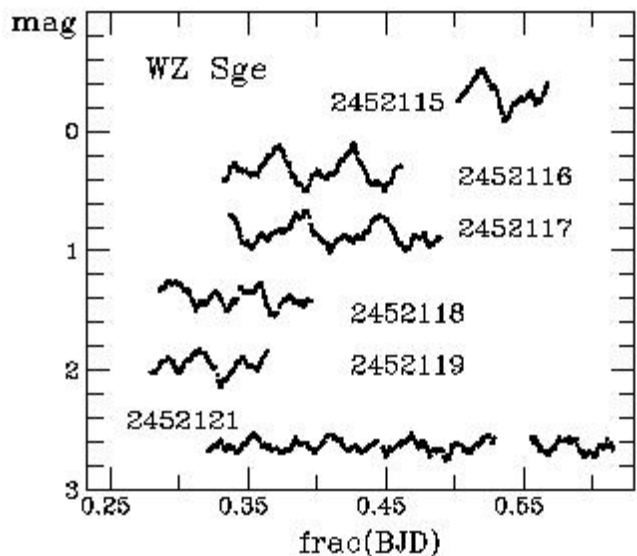


Figure 2: Light curves of WZ Sge for individual nights. The abscissa is a fractional part of barycentric Julian date. The integer part is shown near corresponding curves. The magnitude is expressed as "variable-comparison". The magnitude shift between the subsequent curves is 0.^m4.

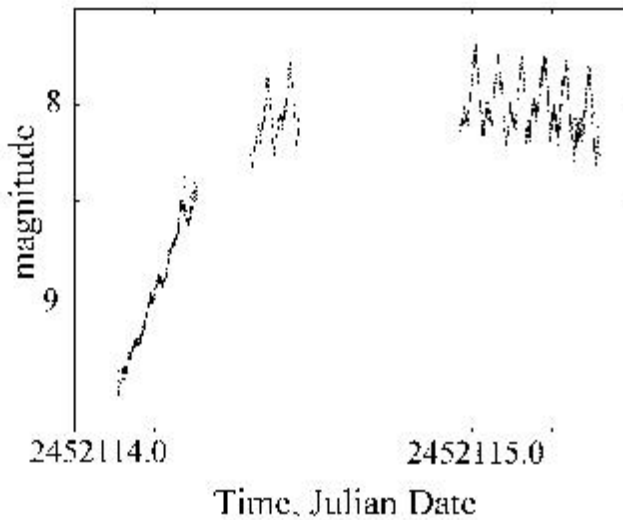


Figure 3: Rise to the maximum and the early evolution of the light curve from the VSNET observations (www.kusastro.kyoto-u.ac.jp/vsnet/DNe/wzsg01.html). Our observations started 4 hours after these data, when the night moved from Japan to Europe.

4. Multi-harmonic analysis with a linear trend

Because of fast non-linear variations of the mean brightness and the light curve, the periodogram analysis for all data gives us some "effective" values of the parameters, which are highly biased by such instability. The preliminary analysis shows, that, the decrease of the interval allowed to decrease systematic errors owed to non-linear variations of the mean brightness. Thus we have used a trigonometric polynomial of order s superimposed onto the polynomial trend of order p . The mathematical model is

$$z_C(t) = C_1 + \sum_{k=1}^s (C_{2k} \cos(k\omega\bar{t}) + C_{2k} \sin(k\omega\bar{t})) + \sum_{k=1}^p C_{2s+1+k} \bar{t}^k, \quad \bar{t} = t - \bar{t}, \quad (1)$$

where \bar{t} is the mean value of the times of observations, and $\omega = 2\pi/P$ is an angular frequency corresponding to the trial period P . The corresponding computer code extends the programs for separate multi-harmonic and polynomial approximations described by Andronov (1994). The preliminary value of the period is then changed to the value optimal for given degrees s and p for trigonometric and ordinary polynomials, respectively, using the method of differential corrections. The optimal values of s and p are determined using analysis of variances (the Fischer's criterion).

For the "shortened" data set, the values $s = 3$ and $p = 1$ are statistically significant. The "false alarm

probability" of obtaining the wave at a period P/s of given amplitude, assuming the signal is white noise, is only $2 \cdot 10^{-4}$. The mean slope $C_{2s+2} = d\langle m \rangle / dt = (0.1481 \pm 0.0007)$ mag/days corresponds to a characteristic decay time $\tau = (d\langle m \rangle / dt)^{-1} = (6.75 \pm 0.03)$ days/mag. Here

$$\langle m \rangle = C_1 + \sum_{k=1}^p C_{2s+1+k} \bar{t}^k \quad (2)$$

is a time-dependent zero-point of variations (trend value). For $p = 1$, it coincides with the orbit-average of the fit.

The time of the exponential decay $\tau_e = 2.5\tau / \ln 10 = 1.0857\tau = 7.33 \pm 0.03$ is well consistent with the range 4...12 days/mag over the first 15 days of the outburst estimated by Cannizzo (2001). The mean brightness $v - c = 0.2433 \pm 0.0014$ at the mean time of observations $\bar{t} = 2452118.77$. The best fit frequency $P^{-1} = 17.6518 \pm 0.0007$ cycles/day corresponds to the period $P = 0.0566513 \pm 0.0000022$. The light curve is highly asymmetric with a mean maximum at BJD 2452118.7483 ± 0.0003 with a trend-corrected value $v - c = 0.2130 \pm 0.0004$ and minimum at BJD 2452118.7670 ± 0.0002 with $v - c = 0.2348 \pm 0.0004$. Thus the total amplitude of the fit $\Delta m = 0.2218 \pm 0.0004$, asymmetry 0.670 ± 0.009 .

Often the coefficients of trigonometric polynomial are studied instead of the real brightness values for variable stars of various types (e.g. Kukarkin and Parenago, 1937; Niarchos, 1978; Kopal, 1986; Petersen, 1986). In this case, the term

$$C_{2k} \cos(k\omega\bar{t}) + C_{2k} \sin(k\omega\bar{t}) = -r_k \cos(k\omega(t - T_0) - 2\pi k\varphi_k) \quad (3)$$

Here T_0 is initial epoch (we use that corresponding to the brightness maximum, i.e. the minimum of the magnitude fit), and φ_k is the phase of maximum of the contribution. These characteristics are listed in the following table:

Table 1. The amplitudes r_k and phases φ_k of the contributions with a period P/k .

k	r_k	φ_k
1	0.0746 ± 0.0020	-0.051 ± 0.004
2	0.0538 ± 0.0020	0.055 ± 0.006
3	0.0087 ± 0.0020	-0.417 ± 0.037
	r_k/r_1	$\varphi_k - k\varphi_1$
1	1.000 ± 0.000	0.000 ± 0.000
2	$.722 \pm .033$	0.158 ± 0.010
3	$.117 \pm .027$	-0.263 ± 0.039

The phase light curve and the best fit are shown in Fig.4. Despite the scatter of the individual curves is rather small, there are physical variations of the shape of the light curve.

5. Superhumps

The scatter in the phase curves is caused by real variability of the shape. One mechanism is the luminosity dependence of the phase curve, which could be studied separately. Another important mechanism is a possible of superhumps - periodic waves with a period larger than the orbital one.

Kato et al. (2001) reported that superhumps became dominating over the orbital variability on Aug.4.53 with an amplitude 0.10 mag and a period $0^d.057143 \pm 0^d.000046$. Their later observations during next two nights "have shown further development of superhumps up to 0.23 mag and give a mean period of 0.058876 ± 0.000025 day". They called these superhumps as "genuine", contrary to the "early superhumps" which they called the prominent hump structure of the orbital variations.

To look for possible "genuine" superhumps at the beginning of outbursts, we have made a periodogram analysis of the residuals "O-C" of the data from the fit (1). The periodogram shows three distinct groups of peaks caused by daily aliases. The most prominent peak occurred at the period $0^d.0611$, far from the value achieved for "genuine" superhumps. However, the second peak with a height differing from the first one by only one per cent. The corresponding period is $0^d.057435 \pm 0^d.000046$, in an excellent agreement with the superhumps. The initial epoch $T_{max,sh} = \text{BJD } 2452117.6830 \pm 0^d.0008$, and a semi-amplitude $0^m.208 \pm 0^m.0018$. Thus one may conclude that "genuine" superhumps started at least two days after the outburst.

Two other groups of peaks correspond to frequencies 57.88 and 67.80 cycles/day (21-25 minutes) and equal semi-amplitudes of $0^m.014 \pm 0^m.02$. The frequency difference between the highest peaks from these groups, ~ 10 cycles/day does not correspond to the orbital frequency of the system (17.65 cycles/day). These frequencies are also much larger than the frequency 3100 cycles/day of the coherent 27.87-second oscillations. Thus possibly this variability is caused by some quasi-periodic oscillations and needs additional study.

6. Results

Our observations started $\sim 1^d$ after the outburst, where the mean light curve behaved non-linearly. Such a decrease of dm/dt was interpreted by Cannizzo (2001) as a consequence of increase of viscous time scale with decreasing mass of the accretion disk. He interpreted the outburst as a consequence of the sudden accretion of 10^{24} g of gas onto the white dwarf.

We present results of the "multiharmonic+trend" fit of the orbital variation, report on the presence of superhumps much before their amplitude became dominating. An interesting phenomenon are 21-25 minute waves.

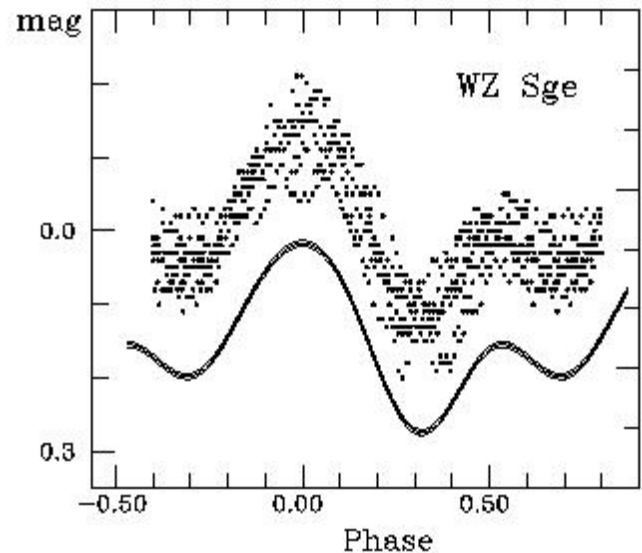


Figure 4: Phase light curve of WZ Sge for 4 nights used for the fit. The data are trend-corrected. The 3rd-order trigonometric fit and its $\pm 1\sigma$ limits are shown as solid lines shifted by $0^m.15$ from the data points.

Acknowledgements. The authors are thankful to Profs. F.Meyer and Y.Osaki for helpful discussions. This work was partially supported by the grant 02/07/451 of the Ukrainian State Fund of Fundamental Research.

References

- Andronov I.L.: 1994, *Odessa Astron. Publ.*, 7, 49.
 Cannizzo J.K.: 2001, *ApJ*, 561, 175.
 Faulkner J.: 1971, *ApJ*, 170, L99.
 Gilliland R.L., Kemper E.: 1980, *ApJ*, 236, 854.
 Greenstein J.L.: 1957, *ApJ*, 126, 23.
 Kato T., Ohashi H., Ishioka R., et al.: 2001, *IAUC*, 7680.
 Kopal Z.: 1986, *Vistas in Astronomy*, 29, 295.
 Krzeminski W.: 1962, *PASP*, 74, 66.
 Krzeminski W., Kraft R.P.: 1964, *ApJ*, 140, 921.
 Kukarkin B.W., Parenago P.P.: 1937, *AZh.*, 14, 337.
 Niarchos P.G.: 1978, *Ap.Space Sci.*, 58, 301.
 O'Donoghue D.: 2000, *New Astr. Rev.*, 44, 45.
 Osaki Y.: 1995, *PASJ*, 47, 470.
 Patterson J.: 2001, *PASP*, 113, 784, 736.
 Patterson J., McGraw J.T., Coleman L., Africano J.L.: 1981, *ApJ*, 248, 1067.
 Patterson J., Richman H., Kemp J., Mukai K.: 1998, *PASP*, 110, 746, 403.
 Petersen J.O.: 1986, *As.Ap.*, 170, 59.
 Ritter H., Kolb U.: 1998, *As.Ap.Suppl.*, 129, 83.
 Tutukov A.V., Yungelson L.R.: 1979, *Acta Astr.*, 29, 665.
 Warner B., Nather E.R.: 1972, *MNRAS*, 156, 297.

PHOTOMETRICAL STUDY OF SU UMA-TYPE BINARY RZ LMI DURING THE SUPEROUTBURST IN 2001

A. V. Baklanov¹, E.P. Pavlenko²

¹ Department of Astronomy and Astronomical Observatory
Odessa National University, Odessa 65014 Ukraine

² Crimean Astrophysical Observatory, Nauchny, Crimea, 98409 Ukraine

ABSTRACT. We perform the photometry of the SU UMa-type binary, RZ LMi during the superoutburst in 2001. The star displayed the superoutburst decay with a rate $\sim 0^m07/\text{day}$. We detected the superhumps with an amplitude up to 0^m2 . Some of the superhumps show the eclipse-like feature. The ephemeris for maxima is $\text{HJD} = 2451933.5939(6) + 0.059296(40) \cdot E$.

Key words: Stars: variable: cataclysmic: UG SU: RZ LMi

1. Introduction

RZ LMi was discovered as a variable star by Lipovetskiy and Stepanian (1981). Green et al. (1986), Szkody and Howell suggested RZ LMi to be a dwarf nova. Robertson et al. showed that behaviour of this dwarf nova is similar to those of ER UMa and V1159 Ori. Pikalova and Shugarov (1995) on the base of inspection of 300 photoplates from the SAI collection found that within $JD = 2446019 - 2446208$ RZ LMi displayed the brightness variations with extremely short cycle 21.2 days (or 23.3 days). Nogami et al. (1995) found some shorter interval between two neighbour superoutbursts – supercycle length (~ 19 days) and discovered the superhump period (0.05946 days). So RZ LMi is a unique binary among SU UMa type stars at least due to its extremely short supercycle. For example, the shortest supercycle in a "classical" dwarf nova V503 Cyg is 89 days (Harvey et al. 1995). Here we perform the results of our observations of RZ LMi during four nights over one of the superoutburst in 2001, that are the part of a multilongitude campaign organised by J. Patterson.

2. Observations

Our observations of RZ LMi have been carried out at the 380-mm Kassegrain telescope (K-380) of the Crimean astrophysical observatory in the standard Johnson R band. The exposure time was 100^s. The start and the end of observations, number of measurements, maximal and minimal brightness in respect to

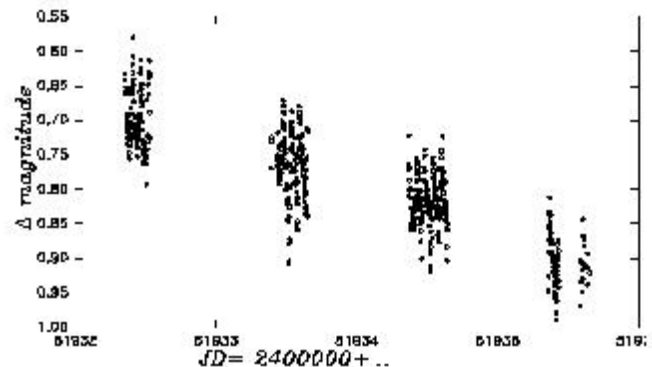


Figure 1: The light curve of RZ LMi during the superoutburst 2001

Table 1. Journal of observations.

JD	JD	N	m_{min}	m_{max}
51932.3477	51932.5313	129	0.794	0.580
51933.3906	51933.6523	163	0.908	0.672
51934.3672	51934.6445	198	0.919	0.723
51935.3633	51935.6563	77	0.990	0.813

the comparison star are given in the Table 1. The accuracy of a single measurement was 0^m03 .

3. Results

The known observations of RZ LMi show an extremely short duration of its superoutburst. The plateau of superoutburst in RZ LMi lasts no longer than 7 days (while in another SU UMa type binaries it could reach 14 days). We observed approximately half of the RZ LMi superoutburst duration. The long-term trend corresponded to the plateau of superoutburst decline is shown in Fig.1. The fading of RZ LMi was about $\sim 0^m07/\text{day}$. Note that Nogami et al. (1995) found a rate of plateau brightness fading in V band $\sim 0^m1/\text{day}$ in 1995. The same rate obtained Honneycutt et al. (1995) also in V band for the folded 1992-94 light curve.

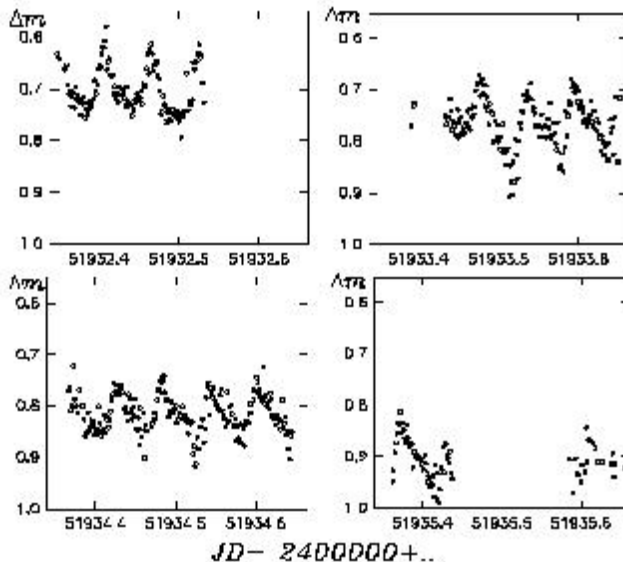


Figure 2: Nightly light curves of RZ LMi

Table 2. Maxima timings for RZ LMi.

JD	O-C (day)	σ
51932.4084	0.0177	0.0014
51932.4654	0.0153	0.0012
51933.4760	0.0150	0.0035
51932.4084	0.0177	0.0014
51932.4654	0.0153	0.0012
51933.4760	0.0150	0.0035
51933.5377	0.0172	0.0008
51933.5931	0.0132	0.0012
51934.4285	0.0161	0.0008
51934.5395	0.0082	0.0019
51934.6008	0.0101	0.0028
51935.3715	0.0078	0.0015

Similar value could be crudely estimated from photographic data by Pikalova and Shugarov (1995).

During the superoutburst, the prominent superhumps have been detected with amplitude up to $\sim 0.2^m$. The original light curves are shown in Fig.2. Over the course of the outburst the profile of the superhump changed from a symmetric shape to an asymmetric one (see Fig.2): The ascending branch became more steep than descending branch. For the superhumps with more steep ascending branch, the appearance of the eclipse-like feature in some minima is seen.

Using the code of Marsakova and Andronov (1996) we calculated the timings of a sharp maxima and the residuals (O-C) according to the ephemeris by Nogami et al. (1995):

$$Max = HJD2449781.009 + 0.05946 \times E \quad (1)$$

The result is presented in Fig.3. The (O-C)s were decreasing during the superoutburst. We fitted our data by the line and by the parabola. The fitting

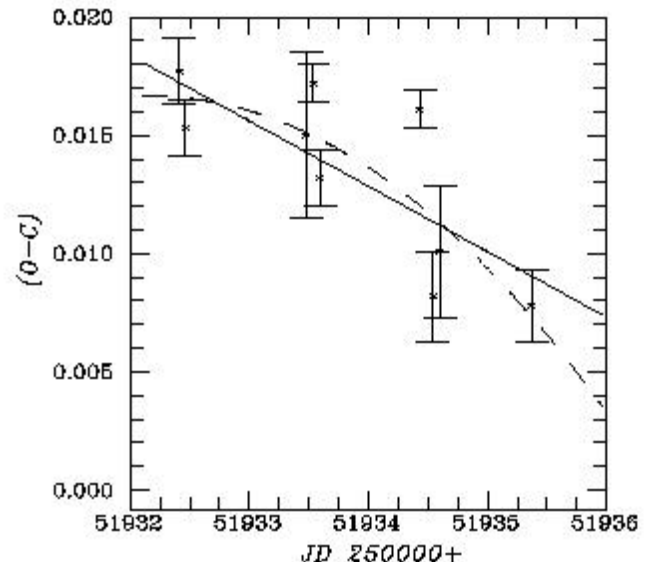


Figure 3: The (O-C) diagram for the time of the maxima calculated using the ephemeris (1). Line corresponds to a new ephemeris (2) and the dashed line - to the parabolic fit.

by parabola is slightly better: we got a less residuals after subtraction it from the original (O-C)s, then if we subtract the straight line. The residuals calculated as standard deviations are 0.00217 for parabola and 0.00223 for line. It could indicate the decrease of the superhump period. However, the quadratic term $Q = (-3.3 \pm 2.6) \cdot 10^{-6} \text{ days/cycle}^2$. Thus the decrease is not statistically significant.

This event often (but not always) is observable in different SU UMa-type stars.

This work was partially supported by the grant 02/07/00451 of the Ukrainian State Fund of Fundamental Research.

References

- Green R.F., Schmidt M., Liebert J.:1986, *ApJS*, **61**, 305.
 Harvey D., Skillman D.R., Patterson J., Ringwald F.A.: 1995, *PASP*, **107**, 551.
 Honeycutt R.K., Robertson J.W., Turner G.W.: 1995, *Cataclysmic Variables*, A. Bianchini, M. Della Valle, M. Orto (Eds.), *A.S.P. Conf. Ser.*, **205**, 75.
 Lipovetskiy V., Stepanjan J.: 1981, *Astrophysics (Armenia)*, **17**, 573.
 Marsakova V.I., Andronov I.L.: 1996, *Odessa Astron. Publ.*, **9**, 127.
 Nogami D., Kato, T., Masuda S., Hirata R., Matsumoto K., Tanabe K., Yokoo T.: 1995, *PASJ*, **47**, 897.
 Pikalova O.D., Shugarov S.Yu.: 1995, *A.S.P. Conf. Ser.*, **205**, 173.
 Szkody P., Howell S.B.: 1992, *ApJS*, **78**, 537.

MR SER: PHOTOMETRIC PORTRAIT OF UNUSUAL POLAR

A.V. Baklanov¹, E.P. Pavlenko²¹ Department of Astronomy and Astronomical Observatory
Odessa National University, Odessa 65014 Ukraine² Crimean Astrophysical Observatory, Nauchny, Crimea, Ukraine

ABSTRACT. Based on the CCD photometry (R) of MR Ser obtained in 1999-2001, the period was corrected with a corresponding ephemeris $\text{Min.HJD} = 2451369.9664 + 0.0787966E$. The phase curve exhibits drastic changes with luminosity.

Key words: Stars: variable: cataclysmic: polar: MR Ser

We present a result of 3-year detailed photometric investigations of the polar MR Ser. Totally 1773 brightness estimates have been obtained during 24 nights. Based on these data, we corrected its photometric period, as listed in the abstract, with the initial epoch corresponding to the season 1999. The data from 1999, 2000 and 2001 folded with this period are shown in Fig. 1. Over 3 year MR Ser displayed light variations up to $2^m.5$ in maximum and up to $1^m.5$ in minimum.

The mean profile for 1999 shows a sharp minimum and wide maximum with two "shoulders", where the right shoulder is higher than the left one. Amplitude of this profile is $1^m.7$. In 2000 the amplitude decreased up by 1^m , the left "shoulder" practically disappeared. The system became brighter. One may note a significant shift of the phase by $\sim 0.1P$, which may be possibly explained by the orientation changes of the magnetic axis of the white dwarf in respect to the rotating line of centers. In the first part of 2001 (2001a) the star was in its lowest brightness state and displayed one-humped profile with an amplitude of $0^m.5$.

In 20 days, it has shown a dramatical change: being unchanged in minimum, it jumped by $\sim 1^m$. At maximum, it approached the brightness maximum in 1999. However the shape of maximum now is different: the left "shoulder" is higher than the right one. The largest instability occurs at the phase ~ 0.7 , and the curve is most stable at the phase ~ 0.4 . All these changes may be explained by variations of the structure and orientation of the accretion column.

Table. Journal of observations.

year	days	N	t_{min}	t_{max}
1999	12	1301	51364.4280	51375.5071
2000	6	330	51665.3759	51748.4307
2001(a)	3	80	52083.4017	52100.4622
2001(b)	3	62	52124.3082	52128.2935

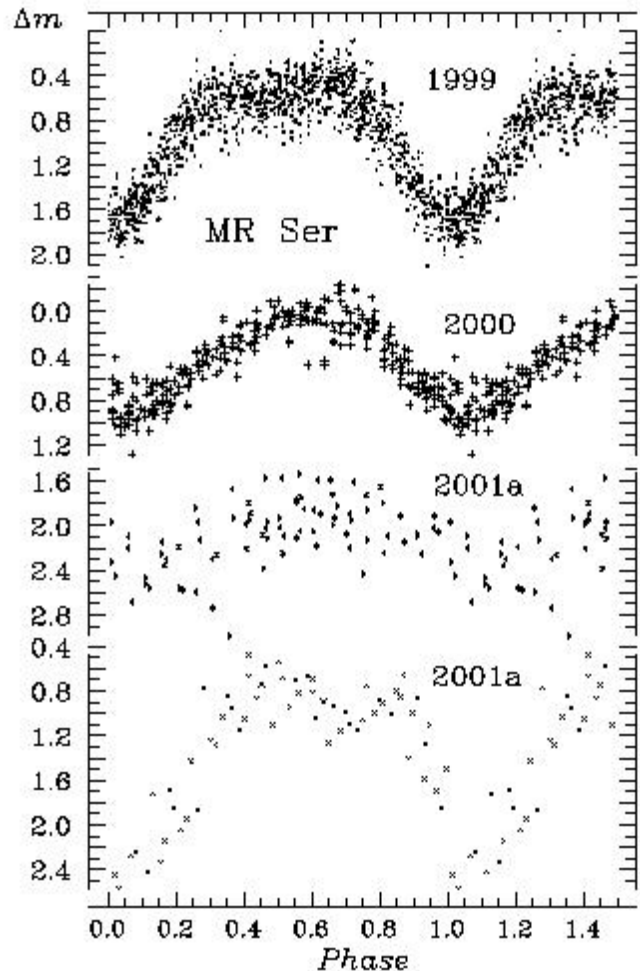


Figure 1: Phase light curves of MR Ser in different seasons

CCD-PHOTOMETRY OF CATAclySMIC VARIABLE ES Dra IN 2001

A.V. Baklanov¹, E.P. Pavlenko², O.I. Dudka³

¹ Department of Astronomy and Astronomical Observatory
Odessa National University, Odessa 65014 Ukraine

² Crimean Astrophysical Observatory, Nauchny, Crimea, 98409 Ukraine

³ Department of Astronomy Kharkov National University, Kharkov 61077 Ukraine

ABSTRACT. On the base of our 34-day photometry of ES Dra we found its ~ 20 -d light variations with amplitude of $1^m.6$ and suggest this star could belong to the nova-like subclass of cataclysmic variable stars.

Key words: Stars: variable: cataclysmic: ES Dra

ES Dra was first discovered by Green et al. (1986). They suspected this star to be cataclysmic variable. In the Catalog of Downes et al. (1997), ES Dra is preliminary classified as the UG - type binary which varies in the region $13^m.9 - 16^m.3$. Several efforts were undertaken in order to get the value of orbital period of this binary. Andronov (1991) found $P = 3h$, however Ringwald (1995) obtained $P = 4.24h$.

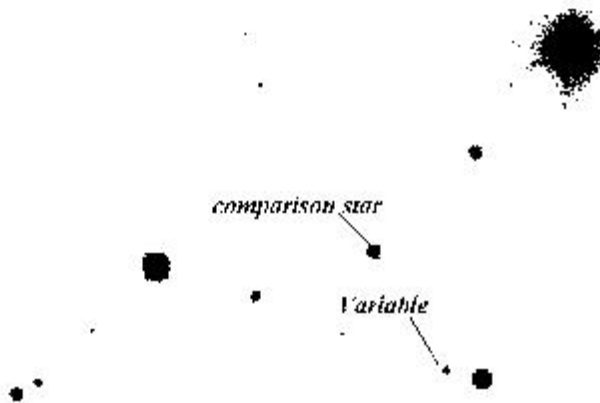


Figure 1: The finding chart of ES Dra. An additional designations of the binary are given accordingly to Downes and Shara (1993).

We made photometric observations of this binary during 34 nights in 2001 at the K-380 Cassegrain telescope of the Crimean astrophysical observatory in unfiltered light. In total we obtained 1732 brightness measurements of the variable and comparison star. We can see that ES Dra displays the long-term light variations with ~ 20 -d typical time and amplitude $1^m.6$.

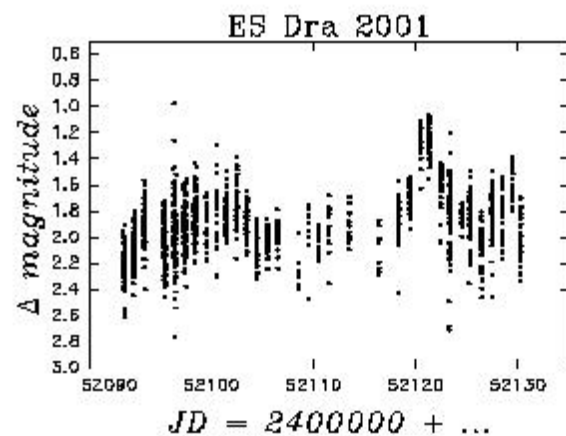


Figure 2: light curve of ES Dra in 2001. The stellar magnitude is given in respect to the comparison star ($m_{ph} = 14^m.8$).

The profile of the brightenings is changing from cycle to cycle. It seems that the ES Dra behaviour could be an attribute of rather nova-like star than that of a dwarf nova. Note that the brightness variations of the similar cycle was found in the SU UMa type binary RZ LMi (19d), classical nova V446 Her = Nova Her 1960 (22d), and nova-like RW Tri (25d) (R.K. Honeycutt et al., 1995). A detail analysis of the variability will be performed later.

This work was partially supported by the grant 02/07/00451 of the Ukrainian State Fund of Fundamental Researches.

References

- Andronov I.L.: 1991, *IBVS*, **3645**.
 Downes R.A., Shara M.M.: 1993, *PASP*, **105**, 127.
 Green R.F., Schmidt M., Liebert J.: 1986, *Ap.J. Suppl.*, **61**, 305.
 Honeycutt R.K., Robertson J.W., Turner G.W.: 1994, *Ap. Space Sci. Libr.*, **205**, 75.
 Ringwald F.: 1995, *private communication*.

DETERMINATION OF THE AGE OF LOW-MASS CLOSE BINARY STARS OF EARLY SPECTRAL CLASSES

I.I. Bondarenko, E.L. Perevozkina

Ural State Pedagogical University

Ekaterinburg, 620151, Russia, *minobr_info@mail.ur.ru*

ABSTRACT. The results of the determination of age of less-massive close binary stars of the early spectral classes are presented.

Key words: Stars: close binary: less-massive of the early spectral classes;

1. Introduction

The determination of age of close binary stars of the early spectral classes (CE) was made for the systems by Bondarenko and Perevozkina (1997). CE-stars with mass of a secondary component less than 3 solar masses belong to the group of less-massive CE. Secondaries of CE have F-K spectral classes. The determination of age was made by three methods: 1) of isochrones by Claret and Gimenez (1992) (isochrones on the diagram $L-T_{eff}$ with the tracks of Claret which were made by G. Dremova); 2) using the relation age-mass of Barrando et al. (1994)

$$\lg T = 9.883 - 2.965 \lg M, \\ \pm 22 \pm 122$$

where T - age of star in years, M - mass in solar masses. This relation is recommended to use for obtaining of age of chromosphere active binary stars (less-massive CE, KW and \sim KW-systems). 3) according to the law of braking of Scumanich (1972)

$$v_e = \lambda \cdot 10^{14} \cdot T^{-0.5}, \quad (1)$$

where T - age of star in seconds, $\lambda = 1.7$. The majority of the secondaries of less-massive CE has spectral class F5 and later, i.e. these components have

well-developed convective envelope. It is able to use the empirical law of Scumanich to calculate age of CE. Adopted, that the orbits are round ($e = 0$), an orbital period P is equal to the period of rotational motion. The equatorial speed v_e is calculated using means of radii of secondaries and means of orbital periods and adopted 4.5 times larger than the mean of speed in Scumanich law, $\lambda = 1.7$. Accounting adopted means Scumanich law is

$$T = 2.86 \cdot 10^{10} \cdot P^2 / R^2, \quad (2)$$

where T - age of star in years, P - orbital period in days, R - radius of star in solar radii. The calculated means of age of primaries by the methods of Barrando et al (1994) and Claret and Gimenez (1992) are accord in limit of 25%. The accordance of means of age of secondaries with use of the methods of Barrando, Claret and Scumanich is in limit of 22%. The calculations, which were made, confirm possibility to use an empirical law of Scumanich for obtaining of age of less-massive binary stars. Less-massive CE-systems have age from million years to ten milliard. Such interval of means of age points to an evolutionary unhomogeneous of CE-stars.

References

- Barrando D. et al.: 1994, *As. Ap.*, **290**, 137.
 Bondarenko I.I., Perevozkina E.L.: 1997, *Contact Stars of Early Spectral Classes: the monography Ural State Pedagogical university. Ekaterinburg*, 146.
 Claret A., Gimenez A.: 1992, *As. Ap. Suppl. Ser.*, **96**, 255.
 Scumanich A.: 1972, *Ap.J.*, **171**, 565.

MULTI-FREQUENCY STUDY OF SYMBIOTIC NOVAE

D. Chochol, T. Pribulla

Astronomical Institute of the Slovak Academy of Sciences
059 60 Tatranská Lomnica, Slovakia, *chochol,pribulla@ta3.sk*

ABSTRACT. Symbiotic novae are subclass of symbiotic stars - interacting binaries with wide orbits, whose photometric history is characterized by a single nova-like outburst lasting decades and caused by a thermonuclear runaway on the surface of a wind accreting white dwarf. Symbiotic novae have been detected in all frequencies from X-rays to radio waves. Multifrequency observations yield complementary information which appears to be crucial for an understanding of the underlying physical processes as an accretion by stellar winds, TNRs on the white dwarf, ionization of the wind from a cool giant, colliding winds, jets and bipolar outflows. The basic properties and multifrequency behaviour of the most studied objects: V1016 Cyg, V1329 Cyg, HM Sge, AG Peg, RT Ser, RR Tel and PU Vul are reviewed.

Key words: Stars: binary: symbiotic novae; stars: individual: V1016 Cyg, V1329 Cyg, HM Sge, AG Peg, RT Ser, RR Tel, PU Vul.

1. Introduction

Symbiotic stars are interacting binaries consisting of a cool evolved mass losing giant and a hot radiation source ($T_{hot} \approx 100\,000$ K), which is either an accreting main sequence star or a hot white dwarf. The hot star ionizes a portion of the giant's wind, giving rise to nebular emission. The nebula is the main source of the optical continuum. The near-IR colours indicate either the presence of normal giant with $T_{eff} \sim 3000-4000$ K (S-type systems) or the combination of reddened Mira and dust with temperature of ~ 1000 K (D-type systems). The distinction between S and D types (Webster & Allen, 1975) is given by orbital separation of the cool and hot component. The binary must have enough room for Mira-variable. Therefore, the orbital periods of D-type systems are expected in the range 20 - 200 years (Whitelock, 1987). The known orbital periods of symbiotic stars are from 227 days (T CrB) to 5300 days (CH Cyg), most of them run between 1-3 years. New catalogue of symbiotic stars include 188 symbiotic stars and 30 objects suspected of being symbiotic (Belczynski et al., 2000).

Symbiotic novae are subclass of symbiotic stars whose photometric history is characterized by a single nova-like outburst lasting decades. The original Allen's (1980) list of symbiotic novae: AG Peg, RT Ser, RR Tel, V1016 Cyg, V1329 Cyg, HM Sge was later complemented by PU Vul. Recent list including 22 objects was published by Munari (1997). As the symbiotic novae are detected in frequencies from X-rays up to radio, their detailed study requires a multifrequency approach.

The behaviour of symbiotic novae is similar to classical novae, except for much longer time scale. While the mass loser in classical novae is Roche lobe filling red dwarf, in symbiotic novae it is an M giant located well inside its Roche lobe. In both cases the accreting object is a white dwarf. The orbital periods of classical novae are smaller than two days, so the radius of the Roche lobe of the hot component is a few R_{\odot} . During thermonuclear runaway the hot component expands to dimensions $> 10 R_{\odot}$ and engulfs the binary system. Common envelope is ejected from the system in a few days or weeks. The orbital periods of symbiotic novae are larger than two years. Therefore both components are well separated, even during the expansion of the outbursting white dwarf to an A-F supergiant. The rise to the maximum luminosity lasts several months so it is slower than in classical novae. The increase of brightness of symbiotic novae due to the outburst does not exceed 7^m in V band. They remain at a steady high luminosity for dozens of years. Typical decline to the precoutburst luminosity lasts about 100 years.

The basic information about the nature of symbiotic novae provides the study of variability of these objects in UV, IR and optical region. Variability can be caused by: the eclipses, the reflection effect, the orbital variations of the emission measure in the nebular continuum, pulsations and/or rotation of the hot and cool component, changes of the structure of the circumstellar matter including accretion and excretion disks, interaction zone of colliding winds, flares, outbursts, dust formation. The most important physical processes which require multifrequency approach are: wind and disk accretion, flares, thermonuclear runaways, ionization of the cool giants winds, colliding winds, jets and bipolar outflows.

2. Basic orbital parameters

Orbital periods of symbiotic novae can be determined either from photometry (periodic brightness variations) or spectroscopy (periodic variations of the continuum or line fluxes, radial velocity curves). The following orbital periods were found from photometry:

V1329 Cyg - 959 days (eclipses in pre-outburst photometry; Stienon et al. (1974)), 956.5 days (post-outburst brightness variations; Schild & Schmid (1997), Chochol et al. (1999)).

RT Ser - 4502 days (post-outburst brightness variations; Pavlenko (1997)).

PU Vul - 4900 days (post-outburst eclipses; Nussbaumer & Vogel (1996), pre-outburst eclipses; Chochol et al. (1997)).

AG Peg - 816.5 days (post-outburst brightness variations; Fernie (1985)).

V1016 Cyg - 5510 days (periodicity in flares; Parimucha et al. (2000)).

The exact determination of the orbital periods of AG Peg and V1329 Cyg found from the photometric minima positions in their light curves is influenced by their apparent changes discovered by Skopal (1998). They are connected with changes of the energy distribution of the hot-star spectrum. The phase shift in the period correlates with the change in the star's brightness. Skopal (2001a) showed that the main source of of the optical continuum is the nebula arising from ionization of the cool giant wind by the hot star radiation. Variation in the emission measure is fully responsible for the observed wave-like modulation of the light curves of symbiotic binaries with the orbital phase. The large amplitude of the orbitally-related wave-like variations, shaping of minima and systematic changes in their positions reject their explanation by the reflection effect. The variation in the optical continuum should always be followed by a similar variation in Balmer emission lines.

Chochol & Wilson (2001) modelled U, B, V light curves of V1329 Cyg in terms of combined wind and chromospheric fluorescence, with eclipses and shadowing of fluorescent regions and conversion of far-ultraviolet energy into the optical bands.

The extended atmosphere of the cool giant scatters the light emitted from the hot component. The dust, Thomson, Rayleigh and Raman scattering play an important role. The previously unidentified emission lines at 6825 Å and 7082 Å were explained by Raman scat-

tering of the far ultraviolet O VI resonance doublet, emitted near the hot compact component, by neutral hydrogen in the extended atmosphere of the cool giant. Periodic changes of the polarization vector due to the orbital motion permit to determine orbital period, inclination and orientation of the orbital plane (Schmid, 1998). Orbital period RR Tel estimated by this method exceeds 100 years.

The 5510 days photometric periodicity in V1016 Cyg was independently confirmed from infrared photometry and UV spectroscopy by Parimucha et al. (2001). They showed that the variations in the $(J - K)$ colour index as well in the UV continuum and O III], N III], C III] and Si III] emission line fluxes exhibit the same periodicity interpreted as the orbital period of the binary (see also Parimucha et al. - this proceedings).

The absolute parameters of AG Peg were determined by Kenyon et al. (1993). Spectroscopic orbits for an M giant and a hot component (found from the radial velocities of He II $\lambda 4686$ Å emission line) provided the component masses $M_{cool} = 2.6 \pm 0.4 M_{\odot}$, $M_{hot} = 0.65 \pm 0.10 M_{\odot}$ and a semimajor axis $A = 2.5 \pm 0.1$ AU for an orbital inclination $i = 50^{\circ}$. The red giant does not fill its Roche lobe. The orbit of the cool M giant was slightly improved by Fekel et al. (2000).

Two objects from our sample show the presence of eclipses: PU Vul and V1329 Cyg.

Two subsequent minima in the post-outburst light curve of PU Vul were explained by Nussbaumer & Vogel (1996) as eclipses in a binary system with the orbital period 4900 days. The eclipses were confirmed by Chochol et al. (1997) from the analysis of the pre-outburst photometry published by Liller & Liller (1979). Chochol et al. (1996) studied the radial velocities of the outbursting white dwarf mimicing an F-supergiant in PU Vul from 1979 to 1987 and found a possible 761 days spectroscopic orbit ($f(m) = 1.6 M_{\odot}$). If confirmed, symbiotic nova PU Vul is a triple system similar to the eclipsing symbiotic triple system CH Cyg (Skopal 1997).

The pre-outburst photographic light curve of V1329 Cyg suggested the presence of eclipses with the period 959 days (Stienon et al., 1974). Grygar et al. (1979) confirmed this period by analyzing the radial velocities of optical emission lines and found extremely large semiamplitude of the orbit resulting in a mass function $f(m) = 23 M_{\odot}$, confirmed by Iijima et al. (1981) from optical spectra and Nussbaumer et al. (1986) from UV spectra. This mass function led to a very large mass of the cool component (at least $24 M_{\odot}$), which did not seem probable. Ikeda & Tamura (2000) argued that only certain portion of the emission-line profile of H α , He II and [O III] represents the true orbital motion and found acceptable $f(m) = 1.2 \pm 0.3 M_{\odot}$. Fekel et al. (2001) used infrared radial velocities of the cool giant and determined $K_2 = 7.85 \pm 0.26$ km/s and $f(m) = 0.0481 \pm 0.0047 M_{\odot}$. Both orbits lead to a mass ratio q

= 2.93 and masses of the components $M_{cool} = 2.2 M_{\odot}$ and $M_{hot} = 0.75 M_{\odot}$ for an orbital inclination $i = 86^{\circ}$ determined by Schild & Schmid (1997).

3. The cool component

Near-infrared region is optimal for the determination of the spectral types of the cool components because it includes the peak emission from the giant and the contamination by thermal dust emission, which dominates in thermal infrared region, is small. The spectral types of the cool giants in symbiotic novae recently determined by Mürset & Schmidt (1999) and Rudy et al. (1999) using infrared TiO and VO molecular bands are as follows: V1016 Cyg: M6-7, HM Sge: M7, V1329 Cyg: M5.5-6, AG Peg: M3, RR Tel: M6, RT Ser: M5.5-6, PU Vul: M4.5-6. The empirically determined dependencies of effective temperature and radius upon spectral type and $V - K$ colour for cool giants and supergiants was published by van Belle et al. (1999). The S-type objects: AG Peg, RT Ser, PU Vul and V1329 Cyg have near-IR colours of a late type giant, the D-type objects: HM Sge, V1016 Cyg, RR Tel indicate presence of a dust shell.

Infrared observations demonstrated that D-type systems contain long-period Mira variables (Whitelock, 1988). Their pulsation periods are in RR Tel: 387 days (Feast et al., 1983), in HM Sge: 527 days (Munari & Whitelock, 1989); 535 ± 5 days (Taranova & Shenavrin, 2000), in V1016 Cyg: 478 days (Munari, 1988); 470 ± 5 days (Taranova & Shenavrin, 2000), 474 ± 6 days (Parimucha et al. - this proceedings). Taranova & Shenavrin (2000) determined the parameters of the cool components in V1016 Cyg: $L_c = 8600 L_{\odot}$, $T_{eff} = 2850$ K, $R_c = 500 R_{\odot}$ and in HM Sge: $L_c = 10\,000 L_{\odot}$, $T_{eff} = 2650$ K, $R_c = 540 R_{\odot}$. They determined the radii of the cool shells in V1016 and HM Sge to be $1400 R_{\odot}$ and $1500 R_{\odot}$ and their masses $(3-3.3) \cdot 10^{-5} M_{\odot}$ and $(4-8) \cdot 10^{-5} M_{\odot}$.

Chochol et al. (1998) found from the R and V band photometry the pulsation period of the AGB component in PU Vul to be 217 days and determined $L_c = 3820 L_{\odot}$, $R_c = 282 R_{\odot}$ and $M_c = 0.76 M_{\odot}$. The photometric data from the 1993-4 eclipse were used by Chochol et al. (1997) and Chochol & Pribulla (2000) to calculate the radius of the cool component $R_c = 0.208 A = 287 R_{\odot}$ in agreement with the radius derived from pulsations. Pavlenko (1997) found the pulsation period of the cool giant in RT Ser $P = 213$ days from the B band photometry.

Cool components are characterized by slow winds with a velocity of about 10-20 km/s. The mass loss rates estimated by Whitelock (1987) and Kenyon et al. (1988) are $\dot{M} \sim 10^{-7} M_{\odot} \text{yr}^{-1}$ and $\dot{M} \sim 10^{-5} M_{\odot} \text{yr}^{-1}$ for S-type and D-type systems, respectively. Radio continuum measurements at 5-15 GHz confirmed this

result (Seaquist & Taylor, 1990).

4. The hot component

The hot components in symbiotic novae have undergone a single outburst lasting decades caused by the TNR on the surface of the wind accreting white dwarf. Historical light-curves of the symbiotic novae based on the published photometry were presented by Mürset and Nussbaumer (1994). We describe the history of the outburst for AG Peg, RR Tel, PU Vul and V1329 Cyg in more details.

AG Peg began the slowest classical nova outburst ever recorded in the mid-1850s, rising from 9^m to 6^m in about decade. The first available spectra from the beginning of 20th century revealed Be-type spectrum with strong P-Cygni profiles of emission lines. Then the hot component slowly shrunk, increased its temperature and in 1980's evolved to a Wolf-Rayet star (WN6 spectrum), a hot subdwarf with $T_{eff} > 100\,000$ K (Kenyon et al., 1993). The IUE observations of AG Peg showed broad He II $\lambda 1640 \text{ \AA}$ and N V $\lambda 1240 \text{ \AA}$ emission line profiles. A mass loss from the hot component by a fast wind in AG Peg was proved by Nussbaumer et al. (1995), who detected with the HST the P Cygni profile of N V line. The wind in 1994 had a terminal velocity of 1000 km/s and a mass-loss rate about $10^{-7} M_{\odot} \text{yr}^{-1}$ (Vogel & Nussbaumer, 1994). Historical data together with IUE spectra showed that the hot component maintained a roughly constant bolometric luminosity $3000 L_{\odot}$ from 1870 till 1985. During 1992-97 the bolometric luminosity declined by a factor 2-3 in comparison with the 1980-85 data (Kenyon et al., 2001).

RR Tel began its outburst in 1944. The mass-loss history was described by Nussbaumer & Dumm (1997). The nova outburst led to an extended atmosphere with a radius of $\approx 90 R_{\odot}$ and no mass loss. Thereafter it slowly shrunk and increased its effective temperature. The transition to the nebular stage was accompanied by a strong mass-loss. The corresponding wind increased its terminal velocity from ≈ 400 km/s in 1949 to ≈ 1300 km/s in 1960. There is no trace of mass loss after 1978. At present, the UV dereddened continuum can be fitted with a black-body emission of $T = 140\,000$ K and $L = 3700 L_{\odot}$, corresponding to a hot star with $R = 0.105 R_{\odot}$. The ROSAT X-ray observations showed that RR Tel exhibits supersoft α pulse height distribution i.e., essentially all counts are below 0.4 keV. The observations can be reproduced by the emission of a white-dwarf model atmosphere with $T_{eff} = 142\,000$ K and $L = 3500 L_{\odot}$ (Jordan et al., 1994).

PU Vul: Liller & Liller (1979) showed that during

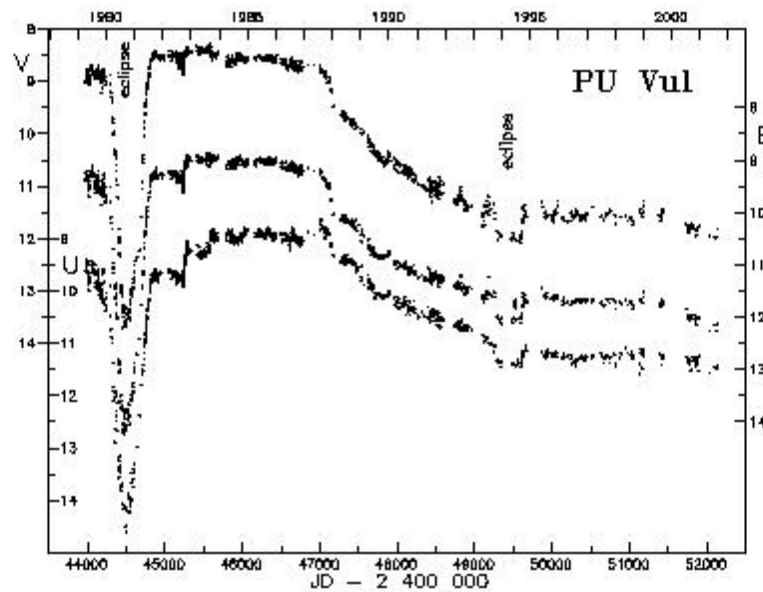


Figure 1: Long-term *UBV* photometry of PU Vul

1898-1956 the brightness of the object fluctuated between 15^m - 16.5^m prior to the slow rise to $B \sim 9.3^m$ in 1977-79. The *UBV* photometry of PU Vul is presented in Fig. 1. In 1979-87 the light curve exhibited almost flat maximum interrupted by an eclipse in 1980-82. The brightness maximum $B \sim 8.9^m$ was reached in 1983. Since 1987 the brightness continuously faded. In 1993-4 another eclipse was detected. During the flat maximum an F supergiant spectrum appeared (Belyakina et al., 1984). In 1987 the wind emerged from the hot star and the envelope was ejected. The nova entered to nebular stage in 1990 showing a rich emission line spectrum. P Cyg profile of Si IV line in IUE spectra taken in 1990-91 gave the evidence for a wind with terminal velocity ≈ 500 km/s (Vogel & Nussbaumer, 1992). Mass loss from the system $\dot{M} = 2.7 \cdot 10^{-7} M_{\odot} \text{yr}^{-1}$ was found by Seaquist et al. (1993) from radio observations. He determined an expansion velocity of the ionized shell to be $\approx 70 \pm 10$ km/s. Chochol et al. (1997) showed that the emission [O III] line profile consists of multiple peaks. They interpreted it as approaching and receding parts of the equatorial ring and polar blobs with the expansion velocities ≈ 80 km/s.

V1329 Cyg: In the years 1891-1964 the brightness of the object fluctuated around 15^m with occasional 2.5^m deep decreases, which repeated with a period 959 days (Stienon et al., 1974), interpreted as eclipses of the hot component by a red giant. The nova-like outburst started in 1964. The brightness maximum of 11.5^m was reached in 1966. The brightness decline was accompanied by wave-like variations with the orbital period 956.5 d. The spectral evolution after the discovery of the object in 1979 was characterized by the

gradual increase of the ionization level of the emission line spectrum. Crampton et al. (1970) found broad WR emission features with an expansion velocity of ~ 2300 km/s and a multiple structures of [Ne III] and [O III] emission lines with peaks extending from -240 to +250 km/s. Grygar et al. (1979) explained these structures by existence of ejected polar caps and an equatorial ring. Tamura (1977) noted the appearance of [Fe VII] emission lines and strengthening of the He II line in 1974-76.

Observations of symbiotic novae during outburst show the presence of fast winds from their hot components. Very broad WR emission features of He II, N III, C III, N V lines during nebular stage can be attributed to this wind.

Symbiotic novae fall into two classes with quite distinct spectral behaviour. In V1016 Cyg, V1329 Cyg and HM Sge the outburst led straight to a nebular emission spectrum. The photosphere of the outbursting white dwarf reached in maximum only few R_{\odot} . In AG Peg, RT Ser, RR Tel and PU Vul outbursting star remains several years in A-F supergiant state before entering the nebular phase. The outburst of symbiotic nova occurs when unstable hydrogen shell burning causes a white dwarf to expand to a radius of 1-100 R_{\odot} . This model predicts a long-duration, constant luminosity phase following the visual maximum. The evolution of luminosity and temperature during the outbursts of symbiotic novae was studied by Mürset & Nussbaumer (1994). They found the peak luminosities in the range 3700 - 37000 L_{\odot} and slowly increasing temperatures up to 200 000 K during their decline from visual maxima. Different behaviour of two types of symbiotic novae can be explained in terms of degenerate and non-

degenerate flashes. White dwarfs undergoing strong, degenerate flash evolve into A-F supergiant resembling the classical novae in maximum. Objects undergoing weak, non-degenerate flash remain at high effective temperatures and resemble planetary nebulae at visual maximum (Iben, 1982; Kenyon & Truran, 1983). The strong degenerate flashes occur at low accretion rates $\dot{M} < 10^{-9} M_{\odot}\text{yr}^{-1}$, while non-degenerate flashes at high accretion rates $\dot{M} > 10^{-8} M_{\odot}\text{yr}^{-1}$ (Iben, 1982).

Luminosities of the hot components at plateau portion of a white dwarf cooling curve are directly related to their masses by the core mass-luminosity relation (Paczynski, 1971; Joss et al., 1987). The masses of the white dwarfs in M_{\odot} , calculated by Mikolajewska & Kenyon (1992)⁽¹⁾ and Mürset & Nussbaumer (1994)⁽²⁾ are as follows: V1016 Cyg (1.1^(1,2)), HM Sge (0.9⁽¹⁾; 0.95⁽²⁾), V1329 Cyg (0.68⁽¹⁾; 0.81⁽²⁾), AG Peg (0.55⁽¹⁾; 0.54⁽²⁾), RR Tel (0.7⁽¹⁾; 0.85⁽²⁾), RT Ser (0.99⁽²⁾), PU Vul (0.9⁽¹⁾; 0.54⁽²⁾). The derived luminosities in plateau phase are responsible for differences in white dwarf masses presented in both papers. The distances to the systems which can resolve the problem are poorly known.

5. The nebula

The rich emission-line optical and UV spectra indicate the presence of a circumstellar ionized nebula formed by a mass loss from one or both components of the symbiotic nova. The diagnostic of the physical conditions within the nebula (electron densities and temperatures) can be accomplished using the forbidden and intercombination emission line fluxes (Viotti & Hack, 1993 and references therein). S-type symbiotics are surrounded by nebulae with electron densities $N_e \sim 10^8 - 10^{10} \text{ cm}^{-3}$, while the densities of nebulae in D-type systems are $N_e \sim 10^6 \text{ cm}^{-3}$ (Kenyon, 1986). Electron temperatures can be derived also from fitting of spectral energy distribution in the continuum between 0.12 and 5 μm by a three-component model of radiation. Two stellar components are approximated by Planck functions, while the nebular spectrum is represented by the free-bound and free-free emission from hydrogen (Skopal, 2001b). Application of this method allowed to determine electron temperatures of AG Peg and V1329 Cyg as $T_e = 17\,200 \text{ K}$ and $T_e = 19\,500 \text{ K}$, respectively (Skopal, 2001c).

Taylor (1988) reviewed the radio imaging of symbiotic stars and categorized ionized nebulae into two types: outburst ejecta with strong tendency for bipolar or jet morphology and stellar winds. V1016 Cyg and HM Sge show the characteristics of both types. Extended nebulae can be resolved by radio-interferometric observations and high-resolution CCD imaging. The nebulae of HM Sge, V1016 Cyg and AG Peg were resolved both at radio and optical wave-

length (Corradi et al., 1999a and references therein), V1329 Cyg by the HST at optical wavelength (Schild & Schmid, 1997). The UV images of HM Sge were taken by the HST (Hack & Paresce, 1993). Direct images of the extended nebular structures around D-type symbiotics show bipolar geometry. The detailed study of the optical nebulae around HM Sge and V1016 Cyg (Corradi et al., 1999b) shows the evidence of elongated and collimated outflows. HM Sge possesses a curved collimated string of knots as a result of a fast collimated wind from the white dwarf and precessing accretion disk. The bipolar outflow velocities of 120 km/s for V1016 Cyg and 200 km/s for HM Sge were found from long-slit spectroscopic imaging (Solf, 1983; 1984).

The matter lost by a cool giant escapes from the system directly by conventional stellar wind or during the accretion process onto the hot component. This component loose the mass by wind which can be collimated by an accretion disk or by the ejection of the envelope due to the outburst. Binary model for the creation of bipolar circumstellar outflows was proposed by Morris (1987). The wind of the red giant forms an accretion disk around the secondary component and an excretion disk encompassing the whole system. A second wind arises from the interior of the accretion disk. The presence of accretion and excretion disk in V1329 Cyg was proposed by Chochol & Vittone (1986). Long-term photometry of this object shows that the orbital brightness variations are modulated by a secondary period of 553 days and a possible cycle of ≈ 5300 days (Chochol et al., 1999), probably caused by the precession and nutation of the accretion disk. The existence of the accretion disk is supported by the 3D simulation of the wind accretion by compact star (Theuns & Jorissen, 1993) as well as by the 2D gas dynamic simulation of a mass-transfer by stellar wind in symbiotic stars (Bisikalo et al., 1997).

In the standard model (Seaquist et al., 1984; Taylor & Sequist, 1984; Nussbaumer & Vogel, 1987) the nebula is generated in the wind from the cool giant and part of this wind is photoionized by the hot star. Ionized region can be either completely enclosed by neutral material or the cone of ionized material sweeps over the one of the components.

In the colliding-wind model the wind from the hot component interacts with the wind of the cool giant (Wallerstein et al., 1984; Girard & Willson, 1987; Nussbaumer & Walder, 1993). The winds from two components approach from opposite directions colliding head-on in the region between the stars and head-on-tail outside. As a result, the reverse shock propagating in the direction of the white dwarf and expanding shock propagating towards and beyond the giant appear.

Detailed 3D simulations of colliding winds in symbiotics performed by Walder (1998) show the presence of the spiral-shaped interaction zone of the two winds. It consists from the driving part, where the hot-star wind

crashes into the slow, dense wind of the cool giant and lagging part characterized by a huge rarefaction of the cold wind.

For the collision region, temperatures of a few million K and consequently X-ray emission are expected. Symbiotic novae V1016 Cyg and HM Sge were detected as bright X-ray sources by Allen (1981) using the EINSTEIN satellite. The same objects as well as AG Peg and PU Vul were detected also by ROSAT. These objects exhibit harder β pulse height distribution that typically peaks at 0.8 keV and can be reproduced with the emission from a very hot optically thin plasma heated by the shocks in the collision of two stellar winds (Mürset et al., 1995, 1997). All β -type observations were fitted with one point Raymond-Smith type plasma model and temperatures 3.1 - 6.3 millions K were derived.

The colliding wind model was successfully applied to the calculation of the line and continuum spectra of HM Sge (Formigini et al., 1995), AG Peg (Contini, 1997) and RR Tel (Contini & Formigini, 1999). The model fits the high- and low-ionization emission lines taking into account both the shock created by the winds and photoionization flux from the hot star.

Kenny & Taylor (1998) applied a model of orbital colliding winds developed by Kenny (1995) to explain radio observations of HM Sge. They derived the orbital period of HM Sge as 80^{+60}_{-20} years. Richards et al. (1999) used the MERLIN and VLA radio observations to show that emission peaks appear to be corotating with the binary orbit as the ionization front and the hot wind from the white dwarf interact with the Mira wind. The development of the radio structure over 5 years allowed to estimate the binary separation $A = 50$ AU if the distance is $d = 1250 \pm 280$ pc. Eyres et al. (2001) used HST and VLA observations to measure for the first time the positions of the binary components of a symbiotic star HM Sge directly. They estimated the projected angular binary separation to be 40 ± 9 mas. The colliding winds model was successfully applied also for explanation of the MERLIN radio observations of V1016 Cyg (Watson et al., 2000).

Acknowledgements. This work was supported by VEGA Grant No. 1157 of the Slovak Academy of Sciences.

References

- Allen D.: 1980, *MNRAS*, **190**, 75.
 Allen D.: 1981, *MNRAS*, **197**, 739.
 Belczynski K., Mikolajewska J., Munari U., Ivison R.J., Friedjung M.: 2000, *As.Ap.S*, **146**, 407.
 Belyakina T.S., Bondar N.I., Chochol D., Chuvpav K.K., Efimov Y.S., Gershberg R.E., Grygar J., Hric L., Krasnobabtsev V.I., Petrov P.P., Pürola V., Savanov I.S., Shakhovskaya N.I., Shakhovskoy N.M., Shenavrin V.I.: 1984, *As.Ap.*, **132**, L12.
 Bisikalo D.V., Boyarchuk A.A., Kuznetsov O.A., Chechetkin V.M.: 1997, in *Physical Processes in Symbiotic Binaries and Related Systems*, J. Mikolajewska (ed.), CFFA Warszawa, p. 83.
 Chochol D., Andronov L.L., Arkhipova V.P., Chinanova L.L., Mattei J., Shugarov S.Y.: 1999, *Contrib. Astron. Obs. Skalnaté Pleso*, **29**, 31.
 Chochol D., Pribulla T.: 2000, in *The Impact of Large-Scale Surveys on Pulsating Star Research*, L. Szabados & D.W.Kurtz (eds.), ASP Conf. Ser. **203**, p. 125.
 Chochol D., Pribulla T., Tamura S.: 1998, *IBVS*, **4571**.
 Chochol D., Pribulla T., Tamura S., Tajitsu A., Kanamitsu O.: 1997, in *Physical Processes in Symbiotic Binaries and Related Systems*, J. Mikolajewska (ed.), CFFA Warszawa, p. 127.
 Chochol D., Tamura S., Kanamitsu O., Pribulla T., Tajitsu A.: 1996, in *Cataclysmic Variables and Related Objects*, A.Evans & J.H.Wood (eds.), Kluwer Academic Publishers, p. 343.
 Chochol D., Vittone A.: 1986, *Ap.Sp.Sci.*, **121**, 225.
 Chochol D., Wilson R.E.: 2001, *MNRAS*, **326**, 437.
 Contini M.: 1997, *ApJ*, **483**, 886.
 Contini M., Formigini L.: 1999, *ApJ*, **517**, 925.
 Corradi R.L.M., Brandi E., Ferrer O.E., Schwarz H.E.: 1999a, *As.Ap.*, **343**, 841.
 Corradi R.L.M., Ferrer O.E., Schwarz H.E., Brandi E., Garcia L.: 1999b, *As.Ap.*, **348**, 978.
 Crampton D., Grygar J., Kohoutek L., Viotti R.: 1970, *Astrophys. Lett.*, **6**, 5.
 Eyres, S.P.S., Bode M.F., Taylor A.R., Crocker M.M., Davis R.J.: 2001, *ApJ*, **551**, 512.
 Feast M.W., Whitelock P.A., Catchpole R.M., Roberts G., Carter B.S.: 1983, *MNRAS*, **202**, 951.
 Fekel F.C., Hinkle K.H., Joyce R.R., Skrutskie M.F.: 2001, *AJ*, **121**, 2219.
 Fekel F.C., Joyce R.R., Hinkle K.H., Skrutskie M.F.: 2000, *AJ*, **119**, 1375.
 Fernie J.D.: 1985, *PASP*, **97**, 653.
 Formigini L., Contini M., Leibowitz E.M.: 1995, *MNRAS*, **277**, 1071.
 Girard T., Wilson L.A.: 1987, *As.Ap.*, **183**, 247.
 Grygar J., Hric L., Chochol D., Mammano A.: 1979, *BAC*, **30**, 308.
 Hack W.J., Paresce F.: 1993, *PASP*, **105**, 1273.
 Iben I.: 1982, *ApJ*, **259**, 244.
 Iijima T., Mammano A., Margoni R.: 1981, *Ap.Sp.Sci.*, **75**, 237.
 Ikeda Y., Tamura S.: 2000, *PASJ*, **52**, 589.
 Jordan S., Mürset U., Werner K.: 1994, *As.Ap.*, **283**, 475.
 Joss P.C., Rappaport S., Lewis W.: 1987, *ApJ*, **319**, 180.
 Kenny H.T.: 1995, *PhD thesis*, Univ. Calgary, Canada.

- Kenny H.T., Taylor A.R.: 1998, *J. R. Astron. Soc. Canada*, **92**, 317.
- Kenyon S.J.: 1986, *The Symbiotic Stars*, Cambridge University Press.
- Kenyon S.J., Fernandez-Castro T., Stencel R.: 1988, *AJ*, **95**, 1817.
- Kenyon S.J., Mikolajewska J., Mikolajewski M., Polidan R.S., Slovak M.H.: 1993, *AJ*, **106**, 1573.
- Kenyon S.J., Proga D., Keyes C.D.: 2001, *ApJ*, **122**, 349.
- Kenyon S.J., Truran J.W.: 1983, *ApJ*, **273**, 280.
- Liller M.H., Liller W.: 1979, *AJ*, **84**, 1357.
- Mikolajewska J., Kenyon S.: 1992, *MNRAS*, **256**, 177.
- Morris M.: 1987, *PASP*, **99**, 1115.
- Munari U.: 1988, *As.Ap.*, **200**, L13.
- Munari U.: 1997, in *Physical Processes in Symbiotic Binaries and Related Systems*, J. Mikolajewska (ed.), CFFA Warszawa, p. 37.
- Munari U., Whitelock P.A.: 1989, *MNRAS*, **237**, 45.
- Mürset U., Jordan S., Walder R.: 1995, *As.Ap.*, **297**, L87.
- Mürset U., Nussbaumer H.: 1994, *As.Ap.*, **282**, 586.
- Mürset U., Schmid H.M.: 1999, *As.Ap.S*, **137**, 473.
- Mürset U., Wolff B., Jordan S.: 1997, *As.Ap.*, **319**, 201.
- Nussbaumer H., Dumm T.: 1997, *As.Ap.*, **323**, 387.
- Nussbaumer H., Schmitz W., Vogel M.: 1986, *As.Ap.*, **169**, 154.
- Nussbaumer H., Schmitz W., Vogel M.: 1995, *As.Ap.*, **293**, L13.
- Nussbaumer H., Vogel M.: 1987, *As.Ap.*, **182**, 51.
- Nussbaumer H., Vogel M.: 1996, *As.Ap.*, **307**, 470.
- Nussbaumer H., Walder R.: 1993, *As.Ap.*, **278**, 209.
- Paczynski B.: 1971, *Acta Astron.*, **21**, 417.
- Parimucha Š., Arkhipova V.P., Chochol D., Kroll P., Pribulla T., Shugarov S.Y., Ulyanikhina O., Chinarova L.L.: 2000, *Contrib. Astron. Obs. Skalnate Pleso*, **30**, 99.
- Parimucha Š., Chochol D., Pribulla T., Buson L.M., Vittone A.: 2001, *As.Ap.*, submitted.
- Pavlenko E.P.: 1997, in *Physical Processes in Symbiotic Binaries and Related Systems*, J. Mikolajewska (ed.), CFFA Warszawa, p. 205.
- Richards A.M.S., Bode M.F., Eyres S.P.S., Kenny H.T., Davis R.J., Watson S.K.: 1999, *MNRAS*, **305**, 380.
- Rudy R.J., Meier S.R., Rossano G.S., Lynch D.K., Puetter R.C., Erwin P.: 1999, *As.Ap.S*, **121**, 533.
- Sequist E.R., Krogulec M., Taylor A.R.: 1993, *ApJ*, **410**, 260.
- Sequist E.R., Taylor A.R., Button S.: 1984, *ApJ*, **284**, 202.
- Sequist E.R., Taylor A.R.: 1990, *ApJ*, **349**, 313.
- Schild H., Schmid H.M.: 1997, *As.Ap.*, **324**, 606.
- Schmid H.M.: 1998, *Rev. Modern Astronomy*, **11**, 297.
- Stienon F.M., Chartrand M.R., Shao C.: 1974, *AJ*, **79**, 47.
- Skopal A.: 1997, in *Physical Processes in Symbiotic Binaries and Related Systems*, J. Mikolajewska (ed.), CFFA Warszawa, p. 99.
- Skopal A.: 1998, *As.Ap.*, **338**, 599.
- Skopal A.: 2001a, *As.Ap.*, **366**, 157.
- Skopal A.: 2001b, *Contrib. Astron. Obs. Skalnate Pleso*, in press.
- Skopal A.: 2001c, in preparation.
- Solf J.: 1983, *ApJ Lett.*, **266**, 113.
- Solf J.: 1984, *As.Ap.*, **139**, 296.
- Tamura S.: 1977, *Astrophys. Lett.*, **19**, 57.
- Taranova O.G., Shenavrin V.I.: 2000, *Astron. Lett.*, **26**, 600.
- Taylor A.R.: 1988, *The Symbiotic Phenomenon*, J. Mikolajewska, M. Friedjung, S.J. Kenyon & R. Viotti (eds.), Kluwer Academic Publ., p. 77.
- Taylor A.R., Sequist E.R.: 1984, *ApJ*, **286**, 261.
- Theuns T., Jorissen A.: 1993, *MNRAS*, **265**, 946.
- Van Belle G.T., Lane B.F., Thompson R.R., Boden A.F., Colavita M.M., Dumont P.J., Mobley D.W., Palmer D., Shao M., Vasisht G.K., Wallace J.K., Creech-Eakman M.J., Koresko C.D., Kulkarni S.R., Pan X.P., Gubler J.: 1999, *AJ*, **117**, 521.
- Viotti R., Hack M.: 1993, in *Cataclysmic Variables and Related Objects*, M. Hack & C. la Dous (eds.), NASA SP-507, p. 663.
- Vogel M., Nussbaumer H.: 1992, *As.Ap.*, **259**, 525.
- Vogel M., Nussbaumer H.: 1994, *As.Ap.*, **284**, 145.
- Walder R.: 1998, *Ap.Sp.Sci.*, **260**, 243.
- Wallerstein G., Willson L.A., Salzer J., Brugel E.: 1984, *As.Ap.*, **133**, 137.
- Watson S.K., Eyres S.P.S., Davis R.J., Bode M.F., Richards, A.M.S., Kenny H.T.: 2000, *MNRAS*, **311**, 449.
- Webster B.L., Allen D.A.: 1975, *MNRAS*, **171**, 171.
- Whitelock P.A.: 1987, *PASP*, **99**, 573.
- Whitelock P.A.: 1988, *The Symbiotic Phenomenon*, J. Mikolajewska, M. Friedjung, S.J. Kenyon & R. Viotti (eds.), Kluwer Academic Publ., p. 47.

OBSERVED PROPERTIES OF CONTACT BINARY SYSTEMS

A. Kalimeris, H. Rovithis-Livanidou

Section of Astrophysics, Astronomy & Mechanics, Dept. of Physics, Athens University,
Panepistimiopolis, Zografos 157 84, Athens, Greece *elivan@cc.uoa.gr*

ABSTRACT. A group of close eclipsing systems, which continues to pose a challenge in many subjects of modern astrophysics, is that of contact binaries. In this study, using the most recent observational data of a large sample of such systems, a review concerning their properties is presented. Except from the basic graphs, appeared so far in similar reviews, some new diagrams for their angular momentum, horizontal energy transfer, and corrected mass- radius relations are given. From them, some new important properties of contact binaries are derived.

Key words: Stars: binaries: contact

1. Introduction

Regardless the large number of papers referred to contact binaries -and especially to those of W UMa-type, that is to the late type ones- which have been presented up to now (e.g. Hazlehurst 1970, Mochnacki 1981, 1985, van Hamme 1982, Duerbeck 1984, Kaluzny 1985, Rucinski 1985, 1992, Maceroni et al. 1985, Kähler 1989, 1997, Rovithis-Livanidou et al. 1992, Maceroni, van't Veer 1996), a lot of problems, concerning their structure and evolution are still open. Lucy (1968) was the first to make serious attempt to construct equilibrium models of contact binaries that take into account Kuiper's paradox; and it had proved surprisingly difficult to construct contact systems, that satisfy all the observational constrains. Later, Biermann and Thomas (1972, 1973) proposed some models; while, various theories and other models were developed and suggested by many investigators concerning the structure and evolution of contact binaries, as well as their general properties (e.g. Vilhu 1973, Vilhu and Rahunen 1976, Hazlehurst 1976, Rahunen and Vilhu 1977, 1982, Shu 1980, Shu and Lubow 1981, Hazlehurst et al. 1973, 1980, 1982, 1984, Rahunen 1983, Smith 1984, Rucinski 1985, 1992, Webbink 1977, Rucinski and Kaluzny 1994, Karetnikov 1996).

Binnendijk (1970) divided the late type contact systems to two sub-classes: A and W, according to their light curves properties, while a third sub-class (known as E) was added to include the early type contact binary systems.

In the present study the properties of contact binaries will be presented, based on the latest observational data of a large sample of such systems. Special attention will be paid to the late type systems, since a larger number of them, compared to those of early type, have been observed and analyzed so far, and thus they yield to more reliable results.

2. Observational Data

The observational material used in the present study is mainly come from the photometric observations of these systems, and their subsequent analysis using modern techniques, based on the Roche geometry. Spectroscopic data were also used where available. Thus, eighty (80) contact binaries, with well observed light curves, were included in our study. From them, 38 belong to the W sub-class, 30 to A, and 12 are early type contact systems. The mass ratios range from $q = 1$ (for V701 Sco) to $q = 0.072$ (for AW UMa).

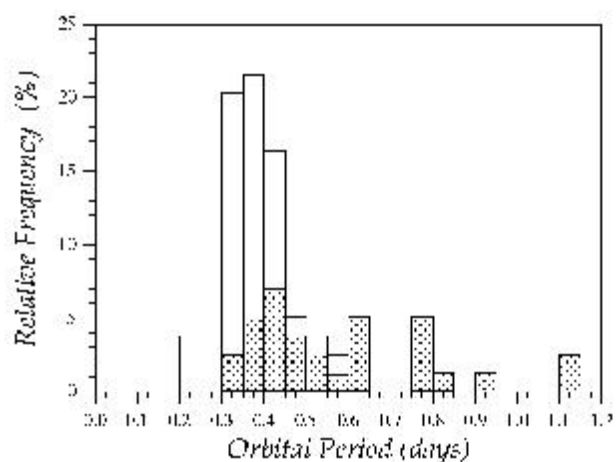


Figure 1: Orbital periods distribution of contact binaries.

3. General Observed Properties

3.1. Orbital Periods and Spectral Types

The orbital period distribution of contact binaries, in groups of 0.5 days, are presented in Fig.1, where dashed

blocks denote the A sub-class systems, blank these of W, and dashed-tilde blocks those of E. The same symbolism will be kept in all other diagrams, where the relative frequency is involved. From this figure, one can notice that the periods of the W sub-class systems range from 0.22 to 0.65 days; these of the A are greater than 0.3, while those of E are greater than 0.8 days.

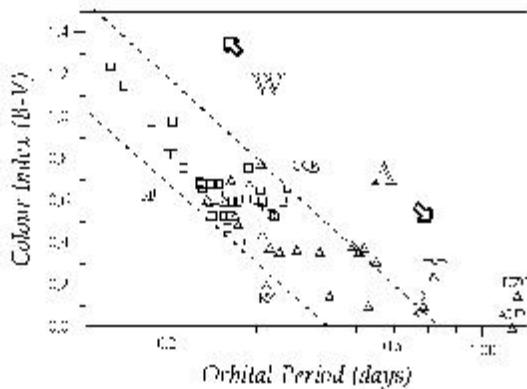


Figure 2: The period colour diagram of contact binaries.

Moreover, a relation exists between the colour index (B-V) and the orbital period P, known as the colour-period diagram, or Eggen's relation (Eggen 1961, 1967, Lucy 1968). For the sample used in our study, this relation is presented in Fig.2. Most of the contact systems lie within a zone -Eggen's zone- of 0.15 day width, with the W sub-class systems being at upper left part of the diagram, and the A, at right lower part; while, there is a mixing of the two sub-classes from F7 to G7 spectral types.

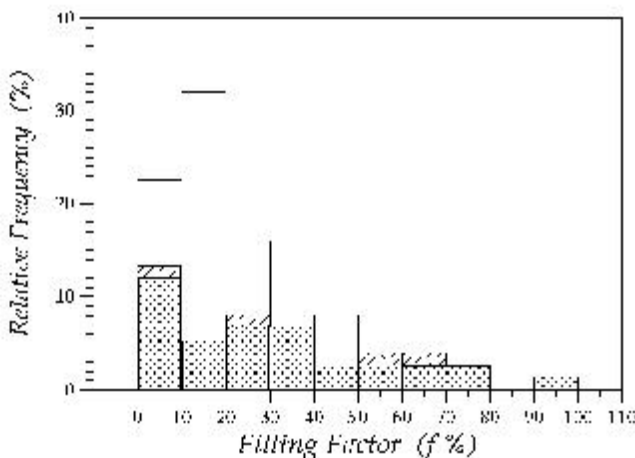


Figure 3: The filling factor distribution for contact binaries.

According to Hazlehurst (1970), the zone is extended in both sides of the line: $(B - V) = -0.55 - 2.26 \log P$; while a different description is given by Kähler & Fehlberg (1991): $1.5 \log T_{eff} - \log P = c$, where c varies

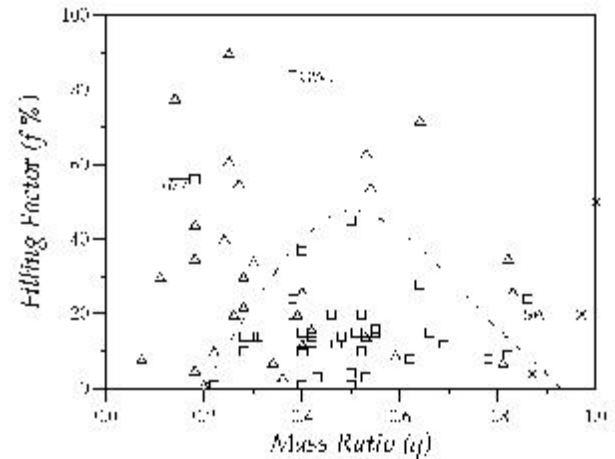


Figure 4: The filling factor mass-ratio relation of contact binaries. Squares denote the W, and triangles the A sub-class; while crosses the early type systems, E.

from 5.975 to 6.15.

3.2. Mass-ratio and Filling Factor

Fig.3 presents the filling factor f (Mochnacki, 1981), distribution of contact systems.

All W UMa-type systems have small filling factors, generally less than 25%. More specifically, in most of the W sub-class, f is around 15%, and in most of the A's f is around 5%. It seems that there is no contact system to be in complete over-contact (having $f = 100\%$). The f values are less than 84%, with one exception, the UZ Leo system, for which f was found to be equal to 90%; but, the accuracy of its elements is not as high as that of other systems.

Fig.4, shows the filling factor mass-ratio relation, f - q , where squares denote the W sub-class systems, triangles these of A, and crosses those of E. This symbolism will be kept from here on. From Fig.4 one can notice that the W sub-class systems, with the exception of 3, that is: of SW Lac, V677 Cen and GW Cep, are bounded by the dashed line.

From Fig.4, is also obvious that W systems, are getting greater filling factor values, when mass ratio q is around 0.5, and smaller for $q < 0.3$ & $q > 0.8$. On the contrary, the A sub-class systems are uniformly spread all over the f - q diagram, and appear to develop greater f values towards smaller mass-ratio q 's.

3.3. Masses and Radii

The masses of the late type contact binaries are generally small. The masses of their primary components are less than $2.4M_{\odot}$, and these of their secondary stars less than $1.2M_{\odot}$, M_{\odot} being the solar mass.

On the other hand, the radii of most of the primary stars of W UMa-type systems are very little above

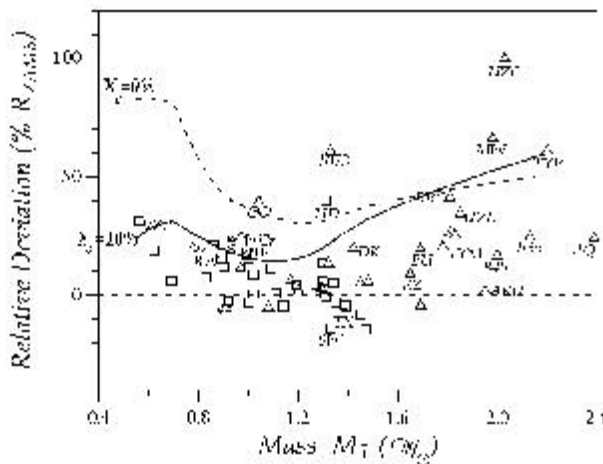


Figure 5: Relative deviation of primary stars radii of contact binaries, from ZAMS and TAMS. (Models by Mengel et al. 1979).

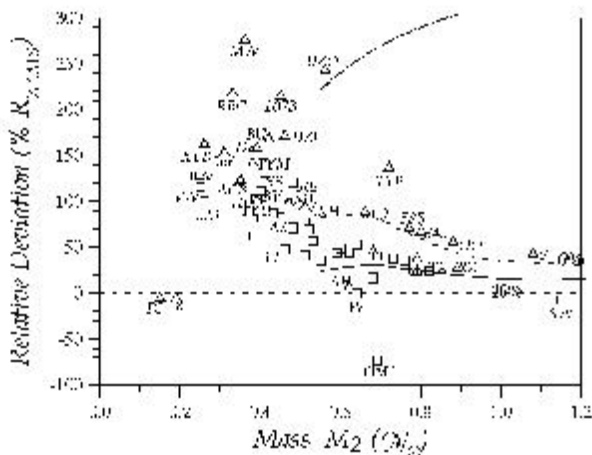


Figure 6: Same as Fig.5, but for the secondary components of contact systems. Moreover, the dashed-dot line denotes the radius value of an ordinary star, before entering the giant branch.

ZAMS (Fig.5); while, that of their secondaries are very much above it: from 30 to 300%, greater than ZAMS (Fig.6). It is worthwhile to mention that the relative deviation of the secondaries' radii is greater towards the smaller mass values.

In Figs.5 and 6, the thick dashed line denotes TAMS (when hydrogen in the star's nuclei is zero, 0%), while the continuous one stands for the luminosity of an ordinary star, when its hydrogen has been reduced to 10%. The same symbolism is used in Figs. 9, 10, 12 and 13, too.

3.4. Temperature Differences

The temperature difference appeared on the surface of the common photosphere of late type contact systems of W UMa-type, has been attributed to two absolutely

different causes: 1) to the physical processes of their common envelope or 2) to the presence of dark spots, similar to those of our Sun. Assuming that the temperature differences are real, then from the light and colour curves analysis of these systems, it comes out that their values range from -450 to +550 K, as is shown in Fig.7. From this figure, we notice that in the early type contact systems the temperature differences are very small (of the order of ± 50 degrees).

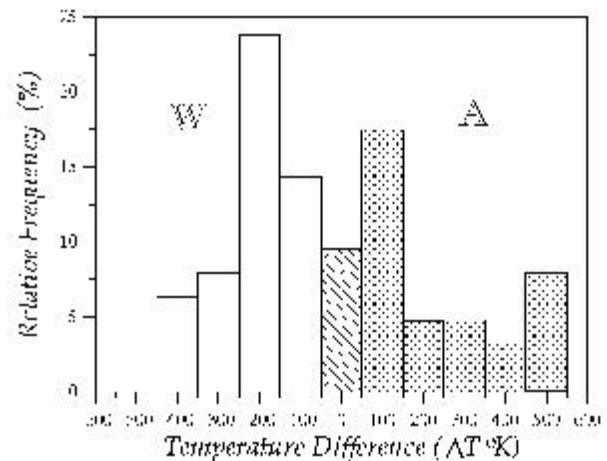


Figure 7: The temperature difference for the two basic sub-classes W and A, of contact binaries of W UMa-type.

Moreover, in Fig.8 the temperature difference versus the colour index (B-V) is shown. From this, is obvious that almost all W UMa-type systems with colour index greater than 0.5, (that corresponds to spectral types later than F7-8), have secondaries with much greater T_{eff} values than their primary components.

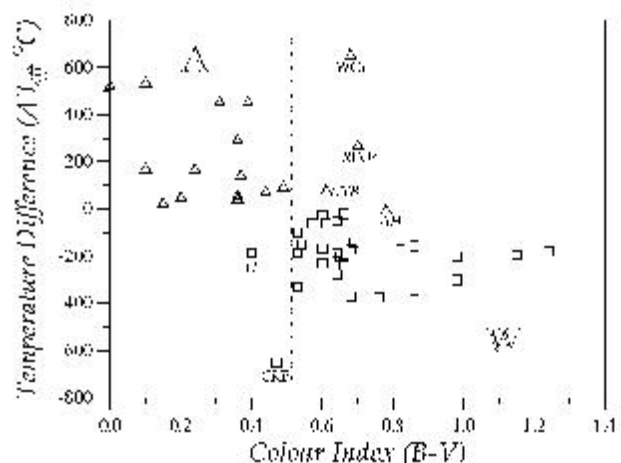


Figure 8: Relation between temperature differences and colour index (B-V), for the two basic sub-classes of contact binaries of W UMa-type.

3.5. Luminosities

The real luminosities of the two components of W UMa-type systems, can not be measured directly from observations, due to large amounts of energy transfer ΔL from primaries to the secondaries stars.

The total energy $L_1 + L_2$, coming out from the two components photospheres, is equal to the total energy $L_{1,e} + L_{2,e}$, produced by their nuclei, if the amount of energy lost by the primary is added to the secondary component. In Figs.9 and 10, the observed luminosities versus the ZAMS nuclear luminosities, for the primary and secondary stars of a contact binary are presented, respectively. The dashed diagonal line, denotes the relation $L_{1,ob} = L_{1,e}$ and $L_{2,ob} = L_{2,e}$, respectively, without energy transfer, and for zero age components. $L_{i,ob}$, $i=1,2$, stands for the observed luminosity of the two stars of the system.

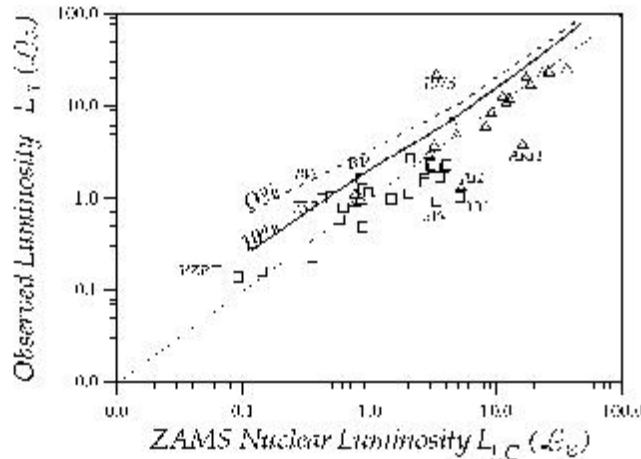


Figure 9: Comparison of the observed luminosity versus ZAMS nuclear luminosity for the primary components of late type contact binaries.

As is obvious from Fig.9, primary components follow in general the ZAMS mass-luminosity relation, although a large number is below it. On the other hand, Fig.10, shows that almost all secondaries have much larger luminosities than ZAMS, and in some cases, even TAMS values; with bigger deviations to those of A subclass.

4. The Energy Transfer

The energy transfer ΔL , is not a directly measured quantity. It can be computed, assuming that the energy lost by the primary star, is added to the secondary component to yield to an isothermal common photosphere. In such a case:

$$L_{1,ob} = L_{1,e} - \Delta L, \text{ and}$$

$$L_{2,ob} = L_{2,e} + \Delta L.$$

Using Stefan-Boltzmann, and Planck laws, we get: $((L_{1,e} - \Delta L)/(\sigma A_1))^{1/4} = ((L_{2,e} + \Delta L)/(\sigma A_2))^{1/4} = \Delta T_{eff}$, where A_i , $i=1,2$ is the area of the outer envelope of the i -component. This quantity can be arithmeti-

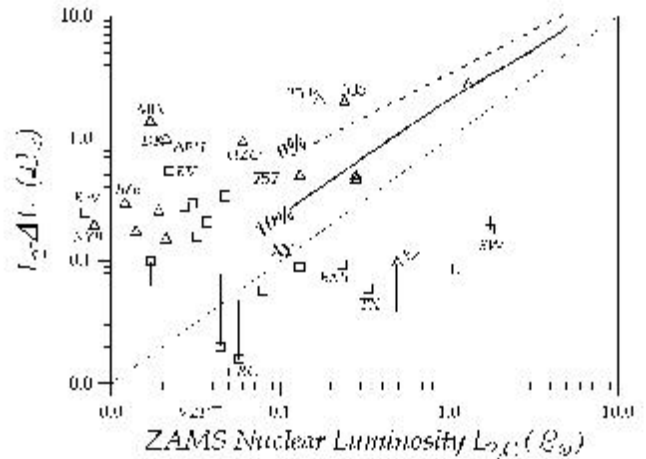


Figure 10: Same as Figure 9, but for the secondary components.

cally calculated through the Roche model, when the filling factor, the period and the two stars' masses are known. In this way ΔL was calculated and in Fig.11 has been plotted versus the mass-ratio q . Moreover, the following relation was found:

$$\log(\Delta L/L_{2,e}) = 2.66 - 3.5 \cdot q$$

for the secondary components.

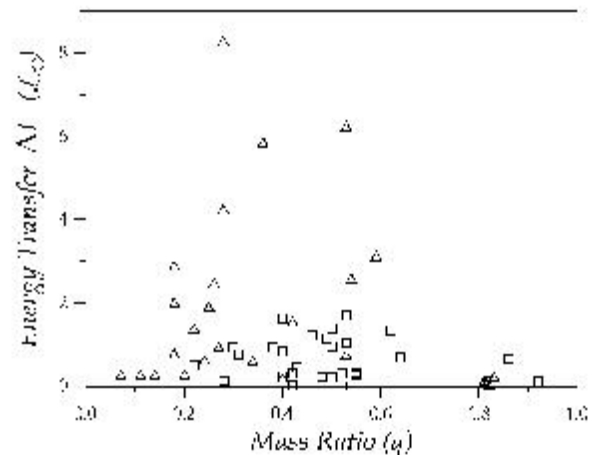


Figure 11: Energy transfer versus mass-ratio q , for the two basic sub-classes of contact binaries of W UMa-type.

A first estimation of the amounts of energy produced at the two stars' nuclei, is also possible since: $L_{1,e} = L_{1,ob} + \Delta L$ and $L_{2,e} = L_{2,ob} - \Delta L$, for the primary and the secondary components, respectively. Figs.12 and 13 present the corrected luminosities of primary and secondary components, respectively towards their ZAMS nuclear luminosities. Again, most primaries are very close to ZAMS, and with the exception of one (the V1073 Cyg system), no one is above TAMS. Five, (the DK Cyg, U Peg, BV Dra, BW Dra, and VS Psc) are on TAMS; while four, (the SW Lac, YY Eri, AH Vir,

AK Her), are below ZAMS.

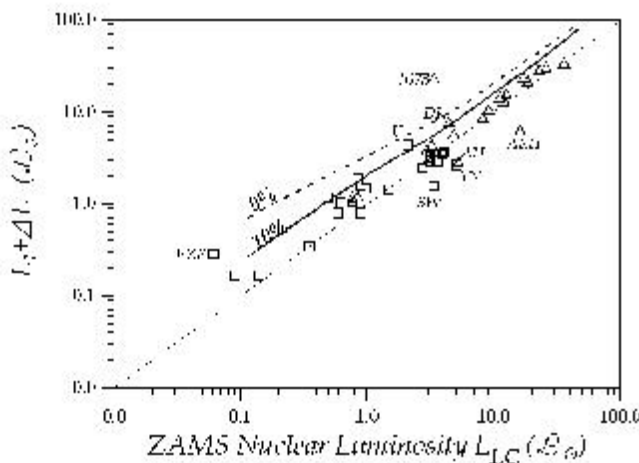


Figure 12: Comparison of the corrected luminosity towards ZAMS nuclear luminosity for primary components of the two basic sub-classes of late type contact binaries.

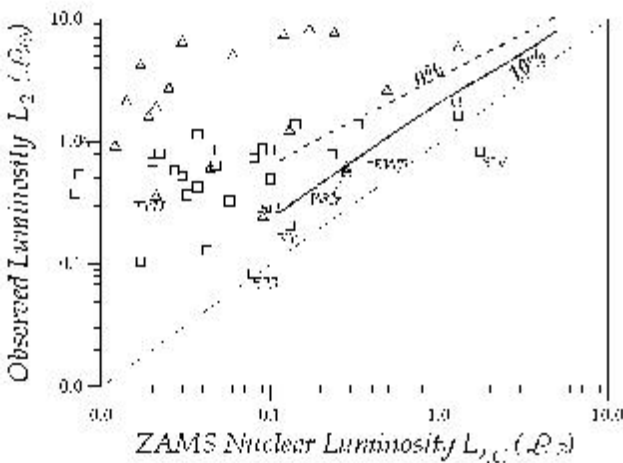


Figure 13: Same as figure 12, but for the secondary components.

On the contrary, a significant large number of secondaries (especially of the A sub-class), are on ZAMS, or even above it. Due to big errors, this result is not certain; and although the whole picture can not be considered as clear, it seems that there are some weak indications according to which some of them (about 20%), is possible to be above ZAMS.

Acknowledgements. H. R-L acknowledges the financial support of the University of Athens.

References

Biermann P., Thomas H-C: 1972, *As.Ap.*, **16**, 60.
 Biermann P., Thomas H-C: 1973, *As.Ap.*, **23**, 55.
 Binnendijk L.: 1970, *Vistas in Astron.*, **12**, 217.
 Durbeck H.D.: 1984, *Mitt. Astron. Gesellschaft*, **62**, 17.
 Eggen O.: 1961, *Roy. Obs. Bull. Ser.*, **31**, 101.
 Eggen O.: 1967, *MemRAS*, **70**, 111.
 Hazlehurst J.: 1976, in *Structure and Evolution of Close Binary Stars*, eds. P.Eggleton et al., p.323.
 Hazlehurst J.: 1970, *MNRAS*, **140**, 129.
 Hazlehurst J., Meyer-Hofmeister E.: 1973, *As.Ap.*, **24**, 379.
 Hazlehurst J., Refsdal S.: 1980, *As.Ap.*, **84**, 200.
 Hazlehurst J., Hoepfner W., Refsdal S.: 1982, *As.Ap.*, **109**, 117.
 Hazlehurst J., Refsdal S.: 1984, *As.Ap.*, **133**, 63.
 Kähler H.: 1989, *As.Ap.*, **209**, 67.
 Kähler H.: 1997, *As.Ap.*, **326**, 161.
 Kähler H., Fehlberg H.: 1991, *As.Ap.*, **252**, 137.
 Kazny J.: 1985, *Acta Astron.*, **35**, 313.
 Karetnikov V.G.: 1996, *Ap.S.S.*, **246**, 309.
 Lucy L.B.: 1968, *Ap.J.*, **151**, 1123.
 Maceroni C., Milano L., Russo G.: 1985, *MNRAS*, **217**, 843.
 Maceroni C., van't Veer F.: 1996, *As.Ap.*, **311**, 523.
 Mengel J.G., Demarque P., Sweigart A.V., Gross P.G.: 1979, *Ap.J.S.*, **40**, 733.
 Mochnacki S.W.: 1981, *Ap.J.*, **245**, 650.
 Mochnacki S.W.: 1985, in *Interacting Binary Stars*, eds. J.Pringle and R.Wade, Cambridge University Press, p. 51.
 Rahunen T.: 1983, *As.Ap.*, **117**, 235.
 Rahunen T., Vilhu O.: 1977, *As.Ap.*, **58**, 99.
 Rahunen T., Vilhu O.: 1982, in *IAU Coll. No.69*, eds. Z.Kopal and J.Rahe, D. Reidel, Dordrecht, Holland, p. 289.
 Rucinski S.M.: 1985, in *Interacting Binaries*, eds. P.Eggleton and J.Pringle, D. Reidel, Dordrecht, Holland, p. 115.
 Rucinski S.M.: 1992, *A.J.*, **103**, 960.
 Rucinski S.M., Kazny J.: 1994, *Mem.S.A.B.*, **65**, 113.
 Shu F.H.: 1980, in *IAU Symp. No. 88*, eds. M.Plavec et al., D. Reidel, Dordrecht, Holland, p. 477.
 Shu F.H., Lubow S.H.: 1981, *Ann. Rev.As.Ap.*, **10**, 277.
 Smith R.C.: 1984, *Q. Jl. R. Soc.*, **25**, 405.
 van Hamme W.: 1982, *As.Ap.*, **116**, 27.
 Vilhu O.: 1973, *As.Ap.*, **26**, 267.
 Vilhu O., Rahunen T.: 1976, *IAUS*, **73**, 337.
 Webbink R.F.: 1977, *Ap.J.*, **215**, 851.

ON THE ESTIMATION OF THE LIFETIME OF THE ACCRETION DISK IN THE SEMIDETACHED BINARIES

A.A. Kilpio

Institute of Astronomy, Moscow, Russia, *skilpio@inasan.rssi.ru*

ABSTRACT. The results of 3D numerical simulations of mass transfer in semidetached binaries after the mass transfer termination are presented. On the first stage the 3D gasdynamical simulation of mass transfer for the case of constant rate of mass transfer has been conducted up to the steady-state solution. Then the matter outflow was adopted to be terminated and the dependency of the lifetime of residual disk on numerical viscosity has been considered.

Key words: Stars: binary: cataclysmic; stars: accretion disk.

1. Problem setup

The purpose of this work is to investigate the flow structure in a semidetached binary after the mass transfer termination. On the first stage the 3D gasdynamical simulation of the gaseous flows for the case of constant rate of mass transfer has been conducted up to the steady-state solution. Then it was adopted that matter outflow is terminated and the fate of residual disk was considered. It is well known that the evolution of accretion disk is controlled by physical processes responsible for the redistribution of the angular momentum in the disk. To investigate the influence of viscosity we conduct 3 runs for various values of viscosity, these ones corresponding to the following effective values of parameter α in terms of the α -disk (Shakura and Syunyaev 1994): $\alpha \sim 0.08 \div 0.1$, $0.04 \div 0.06$ and $0.01 \div 0.02$.

Let us consider a semidetached binary system and adopt that accretor has the mass M_1 , the mass-losing star has the mass M_2 , the separation of the binary system is A , and angular velocity of orbital rotation is Ω . The flows of matter in this system can be described by Euler equations with equation of state for ideal gas $P = (\gamma - 1)\rho e$, where P - pressure, ρ - density, e - specific internal energy, γ - adiabatic index. To mimic the radiative loss of energy we adopt the value of γ close to 1: $\gamma = 1.01$, which corresponds to the near-isothermal case (Bisikalo et al. 1997, Molteni et al. 1991).

To obtain the numerical solution of the system of equations we used the Roe-Osher TVD scheme of a high order of approximation (Roe 1986, Chakravarthy and Osher 1985) with Einfeldt modification (Einfeldt 1988). The original system of equations was written in a dimensionless form. To do this, the spatial variables were normalized to the separation A , the time variables were normalized to the reciprocal angular velocity of the system Ω^{-1} , and the density was normalized to its value in the inner Lagrangian point L_1 . The gas flow was simulated over a parallelepipedon $[-^{1/2}A \dots ^{1/2}A] \times [-^{1/2}A \dots ^{1/2}A] \times [0 \dots ^{1/4}A]$ (due to the symmetry of the problem calculations were conducted only in the top half-space). The sphere with a radius of $^{1/100}A$ representing the accretor was cut out of the calculation domain.

The boundary and the initial conditions were determined as follows:

- the donor star fills it's Roche lobe;
- we adopted free-outflow conditions at the accretor and at the outer boundary of the calculation domain;
- on the first stage in gridpoint corresponding to L_1 we injected the matter with parameters $\rho = \rho(L_1)$, $V_x = c(L_1)$, $V_y = V_z = 0$, where $c(L_1) = 10^{-1}$ - is a gas speed of sound in L_1 ;
- on the second stage when steady-state regime was reached at the moment of time $t = t_0$ we adopted free-outflow conditions at the accretor and at the outer boundary of the calculation domain.

The initial conditions corresponded to the background gas with the following parameters were used:

$$\rho_0 = 10^{-5} \rho(L_1), \quad P_0 = 10^{-4} \rho(L_1) c^2(L_1) / \gamma, \quad \mathbf{V}_0 = 0.$$

2. Estimation of the lifetime of the residual disk for different values of viscosity

To evaluate the influence of the viscosity on the solution, three runs with different spatial resolution were conducted. The Euler equations don't include

physical viscosity so we varied the numerical viscosity by virtue of changing of computational grid. Three grids were chosen for the simulation: $31 \times 31 \times 17$ ("A"), $61 \times 61 \times 17$ ("B") $91 \times 91 \times 25$ ("C"). The used grids were uniform for all the runs. In terms of the α -disk the numerical viscosity for runs "A", "B", "C" approximately corresponds to $\alpha \sim 0.08 \div 0.1$, $0.04 \div 0.06$ and $0.01 \div 0.02$.

Prior to simulation of the flow structure with stopped mass transfer the near-steady-state solutions for the case of constant non-zero rate of mass transfer were obtained and used as initial conditions. At the moment of time $t = t_0$, the rate of mass transfer was decreased in five order of magnitude, which corresponds to the termination of the mass transfer.

Calculations of runs "A" and "B" were lasted until the density of gas becomes less than the background density $\rho_0 = 10^{-5} \rho(L_1)$. This corresponds to the full vanishing of matter due to accretion and outflow through outer boundary. The durations of these two runs correspond to $5P_{orb}$ and $12P_{orb}$ after the moment of time t_0 . Run "C" has the best resolution and the minimal numerical viscosity. Nevertheless, this run was conducted to $10P_{orb}$ only, since this run is very computer-time-consuming while the time when disk vanishes can be estimated as $\sim 50P_{orb}$. We extrapolated the results of calculation of run "C" for $t > 10P_{orb}$.

To evaluate the lifetime of the residual disk we used the estimation of the gas mass change $\dot{m} = \iiint \rho dx dy dz$, which is shown on Figures 1 and 2. In Fig. 1 the time variation of the total mass of the calculation domain is presented. Fig. 2 demonstrates the change of the mass of the accretion disk zone versus time. The accretion disk sizes change from runs to runs; therefore, for the sake of comparison of results of different runs we calculate not the exact mass changes in the accretion disk but the mass changes in the domain $r < 0.1, h < 0.05$, which is rather close to the accretion disk sizes for all the three runs. The lower limit of the density of gas is the background density ρ_0 , therefore the mass of the uniform matter with $\rho = \rho_0$ calculated for the whole computation domain and for the disk zone are asymptotic lines for graphs $m(t)$. These lines are shown in the corresponding figures by dashed lines.

The analysis of the data presented in the figures shows that the lifetime of the residual disk is increased with the decrease of the numerical viscosity: for the run "A" ($\alpha \approx 0.1$) $\tau_{disk} \approx 5P_{orb}$; for the run "B" ($\alpha \approx 0.05$) $\tau_{disk} \approx 12P_{orb}$; for the run "C" ($\alpha \approx 0.01$) he extrapolation of the result of simulation shows that the lifetime of the residual disk exceeds 50 orbital periods. It is pertinent to note that the value $\alpha \approx 0.01$ is typical for observable accretion disks (Lynden-Bell and Pringle 1974, Meyer-Hofmeister and Ritter 1993, Tout 1996, Armitage and Livio 1996). Consequently,

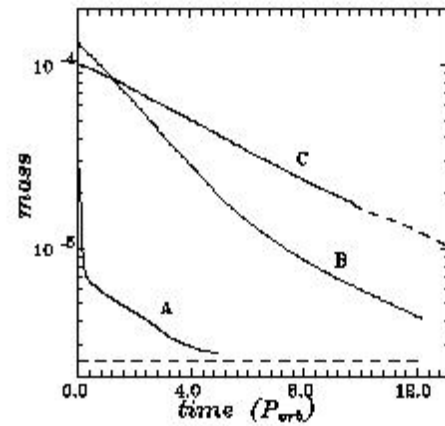


Figure 1: Time evolution of the total mass of the calculation domain for "A" ($\alpha \approx 0.1$), "B" ($\alpha \approx 0.05$), and "C" ($\alpha \approx 0.01$) runs. The mass of the uniform matter corresponding to the background density $\rho = \rho_0$ is shown by the dashed line.

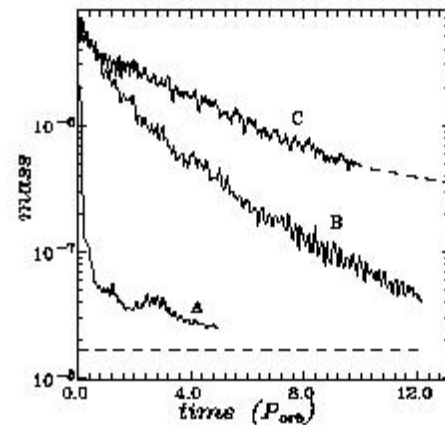


Figure 2: Time evolution of the mass of the accretion disk zone for "A" ($\alpha \approx 0.1$), "B" ($\alpha \approx 0.05$), and "C" ($\alpha \approx 0.01$) runs. The mass of the uniform matter corresponding to the background density $\rho = \rho_0$ is shown by the dashed line.

we can expect the lifetime of residual disk after the termination of mass is of order 50 orbital periods (near a week) for typical dwarf novae.

3. Conclusions

The 3D numerical simulations of structure of the accretion disk after the mass transfer termination reveals an essential increase of its lifetime with the decrease of viscosity. For effective $\alpha \sim 0.05$ the lifetime of the residual disk exceeds 12 orbital periods and for $\alpha \sim 0.01$ (that is typical for observable accretion disks) the lifetime of the residual disk is as much as 50 orbital periods.

Acknowledgements. This work has been partially funded by the RFBR grants 99-02-17619 and 01-02-06106, grants of the President of Russian Federation 00-15-96722 and 99-15-96022 as well as by the INTAS grant 00-491.

References

- Armitage P.J., Livio M.:1996, *Ap.J.*, **470**, 1024.
Bisikalo D.V., Boyarchuk A.A., Kuznetsov O.V.,
Chechyotkin V.M.: 1997, *Astron. Rep.*, **41**, 786.
Chakravarthy S., Osher S.: 1985, *AIAA Pap.*, **85**, 363.
Einfeldt B.: 1988, *SIAM J. Numer. Anal.*, **25**, 294.
Lynden-Bell D., Pringle G.E.: 1974, *M.N.R.A.S.*, **168**,
603.
Meyer-Hofmeister E., Ritter H.: 1993, in *"The
Realm of Interacting Binary Stars"*, eds J.Sahade,
G.E.McCluskey, Jr., Y.Condo., 143.
Molteni D., Belvedere G., Lanzafame G.: 1991,
Monthly Notices Roy. Astron. Soc., **249**.
Roe P.L.: 1986, *Ann. Rev. Fluid Mech.*, **18**, 337.
Shakura N.I., Syunyaev R.A.: 1994, *Sov. Astron.*,
1972, **16**, 756.
Tout C.:1996, in *"Cataclysmic Variables and Related
Objects"*, eds A.Evans, J.H.Wood., 97.

2D MODELLING OF THE GAS FLOW STRUCTURE IN THE SYMBIOTIC STAR Z ANDROMEDAE

E.Yu. Kilpio

Institute of Astronomy RAS, Moscow, Russia, *lena@inasan.rssi.ru*

ABSTRACT. The 2D gasdynamical simulations of gas flow structure in the symbiotic star Z And have been carried out for different stellar wind regimes. Since the mechanisms of gas acceleration in stellar atmospheres are not well studied, the parametric representation of gas accelerating force was used. The calculations for various stellar wind velocity regimes have shown that for realistic cases the accretion discs in the system were formed.

Key words: Stars: binary: symbiotic; stars: gas flow; stars: individual: Z And.

1. Problem setup

Z Andromedae is one of the most famous representatives of symbiotic stars. It is generally admitted to be the binary system with the components not filling the Roche lobe. Therefore, the mass exchange in Z And should be driven by the stellar wind. Previous studies (e.g. Bismovaty-Kogan et al. 1979, Bisikalo et al. 1994, Bisikalo et al. 1996) have shown that the general structure of the gas flow in binary systems with components not filling the Roche lobe, is defined first and foremost by the stellar wind parameters and it is very important to fix the velocity regime of the stellar wind.

Unfortunately, the wind velocity regime is not well-known due to the absence of an avowed mechanism of gas acceleration in stellar atmospheres. To avoid this ambiguity we use in the model the additional artificial force that accelerates gas. This force can be written in the following form:

$$\mathbf{F} = \alpha \frac{GM_1}{r^2} \frac{\mathbf{r}}{|\mathbf{r}|}$$

where M_1 is the mass of the primary component, G - gravitational constant, r - distance from the center of the primary component, α is the dimensionless parameter. This force has been included in the original Roche potential and all the simulations were carried out using the modified Roche potential.

This approach allowed us to obtain all possible stellar wind velocity regimes by varying the parameter α

without taking into account the detailed mechanisms of gas acceleration.

In this work the results of 2D gasdynamical calculations for $\alpha = 0.3, 0.5, 0.7, 0.8, 0.9$ are presented.

2. The model

In the gasdynamical model we use the 2D system of Euler equations in rotational coordinate frame:

$$\frac{\partial \rho}{\partial t} + \frac{1}{r} \frac{\partial(r\rho u)}{\partial r} + \frac{1}{r} \frac{\partial(\rho v)}{\partial \varphi} = 0$$

$$\begin{aligned} \frac{\partial(\rho u)}{\partial t} + \frac{1}{r} \frac{\partial(r\rho u^2 + rP)}{\partial r} + \frac{1}{r} \frac{\partial(\rho uv)}{\partial \varphi} &= \\ &= \frac{P}{r} - \rho \frac{\partial \Phi}{\partial r} + \rho \frac{v^2}{r} + 2\Omega v \rho \end{aligned}$$

$$\frac{\partial \rho v}{\partial t} + \frac{1}{r} \frac{\partial \rho uv}{\partial r} + \frac{1}{r} \frac{\partial(\rho v^2 + P)}{\partial \varphi} = -\frac{\rho}{r} \frac{\partial \Phi}{\partial \varphi} - \rho \frac{uv}{r} - 2\Omega u \rho$$

$$\frac{\partial(\rho E)}{\partial t} + \frac{1}{r} \frac{\partial(r\rho uh)}{\partial r} + \frac{1}{r} \frac{\partial(\rho vh)}{\partial \varphi} = -\rho u \frac{\partial \Phi}{\partial r} - \rho \frac{v}{r} \frac{\partial \Phi}{\partial \varphi}$$

here ρ denotes density, u and v are r and φ components of the velocity vector respectively, P is the pressure, $E = \varepsilon + \frac{|u|^2}{2}$ - total specific energy, ε - specific internal energy, Ω is the system's angular velocity.

The modified Roche potential after including the accelerating gas force has the following form:

$$\Phi(\mathbf{r}) = -\frac{GM_1}{|\mathbf{r} - \mathbf{r}_1|} + \alpha \frac{GM_1}{|\mathbf{r} - \mathbf{r}_1|} - \frac{GM_2}{|\mathbf{r} - \mathbf{r}_2|} - \frac{1}{2} \Omega^2 (\mathbf{r} - \mathbf{r}_c)^2$$

where \mathbf{r}_1 , \mathbf{r}_2 are radius-vectors of centers of components, \mathbf{r}_c - radius-vector of the mass center of the binary system, M_2 is the mass of the secondary component (accretor).

We restricted our consideration to an ideal gas model with adiabatic index $\gamma = 5/3$ and equation of state:

$$P = (\gamma - 1) \rho \varepsilon$$

To solve this system of equations the explicit finite-difference Roe scheme with restrictions of flows in Osher forms (Roe 1986, Chakravarthy and Osher 1985) was used.

The boundary and the initial conditions were determined as follows:

- The gas is injected from the donor's surface with radial velocity $v = 25 \text{ km/s}$;
- We adopted free-outflow conditions at the accretor and at the outer boundary of the calculation domain;
- The initial conditions corresponded to the background gas with the following parameters were used:

$$\rho_0 = 10^{-5} \rho(R_1), \quad P_0 = 10^{-4} \rho(R_1) c^2(R_1) / \gamma,$$

$$\mathbf{V}_0 = 0.$$

where R_1 is the radius of the donor.

The coordinate system was defined as follows: the origin of coordinates is located in the center of the mass-losing star, X -axis is directed along the line connecting the centers of stars, from the mass-losing star to the accretor, Y -axis is directed along the orbital movement of the accretor. The calculations region was adopted as $[-A \dots 2A] \times [-\frac{3}{2}A \dots \frac{3}{2}A]$. All the calculations were carried out for 301×301 computational grid.

The parameters for Z And required for our calculations were taken from the work by Fernandez-Castro et al. (1988): the mass of the primary (mass-losing) component $M_1 = 2M_\odot$ and its radius $R_1 = 77R_\odot$, the mass of the secondary component $M_2 = 0.6 M_\odot$ and the radius $R_2 = 0.07R_\odot$, the orbital period of the system $P = 758.8$ days, separation between the components $A = 482.53R_\odot$. These parameters result in the Roche lobe radius $(R/A) = 0.48$. The orbital velocity of the system $V_{orb} = 32 \text{ km/s}$.

3. Results

The results of numerical simulations for different values of α parameter show that up to $\alpha=0.8$ there are no steady state solution. The matter firstly injected into the system falls back to the donor's surface and finally there is no matter left to form the disk (the obtained densities don't exceed the background value). The situation is rather different for greater values of $\alpha \geq 0.8$ – here the stationary regime takes place in few orbital periods. The accretion disk and the bow shock wave in front of the secondary component are formed. Here the gas densities are significantly greater than the background values.

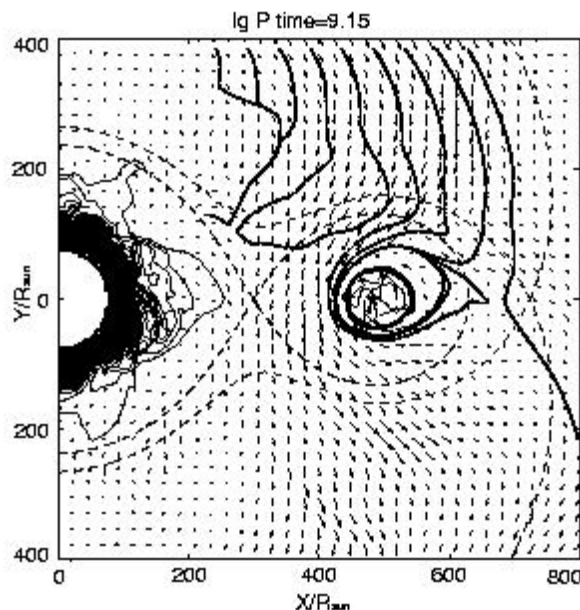


Figure 1: Fields of pressure and velocity vectors in equatorial plane for run with $\alpha=0.7$. The length of the longest arrow corresponds to the velocity value of 100 km/s

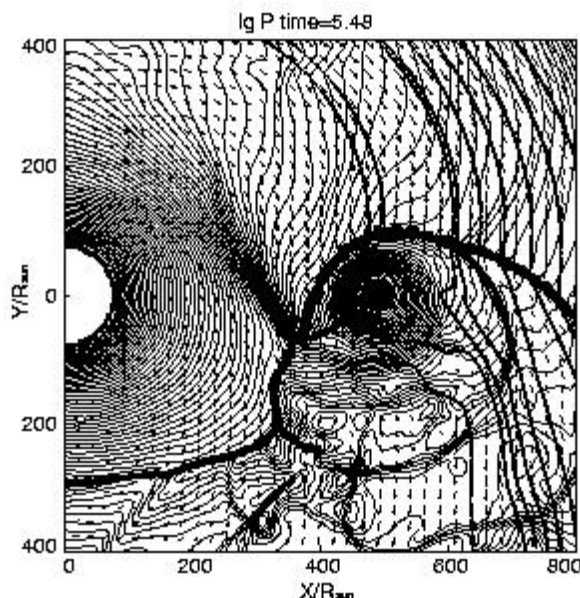


Figure 2: Fields of pressure and velocity vectors in equatorial plane for run with $\alpha=0.9$. The length of the longest arrow corresponds to the velocity value of 100 km/s

Table 1: Radial velocities and accretion rates

1	2	3	4
α	T	v_{rad}	Accr. rate
0.3	10.94	60	$< 10^{-5}$
0.5	6.53	65	$< 10^{-5}$
0.7	5.60	65	10^{-5}
0.8	5.69	63	4×10^{-4}
0.9	5.48	71	5×10^{-3}

These conclusions are illustrated by Figures 1,2. In these figures fields of pressure in the equatorial plane are presented for two values of α parameter ($\alpha=0.7$ and $\alpha=0.9$). All the distances are given in the units of solar radius. The radius of the circle with center at the origin of the coordinate frame corresponds to the donor's surface. The flow lines are shown by solid lines. The flows are directed along the velocity vectors (shown by arrows). The dashed lines mark the Roche equipotentials. The accretor is marked by the asterisk.

In the Figure 1 the non-steady case with $\alpha=0.7$ is presented. Here we can see that by the moment of 9.15 orbital periods there are no matter between the components (the observed picture corresponds to the densities less then background value). The gas is concentrated near the donor's surface. In this case almost all the gas ejected has returned to the donor's surface.

Figure 2 illustrates the case of $\alpha=0.9$ where the steady state picture with the disk and the bow shock wave (the bold line resulting from the isobars condensation) located in front of the accretor on the way of it's orbital motion takes place. The figure corresponds to the time of 5.48 orbital periods. The calculations for values of $\alpha > 0.8$ also showed that the disc size was greater for the smaller value of α .

The relative accretion rates and radial velocities at infinity have been also calculated. The radial velocities are all of the order of 60–70 km/s. The accretion rates don't exceed the values 5×10^{-3} . These results are presented in the Table 1. Here 1st column – the value of α parameter, 2nd column – T – time in orbital periods, 3rd column – V_{rad} – radial velocity at infinity (km/s), 4th column is the relative accretion rate.

4. Conclusions

Different gas flow regimes for the symbiotic system Z And have been considered within the framework of 2D gasdynamical model. Calculations for the various stellar wind velocity regimes ($\alpha = 0.3, 0.5, 0.7, 0.8, 0.9$) have been carried out.

The results show that for small stellar wind velocities ($\alpha < 0.8$) no steady disk can be formed. Solutions with $\alpha < 0.8$ are not steady state ones. The gas ejected during the first phase falls down to the donor star. This process is rather slow and at the time $T \sim 5 - 10 P_{orb}$ we still have some matter in the system.

The calculations for $\alpha = 0.8$ and 0.9 show the presence of the disk as well as of bow shock waves located in front of the compact star on the way of its orbital motion. For these runs ($\alpha \geq 0.8$) we have found that:

- the disk size decreases with increasing of α ;
- the accretion rate does not exceed 0.5 % that is smaller than the value of 5% estimated in Bisikalo et al. (1996) for symbiotic systems. This may be due to the difference in the considered parameters. It is also smaller than the value 2% obtained by Fernandez-Castro et al. (1988) for Z And.

Acknowledgements. This work has been partially funded by the RFBR grants 99-02-17619 and 01-02-06104, grants of the President of Russian Federation 00-15-96722 and 99-15-96022 as well as by the INTAS grant 00-491.

References

- Bisnovatyi-Kogan G. S., Kazhdan Ya. M. et al.: 1979, *Soviet Astronomy*, **23**, 201.
- Bisikalo D. V., Boyarchuk A. A. et al.: 1994 *Astronomy Reports*, **38**, 4, 494.
- Bisikalo D. V., Boyarchuk A. A. et al.: 1996, *Astronomy Reports*, **40**, 5, 653.
- Fernandez-Castro T., Cassatella A., et al.: 1988, *Ap.J.*, **324**, 1016.
- Roe P.L.: 1986, *Ann. Rev. Fluid Mech.*, **18**, 337.
- Chakravarthy S., Osher S.: 1985, *AIAA Pap.*, **85**, 363.

RR Tel: MASS LOSS RATE OF THE COOL COMPONENT

D. Kotnik-Karuz¹, M. Friedjung²¹ Department of Physics, University of Rijeka
Omladinska 14, Rijeka 51000 Croatia, *kotnik@mapef.pefri.hr*² Institut d'Astrophysique
98bis Boulevard Arago, Paris 75014 France, *fried@iap.fr*

ABSTRACT. The Fe II emission lines in the optical spectrum of the symbiotic star RR Tel, observed by Crawford et al. (1999), have been analysed applying the SAC method. We obtain information about the relative populations of the lower levels of the lines and, assuming them to be in LTE, we determine the column densities of Fe+ and of H. The mass loss rate has been calculated using the mean cool component radius obtained from the bolometric properties of Mira variables with a pulsation period similar to that of the cool component of RR Tel.

Key words: Stars: binary: symbiotic; stars: individual: RR Tel.

1. Introduction

The symbiotic nova RR Tel had one single observed major outburst in 1944, followed by a long recovery phase which has not yet finished. Extensive spectroscopic investigations during this period have indicated that it is an interacting binary, consisting of a Mira variable of a late spectral type and a white dwarf. There is evidence of a planetary nebula-like plasma and additional hot plasma due to colliding winds from the two components as well as a circumstellar dust shell due to which RR Tel has been classified as a D-type symbiotic. The Mira variable loses mass at high rates via a spherically symmetric stellar wind which expands at low velocity and is ionized by the hot component. The mass loss rate is important for the evolution of the binary system and may play a causal role in producing its symbiotic behaviour.

The mass loss rate for RR Tel has been determined by use of different methods: from the flux of thermal radio emission (Seaquist et al. 1993), by use of infrared flux ratios derived from IRAS satellite observations (Kenyon et al. 1988), from a mean relation for miras involving their luminosities (Whitelock et al. 1994) and from the proportion of O VI resonance line emission which is Raman scattered in parts of the wind where hydrogen is neutral (Birriel et al. 2000).

In our present approach we find a limit to the mass

loss rate of the cool mira in RR Tel by the Self Absorption Curve (SAC) method.

2. Observations

We have analysed the flux calibrated high resolution optical spectrum of RR Tel observed in 1996 (Crawford et al. 1999) in the $\lambda\lambda 3180 - 9455 \text{ \AA}$ spectral region.

The spectrum displays a large number of narrow emission lines including those of singly ionized iron which have been analyzed in this work.

The database of Crawford et al. was checked critically regarding the line identifications (Selvelli and Bonifacio 2000) as well as the line intensities (Keenan 2001, Mc Kenna et al. 1997). A total number of 131 permitted and forbidden Fe II lines with reliable atomic parameters have been selected for this study. They belong to different multiplets and originate from transitions between the lowest levels with an excitation potential up to 9 eV.

3. Methods

The mass loss rate can be calculated by use of the continuity equation:

$$\dot{M} = 4\pi r^2 \rho(r) v(r) \quad (1)$$

which can be expressed in terms of hydrogen column density N_H by

$$\dot{M} = 4\pi r N_H m_H v(r) \quad (2)$$

where $N_H = r n(r)$ and $n(r) = \rho(r) / m_H$. m_H is the mass of the hydrogen atom, $n(r)$ the hydrogen number density and $v(r)$ the outward velocity which can be directly measured as the mean velocity broadening of the line profile. The remaining two unknowns in the expression for \dot{M} (2), r and N_H , have been determined by use of the SAC method which has proved to be effective in determining limits to relative populations of upper and lower terms, as well as in deriving other information

about the line formation region (Friedjung and Muratorio 1980, Friedjung and Muratorio 1987, Muratorio and Friedjung 1988, Baratta et al. 1998).

The Self Absorption Curve (SAC), whose shape is determined by self absorption effects, is the observational log-log plot of the quantity $F\lambda^5/gf$ versus $(gf\lambda)$. F is the line flux emitted in a transition which is related to the optical thickness of that transition.

Simple theory gives

$$\log \frac{F\lambda^5}{gf} = \log \left(\frac{2\pi^2 e^2 h R^2}{m_e d^2} \right) + \log \left(\frac{N_u}{g_u} \right) + Q(\tau_0) \quad (3)$$

and

$$\log \tau_0 = \log(gf\lambda) + \log \frac{N_l}{g_l} + \log \frac{\pi e^2}{m_e c} - \log v_d \quad (4)$$

$Q(\tau_0)$ is the self absorption function depending on the optical thickness τ_0 ; N_u and N_l are the column densities of the upper and the lower level and g_u , g_l their statistical weights. R is the size of the emitting region perpendicular to the line of sight and d the distance of the star. A type of excitation temperature of the line emitting region can be defined by

$$\frac{\frac{N_u}{g_u}}{\frac{N_l}{g_l}} = e^{-\frac{E_u - E_l}{kT}} = e^{-\frac{1}{kT}} \quad (5)$$

4. Results

4.1. Determination of R

The lower and upper limits to the radius of the emitting line region of RR Tel have been determined by the SAC method in the previous paper (Kotnik-Karuzza and Friedjung 2001), yielding values of 26 and 2300 solar radii respectively. However, when estimating the mass loss rate, it is more realistic to take for r in equation (1) the radius of the cool component instead of the minimum radius of the line emitting region. Using bolometric corrections to the K magnitude for M giants (Houkashelt et al. 2000), measured properties of "group 1" Mira variables with a 387 day pulsation period (Barthès et al. 1999) and an M7 spectral class of the cool component (Mürset and Schmid 1999), we can expect a mean cool component radius of the order of $1.5 \cdot 10^{15}$ cm to $3.0 \cdot 10^{15}$ cm which gives a mean value of about $300 R_\odot$. The smaller of these radii is less than the maximum radius obtained by the SAC method. In fact we expect line formation outside the region of dust condensation (Kotnik-Karuzza et al. 2001), which is expected to be at 5 mira radii or averaging 1500 solar radii. We take it for justified to calculate the mass loss rate by assuming this value of $r = R$.

Table 1: Parameters of the cool component of RR Tel from this work

R_{dust} (cm)	$N_{H\alpha min}$ (cm^{-2})	v (kms^{-1})	\dot{M}_{min} ($M_\odot yr^{-1}$)
$1.0 \cdot 10^{14}$	$7.5 \cdot 10^{22}$	14	$3 \cdot 10^{-6}$

4.2. Column density

The column density has been obtained starting from the SAC of multiplet 27 (Fig.1).

The minimum optical thickness of 1 at $\log(gf\lambda)=1$ leads from (4) to a minimum N_l/g_l of $5.3 \cdot 10^{14} cm^{-2}$ for the lower metastable term at 2.68 eV. This term is the upper term of the forbidden line multiplet 4F, so we obtain from (5) the ground level N/g of $5.9 \cdot 10^{16}$ atoms cm^{-2} . In this calculation we used the temperature of 6600 K which is an upper limit to the permitted line region temperature (Kotnik-Karuzza and Friedjung 2001) and is near to the maximum temperature of the forbidden line formation region. The latter was obtained by plotting $\log \frac{F\lambda^5}{gf}$ versus upper level excitation potential for all forbidden lines, assumed to be optically thin (Fig.2).

This temperature of 6600 K, being an upper limit to the permitted line region excitation temperature, together with the interpolated value of the partition function of antilog 1.71 at this temperature, leads to a minimum column density of $3.0 \cdot 10^{18}$ atoms cm^{-2} for Fe+ and so for Fe since iron is present also in higher degrees of ionization. By assuming standard abundances we obtain $7.5 \cdot 10^{22}$ atoms of hydrogen per cm^2 .

4.3. Mass loss rate

By inserting the calculated parameters and the value of $14 kms^{-1}$ for the mean velocity broadening of the emission line profile in (2), we obtain $3 \cdot 10^{-6} M_\odot yr^{-1}$ for the minimum mass loss rate of the cool component as shown in Table 1.

An agreement with estimates by other authors, using other methods, can be seen from Table 2.

The adopted geometry of RR Tel which agrees with the model of Taylor and Seaquist (Taylor and Seaquist 1984), is represented in Fig.3. Beside the determined sizes, it shows clearly that Fe II is especially present near the boundary of the ionized and neutral regions. While the permitted lines are formed not too far from the boundary of the ionized zone, the forbidden lines are most probably formed further out, in that part of an accelerated wind which is ionized by the hot component. The ionization front cannot penetrate the dust region. Our determinations are consistent with line formation in the cool star wind.

PROPERTIES OF CLASSICAL Be STARS FROM ANALYSIS
OF HIGH-RESOLUTION H α PROFILESA.S. Miroshnichenko^{1,2}, K.S. Bjorkman¹, V.D. Krugov³, I.A. Usenko⁴¹ Ritter Observatory, University of Toledo, Toledo, Ohio, 43606, USA² Pulkovo Observatory, Saint-Petersburg, 196140, Russia³ Main Astronomical Observatory, Kiev, Ukraine⁴ Astronomical Observatory, Odessa National University, Odessa, 65014, Ukraine

ABSTRACT. We summarize results of the 25 year period of observations of Be-stars. We suggest that Be stars with moderate and strong H α emission are good candidates to search for binary systems.

Key words: stars: Be-stars - stars: binary.

Long-term high-resolution spectroscopic observations of classical Be stars in the H α region are important for understanding the nature of the Be-phenomenon, which is still controversial. We carried out an analysis of published data and more than 1000 spectra obtained at the Ritter Observatory of the University of Toledo (USA) and Main Astronomical Observatory of the Ukrainian Academy of Sciences over a total period of about 25 years. Our study revealed that 50% of Be stars brighter than 4 mag. show evidence (mostly from spectroscopy or interferometry) of being binary systems. This fraction is smaller for fainter objects (22% for $V \leq 7$ mag.) probably due to selection effects. The secondary components are usually a few magnitudes fainter than the primaries. We also found that H α line profiles in high-resolution spectra (resolving power $R \geq 20000$) of many Be stars have a complex structure (3 or more emission peaks rather than the 2 peaks, typically seen at a lower resolution). A noticeable fraction of Be stars with such complex profiles turned out to be recognized binaries. Taking into account that expected separations of the companions in Be binaries are of the order of a few milliarcseconds (which is still beyond the limits of speckle interferometry), we suggest that high-resolution spectroscopy remains the best method to search for Be binaries. It is difficult to detect spectral lines of the secondary com-

ponents, and hence periodic radial velocity variations of the primaries' spectral lines is the main evidence of the orbital motion in most cases. Amplitudes of such variations are of the order of a few to a few tens km s^{-1} , and therefore spectroscopy with $R \geq 15000$ is needed to detect them. The H α line is usually the strongest feature in the spectra of Be stars which often reflects the orbital motion. Observations in this spectral region are very useful to search for signs of binarity and to monitor the behaviour of the circumstellar envelopes. However, the profiles' fine structure can be resolved only with a much higher resolution ($R \geq 50000$).

We suggest that Be stars with moderate and strong H α emission are good candidates to search for binary systems. Our analysis shows that Be binaries with stronger H α lines have larger orbital periods, as was previously found for Be/X-ray binaries by Reig, Fabregat and Coe (1997). For example, stars with primaries of early B-types (B0–B3) with a maximum H α equivalent width of 20–30 Å have orbital periods of 100–200 days (e.g., ϕ Per, ζ Tau, and γ Cas). However, binaries with later-type primaries and similar periods usually have weaker H α lines (e.g., σ And, β CMi, and 4 Her). Thus, regular spectroscopic observations over a period of a few years are capable of determining how frequent binary systems among Be stars are.

We thank Reinhard Hannschik for providing us with the ESO high-resolution spectra of Be stars. A.M. and K.B. acknowledge support of the NASA Long-Term Space Astrophysics grant NAG5–8054.

References

Reig P., Fabregat J., Coe M.J.: 1997, *As.Ap.*, **322**, 193

2D AND 3D MASS TRANSFER SIMULATIONS IN β LYRAE SYSTEM

V.V. Nazarenko, L.V. Glazunova, V.G. Karetnikov

Astronomical Observatory, Odessa State University
T.G.Shevchenko Park, Odessa 65014 Ukraine, *val@dneb.odessa.ua*

ABSTRACT. 2D and 3D mass transfer simulations of the mass transfer in β Lyrae binary system. We have received that from a point L_3 40 per cent of mass transfer from L_1 -point is lost. The structure of a gas envelope, around system is calculated. 3-D mass transfer simulations has shown presence the spiral shock in the disk around primary star's and a jet-like structures (a mass flow in vertical direction) over a stream.

Key words: Starsinteract binary systems; simulation.

The second brightest star of summer constellation β Lyra, β Lyrae, has been studying astronomers for the past 200 years. β Lyrae (10 Lyr, HR 7106, HD 174638, BD+33 3223, ADS 11745A) is the brightest member (component A) of an optical system of six star and 13.086d spectroscopic and eclipsing binary with the ample evidence of circumstellar matter within and around the system. Now, it is existing two models of the envelope in β Lyrae: that of Wilson (1974) who argued that disk around the mass accreting star (the primary) is massive (of the order of a solar mass), modelled it as a very flattened ellipsoid.

Hubeny,Plavec (1991) presented a different quantitative model of disk, assuming explicitly that the disk is an accreting disk and treating its vertical structure as to be self-consistently. This disk model has a negligibly small mass and is in the form of a normal Keplerian disk bounded from outside by a half-torus. Its 'height' (i.e. thickness in the direction perpendicular to the orbital plane) grows with the distance from the primary. Comparing their model with the various data and using the geometrical constrains, Hubeny and Plavec concluded that the disk have the radius of about $25 R_{\odot}$ and height of about $6 R_{\odot}$.

Here we present 2d and 3d simulations of the mass transfer in the β Lyrae binary system.

Our approach to the mass transfer is based on two points: i. to obtain the initial stream structure (the one in L_1) we will simulate the stream formation process instead to use Lubow and Shu model (Lubow and Shu, 1975 hereafter LS). ii. to set up the secondary internal structure in the vicinity of L_1 point we will use the

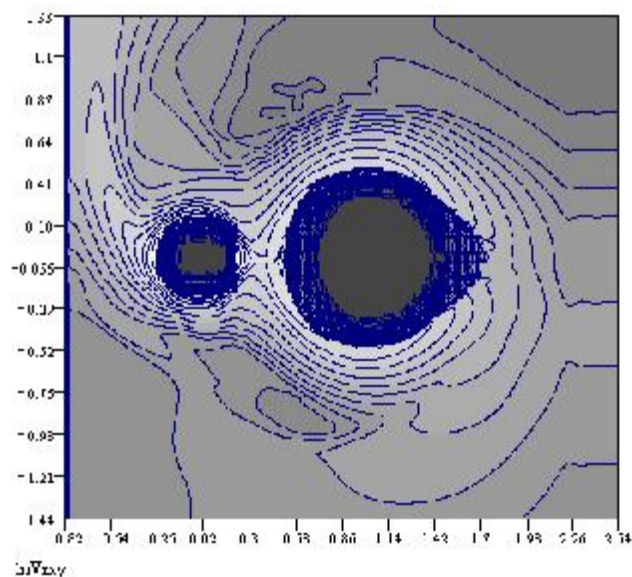


Figure 1: The density contours for the primary's radius equal to 0.5, $fv=0.1$.

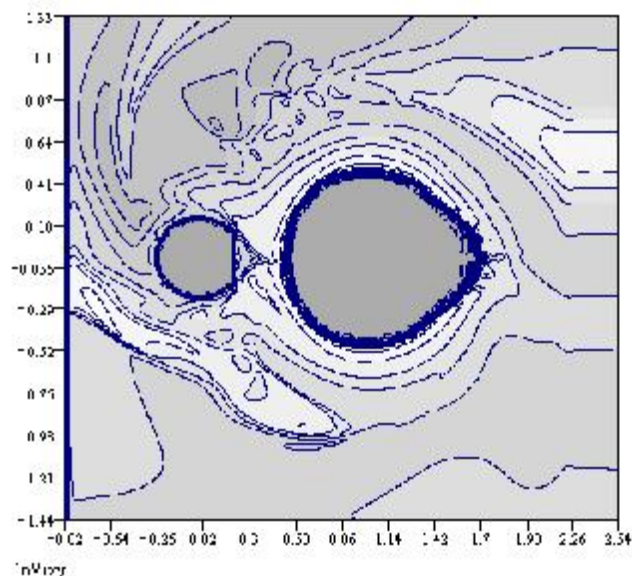


Figure 2: The temperature contours for the primary's radius equal to 0.5, $fv=0.1$.

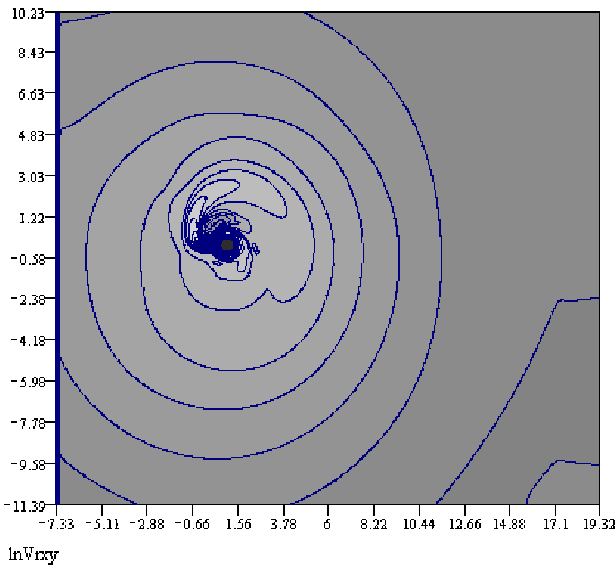


Figure 3: The density contours for the very large grid the 2d-model of the outer envelope.

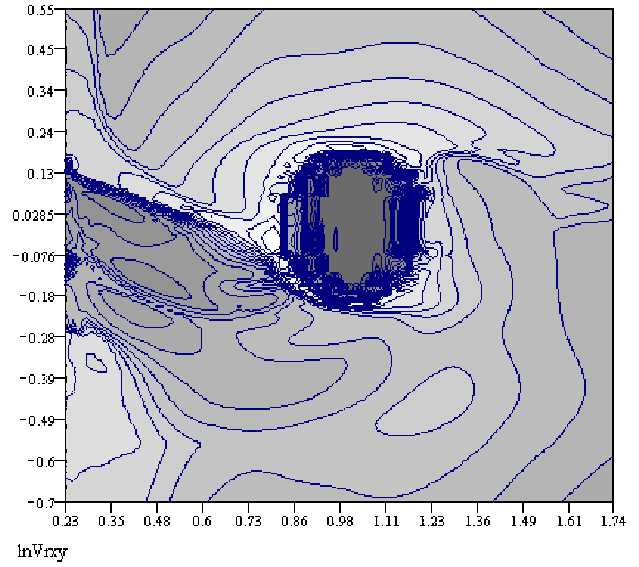


Figure 5: The temperature contours in orbital plane for 3d-simulations, $R_{\text{prim}}=0.2$, $fV=0.5$.

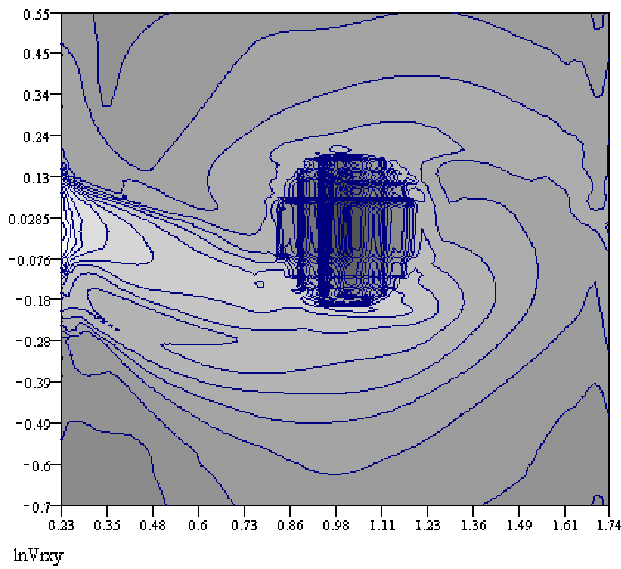


Figure 4: The density contours in orbital plane for 3d-simulations, $R_{\text{prim}}=0.2$, $fV=0.5$.

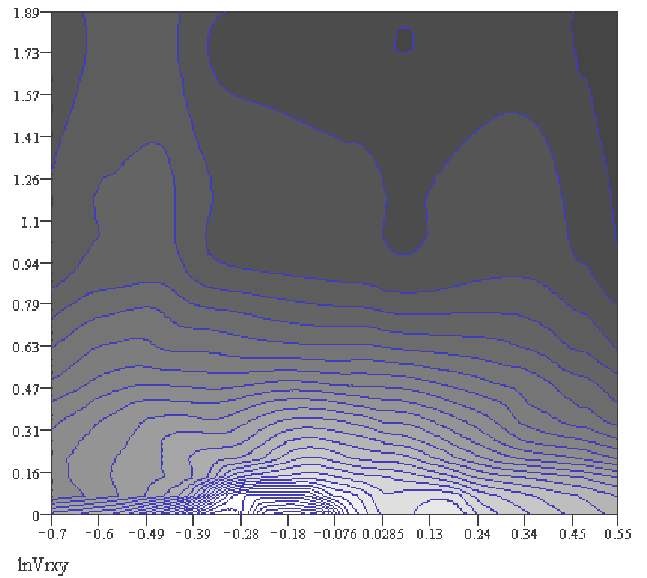


Figure 6: The density contours in zy-plane, lying on the spiral shock I.

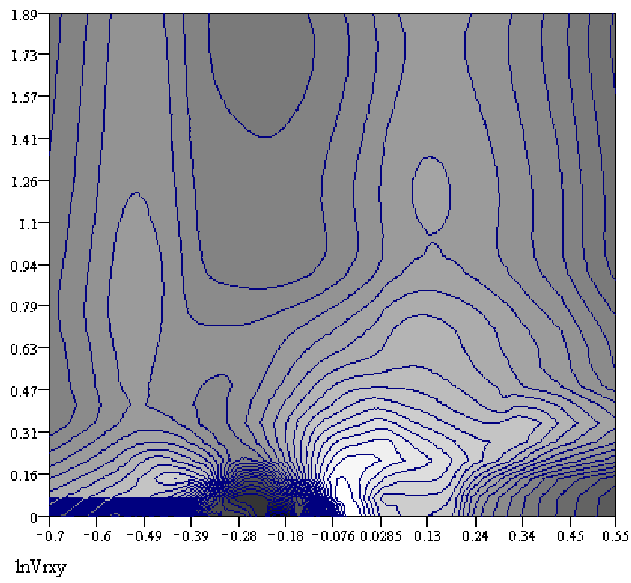


Figure 7: The temperature contours in zy -plane, lying on the spiral shock I.

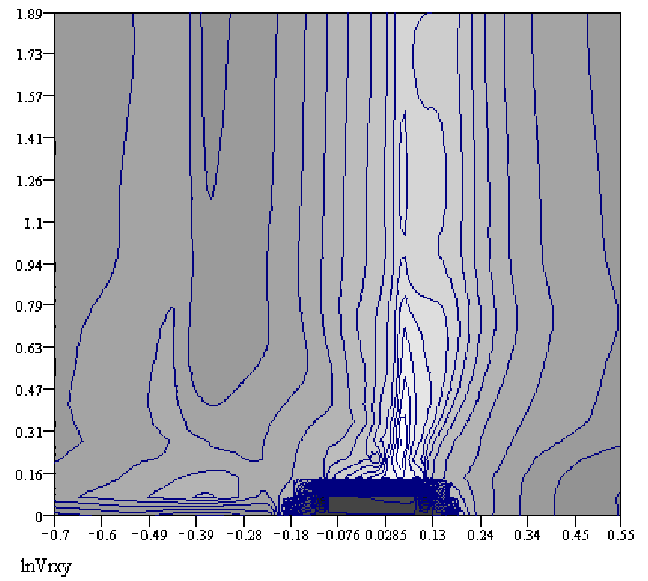


Figure 9: The temperature contours in zy -plane, lying on the mass accreting star.

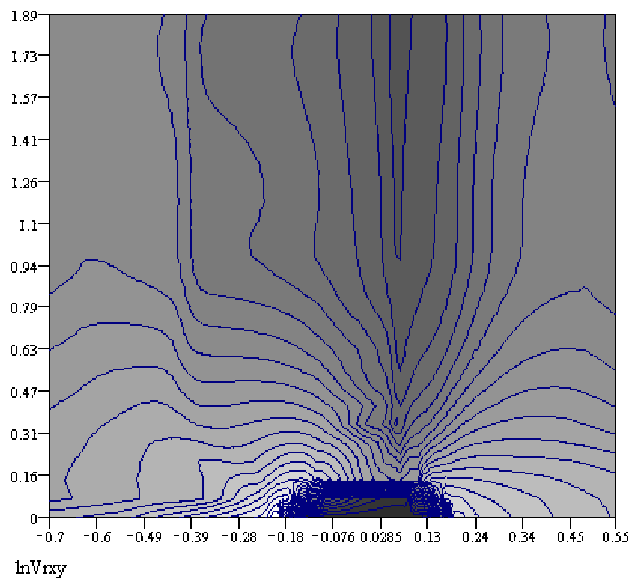


Figure 8: The density contours in zy -plane, lying on the mass accreting star.

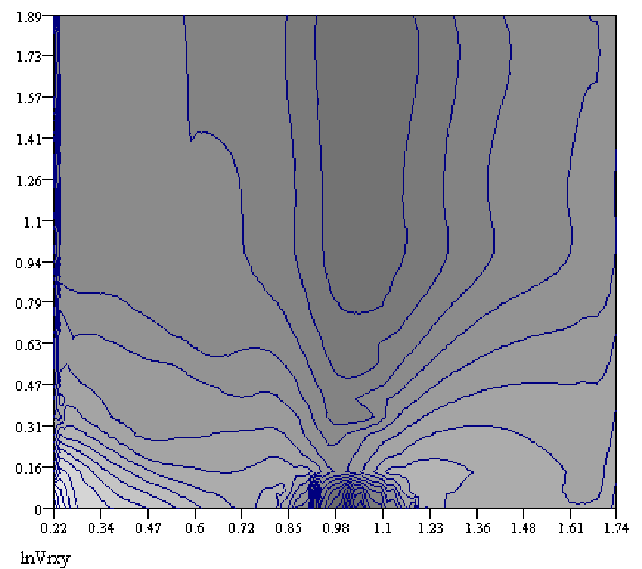


Figure 10: The density contours in zx -plane, lying on line of centres.

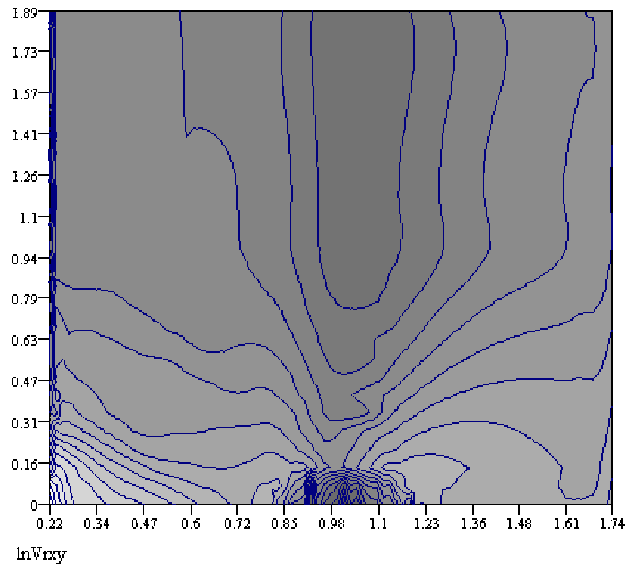


Figure 11: The temperature contours in zx -plane, lying on line of centres.

Kurucz's grid (Kurucz, 1979)

To calculate the mass flow we use non-stationary Euler-hydrodynamics equations which are resolved by 'big-particles' code developed by Belotserkovskii and Davydov (Belotserkovskii and Davydov, 1982) at the computer center of Academy of Science of SU. We use such the code version where the artificial viscosity is implemented at the first time substep and which is two order accuracy in time and space. The simplicity of algorithm organization and high stability in calculation allow to use PC to calculate the mass transfer in CBS. We have used in simulations PS-Pentium 3 of Odessa Astronomical Observatory of Odessa State University. On practice the CPU time of every time step take about 2.6-3.5 sec. and total required number of the time step to obtain the steady state in the solution is order of 300,000 -500,000.

Our treatment of binary model is standard since we consider: the synchronization rotation of the spin rotation of the binary components with their orbital motion when we shall simulate the stream formation near L_1 -point and its motion further in a calculation area; We use the Roche lobe model of the binary component gravitation and all the effects of the orbital rotation in the binary (the centrifugal and Coriolis forces); circular orbits of the binary components. We account a gas as perfect one consisting from hydrogen for the simplicity.

We drop the specific heats ratio to 1.3-1.4 to take into account the possible radiative cooling effect in mass flow. This is usual way to take in account this radiative effects (see for example Molteni et, al 1991; Bisikalo et.al. 1999). We adopt the binary parameters to be: mass of the mass losing star (the secondary) equal to $2 M_{\odot}$, mass of mass accreting star is $12 M_{\odot}$, orbital pe-

riod of 13.086 days. The peculiarity of mass transfer in binaries with the binary components - normal stars is the problem to describe stream-the primary star interaction. We decide this problem introducing the special coefficient on the primary surface, F_v , which decreases the gas velocity here relatively velocity in surrounding cells. By such the way if the velocity in cells surrounding the primary's surface is V than the velocity on the primary's surface is $F_v \cdot V$ where $F_v \leq 1$. The case $F_v=1$ describes the entirely free flow of gas via the primary, maximum of accretion process; the case $F_v \leq 1$ describes partially reflecting and partially absorbing boundary conditions; the case of $F_v=0$ shows the absent accretion process on the primary, the entirely reflecting boundary conditions.

Taking into account the inevitable indefinite in the binary parameters (We have in mind in the first turn the primary radius) We calculate 2d- and 3d-models for the various primary radius:- 0.5 for 2d-simulations and 0.2 for 3d simulations (hereafter all the distance will be given in units of the orbital separations). We choose the F_v -coefficient to be equal to 0.1 for 2d-model and to be 0.5 for 3d-model.

The 2d-model we show in Fig.1a and Fig.1b where the density and temperature contours are plotted. As one can see from this Figure the mass flow with large primary radius and strong reflection of a stream from the primary produces the contact envelope around the binary components. The peculiarity of this mass transfer variant is that a gas of a stream reflecting from the primary is going back to L_1 -point and interacts with a gas placed here. As result of this the mass transfer rate in L_1 -point decrease on the appreciable value in 5-7 time. The another peculiarity of this model is the mass outflow from another side of the secondary in the vicinity of L_3 -point. This take place due to considerable size of the secondary's atmosphere which penetrates beyond L_3 -point. The mass transfer in L_3 -stream is 40 per cent of mass transfer from L_1 -point. In order to show how L_3 -stream moves out of the system we calculate the mass transfer in the system on the very larger grid, where x -coordinates range in the interval $-8 \div +19$ and y -coordinate range in the interval $-8 \div +9$. Such outer envelope produced by L_3 -stream is shown in Fig.2 where the density contours are plotted. It is clear seen how the L_3 stream is moving under Coriolis forces and regularly transform in the outer envelope. Thus, L_3 -stream originates the binary system wind blowing from the system with the velocity 50-350 km. sek^{-1} and density less than 10^9 cm^{-3} on the distance more than 2-3 from center mass of the system. We also think that z -thickness of this wind is increased with increasing of the distance from center mass of the system.

We present 3d-model of the mass transfer in β Lyrae in Fig.3-6. In Fig.3 the density and temperature contours are plotted in the orbital plane of the system.

We clearly see the place where a stream interacts with the primary, the spiral shock I when a gas orbiting the primary strikes a stream moving from L_1 -point, a thin ring of high temperature in internal parts of accreting disk close to the primary's surface. We also see the spiral shock II (these notations of spirals shocks are given in that of Bisikalo's paper, 1999) that is placed upper and right of the primary star. Thus a mass flow in 3d-simulations produces the spiral shocks I and II, accreting disk, the place of star-stream interaction (PS-SI) and outer envelope. The cross-sections of a stream and spiral I in the z - y plane near PS-SI in the directions perpendicular to the stream motion are shown in Fig.4 a and b where density and temperature contours are plotted. As one can see from this Figure y -size of a stream is about 0.2 and z -size is almost 0.08 that show that y - z cross section of a stream is elliptical. The Fig.4b show that spiral I reflects from a stream and have the complicated form of the standing wave. The Fig.4b also show that a stream is very cool in respect to surrounding a gas in a disk and envelope. The Fig.4c show the velocity field in y - z cross section stated above. This velocity fields has a jet-like structures (a mass flow in vertical direction) over a stream. It confirms the suggestion of Harmanec et al. (1996) and numerical simulations of Bisikalo et al. (2000) about jet-like structures in β Lyrae.

The Fig. 5 and 6 show the y - z cross-section lying on the center of the primary and x - z cross-section lying on line of center respectively. These Figures show that upper the primary a pillar of a gas exists with a small density and high temperature. This pillar is a result

from an accreting of a gas on the primary. Its structure also originates jet-like structure (upper the primary).

It shows that jet-like structure in β Lyrae is more complicated than was supposed and was calculated in Harmanec et al.(1996) and Bisikalo et al.(2000) papers. As one can see from Figures 5 and 6 circumstellar envelope consists of two parts: accreting disk that have the form of torus and outer envelope in which z -thickness of a gas is increased with an increasing of distance from the primary. The essential part of outer envelope has the size of $12 R_{\odot}$ although to define exactly 'size' of the envelope is hard problem (it is necessary to define optical thickness in 3d-medium).

References

- Belotserkovskii O.M., Davydov Yu.M.: 1982, "*The big particles code in gas dynamics*", Moskau, Scientist
- Bisikalo D.V., Boyarchuk A.A., Chechetkin V.M., Kuznetsov O.A., Molteni D.: 1999, *Astron. Reports*, **43**, 797
- Bisikalo D.V., Harmanec P., Boyarchuk A.A., Kuznetsov O.A., Hadrava P.: 2000, *As.Ap.*, **353**, 1009
- Harmanec P., Morand F., Bonneau D., et al.: 1996, *As.Ap.*, **312**, 879
- Hubeny L., Plaves M.J.: 1991, *A.J.*, **102**, 1156
- Kurucz R.L.: 1979, *Astrophys.J.Suppl.Ser.*, **40**, 1
- Lubow S.YH., Shu F.H.: 1975, *Ap.J.*, **198**, 383
- Molteni D., Belvedere G., Lanzafame G.: 1991, *MNRAS*, **249**, 748
- Wilson R.E.: 1974, *Ap.J.*, **189**, 319

ECLIPSING BINARY STARS : LIGHT CURVE MODELS AND SOFTWARE

P.G. Niarchos

Department of Astrophysics, Astronomy and Mechanics, University of Athens,
GR 157 84 Zografos, Athens, Greece, *pniarcho@cc.uoa.gr*

ABSTRACT. The importance of studying Eclipsing Binary Stars for the determination of fundamental stellar data is sketched. The eclipsing binaries, originally classified phenomenologically, are now understood on the basis of much firmer physics and the improved understanding has led to a morphological basis of classification. The main light curve models developed since Russell's era are presented along with the respective programs for analysis (Kallrath & Milone 1999). These models are based on the geometric effects due to eclipses and on physical proximity effects between the components. Significant progress was made in the early 1970s, when models and programs were developed to compute (synthetic) light and velocity curves directly. Such models and programs were based on spherical stars, ellipsoidal geometry and on Roche geometry. During the last 25 years the analysis of photometric and spectroscopic data of eclipsing binaries has been performed by means of synthetic light curve programs based on Roche geometry. The synthetic light curve programs, based on physical models, have contributed to our understanding of physical processes in stars and have been used to solve several important astrophysical problems. A desirable feature of a light curve program is the ability to incorporate additional astrophysics. There is a continuing need to improve the model physics, as we become more aware of the observational properties of stars.

Key words: Stars: binary: eclipsing: light curve models: light curve analysis.

1. Introduction

There are several reasons why the study of Binary stars is so important:

- they are as common as single stars in the Universe. In the solar neighborhood the frequency is more than 50%
- they are the primary source of our knowledge of the fundamental properties of stars. Their study allows direct determination of stellar masses, stellar radii and stellar luminosities

- they are distant indicators for nearby galaxies
- the evolution of binary stars helps to explain a host of diverse and energetic phenomena such as : X-ray binaries, cataclysmic variables, novae, symbiotic stars and some types of supernovae
- these binaries are classic examples of the fundamental contribution that stellar astrophysics makes to our general understanding of physical processes in the universe.

2. Classification of Eclipsing Binaries and Importance of their Study

2.1 Phenomenological classification

2.1.1 EA Light Curves (*Algol type*)

- they show clearly defined eclipses with obvious start and end times
- the outside eclipses parts are flat-topped, suggesting that the effects due to proximity of the two components are small
- there is large difference between the depths of the two minima
- the reflection effect is pronounced.

2.1.2 EB Light Curves (*β Lyrae type*)

- they show well-defined eclipses
- the variation is continuous (ellipsoidal variation)
- they are characteristic of tidally distorted components
- the large difference in depths of minima indicates components of quite different surface brightness.

2.1.3 EW (or *W UMa*) Light Curves

- a continuous variation of brightness is present
- there is small difference in depths of the minima

- proximity effects are pronounced (mainly tidally distorted shapes of the stars)

Studies of eclipsing binaries show the value of treating all aspects of the light of the systems in light curve analysis, and not only their geometric characteristics. Eclipsing binary analysis is a formidable astrophysical task. The field includes radiation physics and sometimes hydrodynamics. It borrows methods from celestial mechanics, thermodynamics, and other branches of physics. Physical models are required for radiation transport in the component's atmospheres and for the dynamic forces controlling the stellar mass distribution.

2.2 Morphological classification

The concept of the equipotentials in the Roche geometry allows us to separate eclipsing binaries into morphological classes :

- *detached systems*, if neither component fills its Roche lobe
- *Semidetached systems*, if one component fills its Roche lobe and the other does not
- *Over contact systems*, if both components exceed their Roche lobes and a common envelope is formed
- *Double contact system*, where each component fills its lobe exactly, and at least one rotates supersynchronously. The two components fill their limited lobes but do not touch each other (Wilson 1979).

There is a correspondence between the morphological classification and the phenomenological classification. The Algol-type light curves are produced by semi-detached systems and the W UMa-type light curves by over contact systems.

The phenomenological classification of β Lyrae-type light curve has no morphological counterpart. Sometimes, β Lyrae-type light curves are produced by detached systems, sometimes by semi-detached systems and sometimes also by systems having marginal over-contact.

2.3 Why data derived from eclipsing binaries are important

A light curve can provide : the orbital inclination, the relative radii in units of the separation, the ratio of luminosities and the photometric mass ratio.

The radial velocity curves can provide : the mass ratio, the separation α in physical units (if inclination is known), the orbital dimensions (if inclination is known), the period P (also known from light curve).

The spectroscopic observations can provide: the spectral classification, the chemical composition and the temperatures of the two components.

The full determination of absolute eclipsing binary parameters requires both a light curve and a radial-velocity curve for each component. A combination of the above observations yields the fundamental source of information about sizes, masses, luminosities and distances or parallaxes of stars. This information provides the means : to test stellar structure and stellar evolution theories, to improve our understanding of such exotic objects as X-ray binaries, novae and Wolf-Rayet stars and to get a great wealth of knowledge from binaries in globular clusters.

3. Methods of Light Curve Analysis

3.1 The age of geometrical models

H.N. Russell (1887-1957) spoke about the Royal Road of Eclipses. Traveling this road entails the decoding of the messages encrypted in the light curves of eclipsing variables. As a rule, the light curve is determined by geometric effects due to eclipses and by physical proximity effects. The effects of ellipticity and reflection effect can be treated through the rectification procedure and the solution is made for spherical mode (Russell- Merrill method, 1952). Computer programs based on rectifiable models were developed by Jurkevich (1970) and Proctor and Linnell (1972). The solutions are possible only for well-separated detached systems, but not for semi-detached and over-contact systems.

3.2 The age of computational Astrophysics

Significant progress in the fields was made in early 1970s. Models and programs were developed to compute (synthetic) light and velocity curves directly. Such programs are : the EBOP, based on spherical stars (Etzel 1993), the WINK, based on ellipsoidal geometry (Wood 1971), and models and programs based on Roche geometry developed by Lucy (1968), Hill and Hutchings (1970), Wilson and Devinney (1971) and Mochnacki and Doughty (1972). These new approaches permitted the computation of light curves on the basis of complex physical models describing the dynamic forces controlling the stellar mass distribution and the radiation transport in the component's atmospheres.

Physical models based on equipotentials and Roche geometry were implemented in the Wilson-Devinney program (Wilson & Devinney 1971, Wilson 1979) and in LIGHT2 program (Hill & Rucinski 1993). Physical models and programs led to least-squares determinations of the light curve parameters (Wilson & Devinney 1971, 1972, 1973) and Lucy (1973). The computational implementation of Roche models coupled with least-squares analyses really started the age of computational astrophysics in eclipsing binary research. Other programs based on physical models are those of Hill & Rucinski (1993), Linnell (1984), Hadrava (1997)

and others.

3.3 Astrophysical problems solved by Light Curve Methods

- the Algol paradox
- the structure of W UMa-type stars
- bolometric albedos of convective envelopes
- undersized subgiants (Wilson 1994)
- understanding intriguing binaries such as ϵ Aurigae and β Lyrae by including gas streams and discs in the light curve modelling
- understanding of physical processes in stars
- successful modelling of W UMa stars as over-contact systems
- understanding evolution subsequent to mass transfer episodes through observations of binaries with major circumstellar mass flows. Examples : β Lyrae, V356 Sge, KU Cyg, AX Mon and many symbiotic stars

4. Models for computing eclipsing binary observables and Software

4.1 A general approach to modeling Eclipsing Binaries

We define an eclipsing binary observable curve O

$$O := [(t_k, o_k) \mid 1 \leq k \leq n]$$

a set of n elements in which each element is a pair, (t, o) , where t represents an independent, time-related quantity and o is the corresponding observable (Kallrath & Milone 1999). The quantity t may either represent the *time* or the *photometric phase* Φ (traditionally used). The term light is usually used in the abstract sense and may represent not only the photometric brightness but any observable, such as :

- the light at a given wavelength
- the radial velocity
- polarisation
- photospheric spectral line profile
- spectral distributions due to circumstellar flows, and
- any other quantity associated with the phase, but also other quantities independent of phase which we call systemic observables.

It may represent a measured value of an observable, and/or a value derived from a light curve program.

Thus an 'observable curve' may be, for instance:

- an observed light curve O^{obs}
- a calculated light curve O^{cal}
- a wavelength-dependent light curve O^λ
- a radial velocity curve O^{vel}
- a polarization curve O^{pol}
- a set of output arrival times O^{pul}

Before 1970 an observed light curve O^{obs} of an eclipsing binary was analyzed following rectification procedures. However, the underlying physical models were relatively simple and neglected effects which later turned out to be relevant. Photometric and spectroscopic data were analyzed separately and with different methods. Today's methods permit analysis of photometric, spectroscopic, and other data simultaneously.

4.2 Direct problem

If the vector \mathbf{x} represents all relevant eclipsing binary parameters, then for a given set of phases a whole observable curve $O^{cal}(\mathbf{x})$, or a set of several curves $O^{cal}(\mathbf{x}^*)$ can be computed. Such a computation consists of three major parts:

1. The physics and geometry of orbits and components
2. The computation of local radiative surface intensity as a function of local gravity, temperature, chemical composition, and direction. The proper formulation of the radiative physics requires the use of accurate model atmospheres
3. The computation of the integrated flux in the direction of the observer. This computation must take eclipses into account. The inclusion of other effects such as circumstellar matter, i.e., gas streams, disks, attenuating clouds, etc., may be desirable.

4.3 Inverse problem

Determine a set of parameters \mathbf{x}^* from a set of eclipsing binary observations by the condition that the set of curves $O^{cal}(\mathbf{x}^*)$ best fits a set of observed curves O^{cal} . The system parameters x are modified according to an iterative procedure until the deviation between the observed curves O^{obs} and the calculated curves $O^{cal}(\mathbf{x}^*)$ becomes minimal in a well-defined sense. The system parameters \mathbf{x}^* , corresponding to the observed curves O^{obs} , are ordinarily regarded as the solution of non-linear least-squares problem. The least squares techniques used in Eclipsing Binary Data Analysis are:

1. The classical Differential Corrections
2. Multiple Subset Method and Interactive Branching
3. Damped Differential Corrections
4. The Simplex Algorithm
5. Other approaches.

4.4 Distinction Between Models and Programs

A *model* is a set of mathematical and physical relations which enables the mapping of a set of eclipsing binary parameters \mathbf{x} to a light curve L^{cal} for a given set of phase values, while a *light curve code or program* is the software implementation of such a model.

While the model is abstract and generic and relates a stellar system's physical attributes (gravitational potential, eclipse conditions, etc.), the program requires a choice of coordinates, integration or summation procedures and matrix inversion routines. The degree of realism of the model fundamentally determines the reliability of the predicted light curve. However the program itself constrains the accuracy of the result as well as the efficiency with which the result is reached. Therefore, it seems reasonable that those who develop light curve models maintain close contact with those who write and upgrade the program.

A desirable feature of the a light curve program is an ability to incorporate additional astrophysics. There is a continuing need to improve the model physics, as we become more aware of the observational properties of stars. It should also be structurally well defined but especially expandable.

5. Synthetic Light Curve Models

The Russell-Merrill Model and Technique

- Basic assumptions : spherical stars and in subsequent versions ellipsoidal in shape. The technique is described in Russell and Merrill (1952).
- The geometrical model for distorted stars is a tri-axial ellipsoid.
- Light curves of stars showing evidence of tidal distortion and reflection are transformed by rectification process into those of spherical stars.
- The physics is limited to Planckian radiation, linear limb darkening law, gravity darkening and simple treatment of reflection effect.
- Manual techniques continued to be used till 1970.
- Computerized versions were developed by Jurkevich (1970) and Proctor and Linnell (1972).

The eclipsing Binary Orbit Program EBOP

- A FORTRAN program based on spheroidal model (Etzetel 1981), known as NDE model (Nelson and Davis 1972).
- Suitable for detached systems, not for deformed components.
- Provides options to implement further physics.
- Makes use of spheroidal stars moving in circular or eccentric orbits.
- Linear limb darkening law is used.

The Wood model and the WINK program

- Assumes the components of the binary system to be triaxial ellipsoids (Wood 1971, 1972).
- Suitable for systems with moderate oblateness and reflection effect.
- It is not in use any more.

PHYSICAL MODELS :

ROCHE GEOMETRY BASED PROGRAMS

Binnendijk's Model

- Synthetic light curve program for contact binaries, based on Roche model with cylindrical coordinates (Nagy 1975, Binnendijk 1977).
- Good exposition of the physical principles behind the model.
- Binnendijk stressed the importance of surface brightness as a radiation parameter and emphasized the importance of radial velocity, line profile, and spectrophotometric data and therefore he foresaw many of the modern advances that have been made.

Hadrava's Program FOTEL

- Suitable for simultaneous solution of light curves and radial velocity curves of eclipsing binaries (Hadrava 1997).
- It uses a very simplified model of physics and geometry for the flux calculations.
- Designed to handle a large number of original observational data and to run on a PC.
- It can take into account a third body or component.

- The code uses a Simplex algorithm combined with a direct least-squares solution of multiplicative parameters.
- Errors and cross-correlations of all fitted parameters are included.

Hill's Model and its Program LIGHT2

- Based on Roche model;
- Black-body, color-index based, and theoretical atmosphere fluxes;
- Differential corrections based on Marquardt method;
- Multiple (≤ 10), elliptical spot structures;
- Line profiles are calculated;
- For complete review and current capabilities see Hill and Rucinski (1993).

Linnell's model

- Based on Roche geometry (Linnell 1984, 1993);
- Assumes circular and eccentric orbits;
- The software package consists of a series of programs;
- Monochromatic light curves are calculated;
- Calculates theoretical light curves at the times of observations;
- Permits placement of dark (bright) spots on the component photospheres;
- Synthetic spectra are calculated (Linnell et al. 1998);
- Can handle multicolor light curves;
- Impractical implementation of the whole synthetic photometry program except for the division of the entire project into separate programs.

Rucinski's Model

- Free of systematic errors related to uneven distribution of integration points;
- Roche model;
- Differential corrections via Rucinski's least-squares program;
- No spots are modelled;

- Line profiles are calculated;
- Extreme simplicity and modular structure permit easy modification;
- Input through a separate file;
- The code (in FORTRAN) is not supported generally and has restricted distribution.

The Russian school's Models

- Strong focus on eclipsing binaries with extended atmospheres (Wolf-Rayet binaries and X-ray binaries) (Cherepashchuk 1966, 1975);
- Spherical models with enhanced features for atmospheric eclipses and disks;
- Methods used are based on the regularization algorithms by Tikhonov (1963); Strong mathematical background;
- Unique solutions are determinable only in certain cases;
- X-ray systems are among the principal binaries studied by the Russian school (Bochkarev & Karitskaya 1983, Bochkarev et al. 1975, Goncharsky et al. 1991, Antokhina et al. 1992, 1993).

Wilson-Devinney's Model and Program

- Extended in many publications and software releases (Wilson and Devinney 1971, Wilson 1979, 1990, 1993).
- Supports elliptical orbits with eccentricity and non-synchronous rotation of components;
- The most recent version includes Kurucz stellar atmospheres models;
- Simple reflection effect is considered;
- Different laws of limb-darkening can be used;
- Several modes are provided to specify the geometry of a binary system or to add constraints or relations between parameters;
- Gravity darkening and albedos can be treated either as fixed parameters or adjusted ones;
- It consists of two main programs named LC and DC, where two dozen subroutines are utilized.
- Relative dimensions of the components are derived and many quantities and parameters in the model are dimensionless.

Other approaches*Budding's Eclipsing Binary Model*

- Spherical model, circular orbits, circular spots;
- Original light curves are cleaned from the effects of spots.

Kopal's Frequency Domain Method

- Kopal's contributions to the field of modern light curve analysis were crucial;
- The basic aspects of the technique are described in Kopal (1979, 1990);
- Methods in great mathematical depth are used for the representation of the fractional loss of light in symmetric eclipsing binary light curves in terms of integral transforms, especially Hankel and Fourier transforms, and discuss the asymptotic properties of finite sums of the latter;
- Corrections are applied for limb- and gravity-darkened tidally distorted non-spherical stars with light curve perturbations;
- Superiority of the method, since allows direct determination of the parameters from the observations;
- Main disadvantages:
 1. components are assumed to be spheres, or corrected spheres
 2. it is doubtful whether a few Fourier coefficients can contain all the information in a light curve
 3. the angle of the external tangency must be specified
 4. it is not easy to introduce additional physical effects into the model in this analysis.
 5. the method becomes complicated in the case of partial eclipses.

Mochnacki's General Synthesis Code, GENSYN

- GENSYN was developed by Mochnacki and Doughty in the early 1970s and further improved around 1983. It was intended to do both light curve and line profile synthesis;
- Uses cylindrical coordinate scheme;
- It was the first Roche-geometry based light curve code to incorporate full mutual irradiation by mapping each surface element to all those illuminating it.

Collier-Mochnacki-Hendry Spotted General Synthesis Code

- Combination of the programs SPOTTY (Collier) and GENSYN (Mochnacki) in 1987 to analyze spotted eclipsing systems (Hendry and Mochnacki 1992);
- Allows determination of the most likely spot distribution making use of the maximum entropy algorithm (Hendry et al. 1992);
- More recently, Hendry wrote a program to fit both orbital elements and spot distributions to photometric and spectroscopic data.

THE WILSON-DEVINNEY PROGRAM

The Wilson-Devinney program is the most widely used of all the synthetic and analytic light curve modeling codes. It is appropriate to describe its features, capabilities, and continuing developments in some detail. It has seen continual improvements and the 1998 version provides powerful features.

Current Capabilities of the WD program

- Full functionality of the WD-Program (version distributed before 1995);
- Kurucz atmospheres;
- Initial parameter search with the Simplex algorithm;
- Automatic differential corrections;
- Damped Levenberg-Marquardt scheme;
- Spectral line profiles can be computed; they can be associated with specific regions of the stars, permitting an analysis of chromospheric fluorescence and also lines from spots;
- Either time or phase can be independent variable;
- Output data can be used as input to any commercial or private plotting program;
- The program is now entirely in double precision;
- The LC input/output format is determined by a control integer allowing certain decisions about what will be computed;
- The parameter error estimates are now standard deviations;
- Shell-based I/O interface.

Several improvements await incorporation

1. Polarimetry is a ripe field for exploitation in the light curve analysis. The existing data are scarce but the means to incorporate them into analytical methods could encourage further observations in this demanding field;
2. Atmospheric eclipses for components with extended atmospheres;
3. Improved accuracy.

Atmospheric Options

1. Kurucz new stellar atmospheres incorporate computed opacities from a comprehensive list of 58 million lines and for 56 temperatures in the range 2000 to 200,000 K.
2. The models range from 3500 K to 50,000 K and over a large range in $\log g$, but not over the entire range of opacities;
3. The atmospheres were integrated over the standard passbands UBVRJIIJ, RCIC, and uvby, the nominal extended Johnson infrared passbands JHKLMN, the improved infrared bands, iz, iJ, iH, iK, iL, iL', iM, iN, in, and iQ, and for a range of narrow, square-edged passbands centered on wavelengths in the far-ultraviolet, appropriate for IUE, HSP, or other space platforms with far-ultraviolet detectors.

Applications and Extensions

The intention is to provide hints about what can be achieved and how various extensions can be used to derive astrophysical results;

1. The eclipsing X-ray Binary HD 77581 / Vela X-1
 - The binary contains an X-ray pulsar, while the ellipsoidal variable HD 77581 / GP Velorum is the optical counterpart of the pulsed, eclipsing X-ray source Vela X-1
 - A BO.5 supergiant and a neutron star move in an eccentric orbit of about $e=0.1$ and a period of 8.96 days
 - The pulse arrival times are an additional observable used in a simultaneous analysis
 - B, V light curves, optical radial velocities, pulse arrival times and estimations of the X-ray eclipse duration are used in a simultaneous analysis to ensure a self-consistent solution (Wilson & Terrell 1998).

2. Eclipsing binaries in Clusters

The objective is to analyze eclipsing binary systems in well studied clusters in a boot-strap program to increase knowledge of both binaries and clusters and test evolution models.

3. Fitting of Line Profiles

Mukherjee et al. (1996) combined the theory of stellar line broadening for local profiles with the WD program and used it to estimate rotation rates of Algol binaries by fitting line profiles to observed data.

6. The Structure of the Future Light Programs

The aspects of a general light curve program include:

- the light curve models (provided by astronomers);
- capabilities of the least-squares solvers (could be implemented by astronomers, mathematicians, computer scientists);
- user-friendly front-ends (the development requires the expertise of a software engineer rather than an astronomer or mathematician. Of course many gifted individuals are capable of fulfilling more than one of these roles).
- the above three components need to be linked appropriately. Such a program is expected to emerge in the future.

Prospects and expectations

- Modern light curve analysis was born early in the twentieth century with the pioneering work of Henry Norris Russell;
- Thanks first to the theoretical investigations of Zdenek Kopal beginning in the 1940s, and second to a number of workers who developed practical computer applications, two decades later;
- The WD program has become the light curve analysis tool of choice by the majority of the community;
- The number of observed light curves will continue to exceed the number analyzed (use of CCDs etc.);
- New techniques of analyzing data should be invented (Neural network techniques);
- The quality of light curve analyses can also be expected to improve;
- Phenomena of extended atmospheres, semi-transparent atmospheric clouds, variable thickness disks, and gas streams will be treated by such programs;

- Targets of modeling work : besides the determination of orbits, stellar sizes and masses, it seems likely that the detailed physics of stellar surfaces, including those arising from activity cycles will be included.

Close binary research might initiate projects involving complicated physics and requiring sophisticated mathematics and numerical methods.

Recommendations to Observers

1. Mid-range to long-period binaries ($P > 5d$, but especially $P > 50d$) need observations of all kinds. The longer period binaries are nearly unexplored territory;
2. Infrared light curves are especially needed for binaries with large temperature differences between the two components. Simultaneous observations in the optical and infrared are critically important;
3. Individual observations should be published or archived with easy access to them;
4. Binaries with active mass flow need to be followed continuously over at least several orbits. Suitable targets for APTs.
5. Polarimetric observations are equally important. Although light curves are nearly periodic, polarization curves mainly show transient events. Absolute time of observations should be given;
6. X-ray binaries are a major and important new area. Again absolute time should be published. X-ray binaries provide excellent data for simultaneous fitting of multiband light curves, optically determined radial velocities, and pulse arrival times.
7. Spectrophotometry provides an even greater potential bounty, and, in principle, thousands of light curves, if proper star spectra are taken (not easy and seldom done).

References

- Antokhina E.A., Seyfina E.V., Cherepashchuk A.M.: 1992, *Sov. Astron.*, **36**, 143.
- Antokhina E.A., Pavlenko E.P., Cherepashchuk A.M., Shugarov S.Y.: 1993, *Astron. Rep.*, **37**, 407.
- Binnendijk L.: 1977, *Vistas*, **21**, 359.
- Bochkarev N.G., Karitskaya E.A., Shakura N.I.: 1975, *Sov. Astron. Lett.*, **1**, 118.
- Bochkarev N.G., Karitskaya E.A.: 1983, *Sov. Astron.*, **27**, 421.
- Cherepashchuk A.M.: 1966, *Sov. Astron.*, **10(3)**, 227.
- Cherepashchuk A.M.: 1975, *Sov. Astron.*, **19(1)**, 47.
- Etzel P.B.: 1981, in E.B. Carling and Z. Kopal (eds.), *Photometric and Spectroscopic Binary Systems*, 111, D. Reidel, Dordrecht, Holland.
- Goncharov A.V., Romanov S.Y., Cherepashchuk A.M.: 1991, *Finite-Number Parametric Inverse Problems of Astrophysics*, Moscow University Press, Moscow, Russia (In Russian).
- Hadrava P.: 1997, *FOTEL 3 - User's Guide*, Technical report, Astronomical Institute of the Academy of Sciences of the Czech Republic, 25165 Ondrejov, Czech Republic.
- Hendry P.D., Mochnacki S.W.: 1992, *ApJ*, **338**, 603.
- Hendry P.D., Mochnacki S.W., Cameron A.C.: 1992, *ApJ*, **399**, 246.
- Hill G., Rucinski S.M.: 1993, in E.F. Milone (ed.), *Light Curve Modeling of Eclipsing Binary Stars*, 135.
- Jurkevich I.: 1970, *The Henry Norris Russell Memorial Volume*, Vol. 12 of *Vistas*, 63, Pergamon Press, Oxford, UK.
- Kallrath J., Milone E.F.: 1999, *Eclipsing Binary Stars*, Springer-Verlag, New York, Inc.
- Kopal Z.: 1979, *Language of the Stars*, D. Reidel, Dordrecht, Holland.
- Kopal Z.: 1990, *Mathematical Theory of Stellar Eclipses*, Kluwer Academic Publishers, Dordrecht, Holland.
- Linnell A.P.: 1984, *ApJ Suppl.*, **54**, 17.
- Linnell A.P.: 1993, in E.F. Milone (ed.), *Light Curve Modeling of Eclipsing Binary Stars*, 103, Springer, New York.
- Linnell A.P., Etzel P.B., Hubeny I., Olson E.C.: 1998, *ApJ*, **494**, 773.
- Mukherjee J.D., Peters G.J., Wilson R.E.: 1996, *MNRAS*, **283**, 613.
- Nagy T.E.: 1975, *Bull. Amer. Astr. Soc.*, **7**, 533.
- Nelson R.H., Davis W.D.: 1972, *ApJ*, **174**, 617.
- Proctor D.D., Linnell A.P.: 1972, *ApJ Suppl.*, **24**, 449.
- Russell H.N., Merrill J.E.: 1952, *Princeton Obs. Contr.*, **26**, 1.
- Tikhonov A.N.: 1963, *Dokl. Akad. Nauk USSR*, **153**, 49.
- Wilson R.E.: 1979, *ApJ*, **234**, 1054.
- Wilson R.E.: 1990, *ApJ*, **356**, 613.
- Wilson R.E.: 1993, in J.C. Leung and I.-S. Nha (eds.), *New Frontiers in Binary Star Research*, Vol. 38 of ASP Conference Series, 91, Astronomical Society of the Pacific, San Francisco, CA.
- Wilson R.E., Devinney E.J.: 1971, *ApJ*, **166**, 605.
- Wilson R.E., Terrell D.: 1998, *MNRAS*, **296**, 33.
- Wood D.B.: 1971, *AJ*, **76**, 701.
- Wood D.B.: 1972, *A Computer Program for Modeling Non-Spherical Eclipsing Binary Star Systems*, Technical Report X-110-72-473, GSFC, Greenbelt, MD.

SYMBIOTIC NOVA V1016 CYG AS INTERACTING BINARY

Š. Parimucha^{1,2}, D. Chochol², T. Pribulla²

¹ Faculty of Natural Sciences, Department of the Theoretical Physics and Geophysics, University of P.J. Šafárik, 040 01 Košice, Slovakia, *parimuch@ta3.sk*

² Astronomical Institute of the Slovak Academy of Sciences, 059 60 Tatranská Lomnica, Slovakia, *chochol, pribulla@ta3.sk*

ABSTRACT. Long-term *UBV* photoelectric and photographic photometry of the symbiotic nova V1016 Cyg is discussed. The pre-outburst brightening in 1949, main nova-like outburst in 1964 and two small brightenings in 1980 and 1994 suggest 15.1 ± 0.2 years period of activity. It is shown that a variation in the $(J - K)$ colour index as well as that in the UV continuum and emission line fluxes in the IUE, HUT and HST spectra exhibit the same periodicity, which is interpreted as the orbital period of the binary on an eccentric orbit. The basic parameters of the system are given.

Key words: Stars: symbiotic, stars: individual - V1016 Cyg, stars: photometry, stars: UV spectroscopy

1. Introduction

V1016 Cyg is a member of a small subgroup of symbiotic novae, also including V1329 Cyg and HM Sge, in which the outburst leads to a nebular spectrum (Mürset & Nussbaumer, 1994). Symbiotic novae are wide interacting binaries, where matter from a late-type giant is transferred onto the surface of the more compact companion. The nova-like optical outburst ($\Delta m \sim 5 - 7$ mag), lasting decades, is caused by a thermonuclear runaway on the surface of a wind accreting white dwarf after the critical amount of material has been accumulated (e.g., Mikolajewska & Kenyon, 1992). V1016 Cyg underwent such nova-like outburst in 1964 (McCuskey, 1965). The object is classified as a D-type symbiotic. The cool component is the Mira variable embedded in the dust envelope. Its pulsation period of ~ 478 days was determined by Munari (1988). Episodic formation of the dust in the system in 1983 was reported by Taranova & Yudin (1986).

Previous estimates of the orbital period of the symbiotic binary V1016 Cyg were not successful. Taranova & Yudin (1983) used an increase of Balmer emission lines in combination with the appearance and disappearance of FeII lines to estimate the orbital period of ≈ 20 years.

Nussbaumer & Schmid (1988) proposed the orbital period of 9.5 years on the basis of periodicity in the UV fluxes of OI and MgII lines observed by IUE satellite. However they have not observed any two subsequent maxima or minima indicating that a phenomenon repeats with time. Munari (1988) analyzed IR observations and proposed 6-year orbital period based on modeling of the dust obscuration episodes related to the passage of the Mira at the inferior conjunction in the system. Wallerstein (1988) suggested that the sharp FeII emission lines are formed in the chromosphere of the cool star and reflect the orbital motion. Their radial velocities between 1978-1985 limit any orbit of high inclination to a period greater than 25 years or to a large eccentricity. Schild & Schmid (1996) concluded from analysis of spectropolarimetric data taken from 1991-94, that the orbital period is about 80 ± 25 years. However, new observations in 1997 put this result into question (Schmid, 1988).

Long-term photographic, photoelectric and visual photometry of the object gathered and analysed by Parimucha et al. (2000), led to the discovery of 15-year periodicity of activity, interpreted as the orbital period. The aim of the present paper is to confirm this period using available IR photometry and the IUE, HUT and HST spectroscopic observations and to determine the basic parameters of the system.

2. *UBV* photoelectric and photographic photometry

The historical light curve of V1016 Cyg based on the photographic and *UBV* data gathered by Parimucha et al. (2000) is presented in Fig. 1. The light curve suggests four stages of activity marked by arrows in the figure: the pre-outburst flare *a* in 1949, the main nova-like outburst *b* in 1964 and two post-outburst flares *c* and *d* in 1980 and 1994, respectively. The ephemeris for maxima of activity calculated in Parimucha et al. (2000) is as follows:

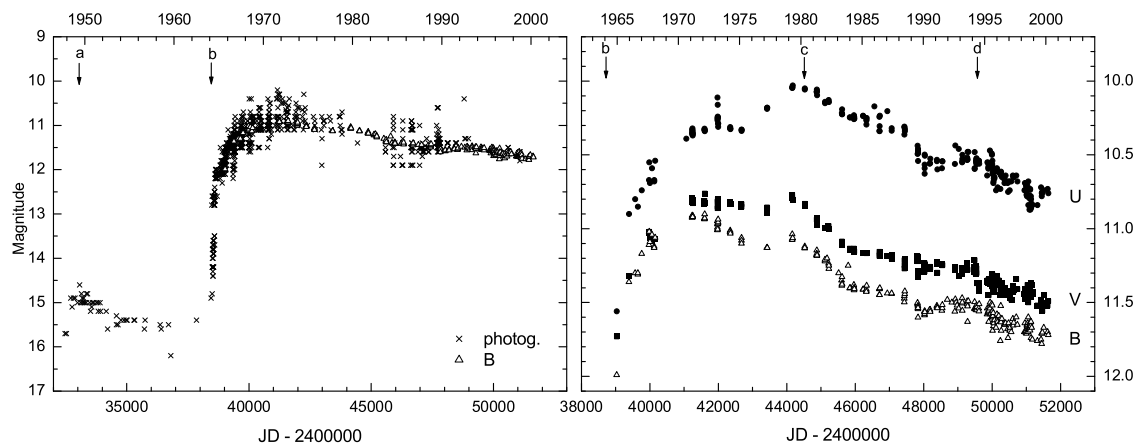


Figure 1: Long-term photographic and photoelectric UBV observations

$$\text{JD}_{max}^{phot} = 2427590 + 5510 \times E. \quad (1)$$

$$\pm 250 \quad \pm 90$$

The brightness maxima in 1980 and 1994 followed the well detected brightness decreases as possible signatures of an enhanced mass transfer from the cool to the hot component. Similar effect was detected in the light curve of very slow classical nova V723 Cas (Chochol & Pribulla, 1998).

3. Infrared photometry

We have used all available infrared photometry (for complete list of the observations see Parimucha (2001)) to improve the period of pulsation of the Mira variable present in the system. The Fourier period analysis applied to the JHK data, after the trend removal, led to the mean period $P = 474 \pm 6$ days (Fig. 2). Corresponding phase diagrams are presented in Fig. 3.

According to Whitelock (1987), the $(J - K)$ color index in symbiotic Miras is little affected by the Mira pulsation but it is very sensitive to the circumstellar dust around cool component. The transient dust obscuration episodes are orbitally related, so they could be used to find the orbital period. It is well known, that the dust can be formed also in the ejecta of novae (e.g., Bode, 1993).

The long-term behaviour of the $(J - K)$ color index of V1016 Cyg using all available infrared data is presented in Fig. 4. The most interesting feature is a short-term but strong dust formation episode in 1983 detected by Taranova & Yudin (1986), which occurred three years after the brightness maximum of the nova in U passband. We interpret this by a dust formation in the ejecta of the symbiotic nova. Detailed in-

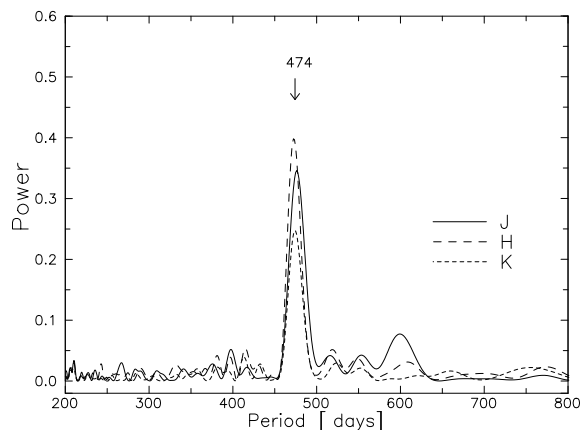


Figure 2: The Fourier power spectra of the pulsation period of Mira in the JHK data

spection of the behaviour of the $(J - K)$ index shows wave-like variation with the maxima in 1988 and possibly in 1973 (marked by o and $o?$) and minima in 1992 and possibly in 1977 (marked by b and $b?$). It suggests the ≈ 15 -years periodicity in agreement with that found from UBV photometry. The $(J - K)$ index is influenced also by a dust formation due to the activity of the hot component and possible mass transfer bursts in the periastron of eccentric orbit. Combination of all these effects leads to ≈ 6 -year periodicity interpreted by Munari (1988) as the orbital period of the binary.

4. Ultraviolet spectroscopy

We have analyzed low and high dispersion IUE (International Ultraviolet Explorer) spectra, HUT (Hopkins Ultraviolet Telescope) spectrum taken on March 6, 1995 and two HST (Hubble Space Telescope) spectra taken on March 24, 2000 (for complete list see

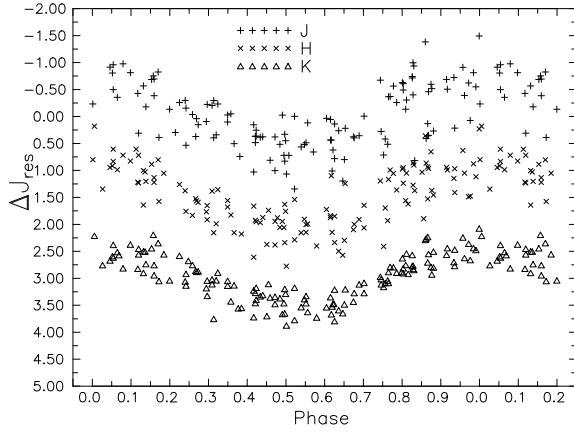


Figure 3: The JHK residual light curves phased with the ephemeris $JD_{max} = 2447442 + 474 \times E$. The ΔH_{res} and ΔK_{res} are shifted by 1.5 and 3.0 mag, respectively

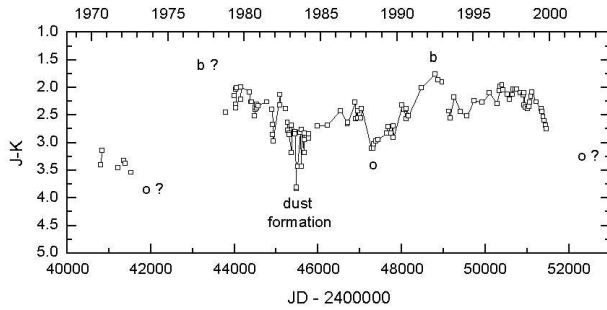


Figure 4: $(J - K)$ color index of V1016 Cyg

Parimucha (2001)). We have excluded saturated spectra or saturated lines and bad pixels. The low dispersion IUE spectra and the HST spectra were used to determine the continuum flux. To establish the continuum behaviour, we measured average fluxes in 20\AA bins free from emission lines. The high dispersion IUE spectra, the HUT and HST spectra were used to determine the fluxes of the emission lines. The spectra were dereddened with $E(B - V) = 0.28$ (Nussbaumer & Schild, 1981). Fluxes of non-saturated lines were determined by fitting Gaussian profiles.

The temporal behaviour of the continuum and line fluxes are shown in Figs. 5 and 6, respectively. We have found the ephemerides for the maxima of the continuum and line fluxes as follows:

$$JD_{max}^{cont} = 2444150 \pm 120 + 5400 \pm 200 \times E. \quad (2)$$

$$JD_{max}^{lines} = 2444650 \pm 240 + 5630 \pm 300 \times E. \quad (3)$$

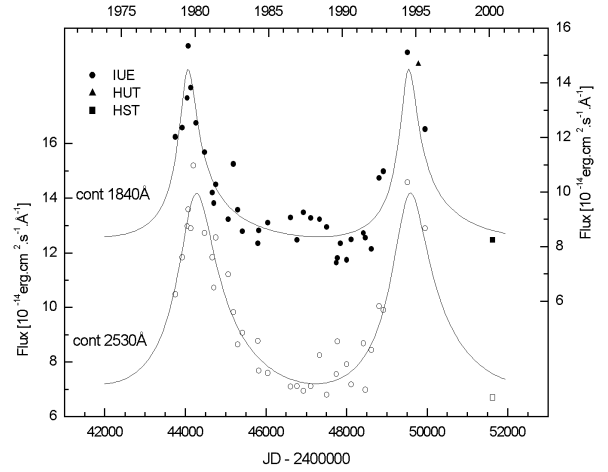


Figure 5: Fluxes of the UV continuum

The maximum of the continuum flux agrees within the uncertainty with that detected photometrically (see ephemeris (1)). On the other hand, the maximum of emission lines occurred 1.4 years after the maximum of the continuum. Nevertheless, the ≈ 15 -year period is clearly present in all sets of data.

4. Basic parameters of the binary system

The period of Mira star pulsation in V1016 Cyg allows to determine basic parameters of the cool component using the standard pulsation equation, period-luminosity relation, period- T_{eff} relation and Stephan-Boltzmann law (Cox, 2000; Glass & Feast, 1982): $L_c = 7600 \pm 100 L_\odot$, $T_{eff} = 2450 \pm 50$ K, $R_c = 485 \pm 20 R_\odot$, $M_c = 0.81 \pm 0.11 M_\odot$. If we accept the orbital period of the binary 5510 days and the mass of the hot component $1.1 M_\odot$ estimated by Mürset & Nussbaumer (1994) and Mikolajewska & Kenyon (1992), the semi-major axis of the system is $1630 R_\odot$. Then, the Roche lobe radius of the cool component is $R_{Roche} = 576 R_\odot$. The possible small eccentricity of the orbit can cause the pulsating Mira variable to fill-up the Roche lobe near periastron, so the matter is easy transferred to the hot component. The distance to V1016 Cyg derived from IR photometry by Parimucha (2001) is 2.9 ± 0.7 kpc.

5. Discussion

Symbiotic nova V1016 Cyg is a wide-orbit binary consisting of a pulsating Mira and a white dwarf that after prolonged accretion underwent a thermonuclear outburst in 1964 leading straight to a nebular spectrum. According to the ionization model of symbiotic binaries, the hot luminous component ionizes the neu-

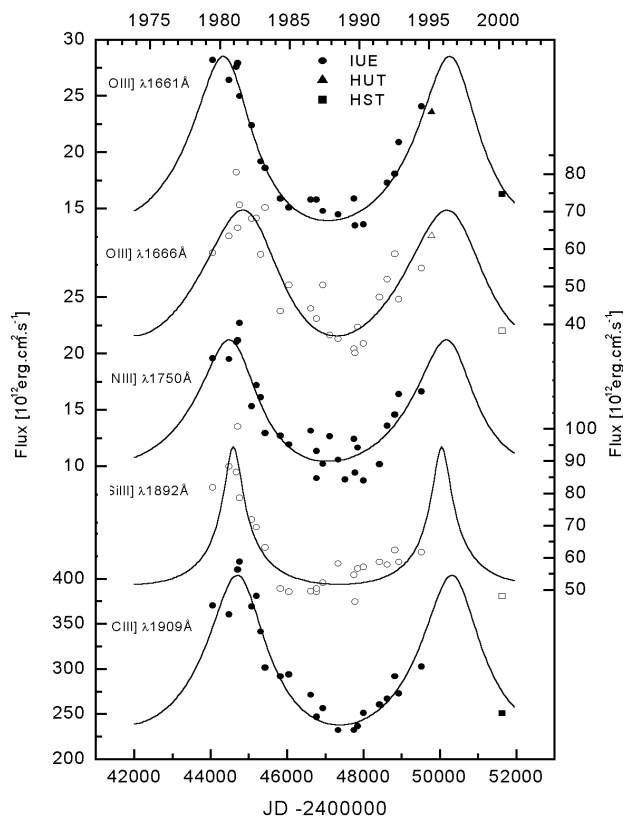


Figure 6: Fluxes of the emission lines

tral wind of the giant giving rise to the nebula in the system. The times of brightness maxima in the U pass-band observed in 1980 and 1994 agree with that in the ultraviolet continuum. This suggests that the nebula is responsible for both continua. The periodic variations of the optical and UV continuum can be caused by the different contribution of the nebula to the brightness of the system along the orbital cycle (Skopal, 2001) and individual flares originated in the accretion disk of the white dwarf. These flares are triggered by enhanced mass transfer bursts from the Mira during the periastron passage of the hot object on the 15-year eccentric orbit. The pre-outburst flare in 1949 could be of the same nature. The 1.4 years delay of the maxima of the OIII], CIII], NIII] and SiIII] UV emission line fluxes in comparison with the maximum in the UV continuum shows that the lines are excited in the surrounding nebula collisionally when the fast wind from the hot object interacts with the slow wind from the Mira variable.

Present analysis of the photometry and UV spec-

troscopy shows that V1016 Cyg is a binary system with the orbital period 15.1 ± 0.2 years (Parimucha et al., 2001). V1016 Cyg is the first D-type symbiotic system in which the orbital period was determined.

Acknowledgements. This work was based on INES data from the IUE satellite and on observations made with the NASA/ESA Hubble Space Telescope, obtained from the data archive at the Space Telescope Science Institute. STScI is operated by the Association of Universities for Research in Astronomy, Inc. under NASA contract NAS 5-26555. This work was accomplished as a part of a PhD thesis of Š.P. and has been supported by VEGA Grant 2/1157 of the Slovak Academy of Sciences.

References

- Bode M.F.: 1995, in *Wolf-Rayet Stars: Binaries, Colliding winds, Evolution*, K. A. van der Hucht & P. M. Williams (eds.), Kluwer, Dordrecht, 363.
- Chochol D., Pribulla T.: 1998, *Contrib. Astron. Obs. Skalnaté Pleso*, **28**, 121.
- Cox A.N. (ed.): 2000, *Allen's Astrophysical Quantities*, AIP Press, New-York.
- Glass I.S., Feast M.W.: 1982, *MNRAS*, **199**, 245.
- McCuskey S.: 1965 *IAU Circ.*, 1916.
- Mikolajewska J., Kenyon S.J.: 1992, *MNRAS*, **256**, 177.
- Munari U.: 1988, *As.Ap.*, **200**, L13.
- Mürset U., Nussbaumer H.: 1994, *As.Ap.*, **282**, 586.
- Nussbaumer H., Schild H.: 1981, *As.Ap.*, **101**, 118.
- Nussbaumer H., Schmid H.M.: 1988, *As.Ap.*, **192**, L10.
- Nussbaumer H.: 2001, private communication.
- Parimucha Š., Arkhipova V.P., Chochol D., Kroll P., Pribulla T., Shugarov S.Y., Ulyanikhina O., Chinarova L.L.: 2000, *Contrib. Astron. Obs. Skalnaté Pleso*, **30**, 99.
- Parimucha Š.: 2001, *PhD Thesis* (in Slovak).
- Parimucha Š., Chochol D., Pribulla T., Buson L.M., Vittone A.A.: 2001, *As.Ap.*, submitted.
- Skopal A.: 2001, *As.Ap.*, **366**, 157.
- Taranova O.G., Yudin B.F.: 1983, *As.Ap.*, **117**, 209.
- Taranova O.G., Yudin B.F.: 1986, *AZh*, **63**, 317.
- Schmid H. M.: 1998, *Rev. in Modern Astronomy*, **11**, 297.
- Schild H., Schmid H.M.: 1996, *As.Ap.*, **310**, 211.
- Wallerstein G.: 1988, *As.Ap.*, **197**, 161.
- Whitelock P.A.: 1987, *PASP*, **99**, 573.

DV AQUARI REVISITED

G. Połubek

Astronomical Institute of the Wrocław University,
Kopernika 11, 51-622 Wrocław, Poland, *polubek@astro.uni.wroc.pl*

ABSTRACT. This work presents a new solution for the close binary system DV Aqr (HD 199603, HR 8024) based on archival International Ultraviolet Explorer observations, ground-based photometric light curves and radial velocity data. The solution is obtained as the best fit of the theoretical model to all these observations simultaneously. Roche geometry of the binary system is assumed and a grid of the newest Kurucz models of stellar atmospheres is used in the calculations.

Key words: Stars: close binary; stars: individual: DV Aqr.

1. Introduction

The energy flux distributions, light and radial velocity curves of a binary contain information about the basic parameters of the system. To obtain these parameters a separate treatment of different types of data is usually made. In this work all observations are analyzed simultaneously giving only one set of model parameters. For this purpose we construct models which allow us to calculate energy flux distributions, light curves in different wavelengths, and radial velocity curves, according to prescriptions given by Połubek (1998). The main properties of the model are the following:

- Roche model is assumed for the system geometry,
- irradiation effect is taken into account,
- synchronous rotation of both components is assumed,
- newest Kurucz (1996) models of stellar atmospheres are included.

We use a differential correction scheme to derive the basic parameters of the system. This scheme is equivalent to the chi-square value minimization procedure (cf. Numerical Recipes in Fortran, Chapter 15):

$$\chi^2 = \sum_k^{N_{\text{obs}}} \left(\frac{C^{\text{obs}}(k) - C^{\text{cal}}(k, \vec{p})}{\sigma_k} \right)^2,$$

where $\vec{p} = (p_1, p_2, \dots, p_{N_{\text{par}}})$ is the vector of model parameters, $C^{\text{obs}}(k)$ and $C^{\text{cal}}(k, \vec{p})$ correspond to the observed and theoretical values of different types of data, respectively; σ_k is the error of k -th point and N_{obs} is the number of observations. The vector \vec{p} must include, in general, geometrical parameters of the system, as well as parameters describing the radiation field. Our choice of \vec{p} is the following:

$$\vec{p} = (d, T_{\text{eff}}^P(\text{pole}), T_{\text{eff}}^S(\text{pole}), q, U^P, U^S, i, M_{\text{tot}}, P, E(B-V), \gamma, v_{\text{turb}}, \left[\frac{m}{H} \right]),$$

where d is the distance to the system, $T_{\text{eff}}^P(\text{pole})$ and $T_{\text{eff}}^S(\text{pole})$ are polar temperatures of the primary and secondary components of the binary system, respectively, q is the mass ratio, U^P and U^S are the surface physical potentials of the components, i is the binary inclination angle, M_{tot} is the total mass of the system, P is the orbital period, $E(B-V)$ is the colour excess, γ is the radial velocity of the barycentre, v_{turb} is the turbulent velocity, and $\left[\frac{m}{H} \right]$ is the metallicity. In our case

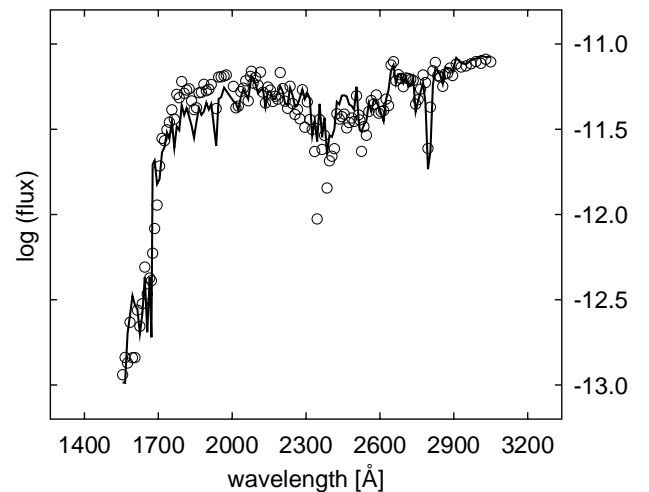


Figure 1: Observed (symbols) and synthetic (solid line) flux distributions of DV Aqr.

the minimization of chi-square χ^2 must be achieved by an iterative scheme. We have to find corrections $\Delta\vec{p}$, which added to the current approximation of the sys-

Table 1: Archival IUE observations of DV Aqr.

image identifier	dispersion	aperture	date and time	integration time in seconds
SWP52093	low	large	1994-09-12 07:44:38	359.5
LWP29159	high	large	1994-09-12 08:00:38	2159.7
SWP52160	low	large	1994-09-20 07:50:30	119.5

tem parameters \vec{p}_{cur} give smaller value of χ^2 .

2. Observational material

Observational material used in our analysis consists of:

- International Ultraviolet Explorer spectra listed in Table 1;
- B and V light curves of Okazaki & Yamasaki (1985);
- radial velocity curve of the primary component taken from Paffhausen & Seggewiss (1976).

Orbital phases are calculated assuming the ephemeris given by Strohmeier (1965):

$$\text{Min.I : HJD}2426160.500 + 1^{\text{d}}575531 \times E.$$

3. Analysis

Okazaki & Yamasaki (1985) found photometric value of the mass ratio $q = 0.6$ and our first solution assumes this value.

Table 2: Parameters of DV Aqr.

Parameter	Value
d	$91 \text{ pc} \pm 12 \text{ pc}$
$T_{\text{eff}}^P(\text{pole})$	$7905 \text{ K} \pm 320 \text{ K}$
$T_{\text{eff}}^S(\text{pole})$	$6056 \text{ K} \pm 240 \text{ K}$
q	$0.6 *$
U^P	$1.474\text{E}15 \pm 0.085\text{E}15 \text{ cgs}$
U^S	$2.255\text{E}15 \pm 0.181\text{E}15 \text{ cgs}$
i	$83^{\circ}18 \pm 0^{\circ}11$
M_{tot}	$2.76 \pm 0.04 M_{\odot}$
P	$1^{\text{d}}575531 *$
$E(B - V)$	0.04 ± 0.03
γ	$10.0 \text{ km s}^{-1} \pm 2.3 \text{ km s}^{-1}$
v_{turb}	$2.0 \text{ km s}^{-1} *$
$\left[\frac{m}{H}\right]$	$0.0 *$

*) assumed value

Model parameters derived from the best fit procedure are shown in Table 2. Table 3 gives additional

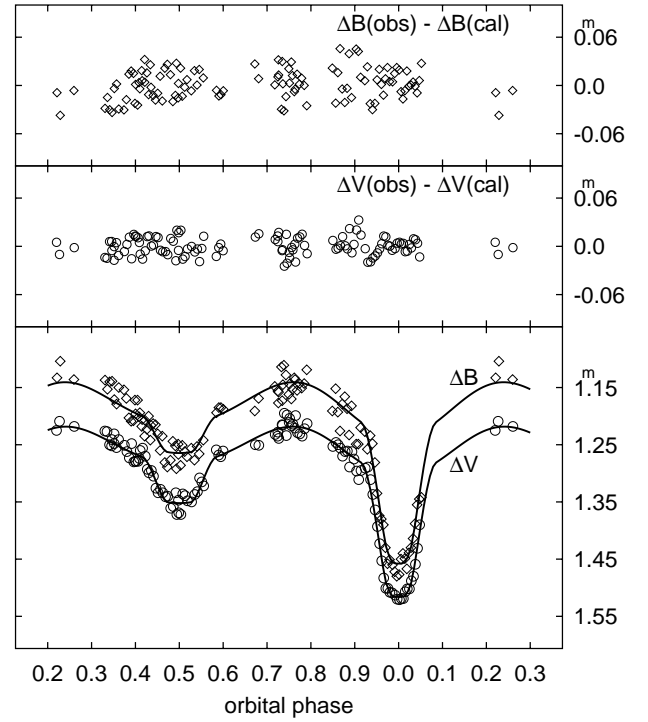


Figure 2: Lowest panel shows B and V light curves of DV Aqr (open symbols) with the best fit synthetic curves (solid lines). Upper two panels show the residuals.

information about the binary system. Observed energy flux distributions, light curves and radial velocity curve are marked in Figures 1 – 3 as open symbols, while solid lines represent theoretical values. DV Aqr appears to be a detached system just as in the solution of Okazaki & Yamasaki, but model parameters of our solution are significantly different from those of Okazaki & Yamasaki. In contrast, light curves minima are flat in our solution (see Figure 2) and dimensions of secondary component are considerably smaller. Our estimate of the inclination angle is $i = 83^{\circ}18$, while Okazaki & Yamasaki give $i = 70^{\circ}$.

To check quality of the solution we compare the rms residuals of the light curves. For scatter of the observations from synthetic light curves Okazaki & Yamasaki report $\sigma_{\Delta V} = 0.019 \text{ mag}$ and $\sigma_{\Delta B} = 0.033 \text{ mag}$ for V

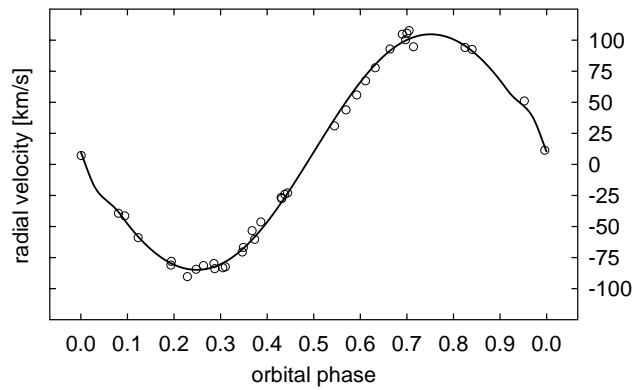


Figure 3: Observed radial velocities (open symbols) and the synthetic curve of the best fit solution (solid line).

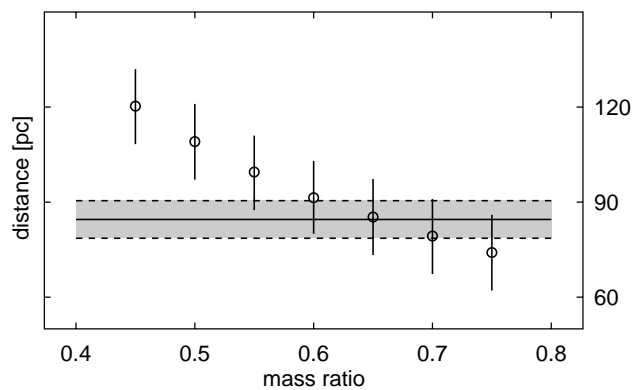


Figure 4: Distance to the DV Aqr as a function of mass ratio. Solid line corresponds to the Hipparcos parallax of the system.

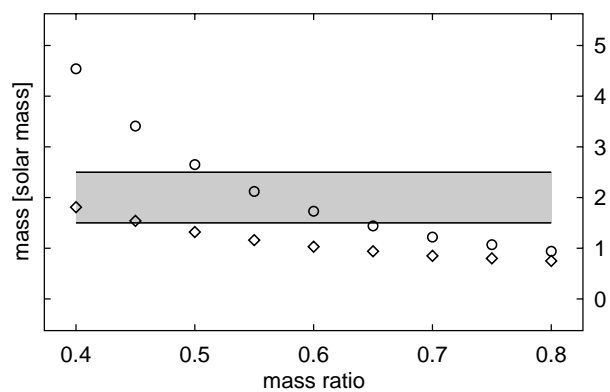


Figure 5: Mass of primary (circles) and secondary (diamonds) component of DV Aqr as a function of mass ratio. Shaded region corresponds to mass range of δ Scuti variable stars.

Table 3: Other characteristics of DV Aqr.

	Primary	Secondary
Roche potentials	3.467	8.603
Radius*		
pole	0.345	0.144
point	0.384	0.146
side	0.357	0.144
back	0.371	0.145
Radius**		
pole	2.756	1.149
point	3.067	1.164
side	2.854	1.154
back	2.963	1.162
Temperature		
pole	7905	6059
point	7613	6289
side	7815	6052
back	7721	6035
log g		
pole	3.803	4.334
point	3.585	4.312
side	3.742	4.327
back	3.676	4.315

*) fractional radius (in separation units)

**) radius in solar units

and B bands, respectively. Our solution is much better since $\sigma_{\Delta V} = 0.011$ mag and $\sigma_{\Delta V} = 0.018$ mag.

In the next step we search for a photometric value of the mass ratio, q . For this purpose, a sequence of solutions is calculated for different values of q in the range from 0.4 to 0.8. In all cases we get a detached configuration. However, no unique minimum can be reached. Thus, photometric value of q cannot be determined with reasonable accuracy.

Alternative way to find the mass ratio is the following. Different values of q give different values of distance to the system. Figure 4 shows a distance to DV Aqr as a function of q . The solid line represents the Hipparcos (ESA 1997) data, viz. $d = 84.5 \pm 6.0$ pc. As can be seen from this comparison, the value of q consistent with the Hipparcos distance is in the range from 0.55 to 0.8.

Additional constraint on the mass ratio may be secured from H_{β} observations of DV Aqr (Kilambi 1975). These data suggest that the binary system contains a pulsating star of δ Scuti type. Mass of such a star must be in the range from 1.5 to 2.5 M_{\odot} (cf. Gautschy & Saio 1995). Figure 5 shows masses of the primary and secondary components as a function of q . Formal errors of the mass determinations are small (they are comparable to the size of symbols used in Figure 5). As can be seen, the secondary component may be a δ Scuti variable only for $q < 0.45$. It is inconsistent with the

mass ratio determination from the Hipparcos parallax. This indicates that only the primary component may be a δ Scuti variable. In this case the mass of the primary component lies in the range from 1.5 to 2.5 M_{\odot} for $q = 0.50 - 0.65$. This indicates that the Okazaki & Yamasaki value of q is reasonable estimation of the mass ratio.

Acknowledgments This work was supported by the Wrocław University grant 2041/W/IA/01.

References

- ESA, 1997, *The Hipparcos and Tycho Catalogues*, ESA SP-1200
Gautschy A., Saio, H.: 1995, *ARA&A*, **33**, 75
Kilambi G.C.: 1975, *IBVS*, No 1024
Kurucz R.L.: 1996, CD-ROM No. 19
Okazaki A., Yamasaki, A.: 1985, *PASP*, **97**, 620
Paffhausen W., Seggewiss, W.: 1976, *A&AS*, **24**, 29
Polubek G.: 1998, *ASP Conf. Ser.*, Vol. **145**, 19
Press W.H., Flannery B.P., Teukolsky S.A., Vetterling W.T.: 1989, *Numerical Recipes in Fortran*, Cambridge University Press
Strohmeier, W.: 1965, *IBVS*, No. 89

PHOTOELECTRIC MONITORING OF ACTIVE CLOSE BINARIES

T. Pribulla¹, D. Chochol¹, Š. Parimucha¹, P. Rovithis², H. Rovithis-Livanou³, J. Tremko¹

¹Astronomical Institute of the Slovak Academy of Sciences,

059 60 Tatranská Lomnica, Slovakia, (*pribulla,chochol,parimuch,tremko*)@ta3.sk

²National Astronomical Observatory, P.O. Box 20048, GR 11810 Athens, Greece

³Department of Astrophysics, Astronomy and Mechanics, University of Athens,
GR 157 84 Zografos, Athens, Greece, *elivan@cc.uoa.gr*

ABSTRACT. The results of the long-term *UBVR* photoelectric monitoring of active close binaries XY UMa, RT And, VW Cep and SW Lac are presented. The orbital period changes are discussed including light-time effect and apparent changes caused by the surface activity. The presence and effects of other components to the studied close binaries are stressed. Clean light curves are constructed and resulting photometric elements are used to determine the absolute parameters of the systems.

Key words: Stars: binary: contact; stars: individual: XY UMa, RT And, VW Cep, SW Lac

1. Introduction

Surface and super-surface activity in the stars is connected with the presence of magnetic fields. The surface regions with stronger magnetic field, cool spots, are also origin of other manifests of activity like eruptions and flares, coronal transients, stellar wind. Intensity of the surface magnetic field is proportional to the rotational velocity of the star and depends also on the turn-over time of the convective zone. These two quantities are connected by so called Rossby number. It is widely known that magnitude of the stellar activity increases toward late spectral types. Unlike in the Sun ($v_{rot} = 1.8 \text{ km.s}^{-1}$) and other single stars, magnetic braking in close, tidally coupled binaries spins-up rotation of the components. Due to tidal coupling of the rotational and angular momentum rotational velocities of the components in close binaries are often higher than 100 km.s^{-1} .

The present study deals with two separate groups of active close binaries. Short-period RS CVn-like systems are detached binaries with main-sequence components. Their orbital periods are in the range $0.49 < P < 0.9$ days, spectral types F8V-G9V (primary components) and K0V - K5V (secondary components). The activity is displayed as an enhanced Ca II H and K

emissions, flares in visual region and light-curve disturbances up to 0.3 mag. W UMa systems (W-type group, the more massive component is cooler) are contact binaries with very short orbital periods $0.22 < P < 0.40$ days and late spectral types G3V - K5V. The activity is usually lower compared with RS CVn-like binaries of the same spectral type. LC disturbances are observed up to 0.1 mag. The presence of the magnetic field causes also coupling of the magnetic and angular momentum (Applegate, 1992) displayed as the cyclic period, brightness and colour variation. The activity of the eclipsing pairs is probably connected with the presence of other component(s) to the binary systems. In present sample: XY UMa, RT And (RS CVn-like short period group), VW Cep, SW Lac (contact binaries of the W type), the third components were conclusively detected in XY UMa, VW Cep and SW Lac. Important physical parameters of the studied systems are given in Table 1.

2. Long-term multicolour photoelectric photometry

New extensive photoelectric photometry was performed at 0.6m Cassegrain telescopes at the Skalnaté Pleso (*UBVR*) and Stará Lesná (*UBV*) Observatories, 0.6m Cassegrain of the Mt. Laguna Observatory (*BVRI*). XY UMa was observed in 1994-2001, RT And 1997-2000, VW Cep in 1968-9, 1976, 1998-2001, SW Lac from 1998-2001. Selected photoelectric light curves are shown in Fig. 1. The comparison stars are given in Table 1. For RT And additional high-speed photometry was performed to determine the type of the eclipses. For RT And, XY UMa and VW Cep also photometry of all comparison stars used by different observers, necessary for the analysis of the long-term brightness variability, has been performed. All our observations were used to determine times of the minima using Kwee and van Woerden's (1956) method.

Table 1: Fundamental parameters of the studied systems

	RS CVn (SPG)		W UMa - (W-type)	
	XY UMa	RT And	VW Cep	SW Lac
JD ₀	49777.9429	50000.3588	50003.2992	51056.2890
Period [days]	0.47899819	0.62892932	0.27831149	0.32071484
$\Delta P/P$ [10^{-8} year ⁻¹]	+8.66	-22.4	-76.0	+18.9
Interval	1994-2001	1968-2000	1995-2001	1993-2001
Comparison	BD+55 1320	BD+52 3384	SAO 9836	BD+37 4715
$q = M_c/M_h$	0.61	0.74	2.53	1.255
i [°]	80.9	87.6	63.6	80.2
$M_c[M_\odot]$	0.66	0.79	1.16	0.96
$M_h[M_\odot]$	1.10	1.13	0.46	0.78
$R_c[R_\odot]$	0.63	0.89	1.00	1.00
$R_h[R_\odot]$	1.16	1.22	0.66	0.91
(B-V)	0.80	0.50	0.93	0.82
π^{-1} [pc]	66	75	27	81
P_3 [years]	30	–	32	90
P_4 [years]	–	–	19?	23

3. Methods

For the studied systems we gathered all available times of minima from Kraków database (Kreiner et al., 2000). The minima were weighted according to their mean precision: photographic and photovisual $w=3$, photoelectric and CCD $w=10$. Our analysis included Fourier and pdm analysis of the residuals, determination of the orbital elements of the multiple components to the eclipsing pairs including quadratic orbital ephemeris optimization and correlational analysis of the LC asymmetries and (O-C) residuals. The observed period changes and the new linear ephemerides of all four studied systems valid for the coming years are given in Table 1. The ephemerides were up-dated using all available minima (until September 2001) from the last approximately linear part of the (O-C) diagram (Table 1).

All observations were used to construct the clean "unspotted" light curves selecting the brightest points in the 0.01 phase bins. For the determination of the photometric elements we have used the 1992 version of the differential corrections code developed by Wilson and Devinney (1971) (W&D). The clean elements were used to determine also individual spotted light curves assuming circular starspots. The resulting clean photometric elements together with published spectroscopic elements were used to determine the absolute parameters of the studied systems (Table 1). The long-term changes of the maximum brightness were studied for XY UMa, RT And and SW Lac.

4. Results for individual objects

4.1. XY UMa

XY UMa is the most active member among all RS

CVn-like binaries. The system was discovered by Geyer et al. (1955), who later performed extensive photometric and spectroscopic observations. The brightness of XY UMa exhibits night-to-night LC variations, changes from symmetrical to asymmetrical LC shape as well as long-term total brightness and colour changes. The observed period changes were interpreted either by the light-time effect caused by another body in the system (Pojmanski and Geyer, 1998) or Applegate's mechanism (Erdem and Gdr, 1998). The latter possibility was not tested observationally. Pojmanski and Udalski (1997) were first to determine the semi-amplitude of the radial velocities of the secondary component. The spectroscopic elements were later improved by Pojmanski (1998) by analysis of the near-infrared spectra.

Our extensive photometric monitoring (16 LCs) resulted in the determination of the clean photometric elements as well as absolute parameters of the components (Table 1). The observed ($O - C$) diagram was interpreted by the combination of the LITE ($P_3 = 30$ years) and maculation effects. This result was conclusively supported by the correlational analysis of the (O-C) residuals and light-curve asymmetries as well as the eclipse of the binary by the protostellar third body around 1977. The LC asymmetries and (O-C) residuals from LITE were found to display 710 days periodicity. High-dispersion spectroscopy showed the presence of additional chromospheric emission in the H_α . New spectral classification showed discrepancy between the spectral type and observed ($B - V$) colour index. Hipparcos distance $d = 66 \pm 6$ pc was found to be much lower than distance determined from simultaneous analysis of the photometry and spectroscopy

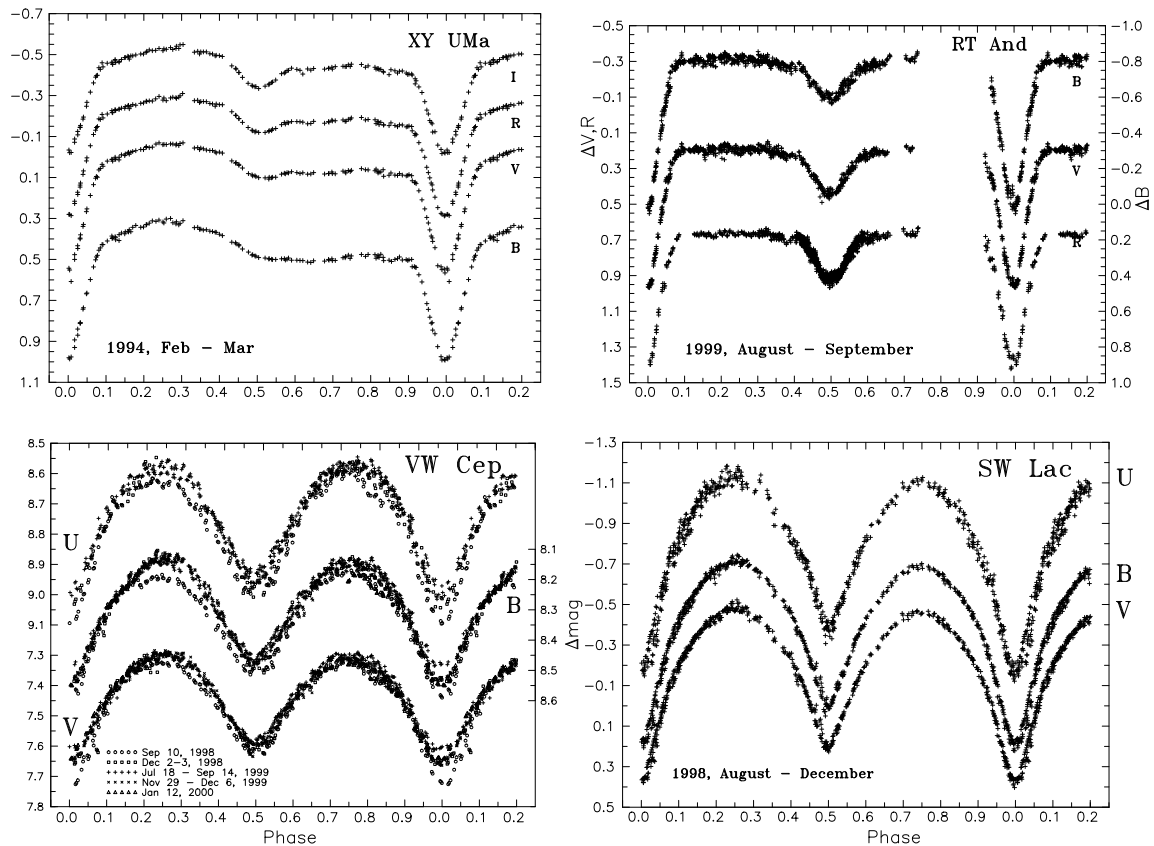


Figure 1: Selected photoelectric light curves of XY UMa, RT And, VW Cep and SW Lac

$d = 86$ pc. New results are presented in Pribulla et al. (2001) and Chochol et al. (1998).

4.2 RT And

Active eclipsing binary RT And has been known from the beginning of the 20th century. Williamon (1974) interpreted observed period decrease by two jumps caused by instantaneous mass exchange bursts. Albayrak et al. (1999) and Borkovits and Hegedüs (1996) explained the long-term period decrease by the LITE caused by the presence of one or two other bodies, respectively. Photometric solutions of the binary lead to the detached configuration with an inclination angle either close to 82 or to 88 degrees and small orbital eccentricity 0.02 - 0.08. The Mg II H and K lines indicate high degree of the chromospheric activity (Budding et al., 1982).

Our analysis of the clean light curve lead to two possible solutions: $i = 82.6^\circ$, $i = 87.6^\circ$. Additional high-speed photometry of the secondary minimum showed that the eclipses are total. Possible small orbital eccentricity was ruled out. It was shown to be only result of the distortion of the RV and LC curves caused by the maculation effects. All published photoelectric LCs were solved individually to find the positions and parameters of the spots. For some LCs the face-to-

face position of the polar starspots on both components was detected, leading to possible interconnection of the magnetic fields - magnetic bridge. The Fourier analysis of the spot longitudes on the primary component showed the presence of the 6.8 year oscillation. The distance to the system determined from photometry and spectroscopy $d = 83$ pc is within error of the Hipparcos distance $d = 75 \pm 6$. Detailed results of our study are given in Pribulla et al. (2000).

4.3 SW Lac

SW Lac is the most extreme representative of W-type W UMa stars and is well known for its variable light curve and period (Brownlee, 1957). Van't Veer (1972) explained period changes by jumps alternated with intervals of constant period. Panchatsaram and Abhyankar (1981) explained (O-C) diagram by the presence of double sinusoids, interpreted as the LITE in a quadruple system. Zhang and Lu (1989) reliably determined spectroscopic elements. Rucinski et al. (1984) found strong chromospheric and coronal activity of the system. The presence of another component to the system was conclusively shown by Hendry and Mochnacki (1998).

The (O-C) diagram constructed using all available photographic and photoelectric times of minima (in-

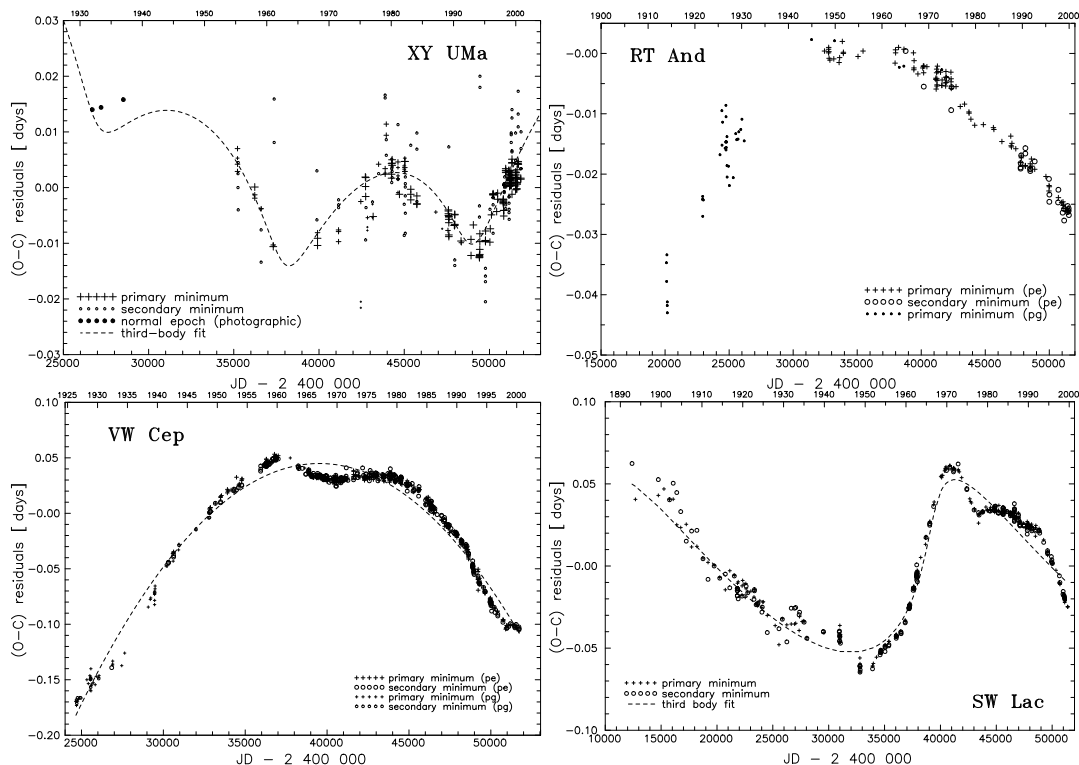


Figure 2: (O-C) diagrams from the mean linear ephemeris for XY UMa, RT And, VW Cep and SW Lac. LITE fits are shown for XY UMa and SW Lac.

cluding our 12 determinations) was explained by a secular period increase $\Delta P/P = 1.89 \cdot 10^{-7} \text{ year}^{-1}$ and light-time effect due to the presence of another two bodies in the system with orbital periods $P_3 = 23$ and $P_4 \approx 90$ years. The minimum masses of these bodies are $M_3 = 0.41 M_\odot$ and $M_4 = 1.47 M_\odot$. The observed *UBV* light curves of the system were found to be quite asymmetric: max I (phase 0.25) was about 0.02 mag brighter than max II (phase 0.75). All observations were used for the LC analysis. The resulting elements are given in Table 1. The slight asymmetry of the light curve was explained by a cool spot on the primary component facing the observer in phase 0.75. We have checked also possibility that the light curve is affected by the third light caused by the other components to the binary. The third light was found to be negligible. The geometric elements $i = 80.2^\circ$ and fill-out factor $F = 0.39$, obtained from our observations are close to that determined by Leung et al. (1984). Our results are presented in Pribulla et al. (1999).

4.4 VW Cep

VW Cep is a very bright ($V_{max} = 7.3$ mag) chromospherically active system. The pronounced variations of the light curve and presence of the third body have caused it to be one of the most observed variable stars. The system was the subject to the multi-site international campaign organized by Kwee (1966) and exten-

sive observations by Pustyl'nik and Sorgsepp (1976). Many alternative models were proposed to explain the light-curve disturbances including a circumstellar ring, hot spot due to a gas stream and dark starspots. The starspot model is supported by an enhanced surface activity indicated by flare events and increased H_α emission. The presence of the third body affecting observed times of minima was conclusively proved by astrometric observations (Hershey, 1975). Hendry and Mochnacki (2000) performed a detailed analysis of the simultaneous *UBVRI* photometry and high-dispersion spectroscopy. Except the reliable determination of the absolute parameters (see Table 2), maximum entropy images of the eclipsing pair show rather high spot coverage of both components.

The detailed analysis of the (O-C) diagram revealed the continuous period decrease explained by the mass transfer from the more to less massive component and/or the magnetic braking process. A mass transfer rate of $(1.38 \pm 0.01) \cdot 10^{-7} M_\odot \text{ y}^{-1}$ fully explains the period decrease. (O-C) residuals from the parabolic fit show the light-time effect due to the third body on the 30-years orbit and 19-years wave-like variation caused either by the fourth body orbit or by the Applegate's mechanism. The latter possibility should be tested, however, by the analysis of the long-term changes of the brightness and colour of the eclipsing pair. If VW Cep is a quadruple system the minimum masses of the

components are $m_3 = 0.49 M_{\odot}$ ($P = 31.3$ years) and $m_4 = 0.19 M_{\odot}$ ($P = 18.6$ years). The mass of the third body is still incompatible with the observed third light and intensity of the third-component lines in the spectrum. Hence, it is possible that the observed period changes are partly caused by the intrinsic processes in the system. The preliminary results of our period study are given in Pribulla et al. (1999).

Although our analysis of the (O-C) diagram are not conclusive, it is probable that VW Cep is a multiple system. For the reliable detection of all components more extensive and precise observations are needed. The orbital elements of the third and fourths components should be determined by simultaneous fitting of the astrometric data and observed times of the minimum light. A detailed analysis of the observed light curves is under preparation.

5. Conclusions

Analysis of the (O-C) diagrams of several close active binaries of the RS CVn-like and W-type W UMa type has shown that incidence and importance of the multiple systems is higher than previously thought. The existence of other components to the studied pairs was independently proved by an infrared excess (XY UMa), visual detection (VW Cep) and spectral lines (SW Lac, VW Cep). On the other hand, so called Applegate's orbital - magnetic momentum coupling mechanism was not found to be important for XY UMa.

Analysis of new and published light curves led to the determination of the reliable clean photometric elements for RT And and XY UMa. Variations of the LCs were found to occur on the time scales of months. The night-to-night variations are seldom and not important. The asymmetry of the LCs was found to change on a time scale of months (XY UMa). Surface mapping of the active systems (XY UMa, RT And, SW Lac) using circular starspots model did not support the active longitude belts hypothesis (Zeilik et al., 1989). The occurrence of the facing polar spots indicates possibility of the complicated magnetic connection of the components.

Activity of the short-period RS CVn-like systems is higher than W-type W UMa systems of the same spectral type. The maximum observed differences in the maxima heights are: 0.10 mag in SW Lac, 0.27 in XY UMa 0.27 mag, 0.11 in RT And and 0.05 mag in VW Cep.

The spectral type of XY UMa was found to be later than previously thought. Its spectral classification is negatively influenced by the enhanced chromospheric emission, filling of the spectral lines, presence of the cool spots on the surface. Hence, one has to be careful in spectral classification of the chromospherically active systems since amount of the detected extra emission depends on the accepted spectral type.

Acknowledgements. This study was supported by VEGA grant 2/1157 of the Slovak Academy of Sciences.

References

- Albayrak B., Özeren F.F., Ekmenci F., Demircan O.: 1999, *Rev. Mex. A.A.*, **35**, 3.
- Al-Naimiy H.M.: 1978, *Ap.Space Sci.*, **53**, 181.
- Applegate J.H.: 1992, *ApJ*, **385**, 621.
- Borkovits T., Hegedüs T.: 1996, *As.Ap.Suppl.*, **120**, 63.
- Brownlee R.R.: 1957, *ApJ*, **172**, 372.
- Budding E., Kadouri T.H., Giménez A.: 1982, *Ap.Space Sci.*, **88**, 453.
- Chochol D., Pribulla T., Teodorani M., Errico L., Vittone A.A., Milano L., Barone F.: 1998, *As.Ap.*, **340**, 415.
- Erdem A., Güdür N.: 1998, *As.Ap.Suppl.*, **127**, 257.
- Geyer E.H., Kippenhahn R., Strohmeier W.: 1955, *Kleine Veroff. Remeis Sternwarte Bamberg* No. 9.
- Hendry P.D., Mochnacki S.W.: 1998, *ApJ*, **504**, 978.
- Hershey J.L.: 1975, *AJ*, **80**, 662.
- Kreiner J.M., Kim C.H., Nha I.S.: 2000, *An atlas of (O-C) diagrams of eclipsing binary stars*, Wydawnictwo Naukowe Akademii Pedagogicznej, Kraków.
- Leung K.C., Zhai D., Zhang R.: 1984, *PASP*, **96**, 634.
- Kwee K.K., Van Woerden H.: 1956, *Bull. Astron. Inst. Netherl.* **12**, 327.
- Kwee K.K.: 1966, *Bull. Astron. Inst. Netherl. Suppl. Series*, **1**, 265.
- Panchatsaram T., Abhyankar K.D.: 1981, *Bull. Astron. Soc. India*, **9**, 31.
- Pojmanski G.: 1998, *Acta Astron.*, **48**, 711.
- Pojmanski G., Geyer E.H.: 1990, *Acta Astron.*, **40**, 245.
- Pojmanski G., Udalski A.: 1997, *Acta Astron.*, **47**, 451.
- Pribulla T., Chochol D., Parimucha Š.: 1999, *Contrib. Astron. Obs. Skalnaté Pleso*, **29**, 111.
- Pribulla T., Chochol D., Tremko J., Parimucha Š., Vaňko M., Kreiner J.M.: 2000a, *Contrib. Astron. Obs. Skalnaté Pleso*, **30**, 117.
- Pribulla T., Chochol D., Milano L., Errico L., Vittone A.A., Barone F., Parimucha Š.: 2000b, *As.Ap.*, **362**, 169.
- Pribulla T., Chochol D., Heckert P.A., Errico L., Vittone A.A., Parimucha Š., Teodorani M.: 2001, *As.Ap.*, **371**, 997.
- Pustyl'nik I., Sorgsepp L.: 1976, *Acta Astron.*, **26**, 319.
- Rucinski S.M.: 1984, *MNRAS*, **208**, 309.
- van't Veer F.: 1972, *As.Ap.*, **20**, 131.
- Williamson R.M.: 1974, *PASP*, **86**, 924.
- Wilson R.E., Devinney E.J.: 1971, *ApJ*, **166**, 605.
- Zeilik M., Cox D., De Blasi C.: 1989, *ApJ*, **345**, 991.
- Zhang D., Lu W.: 1989, *Chinese As.Ap.*, **13**, 350.

AN ACTIVE TRIPLE SYSTEM 44i BOOTIS

T. Pribulla¹, J. Tremko¹, H. Rovithis-Livaniou², P. Rovithis³

¹Astronomical Institute of the Slovak Academy of Sciences,

059 60 Tatranská Lomnica, Slovakia, (*pribulla,tremko*)@ta3.sk

² Section of Astrophysics, Astronomy & Mechanics, Dept. of Physics, University of Athens,

GR 15784, Zografos, Greece, *elivan@cc.uoa.gr*

³ Astronomical Institute, The National Observatory of Athens, P.O. Box 20048,

GR 11810 Athens, Greece

ABSTRACT. The long-term *UBVR* photoelectric monitoring of 44i Boo performed at the Skalnaté Pleso, Stará Lesná and Kryonerion observatories is presented. The orbital period changes are discussed including light-time effect caused by the visual companion. The radial velocity of the visual companion as well as observed period change conclusively determine the ascending node of the visual orbit to be in the first quadrant. The light curve of the system was found to be quite stable but asymmetric: maximum in the phase 0.25 has always been fainter than maximum in the phase 0.75. Light-curve analysis of the V observations since 1998 provided new inclination angle $i = 73.66 \pm 0.14^\circ$. Combination of the inclination angle with the published spectroscopic elements gave reliable masses of the components: $m_1 = 0.861 \pm 0.008 M_\odot$ and $m_2 = 0.419 \pm 0.11 M_\odot$.

Key words: Stars: binary: contact; stars: individual: 44i Boo

1. Introduction

Triple system 44i Boo ($V = 4.76$, sp. K2V) composed of a W-type contact binary star and a main sequence companion forms a visual double star ADS9494 ($P_{123} = 206$ years). The system is unique since it has precisely known astrometric orbit and it is our closest W UMa neighbour ($\pi = 0.0784''$). The contact pair shows enhanced photospheric activity displayed as the differences in the maxima heights and brightenings in the UV region. Because of its brightness the system has been subject to numerous photometric observations. Unfortunately, the precise determination of the photometric elements is complicated not only by the photospheric activity but also low inclination angle ($\approx 69-73^\circ$) and considerable third light making the amplitude of the light variation as small as $\Delta V = 0.17$ mag.

Lu et al. (2001) performed extensive high-dispersion

Table 1: Spectroscopic elements of the contact pair (Lu et al., 2001) and the orbital elements of the relative 12-3 orbit (Söderhjelm, 1999). Errors are given in the parentheses.

Spectroscopic orbit 12		Visual orbit 12-3	
V_0 [km.s ⁻¹]	-17.9(4)	$\sum m$ [M_\odot]	2.70(16)
K_2 [km.s ⁻¹]	231.3(6)	P_{123} [year]	206(2)
K_1 [km.s ⁻¹]	112.7(5)	a ["]	3.8
q_{12}	0.487(6)	e	0.55
$m_{12} \sin^3 i$ [M_\odot]	1.132(11)	i [°]	84
P_{12} [day]	0.267818	ω [°]	45
		T_0 [year]	2013
		Ω [°]	57

spectroscopic observations of the system. A thorough analysis of the broadening functions resulted in new reliable spectroscopic elements of the contact pair (see Table 1). Söderhjelm (1999) used all Hipparcos and Earth-bound astrometry and re-computed the relative visual orbit (Table 1).

2. New observations

In our paper we present three sets of *UBVR* photoelectric observations. In all three cases the combined light of the visual pair was measured. The first set of data are *UBV* observations obtained at the Skalnaté Pleso (SP) observatory of the Astronomical Institute of SAS in 1968 (3 nights) and in 1969 (4 nights only in *V*). The second set of data was obtained with the 1.2m Cassegrain reflector at the Kryonerion Astronomical Station (KAS) of the Athens National Observatory on 5 nights from May 1994 to May 1996. Standard *BV* filters and a two-beam, multi-mode, nebular-stellar photometer was used. 54 Boo served as the comparison star. The system was also observed on 18 nights from

Table 2: New times of the primary (p) and secondary (s) minima. The standard errors are given in parentheses

JD _{hel} 2400000+	Fil.	JD _{hel} 2400000+	Fil.
p 39222.5889(2):	B	p 50204.4309(1)	V
p 39222.5851(3)	V	s 50204.5613(1)	V
p 39887.5749(4)	U	s 50204.5620(2)	B
p 39887.5755(2)	B	s 50205.3654(1)	B
p 39887.5744(1)	V	s 50205.3645(1)	V
s 39940.4618(5):	U	p 50205.4996(1)	B
s 39940.4650(3)	B	p 50205.5017(1)	V
s 39940.4651(5)	V	s 52001.3670(8)	B
p 39995.4973(3):	U	s 52001.3675(5)	V
p 39995.5000(8)	B	p 52097.3817(1)	B
p 39995.5021(7)	V	p 52097.3816(1)	V
p 40286.6217(3)	V	p 52123.3557(1)	B
p 50204.4286(2)	B	p 52123.3572(6)	V

February 1998 to August 2001 at the Stará Lesná (SL) and SP observatories of the Astronomical Institute of the SAS. At both observatories a single-channel photoelectric photometer installed at the Cassegrain focus of the 0.6m reflector was used. The standard *UBV* and *UBVR* filters were employed at SL and SP, respectively. 47 Boo was used as the comparison star.

Our observations led to the determination of 31 minima times. They have been calculated separately for each passband using Kwee & van Woerden's (1956) method. Twelve previously unpublished minima times are listed in Table 2.

3. Period Analysis

The orbital period of the system was analysed by many investigators. Part of them correctly included the light-time effect (hereafter LITE) caused by the presence of the third component, others ignored the LITE in their analysis entirely. Hill et al. (1989) tried to re-analyse the times of the minima including the LITE. The authors, however, computed the scale factor *s* erroneously.

The analysis of the orbital period changes of the contact pair has no meaning without proper subtraction of the LITE. The mass ratio $q_{123} = m_3/(m_1 + m_2 + m_3)$, necessary for the determination of the semi-amplitude of the LITE, can be determined from the total mass of the system determined from the visual orbit (Söderhjelm, 1999) and the simultaneous spectroscopic (Lu et al., 2001) and photometric analysis of the contact pair. From Table 1 we have $m_1 + m_2 + m_3 = 2.70 \pm 0.16 M_\odot$ and $(m_1 + m_2) \sin^3 i = 1.132 \pm 0.011$

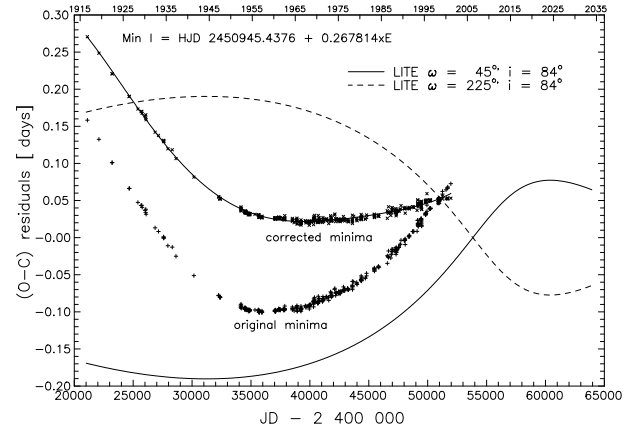


Figure 1: (*O* - *C*) diagram of 44i Boo from the mean linear ephemeris. The theoretical LITE curve corresponds to the visual orbit and parallax given in Table 1 and $q_{abc} = 0.52$

M_\odot . If we take the orbital inclination $i = 73.7^\circ$ (see Section 4), we get $q_{123} = 0.52 \pm 0.03$.

The theoretical LITE correction with respect to the center of the mass of the triple system can be computed as follows:

$$\Delta T = \frac{a'' q_{123}}{c\pi} \sin i_{123} \frac{1 - e^2}{1 + e \cos \nu} \sin(\nu + \omega), \quad (1)$$

where a'' is the semi-major axis in arcsec, e eccentricity, ω longitude of the periastron, ν true anomaly and i_{123} inclination of the relative orbit, c is the velocity of light and π is the parallax of the system.

The contact pair revolves the third component in the direct orbit. Unfortunately, the positional measurements do not allow to distinguish between two possible positions of the ascending node¹: either in the first or third quadrant. Both cases computationally differ in the longitude of the periastron ω . If the ascending node is positioned in the first quadrant, then $\omega = 45^\circ$. In the second case $\omega = 45 + 180 = 225^\circ$.

To analyse the orbital period changes of the contact pair we have gathered all available minima mainly from Hill et al. (1989) and Kreiner et al. (2001). The minima were weighted according to Kreiner et al. (2001): photographic and photovisual $w = 3$, photoelectric $w = 10$. The (*O* - *C*) diagram from the mean weighted linear ephemeris $Min I = 2450945.4376 + 0.26781558 \times E$ is presented in Fig. 2. The general course of the observed times of minima (mainly since 1955) as well radial velocity of the third component indicates that the ascending node is in the first quadrant i.e., the contact pair is now receding from the Sun. Although the LITE correction to the minima cannot be

¹where the fainter component (contact pair) crosses the plane of the sky while receding from the observer

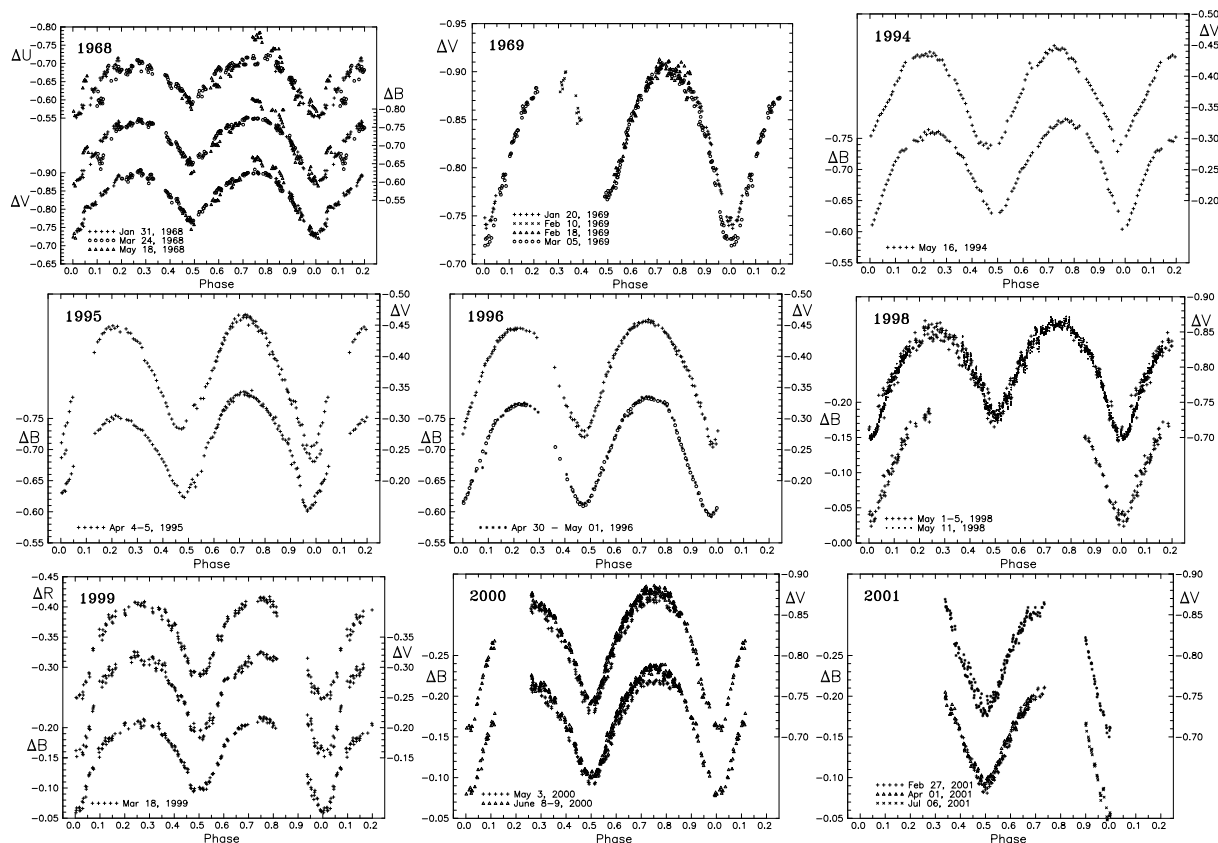


Figure 2: Selected *UBVR* photoelectric light curves of 44i Boo

neglected, the corrected ($O - C$) residuals still show steady period increase.

The ($O - C$) diagram for the corrected times of the minima can be divided into two parts (i) till \approx JD 2431000 when the orbital period seemed to be constant: $Min I = 2450945.078(6) + 0.26780838(7) E$ and (ii) since JD 2431000 when the orbital period is increasing at an approximately constant rate: $Min I = 2450945.4910(5) + 0.26781565(3) E + 2.21(5) 10^{-11} E^2$. Although the ephemerides describe the general trend well, the individual minima show large scatter (caused most probably by the photospheric activity) and small intermittent period changes. Hence our light curves (hereafter LCs) were phased using minima in short intervals around observations.

4. Light-curve analysis

In the present paper we have aimed at the determination of the geometrical elements necessary for the absolute parameters determination. Hence we tried to remove the photometric disturbances caused by the activity on the surface of the contact pair. The most stable and best covered is the *V* passband LC. *U* and *B* passband observations are negatively influenced by the chromospheric, flare and spot activity on the surface.

R passband observations are rather scanty. Hence we have analysed only the *V* LC.

It is interesting to note that all *V* LCs observed at the SP and SL observatories since 1998 are very similar and stable (see Fig. 2). Therefore, we used them for the determination of the photometric elements. These LCs only slightly differ mainly in the maxima heights. The maximum I (phase 0.25) has been always observed to be fainter by 0.004 - 0.017 mag than maximum II (phase 0.75). If we assume that the component 3 is not variable and we correct the LCs for its light, the corresponding maxima differences are 0.012 - 0.052 mag. The most stable part of the LC was around the maximum I. Assuming the presence of dark starspots on the surface we have used only the brighter half of the LC around the maximum II. All *V* passband observations in this phase interval were used to form 89 normal points by the running parabolae method.

For the determination of the photometric elements we have used the 1992 version of the differential corrections code developed by Wilson & Devinney (1971) (W&D). Since the spectroscopic elements are reliably known, we have fixed the mass ratio $q = 0.487$ (Lu et al., 2001). Mode 3 of the W&D code appropriate for the contact binaries was employed. For the computation of the monochromatic luminosities we have used the approximate atmospheric model option of the

W&D program. Coefficients of the gravity darkening $g_1 = g_2 = 0.32$ and bolometric albedo $A_1 = A_2 = 0.5$ were fixed as appropriate for the convective envelopes. The limb darkening coefficients were interpolated from Table 1 of Al-Naimiy (1978). The mean temperature of the primary (the more massive and cooler component) was taken 4830 K corresponding to the $(B - V)$ colour of the contact pair. Fabricius & Makarov (2000) give $V_{12} = 6.12$ (average) and $V_3 = 5.28$. The corresponding maximum V magnitude of the contact pair is 6.05 and the third light is $l_{3V} = 0.676$. The resulting geometrical elements are: $i = 73.66^\circ \pm 0.14^\circ$, $\Omega = 2.8020 \pm 0.0038$ (fill-out = 0.167 ± 0.013). The temperature of the secondary (hotter and smaller component) is $T_2 = 5174 \pm 10$ K. The corresponding fit of the V LC is depicted in Fig. 3 by the solid line.

Using "clean" geometric elements we have tried to solve the whole V LC assuming that the cool circular spot is positioned on the primary component. Due to the fact that the spot is not eclipsed we have fixed its latitude on the stellar equator. The best fit was obtained for the spot positioned at the longitude $l = 68^\circ$ with radius $r_{spot} = 20^\circ$ and the temperature factor $k = 0.937$. Fitting the one-passband photometry we must be aware that the radius and temperature factor of a spot are quite correlated. The resulting spot fit is depicted in Fig. 3 by the dashed line in the residuals.

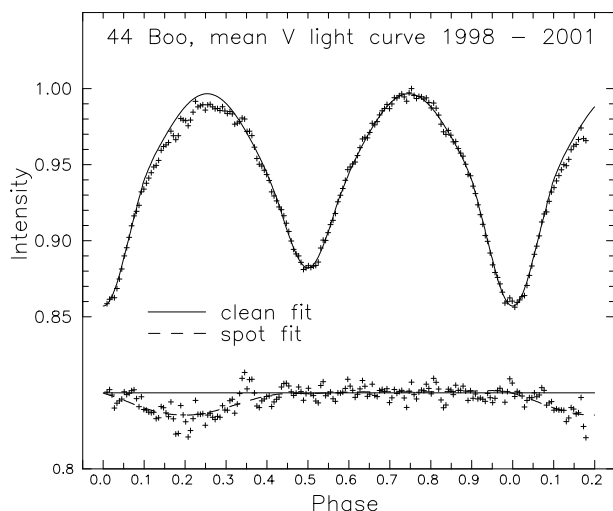


Figure 3: Best fit of the mean V LC constructed from observations since 1998. The spot fit corresponds to a dark spot positioned on the primary component.

5. Absolute parameters of the components and conclusion

Using our new determination of the inclination angle $i = 73.7^\circ$, new spectroscopic elements of the contact pair (Lu et al., 2001) and the elements of the visual orbit, we have computed masses of the components

$m_1 = 0.816 \pm 0.008 M_\odot$ and $m_2 = 0.419 \pm 0.003 M_\odot$. If we accept the total mass of the system as $2.70 \pm 0.16 M_\odot$ (Söderhjelm, 1999) we have the mass of the third component $m_3 = 1.42 \pm 0.16 M_\odot$. As this component is much more massive than expected for its spectral type (G5V), it can be a binary system.

Including the semi-major axis $a_{12} = 1.898 \pm 0.006$ in the W&D code we have obtained the absolute visual magnitude of the contact pair as $M_{12}^{bol} = 5.31$. Using the appropriate bolometric correction $BC = -0.46$ we obtained absolute visual magnitude $M_{12} = 5.77$. Since the distance to the system is precisely known, we can determine the absolute magnitude from the observed maximum visual brightness $V_{12} = 6.05$ assuming zero interstellar absorption. The resulting absolute visual magnitude 5.52 is much lower than that obtained from the spectroscopic and photometric data. The luminosity of the contact pair increases with the semi-major axis (and masses) of the components. Hence, it is possible that the most recent determination of the spectroscopic elements (Lu et al., 2001) is still negatively influenced by the third component.

Our monitoring of the eclipsing system 44i Boo shows that the system's LC suffers small seasonal variations but the general shape of the LC remains stable. It is interesting to note that the asymmetry in the maxima heights (maximum II brighter) was persistent during our observations since 1968.

The orbital period of the system is variable. Apart from the LITE caused by the third component on the 206 years orbit, the orbital period of the system continuously increases. The large scatter of minima times, highly exceeding the standard errors of the minima, is probably caused by the LC disturbances.

The detailed analysis and revision of both LC and period changes is under preparation.

Acknowledgements. This study was supported by VEGA grant 2/1157 of the Slovak Academy of Sciences. The authors are indebted to D. Chochol for critical reading of the manuscript.

References

- Al-Naimiy H.M.: 1978, *Ap.Space Sci.*, **53**, 181.
- Fabricius C., Makarov V.V.: 2000, *As.Ap.*, **356**, 141.
- Hill G., Fisher W.A., Holmgren D.: 1989, *As.Ap.*, **211**, 81.
- Kreiner J.M., Kim C.H., Nha I.S.: 2001, *An atlas of (O-C) diagrams of eclipsing binary stars*, Wydawnictwo Naukowe Akademii Pedagogicznej, Kraków.
- Kwee K.K., Van Woerden H.: 1956, *Bull. Astron. Inst. Netherl.*, **12**, 327.
- Lu W., Rucinski S.M., Ogloza W.: 2001, *AJ*, subm.
- Söderhjelm S.: 1999, *As.Ap.*, **341**, 121.
- Wilson R.E., Devinney E.J.: 1971, *ApJ*, **166**, 605.

WHY NS AND BH MASS DISTRIBUTION IS BIMODAL?

M.E. Prokhorov, K.A. Postnov

Sternberg Astronomical Institute, Moscow State University,
 Universitetskii pr. 13, Moscow 119899 Russia,
mystery@sai.msu.ru; pk@sai.msu.ru

ABSTRACT. The observed mass distribution for the compact remnants of massive stars (neutron stars and black holes) and its relationship to possible mechanisms for the ejection of the envelopes of type II and Ib/c supernovae is analyzed. The conclusion is drawn that this distribution can be obtained only by a magneto-rotational mechanism for the supernovae with sufficiently long time of the field amplification, and a soft equation of state for neutron stars with limiting masses $\sim 1.5\text{--}1.6 M_{\odot}$. Some consequences of this hypothesis are discussed.

Key words: Stars: neutron, black holes, supernova.

1. Introduction

The observed masses of white dwarfs lie in a wide range from several tenths of a solar mass to nearly the Chandrasekhar limit ($\sim 1.2M_{\odot}$), with low-mass white dwarfs encountered more often. We are not concerned with these objects here, and will not consider them further. The masses of neutron stars (NS) measured so far lie within a very narrow interval: the masses for 26 NS radio pulsars in binary systems are consistent with a normal distribution with mean mass $1.35M_{\odot}$ and dispersion $0.04M_{\odot}$ (Thorsett and Chacrabarty 1999). As noted by Thorsett and Chacrabarty, there is currently not a single pulsar in a binary system whose mass exceeds $1.45M_{\odot}$. The recently obtained upper limit on the NS mass in millisecond pulsar PSR J2019+2425 is $M_{\text{NS}} < 1.51 M_{\odot}$ (Nice et al 2001). If we add the less accurately determined masses of NS in X-ray binaries (Cherepashchuk 2000) to this sample, the observed mean mass of NS is $M_{\text{NS}} = (1.35 \pm 0.15) M_{\odot}$ (the same mean as above with a larger dispersion).

More than a dozen of black hole (BH) candidates in close X-ray binary systems are known (see Cherepashchuk (1996, 2000) and references therein). The masses of these objects are determined using radial velocity curves of optical counterparts of binary systems. According to current data, the masses of BH candidates fill the interval $\sim 3\text{--}40 M_{\odot}$, with a mean value of about $10 M_{\odot}$.

In addition to the reliable dynamical determinations

of the NS and BH masses in binary pulsars and X-ray novae, there are a number of less accurate mass estimates for compact objects in X-ray binaries. (1) The mass of NS in the low-mass X-ray binary Cyg X-2 is determined by Orosz and Kuulkers (1999) to be $1.8 \pm 0.2 M_{\odot}$. (2) X-ray pulsar Vela X-1: $M_{\text{NS}} \sim 1.9 M_{\odot}$, according to van Kerkwijk et al (1995), but $M_{\text{NS}} \sim 1.4 M_{\odot}$ according to Stickland et al (1997). (3) The eclipsing low-mass X-ray binary 4U 1700-37: $M_{\text{NS}} = 1.8 \pm 0.4 M_{\odot}$ according to Heap and Corcoran (1992), but it could be a low-mass BH (Brown et al 1996). Until the high masses of these NS are independently verified, we will consider them to be uncertain.

Thus, we assume that current reliable measurements of NS masses lie in a narrow interval $M_{\text{NS}} = (1.35 \pm 0.15) M_{\odot}$, masses of BH lie in a wide range $M_{\text{BH}} > 3M_{\odot}$, and *not a single* NS has currently been reliably detected to have mass in the gap between 1.5 and $3M_{\odot}$, and the number of BH with such small masses is small (the total absence of such BH *is not required*).

This picture is in a dramatic disagreement with both a monotonic distribution of the initial masses of main-sequence stars and the monotonic distribution of masses of carbon and iron cores that are developed during nuclear evolution of massive stars. If a massive star is deprived of its hydrogen envelope during evolution, its carbon core is observed as a Wolf-Rayet star. The current observations show that their masses lie in a wide range from $\sim 3M_{\odot}$ to $\sim 50M_{\odot}$ (Cherepashchuk 2001, 2000, 1998). According to calculations Timmes et al (1996), the masses of the iron cores before collapse lie in the interval from 1.25 to $2.05M_{\odot}$. Both the carbon and iron cores depend monotonically on the initial masses of the stars.

2. The envelope ejection

In sufficiently massive stars ($> 8\text{--}10M_{\odot}$), which can produce NS and BH, the nuclear evolution ends up with the core collapse which can be accompanied by the envelope ejection, leading to the supernova type II or Ib/c. If the shell is ejected "efficiently" (i.e., it receives an energy of the order of the binding energy of the

remnant), it expands in the surrounding medium and a low-mass compact object forms with a mass of order the mass of the collapsed core of the pre-supernova. If the shell is ejected "inefficiently", a large fall of matter from the envelope to the forming compact object is inevitable. As a result, the mass of the latter can substantially grow and approach the pre-supernova mass.

There can be a continuous transition between these two limiting cases. However, if we suppose that *the ejection of the envelope during the supernova explosion is sharply* (even in a step-like manner) *weakened for pre-supernova core masses above some threshold*, the continuous sequence of the pre-supernova masses would give rise to two types of objects with sufficiently different masses.

3. The core collapse

The formation of a compact object during the core collapse can occur in two ways.

(1) The direct collapse into a BH, bypassing an intermediate stage of a hot proto-neutron star, if its mass is above some threshold $M_{dir} > M_{OV}$ (see Prakash et al (2000) and references therein for a more detailed description of this process).

(2) Via the intermediate stage with hot proto-neutron star lasting several seconds or tens of seconds, in which there is intense radiation of thermal energy by the neutrino flux, after which the hot proto-neutron star "cools" or, if its mass exceeds the Oppenheimer-Volkoff limit for neutron star matter M_{OV} , collapses into a black hole.

The modern calculations of core collapses show that $M_{dir} - M_{OV} \approx 0.3-1M_{\odot}$ (Strobel and Weigel (2000) and references therein). Clearly, that for a *static* NS M_{dir} is always larger than M_{OV} .

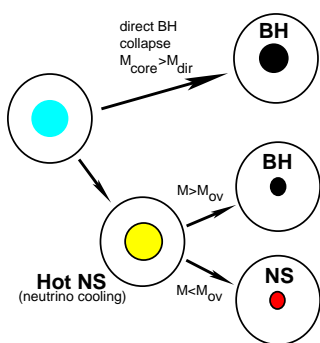


Figure 1: The scheme of the core collapse

The possible ways of the core collapse are schematically shown in Fig. 1.

4. Supernova mechanisms

Let us now consider various mechanisms for super-

nova explosions to find a qualitative shape of the resulting mass distribution of compact objects. The consideration will be based on the illustration with the scheme of Fig. 1 to the left, completed with details of various SN mechanisms, and by the compact mass distribution plot turned counterclockwise to the right.

Excluding exotic models, currently there are three different mechanisms for supernova explosions: (1) The standard mechanism, in which a shock wave appears as a result of the bounce of the matter flux from the "solid" core; the shock wave propagation is sustained by the neutrino flux. (2) The mechanism proposed by Imshennik (1992) is associated with the division of the rapidly rotating collapsing stellar core into two parts. (3) Magneto-rotational mechanism of envelope ejection (Bisnovatyi-Kogan 1970). Let us consider these mechanisms in turn.

Note that none of these mechanisms can presently explain all the facts related to supernova phenomenon. So *a priori* all these mechanism may be equally applicable.

4.1. The standard (neutrino) supernova mechanism

In the standard model, the energy is transferred from the hot compact remnant to the envelope by the neutrino flux. Unfortunately, this mechanism is unable to eject the supernova shell either in the spherically symmetric or the axially symmetric (with rotation) case (Janka 2001). There is some hope that the situation can be saved by large-scale neutrino convection (Herant et al 1994, Mezzacappa et al 1998).

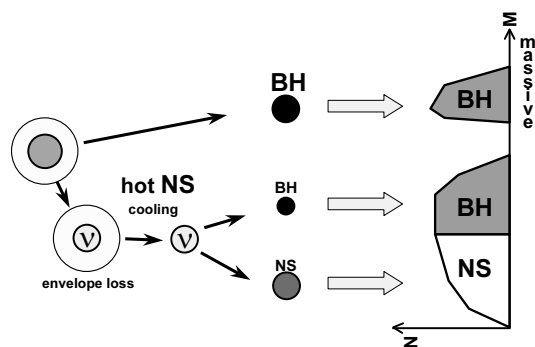


Figure 2: The standard (neutrino) mechanism

The envelope ejection, if any, must occur on the first stage of the hot NS with most intensive neutrino emission (this stage lasts for several seconds). The neutrino fluxes from hot NS with a mass below and above M_{OV} are not strongly different. In a direct collapse, the hot stage is appreciably shorter (of the order of the dynam-

ical time scale for the collapse), and, consequently, is less efficient.

The resulting mass distribution consists of a class of massive BH formed during the direct collapse and a comparable number of NS and low-mass BH (see Fig. 2). This distribution does not match with observations.

4.2. Imshennik's mechanism (the double core)

This mechanism is associated with the division of a rapidly rotating collapsing stellar core into two parts, at least one of which must be a NS. The parts of the binary core then approach due to the emission of gravitational radiation, until the component with the smaller mass (and larger size) fills its Roche lobe. Further, there is an exchange of mass until the mass of the smaller component reaches the lower limit for the mass of a neutron star (about $0.1M_{\odot}$), at which point there is an explosive de-neutronization of the low-mass neutron star. This mechanism was first suggested by Blinnikov et al (1984) and applied to supernova explosions by Imshennik (1992). This additional release of energy fairly far from the center of the collapsing star can efficiently eject its envelope. This mechanism can act only for the most rapidly rotating supernova precursors.

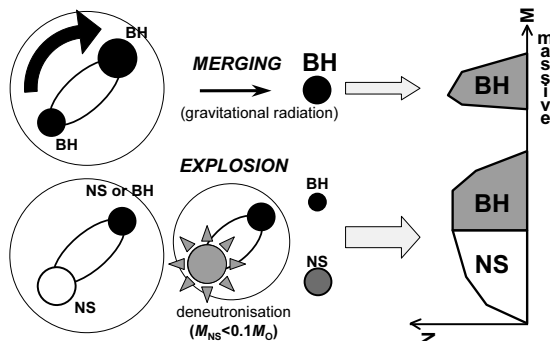


Figure 3: Imshennik's supernova mechanism

The approach of the binary core up to its merging could last from several minutes to several hours; i.e., appreciably longer than the hot neutron star can exist. The scheme of the collapse shown in Fig. 3 is somewhat different: here *massive* is the binary system in which both parts of the core become BH. In this case the process results in a "quiet" coalescence of BH with a concomitant accretion of matter from the envelope.

The processes which take place in the *low-mass* situation are described above and their result is weakly dependent on the mass and type of the compact remnant. As a result, the same mass distribution as for

the neutrino mechanism is obtained, in contradiction with observations.

4.3. Magneto-rotational mechanism

This mechanism was proposed by Bisnovatyi-Kogan (1970). The supernova shell is expelled by the magnetic field at the expense of the rotational energy of the newborn NS. The process occurs in two stages. At the first stage, a toroidal magnetic field appears and linearly grows with time. The duration of this stage depends on the NS rotational velocity and its initial magnetic field value and can vary from fraction of a second to hours. When the magnetic field strength approaches some critical value ($\sim 10^{16}$ – 10^{17} G), the magneto-rotational explosion occurs which accelerates and expels the envelope in 0.01–0.1 s (see Ardeljan et al (1998)). For this mechanism to operate, the star should have a sufficiently rapid (but not limiting) rotation.

Depending on the relation between the time of the magnetic field amplification t_B (time before the explosion) and the hot NS cooling time scale t_{ν} , different compact object mass distributions appear.

During the direct core collapse into BH, the magnetic field amplification never starts and the envelope are not ejected. In contrast, on the branch leading to NS formation, the magneto-rotational mechanism ultimately leads to the explosion and the envelope ejection.

The difference between the two variants concerns only objects with masses $M_{OV} < M < M_{dir}$, in which initially a hot NS forms and after cooling collapses into BH. If the explosion occurs at the stage of a hot NS ($t_B < t_{\nu}$), the envelope is ejected before stars with $M > M_{OV}$ collapse; they form low-massive BH. Therefore, we for the third time obtain the mass distribution in disagreement with observations.

In contrast, if the field amplification proceeds slowly ($t_B > t_{\nu}$), the objects with $M_{OV} < M < M_{dir}$ collapse into BH, after which the field amplification stops. No magneto-rotational explosion, and hence, envelope ejection occurs, so masses of these BH will be weakly different from those formed during the direct collapse. The mass distribution will consist of only two groups of objects: NS and massive BH.

Note one very important corollary of the scheme considered: the upper boundary of the NS mass distribution must coincide (to the mass defect) with M_{OV} . Thus the current observations suggest that NS should have a *very soft* EOS with $M_{OV} \simeq 1.5$ – $1.6M_{\odot}$ (such equation are possible, e.g. GS1, PAL6 and PCL2 in Lattimer and Prakash (2000)).

The magneto-rotational explosion is illustrated in Fig. 4.

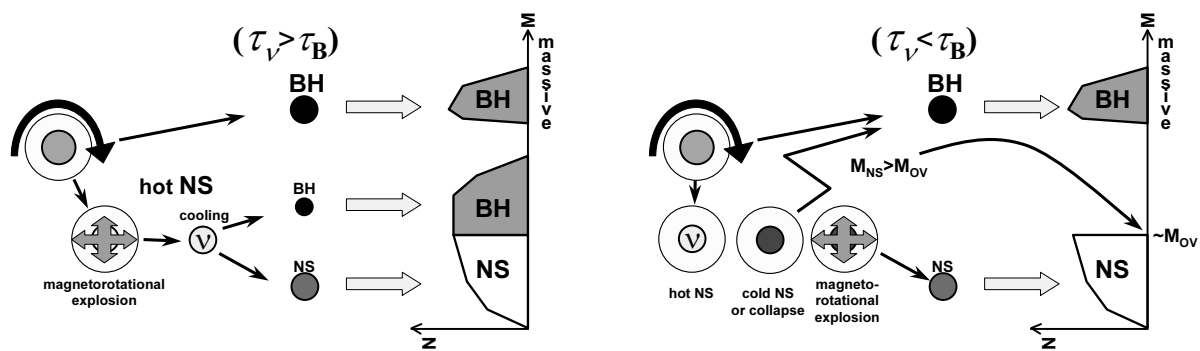


Figure 4: Two ways of the magneto-rotational mechanism for SN explosion

5. Conclusions

We have shown that the magneto-rotational mechanism for supernova explosions, with the additional requirements that the time before the explosion is larger than the cooling time of a proto-NS ($\tau_B > \tau_\nu$) with a soft equation of state of NS matter ($M_{OV} \simeq 1.5\text{--}1.6 M_\odot$), leads naturally to the mass distribution of compact objects similar to what is currently observed. To eject the envelope, the NS rotational energy should be above $\sim 10^{50}$ ergs (period of rotation < 10 ms). Unless the magnetic coupling between the pre-collapse core and envelope is strong enough to preclude rapid rotation of the core, as was suggested in Spruit and Phinney (1998), the magneto-rotational supernova explosion is very attractive mechanism. This hypothesis has a number of additional predictions, which can be verified by observations:

(1) Accretion-induced BH with masses of about M_{OV} should exist. They could be detected in low-mass transient X-ray binaries.

(2) Supernova remnants containing BH must be less energetic evidencing less energetic supernova explosions. Supernova remnants with NS should be axially symmetric.

(3) The coaxiality of the angular momentum and the space velocity of a pulsar, as observed in Crab and Vela pulsars, must be a common property of all radiopulsars.

(4) BH should have very small space velocities in comparison with pulsars.

Reliable measurements of the NS mass substantially above $1.6 M_\odot$ would be a *direct refutation of the proposed hypothesis*.

Acknowledgments. The work is partially supported by RFBR grants 99-02-16205, 00-02-17164, and 01-15-99310.

References

- Ardeljan N.V., Bisnovaty-Kogan G.S., Moiseenko S.G.: 2000, *As.Ap.*, **355.**, 1181.
- Bisnovaty-Kogan G.S.: 1970, *Astron. Zhurn.*, **47.**, 813.
- Blinnikov S.I., Novikov I.D., Perevodchikova T.V., Polnarev A.G.: 1984, *Pisma Astron. Zhurn.*, **10.**, 177.
- Brown G.E., Weingartner J.C., Wijers R.A.M.J.: 1996, *Ap.J.*, **463.**, 297.
- Cherepashchuk A.M.: 1996, *Phys. Usp.*, **39.**, 753.
- Cherepashchuk A.M.: 1998, In Proc. Int. Conf. in Honour of Prof. A.G.Massevitch, "Modern Problems of Stellar Evolution", Ed. D.S.Wiebe, Moscow.
- Cherepashchuk A.M.: 2000, *Space Sci. Rev.*, **93.**, 473.
- Cherepashchuk A.M.: 2001, *Astron. Rep.* **45.**, 120.
- Heap S.R., Corcoran M.F.: 1992, *Ap.J.*, **387.**, 340.
- Herant M., Benz W., Hix J., Fryer C.L., Colgate S.A.: 1994, *Ap.J.*, **435.**, 339.
- Imshennik V.S.: 1992, *Pisma Astron. Zhurn.*, **18.**, 489.
- Janka H.-Th.: 2001, *As.Ap.*, **368.**, 527.
- Mezzacappa A. et al.: 1998, *Ap.J.*, **495.**, 911.
- Nice D.J., Splaver E.M., Stairs I.H.: 2001, *Ap.J.*, 516.
- Orosz J.A., Kuulkers E.: 1999, *MNRAS*, **305.**, 132.
- Prakash M., Lattimer J.M., Pons J.A., Steiner A.W., Reddy S.: 2000, *astro-ph/0012136*.
- Spruit H., Phinney S.: 1998, *Nature*, **393.**, 139.
- Stickland D., Lloyd C., Radzuin-Woodham A.: 1997, *MNRAS*, **296.**, L21.
- Strobel K., Weigel M.K.: 2001, *As.Ap.*, in press (*astro-ph/0012321*).
- Thorsett S., Chacrabarty D.: 1999, *Ap.J.*, **512.**, 288.
- Timmes F.X., Woosley S.E., Weaver T.A.: 1996, *Ap.J.*, **457.**, 834.
- van Kerkwijk M.H., van Paradijs J., Zuiderwijk E.J.: 1995, *As.Ap.*, **303.**, 497.

ON THE OBSERVED PHYSICAL PROPERTIES AND EVOLUTIONARY TRENDS OF HOT SUBDWARFS IN BINARY SYSTEMS

I. Pustynnik,

Tartu Observatory
Estonia, *izold@aai.ee*

ABSTRACT. In our brief review we summarize the latest advances in studies of white dwarfs both as single objects and the components of binary systems. We discuss the observed properties of the hot subdwarfs (sdws), the various techniques of their discovery and some peculiarities of their evolution following the final stages of AGB, both for single stars and binary cores of PN. We find that the observed statistics of sdws clearly point to drastically different evolutionary histories for sdws belonging to very wide pairs and those found in close binaries.

Key words: stars: binary: AGB; stars: evolution- stars: mass loss; stars: rotation-white dwarfs.

1. Introduction

In the last twenty years we witness an ever increasing interest among astronomers in studying physical properties and final stages of evolution of medium mass stars leading to formation of wide dwarfs (WD). Roughly during one generation observational and theoretical research of WD transformed into one of the most flourishing branches of modern astrophysics, a cosmic laboratory for a detailed verification of the predictions of WD theory, more specifically mass-radius relation derived by S.Chandrasekhar almost seventy years ago (for the most recent successes in this field see articles by Wood (1995), Shipman *et al*(1997), Shipman and Provencal (1999), Provencal *et al*(2001). There are several important reasons behind these spectacular achievements and the most impressive of them deserve at least a brief enumeration.

1) Although even today the bulk of all known to us WD lie within 25 pc from us, the number of the newly discovered WD is rapidly growing and the latest McCook & Sion *Villanova Catalogue of Spectroscopically Identified White Dwarfs* (see McCook & Sion (1999) contains entries for 2249 WD stars (for more details on catalogues, data bases and Websites of WD see the paper by Holberg *et al*(2001).

2) It is universally acknowledged that WD-s are the end product of evolution of stars with initial masses between $0.5m_{\odot}$ and $8m_{\odot}$ which implies that 98% of all stars are or will be WD-s (if one applies the standard "Salpeter mass function" to estimate the fraction of total stellar mass contained in existing and "would be" WD-s).

3) Since the seminal paper by I.Shklovski who first noticed the rough coincidence between the velocity of expansion of planetary nebulae (PN) and the terminal wind velocities for red giants and conceived its deep evolutionary implication, a remarkable progress has been achieved in both observational and theoretical investigations of the internal structure and evolution of AGB stars leading to superwind, ejection of the extended convective envelope which finally becomes visible as PN illuminated by the bare core - emerging hot subdwarf (sdw) star, the progenitor of future WD. This in its turn inspired both observers and theoreticians to study even more closely the questions of morphology and kinematics of PN, to look for the role of duplicity of illuminating stellar source in shaping PN-s, to explore the physical mechanisms governing the formation of novae and more generally cataclysmic binaries from initially wide pairs.

4) Because the theoretical treatment of the cooling of WD stars is relatively simple (at least for the early stages before effects of crystallization in the interiors of WD become important) it soon became clear that WD can serve as a powerful tool for measuring the age of Galactic disc population provided that one possesses a statistically sufficient observed population of WD-s of different ages. This is due to the fact that the cooling time of WD is inversely proportional to its intrinsic luminosity, therefore we should see more and more WD-s as we proceed to the fainter objects until the luminosity function turns down because of the finite age of the Galaxy. In addition the location of the turning point of the evolutionary tracks on the $H - R$ diagram at the onset of the cooling process of the new borne hot sdws

appears to be very similar for PN-s discovered in other galaxies thereby making the so-called PN luminosity function a useful tool for measuring distances to the extragalactic PN-s (for a detailed discussion of these and related problems see, for instance, the articles by Jacoby (1989)), Iben, Laughlin (1989), Wood (1992)).

5) In addition to the galactic and extragalactic outreach of WD research discovery of rapid oscillations in WD like PG 1159 stars opened up the new horizons for probing both the deep interiors and the thin "crust" of the evolved WD. This new branch has culminated in project WET enabling to achieve an unprecedented accuracy in measuring the masses of individual WD through a detailed study of their oscillation spectra (for a more recent progress in astroseismology of WD see, for instance, detailed discussion of the current state of WET in the article by Kleinman (1999) and references therein, also a number of articles "Variable White Dwarfs" in the Proceedings of the 12th European Conference on White Dwarf Stars (2001), see the list of references to this article).

Until recently the observed statistics of binaries with the hot sdw primaries has been significantly biased since a number of observational selection criteria favors discovery of strongly interacting binaries with short orbital periods. In a striking contrast to this trend peculiarities of the wide pairs up to most recent times remained largely non-explored (with an exception of a limited number of symbiotic stars).

The so-called precataclysmic binaries (PCB) provide an important link between the short period cataclysmic variables and wide pairs. PCB-s is a small group of detached close binary systems, which are observed at centre of planetary nebula, consisting of a hot white dwarf or a subdwarf accompanied by an essentially unevolved low mass cool companion $m_2 \leq 1m_{\odot}$. PCB orbital periods are so short (typically less than two days) that they can only have been formed via a common envelope evolution (see, for instance, Bond et al 1991, Ritter 1986). Despite the fact that PCB-s have been intensively studied for the last twenty years a number of important problems remains open. PCB-s are discovered mostly due to a pronounced irradiation effect (conveniently called "reflection effect"). Since the early paper by Paczynski and Deaborn (1980) the problem of anomalously high reflection effect amplitude remains unsolved (see a discussion in paper by Hildtich (1994)). It seems that the key to the solution of this problem lies in the reprocessing of Lyman continuum of hot sdws in the uppermost atmospheric layers of the late type unevolved companion (for more details see the paper by Pustynki, Pustynnik and Kubat (2001)).

2. Statistics of the Hot Subdwarfs in Binaries

To understand better the difference between the single sdws and their counterparts in binary systems sev-

eral groups of investigators have undertaken systematic searches for the late-type companions of sdws. Thus, Saffer, Green and Bowers (2001) have studied a sample of 70 bright B type subdwarfs (SdB) and obtained accurate radial velocities for them. According to these authors SdB stars fall into three distinct groups based on their kinematic and spectroscopic properties. No detectable spectral lines from a cool companion have been found in Group I and only insignificant velocity variations have been detected. These objects constitute around 35% of all SdB stars in Saffer's *et al* sample and this estimate sets an upper limit for the total fraction of non-binary SdB-s. Group II SdB-s are single-lined spectroscopic binaries, comprising about 45% of the objects from the same sample. The remaining 20% of SdB-s are binaries which indicate the presence of additional spectral lines from a cool MS or a subgiant companion. In this Group III all systems reveal slowly varying or nearly constant radial velocities indicating orbital periods ranging from many months to several years. According to Saffer et al "the current data are insufficient to rule out the possibility that some SdB-s in Group I may be analogs of the wide binaries in Group III with undetectable faint companions. The clear division into three groups with such disparate properties suggests very different evolutionary histories even though the current physical status are essentially indistinguishable". These results may be confronted with those of Maxted, Marsh and North (2001) who found 23 stars in a sample consisting of 44 SdB stars definitely to be short period binaries. This conclusion corroborates an earlier estimate of 54% – 66% obtained by Allard *et al* (1997) based on circumstantial evidence from *UBVRI* colours of sdws (in fact Bergeron *et al* (1995) have demonstrated that model atmosphere calculations reproduce quite successfully observed $M_v - (V - I)$ diagram for DA and non-DA white dwarfs).

Several observational tests can be proposed to discriminate between different evolutionary scenarios leading to formation of WD-s. In particular statistically more rapid axial rotation is expected for hot sdws in binaries (when compared to single objects). In reality Koester *et al* (1999) have determined $v \sin i$ for 26 WD by fitting H_{α} rotationally broadened profiles to the observed ones. Only in 3 cases $v \sin i$ definitely exceeded 50 km/s (in all these cases magnetic field higher than 40 KG was detected), only in one case the presence of a companion was established beyond any doubt (similar results have been obtained earlier by Heber *et al* (1997)). These results are in accord with the theoretical predictions of Spruit (1998) who presented numerous arguments favouring the idea that the rotation of WD is not a remnant of the angular momentum of their MS progenitors but a result of the mass loss process during the AGB stage. According to this author strictly axisymmetric mass loss during

the AGB stage from uniformly rotating stars would lead to WD with rotation periods $P > 10y$ but small random non-axisymmetry of order 10^{-3} in the mass loss process add sufficient angular momentum to produce observed rotation of order 1 day. Unfortunately up to now the existing data on radial velocities of sdws in binaries remains scarce and scattered. On the other hand, two ultra-rapid K-dwarfs *2REJ004 + 093* and *2REJ0357 + 287* (projected velocities respectively $90km/s$ and $140km/s$) have been discovered in wide binaries with hot sdws (see Jeffries and Stevens (1996)). Jeffries and Stevens propose a model which explains the origin of such systems as the consequence of the spinning up late type components due to accretion of the slow wind from the AGB progenitor.

Different evolutionary histories for very wide pairs and relatively close binaries with hot sdws may solve a certain controversy concerning the role of binarity in the observed diversified morphology of PN-s. According to Tutukov, Yungelson and Livio (1993) the fraction of all PN-s possessing binary cores is $\sim 22\%$ whereas Schwarz and Corradi (1995) find 11% among the bipolar PN-s. Bond and Livio (1990) who studied 10 precataclysmic binaries MT Ser, UU Sge, V477 Lyr, V664 Cas, VW Pyx, V 651 Mon, Abell-35, LSS 2018, LoTr1, LoTr5 and their environments derive the following conclusions: 1) in nebulae with binary central cores no double shells have been detected typical for PN-s, 2) roughly in 50% of PN-s elliptical or bipolar structures have been observed, 3) morphology of at least three PN-s unambiguously points to the interaction effects with interstellar medium. The fraction of PN-s with such features is higher for binary cores in comparison with single objects.

Bearing in mind results of Saffer *et al* (2001) it is clear that actual fraction of PN-s with binary cores may be significantly underestimated for wide pairs. Although the original interacting winds model of Kwok, Purton and Fitzgerald (1978), later generalized by Kahn and West (1985) and by Balick (1987) does not invoke specifically the effects of binarity to explain elliptical and bipolar shape of PN, it is evident that even in very wide systems the presence of a companion should influence both the overall distribution of circumstellar material and its chemical composition due to effects of accretion of ejecta (see also a discussion of various scenarios for production of elliptical and bipolar shapes of PN-s in Hrivnak (2001)).

There are several independent methods of discovery of the faint late type components accompanying hot sdws. One of the most promising technique lies in the detection of infrared flux excesses in the spectra of hot sdws through application of *JHK* photometry of sdws in combination with the *IUE* data for spectral distribution of sdws. Although this technique has its limitations (it implies a reliable knowledge of the gravity acceleration for sdw which suffers from the uncertain-

ties in the radii values, also it is a common practice to assume the average values of $m_{sdw} = 0.55m_{\odot}$) it enabled to discover 88 new binaries with sdws as the primaries (for details see the papers by Thejll *et al*(1995) and Ulla, Thejll (1998)). A circumstellar origin of IR excess has been excluded by Thejll *et al*(1995). Essentially the same method has been applied the other way round: by inspecting the spectral energy distribution of late type MS stars in far UV it is possible to detect the signatures of the hot companions shortward of 1600\AA . Nine such systems have been identified through *ROSAT*, *EUVE* and *IUE* observations summarized by Barstow *et al* (1994). Unfortunately, these indirect methods cannot provide data on orbital parameters without follow-up spectroscopic and photometric observations. At least for some of these objects inspection of *HIPPARCOS* data should give the distances to these binaries, while in absence of eclipses and pronounced irradiation effects one can get at least the lower limits to separation between the components and the order of magnitude estimate of anticipated orbital period.

3. Different Evolutionary Histories for Moderately Wide Binaries and Wide Pairs ?

In Table I reproduced from paper by Burleigh *et al* (2001) the estimated separations and orbital periods of some binary systems resolved by HST with the hot subdwarfs primaries and the late type MS stars or subgiants as the secondaries are given. We use this small sample for making rough estimates of the plausible orbital parameters of the progenitors of these systems.

To see more distinctly the differences between the consequences of disparate evolutionary histories for WD in close and wide binaries we compare the cooling time t_{cool} of WD and the time scale for the mass loss during the final stages of AGB immediately preceding the emergence of the hot sdw from the ejected envelope of AGB star.

$$t_{cool} \approx 9.41 \cdot 10^6 yr \left(\frac{A}{12}\right)^{-1} \mu^{-2/7} \left(\frac{\mu_e}{2}\right)^{4/3} \left(\frac{m}{m_{\odot}}\right)^{5/7} \left(\frac{L_{\odot}}{L}\right)^{5/7}$$

Here μ is the mean molecular weight of the giant's envelope, μ_e is the mean molecular weight per electron in the core, A is the atomic weight of the matter in the core. Assuming that the masses and luminosities of the WD in wide pairs like HD27483 or 14 Aur C are comparable to those typical for such PCB-s like UU Sge or V477 Lyr (see Polacco and Bell (1993),(1994)) we estimate t_{cool} as $7.7 \cdot 10^5 yr$ and $10^4 yr$ for masses of WD respectively $0.51m_{\odot}$ and $0.63m_{\odot}$ and luminosities of the hot sdws taken from papers of Polacco and Bell. Confronting these values t_{cool} with the time scales of increase the temperature of the hot sdw due to the

Table 1: Estimated physical parameters for the resolved binaries

System	Sp.type	Dist(pc)	$P(yr)$	$a(R_\odot)$
HD2133	F7V+DA	140	590	$1.7 \cdot 10^4$
HD27483	F6V+DA	46	260	10^4
14 Aur C	F4V+DA	82	1307	$2.9 \cdot 10^4$
RE J1925-566	G7V+DA	110	95	5100
HD223816	F8V+DA	92	290	$1.1 \cdot 10^4$
56 Per	F4V+DA	42	47	3190
MS 0354.6-3650	G2V+DA	400	6200	$8.3 \cdot 10^4$
ζCyg	G8IIIp+DA	46	18	1680

decrease of the mass of hydrogen envelope τ_{nuc}

$$\tau_{nuc} \approx 6 \cdot 10^4 yr \left(\frac{L}{1000L_\odot} \right)^{-1} \left(\frac{m_{env}}{10^{-3}m_\odot} \right)$$

and time scale $\tau_{\dot{m}}$ of the mass loss during the phase of superwind

$$\tau_{\dot{m}} \approx 3 \cdot 10^4 yr \left(\frac{\dot{m}}{10^{-8}m_\odot/yr} \right)^{-1} \left(\frac{m_{env}}{10^{-3}m_\odot} \right)$$

we see that $t_{cool}, \tau_{nuc}, \tau_{\dot{m}}$ are all roughly of the same order magnitude and less or comparable to τ_{therm} for the cool companion of the hot sdw. This means that during the phase of superwind and after emergence of the hot sdw following "shedding" of the envelope the distant companion in a binary had no time enough for accreting appreciable portion of the material lost from sdw. We use this fact to estimate the initial separation between components of the binaries shown in Table I.

For very wide pairs with the estimated orbital periods $10^2 - 10^3$ yr the size of the orbit found from the Kepler's third law $a = 214R_\odot m_1^{1/3} (1+q)^{1/3} P_{yr}^{2/3}$ is indicated in the last column of the Table I (assuming $m_1 = 1m_\odot$ and $q = 0.5$). For half of the systems in the Table I the size of orbit is $a \geq 10^4 R_\odot$. This means that such wide pairs most probably escaped in past the phase of common envelope because even during the AGB stage the progenitor of WD had no chance to fill in its Roche lobe or because due to the very large size of the orbit the magnetic braking and the ensuing orbital decay could not operate efficiently. Arguing in that way we ignore the evolution of the orbit in the past. If, on the other hand, we make an assumption of the net mass loss from the AGB star without a considerable accompanying angular momentum loss, then using the relation $PM^2 = const$ (M being the total mass of a binary) for $M \simeq 5m_\odot, q = 0.5$ and $m_{wd} = 0.6m_\odot$ we find that initial separation between the components was of order $10^3 R_\odot$. Thus, the validity of conventional concept about the Roche lobe overflow and subsequent formation of common envelope in application to such binaries looks problematic.

A reasonable estimate of an impact caused by a distant companion upon the properties of stellar wind

from AGB can be found using the recently published results of Frankowski and Tylanda's investigation(2001) of stellar wind peculiarities in a binary.

Frankowski and Tylanda (2001) have explored the influence of a companion on the wind from the giant in the AGB stage in a binary system. They have derived a simple relation for the equatorial-to-polar wind intensity contrast

$$\frac{\dot{m}_{eq}}{\dot{m}_{pol}} = 1 + \frac{(a - 4ab - 4c)}{4\gamma} (2 + 5q)\xi(q)^3 \left(\frac{R}{R_L} \right)^3$$

Here q - is the mass ratio, R -the radius of a giant, $\xi = R_L/A$, A being a semi-major axis of the relative orbit, R_L - the radius of the Roche lobe. γ is a free parameter describing the effectiveness of the Newtonian gravitational force (it accounts for the effects of pulsation, radiative pressure and convective motions all acting to diminish the gravity on the giant's surface), α is a parameter describing the effect of gravity darkening ($\alpha = 0$ for uniform temperature distribution and $\alpha = 0.25$ for the atmosphere being in a state of strict radiative equilibrium according to von Zeipel's theorem), parameters a, b, c are determined from the power law approximation of the mass loss rate $\dot{m} \sim R^a T_{eff}^b g^c$ and found from the model of stellar wind for AGB stars (for example, in case of the models by Arndt *et al* (1997), $a = -4.70, b = -2.14, c = -2.88$). For reasonable combinations of parameters a, b, c, γ, α Frankowski and Tylanda find the effect of the contrast $(\dot{m}_{eq}/\dot{m}_{pol} - 1)$ ranging between $10^{-4} - 10^{-3}$ for $(R/R_L \ll 1)$ up to 1-5 for $R/R_L \sim 1$. Using the above-given expression for $\frac{\dot{m}_{eq}}{\dot{m}_{pol}}$ we can easily verify that effect of the wind contrast between equator and pole will not influence appreciably the above-given estimate of the initial separation between the components. Thus, the following conclusion seems to be unavoidable: evolutionary history for very wide pairs (with $P_{orb} \geq 100yr$) should be drastically different from binaries with initial orbital periods $P_{orb} \ll 100yr$. In view of the above-stated a comparative study of the evolutionary history for binaries with moderate masses ($M \leq 10m_\odot$) and orbital periods ($P_{orb} \sim 10 - 100yr$) deserves a special investigation.

Acknowledgements. We acknowledge with gratitude support of this research by Grant 4701 of Estonian Science Foundation.

References

- Allard F., Wesemael F., Fontaine G., Bergeron P., Lamontagne R.: 1997 *Astron.J* **107**, 1565.
- Arndt T.U., Fleischer A.J., Sedlmayr E.: 1997, *As.Ap.*, **327**, 614.
- Balick B.: 1987, *Astron.J.*, **94**, 671.
- Barstow M.A., Hollberg J.B., Fleming T.A., Marsh M.C., Koester D., Wonnacott D.: 1994, *MNRAS*, **279**, 180.
- Bergeron P., Wesemael F., Beauchamp A.: 1995, *PASP*, **107**, 1047.
- Bond H.E., et al: 1991, in: "Evolutionary Processes in Interacting Binary Stars eds. Y.Kondo et al, 240.
- Bond H.E., Livio M.: 1990, *Astrophys. J.*, **355**, 568.
- Burleigh M., Barstow M., Bond H.E., Holberg J.: 2001, in: *12th European Workshop on White Dwarf Stars ASP Conference series*, **226**, eds. Provencal J.L., Shipman H.L., McDonald J., Goodchild S., 222.
- Frankowski A., Tylenda R.: 2001, *As.Ap.*, **367**, 513.
- Heber U., Napiwotzki R., Reid I.N.: 1997, *As.Ap.*, **323**, 819.
- Hiltich R.W.: 1994, *Observatory*, **114**, 214.
- Holberg J.B., McCook G.P., Sion M., Oswalt T., Burleigh M.: 2001, in: *12th European Workshop on White Dwarf Stars ASP Conference series*, **226**, eds. Provencal J.L., Shipman H.L., McDonald J., Goodchild S., 359.
- Hrivnak B.: 2001, in: *12th European Workshop on White Dwarf Stars ASP Conference series*, **226**, eds. Provencal J.L., Shipman H.L., McDonald J., Goodchild S., 3.
- Iben I.Jr., Laughlin G.: 1989, *Astrophys.J.*, **341**, 312.
- Jacoby G.: 1989, *Astrophys.J.*, **339**, 39.
- Jeffries R.D., Stevens I.R.: 1996, *MNRAS*, **279**, 180.
- Kahn F., West K.A.: 1985, *MNRAS*, **212**, 837.
- Kleinman: 1999, in: *11th European Workshop on White Dwarf Stars ASP Conference series*, **169**, eds. J.-E.Solheim and Meistas E.G., 71.
- Koester D., Dreizler S., Weidemann V., Allard N.F.: 1999, in: *11th European Workshop on White Dwarf Stars ASP Conference series*, **169**, eds. J.-E.Solheim and Meistas E.G., 415.
- Kwok S., Purton C.R., Fitzgerald P.M.: 1978, *Astrophys. J.*, **219**, L127.
- Maxted P.F.L., Marsh T.R., North R.C.: 2001, in: *12th European Workshop on White Dwarf Stars ASP Conference series*, **226**, eds. Provencal J.L., Shipman H.L., McDonald J., Goodchild S., 187.
- McCook G.P., Sion E.M.: 1999, *Astrophys. J.Suppl*, **121**, 1.
- Paczynski B., Deaborn D.S.: 1980, *MNRAS*, **190**, 395.
- Polacco D.L., Bell S.A.: 1993, *MNRAS*, **262**, 377.
- Polacco D.L., Bell S.A.: 1994, *MNRAS*, **267**, 452.
- Provencal J.L., Shipman H., Koester D., Wesemael F., Bergeron P.: 2001, in: *12th European Workshop on White Dwarf Stars ASP Conference series*, **226**, eds. Provencal J.L., Shipman H.L., McDonald J., Goodchild S., 228.
- Pustynnik I, Pustynski V.V.: 2001, in: *12th European Workshop on White Dwarf Stars ASP Conference series*, **226**, eds. Provencal J.L., Shipman H.L., McDonald J., Goodchild S., 253.
- Pustynski V.-V., Pustynnik I., Kubat J.: 2001, (this volume)
- Ritter H.: 1986, *As.Ap.*, **169**, 139.
- Saffer R.A., Green E.M., Bowers T.: 2001, in: *12th European Workshop on White Dwarf Stars ASP Conference series*, **226**, eds. Provencal J.L., Shipman H.L., McDonald J., Goodchild S., 408.
- Schwarz H.E., Corradi R.L.M.: 1995, in: *Ann. of the Israel Physical Society, Asymmetrical Planetary Nebulae*, **11**, eds. Harpaz A. and Soker N., Haifa, Israel, 113.
- Shipman H.L., Provencal J.L., Hog.E, Thejll, P.: 1997, *Astrophys. J.*, **488**, L43.
- Shipman H.L., Provencal J.L.: 1999, in: *11th European Workshop on White Dwarf Stars ASP Conference series*, **169**, eds. J.-E.Solheim and Meistas E.G., 15.
- Spruit H.C.: 1998, *As.Ap.*, **363**, 603.
- Thejll P., Ulla A., McDonald J.: 1995, *As.Ap.*, **303**, 773.
- Tutukov A.V., Jungelson L.R., Livio M.: 1993, *Astrophys.J.*, **418**, 794.
- Ulla A., Thejll P.: 1998, *As.Ap.S.*, **132**, 1.
- Wood M.: 1992, *Astrophys.J.*, **386**, 539.
- Wood M.A.: 1995, in: *Proceedings of 9th European Workshop on White Dwarfs*, ed. Koester D., Werner K. (Berlin,:Springer), 41.

REPROCESSING OF L_c IN IRRADIATED ATMOSPHERES OF UNEVOLVED COMPANIONS IN PRECATAclySMIC BINARIES (PCB) AS A SENSITIVE TOOL OF MEASURING THE TEMPERATURES OF HOT SUBDWARF PRIMARIES

I. Pustyl'nik¹, V. Pustynski², J. Kubat³

¹ Tartu Observatory
Estonia, *izold@aai.ee*

² Tartu University
Estonia, *vladislav@aai.ee*

³ Astronomický ústav, Akademie věd České republiky,
CZ-251 65 Ondřejov, Czech Republic, *kubat@sunstel.asu.cas.cz*

ABSTRACT. We report results of modeling physical processes in the outermost layers of strongly irradiated atmospheres of low mass companions in PCBs where L_c radiation coming from the hot subdwarf (sdw) primary is reprocessed. We solve explicitly a set of equations of hydrostatic, ionization and thermal equilibrium and calculate the intensity of reprocessed emergent radiation in recombinations for optically thin plasma. For purely hydrogenic atmosphere and typical for PCBs values of incident fluxes, densities, gas pressures of irradiated upper atmospheric layers we find that L_c will be absorbed and re-emitted in recombinations within the column of effective thickness $(10^6 - 10^8)cm$ of HII depending on the electron density and the effective temperature of sdw. The most interesting and non-trivial result of our model computations lies in the overheating of the uppermost layers of irradiated atmosphere: the equilibrium temperature of gas turns out to be considerably higher than the value of radiative temperature in the black body approximation following from the total irradiating flux of the diluted incoming radiation of sdw. This result enables one to explain the abnormally high values of albedos following from the conventional analysis of the light curves of PCBs (amplitudes of the light curves correspond to albedo values typically amounting to 3 – 5 for well-studied systems like *V477Lyr*). The effect of overheating is determined solely by the effective temperature of irradiating source. Thus, we indicate how the effect of reprocessing of L_c radiation can be used as a sensitive tool for a more rigorous determination of the effective temperature of the sdw primaries in PCBs.

Key words: Stars: binary: precataclysmic, reflection effect.

1. Introduction

PCBs is a group of close binary systems composed of a sdw or a white dwarf precursor (primary star) and an unevolved secondary star, usually a red dwarf. Periods of these systems are very small, varying from several days to several hours, and separations between the components are also small, so systems are close. Nonetheless, they are still not close enough for the secondary's Roche lobe to be filled, so cataclysmic activity hasn't yet started. PCBs are frequently found to be the cores of planetary nebulae.

It is generally accepted now that such systems originate from wider binaries as a result of the common envelope stage that once took place in course of their evolution. The common envelope originates, when the more massive primary fills its Roche lobe and begins to loose matter forming a shell embracing the system and effectively brakes it down, forcing the secondary to spiral down towards the common gravity center. Thereafter the matter is expelled from the system and is observed as a planetary nebula.

One of the most spectacular particularities of PCBs is an extremely high reflection effect. Being only a second order effect in common semi-detached systems, it is often the main cause of optical variability in such close systems as PCBs. Due to the fact that the distance between the components is very small (about some units of solar radius) and that the effective temperature of the primary is extremely high (tens of thousands Kelvins), the hemisphere of the secondary facing the primary star is highly overheated. The physics standing behind the emergent radiation transformations in the overheated photosphere of the secondary, is very complicated; that is why we cannot treat the flux es-

caping from the secondary's illuminated hemisphere as simply as it is usually done in conventional models of reflection effect in ordinary semi-detached systems (see, for instance, Paczynski and Dearborn 1980).

An adequate model of the processes involved in the transformation of the incoming hot radiation in the photosphere of the secondary star would let one to obtain independent estimations of the system's parameters, including so important one as temperature of the white dwarf. Such model would also help us to predict the future evolution of the system, to answer the question if it has enough time to start cataclysmic activity. Some specific questions, like an unusually high reflection albedo found from observations, could also be answered (see for instance, Pustynnik and Pustynski 1999).

2. Model for upper layers of irradiated atmosphere.

We developed a theoretical model of the upper photosphere of the secondary.

As already mentioned above, effective temperatures of the primary correspond to absolutely black body temperatures of some tens thousands Kelvins. It means that a significant portion of the incoming flux energy is concentrated in the far ultraviolet portion of the spectrum, namely in the band with wavelengths shorter than Lyman limit. This hard flux falls onto rarefied layers of the secondary's photosphere, and processes in these layers are somewhat similar to the processes taking place in planetary nebulae. This fact justifies application of similar methods in our model. It is intuitively clear that there shouldn't exist local thermal equilibrium in such overheated medium. To escape sophisticated non-LTE calculations that would make our reflection effect model extremely complicated, we suppose upper non-LTE layers to be purely hydrogenic and describe them generally in the on-the-spot approximation by the system of three equations: the equation of ionization balance

$$N_0(r) W_\delta \int_{\nu_{Ly}}^{\infty} \frac{B_\nu(T_1) k_\nu[T(r)] \exp(-\tau_\nu(r))}{h\nu} d\nu = N_e(r) N^+(r) \alpha[T(r)] .$$

the equation of thermal equilibrium

$$N_0(r) W_\delta \int_{\nu_{Ly}}^{\infty} \frac{B_\nu(T_1) k_\nu[T(r)] \exp(-\tau_\nu(r))}{h\nu (h\nu - h\nu_{Ly})^{-1}} d\nu = 4\pi \int_0^{\nu_{Ly}} \epsilon[T(r), N_e(r)] [1 + \tau_\nu(r)] d\nu ,$$

and the equation of hydrostatic equilibrium

$$N(r) = \frac{P_{r=0}}{[1 + X(r)] k T(r)} \exp\left(\frac{m_p G_\delta r}{[1 + X(r)] k T(r)}\right)$$

Here

$$X = 1 - \frac{N_0}{N_0 + N_e + N^+}$$

stands for ionization degree (it is unit when all hydrogen is ionized and is zero when all hydrogen is neutral), α is the recombination coefficient to all levels except the first one, ϵ is the total emission coefficient for recombinations, N_0 , N_e , N^+ are respectively the number density of neutral H atoms, of free electrons and protons, B_ν is the Planckian, W_δ is the local value of dilution factor, δ being the angular distance from substellar point of irradiated component, $\tau_\nu(r)$ - the monochromatic radial optical depth counted from the surface of the star, P is the gas pressure (the meaning of other notations is self-explanatory). We neglect the number of ionizations from upper levels in equation of ionization equilibrium. We add the optical depth-dependent coefficient into the right-hand-side integrand of the thermal equilibrium equation to take into account approximately contribution from diffuse radiation. In the formula for hydrostatic equilibrium we take into account the dependence of effective gravity acceleration G on coordinates of the selected point upon the secondary's surface. The applicability of such simplified description was checked by our numeric estimations which showed, that the upper layer of the irradiated atmosphere is opaque for Lyman continuum photons, at the same time photons with lower energy penetrate freely through the same layer practically without being absorbed; so, the non-LTE layer in the first approximation may be considered transparent for radiation in optical wave-band.

When the above-mentioned system of equations is solved, we obtain models of the upper photospheric layer of the heated secondary's hemisphere. As it could be expected, they demonstrate a certain qualitative analogy with models of planetary nebulae.

It is seen that the radiation penetrates into the photosphere until a certain depth, while ionization degree remains close to unity. Thereafter almost whole flux is absorbed in relatively very thin layer of practically neutral hydrogen.

From our models one may conclude that the greatest portion of the Lyman continuum flux is absorbed in the rarefied upper layer, and the energy of Lyman continuum photons is reprocessed into energy of less-energetic quanta, as a result of hydrogen ionization from the ground level and subsequent recombinations onto upper levels, and in addition is expended on heating electron gas. Thus, the reprocessed radiation has a

typical recombination spectrum, and its intensity may be obtained from the equation

$$\epsilon[T(r), N_e(r)] = \frac{N_e^2}{T(r)^2} \Phi_\nu[T(r), N_e(r)] \exp\left(-\frac{h\nu}{kT(r)}\right),$$

where

$$\Phi_\nu = 5.4(F_\nu[T(r)] + G_\nu[T(r), N_e(r)]).$$

Here $F_\nu[T(r)]$ is the Gaunt factor for free-free transitions and $G_\nu[T(r), N_e(r)]$ is the Gaunt factor for bound-free transitions. The normalization coefficient, introduced into this equation to keep emitted energy rate equal to absorbed energy rate, is omitted in this formula. This coefficient differs from unity in our model due to the fact, that the model doesn't include self-absorption that may be important at large wavelengths and its value is found by equalizing the total energy emitted in recombinations to the local value of the incident flux from sdw.

Next we should analyze physical processes involved in transformation of radiation with longer wavelengths. This is the radiation coming directly from the primary star and penetrating through the upper layers nearly without attenuation, and also the radiation reprocessed in the upper layer and penetrating deeper into the photosphere.

The numeric estimations show that the deeper layers may be treated as medium with LTE, and thus we may use diffusion (Eddington) approximation to model them. Following Basko and Sunyaev 1973, we write the Eddington equation in the following form:

$$F_0 + F(y) = -\frac{16\sigma x_H \rho(r) T(r)^3}{3 m_p k[T(r), P(r)]} \frac{dT}{dy},$$

where variable y is defined as follows:

$$y(r) = -\frac{x_H}{m_p} \int_0^r \rho(r) dr$$

and

$$F(y) = \exp\left(-\frac{2}{3\mu}\right) \int_{\lambda_{Ly}}^\infty F_{inc} \exp[-yNk(\lambda, T, P)] d\lambda.$$

This equation is solved numerically together with hydrostatic equilibrium equation

$$\frac{d}{dr} P(r) = G_\delta \rho(r),$$

and the results of the solution may be expressed as temperature, pressure and flux functions of the mean optical depth τ that is introduced with the formula

$$\tau(r) = \int_r^\infty k(r) dr.$$

Having obtained this solution, we may deduce the intensity of emergent radiation from the deeper photosphere:

$$I_\nu(\mu) = \int_0^\infty \frac{1}{\mu} \frac{k_{2/3}(\nu)}{k_{2/3}} B_\nu(T) \exp\left(-\frac{k_{2/3}(\nu)}{k_{2/3}} \frac{\tau_\nu}{\mu}\right) d\tau.$$

This intensity is function of the angle $\arccos \mu$ with the local normal.

In this way we obtain intensities of emergent radiation escaping from the upper non-LTE and deeper LTE layers of the secondary's photosphere. Taking these two intensity components together and integrating them over the whole visible sector of the secondary at a particular orbital phase, we get the total flux intercepted from the secondary by an observer:

$$L_\nu(i, \theta) = 2R_2 \int_{\delta_{min}}^{\delta_{max}} \int_{\chi=0}^{\chi_{max}} I_\nu(\Psi) \sin(\delta) \cos(\Psi) d\chi d\delta.$$

For different phase angles the observable illuminated sector has different shapes, and thus we may construct a smooth light curves by computing the reemitted radiation input into the total system's luminosity at various phases. We normalize the light curves so, that the total relative luminosity in minimum light were unity:

$$l_{norm}(\nu, \theta) = \frac{L_1(\nu) + L_2(\nu, \theta)}{L_1(\nu) + L_2^{min}(\nu)}.$$

3. Results and Conclusions

1. The effective thickness of the column where the total Lc flux is absorbed for typical temperatures $T_{sdw} = (40000 - 70000)K$ and electronic densities $N_e = 10^{13} cm^{-3}$ amounts to $\Delta r = (10^6 - 10^8)cm$. As we can see from the Figure 1, the thickness of the ionized zone is rather strongly dependent both on the values of T_{sdw} and the distance from substellar point. Since the emission measure is proportional to Ne^2 it is clear that the contribution from the zones close to the substellar point will be dominant (both Ne and Δr are higher).

The first attempts to substitute black body spectral distribution of the hot subdwarf by the distributions following from the model atmospheres discussed in (Kubat at al., 1999) demonstrate sensitivity of both temperature and ionization degree runs to Lyman continuum of the irradiating source.

2. One of the observational phenomena that receives a natural explanation in our model is a well-known excess of the secondary's albedo coefficient in optical and infrared bands in comparison with estimates made from the models based on simple black body approximation. In our model this discrepancy is explained by

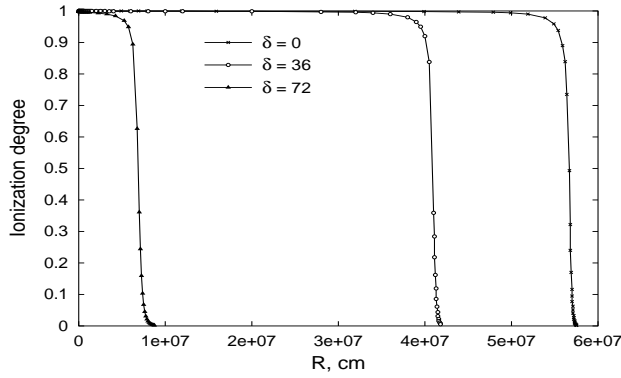


Figure 1: Ionization degree x as function of depth R in irradiated photosphere for different values of angular distance from the substellar point. PCB parameters are: $a = 2R_{\odot}$, $R_1 = 0.01R_{\odot}$, $R_2 = 0.2R_{\odot}$, $M_1 = 0.51M_{\odot}$, $M_2 = 0.15M_{\odot}$, $T_1 = 60000K$, $T_2 = 4000K$, $N_e(0) = 5 \cdot 10^{12}cm^{-3}$.

the fact, that the energy in the ultraviolet part of the spectrum is reprocessed due to recombinational processes into low-energetic quanta, and thus gives rise to the above-mentioned excess.

3. The high values of albedo from irradiated atmospheres follow from the fact that the upper layers where the Lc continuum is absorbed are strongly overheated. This is illustrated in the Figure 2 where the runs of equilibrium temperature T (following from solution of the set of equations of thermal, hydrostatic and ionization equilibrium), T_{saha} (ionization temperature following from Saha formula for a given local values of electron and neutral hydrogen densities), T_{abb} (black body temperature following from the value of total incident flux from sdw) are compared. As we see T is systematically higher than both T_{saha} and T_{abb} , the difference being progressively larger as one moves towards the uppermost layers of the irradiated atmosphere.

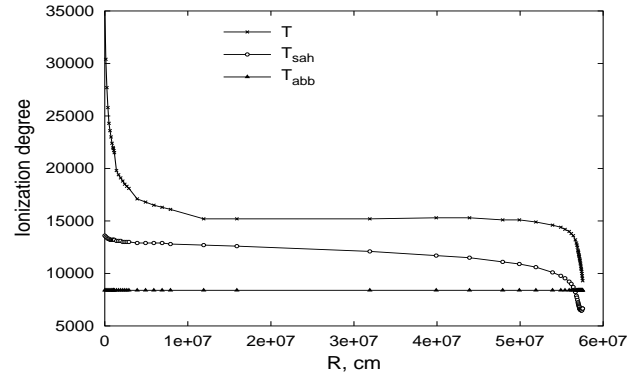


Figure 2: Runs of equilibrium temperature T , ionization temperature T_{sah} and black body temperature T_{abb} in the irradiated photosphere. PCB parameters are the same as in the Figure 1.

Acknowledgements. We gratefully acknowledge support of this research by Grant 4701 of Estonian Science Foundation.

References

- Basko M.M., Sunyaev R.A.: 1973, *Ap.Space Sci.*, **23**, No.1, 117.
 Kubat J., Puls J., Pauldrach A.W.A.: 1999, *As.Ap.*, **347**, 587.
 Paczynski B., Deaborn D.S.: 1980, *MNRAS*, **190**, 395.
 Pustynnik I, Pustynski V.V.: 1999, *11th European Workshop on WD, ASP Conference Series*, **169**, 289.

THE (O-C) DIAGRAMS OF ECLIPSING BINARIES: TRADITIONAL AND NEW WAYS OF TREATMENT

H. Rovithis-Livaniou

Section of Astrophysics, Astronomy & Mechanics, Dept. of Physics, Athens University,
Panepistimiopolis, Zografos 157 84, Athens, Greece *elivan@cc.uoa.gr*

ABSTRACT. In this review, the traditional and the new ways of treatment of the orbital period changes of close eclipsing binaries are presented. Moreover, a comparison is made, and a general discussion is given. All methods are described, in a more or less detail way, and examples are given to prove the inadequacy of the traditional methods. The latter are not only very simple and extremely restrict, but they violate the uniqueness of the solutions. Moreover, it is shown that, although sometimes traditional methods give results close to that found by the continuous methods, and because of this some could conclude that the results coming out from the classic methods and the new ones are equivalent (within observat

ional errors), this is not the case. The big and important difference between traditional and new ways of the (O-C) diagrams' analysis, is their physical interpretation, which in the new ways of treatment is consistent with the physics of close eclipsing binaries and with the physical mechanisms which could produce the observed orbital period variations.

Key words: Stars: eclipsing binaries: orbital period changes

1. Introduction

A basic characteristic of an eclipsing binary, is its orbital period, P_{orb} . If P_{orb} is constant, the time that a primary minimum occurs (an **observed** minimum, hereafter referred as **O**), will coincide with this its appropriate ephemeris formula predicts, (the **calculated** minimum, hereafter referred as **C**); see, for example, Tsessevich (1973).

If, for any reason P_{orb} changes, the observed minimum will be different than the calculated one, and thus the difference (O-C) will not be equal to zero. In such a way an (O-C) diagram is built up.

The appearance of an (O-C) diagram, is strongly depended on the ephemeris formula used to construct it. See for example the (O-C) diagrams of *AM Leo* (Demircan and Derman 1992), of *V566 Oph* (Rovithis-Livaniou et al. 1993); of *ST Per* (Demircan and Selam

1993); of *AB And* (Kalimeris et al. 1994b, or Demircan et al. 1994). For this reason, some investigators are using different ephemeris formulae, as well as different ways of approach to describe an (O-C) diagram.

Traditional analysis ways of an (O-C) diagram, use a *linear*, or a *quadratic* least square fitting, which is sometimes combined with a *sinusoidal* periodic term (Batten 1973, Tsessevich 1973).

On the other hand, three new ways of treatment developed during the last seven years. The new proposed methods are:

- 1) the higher order polynomial method, (HOP), or the first continuous method, (Kalimeris et al. 1994a);
- 2) the state-space model, (SSM), (Koen, 1996), and
- 3) a second continuous method (Jetsu et al. 1997).

The later is considered as a method, although it has been applied to one system only, namely to the *AR Lac*, so far. It is considered so, because it fulfils the basic condition of the new methods; that is, to treat and subsequently analyze an (O-C) diagram as a whole. Actually, the most important difference between traditional and new methods is that the new ones face an (O-C) diagram as a whole. They describe and analyze it in the same continuous way, without deviding it to linear segments, that yield to abrupt period variations which although have been proven to be inconsistent (e.g. Hall 1990, Kalimeris et al., 2001), are still in use (e.g. Qian 2001ab).

Thus, in this review, and after the short description of all methods, (presented in Sections 2 and 3), a general discussion will be given, and a comparison will be made, which will prove the inadequacy of traditional methods of (O-C) diagrams analysis.

2. Traditional Methods

2.1. Linear and Piecewise Approximation

Orbital period, P_{orb} , is not only a basic characteristic of an eclipsing binary, but is also one of its elements calculated with great accuracy. If P_{orb} is known, the time of minimum light (*primary minimum*, or *MinI*), is given by a linear relation of the form:

$$MinI = t_0 + P_{orb} \times E$$

where t_0 stands for the time of the first observed minimum, (*zero epoch*), and E - known as the epoch- is an integer number that denotes the number of the cycles elapsed from t_0 .

The forgoing linear formula is very simple, and predicts the time a primary minimum is expected; thus, is widely used by observers. Especially by those who are mainly interested to minimum times only, and not for the whole light curve of an eclipsing binary.

If the orbital period of an eclipsing binary is constant, let us say: $P_{orb} = P_e$, where P_e will be hereafter used to denote the constant orbital period of an eclipsing binary given by its ephemeris formula (ephemeris period), its (O-C) diagram will be appeared as a straight line. More specifically: if the (O-C) residuals from some assumed ephemeris are plotted versus the number of cycles elapsed, they should be clustered around the line $(O-C)=0$, if the period is chosen correctly. This line will be parallel to the time-axis, if the period is accurately determined; while a positive or a negative slope indicates that the real orbital period is longer or shorter than P_e , respectively (Batten 1973).

In reality things are not thus simple. The (O-C) diagrams of many systems appeared to be quite complicated. A simple glance to the (O-C) diagrams of some eclipsing binaries (e.g. Hall and Kreiner 1980, Kreiner et al. 1994, Kalimeris et al. 1994ab, 1995, Simon 1996, Kim et al. 1997, Mayer 1997, Chochol et al. 1998, Qian 2000), is enough to recognize this fact, which is not due to scatter. (Scatter is expected, since individual points, used for the construction of an (O-C) diagram, usually exhibit small or large discrepancies).

In cases where an (O-C) diagram is impossible to be described by a linear relation -similar to that previously described- the usual way of treatment is to divide it in a number of small linear segments, each one of which is interpreted by a different linear ephemeris. This procedure is known as the *step variation technique*, (e.g. Hall 1975, Yamasaki 1975, Kreiner 1977). Both the **number of segments**, as well as the **choice of time** is not objective and is subject to high-handed acts, according to the investigator wish. In spite of all these, the method is still in use, (e.g. Chambliss 1976, Bakos 1977, Demircan et al. 1990, Kim 1991, Herczeg 1993, Berrington and Hall 1994, Simon 1996, 1997, Kim et al. 1997, Pribulla et al., 1997, Qian et al. 1999a, Qian 2000, Qian and Liu 2000, Qian et al. 2000, Qian 2001ab, Qian and Ma 2001).

2.2. Quadratic Approximation

When the orbital period of an eclipsing binary is variable, and this variation is made at a constant rate, then the quadratic least squares approximation is used to describe an (O-C) diagram. This is the case of the well-known *parabola fitting*. In such a case, the (O-C) differences can be calculated by the relation:

$$(O - C) = 1/2(dP_{orb}/dt)\bar{P}E^2$$

where \bar{P} is the average period over the elapsed time interval.

Many (O-C) diagrams of eclipsing binaries have been treated using the parabola fitting. In some of the cases, this quadratic approximation is enough; but, it is not always the case. Two good examples to explain and present this fact, are the *RT And*, and *AH Vir* systems.

In the *RT And* case (Rovithis-Livaniou et al. 1994), parabola fitting as well as third and fourth order polynomials were used to describe its (O-C) diagram. A comparison of the polynomials coefficients, their RMS errors and the fitting in these three different cases, did not show significant differences. Thus, a second order approximation is good enough for the (O-C) description of *RT And*, yielding to the conclusion that its period varies with a constant rate. (See also Rovithis-Livaniou et al. 1996).

On the other hand, the case of *AH Vir* (Kalimeris et al. 1994a, Rovithis-Livaniou et al. 1996a), shows that quadratic approximation -except the restriction it puts- is not always enough. Indeed, neither a piecewise linear approximation, presented by Demircan et al. (1990), who divided the (O-C) diagram of *AH Vir* in 3 segments, nor the quadratic approximation they used, is good to describe the (O-C) diagram of the system. This is more than obvious from a glance to Figs. 1 and 2 of the foregoing mentioned paper. The division in 3 linear segments, yields to the previously described *step-variation technique*, and the parabola fitting to a continuous variation, with a constant rate. It's not only that none of them is good enough for the description of the (O-C) diagram of *AH Vir*. This is not a simple description's matter. It is very important, because description is related to results concerning the way the system's orbital period varies. Thus, a roughly or not accurate description yields to inaccurate or even to erroneous results.

2.3. Sinusoidal Variation

In some cases the appearance of an (O-C) diagram, yield investigators to include for its description a sinusoidal term, too. In such a case, the time of minimum light is given by an equation of the form:

$$MinI = t_0 + PE + 1/2(dP/dt)PE^2 + \alpha \sin(2\pi E/P_* + \phi)$$

where α is the amplitude of the sinusoidal variation, P_* its periodicity, and ϕ stands for the phase.

See for example the cases of *XX Cep* (Mayer 1984), of *TX Her* (Kreiner and Zola 1989), of *TW Dra* (Abhyankar and Panchatsaram 1984), of *R CMa* (Radhakrishnan et al. 1984), of *AK Her* and *ER Ori* (Abhyankar and Panchatsaram 1982), of *CM Lac*, *AB And*, and *YY*

Eri (Panchatsaram and Abhyankar 1981) and many others, analyzed by various investigators.

In all of the cases mentioned above the presence of a third body in the system was assumed. But, in more recently published papers, another mechanism is also considered; namely, that of magnetic activity cycles (Applegate 1992).

2.4 Combined Methods

In cases of (O-C) diagrams, that have a more or less strange appearance, and since it is well known that this is strongly depended on the ephemeris formula used to construct the diagram, all three previously described methods might be used.

See for an example the case of *ST Per* in the analysis made by Demircan and Selam (1993), where the (O-C) diagram of the system was treated using:

- a linear ephemeris
- using 8 linear segments
- by the combined effect of two sinusoidal variations.

3. New Methods

3.1. The First Continuous Method

According to this new method, the orbital period P_{orb} and its rate of change dP_{orb}/dt are assumed to be **continuous functions of time**, of a **non-prescribed** form. It is also supposed that the calculated time of conjunction is given, at any cycle E , by the usual linear ephemeris:

$$T_c(E) = t_0 + P_e E$$

where E has been used as the time variable, t_0 is a time of conjunction (in Hel.JD), and P_e is the ephemeris period, (which is always constant, as has been already mentioned).

In absence of photometric perturbations (such as spots, flares etc) conjunctions should coincide with primary eclipses. Expressing the $T(E)$ function piecewise, e.g. by least squares, using orthogonal polynomials over a weighting sequence (Kalimeris et al. 1994a), it is found that:

$$\Delta T(E) = \sum_{j=0}^n c_j E_N^j,$$

where the best order of approximation, n , can be chosen by inspection of the error diagram, and E_N^j is defined as: $E_N^j = E/c$, where c is a constant, (*scale constant*), such that: $|max E_{N,min}, E_{N,max}| < 1$

Then, the period of the system at cycle E is equal to the duration of the corresponding cycle E , that is:

$$P(E) = T_{ob}(E) - T_{ob}(E-1) = P_e + \Delta T(E) - \Delta T(E-1)$$

So, the orbital period variations of the system, are calculated with a simple and accurate mathematical way. More details can be found in Kalimeris et al. (1994a) paper. Moreover, the $P(E)$ function shape, -being independent of the ephemeris formula used to construct the (O-C) diagram- can be used to search for periodicities, if any (Kalimeris et al. 1994b).

3.2. A Statistical Method

Koen (1996) used a statistical method to find the orbital period changes from the (O-C) diagrams of some stars. He applied this method to the following 18 variables:

4 Cepheids, the: *S Sge, BW Vul, Y Oph, ζ Gem*,

3 δ Scuti stars, the: *CY Aqu, DY Peg, YZ Boo*,

3 RS CVn's, the: *RS CVn, RT Lac, RT And*,

5 eclipsing binaries, the: *V471 Tau, SV Cam, U Cep, X Tri and ST Per*, to the dwarf nova *V1159 Ori*, to the X-ray source *Cygnus X-3*, and to the RR Lyrae-type system *AR Per*.

The method is the second one that appear to treat an (O-C) diagram as a whole. Koen is continuously working in time series analysis methods. His methods are statistical, and the last one (Koen 2001), was used for the analysis either of the maximum or minimum light of monophasic pulsating stars.

3.3. Another Continuous Method

Another continuous method was proposed to describe and analyze the (O-C) diagram of the RS CVn-type system *AR Lac*, and has not been used to any other eclipsing binary. We considered it as one of the new methods proposed so far for the (O-C) diagrams treatment of eclipsing systems, as has been already mentioned, since it was shown that it is possible to explain the period variations of *AR Lac* without abrupt changes. This is very important, for the reasons explain below, in the next Section.

According to this method, the models for the (O-C) data are given by equation:

$$(O - C)f(T, P_0) = \sum C_i(P_0)T^i$$

where the standard least squares fit method is applied to solve the best value for the free parameters $C_0(P_0), \dots, C_k(P_0)$. Time scale is $T = (t - t'')/T_{scale}$, where t'' is the mid point of the time interval of the data, and the choice of k can be settled by setting all weights to unity, modeling the foregoing equation to different orders, and find where the mean residuals stop decreasing.

4. Mechanisms causing Period Changes

If the (O-C) diagram of an eclipsing binary, is such that it can be described by a linear least squares approximation, the orbital period of the system is constant.

If, on the other hand, it is curved, the orbital period changes. In this case, the main aim of an investigator, is not only to make a good description of the (O-C) diagram, and find the way the orbital period of the system changes; but, to find also the physical mechanisms that might cause it.

As was mentioned before, quadratic approximation is widely used. This is so, because the following three physical mechanisms support such period changes:

- 1) Mass transfer from one star to the other.
- 2) Mass loss through L_2 , or via enhanced stellar wind.
- 3) Tidal interaction of the two members of the binary star.

The description of an (O-C) diagram of an eclipsing binary using a sinusoidal term can be physically supported, too. In such a case, the existence of a third body, the well known *light-time effect*, could be responsible for a sinusoidal variation, (Borkovits and Hegedus 1996).

Another possible explanation for a sinusoidal or any other periodic variation could be the development of magnetic activity cycles, in one or both of the components (Applegate 1992). Applications have been made to many systems (e.g. Lanza and Rodono 1999)

On the other hand, the orbital period changes of many eclipsing systems have been explained as coming from one or the other of these two mechanisms, independently of the way used to describe their (O-C) diagram. More specifically, the systems: *AM Leo* (Demircan and Derman 1992), *AB And* (Kalimeris et al. 1994b, Demircan et al., 1994), *RZ Psc* (Kalimeris et al. 1995), *V505 Sgr* (Rovithis-Livaniou et al. 1996b, Qian et al. 1998a), *UV Psc*, *ER Vul*, and *AR Lac* (Qian et al. 1998b, 1998c, and

1999b, respectively).

Only the abrupt period changes seems to be poorly supported, as is explained below.

Sudden period changes are not suitable for the description of an (O-C) diagram of an eclipsing binary for the following reasons:

- 1) they introduce arbitrary restrictions, since it is suggested to describe a random time-series, as an (O-C) diagram is, with an arbitrary and pre-chosen way.
- 2) the whole procedure is arbitrary, since both the **place** and the **number** of the suspected (or supposed) sudden changes are strongly depended on the **personal choice** of the investigator.
- 3) the mathematical description and the analysis of the observational material, based to a number of small linear parts, is not either self-consistent, nor unique dependent.
- 4) there is not any physical mechanism to produce such sudden period changes. Most of the earlier models proposed (e.g. the rocket effect, the sudden mass transfer, or coronal mass ejections), yielding to abrupt orbital period changes, have been proven to be inconsistent (Hall 1990).
- 5) they require immediately cutting in of the dynamical and thermal perturbations, although there is not any binary that could be back to a totally stable situation just after a sudden change of its orbital period, (e.g. Van't Veer 1972, 1991).

In spite of the foregoing referred reasons, sudden period variations are still in use (e.g. Kim 1991, Demircan and Derman 1992, Demircan and Selam 1993, Simon 1996 and 1997, Qian 2000, Qian et al. 2000ab, 2001ab, and many others).

A possible explanation is that in some cases, the orbital period variation is made in a very short interval of time. Thus, although there are not abrupt orbital period variations, but continuous changes made very rapidly, this rapid change gives the impression of an abrupt period variation. A very good example to see this very clearly is the *X Tri* case. In an analysis of this system, presented by Rovithis-Livaniou et al. (2000a), is shown -(their Fig. 3)- that a big period change occurred in a rather s

mall time interval.

It seems that some of the pioneers in the binary stars field, agree with these statement. For example, Batten (1973), on page 86 of his book, writes for the period variations of *RW Tau*: *the change in period of RW Tau appears to have been abrupt, but there is always sufficient observational error to obscure the distinction between an abrupt change and a very rapid change that was continuous.*

5. Summary Discussion and Conclusions

In this review the traditional as well as the new methods used to analyze an (O-C) diagram of an eclipsing binary were outlined. It was shown that:

Linear approximation is easy in use; moreover, it is very useful, mainly to observers, and especially to some amateurs, who are dealing with observations of minima times only. Linear fitting, on the other hand, can not be used to most of the systems, since it corresponds to constant orbital period, which is usually an exceptional case.

On the other hand, linear approximation can be applied to a small interval of time, if one wants to compute and propose a new ephemeris formula; but, we should keep in mind that this formula might not be valid for long (depending on the rate of period change).

The step variation technique, is absolutely inconsistent with the physics of eclipsing binaries, since there is no any mechanism that could produce abrupt period changes. Those proposed so far, are not valid any more, (Hall 1990), and in general, in most of the cases, there is **plenty of freedom** in choosing the intervals for fitting. Sterken (2000) refers to this subject as: "*the piecewise linear segments can point out the occurrence of a period jump, but cannot reveal exactly when such events do occur*". Moreover, one must be very careful and special attention has to be paid during their construction. In many cases, period jumps may not real, and might come from erroneous computation of the value of epoch E, especially in cases of very short period eclipsing binaries.

Second order approximation, (the classical parabola fitting), corresponds to a continuous period variation, at a constant rate. There is physical support for such a change, but as was shown, it is not suitable in all cases. This seems to be more and more clear, as much more observational material is added. A good example to recognize this is the *XX Cep* case. In this, when newer data were used (Mayer 1984), it was found that the classical parabola fitting that had been earlier applied (Rafert 1982), was not good enough any more.

It is also worthwhile to mention, Wood and Forbes (1963) work, where some (O-C) diagrams of eclipsing binaries were described using a third order approximation. They did so, in cases where this was impossible with any other of the known methods, at that time.

A sinusoidal fitting, although has been satisfactorily used in many cases, is restricted, and this might yield to erroneous results. A good example to present this is the *AK Her* case. In this, when newer times of minimum light were used (Rovithis-Livaniou et al. 1999), it was shown that they did not follow the previously proposed sinusoidal variation (Tunca et al., 1987).

Moreover, sinusoidal variation, in some cases, is not consistent with the presence of a third body (Kreiner et al. 1994). In such cases, magnetic activity cycles can be also used (e.g. Demircan and Derman 1992, Qian et al. 1999b, Rovithis-Livaniou et al. 2000).

Much more cases is expected to be added in the examples previously referred for quadratic approximation, as well as for sinusoidal variations.

These as regards the traditional methods of an (O-C) diagram analysis. Concerning the new ones: this of Koen (1996) is statistical and has been applied so far to a rather small number of eclipsing binaries; that of Jetsu et al. (1997) to one system only.

On the other hand, the first continuous method, has been applied to a large number of eclipsing binaries of every kind. In Kalimeris et al. (1994a), the orbital period variations of four contact binaries were examined; namely of: *GK Cep*, *V502 Oph*, *V566 Oph* and *AH Vir*. The *AB And* system in (Kalimeris et al. 1994b); the *RZ Psc* in (Kalimeris et al. 1995); the *V505 Sgr* by Rovithis-Livaniou et al. (1996b), as well as by Qian et al. (1998a); the *UV Psc*, *ER Vul*, and *AR Lac* by Qian et al. 1998b, 1998c, 1999b, respectively; the *X Tri* (Rovithis-Livaniou et al. 2000); the *AK Her* (Rovithis-Livaniou et al. 2001a), and some semi-detached systems (Rovithis-Livaniou et al. 2001b).

Moreover, this method does not put any restriction, (as quadratic or sinusoidal approximations do), and is well supported by physical mechanisms (Kalimeris et al. 1994b, 1995; Qian et al. 1998a,b,c, 1999b).

Besides, it is worthwhile to mention that the classical way of (O-C) curves analysis emerges as a specific application of Kalimeris et al. (1994a) method. This is obvious from the following:

Suppose that $T(E)$ is given by: $\Delta T(E) = c_1 E_N + c_0$.

Then, $\dot{P}(E) = 0$ and $\Delta P(E) = 0$

That is, the well known fact: *whenever an (O-C) diagram exhibits linear sections, the period remains constant.*

Moreover, suppose that $T(E)$ is given by:

$$\Delta T(E) = c_2 E_N^2 + c_1 E_N + c_0$$

Then:

$$\dot{P}(E) = 2c_2 \text{ and } \Delta P(E) = 2c_2$$

which is another well known result: *whenever an (O-C) diagram exhibits parabolic arcs, the period is changing at a constant rate.*

For the above mentioned reasons, it is clear that the first continuous method proposed and developed by Kalimeris et al. (1994a) is a remarkable and reliable method.

The appearance of an (O-C) diagram, is strongly depended on the ephemeris formula used to construct it. For this reason, some investigators are using different ephemeris formulae, as well as different approaching ways to describe an (O-C) diagram. See for example the *AM Leo* case in the paper by Demircan and Derman (1992), where 1) a linear least square fitting, 2) three linear segments, and 3) a fifth degree polynomial were used for its (O-C) diagram description. Doing so, and because of the strong dependence of the appearance of an (O-C) diagram on the ephemeris formula used, they are hoping that another look will help them to get an idea for a possible hidden periodicity. But this is not a proper way to search for periodicities. Kalimeris et al. (1994b) have shown, (see Appendix I, of their paper), that: *The orbital period $P(E)$, as well as its spectrum, remain invariable -within the errors of least squares description of an (O-C) diagram- irrespective of the ephemeris used to calculate the (O-C) differences.* It is thus suggested that searching for periodicities, one has to analyse the $P(E) - P_e$ function which remains **invariant** and is independent of the ephemeris used, and not the (O-C) diagram which varies according to the ephemeris.

Finally, dealing with (O-C) diagrams of eclipsing binaries, one has to be patient, and do not come to conclusions that may be proven wrong afterwards. Especially when the results are covering a small time interval, and if there is an undetected third companion in the system. Many years of observational material is needed to get reliable results.

Acknowledgements. This work was partly financial supported by Athens University (grant No. 70/4/3305). This work has made use of the Simbad database, operated at CDS, Strasbourg, France.

References

Abhyankar K.D., Panchatsaram T.: 1982, *BASI*, **10**, 315.

- Abhyankar K.D., Panchatsaram T.: 1984, *MNRAS*, **211**, 75.
- Applegate J.H.: 1992, *Ap.J.*, **385**, 621.
- Bakos G.A.: 1977, *BAICz*, **28**, 157.
- Batten A.: 1973, *Binary and Multiple Systems of Stars*, Pergamon Press Ltd.
- Berrington R.C., Hall D.S.: 1994, *A.J.*, **107**, 1868.
- Chochol D., Pribulla T., Rovithis-Livaniou H., Rovithis P., Kranidiotis A.: 1998, *Contrib. Astron. Obs. Skalnaté Pleso*, **28**, 51.
- Borkovits T., Hegedus T.: 1996, *As.Ap.S*, **120**, 63.
- Chambliss C.B.: 1976, *PASP*, **88**, 22.
- Demircan O., Derman E., Akalin A.: 1990, *A.J.*, **101**, 201.
- Demircan O., Derman E.: 1992, *A.J.*, **103**, 593.
- Demircan O., Selam S.O.: 1993, *As.Ap.S*, **98**, 513.
- Demircan O., Derman E., Akalin A., Selam S., MUYESSEROGLU Z.: 1994, *MNRAS*, **267**, 19.
- Hall D.S.: 1975, *Acta Astron.*, **25**, 1.
- Hall D.S., Kreiner J.M.: 1980, *Acta Astron.*, **30**, 387.
- Hall D.S.: 1990, in *Active Close Binaries*, (Ibanoglu Ed), Kluwer Publ. Co., Dordrecht, Holland, 95.
- Herczeg T.J.: 1993, *PASP*, **105**, 911.
- Jetsu L., Pagano I., Moss D., Rodono M., Lanza A.F., Tuominen I.: 1997, *As.Ap.*, **326**, 698.
- Kalimeris A., Rovithis-Livaniou H., Rovithis P.: 1994a, *As.Ap.*, **282**, 775.
- Kalimeris A., Rovithis-Livaniou H., Rovithis P., Oprescu G., Dumitrescu A., Suran M.D.: 1994b, *As.Ap.*, **291**, 765.
- Kalimeris A., Mitrou C.K., Doyle J.G., Antonopoulou E., Rovithis-Livaniou H.: 1995, *As.Ap.*, **293**, 371.
- Kalimeris A., Rovithis-Livaniou H., Rovithis P.: 2001, *As.Ap.*, in press.
- Kim C-H: 1991, *A.J.*, **102**, 1784.
- Kim C-H, Jeung J-H, Demircan O., MUYESSEROGLU Z., Budding E.: 1997, *A.J.*, **114**, 2753.
- Koen C.: 1996, *MNRAS*, **283**, 471.
- Koen C.: 2001, *MNRAS*, **325**, 1124.
- Kreiner J.M.: 1977, in IAU Coll. No. 42, *The Interaction of Variable Stars with their Environment*, eds. Kippenhahn, Rahe and Strohmair, 393.
- Kreiner J.M., Pajdosz G., Tremko J., Zola S.: 1994, *As.Ap.*, **285**, 459.
- Lanza A.F., Rodono M.: 1999, *As.Ap.*, **349**, 887.
- Mayer P.: 1984, *BAICz*, **35**, 180.
- Mayer P.: 1997, *As.Ap.*, **324**, 988.
- Panchatsaram T., Abhyankar K.D.: 1981, *BASI*, **9**, 243.
- Pribulla T., Chochol D., Rovithis-Livaniou H., Rovithis P.: 1997, *IBVS*, **4435**.
- Qian S-B.: 2000, *As.Ap.Suppl.*, **146**, 377.
- Qian S-B.: 2001a, *A.J.*, **121**, 1622.
- Qian S-B.: 2001b, *A.J.*, **122**, 1561.
- Qian S-B, Liu Q-Y.: 2000, *As.Ap.*, **355**, 171.
- Qian S-B, Ma Y.: 2001, *PASP*, **113**, 754.
- Qian S-B, Liu Q-Y, Tan W.: 2000, *Ap.Sp.Sci.*, **274**, 859.
- Qian S-B, Liu Q-Y, Yang Y-L.: 1998a, *Publ. Yunan Obs.*, **75**, 1.
- Qian S-B, Liu Q-Y, Yang Y-L.: 1998b, *Ch.As.Ap.*, **23**, 317.
- Qian S-B, Liu Q-Y, Yang Y-L.: 1998c, *Ap.Sp.Sci.*, **257**, 1.
- Qian S-B, Liu Q-Y, Yang Y-L.: 1999a, *As.Ap.*, **341**, 799.
- Qian S-B, Liu Q-Y, Yang Y-L.: 1999b, *Acta Astron. Sinica*, **40**, 26.
- Qian S-B, Liu Q-Y, Yang Y-L, Yuan L-L.: 2000b, *Acta Astron. Sinica*, **41**, 36.
- Radhakrishnan K.R., Abhyankar K.D., Sarma M.B.K.: 1984, *BASI*, **12**, 182.
- Rafert J.B.: 1982, *PASP*, **94**, 485.
- Rovithis-Livaniou H., Niarchos P.G., Rovithis P.: 1993, *IBVS*, No. **3861**.
- Rovithis-Livaniou H., Rovithis P., Kalimeris A., Oprescu G., Dumitrescu A., Suran M.D.: 1994, *Rom. Astron. J.*, **4**, 135.
- Rovithis-Livaniou H., Rovithis P., Kalimeris A.: 1996a, *Odessa Astron. Publ.*, **9**, 51.
- Rovithis-Livaniou H., Kranidiotis A., Rovithis P., Kalimeris A.: 1996b, in *Physical Properties in Interacting Binaries*, (Chochol et al. Eds.), 14.
- Rovithis-Livaniou H., Rovithis P., Kranidiotis A., Chochol D., Pribulla T.: 1998, *IBVS*, **4563**.
- Rovithis-Livaniou H., Kranidiotis A., Fragouloupoulou E., Sergis N., Rovithis P.: 1999, *IBVS*, **4713**.
- Rovithis-Livaniou H., Kranidiotis A., Rovithis P., Athanassiades G.: 2000, *As.Ap.*, **354**, 904.
- Rovithis-Livaniou H., Fragouloupoulou E., Sergis N., Rovithis P., Kranidiotis A.: 2001a, *Ap.Sp.Sci.*, **275**, 337.
- Rovithis-Livaniou H., Kalimeris A., Kranidiotis A., Athanassiades G., Rovithis P.: 2001b, in *Evolution of Binary and Multiple Star Systems*, 229.
- Selam S.O., Demircan O.: 2000, in *Variable Stars as Essential Astrophysical Tools*, (Ibanoglu Ed), Kluwer, Dordrecht, Holland, 605.
- Simon V.: 1996, *As.Ap.*, **311**, 915.
- Simon V.: 1997, *As.Ap.*, **319**, 886.
- Sterken C.: 2000, in *Variable Stars as Essential Astrophysical Tools*, (Ibanoglu Ed), Kluwer, Dordrecht, Holland. 529.
- Tunca Z., Keskin V., Acan C.M., Evren S., Ibanoglu C.: 1987, *Ap.Sp.Sci.*, **136**, 63.
- Tsesevich V.P.: 1973, *Eclipsing Variable Stars*, J. Wiley, New York.
- van't Veer F.: 1972, *As.Ap.*, **20**, 131.
- van't Veer F.: 1993, *As.Ap.*, **250**, 84.
- Wood D.B., Forbes J.E.: 1963, *A.J.*, **68**, 257.
- Yamasaki A.: 1975, *Ap.Sp.Sci.*, **34**, 413.

CCD OBSERVATIONS OF THE POLAR AM HERCULIS

S.Yu. Shugarov¹, N.I. Ostrova²¹ Sternberg State Astronomical Institute, Moscow State University, Moscow 119899 Russia² Department of Astronomy, Odessa National UniversityT.G.Shevchenko Park, Odessa 65014 Ukraine, *astro@paco.odessa.ua*

ABSTRACT. Results of two CCD runs of V observations of AM Her obtained on August 1 and 2, 1998 are reported. The moment of minimum brightness at $HJD\ 2451027.4014 \pm 0.^d0012$ is in a good agreement with an ephemeris by Andronov et al. (2001).

Key words: Stars: binary: cataclysmic; stars: individual: AM Her

AM Her was observed at the 38cm telescope of the Crimean Astrophysical Observatory equipped with a CCD camera ST-7 in the V filter with the exposure varying from 60 to 90 sec. These runs were obtained on August 1 (HJD 2451027.3369 – .4234) and 2 (HJD 2451028.3423 – .3914), 1998 as a part of the campaign of the observations simultaneous with that obtained at the 6m telescope of the Russian Academy of Sciences by N.N.Somov and T.A.Somova.

The star was in its intermediate state, varying in the range Δm from $0.^m76$ to $2.^m04$ during the first run and $0.^m68$ – $1.^m19$ during the second run. The amplitude in the second interval is underestimated, as the observations cover only 0.4 of the cycle, being close to the maximum of brightness. The comparison star is "d" (Liller, 1977) with $V = 13.^m10$.

We have used the recent ephemeris

$$Min.HJD = 2446637.0510(6) + 0.12892711(3)E \quad (1)$$

(Andronov et al., 2001), which was based on 267 timings. The latest review on AM Her may be found in this volume (Andronov, 2001). The extensive multi-wavelength photometric and polarimetric study of AM Her is presented by Shakhovskoy et al. (2001).

The light curve is shown in Fig. 1. To avoid systematic differences of the fits owed to various methods, we have used the method of "Running parabolae" with a filter half-width $\Delta t = 0.^d035$ adopted in previous studies (Shakhovskoy et al., 2001).

The broad minimum was observed at $HJD\ 2451027.4014 \pm 0.^d0012$ $\Delta m = 2.^m043 \pm 0.^m014$ at the phase -0.035 ± 0.009 , i.e. in an excellent agreement with the ephemeris. At the second night, the secondary minimum occurred at $HJD\ 2451028.3708 \pm 0.^d0044$ ($\Delta m = 0.^m965 \pm 0.^m026$) at the phase 0.485 ± 0.034

close to 0.5. However, during the first run, at the same phase the *maximum* is observed, which is followed by an interesting narrow minimum at $HJD\ 2451027.353$ at the phase 0.59. If interpreting both secondary minima as eclipses of the column of the same nature, the phase difference of $0.1P$ corresponds to the angle difference of $\sim 36^\circ$. Such drastic changes of the structure and position of the accretion column may be owed to the instability of the trajectory of the flow, rather than to the years-scale variations of the orientation of the magnetic axis of the white dwarf.

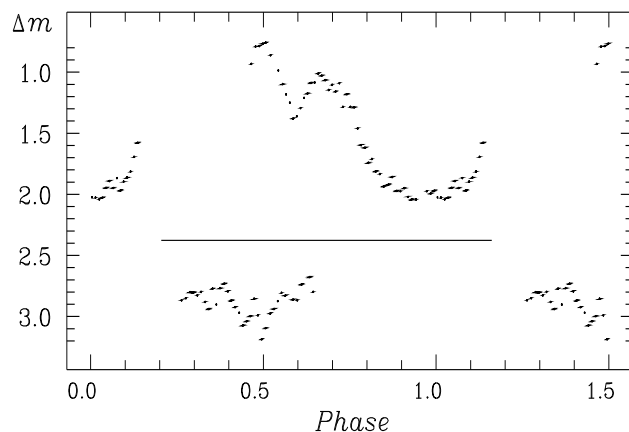


Figure 1: Light curves of AM Her on August 1 (up) and 2 (bottom), 1998. The bottom curve is shifted by $2.^m$ to avoid overlapping.

Acknowledgements. The authors are thankful to I.L.Andronov and V.P.Goranskij for their programs for time series analysis and CCD reduction, respectively.

References

- Andronov I.L.: 2001, *Odessa Astron. Publ.*, **14**, ??.
 Andronov I.L., Kolesnikov S.V., Shakhovskoy N.M.: 2001, *A.S.P. Conf. Ser.* (in press).
 Liller W.: 1997, *Sky Tel.*, **53**, N 5, 351.
 Shakhovskoy N.M., Andronov I.L., Kolesnikov S.V.: 2001, "Atlas and catalogue of the polarimetric and photometric characteristics of the magnetic cataclysmic variable star AM Her", Odessa, Astroprint, 240pp. (in preparation).

THE AM CVN SYSTEMS - THE FINAL STAGE OF BINARY WHITE DWARF EVOLUTION

J.-E. Solheim, M.R. Nasser

Department of Physics, University of Tromsø, 9037 Tromsø, Norway, *janerik@phys.uit.no*

ABSTRACT. The last decade has shown a surge in research on the Interacting Binary White Dwarf s (IB-WDs), or Helium CVs, also called AM CVn systems. We have witnessed long photometric campaigns, time resolved spectroscopy, UV and X-ray observations, and modelling of disc structure, disc atmosphere and their evolution. Recently several new members of the AM CVn family have been added, and a new subclass - double degenerate polars has been identified. A review of the research on AM CVn systems during the last decade is given, and some problems to be solved in the future are presented.

Key words: Stars: binary: cataclysmic; interacting; helium cataclysmic; stars: individual: AM CVn, HP Lib, V803 Cen, CR Boo, CP Eri, GP Com, CE 315, RX J1914+24

1. Introduction

The AM CVn objects are helium-rich analogues to the ER UMa cataclysmic variables - they have short orbital periods and a low mass secondary, transferring mass through the L1 point between the stars.

They evolve through common envelope phases to a close binary system, where the secondary appears as a low mass stellar core, either degenerate or semi-degenerate. Because of the close orbits, angular momentum is lost by gravitational radiation, and the orbits shrink until mass transfer takes place and the orbits again increase. During the common envelope phase the outer hydrogen atmosphere is lost, and we get systems with almost pure helium - at least in the outer parts.

Observations show that the AM CVn stars have orbital periods between 9 and 65 minutes, and that their orbits are increasing while the mass transfer rate is decreasing (Patterson et al. 2001). For the objects with periods more than 15 minutes the mass is transferred through an accretion disc which is made of almost pure helium. For periods between 15 and 30 minutes the discs show signs of non-circularity and thermal and tidal instabilities. Recently the first magnetic AM CVn object type polar, RX J1914+24 has been discovered (Cropper et al. 1998), with an orbital period of

only 9.5 min. This is an exciting discovery, and more possible polars are under investigation.

In the following we will give a review of the status of the research on the AM CVn objects, basically after 1994, when an extensive review was given by Warner (1995). We will start with a presentation of new research related to old and new members of the AM CVn family, and then discuss models for their evolution and challenges for future research.

2. The Family Members

Photometry shows that they have nova or dwarf nova like variability. Two of the objects (AM CVn and HP Lib) are stuck in a high, superoutburst state. For the objects with discs the light curve is modulated by a fundamental period, interpreted as the superhump period, and the FT of the light curve shows a series of harmonics, which are related to structures in the disc (Solheim & Provencal 1998)

Warner (1995) argued that the two members AM CVn and HP Lib are equivalent to H-rich nova-like variables with high mass transfer rate \dot{M} , which leads to a stable high state disc, and V803 Cen, CR Boo and CP Eri are the helium analogues of the VY Scl stars, moving from high to low states as a result of variations in \dot{M} (2), and that GP Com is probably a SU UMa analogue, spending long time in the low state with very infrequent superoutbursts. Skillman et al. (1997) argued that CR Boo is a "helium Z Cam star" (standstill slightly below maximum light) and a "helium ER UMa star" (very frequent short maxima) as well as a "helium SU UMa star" (superoutbursts punctuated by common superhumps). The same nomenclature may be used for V803 Cen and CP Eri.

Some of the AM CVn stars: AM CVn, CR Boo and GP Com are weak, soft X-ray emitters (Ulla 1995). The X-rays come from the accretor or the inner part of the accretion disc and is evidence for non-magnetic behaviour (Teeseling et al. 1996). A reanalysis of the ROSAT Position Sensitive Proportional Counter (PSPC) data for AM CVn gave as a best fit a black-body source of temperature $\sim 3 \times 10^6$ K from a hot boundary layer between the disc and the white dwarf

Table 1: Basic data for for AM CVn family members.

Object	V	P_{orb}	P_{sh}	q
RX J1914+24	>19.7	569		
AM CVn	13.7-14.2	1029	1051	.084
HP Lib	13.7	1103	1119	.060
CR Boo	13.0-18.0	1471	1488	.037
V803 Cen	13.2-17.4	1611	1618	.014
CP Eri	16.5-19.7	1701	1716	.029
KL Dra	16.8-20	unknown		
GP Com	15.7-16.0	2790		.02
CE 315	17.5	3906		.022

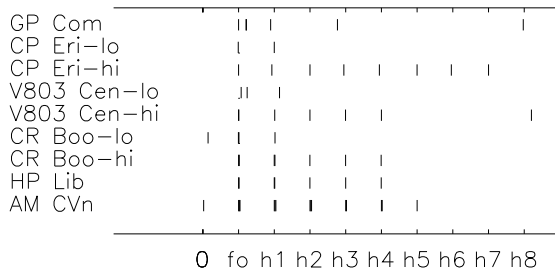


Figure 1: Modulation frequencies observed for AM CVn objects. Frequencies detected are shown relative to a fundamental frequency f_0 which is the superhump frequency if that is detected, otherwise the orbital frequency. Thicker bars tell that closely spaced signals in frequency exists.

(Kellogg et al. 2000). GP Com also shows X-ray modulations both in flux and hardness ratio with its orbital period (Teeseling & Verbunt 1994), which may be explained by modulations of the accretion stream on to the accreting object.

Table 1 gives some basic data for the AM CVn family. In this table P_{orb} is the orbital period, P_{sh} is the superhump period, and $q = M(2)/M(1)$ which is determined by the formulae (1) in Warner (1995), except for GP Com and CE 315 where q is determined by spectroscopy. References for each object are given in the subsections below. Data for orbital and superhump periods are mostly from Patterson (2001) and Patterson et al. (2001).

Figure 1 shows the modulation frequencies observed for the AM CVn systems. f_0 is the fundamental frequency, which for the disc-objects is the superhump frequency, and hn is the harmonics of number n .

2.1. The Novalike: AM CVn And HP Lib

For AM CVn there has long been a controversy on

what is the orbital period and what is the superhump period. Based on WET observations in 1990, Provencal et al. (1995) and Solheim et al. (1998), concluded that the period 1051 s was stable over time and should therefore be the orbital period, even if the period itself was not detected in the FT of the light curve, while the low amplitude 1029 s peak was the superhump period, classifying AM CVn as a negative superhumper.

Harvey et al. (1998) proposed $P=1029$ s as the orbital period. Skillman et al. (1999) observed the star for 670 hr over 227 nights in the period 1992-1999, and concluded that $P=1029$ s is the orbital period and $P=1051$ s is the superhump period, with 5 harmonics and sidebands representing periods of *apsidal advance* Ω and *nodal regression* N of 13.36 and 16.69 hr, respectively.

The controversy is finally put to rest with the detection of a clear S-wave in spectra folded on the 1029 s period, and at the same time Doppler tomography showing a prominent hot spot superimposed on a weak disc emission when folded on this period (Nelemans et al. 2001a).

So far secondary objects in any AM CVn system have not been observed in their spectra. The reason for this is that they are sub-luminous, and do not show up as infrared objects as normal CV secondaries do. The short orbital periods bring them close to the hot disc and the hot primary, and their atmospheres are irradiated and heated up to the same temperature as the outer part of the disc (Nymark 1997). Figure 2 shows how the secondary and the disc spectrum adds up in the AM CVn case.

For the second nova like, HP Lib, a 70 hr photometric campaign revealed the 4 harmonics of the fundamental periods, and its similarity with AM CVn (Aminzade et al. 1999). A more substantial campaign covering 720 hr over 185 nights, reported by Patterson et al. (2001) shows that the main photometric signal varies between 1118.89 and 1119.14 s on a time scale of a few years, and displays a waveform characteristics of superhumps. After subtracting the main signal they found a weak residual signal at 1102.70 s, which they interpreted as the underlying orbital period of the binary. The full amplitude of this variation is just 5 mma, which makes it the weakest orbital signal yet found in a CV. The star showed remarkable constancy in magnitude and superhump behaviour, and displayed sidebands giving a precession period of $\Omega = 21$ hr. It has much more power in the fundamental period and much less power in the harmonics than AM CVn. This may be related to their different angles of inclination and different disc structures.

2.2. The Dwarf Novae

Six of the AM CVn systems are helium dwarf novae

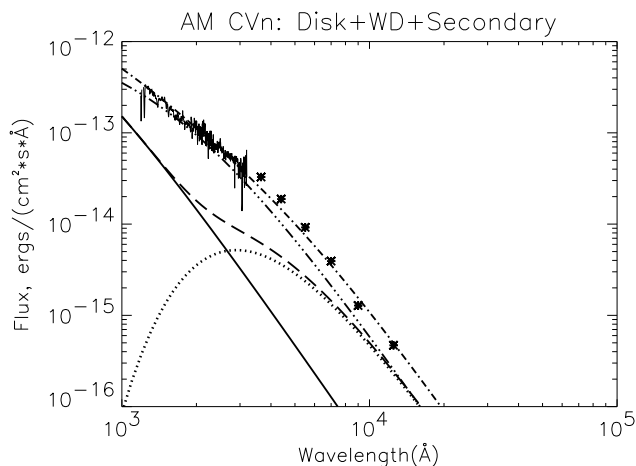


Figure 2: A combined model spectrum (dash-dot) consisting of a blackbody disc model (dash-triplet dots), an irradiated secondary star (dots) and a hot accreting white dwarf (solid line), that fits the observed IUE spectrum plus photometric points for AM CVn. The model parameters are $M_1 = 1.1M_\odot$, $\dot{M} = 3 \times 10^{-9}M_\odot/\text{yr}$, $R_{in} = 1.4R_1$, $R_{out} = 15R_1$, $i = 45^\circ$, $d = 288$ pc, $T_{eff} = 10\,000\text{K}$ for the secondary star and for the central star $T_{eff} = 1.0 \times 10^5$ K (Nasser et al. 2001).

analogues. 4 of these have frequent dwarf nova outburst and two are SU UMa analogues, spending a long time in the low state with very infrequent superoutbursts. Due to the rapid variability – the changes can be of the order 0.1 mag/hr – stable light curves over long periods of time are difficult to obtain, and spectra change continuously.

2.1.1 Dwarf Novae: CR Boo, V803 Cen CP Eri

An intensive photometric campaign for CR Boo in 1996 (Patterson et al. 1997) confirmed the orbital period of 1471 s which was found in the first WET campaign (Provencal et al. 1997). This signal kept its phase and amplitude despite erratic variations of the total brightness. In addition Patterson et al. (1997) proved that the signal with period 1486 – 1494 s is the superhump period, which at the end of an outburst stabilised itself at $P=1487.29$ s. They also found that CR Boo for two weeks went into a quasi periodic *cycling stage* with $P \sim 19$ hr between the high and low states. From the beat between the superhump period and the orbital period an eccentric precession of the accretion disc with period $P \sim 36$ hr can be calculated. This was also observed as a skewness variation in absorption lines (Patterson et al. 1997).

Photometry of V803 Cen in the period 1992-1999 (Patterson et al. 2000) showed a strong periodic signal at $P=1618$ s with harmonics, which resembles the superhumps associated with the other AM CVn ob-

jects. However, it is unusual because it appears to endure through all brightness states, even down to $V=17$. The system also shows some times a periodic signal at $P=1612$ s which by Patterson (2001) is interpreted as the orbital period. The star is occasionally stuck in a cycling stage with a quasi period of $P \sim 22$ hr in the magnitude range 13.4–14.5 and shows in addition a period of ~ 5 days between outbursts from the lowest state at $V=17.2$ (Patterson et al. 2000).

Spectroscopy is done of CP Eri in its low state by Groot et al. (2001). They found a spectrum dominated by He I emission lines, as observed for GP Com and CE 315. All clearly identified lines were double-peaked, which is an indication of lines formed in a rotating accretion disc. One marked difference was observed with respect to GP Com and CE 315: No central low radial velocity amplitude peak was seen in the He I line profiles, and the presence of Si II lines points to a progenitor with solar metallicity (Marsh et al. 1991). They conclude that CP Eri has lower than solar metallicity but is certainly not as metal poor as GP Com and CE 315.

The helium accretor GP Com has been studied by Marsh (1999) and he confirms the S-curve with period 46.52 min and the absence of hydrogen and the presence of strong helium and nitrogen emission lines. This is consistent with seeing material from the core of a star that has undergone hydrogen burning and CNO-cycle processing of most of the carbon and oxygen into nitrogen. Marsh (1999) also found erratically variability in the emission lines. The He II line at 4686 Å changed most, which is consistent with X-ray driven photoionization. The flaring part of the line profiles are broader than the average, as expected if they originate in the inner, unstable, 1/4 of the disc. Marsh (1999) also detected a small radial velocity variation with a semi-amplitude of ~ 10 km s $^{-1}$ in the sharp component in the centre of the emission lines, which indicates that it comes from the accreting star. He found q of the order 0.02, as expected on evolutionary grounds.

2.1.2 New Members: KL Dra and CE 315.

KL Dra was first identified as a supernova (SN 1998di), but a spectrum showing shallow He I absorption features at zero relative velocity, made an identification as an AM CVn object of the dwarf nova type in outburst more likely (Jha et al. 1998). The magnitude at discovery was 16.8. Because of its variability we expect an orbital period between 20 and 40 minutes.

A new member of the family, CE 315 – much like GP Com – was discovered during a spectroscopic follow up of proper-motion stars in the Calán-ESO Catalog (Ruiz et al. 2001). The object was found to have a spectrum consisting of a blue continuum with strong emission lines of He I and He II, with a handful of faint lines

of nitrogen. The He lines exhibit triple peaked profiles with remarkably broad widths of $\sim 2000 \text{ km s}^{-1}$. Ruiz et al. (2001) find an orbital period of 65.1 min and a mass ratio $q=0.022$. The line profiles consists of a double peaked profile from the disc, and a central, occasionally quite strong peak, which may originate from the accreting object.

2.3. New Class Of Members: AM CVn Polars

The X-ray object RX J1914+24 was identified as a polar with a degenerate secondary object by Cropper et al. (1998) on the basis of ROSAT observations with the PSPC and the High Resolution Imager (HRI). The object has an X-ray light curve with a single strong modulation at 569 s, which is interpreted as the orbital period of a synchronized binary system. I-band observations with the Nordic Optical Telescope (NOT) show the same period but with maximum out of phase with the X-ray peak flux (Ramsay et al. 2000). The I-band flux must be from the face of the donor star irradiated by the X-ray flux from the accreting region of the primary star. Since only one period is observed, a disc is not present, and the short period makes a double degenerate system the only possibility. In order to become a stable synchronized system the accretion torque must be balanced by a MHD torque from a magnetic field of the order a few MG (Ramsay et al. 2000).

This polar may be the first example of an electric powered star. Because of the short orbital period and large mass of the primary, huge electric currents are driven between the stars, and the energy of these currents is liberated at the magnetic poles of the magnetic white dwarf and X-rays are generated. Much of the observed flux may come from this energy source (Wu et al. 2001).

Another source RX J0806+1527 has similar X-ray characteristics, showing a single period $\sim 321 \text{ s}$ pulsation. It has $B=20.5$ with no red counterpart (Israel et al. 1999), and may be another member of the polar branch of the AM CVn family.

3. Disc Atmosphere And Structure

A remarkable paper on the spectral properties of AM CVn was published by Voikhanskaya (1982). She observed in the prime focus of the six-meter telescope in 1978 and 1980 and noted many details in the spectrum which have much later been confirmed. In addition to the broad He I lines, she identified an emission feature at $\lambda 4640 \text{ \AA}$ as the C III–NIII blend, which is also observed in many X-ray sources, and also the faint He II emission at $\lambda 4686 \text{ \AA}$. She also noted emission peaks inside the He I absorption lines which moved with time, and that the absorption line edges also moved with

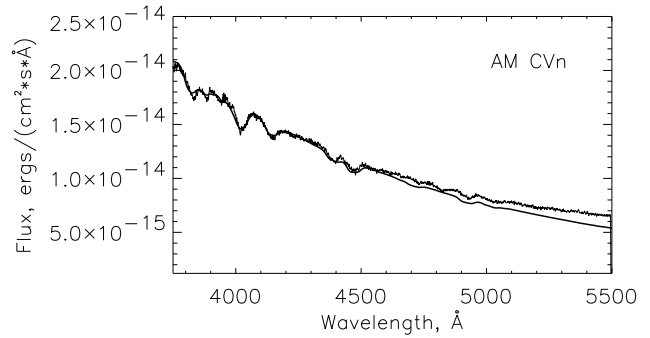


Figure 3: Observed AM CVn spectrum (thin line) fitted with NLTE a pure helium disc atmosphere model (thick line) with the following parameters: $M(1) = 1.1M_{\odot}$, $\dot{M} = 3 \times 10^{-9} M_{\odot}/\text{yr}$, $R_{in} = 1.4R_1$, $R_{out} = 15R_1$, $i = 45^{\circ}$ and $d = 288 \text{ pc}$. R_1 is the radius of the central star. The excess flux beyond 5000 \AA may be a sign of the donor star (Nasser et al. 2001).

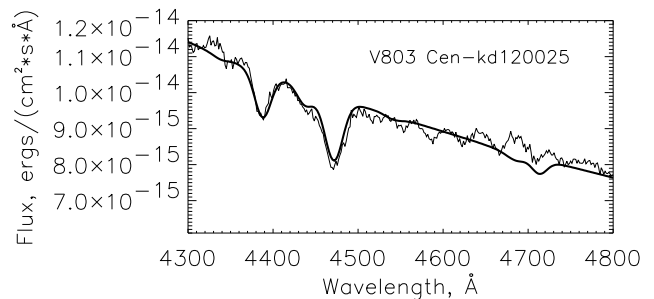


Figure 4: Observed V803 Cen (thin line) fitted with a pure helium NLTE disc atmosphere model (thick line) with the following parameters: $M(1) = 1.2M_{\odot}$, $\dot{M} = 3 \times 10^{-9} M_{\odot}/\text{yr}$, $R_{in} = 1.4R_1$, $R_{out} = 15R_1$, $i = 5^{\circ}$ and $d = 380 \text{ pc}$. (Nasser 2001).

time. Recently it is found that the emission peak variability shows an S-wave with period 1029 s identified as the orbital period (Nelemans et al. 2001a), and the movement of the absorption line edges has revealed the 13.4 hr precession period of the disc (Patterson et al. 1993).

3.1. Disc Atmosphere Models

The main contribution to the flux observed in the optical region for the AM CVn objects is from the disc (Figure 2). Disc spectra can be calculated for geometrical thin discs and depend on the following parameters: The mass of the accreting star: $M(1)$, the mass transfer rate: \dot{M} , and the inner and outer radii of the disc: R_{in} and R_{out} , and the disc inclination: i . In addition the abundance, in particular the H/He ratio is important.

El-Khoury and Wickramasinghe (2000) has calcu-

lated synthetic disc spectra for a range of parameters and fitted them to observed spectra of AM CVn and CR Boo. They use a χ^2 minimisation technique to determine the best fit in a grid of acceptable models, but reduce their number of free parameters by keeping the disc size between the Roche Lobe radius R_{L1} and the maximum radius for the last stable orbit in the restricted three body problem R_{st} . Their best fits for AM CVn and CR Boo are given in table 2. In addition they find upper values for the hydrogen to helium number density ratios to be 10^{-2} to 10^{-3} , which they claim is consistent with a helium-degenerate donor surrounded by a helium-rich envelope. The mass transfer rates determined place the objects in the region of a thermally-stable disc for AM CVn and thermally unstable for CR Boo.

Another approach has been taken by Nasser et al. (2001) who used the TLUSDISK code to calculate NLTE accretion disc models. NLTE models give differences in line equivalent widths between 10 and 40 per cent for certain temperatures or mass transfer rates, and may be a better approximation than the LTE models.

We observed 4 of the AM CVn systems with the NOT during 3 observing seasons, and determined the best set of parameters that fitted the observed spectra. Figures 3 and 4 give examples of the best fits for two of the objects: AM CVn itself and V803 Cen. For this model fitting procedure the inner and outer radius of the disc and the mass of the accretor is determined from photometry, and only allowed to vary within the uncertainty limits. The parameters determined from the spectra are given in table 2 and shown in Figure 5. In none of the spectra the H_γ is detected, and the model calculations show that this gives us an upper limit of the number density of H/He of 10^{-5} . For all the observed objects the mass transfer rate is so high that it indicates a stable disc, which is not obviously true for the dwarf nova like objects CR Boo and V803 Cen. This discrepancy may be due to the observations done only in the outburst state, and that the objects on the average have lower mass transfer rates.

3.2 Disc Structure

The AM CVn systems have all a mass ratio, $q < 0.1$. Simulations have shown (Whitehurst 1988) that discs with such small mass ratios will develop asymmetries due to tidal stress produced by parametric resonance between particle orbits and an orbiting secondary star with a 1:3 period ratio. The initially circular disc is deformed into a slowly precessing disc. Hirose and Osaki (1990) found a similar result and in addition noted that the difference between the superhump period and the orbital period is a function of the mass ratio: q . Using this relation, and a mass-radius relationship for the

secondary, which radius is determined from the Roche Lobe size at a given period, the mass of the primary object can be determined (Warner 1995).

For the AM CVn stars 3-D SPH models of helium accretion discs with small q values have been calculated by Wood and Simpson (1995), and they have also computed the energy production time series that display remarkable similarities with the observed light curves (Simpson & Wood 1998). These calculations show that the disc during one orbital revolution changes its shape from circular to elliptical, and that the stress in the disc when it is non-circular produces more energy, which leads to a pulse profile which can be compared with the observed profiles from the light curves. The pulse will change with time, giving a more triangular shape of *young* pulses from a newly formed disc, than for the more pulses from more mature (*old* discs which are confined to a smaller part of the period).

From the SPH calculations it is also found that spiral shocks appear near the outer edges of the discs, and that the appearances of spiral shocks will have a noticeable effect on the light curve, producing the higher harmonics in the FT of the light curve (Simpson et al. 1998). They also show that the amplitudes of the harmonics are very sensitive to the angle of inclination, and that the time series amplitude spectra for inclination angles $i < 45^\circ$ are dominated by the superhump frequency, but that linear combinations of the superhump and orbital frequencies appear at higher inclinations.

3.2.1 Discoseismology

A special feature of the photometric light curves of the AM CVn stars with discs is the appearance of harmonics in the times series amplitude spectra as shown in Figure 1. The number of harmonics and their relative amplitude is obviously a function of properties of the disc. For AM CVn itself 13 modulation frequencies were detected in the WET campaign in 1990 (Solheim et al. 1998). These frequencies are all related to 3 independent frequencies: ω , Ω , and N with harmonics of the orbital frequency ω and sums and differences of the type $n\omega - m\Omega$, where $m = 1, \dots, n$ are a manifestation of the positive superhump, and this $\pm N$ demonstrate the negative superhump (Skillman et al. 1999).

Simulations as described in the section above (Simpson et al. 1998), show that the synthetic light curve produced also show harmonics, in particular for high values of inclination, and we expect that the relative amplitudes of the harmonics may be related to the visibility of the spiral shocks that appear in the discs (Solheim & Provencal 1998). The relation between the harmonics and disc structure may be a way to investigate discs, we may call it *discoseismology*, and should be explored in more detail (Solheim 1999).

Table 2: Parameters determined from disc spectra.

Object	$M(1)/M_{\odot}$	$\log(\dot{M}(M_{\odot}/\text{yr}))$	i	B
AM CVn ¹	0.84	-8.8	45°	
AM CVn ²	1.1	-8.5	45°	
HP Lib ²	1.1	-8.4	28°	
CR Boo ¹	0.94	-8.9	44°	
CR Boo ²	1.0	-8.4 to -8.2	30°	14.7-13.9
V803 Cen ²	1.2	-8.5 to -8.3	5°	14.8-14.3

Notes: 1. El-Khory & Wickramasinghe 2000; 2. Nasser 2001

Figure 1 shows that there is a difference in the pattern of the harmonics when objects go from the high state to the low state. This must reflect changes in the structure or size of discs. Discoseismological studies of AM CVn dwarf nova type objects which go from high to low states and back may reveal how disc structures evolve through an outburst.

4. Evolution – From Common Envelope to Helium CV

One model for formation of AM CVn systems (Tutukov & Yungelson 1996) is the formation of close white dwarfs during two phases of common envelope evolution in which a substantial mass is lost from the system. The initial mass of the primary is between 1.5 and 6 M_{\odot} . The emission of gravitational waves will subsequently bring the two white dwarfs in a semi-detached phase and mass transfer will start. The Tutukov & Yungelson (1996) evolution calculations predict that at the time of the start of stable mass transfer the secondary white dwarfs must have masses between ~ 0.3 and $\sim 0.13M_{\odot}$ and the mass function for the accretors peaks at 0.65-0.75 M_{\odot} , which is 0.05 M_{\odot} higher than the normal WD mass distribution peak.. They claim that a non-degenerate secondary is not possible, but allow for a larger radius for the secondary than a zero temperature white dwarf has.

An alternative route of evolution is that the donor star is replaced by a helium star that becomes semi-degenerate and dim during the mass transfer (Iben & Tutukov 1991). A population synthesis (Nelemans et al. 2001b) has compared the two models for AM CVn stars evolution. They find that for the first route possibly no accretion disc forms at the onset of the mass transfer. The stability and the rate of mass transfer then depend on the tidal coupling between the accretor and the orbital motion. If this coupling is not efficient most systems merge, and the formation rate of AM CVn stars becomes very low. In this case the magnetic coupled systems are almost the only ones to survive. RX J1914+25 may be such a system. In the

second channel of formation – from a helium star that stops burning – the formation of AM CVn stars may be prevented by explosive burning of the helium layer which may cause detonation of the CO white dwarf accretor and the disruption of the system.

Nelemans et al.(2001b) combine their population synthesis results into two models, one *efficient*, in which the stability of mass transfer is not affected by the absence of an accretion disc and explosive helium burning happens when 0.3 M_{\odot} has accumulated, and one *inefficient* model in which the the absence of an accretion disc is very important and the explosive helium burning disruption starts already when 0.15 M_{\odot} has accumulated. In the inefficient model only one in 30 potential AM CVn systems evolve from double white dwarfs. In the efficient route both progenitor families produce a comparable number of observable system.

4.1 Comparison Of Two Routes Of Evolution

It is now possible to test the evolutionary scenarios in a more direct way, by comparing the calculated relations between orbital periods and mass transfer rates for the two routes of evolution with the mass transfer rates determined from spectra (Tables 1, 2). The result is shown in Figure 5 where we have drawn the evolutionary relations for degenerate and semi-degenerate secondaries and show the mass transfer rates calculated from our spectra as diamonds with error bars. The error bars also include systematic errors in determining the rate, and are quite long for the dwarf nova objects since they are observed only in a high state. The figure also include the results of El-Khory & Wickramasinghe (2000) for the two objects AM CVn and CR Boo. In the figure we have also drawn the the border line between stable and unstable discs according to the thermal-tidal instability calculated by Tsugawa & Osaki (1997). The conclusion is that all the 4 objects with discs have mass transfer rates far too high to have degenerate secondaries. The only evolutionary route for these is the helium secondary that becomes semi-degenerate.

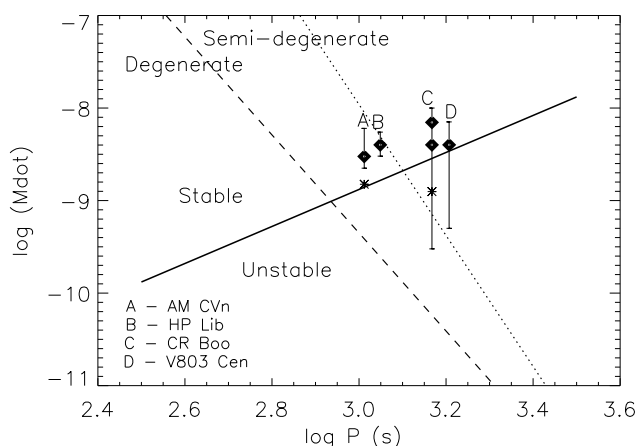


Figure 5: The mass transfer rate versus period for the AM CVn objects as calculated by Nasser et al (2001) and Nasser (20001) are shown as diamonds with error bars representing the systematic errors due to the observations done at a particular phase. Also the results of El-Khory & Wickramasinghe (2000) are included as stars. The solid line is the border between the thermally stable (upper part) and unstable discs (lower part) (Tsugawa & Osaki 1997). The dashed line is the evolution calculated for systems with a white dwarf secondary and the dotted line is the evolution of systems with a semi-degenerate pure helium atmosphere secondary with a C-O core (Nelemans et al. 2001b).

4.2. Future Evolution

Some time in the future the accretion will cease, and the stars will again come closer by loss of angular momentum by Gravitational Radiation. A new period of low mass transfer may take place. Finally the degeneracy of the secondary will be completely lifted, and no material can be transferred. The end product can be a helium type white dwarf (DB) with a small object, maybe planet or brown dwarf, in orbit. A search for such objects has started, but no convincing example has been found yet.

The accreting object may have undergone several helium flashes, and this may make the stellar interior different from normal stars. We may also find signs of magnetic field and circumbinary matter for some of the objects (Solheim & Sion 1994).

5. Conclusions

The smallness of these systems, and the closeness of the secondary, makes these systems laboratories for exciting physics. In the future we expect Gravitational Radiation to be detected from a large no of AM CVn systems by space borne devices. Hydrodynamic simulation of the particle flow through the discs and to the

accreting object may also be done. One day we may also discover a pulsating accreting AM CVn object, and get a possibility to test directly how the accretion can change the structure of a star.

The metallicity variations observed in the emission line objects CP Eri (low state), GP Com and CE 315 opens the possibility of constraining the evolutionary history of these system from the chemical composition of the transferred material. One remaining question is if some AM CVn systems have already evolved into DBs. This is related to the age of the Universe - at least the age of the nearby population in our galaxy.

Acknowledgements. This research is supported by a grant from the Norwegian Research Council. Observations are made with the Nordic Optical Telescope, operated on the island of La Palma jointly by Denmark, Finland, Iceland, Norway, and Sweden, in the Spanish Observatory del Roque de los Muchachos of the Instituto de Astrofisica de Canarias. The data presented here have been obtained using ALFOSC, owned by the Instituto de Astrofisica de Andalucia (IAAA) and operated at the Nordic Optical Telescope under agreement between IAA and the NBIfa of the Astronomical Observatory of Copenhagen.

References

- Aminzade R., Sullivan D.J., Jiang X. et al.: 1999, in 11th European Workshop on White Dwarfs eds J.-E. Solheim and E.G. Meištas, *ASP Conf Series*, **169**, 305.
- Cropper M., Harrop-Allin M.K., Mason K.O. et al.: 1998, *MNRAS*, **293**, L57.
- El-Khory W., Wickramasinghe D.: 2000, *As.Ap.*, **358**, 154.
- Groot P.J. Nelemans G. Steeghs D., Mash T.: 2001, *Ap.J.*, **558**, L127.
- Hirose M., Osaki Y.: 1990, *PASJ*, **42**, 135.
- Iben I. Jr., Tutukov A.V.: 1991, *Ap.J.*, **370**, 615.
- Israel G.L., Panzera M.R., Campana S. et al.: 1999, *As.Ap.*, **349**, L1.
- Jha, S., Garnavich P., Challis P. et al.: *IAU Circ.*, 6983.
- Kellogg E.M., González Pérez J.M., Solheim J.-E.: 2000, <http://www.astro.keele.ac.uk/workshop/xray/main.htm>
- Marsh T. R., Horne K., Rosen K.: 1991, *Ap.J.*, **366**, 535.
- Marsh T.R.: 1999, *MNRAS*, **304**, 443.
- Nasser R.M.: 2001, PhD thesis, University of Tromsø.
- Nasser R.M., Solheim J.-E., Semionoff D. A.: 2001, *As.Ap.*, **373**, 222.
- Nelemans G., Steeghs D., Groot P.J.: 2001a, *MNRAS*, **336**, 621.
- Nelemans G., Portegies Zwart S.F., Verbunt F., Yungelson L.R., 2001b, *As.Ap.*, **368**, 939.

- Nymark T.: 1997 in White Dwarfs eds J. Isern, M. Hernandez and E. García-Berro, Kluwer, 345.
- Patterson J., Halpern J., Shambrook A.: 1993, *Ap.J.*, **419**, 803.
- Patterson J., Kemp J., Shambrook A. et al.: 1997, *PASP*, **109**, 1100.
- Patterson J.: 2001, *PASP*, **113**, 736.
- Patterson J., Fried R.A., Rea R. et al.: 2001, *PASP*, submitted
- Provencal J.L., Winget D.E., Nather R.E. et al.: 1995, *Ap.J.*, **445**, 927.
- Provencal J.L., Winget D.E., Nather R.E. et al.: 1997, *Ap.J.*, **480**, 383.
- Ramsay G., Cropper M., Wu K. et al.: 2000, *MNRAS*, **311**, 75.
- Ruiz M.T., Rojo P.M., Garay G., Maza J.: 2001, *Ap.J.*, **552**, 679.
- Simpson J.C., Wood M.A., Burke C.J.: 1998, *Baltic Astronomy*, **7**, 255.
- Simpson J.C., Wood M.A.: 1998, *Ap.J.*, **506**, 360.
- Skillman D.R., Patterson J., Kemp J. et al.: 1999, *PASP*, **111**, 1281.
- Solheim J.-E., Sion E.M.: *As.Ap.*, **287**, 503.
- Solheim J.-E., Provencal J.L.: 1998, *Baltic Astronomy*, **7**, 277.
- Solheim J.-E., Provencal J.L., Bradley P.A. et al.: 1998, *As.Ap.*, **332**, 939.
- Solheim J.E.: 1999, in *Astrophysics with the NOT*, eds H. Kattunen and V. Pirola, Univ. of Turku, 188.
- Teeseling A., Verbunt F.: 1994, *As.Ap.*, **292**, 519.
- Teeseling A., Beuermann K., Verbunt F.: 1996, *As.Ap.*, **315**, 467.
- Tsugawa M., Osaki Y.: 1997, *PASJ*, **49**, 75.
- Ulla A.: 1995, *As.Ap.* **301**, 469.
- Voikhanskaya N.F.: 1982, *Sov.Astron.*, **26**, 558.
- Warner B.: 1995, *Ap&SS*, **225**, 249.
- Whitehurst R.: 1988, *MNRAS*, **232**, 35.
- Wood M.A., Simpson J.C.: 1995, *Baltic Astronomy*, **4**, 402.
- Wu K. et al.: 2001, *MNRAS*, submitted.

PHOTOMETRIC MONITORING OF SHORT-PERIOD CONTACT BINARIES

M. Vaňko

Astronomical Institute of the Slovak Academy of Sciences,
Tatranská Lomnica 05960 Slovakia, *vanko@ta3.sk*

ABSTRACT. The first photoelectric B, V light curves of the contact binary FU Dra, as well as new B, V light curves of the contact binaries AH Aur, UV Lyn and YY CrB, obtained at the Stará Lesná and Skalnaté Pleso Observatories, are presented. New photometric elements of AH Aur, FU Dra and UV Lyn computed from these light curves were combined with published spectroscopic elements to derive the absolute parameters of the systems.

Key words: Stars: binary: contact; stars: individual: FU Dra, UV Lyn, AH Aur, YY CrB

1. Introduction

Last year we started at the Astronomical Institute of the Slovak Academy of Sciences the program of photometric monitoring of neglected and faint short-period contact binaries. The aim of this program is to obtain the photoelectric light curves (LCs) of contact binaries, to study their orbital period and LCs changes. The LCs analysis provides photometric elements and in combination with published radial velocity curves also the absolute parameters of the studied systems. The LCs of contact binaries and their analysis presented in our paper were obtained in the frame of this program.

2. Our observations

New photoelectric BV observations of UV Lyn, FU Dra, AH Aur and UBV observations of YY CrB were performed from December 2000 to May 2001 at the Stará Lesná (SL) and Skalnaté Pleso (SP) Observatories of the Astronomical Institute of the Slovak Academy of Sciences. At both observatories a single-channel photoelectric photometer installed at the Cassegrain focus of the 0.6m reflector was used. The detailed description of the observational technique and reduction of the data to the international photometric system is given in Pribulla et al. (2001). The stars BD+38°1990, BD+28°1109, GSC 4181-1726 and GSC 3054-640 were used as the comparison stars for

UV Lyn, FU Dra, AH Aur and YY CrB, respectively. Our new photoelectric LCs of these contact binaries are shown in Fig. 1 and Fig. 3.

Our observations enabled us to determine 5 minima times (MT) of UV Lyn, 5 MT of FU Dra, 4 MT of AH Aur (Vaňko et al., 2001) and 3 MT of YY CrB (Vaňko et al., 2002).

3. Interpretation

The W&D (Wilson & Devinney, 1971) code was employed to determine the photometric elements of UV Lyn, FU Dra and AH Aur. We have used the Mode 3 appropriate for the contact configuration. All our BV observations were used to compute about 150 normal points for each passband. The normal points were determined by running averages of phased observations calculated using ephemerides (1), (2) and (3). The standard deviations (σ) used for weighting of the LC in each passband were evaluated as described by Wilson (1979).

For the computation of monochromatic luminosities, the approximate atmospheric models option of the W&D program was used. Since all three systems have late F type spectra, we have assumed coefficients of gravity darkening and bolometric albedo appropriate for convective envelopes ($T_{eff} < 7500$ K). Therefore, we adopted $g_1 = g_2 = 0.32$ (Lucy, 1967) and $A_1 = A_2 = 0.5$ (e.g., Rucinski, 1969). The limb darkening were interpolated from Tab. 1 of Al-Naimiy (1978). The mean temperatures of the primary components were fixed according to their spectral types (UV Lyn-F6V, FU Dra-F8V, AH Aur-F7V, YY CrB-F8V) using the spectral type - T_{eff} calibration of Popper (1980).

The initial parameters of UV Lyn and FU Dra were taken from Maceroni & van't Veer (1996) and Heiner (2000), respectively. Both systems are W-type contact binaries, i.e. the smaller and hotter component is eclipsed during the primary minimum. Hence using the W&D code we have interchanged them shifting the orbital phases by 0.5. Throughout the article we adopted the following notation: the primary com-

ponent is always the more massive one - mass ratios $q = m_2/m_1 \leq 1$. No reliable photometric elements were published for AH Aur.

The resulting photometric and absolute parameters are given in Tab. 1 and Tab 2, respectively.

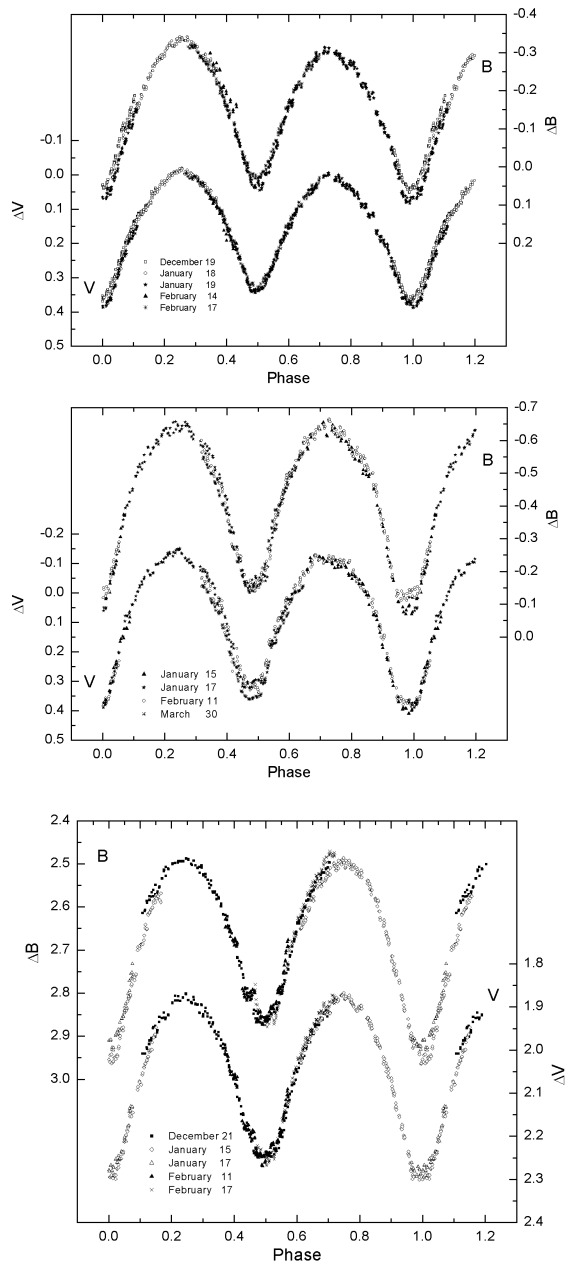


Figure 1: The photoelectric BV LCs of UV Lyn (top), FU Dra and AH Aur (bottom) obtained at the SL and SP Observatories in 2000 and 2001, respectively

2.1. UV Lyn

UV Lyn was discovered to be a variable by Kippenhahn (Geyer et al, 1955). Bossen (1973) classified UV

Lyn as a W UMa type binary with a period 0.415 day, maxima of unequal brightness and the distance of the system $d = 176$ pc. The first spectroscopic orbit of UV Lyn was determined by Lu & Rucinski (1999).

We have collected more than 140 minima times of UV Lyn. The photovisual minima with a very large scatter (about 0.05 day) were only available until 1968. More recent photoelectric and CCD minima times clearly show the increase of the orbital period. The (O-C) diagram of all available minima times from the mean linear ephemeris is shown in Fig. 2.

The period increase $\Delta P/P = (4.88 \pm 0.47) 10^{-7} \text{ year}^{-1}$ can be interpreted by the mass transfer from the less to more massive component. Using the masses of the components given in Tab. 1 we need the mass transfer rate $\Delta m/\Delta t = (1.28 \pm 0.12) 10^{-7} M_{\odot} \text{ year}^{-1}$ to explain the observed period increase. Since the broadening function of the system does not show the third component, an explanation of the observed period change by a light-time effect is questionable.

The recent photoelectric and CCD minima times were used to determine the linear ephemeris:

$$\text{Min I} = 2447000.4197 + 0.41498460 \times E. \quad (1)$$

$\pm 10 \qquad \qquad \qquad \pm 15$

This ephemeris was used for phasing our new photometry and it is suitable for the future minima forecast.

UV Lyn is a W-subtype contact binary (Lu & Rucinski, 1999). During our observations, the BV LCs were clearly asymmetric - the maxima I (phase 0.25) was brighter than the maximum II (phase 0.75) about 0.02 mag in the V and 0.03 mag in the B passband. The depression of the observed LCs was largest around the phase 0.85. The colour index was $\Delta(B - V) = -0.345 \pm 0.005$ and $\Delta(B - V) = -0.324 \pm 0.004$ at the phase 0.25 and 0.85, respectively.

2.2. FU Dra

Contact binary FU Dra was discovered by Hipparcos. Although the system is relatively faint ($V_{max} = 10.55$), it was observed spectroscopically by Lu & Rucinski (2000). On the assumption of the Hipparcos determination of the primary eclipse the authors concluded that the object belongs to W-type binaries. The system is known to have large proper motion (see Rucinski & Lu, 2000). Combining radial velocity of the mass center $V_0 = -11 \text{ km s}^{-1}$ and the Hipparcos proper motions in the right ascension and declination one gets the spatial velocity 195 km s^{-1} .

The system was observed at the Baja Observatory in June 2000 as a part of the diploma thesis (Heiner, 2000). The CCD observations yielded two times of

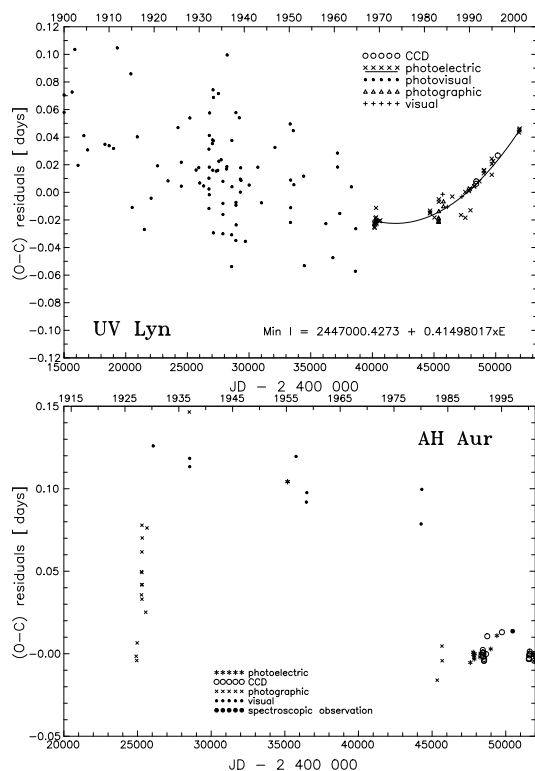


Figure 2: The (O-C) diagrams of UV Lyn (top) and AH Aur (bottom).

the secondary minima and approximate geometric elements: inclination $i = 80.8^\circ$ and fill-out $f=0.05$ assuming the spectroscopic mass ratio $q = 0.25$.

The linear fit to the available 12 minima times provides the following ephemeris:

$$\text{Min I} = 2\,450\,866.2770 + 0.30671686 \times E. \quad (2)$$

± 3 ± 9

The (O-C) residuals do not exceed 0.003 day. Hence the period of the system seems to be stable since its discovery. The ephemeris (2) was used for phasing of our photometry. The maximum I of the LC is about 0.02 mag brighter than the maximum II. We have detected small perturbations of the LC during the primary minimum. The small interval of constant brightness during the primary eclipse suggests that the system is totally eclipsing (subtype W).

2.3. AH Aur

Contact binary AH Aur was discovered by Prager & Guthnick (1929). Photographic LC obtained by Bodokja (1938) shows clear asymmetry of the minima. The system has been neglected since its discovery. The photoelectric observations of AH Aur were published only by Hinderer (1960). The first spectroscopy of the system was performed by Rucinski & Lu (1999).

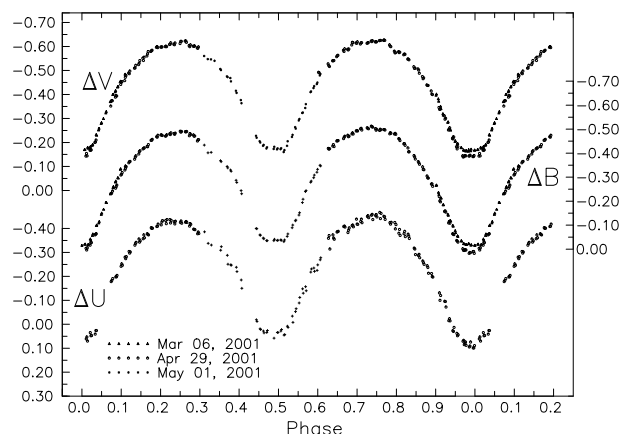


Figure 3: The photoelectric *UBV* LCs of YY CrB obtained at the SL Observatory in 2001. The phases of the light curve correspond to the ephemeris: $\text{Min I} = 2450955.8688(12) + 0.37656421(9) \times E$.

The available minima times consists mainly of the minima published in BAV Mitteilungen (Huebscher et al., 1989, 1990, 1991), minima determined from the Hipparcos photometry (Kreiner, 2000) and our observations. The photoelectric and CCD minima times are rather ample after about JD 2445 000. The weighted linear regression gives:

$$\text{Min I} = 2\,448\,500.3296 + 0.49410834 \times E. \quad (3)$$

± 8 ± 21

The (O-C) diagram for all available minima corresponding to the ephemeris (3) is presented in Fig. 2. The period behaviour before 2445 000 was very unusual. The minima in the interval JD 2426 000 - 2445 000 occurred about one quarter of the period later than predicted by the ephemeris (3). The shift is so large that the primary and secondary minimum could be interchanged. The fact that it is almost impossible to determine the type of the minimum in older observations could cause, that the O-C diagram is ambiguous. The *B* passband LC of Hinderer (1960) suggests, however, that the minima HJD 2435 186.4372 and 2435 191.3788 determined from the Hinderer's photometry by Lichtenknecker (1986) are secondary. Two visual minima just prior to JD 2443 000 and three photographic minima after HJD 2445 000 give orbital period $P = 0.494074(8)$. After HJD 2445 000 period increases by about $\Delta P/P = 6.9 \cdot 10^{-5}$!. Since Rucinski & Lu (1999) did not detect the third component in the broadening functions the LITE explanation is questionable. Also the LC analysis does not indicate the third light. It is possible that the hypothetical third body is not a main-sequence object.

The LC of the system seems to be rather stable. There are only slight variations in the minima depth - the secondary minima are relatively deeper during the

2000 CCD photometry. The short interval of constant light during the secondary minimum indicates that the system is just totally eclipsing.

For the determination of the photometric elements we have used the photoelectric BV observations obtained in December 2000 - February 2001. We have accepted spectroscopically determined mass ratio $q = 0.169$. Due to the fact, that the broadening functions did not indicate the presence of the third component in the system (Rucinski & Lu, 1999), we have fixed the zero third light. Since the mass ratio was also fixed, the differential corrections converged rather fast.

Table 1: Photometric elements and their standard errors (σ). Parameters not adjusted in the solution are denoted by a superscript "a"

Parameter	UV Lyn	FU Dra	AH Aur
i [°]	66.80(12)	78.64(24)	75.46(26)
q	0.367 ^a	0.251 ^a	0.169 ^a
Ω	2.5590(19)	2.3180(16)	2.0805(19)
Fill-out	0.455	0.235(10)	0.674(18)
r_1	0.4821	0.5143(5)	0.5647(7)
r_2	0.3091	0.2788(6)	0.2737(11)
T_1 [K]	6045 ^a	5800 ^a	6215 ^a
T_2 [K]	6262(12)	6133(8)	6141(8)
$L_1^B/(L_1^B + L_2^B)$	0.6769(8)	0.7216(5)	0.8270(2)
$L_1^V/(L_1^V + L_2^V)$	0.6769(7)	0.7290(4)	0.8260(2)
$L_1^R/(L_1^R + L_2^R)$	-	-	-
$\sum(O-C)^2$	0.00073	0.00534	-

Table 2: Absolute parameters and the distance of the observed systems. The masses of the components were derived from spectroscopic elements and new inclination angles (Tab. 1).

	UV Lyn(W)	FU Dra(W)	AH Aur(A)
M_1 [M_\odot]	1.356(19)	1.169(39)	1.683(47)
M_2 [M_\odot]	0.498(8)	0.293(10)	0.284(8)
A [R_\odot]	2.875(13)	2.172(24)	3.294(31)
R_1 [R_\odot]	1.386(6)	1.117(12)	1.853(17)
R_2 [R_\odot]	0.889(4)	0.605(6)	0.891(8)
$\log g_1$ [cm s^{-2}]	4.29	4.41	4.12
$\log g_2$ [cm s^{-2}]	4.24	4.34	3.99
M_V	3.386	4.160	2.831
d [pc]	134	175	282
$\overline{\rho_1}$	0.717	1.181	0.372
$\overline{\rho_2}$	0.998	1.863	0.401

4. Conclusion

The first photoelectric B, V light curves of the contact binary FU Dra, as well as new B, V light curves of the contact binaries AH Aur, UV Lyn and YY CrB

are presented. The absolute parameters of the contact binaries UV Lyn, FU Dra and AH Aur were determined using the published spectroscopic elements and photometric elements computed by the WD code from our photoelectric LCs. The absolute maximum visual magnitudes of the systems were determined from the temperatures of the components (Tab. 1) and absolute radii (Tab. 2) using Popper's (1980) radiative calibration for the main-sequence stars. The distance were computed using the Hipparcos maximum visual magnitudes assuming interstellar or/and circumstellar extinction.

Acknowledgements. This study was supported by VEGA grant 2/1157 of the Slovak Academy of Sciences.

References

Akerlof C., Amrose S., Balsano R. et al.: 2000, *ApJ*, **119**, 1901.
 Al-Naimiy H.M.: 1978, *Ap&SS*, **53**, 181.
 Bodokia V.M.: 1938, *Bull. Abast. Astr. Obs.*, **2**, 11.
 Bossen, H.: 1973, *ApJS*, **10**, 217.
 ESA: 1997, *The Hipparcos Catalogue*, ESA SP-1200, Noordwijk: ESA
 Geyer E., Kippenhahn R., Strohmeier W.: 1955, *Kleine Veröff. Remeis Sternwarte*, Bamberg, No. 9
 Gioia I.M., Maccacaro T., Wolter A.: 1989, *Observ. Cosmology*, eds.: A. Hewitt, G. Burbidge & L. Z. Frang, D. Reidel, Dodrecht, 593.
 Heiner Z.: 2000, *Diploma Thesis*, Szeged University
 Hinderer F.: 1960, *Journal des Observateurs*, **43**, 161.
 Kreiner J.M.: 2000, private communication
 Lichtenknecker D.: 1986, *BAV Rundbrief*, 35, 41.
 Lu W., Rucinski S.M.: 1999, *AJ*, **118**, 515.
 Lu W., Rucinski S.M., Mochnacki S.W.: 2000, *AJ*, **120**, 1133.
 Lucy L.B.: 1967, *Z. Astrophys.*, **65**, 89.
 Maceroni C., van't Veer F.: 1996, *A&A*, **311**, 523.
 Popper D.M.: 1980, *Ann. Rev. Astron. Astrophys.*, **18**, 115.
 Prager R., Guthnick P.: 1926, *Kleine Veröff. Berlin Babelsberg*, **6**
 Pribulla T., Vaňko M., Chochol D., Parimucha Š.: 2001, *Contrib. Astron. Obs. Skalnaté Pleso*, **31**, 25.
 Rucinski S.M.: 1969, *Acta Astron.*, **19**, 245.
 Rucinski S.M.: 1997a, *AJ*, **113**, 407.
 Rucinski S.M.: 1997b, *AJ*, **113**, 1112.
 Rucinski S.M., Lu W.: 1999, *AJ*, **118**, 2451.
 Vaňko M., Pribulla T., Chochol D., Parimucha Š., Kim C.H., Lee J.W., Han J.Y.: 2001, *Contrib. Astron. Obs. Skalnaté Pleso*, (in press)
 Vaňko M. et al.: 2002, (in preparation)
 Wilson R.E., Devinney E.J.: 1971, *ApJ*, **166**, 605.
 Wilson R.E.: 1979, *ApJ*, **243**, 1054.

RAPID OSCILLATIONS IN THE SPECTRUM OF roAp STARS χ PSC AND γ EQU

S.G. Aliev, N.Z. Ismailov
Shemakha astrophysical observatory NAS of Azerbaijan
box1955n@yahoo.com

ABSTRACT. Results of high time and spectral resolution spectral observations with CCD in 1998-1999 for Ap stars χ Psc and γ Equ were presented. Spectroscopic parameters (V_r , W_λ) of spectral lines SiII, CrI, CrII, FeI, FeII, H_α , H_β shows that despite of different value of rotation velocity of χ Psc (180 km/s) and γ Equ (~ 74 years), both stars shows short-time oscillations of spectral parameters, and concern to a subgroup of roAp stars. It is showed that spectroscopic parameters and magnetic field strength variations may be described with short-time pulsation periods ~ 17 min and ~ 12 min for χ Psc and γ Equ correspondingly.

Key words: spectroscopy of stars-roAp stars-stellar magnetism.

On the basis of echelle-spectrums, received with the high time and spectral resolution in spectrometer with application CCD in Cude-focus of 2 telescope of ShAO NAN of Azerbaijan (dispersion 3-5 Å/mm), variations of spectrum Ap stars χ Psc and γ Equ were investigated. The spectral resolution $R = 30000$. For 1998-1999 was received only 84 spectrums for χ Psc and 56 for γ Equ with a signal to noise relation in area $H_\alpha \sim 80-120$. In detail about an observational material and technique of observation was described in works Aliev and Ismailov (2000, 2001).

χ Psc. The changes of equivalent widths and radial velocities of lines H_α and H_β within the first and second night of observations have shown, that the wavy type changes both equivalent widths, and radial velocities of these lines was obtained. In a fig. 1 the time dependence of parameters (radial velocities V_r , equivalent width W_λ) of spectral lines H_α and H_β is given. Pulsation type short time variations of parameters of spectral lines were discovered. On the Fourier analysis of parameters of spectral lines in an interval of frequencies 0-120 d^{-1} , the period of oscillation $P_2 = 0.0119 \pm 0.0008$ day was obtained. Besides it, probably, there is a period $P_3 = 0.0093 \pm 0.0005$ day, and also the period of axial rotation $P_1 = 0.5583 \pm 0.025$ day was found. The different spectral lines show different amplitudes with a short time pulsation, and the largest

amplitudes of changes of radial velocities shows lines of peculiar of elements.

In a fig. 2 the phase diagram of relative equivalent widths of a star χ Psc determined for the period $P_2 \approx 17$ minute is given for different spectral lines.

As shown here, within one year the received results give satisfactory stability on the given period.

In a fig. 3 the phase curve of a magnetic field of a star for the period of a pulsation χ Psc is given. It is shown, that the strength of a magnetic field is satisfactorily described by this period. The measurements of a magnetic field strength were taken from Borra and Landstreet (1980). Though quantity of magnetic field measurements is small, confidently it is possible to tell about periodic changes its with the period of pulsation P_2 . This observational fact shows, that, apparently, main reason of processes of a pulsation also is the magnetic field, though complete understanding of this process encounters difficulty.

The magnetic field of a star varies with a phase also with both period's P_1 and P_2 , though the forms of curves are various. Average curves of radial velocities of lines of peculiar elements show's synchronism of changes with a magnetic field strength. On the rotation velocity of the star are determined an inclination of rotation axis with beam of sight $i = 9^\circ \pm 1^\circ$ and corner of inclination of a magnetic axis of a star to a beam of sight equal $\beta = 63^\circ \pm 1^\circ$. The maximal strength of a magnetic field of a star equal about 1468 ± 200 G is appreciated.

For the first time is shown, that the magnetic field of a star synchronously varies with radial velocity of lines CrII and SiII, and to a lesser degree by other lines. We suggested that this is a result of direct connection of a magnetic field of the star and it peculiar properties.

γ Equ. In the fig.4a for example the change of radial velocities of spectral lines FeI $\lambda 5171\text{\AA}$, MgI $\lambda 5172\text{\AA}$, CrII $\lambda 4836\text{\AA}$ is given for the first night of observation. In the fig. 4b is given change of V_r for the second series of observation, for lines FeI $\lambda 5162\text{\AA}$, FeII $\lambda 5169\text{\AA}$, CrII $\lambda 4836\text{\AA}$ and H_α . From a fig. 4 it would be visible, that two type of changes V_r are observed simul-

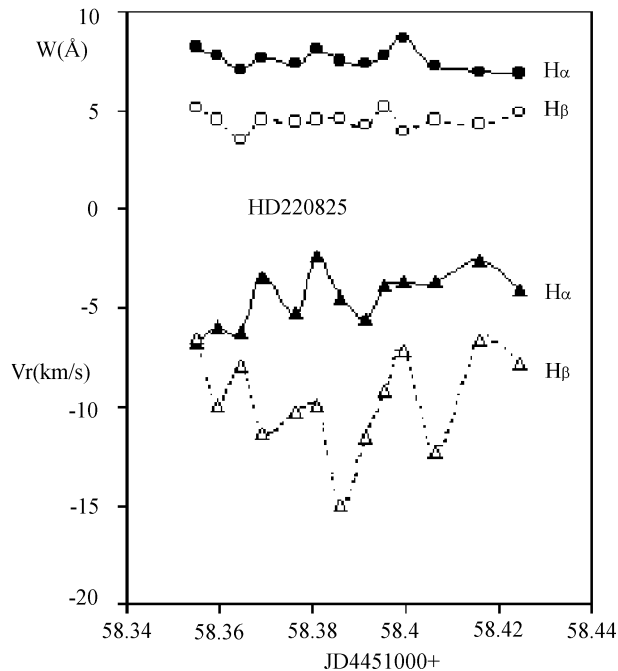
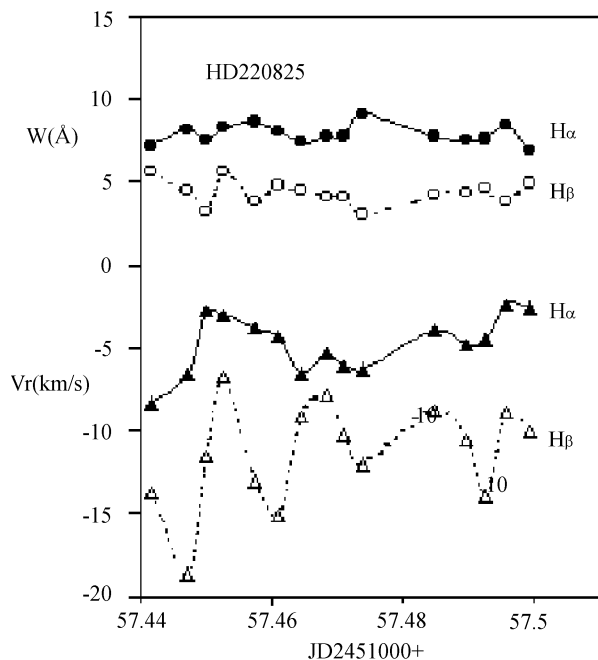


Figure 1: Time variations of spectral parameters W_λ and V_r for hydrogen lines $H\alpha$ and $H\beta$ during two different nights of observations for χ Psc.

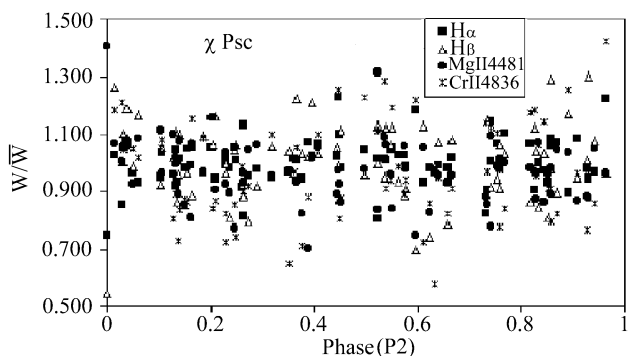


Figure 2: The phase diagram of relative equivalent width of spectral lines of a star χ Psc in phases of pulsation period P2. In ordinate is given of separate relation of equivalent widths meaning to average for the given line.

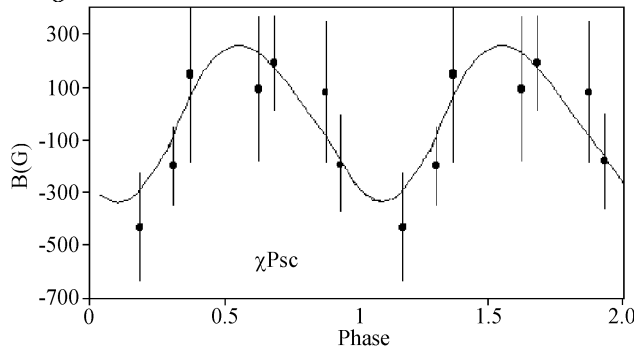


Figure 3: A phase curve of magnetic field strength for χ Psc. Results of a magnetic field measurements are taken from Borra and Landstreet (1980).

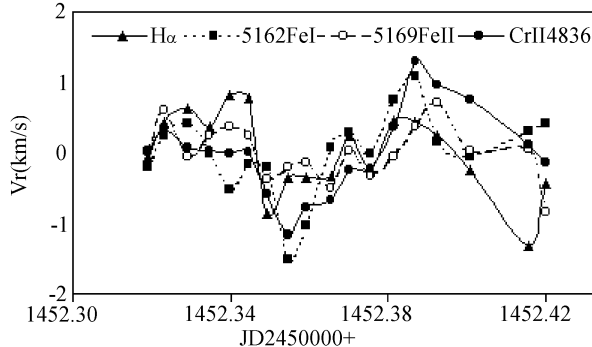
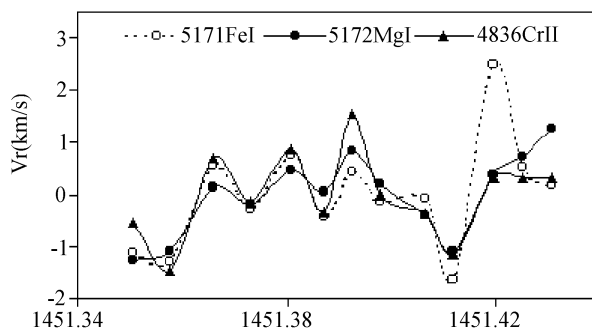


Figure 4: Time variation of radial velocities for separate nights on different spectral lines of γ Equ.

taneously: a) a short-time pulsation type variability, b) rather slow wavy type variation during characteristic time about 1.5 hours. Both types of variations are well appreciable till a fig. 4 both in first, and in the second series of observation: in the first series two minima and one maximum, and in the second series two minima and two maximum are observed. The similar fluctuations of V_r are observed the in other series of observations too.

As a result of frequency Fourier analysis of spectral parameters, from our observation two most probable frequencies ν_2 and ν_4 are revealed which correspond 1324 ± 80 mHz and 1440 ± 70 mHz. These meanings pulsation of modes are very close to meanings of the period given in work Martinez et al. (1996) and on spectral observation, found in Kanaan and Hatzes (1998), and also Malanushenko et al. (1998). As a result of our analysis of a spectrum γ Equ the following basic results are received:

a) The analysis of the data on V_r measurements on different lines showed to existence the pulsation period on a surface of a star γ Equ about $P = 0.^d0080 \pm 0.^d0002$ (~ 12 minutes) and period, contiguous to this meaning. On the radial velocities the separate groups of lines are observed which make pulsation in an antiphase.

b) All spectral parameters (W_λ , V_r , $\Delta\lambda_{1/2}$ (FWHM), R_λ) have shown synchronous change with pulsation period, that confirms a reality of existence oscillations processes as the physical phenomenon on a surface of a star. Two extreme during one pulsation period on all spectral parameters of a star was observed.

c) It is shown, that the magnetic field of a star makes pulsation type fluctuation in an interval ± 350 G. The variations of a magnetic field of the star, on the data of the different authors, will not bad be coordinated with pulsations by the period of the star, and testifies to genetic connection between a magnetic field and processes of oscillations in the atmosphere of the star.

In the conclusion we shall note, that despite of different value of rotation velocity of χ Psc (180 km/s) and γ Equ (~ 74 years), both stars show short-term oscillations of spectral parameters, and concern to a subgroup of roAp stars. It testifies that the origin pulsations processes in atmospheres of roAp stars, apparently, is not a consequence of their axial rotation.

References

- Aliev S.G., Ismailov N.Z.: 2000, *Astronomy Reports*, **44**, 738.
- Aliev S.G., Ismailov N.Z.: 2001, *Fizika*, **7**, N 1, 42.
- Borra F.F., Landstreet J.D.: 1980, *Astrophys. J. Suppl. Ser.*, **42**, 421.
- Martinez P., Weiss W.W., Nelson M.J., Kreidl T.J., Roberts G.R., Mkrtichian D.E., Dorokhov N.I., Dorokhova T.N., Birch P.V.: 1996, *Monthly Notices Roy Astron. Soc.*, **282**, 243.
- Kanaan A., Hatzes A.P.: 1998, *Astrophys. J.*, **503**, 848.
- Malanushenko V., Savanov I.S., Ryabchikova T.: 1998, *IBVS*, N 4650.

DETERMINATION OF CHARACTERISTIC TIME SCALES IN SEMI-REGULAR STARS: COMPARISON OF DIFFERENT METHODS

I.L. Andronov, L.L. Chinarova

Department of Astronomy and Astronomical observatory,
Odessa National University, T.G.Shevchenko park, Odessa 65014 Ukraine,
e-mail: il-a@mail.od.ua, astro@paco.odessa.ua

ABSTRACT. Results of the analysis of the characteristic time scales using the periodogram, scalegram and the wavelet analysis are compared for 173 stars most actively observed by the members of the AFOEV and VSOLJ. The periodogram analysis is more effective for stars with stable nearly coherent pulsations, whereas the wavelet analysis is a better tool for stars with switching pulsational modes, e.g. AF Cyg. The scalegram analysis is effective for non-harmonic and chaotic-like variations. The diagrams of the effective time scales obtained using these methods are analyzed for making additional classification of the stars within subclasses. The use of the test functions for automatic classification is discussed. An example analysis is made for S Aql. Particularly, the ephemeris is determined: $Max.JD = 2443578.9(3) + 146^d.693(6) \cdot E$.

Key words: Stars: variable: semi-regular: S Aql

1. Introduction

Semi-regular variables represent a highly interesting class of long-period pulsating stars, which exhibit a variety of types of observational appearance. Present paper continues the series of articles dedicated to the time series analysis of the patrol visual observations of the members of AFOEV:

ftp://cdsarc.u-strasbg.fr/pub/foev/aql/s
and VSOLJ:

ftp.kusastro.kyoto-u.ac.jp/pub/vsnet/VSOLJ/database/stars/aql.s.jd.

The catalogues of the characteristics of 53 long-period (mainly Mira-type) stars have been published by Marsakova and Andronov (1998, 2000). The catalogue of characteristics of 173 semi-regular variables was recently published by Andronov and Chinarova (2000).

Here we present time series analysis using various methods, using S Aql as an example of data. The complete data set contains 4537 observations in the time interval JD 2422579.98-2451549.20 since 1920.

2. Methods for time series analysis

Taking into account non-stable character of the light curve, it is necessary to use few supplementary methods, which should be optimized for various types of variability. Extensions of the existing methods for astronomical signals with (generally) irregularly spaced arguments are described e.g. in the monographs by Terebizh (1992) and Andronov (2001b).

2.1. Mono-, multi- periodic and multiharmonic variations

The method for determining parameters of harmonic signals is obviously the sine fit

$$m(t) = C_1 - r_1 \cos(\omega(t - T_{01})), \quad (1)$$

where C_1 is the zero-point coinciding with the signal continuously averaged over the complete phase interval. $\omega = 2\pi/P$ is angular frequency, and P is the period of variations, and T_{01} is initial epoch for the maximum (i.e. minimum of the magnitude). For such an analysis, we use the program *Four* by Andronov (1994).

The periodogram for S Aql (Fig.1) shows a highest peak at the periodogram at $P = 146^d.6934 \pm 0^d.0057$, semi-amplitude $r_1 = 0^m.884 \pm 0^m.012$, initial epoch for maximum $T_{01} = 2443578.89 \pm 0^d.31$ and zero-point $C_1 = 10^m.337 \pm 0^m.008$. This value differs from the sample mean for the data $\langle m \rangle = 10^m.284 \pm 0^m.012$ because the data cover the phase interval not homogeneously. The scatter of the data at the phase curve is $\sigma_0 = 0^m.550$, whereas the standard deviation of the data from the mean is $0^m.829$. The test function $S(f)$, which is equal to the ratio of the variance of the signal to the variance of "signal+noise", is equal to 0.544 in our case, i.e. the "noise" only a little bit smaller than the "signal".

There are two other relatively high peaks at the periodogram corresponding to the periods $P_2 = 104^d.64$ and $P_3 = 245^d.23$. It is noticeable, that $P_2/P = 5/7$

and $P_3/P = 5/3$ within few tenth of per cent. So these waves may be formally interpreted as harmonics of the main period $P_4 = 734^d$: $P = P_4/5$, $P_2 = P_4/7$ and $P_3 = P_4/3$. Another formal explanation is that P_2 and P_3 are biases of the primary wave with $P = P_4/5$ with a wave with a period $P_5 = P_4/2 = 367^d = 1$ year.

Thus the star is an excellent example of possibility of misinterpreting the results of the periodogram analysis as a presence of multiple waves with rational period ratio. The cause is that the photometric period of the star deviates from $\frac{2}{5}$ yr by only 0.4% !.

There are no high peaks corresponding to harmonics at periods P/j , where j is an integer, thus one may conclude that the mean light curve is nearly sinusoidal. Otherwise, one could use the program *Fdcn* for determination of the parameters of the trigonometric polynomial, including the statistically significant value of it's order s . Another program was elaborated to determine parameters of the multi-periodic model, including unknown periods (Andronov, 1994).

2.2. Wavelet analysis

To study nearly-periodic and multiperiodic processes with variable shape of the signal, the wavelet analysis is used. Foster (1996) has extended the "Morlet wavelet" method for general case of signals with irregularly spaced arguments. One may name it as a "weighted periodogram analysis with a running window". Andronov (1998, 1999) generalized this approach, adding possibilities to compute weighted mean test functions and to make wavelet smoothing.

In Fig. 2, the test functions used for the wavelet analysis, are shown: *WWZ*, *WWT*, *S* and the wavelet (semi-)amplitude *R* (see Andronov, 1998, 1999 for a complete description). The main peak occurs at $145.^d6$, $146.^d7$, $145.^d3$, $145.^d4$, respectively, corresponding to the test function $S = 0.74$, which is much larger (and closer to unity), than its analog for periodogram analysis (0.54). This shows an advantage of the wavelet analysis for signals with variable shape. Similarly, the mean wavelet amplitude $R = 0.^m98$ is much larger than $0.^m88$ for a coherent sinusoid.

The peak at P_3 is distinguishable, and it corresponds to $R = 0.^m58$. Another interesting feature is maximum at $P = 3520^d$ with $R = 0.^m19$. This period is located between the values $3831^d \pm 20^d$ and $3246^d \pm 29^d$ corresponding to the peaks at the periodogram. Obviously, the peaks so close in frequency may not be separated by the wavelet analysis, as well as that of 104^d and 146^d .

The "wavelet skeleton" is shown in Fig. 3. One may note a large number of low peaks with apparently changing periods. However, the main peak has a relatively smaller scatter in period and a better separation from the low peaks. However, at the time intervals with gaps in the observations, the best fit appar-

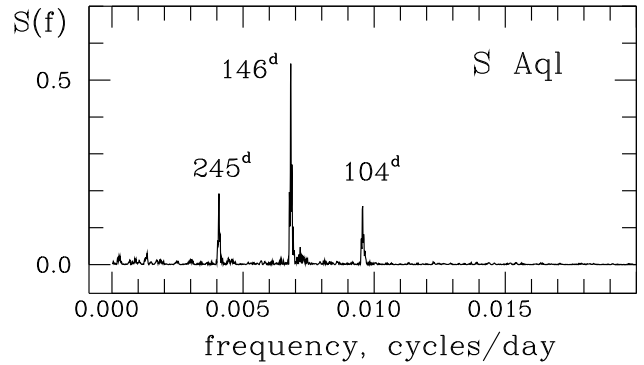


Figure 1: Periodogram of the observations of S Aql.

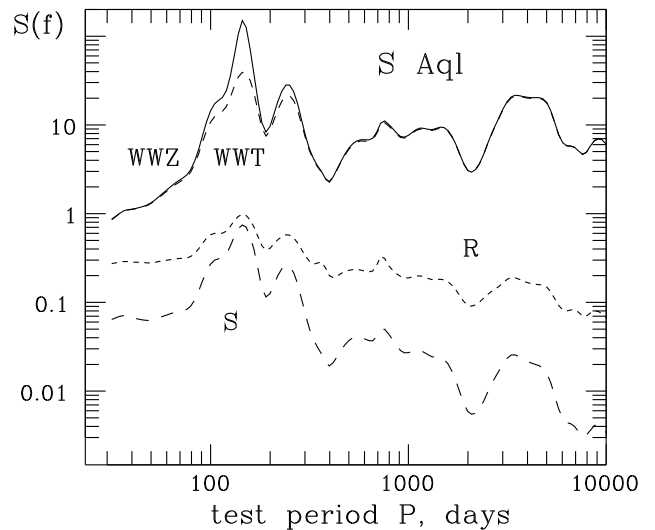


Figure 2: The main test functions for the wavelet analysis averaged over time as described by Andronov (1999).

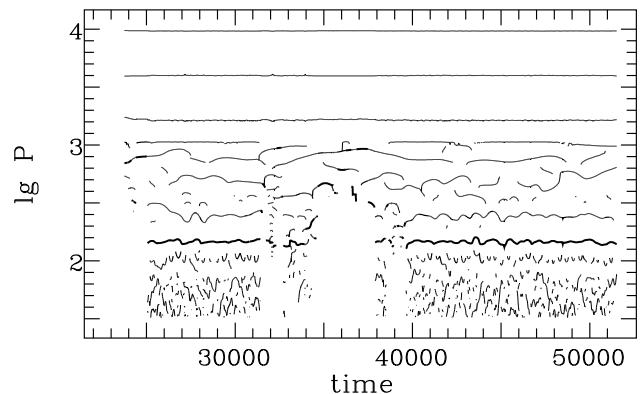


Figure 3: The "wavelet skeleton", i.e. dependence of periods corresponding to local peaks at the wavelet periodogram computed at a mean time t . The highest (at this t) peak is shown by most thick line, the peaks higher than 50% of the highest peak, are shown by an intermediate line, and lower peaks - by a thin line. For the main period value, $\lg P = 2.17$.

ently "switches" to larger values, increasing the effective width of the time filter.

Another effective method intermediate between the periodogram and wavelet analysis is the method of "running sines", where the weight function (time filter) is rectangular, and the period is constant. In this case, the fit (1) is computed for a local interval from $t - \Delta t$ to $t + \Delta t$, where Δt is called "the filter half-width". The parameters zero-point C_1 , semi-amplitude r_1 and the phase (corresponding to T_{01}) are determined as functions of time. Such a method has advantages over the periodogram analysis (owing to study signals of low coherence) and the wavelet analysis (as the phase variations allow to study period variations of much smaller amplitude). An example of application of such a method for variations of UV Aur (symbiotic binary with a pulsating component) is presented by Chinarova (1998). Statistical properties of model parameters are discussed by Andronov (1999).

2.3. Scalegram analysis using "running parabolae"

This method was proposed by Andronov (1997). It may be classified as the Morlet-type wavelet method with $\Delta t/P \ll 1$. Instead of making slow computations of trigonometric functions (few hours of computer time for a typical number of data of few dozens thousand), the polynomials are computed, and the weight function is non-zero only in the vicinities of the center.

In Figure 4, the test functions are shown, i.e. an unbiased error estimate σ_3 of the r.m.s. deviation of the observations from the fit; $\sigma[x_C]$ – the mean squared error estimate of the smoothing function at the arguments of observations; $S/N = \sigma_C/\sigma[x_C]$ – the amplitude signal-to-noise ratio, where σ_C^2 is the variance of the fit values.

As achieved, at small Δt , there is a standstill at the dependence $\sigma_3(\Delta t)$, showing no significant regular variability at high frequencies. The value $\sigma_3 = 0.^m24$ is much smaller than $\sigma_0 = 0.^m55$ corresponding to the harmonic sine fit, and is typical for the scatter of the visual observations from the AFOEV and VSOLJ databases. Thus "running parabolae" are better fit because of variations of the shape of the individual cycles.

The accuracy estimate of the fit $\sigma[x_C]$ reaches its local minimum of $0.^m083$ at $\Delta t = 60.^d5$, despite the global one is at $\Delta t \rightarrow \infty$, i.e., according to this criterion, it is "better" to assume the signal to be constant and to neglect variations. The signal-to-noise ratio is at maximum of 9.3 at $\Delta t = 44.^d8$. This value should be used for further fits.

2.4. "O-C" analysis

This approach allows to study period variations with much smaller level of detectability than the methods of determination of local period. An extensive description and examples one may find e.g. in Kopal and Kurth

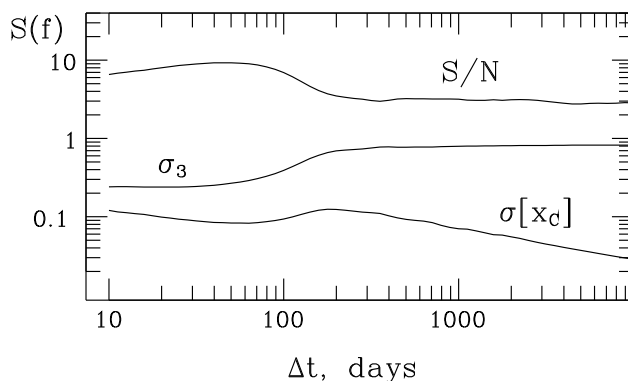


Figure 4: Scalegram for S Aql using "running parabolae".

(1957), Tsessevich (1970) and Kalimeris et al. (1994). The methods of "best accuracy" determination of the moments of "characteristic events" are currently proposed by Marsakova and Andronov (1996) and Chinarova and Andronov (2000). Some methods of study "O-C" diagrams are available using the program OO described in this volume (Andronov, 2001a).

Acknowledgements. The observations were made by the members of the AFOEV and VSOLJ. We thank the amateur astronomers for their intensive studies and E.Schweitzer and D.Nogami for allowing to use these data.

References:

- Andronov I.L.: 1994, *Odessa Astron. Publ. (OAP)*, **7**, 49.
 Andronov I.L.: 1997, *As. Ap. Suppl. Ser.*, **125**, 207.
 Andronov I.L.: 1998, *Kinematika i Fizika Nebesnykh Tel*, **14**, N 6, 490.
 Andronov I.L.: 1999, in: "Self-Similar Systems", eds. V.B. Priezzhev, V.P. Spiridonov, Dubna, JINR, 57.
 Andronov I.L.: 2001a, *OAP*, **14**, 255.
 Andronov I.L.: 2001, *Time Series Analysis of Astronomical Signals* (in Russian), Odessa, Astroprint (in press).
 Andronov I.L., Chinarova L.L.: 2000, *OAP*, **13**, 116.
 Chinarova L.L.: 1998, *Proc. 29th Conf. Variable Star Res.*, ed. J. Dušek, M. Zejda, Brno, p.38.
 Foster G.: 1996, *Astron. J.*, **112**, 1709.
 Kalimeris A., Rovithis-Livaniou H., Rovithis P.: 1994, *As.Ap.*, **282**, 775
 Kopal Z., Kurth R.: 1957, *Z. Astrophys.*, **42**, 90.
 Marsakova V.I., Andronov I.L.: 1996, *OAPubl.*, **9**, 127.
 Marsakova V.I., Andronov I.L.: 1998, *OAPubl.*, **11**, 79.
 Marsakova V.I., Andronov I.L.: 2001, *OAPubl.*, **13**, 82.
 Terebizh V.Yu.: 1992, *Time Series Analysis in Astrophysics* (in Russian), Moscow, Nauka.
 Tsessevich V.P.: 1970: *Variable stars and methods for their study* (in Russian), Moscow, Nauka.

THE PHOTOMETRIC STUDY OF TWO FAINT MIRA-TYPE STARS UX CYG AND AP CYG

Yu.V. Beletskij, A.V. Halevin, L.S. Kudashkina

Astronomical Observatory, Odessa National University,
T.G.Shevchenko Park, 65014 Odessa, Ukraine, astro@paco.odessa.ua

ABSTRACT. Two faint Mira-type stars were investigated on the Moscow and Odessa plates collections. The new ephemerids are $T_{max} = 2426875 + 274.^d8 \cdot E$ for AP Cyg and $2442162 + 568.^dE$ for UX Cyg. For UX Cyg, the multiharmonic variability was detected. Two stars were suspected in variability among the comparison stars.

Key words: Stars: miras; suspected; stars: individual: UX Cyg, AP Cyg.

The stars AP Cyg and UX Cyg have been observed on the Odessa and Moscow collections of the plates. The finding chart is shown in the figure 1. The magnitudes of the 13 comparison stars have been derived from the standard NGC 6633 (Kazanasmas et al., 1981). Their magnitudes are given in the table below. The maximum error estimate for brightest stars reaches $0.^m4$.

Table 1.

Star	m_{pg}	σ	$m_{pg} - m_{vis}$
a	9.40	0.4	+0.6
B	9.62	0.35	+0.3
C	11.35	0.08	+1.85
D	11.50	0.10	+1.6
E	11.63	0.11	+1.7
F	Var.	suspect	
K	12.18	0.12	+1.2
G	12.24	0.11	+1.8
X	12.27	0.10	-
m	12.39	0.15	+0.9
Y	12.43	0.17	-
N	12.51	0.15	+0.5
o	12.75	0.11	+0.15
p	12.95	0.11	-0.25

AP Cyg: The GCVS (1985) data: $20^h52^m23^s$, $+30^\circ25.4$ (eq. 1950.0); $14.^m0 - (15.^m0$ in pg-system; $T_{max} = 2426875$, $P = 274.^d8$, the type - Mira?. Beljawsky (1935) gives the period also $275.^d$

This star is not visible on the Odessa collection plates. Another 38 certain points are available in the AFOEV database.

Only Moscow collection plates were used for the re-

search of the period. The total interval of observation is 31206 days. But two points are very away from the rest. If these points exclude, the interval of observation is only 17374 days. Therefore obtained results are not satisfactory.

For the analysis, the program FO.EXE was used (Andronov, 1994).

UX Cyg: The GCVS data (1985): $20^h53^m00^s$, $+30^\circ13.4$ (eq. 2000.0); $9.^m0-16.^m5$ in visual system; $T_{max} = 2444421$, $P = 565.^d0$, type - Mira, spectral type - M4e-M6.5e. The period is variable. Sometimes rapid light decreases on the ascending branch near maximum are observed.

On the Moscow collection plates, 10 observations have been obtained. These data point to descending branch. On the Odessa collection plates, 189 observations of summary brightness UX Cyg and near star "var1" have been obtained. These objects are not visible separately at one plate. With regard to the investigations "var1" on the Moscow collection plates, the deviations from the mean brightness may think the real variations of light of UX Cyg.

The periodogram analysis has been carried out on the base of the AFOEV (France) and VSOLJ (Japan) data and the multiharmonic variability of UX Cyg has been detected. The parameters of the mean light curve of this star have been calculated used the program FDCN (Andronov, 1994). The light curve is described by a 4^{th} - order trigonometric polynomial with the best fit period $P = 567.^d995 \pm .^d111$; initial epoch for the maximum JD 2442161.8 ± 2.1 ;

initial epoch for the minimum JD 2441953.1 ± 12.5 ; the asymmetry $f = 0.37 \pm 0.02$; $\Delta mag = 4.^m68 \pm .^m08$; The parameters of sharpness:

the ascending branch -

$$dm/dt = -0.058 \pm 0.003; dt/dm = -17 \pm 1;$$

the descending branch -

$$dm/dt = 0.031 \pm 0.003; dt/dm = 32 \pm 3.$$

The amplitude of the wave with main frequency:

$r_1 = 1.^m86 \pm 0.^m08$ and the phase of its maximum: $\phi_{max} = 0^p072 \pm 0^p006$ in respect to the maximum of the light curve.

The amplitudes and the phases of maximum of others: 2: $0.^m99 \pm 0.^m08$; $0^p026 \pm 0^p006$; $r_2/r_1 = 0.53 \pm 0.06$

3: $0^m09 \pm 0^m08$; $-0^p05 \pm 0^p13$; $r_3/r_1 = 0.05 \pm 0.04$
 4: $0^m34 \pm 0^m06$; $-0^p14 \pm 0^p03$; $r_4/r_1 = 0.18 \pm 0.04$

Suspected variables: During the observations of UX Cyg and AP Cyg, two comparison stars were suspected of the variability. These are the stars "v1" and "v2(f)" in the figure 1. The observations are given in the table 2. "v1" shows the variation on 0^m17 , and "v2(f)" shows the variation on 0^m41 during the interval of the observations. However, with regard to the scattering of the magnitudes, the star "v1" may be classified as constant. The variation of the star "v2(f)" is larger, but not exceed 3σ .

Acknowledgements. We thank V.I.Marsakova for useful discussions. The paper is partially based on the observations from the AFOEV and VSOLJ databases.

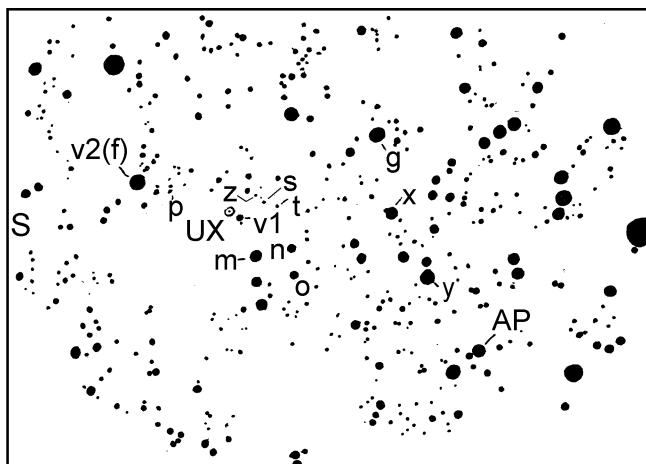


Figure 1: The finding chart for UX and AP Cyg.

Table 2.

v1	v2(f)	JD 243	v1	v2(f)	JD 243
12.69	12.00	9024.383	12.72	12.07	9027.264
12.68	12.07	.348	12.70	11.93	9035.398
12.64	12.13	.311	12.69	12.02	.364
12.74	12.02	.277	12.68	11.83	9034.421
12.72	12.02	.241	12.70	11.99	9033.427
12.72	11.93	9023.400	12.68	11.80	9032.417
12.66	12.04	.371	12.74	11.87	.380
12.68	12.02	.231	12.69	11.99	9031.445
12.72	11.99	9022.370	12.66	11.95	.409
12.72	12.07	.340	12.71	11.84	9030.421
12.78	12.13	9027.235	12.68	11.87	9029.439
12.68	12.02	9026.449	12.70	11.94	40499.251
12.69	11.96	9025.439	12.74	12.01	0478.424
12.65	12.07	.404	12.77	11.97	.389
12.66	12.00	.368	12.79	11.92	0473.416
12.70	12.06	.328	12.76	11.97	.416
12.68	11.98	.279	12.66	11.97	0153.374
12.69	12.02	.235	12.69	12.07	0122.364
12.70	11.91	9024.455	12.68	11.98	0097.537
12.72	12.01	.417	12.75	11.97	0093.507
12.68	12.00	9029.370	12.71	12.16	0071.461
12.71	11.75	9028.4	12.67	12.04	39036.329
12.81	11.94	.38	12.73	11.96	40530.269
12.67	11.97	.3	12.76	11.98	0510.357
12.78	11.99	.27	12.72	12.02	0538.172
12.73	12.02	.231	12.74	11.98	0530.236
12.73	11.97	9027.419	12.69	11.97	0499.286
12.69	11.99	.360	12.79	12.04	0538.206
12.72	11.93	.3			

References

Andronov I.L.: 1994, *Odessa Astron. Publ.*, **7**, 49.
 Beljawsky S.: 1935, *Ponlk.Cm.*, N13.
 Kazanasmas M.S., Zavershneva L.A., Tomak L.F.:
 1981, *Atlas and catalogue of the stellar magnitudes
 of the photoelectric standards*, Kiev, Naukova
 Dumka.
 Kholopov P.N. (et al.): 1985, *General catalogue of
 variable stars 1-3*.

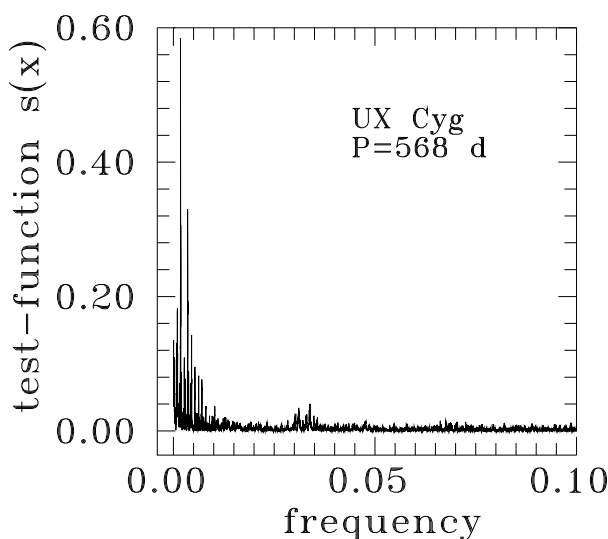


Figure 2: The periodogram for UX Cyg.

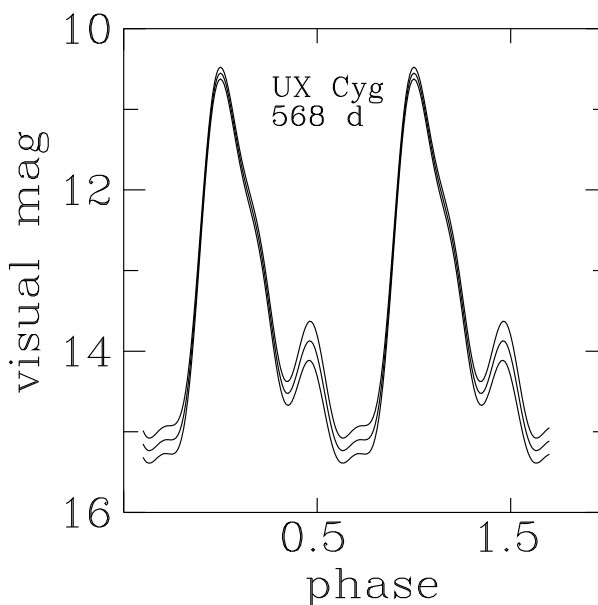


Figure 3: The mean light curve of UX Cyg and $\pm 1\sigma$ limits of the smoothing function.

ON THE PERIODS OF THE β CEPHEI STARS

V.P. Bezdenezhnyi

Astronomical Observatory, Odessa National University, Ukraine
T.G. Shevchenko Park, Odessa, 65014, Ukraine, astro@paco.odessa.ua

ABSTRACT. On the base of GCVS' data the analysis of periods distributions for β Cep stars (BCEP and BCEPS) has been carried out. Identifications for all peaks on the histogram have been performed. There are some overtones and their harmonics. These are related with multiplicity ratios. In addition to GCVS classification it is proposed to extend the range of periods for short-period group (BCEPS) to (0.02 - 0.13) days instead of (0.02 - 0.04) days. We propose a new classification of these stars according to their mode identifications.

Key words: Stars: β Cep, δ Scuti, RR Lyrae, Cepheids, histogram of periods distribution, mode identifications

1. Introduction

The matter of modal content for the pulsating stars has only been solved satisfactory for double-mode Cepheids. The failure to establish the driving mechanism in β Cephei stars is one of the most serious problems in our understanding of stellar pulsations.

We look at the matter the other way round using: 1) statistical data from the fourth edition of the General Catalogue of Variable Stars (Volumes 1-3, hereafter GCVS), considering distribution of periods for these stars; 2) histogram of periods distribution and dependencies of masses, radii and radial pulsation constants, Q , upon period (from Shobbrook's data, 1985); 3) the results of periodogram analysis of individual β Cep stars in NGC 3293 (Engelbrecht, 1986).

2. The analysis of periods distributions from GCVS' data

On the base of GCVS' sampling (75 β Cep stars with the known periods) has been carried out the analysis of periods of these stars. We have constructed a histogram of periods distribution of β Cep variables with interval of periods $\Delta P = 0.02$ days. It is given in Table 2 and shown in Figure 1.

On the base of our analysis of this histogram (Table 2 and Figure 1), we have 10 peaks (maxima) and some steps near to them (see Table 1). The main peak at the mean period of 0.170 days (interval of periods $\Delta P=0.160-0.180$ days) has amplitude $n=12$ stars. If

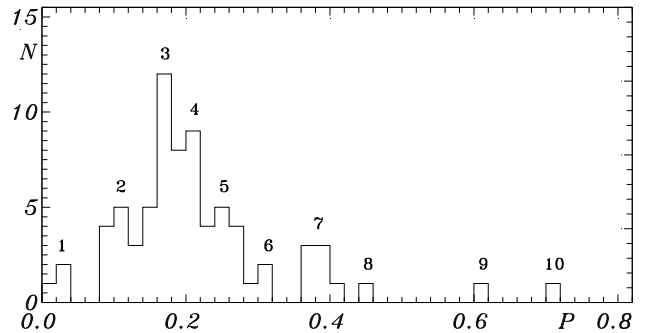


Figure 1: Periods distribution of β Cep stars according to GCVS, total number of stars $N=75$)

Table 1. Results of periods identifications for GCVS' data (m is the number of the peak)

m	i	P_i	n	P_{theor}	Ident.	k_i
1	1	0.0196	1	0.0188	$P_g/4$	1.043
1	2	0.028	2	0.028	$P_f/4$	1.000
2	3	0.08	2	0.084	P_{1H}	0.952
2	4	0.0896	2	0.090	P_e	0.996
2	5	0.101	2	0.100	P_r	1.01
2	6	0.108	1	0.1081	P^*	0.999
2	7	0.11267	3	0.11264	P_f	1.000
2	8	0.12377	1	0.120	$2P_s$	1.031
3	9	0.1378	3	0.135	$2P_{2H}$	1.021
3	10	0.153	4	0.150	$2P_g$	1.02
3	11	0.162	5	0.162	$2P^*_{1H}$	1.000
3	12	0.173	7	0.1728	$2P^*_e$	1.001
3	13	0.1684	12	0.169	$2P_{1H}$	0.996
3	14	0.1846	2	0.180	$2P_e$	1.026
3	15	0.1909	5	0.192	$2P^*_{r}$	0.994
4	16	0.201	6	0.200	$2P_r$	1.005
4	17	0.203	1	0.203	$3P_{2H}$	1.000
4	18	0.2156	4	0.216	$2P^*_f$	0.998
5	19	0.2374	4	0.2400	$4P_s$	0.989
5	20	0.2538	6	0.2535	$3P_{1H}$	1.001
5	21	0.2758	4	0.270	$4P_{2H}$	1.021
6	22	0.305	2	0.300	$3P_r = 4P_g$	1.017
7	23	0.3768	3	0.3755	$5P_g$	1.003
7	24	0.3971	4	0.400	$4P_r$	0.993
8	25	0.4504	1	0.4506	$4P_f = 6P_g$	0.9996
9	26	0.6096	1	0.609	$9P_{2H}$	1.001
10	27	0.7015	1	0.701	$7P_r$	1.001

Table 2. The histogram of β Cep stars' periods distribution ($\Delta P=0.02$ days)

ΔP (days)	N_{stars}						
0.00-0.02	1	0.20-0.22	9	0.40-0.42	1	0.60-0.62	1
0.02-0.04	2	0.22-0.24	4	0.42-0.44	0	0.62-0.64	0
0.04-0.06	0	0.24-0.26	5	0.44-0.46	1	0.64-0.66	0
0.06-0.08	0	0.26-0.28	4	0.46-0.48	0	0.66-0.68	0
0.08-0.10	4	0.28-0.30	1	0.48-0.50	0	0.68-0.70	0
0.10-0.12	5	0.30-0.32	2	0.50-0.52	0	0.70-0.72	1
0.12-0.14	3	0.32-0.34	0	0.52-0.54	0	0.72-0.74	0
0.14-0.16	5	0.34-0.36	0	0.54-0.56	0	0.74-0.76	0
0.16-0.18	12	0.36-0.38	3	0.56-0.58	0	0.76-0.78	0
0.18-0.20	8	0.38-0.40	3	0.58-0.60	0		

we compare it with individual periods in this step, it gives us the mean period 0.1684 days. Its identification (see Table 1) is a double period of the first overtone $2P_{1H}=0.169$ days for a fundamental period $P_f=0.11267$ days (the mean period for three stars) in peak 2. This period is equal to the fundamental period of radial pulsation of the sun $P_f=0.11264$ days. The ratio of these two periods P_i to P_{theor} is $k_i=1.0003!$ The ratio of the period 0.1684 days to the theoretical one $2P_{1H}=0.169$ days is 0.996. The analysis of periods of individual stars in the peak 2 gives us else four mean periods. We identify period 0.08 days (for two stars with equal periods) as the first overtone $P_{1H}=0.084$ days of fundamental period $P_f=0.11264$ days. The ratio of the observed and theoretical periods is equal 0.952. Period 0.0896 days is close to theoretical one $P_e=0.90$ days (the ratio is 0.996) in our extended set of radial modes (see Bezdenezhnyi, 1994a, 1994b, 1997a, 1997b). Period 0.101 days (for two stars with close periods) is identified as period $P_r=0.100$ days (the ratio is 1.01). And period 0.12377 days for one individual star is close to double period P_s : $2P_s=0.120$ days (the ratio is 1.031). For the first peak we have one individual period 0.0196 days near the theoretical one $P_g/4=0.0188$ days (the ratio is 1.04) and one the mean period about 0.028 days (for two stars) identified as $P_f/4=0.028$ days. The main (third) peak has some more three mean periods in its wings (steps on the left and on the right). Period 0.1378 days (for three stars) is close to the theoretical one $2P_{2H}=0.135$ days (the ratio is 1.021), period 0.153 days (for four stars) is identified as $2P_g=0.150$ days (the ratio is 1.02) and period 0.1846 days (for two close periods) - as $2P_e=0.180$ days (the ratio is 1.026). Period 0.1909 days (for five close periods) is not commensurable with $P_f=0.11264$ days but it is so with period 0.108 days (we denote it as P^*). The latter is a minimal of ones in the mean period P_f . Their ratio (P^* to 0.1909) is equal 0.566 (close to the theoretical ratio 0.5625 for double period P_r if we consider P^* as a fundamental one). There is one more

case like that for the mean period 0.2156 days in the next (the fourth) peak. One can identify this period as a double of P^* . We have a splitting of the period P_f and its overtones accordingly. In the fourth peak we have some more two mean periods: 0.201 days (for five close periods) near the theoretical period $2P_r=0.200$ days (the ratio is 1.005) and 0.203 days (an individual period) equal to $3P_{2H}$ (the ratio is 1). These two and the next periods are commensurable with P_f .

The fifth peak has three mean periods. Period 0.2374 days (for four close periods) identified as $4P_s=0.240$ days (the ratio is 0.989), 0.2538 days (for six periods) near the triple P_{1H} ($3P_{1H}=0.2535$ days, the ratio is 1.001), and 0.2758 days (for four periods) near $4P_{2H}=0.270$ days (the ratio is 1.021). The sixth peak has only one mean period 0.305 days (for two close individual periods). It may be identified as the following equal overtones: $3P_r=4P_g=5P_s=0.300$ days (the ratio is 1.017). The seventh peak has two mean periods: 0.3768 days (for three close periods) near $5P_g=0.3755$ days (the ratio is 1.003) and 0.3971 days (for four close periods) near $4P_r=0.400$ days (the ratio is 0.993). Further, three small peaks with single periods follow. Peak 8 has period 0.4504 days near $4P_f=6P_g=0.4506$ days (the ratio is 0.9996). Peak 9 has period 0.6096 days near $9P_{2H}=0.609$ days (ratio is 1.001), and peak 10 has period 0.7015 days near $7P_r=0.701$ days (the ratio is 1.001).

So, we have explained all peaks in the histogram of periods distribution for β Cep stars by means of commensurability with the fundamental period for these stars coincides with the fundamental period of radial pulsation of the sun. Period P^* (with its sequence) is found in other pulsating stars types: δ Sct and SX Phe, for example (from our unpublished data).

3. Identifications of β Cep stars' periods in NGC 3293

Engelbrecht (1986) has studied ten β Cep stars in NGC 3293. All stars are multiperiodic, some showing

Table 3. Results of identifications of β Cep stars' periods in NGC 3293

<i>star</i>	<i>freq</i>	P_i	<i>A, mag</i>	<i>ident</i>	k_i	<i>star</i>	<i>freq</i>	P_i	<i>A, mag</i>	<i>ident</i>	k_i
5	5.64	0.177	.0074	$2P_e$	0.983	16	3.99	0.251	.0267	$3P_{1H}$	0.990
	6.66	0.150	.0050	$2P_g$	1.000		4.92	0.203	.0023	$3P_{2H}$	1.000
	7.17	0.139	.0028	$2P_{2H}$	1.030	18	5.66	0.177	.0136	$2P_e$	0.983
10	5.92	0.169	.0100	$2P_{1H}$	1.000		5.74	0.174	.0094	$2P_{*e}$	1.006
	5.68	0.176	.0061	$2P_{*e}$	1.019	6.58	0.152	.0046	$2P_g$	1.013	
	4.76	0.210	.0043	$2P_{*f}$	0.972	5.77	0.173	.0046	$2P_{1H}$	1.024	
	6.11	0.164	.0034	$2P_{*1H}$	1.012	23	6.17	0.162	.0063	$2P_{*1H}$	1.000
5.46	0.183	.0027	$2P_e$	1.017	5.74		0.174	.0043	$2P_{*e}$	1.007	
11	6.86	0.146	.0065	$2P_{*g}$	1.014	24	6.64	0.151	.0036	$2P_g$	1.004
	6.69	0.149	.0039	$2P_g$	0.993		4.85	0.206	.0065	$3P_{2H}$	1.015
	7.22	0.138	.0034	$2P_{2H}$	1.021	6.25	0.160	.0062	$2P_{*1H}$	0.988	
	7.06	0.142	.0028	$2P_{*g}$	0.986	5.86	0.171	.0052	$2P_{1H}$	1.012	
14	6.61	0.151	.0023	$2P_g$	1.007	27	5.65	0.177	.0034	$2P_e$	0.983
	6.56	0.152	.0045	$2P_g$	1.013		4.40	0.227	.0103	$2P_f$	1.008
	6.33	0.158	.0040	$2P_{*1H}$	0.975	4.33	0.231	.0022	$4P_{*s}$	1.002	
65	5.90	0.169	.0029	$2P_{1H}$	1.000	8.81	0.114	.0030	P_f	1.012	
						9.97	0.100	.0022	P_r	1.000	

from two to five periods. He has found a range of possible non-radial modes identifications. "A roughly equal distribution of radial, dipole and quadrupole modes appears in these stars."

Our identifications give that all ten stars from Table 3 of this work maybe have radial modes (and their harmonics) in our extended system: F (2 times), 1H (5), 2H (4) and the modes R (1), G (6), E (4) introduced by the author (Bezdenzhnyi, 1994a, 1994b, 1997a, 1997b) earlier for RR Lyrae, δ Scuti and for other radial pulsating stars. The sequence of period $P^*=0.1081$ days: $2P_{*1H}$, $2P_{*f}$, $2P_{*e}$, $2P_{*g}$, and $4P_{*s}$ is present too (see Table 3). All the periods we may explain as radial modes for these two main fundamental periods $P_f=0.11264$ and $P_{*f}=0.1081$ days. The presence of these two sequences is the reason that we have so many close frequencies.

We know (GCVS) that the majority of β Cep stars probably show radial pulsations, but some (V649 Per) display non-radial pulsations. Multiperiodicity is characteristic of many of these stars. In our identifications we don't need to attract non-radial pulsations for ten β Cep stars as in original work (Engelbrecht, 1986).

4. The analysis of periods distributions from Shobbrook's (1985) data

On the base of Shobbrook's (1985) data for 47 β Cep variables we have constructed a histogram of periods distribution of these stars with the interval of periods $\Delta P=0.01$ days (Fig.2). Using distributions of individual periods into close groups, we have the following 23 mean periods (see Table 4). 11 periods from 23 ones

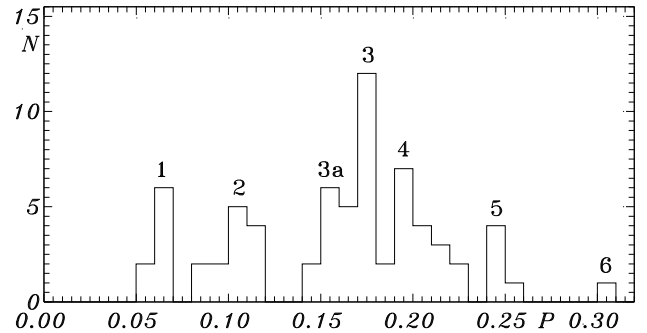


Figure 2: Periods distribution of β Cep stars (Shobbrook, N=47)

are commensurable with period $P^*=0.1081$ days, and the rest 12 periods follow P_f -sequence.

This border at period of 0.133 days has astrophysical bases as it follows from Shobbrook's (1985) data. The mean pulsation constant, Q, has a linear correlation with period and a sharp bend at this period of 0.133 days (see Fig. 3). After this period the slope of the second line is less. Using the pulsation ratio $Q = P \sqrt{\frac{\langle \rho^* \rangle}{\langle \rho \rangle}}$, we estimate mean densities $\langle \rho \rangle_1=0.068$ and $\langle \rho \rangle_2=0.038 \frac{g}{cm^3}$ for the mean lines (before and after period 0.133 days of this sharp bend). This border coincides with a gap between two peaks (2 and 3, see Fig 1 and 2). This gap lies between theoretical periods $2P_{*2H}=0.130$ days and $2P_{2H}=0.135$ days. Mean masses and radii distributions from period have a gap (or minimum) near this period. They change synchronously. So is behavior of $\lg T_e$ and M_{bol} with pe-

Table 4. Periods of β Cep stars' from Shobbrook's data histogram (47 stars)

P_i	<i>ident</i>	k_i									
0.055	$P_f/2$	0.977	0.115	$2P^*_s$	0.997	0.169	$2P_{1H}$	1.000	0.212	$2P^*_f$	0.981
0.061	P_s	1.017	0.118	$2P_s$	0.983	0.174	$2P^*_e$	1.006	0.229	$4P^*_s$	0.993
0.067	P_{2H}	0.991	0.130	$2P^*_{2H}$	theor	0.178	$2P_e$	0.989	0.246	$4P_s$	0.984
0.088	P^*_e	1.017	0.141	$2P^*_g$	0.979	0.191	$2P^*_r$	0.995	0.250	$3P_{1H}$	0.984
0.100	P_r	0.999	0.153	$2P_g$	1.020	0.201	$2P_r$	1.005	0.258	$4P^*_{2H}$	0.995
0.108	P^*_f	0.999	0.161	$2P^*_{1H}$	0.993	0.203	$3P_{2H}$	1.002	0.302	$4P_g$	1.007

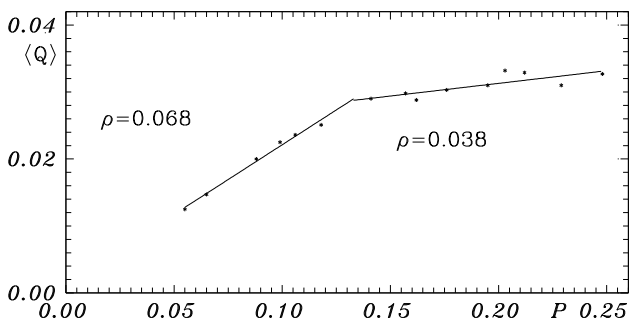


Figure 3: Mean pulsation constant correlation with period

riod as minimum M_{bol} coincides with one for T_e . That behavior of physical parameters before, after and at period of 0.133 days let us to pick out two groups of β Cep stars. It is possible one of them is BCEPS stars group.

In addition to GCVS' classification it is proposed to extend the range of periods for short-period group (BCEPS) to (0.02-0.13) days instead of (0.02-0.04)

days. It is proposed a new classification of these stars according to their mode identifications.

References

Bezdenzhnyi V.P.: 1994a, *Odessa Astron. Publ.*, **7**, 55.
 Bezdenzhnyi V.P.: 1994b, *Odessa Astron. Publ.*, **7**, 57.
 Bezdenzhnyi V.P.: 1997a, *Odessa Astron. Publ.*, **10**, 89.
 Bezdenzhnyi V.P.: 1997b, *Odessa Astron. Publ.*, **10**, 95.
 Engelbrecht C.A.: 1986, *Mon. Not. R. Astr. Soc.* **223**, 189.
 Kholopov P.N. (ed.): 1985a, 1985b, 1987, *General Catalogue of Variable Stars* (Vol. 1-3, abbr. GCVS), Nauka, Moscow.
 Ledoux P., Walraven T.: 1958, *Handbuch der Physics* **51**, 589.
 Shobbrook R.R.: 1985, *Mon. Not. R. Astr. Soc.* **214**, 33.

FREQUENCY ANALYSIS OF PHOTOGRAPHIC OBSERVATIONS OF PULSATING STARS

V.P. Bezdenezhnyi

Astronomical Observatory, Odessa National University, Ukraine
T.G. Shevchenko Park, Odessa, 65014, Ukraine, astro@paco.odessa.ua

ABSTRACT. The Fourier analysis are performed for photoelectric and photographic B-observations (Goranskij and Shugarov, 1979) of RR Lyrae star RW Ari. Besides the main frequency f_0 and four its first harmonics two more frequencies are found: $f_1=f_0/3$ and $f_2=0.711f_0$ c/d. It permits to identify frequencies: f_0 as f_s , introduced by us earlier (Bezdenezhnyi, 1997b) for RR Lyrae star T Sex, and f_2 - as f_{1H} .

Such analysis of photographic author's observations of RR Lyrae star BK Dra is performed too. It is shown that BK Dra is a multiperiodic variable star. Its frequencies identifications are carried out and given.

Three data sets of Cepheid V477 Oph: visual author's (Bezdenezhnyi and Mandel, 1977), photographic Mandel's (1970) observations and (O-C) - residuals (Hacke, 1988) show that V477 Oph apparently can be referred to bimodal Cepheids.

Key words: Stars: RR Lyrae, individual: RW Ari, BK Dra; Cepheids, individual: V477 Oph; Fourier analysis, mode identifications

1. Introduction

By using Breger's (1991) program PERIOD the Fourier analysis for photographic (and some photoelectric and visual) observations of two RR Lyrae stars RW Ari and BK Dra, and Cepheid V477 Oph has been carried out. Identifications for all frequencies have been performed. There are some overtones and their harmonics. These are related with multiplicity ratios.

2. Multiperiodicity of RR Lyrae star RW Ari

The Fourier analysis of photoelectric B-observations (n=132) from Goranskij and Shugarov's work (1979) are performed. The observations have been obtained on 60-cm telescope of Astronomical Institute of Uzbekistan Academy of Sciences (at the Maidanak mountain) and at Crimean Station of Sternberg Astronomical Institute. The main frequency $f_0=2.8222241$ c/d with B-amplitude $A=0.267$ mag has been obtained as well as its first four harmonics: $2f_0=5.6467821$ c/d ($A=0.028$ mag), $3f_0=8.4758498$ c/d ($A=0.021$ mag), $4f_0=11.2864165$ c/d ($A=0.015$ mag) and $5f_0=14.1199694$ c/d ($A=0.016$ mag).

Photographic B-observations (n=122) of the same authors obtained from the plates collection of Sternberg Astronomical Institute also show frequency $f_0=2.8222747$ c/d ($A=0.257$ mag) and the secondary frequency $f_1=0.93564$ c/d ($A=0.039$ mag at amplitude of 0.01 level false alarm probability $a=0.022$ mag). The frequency ratio $f_1/f_0=0.332$ enables to assume that the frequencies be related with the multiplicity ratio $f_0=3f_1$. This value of frequency f_1 is close to that of a triple frequency of the orbital period given by Wisniewski (1971): $3f_{orb} = 0.9448$ c/d. It is because of the multiplicity of these frequencies that the question may have arisen on a possible star binarity.

Photoelectric observations show one more frequency $f_2=2.01018$ c/d ($A=0.029$ mag at amplitude of 0.01 level false alarm probability $a=0.012$ mag) which has not been found when analyzing photographic observations. If it is a real one, then from the ratio $f_2/f_0=0.712$, which is close to the theoretical ratio of a frequency of the first overtone to frequency f_s introduced by us (Bezdenezhnyi, 1997b) for RR Lyrae star T Sex and also observed in other RR Lyrae stars (see for BK Dra in this paper) and in bimodal Cepheids (Bezdenezhnyi, 1997a), we can identify frequencies of RW Ari. Thus, $f_0=f_s$, $f_1=f_s/3$ and $f_2=f_{1H}$. Then rather numerous Penston's (1972) B-observations (n=29) have been added to above set and the Fourier analysis for general photoelectric set (n=161) was performed. The meaning of the frequency $f_2=3.0133114$ c/d ($A=0.029$ mag at $a=0.012$ mag) was revealed.

We can conclude that RW Ari is rather a multimodal of RR Lyrae star than a binary variable. Further analysis of photoelectric Wisniewski's (for 19 nights) and photographic Detre's (1937) observations (n=293) would be needed in order to confirm these results.

3. Multiperiodicity of RR Lyrae star BK Dra

The analysis has been performed of the light variation of BK Dra based on 165 light determination from the Dushanbe plate collection in the interval of 28 years (J.D. 2430166 - 2440448). Range of the brightness variations is 10.59-11.87 mag (pv), the meaning of one degree is 0.05 mag. The observations fit well the lin-

ear elements of General Catalogue of Variable Stars (Kholopov et al., hereafter GCVS, 1985):

$$Max_{hel} = J.D.2425523.305 + 0.5920815 E, \quad (1)$$

acting from 1905 (J.D.2416940). However, before an interval of time J.D. (2414900 - 2416150) another elements were true (GCVS, 1985):

$$Max_{hel} = J.D.2415150.817 + 0.592019 E. \quad (2)$$

For all the observational seasons mean light variation curves have been plotted. There is not any progressive deviation of the maximum light phase from zero but slight variations ranging from 0.99 - 0.02 are possible. The stellar light at minimum is constant, and that at maximum varies and the amplitude does respectively.

The frequency analysis of observations has shown that BK Dra is a multiperiodic star. Besides the main frequency $f_0=1.68896$ c/d ($P_0=0.5920803$ days fits well the linear elements (1)) and its first three harmonics three more frequencies are found. It permitted to identify the main frequency as the one f_s introduced by the author (Bezdenzhnyi, 1997b) for RR Lyrae star T Sex observed in bimodal Cepheids (Bezdenzhnyi, 1997a) too. The main frequency amplitude $A_0=0.36$ mag, its first harmonic $2f_s=3.37793$ c/d ($A=0.17$ mag), the second harmonic $3f_s=5.06687$ c/d ($A=0.10$ mag) and the third one $4f_s=6.75582$ c/d ($A=0.08$ mag).

Three additional frequencies are identified as double frequencies of known ones f_{1H} , f_{2H} and frequency f_e introduced by us earlier (Bezdenzhnyi, 1994) for RR Lyrae star AE Boo. So, these frequencies are: $f_1=2f_{1H}=2.38671$ c/d ($A=0.08$ mag at amplitude of 0.01 level false alarm probability $a=0.04$ mag), $f_2=2f_{2H}=3.00325$ c/d ($A=0.07$ mag) and $f_3=2f_e=4.50194$ c/d ($A=0.08$ mag).

Thus, BK Dra seems to be a multiperiodic RR Lyrae star as AE Boo and T Sex studied by us (Bezdenzhnyi, 1994, 1997b) earlier. But more precise photoelectric observations of this star are needed to confirm these results.

4. The multimodality of Cepheid V477 Oph

In our work (Bezdenzhnyi and Mandel, 1977) from Simeiz photographic observations period of 2.01566917 days was found, the star was classified as Cepheid similar to VZ Aql and V439 Oph. The period found has shown a good agreement for over 17000 days.

Unfortunately, Simeiz observatins are not numerous therefore we added to them photographic Mandel's (1970) observatins obtained from Odessa plates collection. The Fourier analysis of the data ($n=46$) was performed. It gave frequencies: the main one $f_0=0.4961166$ c/d (with amplitude $A=6.9$ degrees at amplitude of 0.01 level false alarm probability $a=0.6$ deg) and two its harmonics $2f_0=0.9921909$ c/d ($A=1.9$ deg), $3f_0=1.4882756$ c/d ($A=1.5$ deg). Two more frequencies were found: $f_1=0.464799$ c/d ($A=1.9$ deg)

and $f_2=1.097299$ c/d ($A=1.1$ deg). The frequency ratio $f_1/f_0=0.737$ is close to the theoretical ratio (0.738) of a frequency f_e to frequency of the first overtone f_{1H} . And the frequency ratio $f_2/f_0=2.212$ approaches the theoretical one (2.25) for double frequency f_g introduced by us (Bezdenzhnyi, 1994). Due to this it is possible to identify these frequencies as $f_0=f_{1H}$, $f_1=f_e$ and $f_2=2f_g$.

The Fourier analysis was done for 98 visual author's observatins (Bezdenzhnyi and Mandel, 1977) covering 17 nights within 363 days. The same frequencies as before has been obtained: the main one $f_{1H}=0.4962053$ c/d ($A=4.4$ deg at $a=0.4$ deg), the first harmonic of this frequency $2f_{1H}=0.9920007$ c/d ($A=3.5$ deg), $3f_{1H}=1.489035$ c/d ($A=2.1$ deg), $f_e=0.4635215$ c/d ($A=3.1$ deg) and $2f_g=1.0980822$ c/d ($A=1.5$ deg).

Then Fourier analysis of 135 (O-C)-residuals within 20439 days (Hacke, 1988) was performed. (O-C)-residuals were given with period $P_0=2.015669$ days ($f_0=0.496113$ c/d) from our work (Bezdenzhnyi and Mandel, 1977). Fourier analysis showed: peak at frequency $2f_0=0.992225$ (that is equal sharp to above our double one) had the biggest amplitude. Two higher harmonics $3f_0$ and $5f_0$ are present too. We have done a fitting with these three frequencies: $2f_0=0.9922261$ c/d ($A=0.403$ days), $3f_0=1.4883391$ c/d ($A=0.192$ days) and $5f_0=2.4805642$ c/d ($A=0.020$ days). After subtraction of this fitting the frequencies $7f_0=3.4728$ c/d ($A=0.006$ days at $a=0.002$ days) and $f_e=0.4673$ ($A=0.004$ days) were found.

Thus, V477 Oph apparently can be referred to bimodal (or even multimodal) Cepheids. To confirm these results the analysis of more precise photoelectric observations of V477 Oph are needed.

References

- Bezdenzhnyi V.P.: 1994, *Odessa Astron. Publ.*, **7**, 55.
 Bezdenzhnyi V.P.: 1997a, *Odessa Astron. Publ.*, **10**, 89.
 Bezdenzhnyi V.P.: 1997b, *Odessa Astron. Publ.*, **10**, 95.
 Bezdenzhnyi V.P., Mandel O.E.: 1977, *Variable stars, Supplement 3*, 227.
 Breger M.: 1991, *Delta Scuti Star Newsletter*, Issue 3, 21.
 Detre L.: 1937, *AN*, **262**, 81.
 Goranskij V.P., Shugarov S.Yu.: 1979, *Variable Stars*, **21**, 211.
 Hacke G.: 1988, *Sonn. Mitt.*, **340**, 146.
 Kholopov P.N. et al.: 1985, *General Catalogue of Variable Stars*, v.1, Nauka, Moscow.
 Mandel O.E.: 1970, *Variable Stars*, **17**, No. 4 (130), 347.
 Penston M.J.: 1972, *M.N.R.A.S.*, **156**, 103.
 Wisniewski W.Z.: 1971, *Acta Astron.*, **21**, 307.

BD +20° 1171 - LONG-PERIODIC VARIABLE STAR

I.S. Brukhanov

Amateur group "Betelgeuse", Republic Center for Technical Art Schoolars, Sudmalis Str.,
16-27, Minsk 220033 Belarus, e-mail: betelgeize-astro@mail.ru

ABSTRACT. BD +20°1171 (= NSV 16732 = TYCHO 1320 91 1 = HD 39785 = SAO 077726) is a long-periodic pulsating variable star of SRc-type with a period of 20930^d, range of variations in B 8.^m8 - 10.^m3, and the most reliable maximum is JD 2443410.5

Key words: Stars: SRc - type: BD +20°1171

The variability of brightness of the star BD +20°1171 ($a = 05^{\circ}55^{\text{m}}37.8^{\text{s}}$, $S = +20^{\circ}28'08''.4$ (2000.0); spectrum K5), has been discovered by An-dronov et al. (1994) and Renault (1984). The highest peaks at the periodogram computed for the measurements on the Odessa Sky Patrol plates (Andronov et al., 1994) correspond to possible periods 13700^d and 50 - 200^d.

The author made an independent research of the star BD +20°1171 on the negatives of the S, T, A series of the Moscow plate collection. Alltogether 90 data points have been obtained. The finding chart and the comparison stars have been kindly given to us by I.L.Andronov. The author determined the brightness of comparison stars according to the standart SA 74 in the photometric system B.

Computer analysis of the observations obtained in the interval 1896-1994 argues for the most satisfactory period $\sim 20930^{\text{d}}$ (Fig. 2) and possible periods of 11500 - 14000^d, 16000 - 18000^d corresponding to lower peaks at the periodogram and also didn't prove periods 50 - 200^d.

Such a discrepancy in results is caused by absence of coherent periodicity and shows variations of the possible period and shape of the pulsations. Much shorter cycles of low coherence of a thousand day (or even shorter) scale are possible.

For the provement of all the reserch results, it is necessary to make an independent research on negatives of the Sonneberg and Harvard photograph libraries in the interval 1900 - 1960.

Acknowledgements. The author is thankful to V.G. Karetnikov and I.L. Andronov for attention and help.

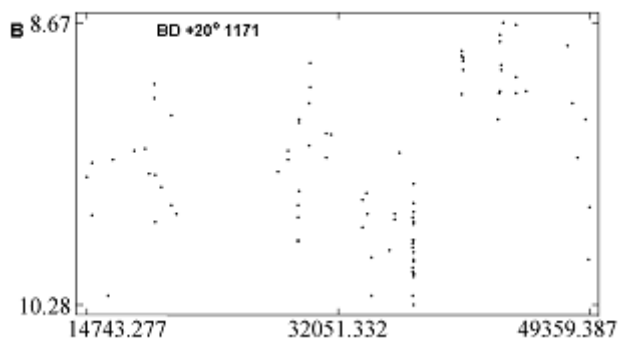


Figure 1: Light curve of BD +20°1171

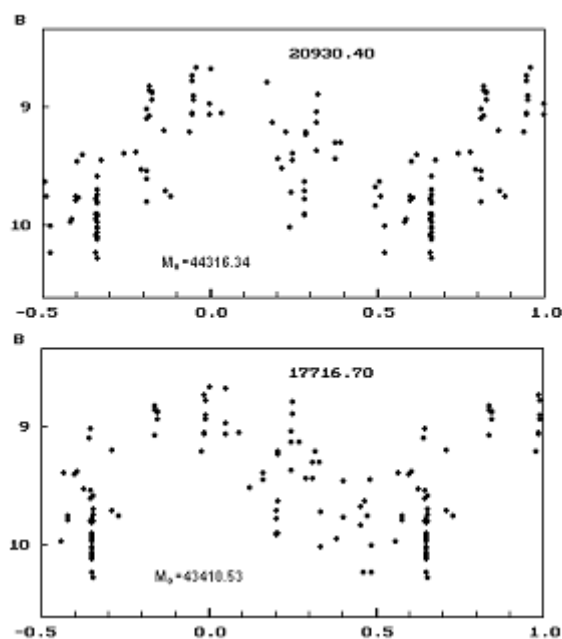


Figure 2: Phase light curves of BD +20°1171

References

- Andronov I.L., Pikhun A.I., Kudashkina L.S.: 1994, *Astron. Tsirk.*, **1554**, 27.
Renault J.: 1984, *Bull. AFOEV*, **27**, 1, 5.

BM ERI - SR-TYPE VARIABLE STAR

I.S. Brukhanov

Amateur group "Betelgeuse", Republic Center for Technical Art Schoolars,
Sudmalis Str., 16-27, Minsk 220033 Belarus, e-mail: *betelgeize_astro@mail.ru*

ABSTRACT. Based on 218 negatives from the Odessa plate collection, BM Eri is classified as an SRa-type star with a $565.^d5$ period; range in pv $6.^m9 - 8.^m5$; spectrum gM6; more probable minima at JD 2439042, 2440183.4, 2446475.

Key words: Stars: SRa - type: BM Eri

The variability of BM Eri was discovered by S. Gaposchkin (1946, 1953). A number of authors proved the discovery. The star was also rediscovered by C. Hoffmeister (1963) in 1959. A small number of measurements lead researchers to a conclusion, that BM Eri is an eclipsing binary with a 15320 - 20000 day period (Kholopov et al., 1987). Independently the variability of BM Eri was rediscovered by V.A. Bartolog (1987) with a minimum at 13.02.1986. A.I. Pikhun's advise led the autor to the decision to do an independent research, using the negatives from the Odessa plate collection.

The star was measured in the photovisual system pv. Visual estimates have been carried out using the method by Nuyland - Blazhko. The finding chart is shown in Fig.1. The brightness of the comparison stars was determined by linking to the photometrical standart Hyades (Kazanasma et al., 1981). The light curve is shown in Fig. 2.

The time series analysis has been carried out using the method by Deeming (1975). The period of $565.^d5$ was detected, which perfectly confirms photometrical measurements of the "Hipparcos" experiment. oreover, the star shows the period of $\sim 9000^d$, the "season of eclipses" - the most noticeable weakenings of brightness with an amplitude from $0.^m5$ to $1.^m5$, which last $\sim 6000^d$; the "season of quasiconstancy" with a small, ($\leq 0.^m4$) amplitude, which lasts for $\sim 3000^d$. This confirms results by Gaposchkin (1946) and Hoffmeister (1963).

Acknowledgements. The author is thankful to A.I. Pikhun, N.N. Samus, I.L. Andronov, V.G. Karetnikov, V.A. Bartolog, M.A. Grishel for attention and help.

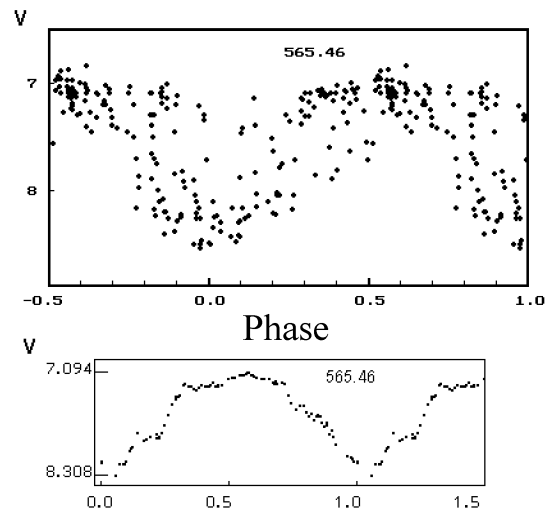
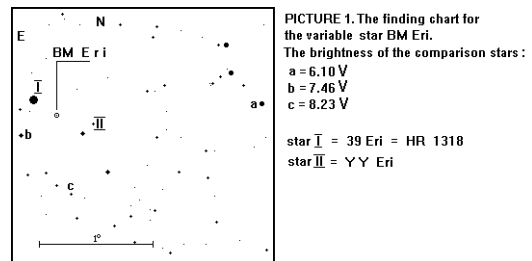


Figure 2: Phase light curve.

References

- Bartolog V.A.: 1987, *Variable Stars*, **22**, 619, 622.
Gaposchkin S.: 1946, *AJ* **52**, 43.
Hoffmeister C.: 1963, *VSS*, **6**, 1.
Kazanasma M.S., Zavershneva L.A., Tomak L.F.: 1981, *Atlas and catalogue of photoelectric standards*, Kiev, Navukova Dumka.
Kholopov P.N. (ed.): 1987, *General catalogue of variable stars*, **2**.

SPECTROSCOPIC NON-ADIABATIC DIAGRAMS FOR MULTIMODAL PULSATING STARS

J. Daszyńska, H. Cugier

Astronomical Institute of the Wrocław University

ul. Kopernika 11, 51-622 Wrocław, Poland, *daszynska@astro.uni.wroc.pl*

ABSTRACT. Recently we proposed a new method of mode identification based on spectroscopic nonadiabatic diagrams (Cugier & Daszyńska 2001, *As.Ap.*, 377, 113). Our results are for β Cephei models. These diagrams involve the amplitude ratios and phase differences calculated from various oscillating parameters measured from line profiles. We found that the spectroscopic observables are especially useful to determine m values. In this paper we investigate the case of multimodal pulsating models.

Key words: Stars: variable: β Cephei, multiperiodic; Line: profiles, Pulsation: mode identification.

1. Introduction

In many β Cephei stars we observe more than one excited mode of pulsation. The mode identification in the multiperiodic variables is of great importance, because the richer spectra of oscillation frequencies constrain potentially much stronger the stellar properties. Unfortunately the frequency spectra of B type stars are sparse, in comparison to the Sun or some white dwarfs, and we need more sophisticated method to derive three quantum numbers, which characterise a given mode of oscillation.

In previous papers we proposed the method of mode identification in β Cephei stars based on the constructing diagrams with amplitude ratios and phase differences derived from various line profile parameters (Cugier & Daszyńska 2001, Daszyńska & Cugier 2001). We adopted the term *spectroscopic nonadiabatic observables* for these quantities. The properties of these observables were investigated from calculated time series of theoretical line profiles of Si III 455.26 nm for Main Sequence stellar models with a mass of $10 M_{\odot}$. All unstable modes were considered in the limit of the single mode of oscillation. In this paper we study the multimode case.

The plan of the paper is as follows. In Section 2 we describe the method of calculations. The results for a MS stellar model of $10 M_{\odot}$ with three unstable modes excited simultaneously are given in Section 3.

2. Model calculations

We calculated time series of Si III 455.26 nm line profiles for the $10 M_{\odot}$ stellar model of $\log T_{\text{eff}} = 4.3693$ and $\log g = 3.9137$. We used results of linear nonadiabatic calculations of Dziembowski & Pamyatnykh (1993), as well as the line blanketed models of stellar atmospheres of Kurucz (1996), see Cugier & Daszyńska (2001) for details. We selected three modes with the periods: $P_1 = 0.^d11846$, $P_2 = 0.^d15633$ and $P_3 = 0.^d17112$, and assumed the corresponding amplitudes of the radius variations of $\varepsilon = 0.015$, $\varepsilon = 0.005$ and $\varepsilon = 0.003$, respectively. The (ℓ, m) -values are $\ell = 0$ for P_1 , $\ell = 2, m = +2$ for P_2 and $\ell = 1, m = -1$ for P_3 .

The data contain 3000 line profiles calculated at equally distant time points with the step of 0.005 day. From these line profiles we measured several characteristics including residual intensities measured at the deepest point of the normalized line profiles (F_{min}), radial velocities corresponding to F_{min} (V_{min}), equivalent widths (EW), full width at the half of maximum ($FWHM$), radial velocities corresponding to $FWHM$ (V_{hm}), line intensities at $\lambda_0 = 455.26$ nm (F_{λ_0}) and line intensities at $\lambda_1 = \lambda_0 - 0.05$ nm (F_{λ_1}). The data span an interval of 15 days.

Now, we search frequency spectra of these time series. For this purpose we compute the least-squares (LS) power spectra using Jerzykiewicz's computing code, which is based on the well-known method of Lomb (1976). The computations were carried out with the step of 0.001 cycles day^{-1} . The results were searched for the maximum values of the power, $p(f)$, over frequency interval up to 30 cycles day^{-1} . The frequency responsible for the highest value of the power was found. After prewhitening with this frequency, we repeated the calculations. In some cases the periodogram analysis reveals the presence of many mixed frequencies in addition to the primary frequencies of modes of oscillations. Finally, for a given set of frequencies we calculated synthetic curves, which fit the best, in the sense of LS, the measured quantities as a function of time.

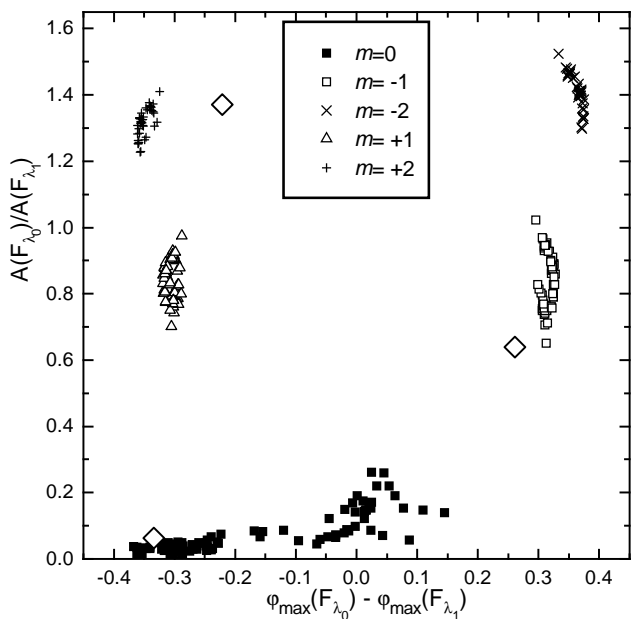


Figure 1: The amplitude ratio *vs.* phase difference for the monochromatic fluxes F_{λ_0} and F_{λ_1} . Modes with different m are marked by various symbols. Big diamonds represent modes retrieved from theoretical calculation for multiperiodic model.

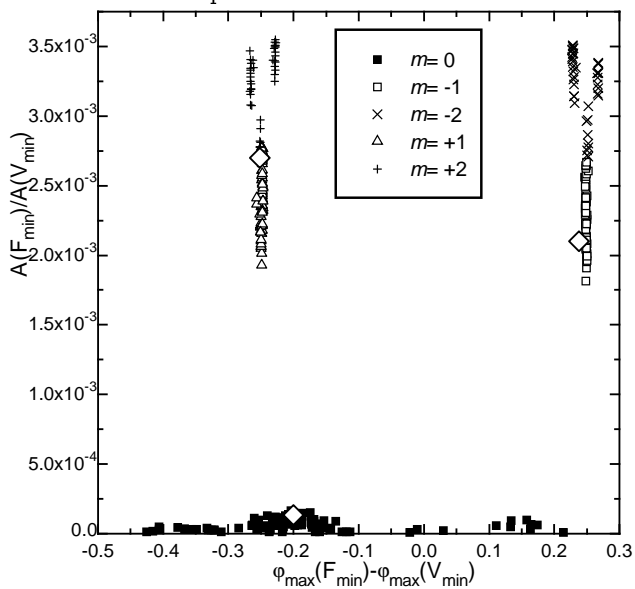


Figure 2: The same as in Fig. 1, but for F_{\min} and V_{\min} .

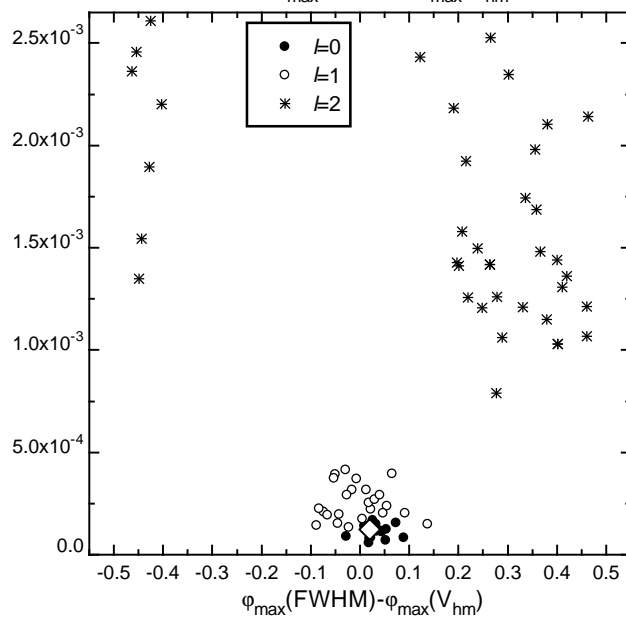
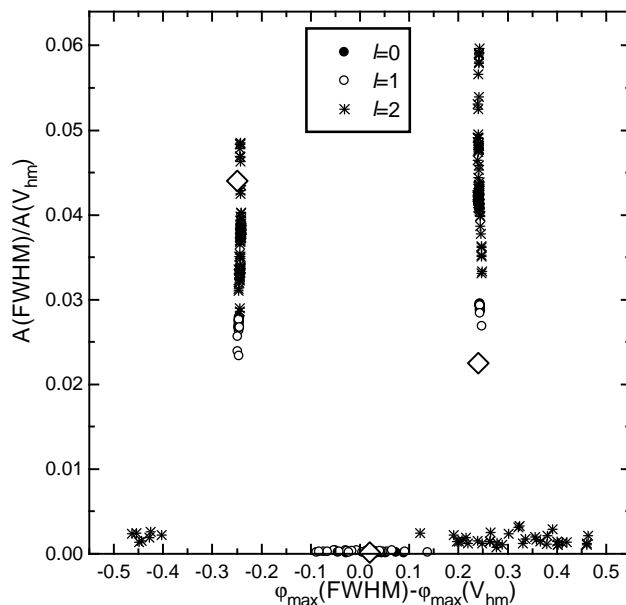


Figure 3: The spectroscopic diagram for the pair $(FWHM, V_{hm})$. Here modes are marked by various symbols with respect to harmonic degree. In the top panel there are all unstable modes with $\ell = 0, 1, 2$, and in the bottom one only zonal modes ($m = 0$).

3. Mode identification for multiperiodic β Cep star

Having frequencies, amplitudes and phases as described in Sect. 2, we constructed various spectroscopic nonadiabatic diagrams in order to check whether it is possible to retrieve the quantum numbers for the modes of oscillations. In Figure 1 we plot the diagram $A(F_{\lambda_0})/A(F_{\lambda_1})$ vs. $\varphi(F_{\lambda_0}) - \varphi(F_{\lambda_1})$. Big diamonds are assigned to the three modes studied in this paper. Here we also show all unstable modes with $\ell = 0, 1, 2, m = -\ell, \dots, +\ell$ for Main sequence models with the mass of $10 M_{\odot}$, at the selected epoch of evolution taken from Cugier & Daszyńska (2001). The modes with different azimuthal order are marked by various symbols. As we can see, the radial mode ($\ell = 0, m = 0$) is in proper place. In the case of the left two modes, ($\ell = 2, m = +2$), ($\ell = 1, m = -1$), we have a good location as far as the amplitude ratio is concerned, but in the values of phase difference they are a little misplaced.

Another example is for the observables F_{\min} and V_{\min} .

Figure 3 illustrates the possibility of deriving the harmonic degree. It turned out that the diagram employing FWHM and radial velocity corresponding to it, V_{hm} , is the best to obtain this quantum number. In Figure 3 we show the location our modes on this diagram, where various symbols are for different ℓ -values. As previously the modes obtained from the "multiperiodic" calculation are marked by big diamonds. In this case we have problem only with the mode of ($\ell = 2, m = +2$), because it is located at the joint of two regions: with $m = +1$ and with $m = +2$.

More detailed discussion will be given in a future paper.

References

- Cugier H., Daszyńska J.: 2001, *As.Ap.*, **377**, 113.
 Cugier H., Dziembowski W.A., Pamyatnykh A.A.: 1994, *As.Ap.*, **266**, 294.
 Daszyńska J., Cugier H.: 2001, *ASP Conf. Ser.*, in press.
 Dziembowski W.A., Pamyatnykh A.A.: 1993, *MNRAS*, **265**, 588.
 Kurucz R.L.: 1996, *CD-ROM No.13* and **19**.

ABOUT 21st RUN OF WET: PG 1336-018

T.N. Dorokhova¹ N.I. Dorokhov¹ J.-E. Solheim², J.M. González Pérez²

¹ Astronomical Observatory, Odessa National University
T.G.Shevchenko Park, Odessa 65014 Ukraine,
tnd@pulse.tenet.odessa.ua

²Department of Physics, University of Tromsø, N-9037 Tromsø, Norway,
janerik@phys.uin.no

ABSTRACT. We briefly communicate about 21st run of the Whole Earth Telescope (WET) in April 2001, where the eclipsing short period binary sdB system PG 1336-018 was the primary target.

Key words: Stars: hot subdwarfs: stars: individual: PG 1336-018, stars: oscillations, stars:: variables: EC 14026

1. The WET

The Whole Earth Telescope (WET) is a collaboration of astronomers who agree to observe a target star in such a way that observations can continue around the globe 24 hours a day, from site to site. The WET was organised in 1988, as an instrument to solve the alias problem which appears when one tries to interpret the time series amplitude spectra for a multimode pulsator from one single observatory. In order to resolve close modes, long nearly continuous coverage is necessary. So both the length of a run and the number of observatories that participate and their distribution in longitudes on the Earth are important parameters. Due to the wish of as global coverage as possible the campaigns are named as XCOVs for EXtended COverage. A summary of the first 10 years of WET operations was given by Kleinman (1999).

So far telescopes of sizes 1-2.5m have been used for the WET. The main instruments during the first 10 years have been two channel (object and comparison star) and 3 channel photometers (object, comparison star and sky background). The experience has shown that the 3 ch photometer can get good data even through light cirrus clouds, and it has been able to extend the length of a nights run with at least one hour, by the continuous measurement of the sky brightness. To be accepted for the WET observers and instruments have to fill requirements given by the WET collaboration.

Now the WET instrumentation is in a transition state as more and more of the observers use CCDs specially programmed for continuous readouts. With such

instruments it is possible to observe fainter stars, and also to correct for thin clouds.

Data are produced as standard ascii files and the WET collaboration has developed a set of PC programs (DOS) for the observations and the data reduction. In addition an interface card with a precise oscillator has been developed to collect the pulses from the photometer and send to the PC as numbers. A group in Lithuania has produced amplifiers, interface cards and complete photometers for the collaboration.

During a campaign a headquarters is organised with some experts that collect the data sent by e-mail from the observers as soon as they finish a night's observations. The headquarters people reduce data as soon as they get their hands on it, and post the results immediately on the internet pages of the WET (<http://wet.iitap.iastate.edu>), so that each observer in the field can follow his or hers contribution to the total light curve and also participate in the running discussion of the analysis of the data. Headquarters people are in daily contact with the observers, asking them about the weather prospects and tell them what to observe. A campaign has usually several targets, and if two observatories at the same longitude have clear weather, the headquarters can decide that one site observe the primary target and another one observe another target. The headquarters also give advice on the observing procedures and in particular check the timing, which has proved to be a problem at some observatories.

All the telescopes involved in WET work as a single instrument, as an orchestra - actually, to run an XCOV could be compared with a piece of music (Kleinman & O'Donoghue, 2000). At the moment Professor Steve Kawaler is the Director of WET, and Reed Riddle is his Deputy Director. They are located at the Iowa State University, Iowa, U.S.A.

Targets are traditionally chosen from the classes of pulsating white dwarfs (ZZ Ceti=DAV, DBV, DOV) and other rapidly (multi-periodic) variable stars, like IBWDs, interacting binaries, δ Scuti and roAp stars,

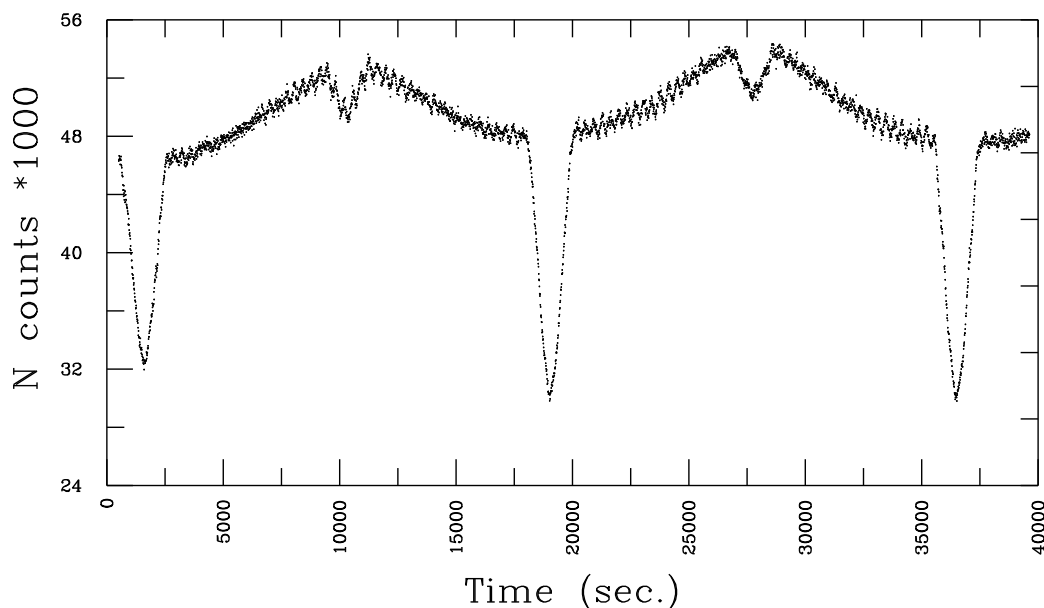


Figure 1: Light curve for PG 1336-018 observed at the Teide Observatory.

and the newly-discovered sdB pulsators.

2. The Target

The pulsating hot subdwarf PG 1336-018 (hereafter PG 1336) was the primary target of XCOV21 from April 15 to May 4 2001. 20 observatories from 16 countries around the globe aimed on this object during the run (Table 1). The list of observatories in Table 1 is sorted accordingly to their East longitudes which were extracted from *Astronomical Almanac* (2001).

The Principal Investigators for this run was Mike Reed from Iowa State University (USA), he observed in CTIO, and Dave Kilkenny from SAAO.

PG 1336 was also the target of XCOV17 in April, 1999, (Reed et al., 2000) and is really remarkable. It is a sdB star ($V=13.4$ mag) in a close binary system with $P=2.4$ hr. The name of the object is derived from Palomar-Green colorimetric survey. Recently some colorimetric surveys focus on the blue subluminoous objects, above all quasars and hot stars different kinds.

Understanding the evolution of sdB stars, the so called prewhite dwarfs, is very important and can be a clue to understanding of many mysteries of the late history of massive stars and population synthesis.

When a group of astronomers from SAAO (Kilkenny et al., 1997) discovered the pulsating sdB stars, it has opened the prospect of using asteroseismology to examine the interiors of these stars. Kilkenny et al. (1997) referred these objects to the EC 14026 stars, because a prototype was discovered in the Edinburgh-Cape survey investigations. According to the 75th namelist of

variable stars (Kazarovets, Samus & Durlevich, 2000) the class has been named RPHS – or "very rapidly pulsating hot (subdwarf B) stars", and the Prototype EC 14026 has been given the variable star designation V361 Hya. The pulsation periods of the EC 14026 stars range from 80 to 500 s and amplitudes are up to 30 mmag.

The 184 s and 141s pulsations of the sdB star, which is the primary of the partially eclipsing binary system PG 1336 were discovered by Kilkenny et al. (1998). As a result of the 17th run of WET Reed et al. (2000) found that the subdwarf pulsates in at least 15 modes - radial and non-radial. The companion is an M4-5 dwarf of approximately the same radius but considerably fainter and in the primary eclipse it covers roughly half of the pulsating star. The XCOV21 run of WET was optimised to search for the pulsations during the eclipses. The investigation of rotational splitting of the modes in eclipse and out of eclipse promises a real opportunity to identify radial and nonradial modes of the pulsations.

3. Some Results from XCOV21

Simulations done before the XCOV21 showed that some modes would be observable *only outside* the eclipses, some would be observable *only during* eclipses, and some both. This would help in classifying the modes. In the campaign it was expected to observe all eclipses during one week (Reed et al., 2001).

The coverage for PG 1336 in the XCOV21 became quite good. According to the WET internet pages (<http://wet.iitap.iastate.edu>) 268 hours were spent on

Table 1: WET XCOV21 observatories and telescopes.

Observatory	Abbr.	Country	Longitude	Tel. (m)
Mauna Kea		Hawaii, USA	-155° 28′	0.6
Southeastern Association	SARA	USA	-111° 36′	0.9
Mt.Lemmon		USA	-110° 48′	1.5
McDonald		USA	-104° 01′	2.1; 0.9
Hard Labor Creed Observatory	HLCO	USA	-83° 36′	0.4
Cierra-Tololo Interamerican Observatory	CTIO	Chile	-70° 49′	1.5
Pico dos Dias (Itajuba)		Brazil	-45° 35′	1.6
Nordic Optical Telescope	NOT	La Palma Spain	-17° 53′	2.6
Teide Observatory	OT	Tenerife, Spain	-16° 30′	0.8
Haute Provence Observatory	OHP	France	+5° 42′	1.93
Loiano		Italy	+11° 20′	1.5
South African Astronomical Observatory	SAAO	South Africa	+18° 28′	1.9; 1
Mt. Suhora		Poland	+20° 04′	0.6
Moletai		Lithuania	+25° 17′	1.65
Turkish Natl. Observatory		Turkey	+32° 47′	1.5
Crimean Astrophysical Observatory	CrAO	Ukraine	+34° 01′	1.25
Wise Observatory		Israel	+34° 46′	1
Uttar Pradesh (Naini Tal)		India	+79° 27′	1
Beijing Astronomical Observatory	BAO	China	+116° 22′	0.85
Mt.Stromlo		Australia	+149° 00′	1.9

PG 1336, and a total of 206 eclipses observed. Fig. 1 shows a long light curve from the Teide Observatory, Tenerife, where we can follow the pulsations into the eclipses which are only partial. The light curve from one of the primary eclipses is shown in more detail in Fig. 2.

However, the coverage in UT or longitude was quite uneven distributed in this campaign. From UT 21hr – to UT 09hr the object was observed 15-17 nights, while the coverage between 9 and 21 hr, corresponding to Asian longitudes, was an average 6 nights on the target, with a minimum of only one night between UT 18 and 19.

Fig. 3 shows the coverage hour by hour, and we note that there is considerable hole in the data set East of the Black Sea all the way to the Pacific Ocean. One could see also returning to Table 1 that from 20 observatories which participated in the run: 10 observatories were in the interval from -35° to $+35^\circ$, 7 ones were in the interval from -35° to -180° , and 3 observatories only - from $+35^\circ$ to $+180^\circ$, so we could make good use of more telescopes in this region.

At the same time on the location of the former Soviet Union stay large and equipped observatories, such as Mt.Dushak-Erekdag ($\lambda = 57^\circ 53'$), Mt. Majdanak ($\lambda=66^\circ 53'$), and Tien-Shan ($\lambda=76^\circ 57'$) observatories. Their modern instrumentation is not in use and decay from the lack or complete absence of local financial support.

We applied for the participation in this run of WET with the 0.8 m telescope and two-star photometer of Odessa Observatory which are situated at the Mt.Dushak-Erekdag in Central Asia (Dorokhov et al., 1997). However, for financial reasons we could not go to the Mt.Dushak-Erekdag and applied instead for an observational time in the Crimean Observatory.

4. The Multi-Colour Observations

The time for the simultaneous UBVR photometry has been given on 1.25 m AZT-11 telescope of the Crimean Observatory with the 5-channel photometer-polarimeter (Efimov et al., 1984). The multi-colour observations of PG 1336 prove useful to the mode identification and the eclipse modeling. Unfortunately the weather was not favourable in Crimea this spring, and only short series of observations could be obtained between the clouds. We selected a short interval of observations of 19 Apr with a bearable transparency and try to reveal the colour amplitudes in the region of principal frequency 5440 Hz, following to Kurtz (1998). The results are shown in Table 2: the filter, the effective length of band, the dominant frequency, the amplitude in mmag and the error of amplitude. Apparently, the results reflect the variability of atmospheric transparency in the Crimean Observatory on that time.

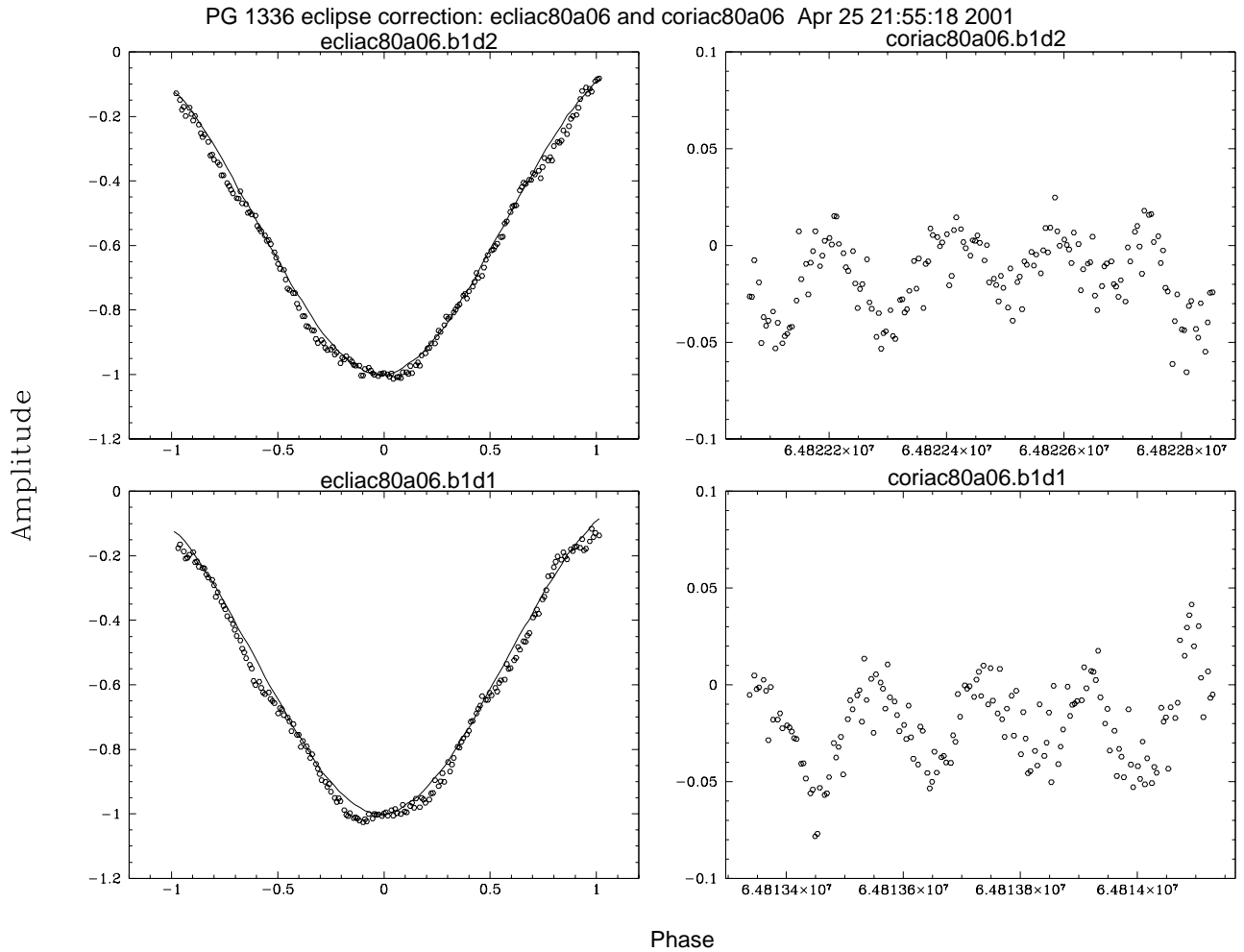


Figure 2: Details of the light curve for PG 1336-018 observed at the Teide Observatory. The curves show how the pulsations continue through two of the eclipses on April 24, 2001. (from wet.iitap.iastate.edu/xcov21/pg1336)

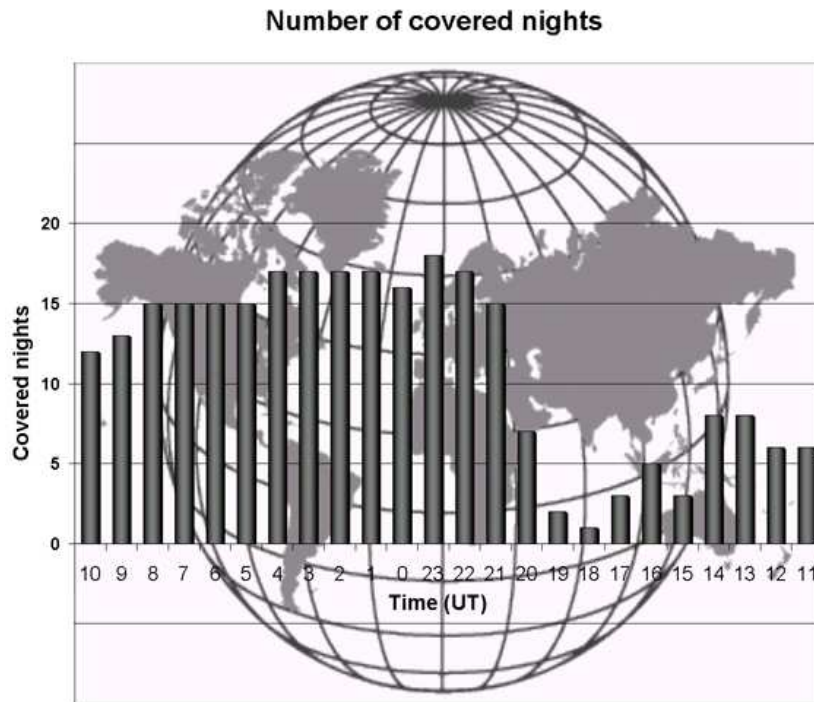


Figure 3: The distribution of the nights observed in particular intervals of UT, or the longitudes' distribution of the observatories. We see a substantial lack of coverage over the Asian continent.

Table 2: The colour semi-amplitudes.

Filter	λ Å	Frequency μHz	Amplitude mmag
U	3670	5675	10 ± 7
B	4360	5710	12.5 ± 5
V	5450	5118	4.5 ± 7
R	6380	5662	6.6 ± 5
I	7970	5611	1.6 ± 10

5. The Future of the WET

The next campaign XCOV22 is planned for May 2002, and in the WET internet pages it will be possible to follow this campaign as it happens (wet.iitap.iastate.edu). The targets selected are PG 1456+103 and PG 1159-035. For this campaign we hope there will be possible to fill the Asian gaps in the coverage we experienced in XCOV21.

Acknowledgements. We thank Steve Kawaler for helpful suggestions in writing this contribution. TND and NID are very grateful to N.M.Shakhovskoy and Nelly Merkulova for the giving observational time at the AZT-11 telescope and the assistance in observations.

References

Astronomical Almanac: 2001, Washington, London.
 Dorokhov N.I., Dorokhova T.N., Komarov N.S., Mukhamednazarov S.: 1997, *Odessa Astronomical Publications*, **10**, 123
 Efimov Yu.S., Piirola V., Shakhovskoy N.M.: 1984, *As.Ap.*, **138**, 62.
 Kazarovets E.V., Samus N.N., Durlevich O.V.: 2000, *IBVS* **4870**.
 Kilkeny D.; Koen C.; O'Donoghue D.; Stobie R. S.: 1997, *MNRAS*, **285**, 640
 Kilkeny D., O'Donoghue D., Koen C., et al.: 1998, *MNRAS*, **296**, 329
 Kleinman S.J.: 1999, in *11th European Workshop of White Dwarfs*, J.-E. Solheim & E.G. Meistas (eds), *ASP Conference Series*, **169**, 71.
 Kleinman S.J., O'Donoghue D.: 2000, *BaltA*, **9**, 3.
 Kurtz, D. W.: 2000, in *Variable stars as essential astrophysical tools / edited by Cafer Ibanoglu*. Dordrecht; Boston : Kluwer Academic Publishers, *NATO science series*, vol. **544**, p.373.
 Nather R.E., Winget D.E., Clemens J.C., et al.: 1990, *ApJ*, **361**, 309.
 Reed M. D., Kilkeny D., Kawaler S. D, et al.: 2000, *BaltA*, **9**, 183.
 Reed M.D., Kawaler S.D., Kleinman S.J.: 2001 in *12th European Workshop on White Dwarf Stars – ASP Conf. Series*, J.L. Provencal & H.L. Shipman, J. MacDonald, S. Goodchild, eds., **226**, 181.

PHOTOPOLARIMETRY OF SOME MIRA-TYPE STARS

Yu.S. Efimov¹, L.S. Kudashkina²¹ Crimean Astrophysical Observatory, p/o Nauchny, Crimea, 98409, Ukraine
*efimov@astro.crao.crimea.ua*² Astronomical Observatory, Odessa National University
T.G. Shevchenko Park, Odessa 65014, *astro@paco.odessa.ua*

ABSTRACT. The variations of the polarization parameters of three Mira-type stars V CrB, S CrB, T Her in the UBVRI bands are presented.

Key words: Stars: late-type: miras; stars: individual: V CrB, S CrB, T Her.

1. Introduction

An existence of dusty circumstellar envelopes is a wide-spread phenomenon. Such envelopes have been detected at R CrB-type stars, red giants and supergiants, T Tau-type stars, hot non-periodic Algol-type stars, IR sources etc.

Visible appearance of the dust existence varies from the existence of great IR excesses and absorption lines to photometric and polarimetric peculiarities. The physics of dusty circumstellar envelopes is a subject for special study.

In spite of the quite a few data on the miras polarimetry and spectropolarimetry one should note its inhomogeneity and fragmentary. Rather detailed information has been obtained for only small number of miras. Besides, most observations has been made at bright stage of stars due to brightness deficiency.

However, observations at the minimum and nearby to the co-called Eruption Point (EP) at the phase 0.8 (Fischer, 1968) are of special interest. That is a reason why at the Crimean Astrophysical Observatory (CrAO) in 1987 have been started the photopolarimetric observations of a sample single miras representing various spectral types and types of variability to study their polarimetric characteristics in minima and nearby to EP.

In this note we present some data of photopolarimetry of mira-type stars T Her (M-type), V CrB (C-type) and S CrB (M-type) based on the observations at CrAO. Everywhere the elements from the GCVS (Kholopov, 1985) were used to calculate the phases of light variations.

2. Observations and data reduction

All our photopolarimetric observations of miras were carried out at CrAO from May, 1987 till June, 1988 with the 125 cm telescope using the computer controlled UBVRI Double Image Chopping Photopolarimeter, developed by V. Pirola (1988).

The instrument provides measurements of the intensity and polarization simultaneously in UBVRI bands centered at 0.36, 0.44, 0.53, 0.69, and 0.83 μ , respectively.

The instrumental polarization in each color, determined from the observations of unpolarized standard stars, was usually very small ($< 0.2\%$). The calibration of the position angle was made observing stars with well known large interstellar polarization (Serkowski, 1974; Coyne et al., 1974; Hsu & Breger, 1982). The duration of observation varied from 15 min till one hour depending on the brightness of the star and sky conditions.

3. T Her

The star belongs to the most numerous class M-type miras. Only communication about the polarimetric observations of the star has been published in 1967 (Zappala, 1967). No polarization has been found. New observations of this star were carried out at the CrAO from May 11, 1987 till August 22, 1988.

Comparison star was SAO 66729 ($V=7.42$, $B-V=0.98$, $U-B=0.87$, $V-R=0.73$, $V-I=1.31$).

No correction for interstellar polarization was applied since the star is located at high galactic latitude ($b=+58^\circ$).

The period of pulsation of this star is one of shortest. It allowed us to monitor the polarimetric and photometric variations in the course of four adjacent cycles of pulsation (practically at all phases in one cycle and in some part of three adjacent cycles).

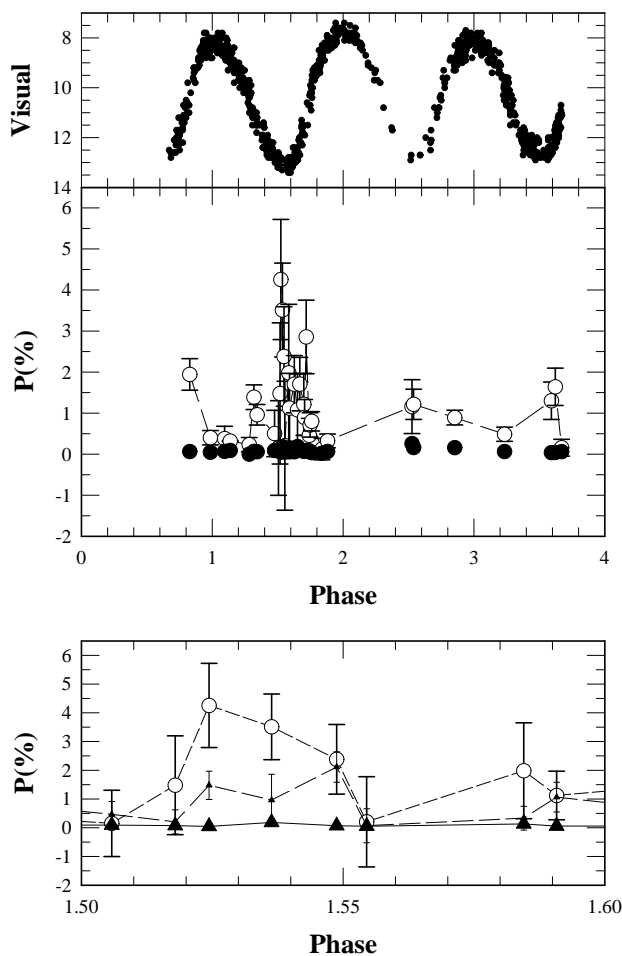


Figure 1: Variations of polarization degree P% (middle and bottom panels) with the phase of light variations in visual band from AAVSO (top panel) for T Her.

The visual light curve from the data of AAVSO is shown in Fig. 1 (upper panel).

In the figure an abscissa shows the phase of light variations and number of cycle calculated from the moment of previous light maximum. The light minimum is at the phase 1.6. A middle panel shows the variations of the degree of polarization P(%) only for two bands: U (open circles) and B (filled circles). The polarization in V,R and I bands is close to zero and does not depicted in the figure to avoid the overlap of the points. It is seen that the polarization is small everywhere except the phase interval between 1.5 and 1.6 which corresponds to the light minimum. In more details the variations of the polarization in this phase interval are shown in lower panel for three bands: U (open circles), B (filled circles) and R (filled triangles). It is seen that in this phase interval the degree of polarization has maximum and rises up to 4% in U-band.

Wavelength dependencies of T Her for some phases are shown in Fig. 2.

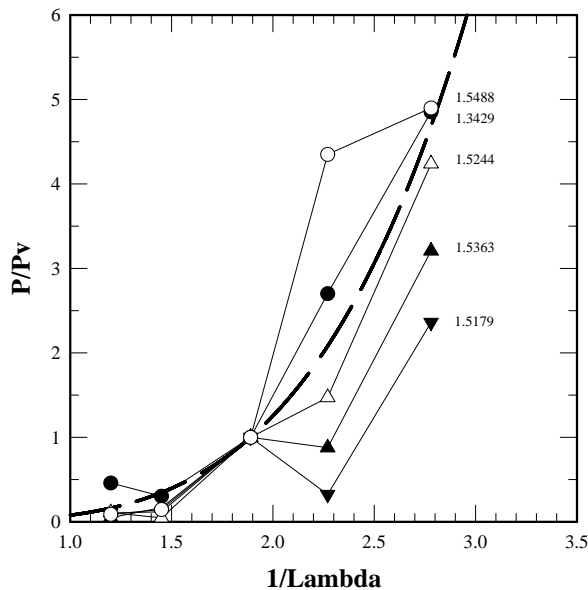


Figure 2: Wavelength dependencies of polarization P of T Her normalized to the degree of polarization P_v in V band. Numbers nearby to the curves indicate the phase of light variations. Thick dashed line corre-

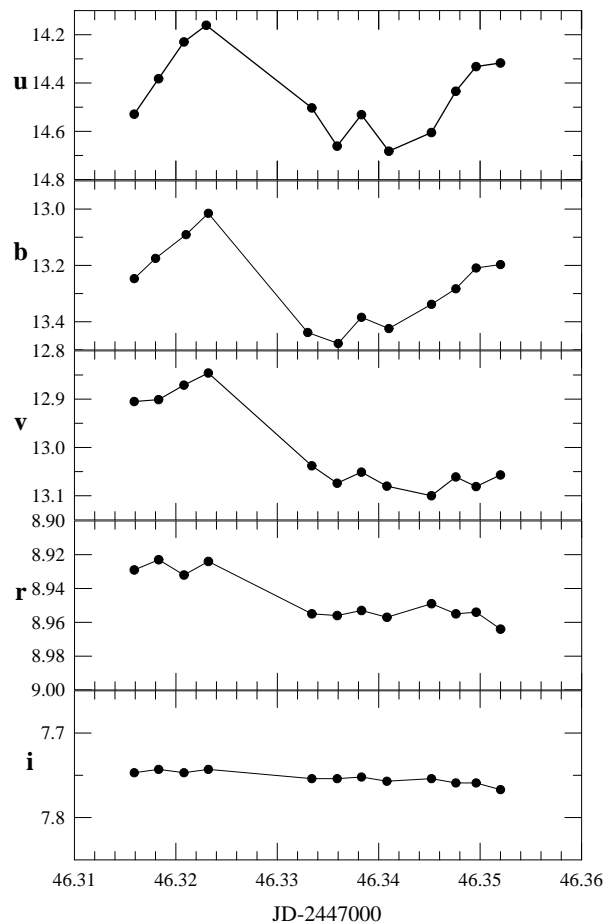


Figure 3: Intraday variations of the brightness of T Her in ubvri bands (instrumental system) on September 7, 1987 (JD 2447046).

It is seen that the shape of these dependencies tends to the the curve of Rayleigh scattering (thick dashed line) as the star approaches to its light minimum. The most prominent maximum of the degree of polarization in U band is also located in this narrow phase interval at the very bottom of the light minimum. So, it seems that the polarization is in fact produced by the scattering the radiation of the star on small dust particles in its circumstellar envelope.

It is well known that late-type stars are unstable on various time scales. In contrast to the longtime variability of miras much less is known about their intraday variations. Fig. 3 shows the brightness variations of T Her during one of night (September 7, 1987) when one can see the different kind of variations.

It is well seen that the maximum amplitude of brightness variations was in U band (about 0.5^m) and decreased toward red light where the amplitude of brightness variations in I band was less than 0.1^m . The time scale of variation was about one hour.

According to the classification by Strelkova (1956) T Her belongs to the II type of light variability, which is characterized by the shortwave colors variations in opposite sense with respect to the brightness variations, i.e. in the phase of minimum the star became bluer due to the decreasing of the TiO absorption bands with the decreasing the stellar temperature. This is well seen in Fig. 4 where we show the colors variations in four adjacent cycles of pulsation.

4. S CrB

The star belongs to the M-class. Previous polarimetric measurements, made by several authors in 1966 – 1970, revealed rather large and variable polarization. It was found that the degree of polarization increased when the brightness of the star goes toward its light minimum. New photopolarimetric observations of the star was made at CrAO from May 12, 1987 till August 11, 1988. The comparison star was SAO 64617 for which we estimated $V=6.86$, $B-V=0.95$, $U-B=1.01$, $V-R=0.75$, $V-I=1.28$. Our results are shown in Figs. 5,6,7.

As it is seen in Fig. 5, the broad polarization maximum, mostly prominent in U-band, locates in the broad light minimum. The position angle of polarization changed in the large interval of angles without any obvious dependence on phase.

The wavelength dependence of polarization is typical for miras, with large scattering in ultraviolet (Fig. 6).

The shortwave color indices changed in accord with the variation of brightness (Fig. 7).

It allows us to place this star into group I by the Strelkova's (1956) classification.

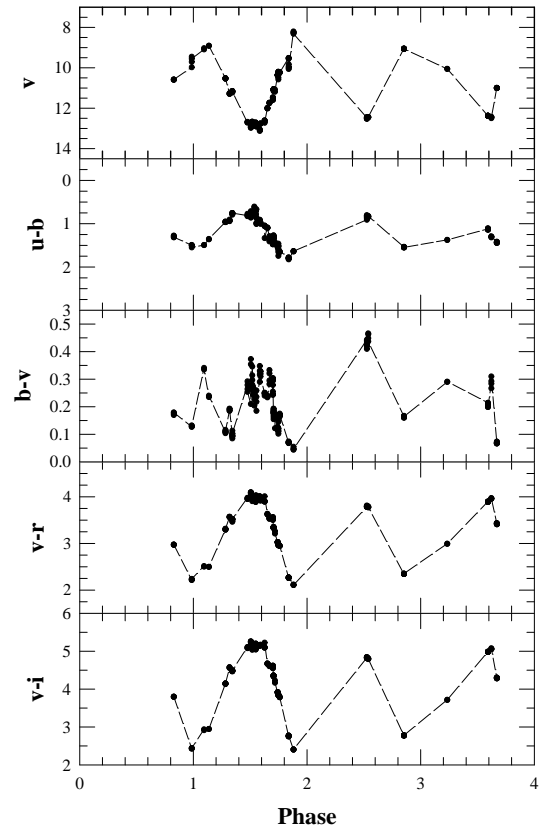


Figure 4: Variations of brightness v and colors $u-b$, $b-v$, $v-r$, $v-i$ of T Her in instrumental system with phase.

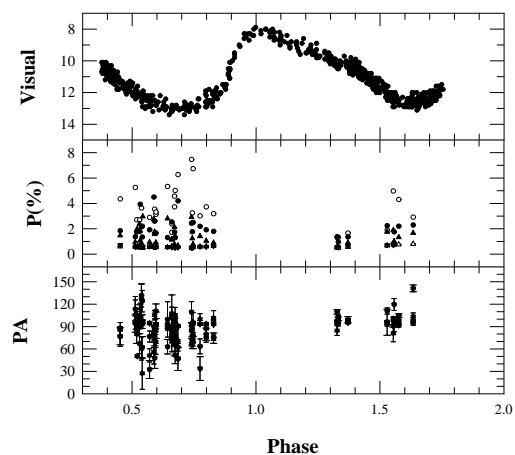


Figure 5: The variations of brightness in visual light from AAVSO (top panel), degree of polarization $P(\%)$ (middle panel) and position angle PA (degrees) (bottom panel) of S CrB in U (open circles), B (filled circles), V (filled triangles) and R (open triangles) bands with the phase of the light variations in two adjacent cycles.

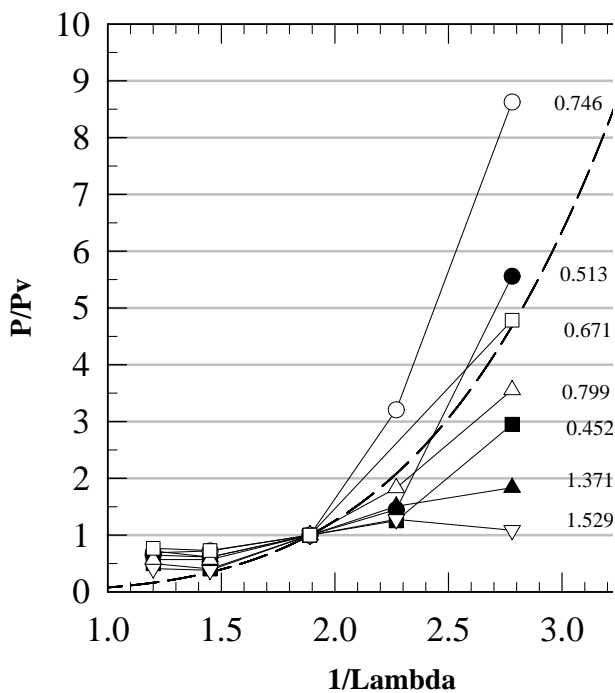


Figure 6: Same as Fig. 2, for S CrB.

5. V CrB

The star belongs to C-class. Previous polarimetry observations of the star made by different observers encompass the wavelength from the blue region to 2 μ . The variation of polarization parameters with time and wavelength was revealed in the sense that the star faded and the degree of polarization increased. Our observations were carried out from June 5, 1987 till June 20, 1988. No correction for interstellar polarization was applied since the star is at high galactic latitude ($b=51^\circ$). The detailed analysis of polarimetric study of V CrB had been published by Efimov (1995). Here we pay attention to some features. Besides the rise in polarization at the brightness minimum, it is seen from Fig. 8 that a rather large (up to 5%) degree of polarization in the B-band was observed at the maximum, in contrast to the polarization in other bands. It is also seen that the polarization plane has a continuous rotation in the course of the pulsation cycle (Fig. 8, bottom panel).

Wavelength dependencies of the degree of polarization in different phases show that the polarization rises toward shortwaves more fast than it may be expected from Rayleigh scattering (Fig. 9).

It is interesting that the behaviour of the position angle of polarization is quite different for two extreme stages of the star: in phase of minimum the orientation of the position angle in all bands is the same. However, the position angles of polarization in the maximum of brightness turn from visual and red to ultraviolet by 90° (Fig. 10). Till now no reasonable explanation was

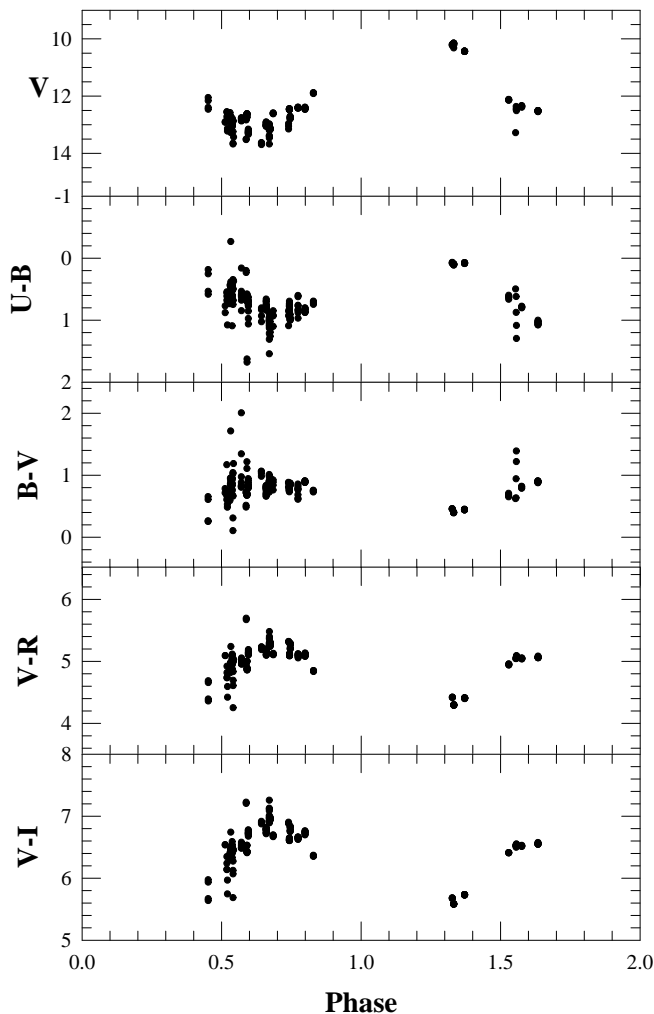


Figure 7: Same as Fig. 4 for S CrB but in standard Johnson system.

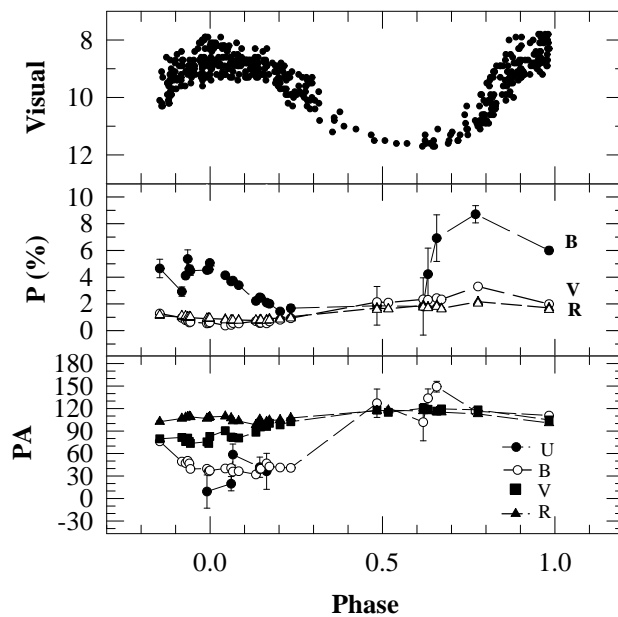


Figure 8: Same as Fig. 5 for V CrB.

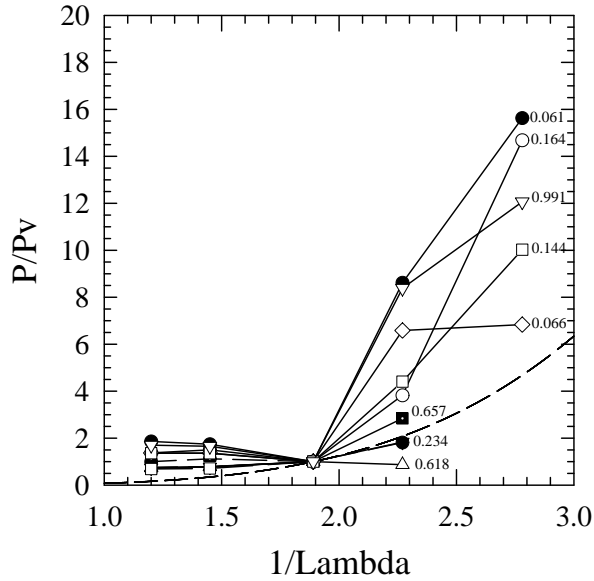


Figure 9: Same as Fig. 2 for V CrB.

suggested.

The results of observations of V CrB may be summarized as follow:

1. There are two different state of polarization. One state is observed at the phase of minimum and characterized by the practically constant orientation of the polarization plane along the spectrum. The other one with strong wavelength dependence of the position angle of polarization is typical for phase of maximum.

2. When star goes from maximum to minimum the degree of polarization increases and the position angle of polarization rotates.

3. The fast increase of the polarization occurred at the phase nearby to 0.6.

6. Discussion

From the study of the polarization variations at α Ceti it was found that its degree of polarization in UV at the phase 0.8 has a rapid increase at the factor two and then falls down. This rise of polarization occurred at the EP in the light curve described by Fischer (1968). This is also the time of the minimum of the U-B color (Serkowski, 1971) and the appearance of hydrogen emission lines. It was suggested that at this point starts the process of fast generation of small (less than 0.05μ) dust particles.

As the distance from the EP increases the size of the particles increases to 0.1μ or more (Materne, 1976) just before the new EP (Shawl, 1975b). However, until now we cannot distinguish between very small dust and gas atoms or molecules, since both give rise to Rayleigh-like scattering.

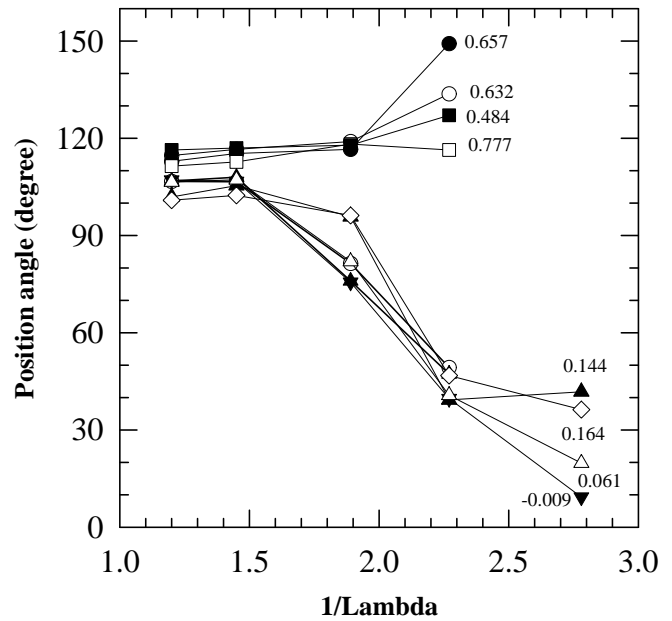


Figure 10: Same as Fig. 2 for V CrB but for position angle.

Three classes of models basing on asymmetry of physical or/and geometrical conditions have been proposed to explain the polarimetric features of miras:

1. Asymmetric distribution of circumstellar silicate dust with ferromagnetic inclusion (Shakhovskoj, 1963; Serkovski, 1971; Shawl, 1975a, 1975b).

2. Photospheric asymmetry, convective cells (Harrington, 1969; Schwarzschild, 1975).

3. Alignment of dust particles by magnetic field (Donn et al., 1966, 1968; Kruszewski, 1971; Dolginov and Mitrofanov, 1977).

The best agreement with observations has a combined model by Marcondes-Machado (1987), suggesting that:

- 1) dust consists of the silicate particles with ferromagnetic inclusions;

- 2) size of particles changes with the distance from the star;

- 3) there is the alignment of particles by the stellar magnetic field;

- 4) the geometry of magnetic field transforms with the distance from the star from dipole near to the stellar surface to the helix one;

- 5) the radiation at different spectral regions is generated at different distances from the star;

- 6) the dust condensation to certain final size occurs at the distance from the star from 3 to 10 stellar radii.

Physical characteristics of miras are strongly changed in the course of the pulsation cycle. Change of temperature exerts influence on the such physical properties of dust particles as their size, shape and compo-

sition which are connected with the optical properties of dust particles. It is clear that the change of these properties at the time of dust formation will change the properties of radiation passed through the dusty envelope. In particular, one may expect the specific changes of the colors and polarization parameters.

These variations will be most significant during the process of the dust formation as it takes place at R CrB-type stars. These changes may be used as the diagnostic tool for the property of circumstellar dust (Grinin, 1988; Efimov, 1988a, 1988b).

7. Conclusion

The comparison of our observations with the data from literature allow to conclude that cycle-to-cycle variations of polarization parameters of optical radiation may occur for stars of the same spectral class. The fast increase the polarization may take place not only at phase 0.8 but at other phases at the minimum brightness of star. There are some evidence on the possible intraday variations of brightness of some miras. To study the process of dust formation one need to estimate the effect of the absorption lines on the the observed photometric behaviour of miras and discriminate between the scattering on dust and gas. The tools to detect and study the dust around stars are the IR radiarion, the comparison of changing the degree of polarization and color indices with variation of brightness. The corresponding data may be obtained from the potopolarimetric monitoring of miras at the stage of dust formation.

Acknowledgements. The authors are thankful to Mrs. N. Petrova for help in the observations and reduction. In this research, we have used, and acknowledge with thanks, data from the AAVSO International Database, based on observations submitted to the AAVSO by variable star observers worldwide.

References

- Coyne G.V., Gehrels T., Serkowski K.: 1974, *AJ*, **79**, 581.
- Dolginov A.Z., Mitrofanov I.G.: 1977, *AZh*, **54**, 1259.
- Donn B., Stecher T.P., Wickramasinghe N.C., Williams D.A.: 1966, *ApJ*, **145**, 949.
- Donn B., Stecher T.P., Wickramasinghe N.C., Williams D.A.: 1968, *ApJ*, **153**, L143.
- Efimov Yu.S.: 1988a, *AZh*, **65**, 807.
- Efimov Yu.S.: 1988b, *AZh*, **65**, 979.
- Efimov Yu.S.: 1990, *Veroff. Sternwarte Sonneberg*, **10**, 28.
- Efimov Yu.S.: 1995, *Izv. CrAO*, **89**, 59.
- Fischer P.L.: 1969, *Ann. Univ. Sternwarte Wien*, **28**, 139.
- Grinin V.P.: 1988, *Pis'ma AZh*, **14**, 65.
- Harrington J.P.: 1969, *ApL*, **3**, 165.
- Hsu J.-C., Breger M.: 1982, *ApJ*, **262**, 732.
- Kholopov P.N.: 1985, *General Catalogue of Variable Stars*, 4th edition, Moscow, Nauka.
- Kruszewski A.: 1971, *Remeis Sternwarte, Bamberg, Veröff.IX*, No 100.
- Marcondes-Machado J.A.: 1987, *As.Ap.*, **188**, 131.
- Materne J.: 1976, *As.Ap.*, **47**, 53.
- Neckel Th., Chini R.: 1980, *As.Ap.Suppl.*, **39**, 411.
- Pirola V.: 1988, in *"Polarized Radiation of Circumstellar Origin"*, Eds. G.V.Coyne, et al., Vatican, 735.
- Schwarzschild M.: 1975, *ApJ*, **195**, 137.
- Serkowski K.: 1971, *Contr. Kitt Peak Obs.*, No 554, 107.
- Serkowski K.: 1974, in *"Planets, Stars and Nebulae Studied with Photopolarimetry"*, Ed. T. Gehrels, Tucson, Univ. of Arizona, 135.
- Shawl S.J.: 1975a, *AJ*, **80**, 8, 595.
- Shawl S.J.: 1975b, *AJ*, **80**, 8, 602.
- Shakhovskoj N.M.: 1963, *AZh*, **40**, 1055.
- Zappala R.R.: 1967, *ApJ*, **148**, L81.

SEARCH OF VARIABILITY OF THE COMPANION OF THE CLASSICAL CEPHEID EV Sct

I.A. Egorova, V.V. Kovtyukh

Astronomical Observatory, Odessa State University
T.G.Shevchenko Park, Odessa 65014 Ukraine, *val@deneb.odessa.ua*

ABSTRACT. Spectroscopic observations of EV Sct obtained on 4m telescope at KPNO showed that the secondary component is probably situated within the instability strip (Kovtyukh & Andrievsky, 1999). Some observers (Pel, 1976; Mermilliod, 1987) have noted a significant data scattering on the light curve. Therefore the companion of EV Sct perhaps is a small amplitude variable star. We present results of photoelectric observations of the EV Sct.

Key words: Stars: Cepheids; stars: individual: EV Sct.

1. Introduction

EV Sct is a famous classical Cepheid ($P=3.091^d$) belonging to NGC 6664 cluster, which was for a long time used for $P - L$ calibration.

2. The observations and analysis

We have observed the EV Sct in June 2000. The observations were made on the 1.25m telescope AZT-11 of Crimean AO. For 9 nights more than 600 UBVR estimates of brightness of the star with accuracy of 0.02-0.03 mag have been obtained. As a standard we used a star "A" NGC 6664 ($V=10.61$; $B-V=0.47$). The time of the exposition was 15 sec. The results are given in Tabl.1. Unfortunately the existing observational data is small and preliminary frequency analysis hasn't confirmed presence of variability of the companion.

The authors would like to thank Dr. N.M.Shakovskoj for his help in the obtaining of the observational data and Dr. N.I.Bondar' for helpful advices.

References

- Kovtyukh V.V., Andrievsky S.M.: 1999, *As.Ap.*, **350**, L55.
Mermilliod J.C., Mayor M., Burki G.: 1987 *As.Ap. Suppl.*, **70**, 389.
Pel J.W.: 1976, *As.Ap.Suppl.*, **24**, 413.

Table 1: UBVR observation

J.D Hel	U-B	B-V	V	R
2415200+				
12.32491	0.751	1.077	10.123	11.131
12.32913	0.768	1.076	10.124	11.130
12.34900	0.764	1.101	10.126	11.113
12.35157	0.766	1.096	10.121	11.110
12.36166	0.791	1.102	10.103	11.094
12.36378	0.791	1.099	10.099	11.097
12.38340	0.779	1.099	10.110	11.114
12.38542	0.797	1.096	10.116	11.120
12.39313	0.805	1.084	10.131	11.125
12.39579	0.792	1.076	10.133	11.122
12.40287	0.799	1.094	10.128	11.118
13.43067	0.852	1.170	10.343	11.178
13.44986	0.871	1.150	10.360	11.181
13.46313	0.861	1.173	10.339	11.169
15.31943	0.699	1.066	10.103	11.085
15.34042	0.680	1.073	10.110	11.085
15.35807	0.665	1.097	10.074	11.074
15.36800	0.696	1.070	10.102	11.080
15.37766	0.709	1.068	10.088	11.078
16.31895	0.598	1.116	10.323	11.082
16.33207	0.600	1.117	10.346	11.131
16.34560	0.567	1.094	10.323	11.110
16.36675	0.587	1.102	10.346	11.120
16.38851	0.620	1.102	10.382	11.131
16.39376	0.611	1.100	10.353	11.116
16.40590	0.603	1.102	10.345	11.117
17.42659	0.652	1.082	10.230	11.130
17.44177	0.671	1.072	10.207	11.112
17.47369	0.652	1.066	10.236	11.143
19.32258	0.806	1.162	10.294	11.181
19.34126	0.772	1.159	10.302	11.191
19.36829	0.731	1.148	10.295	11.200
19.38698	0.706	1.160	10.263	11.184
20.34944	0.823	1.121	10.248	11.137
20.37786	0.803	1.106	10.236	11.135
20.39740	0.802	1.119	10.229	11.130
21.45544	0.774	1.090	10.075	11.094
22.34105	0.866	1.162	10.276	11.164
22.36098	0.872	1.170	10.300	11.187

THERMAL WAVES AND UNSTABLE CONVECTION IN ZZ CETI STARS

N. Falcon, J. Labrador

Departamento de Física, FACYT Universidad de Carabobo
Av. Bolívar Norte, Valencia Apto. Postal 129 (casilla12) CP 2001 Venezuela,
nelsonfalcon@hispanista.com

ABSTRACT. We analyze the stability criteria by convection in ZZ ceti stars when the thermal relaxation times are not negligible. Using the Cattaneo law and the Mixing Length Theory in the degenerate regime, is shown that the heat flux can be propagated by thermal waves and predicts quasi periodic pulses in luminosity. This formalism is consistent with the semi-analytically approaches to temperature variations and several ZZ ceti light curves.

Key words: Stars: interiors, ZZ ceti: convection, stability.

1. Introduction

The thermal properties are responsible of radiation and further evolution of white dwarfs (WD) and ZZ stars. Also, the oscillations and pulsation's (non radial g modes) in DA and ZZ ceti stars are usually attributed to temperature intrinsic variations (Vth et al, 2001; Brickhill, 1992), in which the convection would be an important aspect (Althaus and Benvenuto, 1996; Bergeron et al 1992). Several investigators thinks about these oscillations as "temperatures" waves or heat waves (thought spherical harmonics model in the luminosity variation). However, is necessary to propose some evolutionary pattern of the oscillations observed in the light curves, starting from a formalism based on the usual equations of evolution and stellar structure. But, in standard calculations of the ZZ ceti asteroseismology the possibility of the heat propagation by waves is obviated in the energy transport equation. This simplification will be spurious in the degenerate material because, the relaxation time (the time required for to establish the heat flux when one temperature gradient is switched on) is not negligible. In this article, it is described how the energy transport equation and the luminosity in WD stars change if heat waves are taken into account. To make this, the Maxwell-Fourier law is replaced by the Cattaneo causal law (section 2). A general version of variation of the luminosity and the relaxation time based on the Cattaneo equation and

the heat waves is presented in section 3. Finally, a short discussion of the results, and its application in ZZ Ceti light curve is given in the last section.

2. The Cattaneo Law and the Energy Transport Equation

If the energy in stars is transported though the stellar layer by radiation, conduction and/or convection, the temperature gradient is given, in a good approximation, in the stellar interior in terms of local values of opacity κ density ρ and energy flux F by the energy transport equation (Kippenhahn and Weigert:1990, p.28; Hansen and Kawaler:1994, p.181.):

$$\frac{dT}{dr} = -\frac{3\kappa\rho F}{4acT^3} \quad (1)$$

where $a = 7,5710^{-15} \text{erg.cm}^{-3} \text{K}^{-4}$ is the radiation density constant and c is the light velocity. This relation is just Fourier-Maxwell law for energy flux due to thermal conductivity and/or radiative diffusion:

$$\vec{F}(\vec{x}, t) = -k\vec{\nabla}T(\vec{x}, t) \quad (2)$$

where the coefficient of conduction for the diffusion energy is: $k = \frac{4acT^3}{\kappa}$.

It is well known that Fourier-Maxwell law leads to a parabolic equation for T , according to which perturbations propagate with infinite speed (see Joseph and Preziosi 1989 and references therein). The origin of this non-causal behavior found in Eq. 2 which it is assumed that the energy flux appears at the same time the temperature gradient is switched on. Neglecting the relaxation time (τ) is, in general, sensible thing to do because for most materials it is very small (of the order of 10^{-11} s for the phonon-electron interaction and of the order 10^{-13} s for the phonon-phonon and free electron interaction, at room temperature). There are, however, situations where the relaxation time may not be negligible. For example in neutron star interior the relaxation time τ is the order 10^2 s by temperature the 10^6 K (Herrera and Falcon; 1995a).

The problem of heat propagation for times shorter than the relaxation time has been the subject of lengthy discussions since early work of Maxwell (Joseph and Preziosi 1989 and references therein) and most recently has been introduced in astrophysical scenarios. A heat flux equation leading to a hyperbolic equation is the Cattaneo law (see Joseph and Preziosi, 1984; Herrera and Falcn, 1995b):

$$\tau \frac{\partial \vec{F}}{\partial t} + \vec{F} = -k \nabla T \quad (3)$$

We assume the Cattaneo law for the temperature gradient similarly to the Eq.(1) we obtain:

$$\frac{dT}{dr} = -\frac{3}{4ac} \frac{\kappa \rho}{T^3} \left(\tau \frac{\partial \vec{F}}{\partial t} + \vec{F} \right) \quad (4)$$

If we replace F by the usual luminosity (L) Eq.(4) can be written as

$$\frac{dT}{dr} = -\frac{3}{16ac} \frac{\kappa \rho}{T^3 r^2} \left(\tau \frac{\partial L}{\partial t} + L \right) \quad (5)$$

In case of $\tau \approx 0$ to take notice of the relation (3) and (5) are the "classical" energy transport equation by stellar interior.

3. The Luminosity and the Relaxation Time

The influence and importance of the convection and mixing length theory (MLT) in a study and calculations of the atmosphere model for white dwarf is highly report (Atweh and Eryurt-Ezr, 1992, and references therein). However, the possibility that the time of relaxation is not negligible, in the nucleus of WD, it would bear to the existence of thermal waves. In that case the luminosity change admit quasi periodic variation when the times are less than relaxation time. We now used the Eq. (5) in the convection theory before relaxation (MLT before relaxation) which the luminosity is (Herrera, L. and Falcon, N.; 1995b):

$$L = L^{(d)} f(\chi, \omega) \quad (6)$$

with

$$f(\chi, \omega) = \frac{1}{\omega^2 + 1} \exp \left[\frac{\chi}{2} (\omega^2 - 1) \right] \quad (7)$$

$$\left[(5 + \omega^2) \cos(\omega \chi) - \frac{(3 - \omega^2)}{\omega} \sin(\omega \chi) \right]$$

and

$$\omega^2 \equiv \frac{4\tau}{\tau_d} - 1 \quad (8)$$

$$\chi \equiv \frac{t}{2\tau}$$

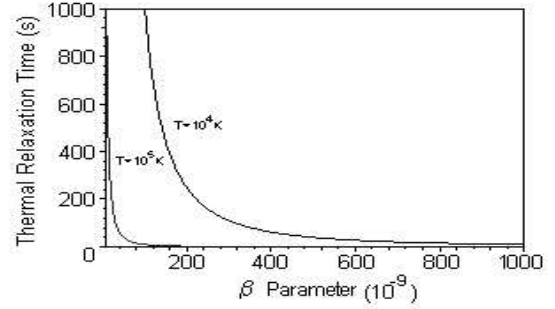


Figure 1: Relaxation Time and Heat Waves Speed to effective temperature interval

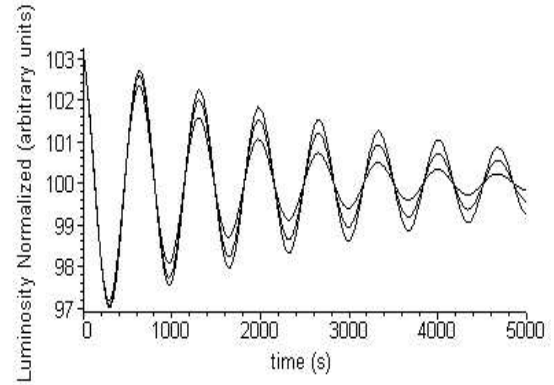


Figure 2: True Luminosity change, for $\omega = 0.94, 0.96, 0.97$ values

This equation (6) connects the standard luminosity (L) of MLT and the luminosity before thermal relaxation ($L^{(d)}$) owing to the heat waves, where f is a function of time t , relaxation time τ and thermal adjust time τ_d . The true luminosity change ($L/L^{(d)}$) is show in the figure 1 for several values of the ω . Note that the luminosity function is a dampen oscillation.

On the other hand, the calculation of the relaxation time can be starting from the relationship (see Herrera and Falcon, 1995a for details):

$$\tau = \frac{k}{V^2 C_V} \approx \frac{10^{-3} T^{-2}}{\beta^2} \quad (9)$$

in the last term it has been used the thermal conductiv-

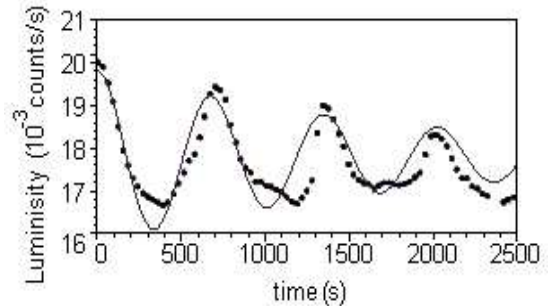


Figure 3: Simulation of the Light Curve of G 29-38

ity (k) for degenerate material (Flower and Itoh, 1979) and the specific heat (C_V) by the Chandrasekhars relationship (Hansen and Kawaler, 1994).

Obviously the relaxation time will depend of the value assumed for the thermal waves speed ($V = \beta c$). The figure 2 shows the relaxation time for diverse values of temperature and several thermal waves speed.

4. Results and Discussion

The luminosity fluctuation, due to the causal propagation of the thermal flow (Eq. 5 and 6) suggest an approximate model for the study of the ZZ Ceti stars. Inside the WD the matter is degenerate and the thermal conductivity is dominated by electrons, therefore the use of the Cattaneo Law is justified.

It can be thought of the existence of statistical fluctuations in the density or in the temperature, in some fluid portion in the stellar deep interior. The aleatory movement of certain convective globule, inside the gradient of temperature, would carry a fluctuation in the temperature and, in consequence a variation in the brightness. The luminosity variation of the convective flow would have, by virtue of the Eq. 6, a dampen oscillatory behavior.

In scales of time comparable to the time of relaxation the stellar total luminosity is due to the contributions of the radiative flow (approximately constant) more the contribution of the convective flow (which is damped oscillatory). According to this model the periods of the luminosity fluctuations would be of the order of the thermal relaxation time. Also, because the convective flow is only an fraction of the total thermal flow, then the luminosity variations would be dampen and small width regarding the intrinsic luminosity. The behavior as erratic function of the ZZ Ceti light curves would be explained in term of the sum of several convective fluctuations along time.

Several convective flows sequentially, each one due to some specific thermal fluctuation, they could reproduce the light curves of some ZZ Ceti stars. Indeed, it is shown in the figure 3, the modeling of the light curve

of the rapid variable G29-38 (data experimental due to McGraw, 1977). Here we used that the relaxation time in order to 1000 second and the thermal wave speed in order to sound speed in degenerate material. The thermal adjust time is account in order to 12 second.

The group of Eq. 6-9 can be used for the modeling of other light curves, using conveniently it values of relaxation time and of the thermal adjustment time. For that should be considered the speed of the thermal waves and the effective temperature by means of the figure 2.

The presented ideas could be good in order to connect the usual stellar evolution formalism with the quasi-analytical approaches (distribution of temperature surface like sum of spherical harmonics) in the study about ZZ Ceti light curve.

References

- Atweh Z.M. & Eryurt-ezr D.: 1992, *Ap.S.S.*, **189**, 27.
- Althaus L.G. & Benvenuto: 1996, *MNRAS*, **278**, 981-984.
- Brickhill A.J. : 1992, *MNRAS*, **259**, 519-528.
- Bergeron P., Wesemael F. & Fontaine G.: 1992, *Ap. J.*, **387**, 288.
- Flowers E. & Itoh N.: 1979, *Ap.J.*, **230**, 847-858.
- Hansen C.J. & Kawaler S.D.: 1994, "*Stellar Interiors Physical Principles, Structure and Evolution*", Springer-Verlag, N.Y.
- Herrera L. & Falcon N.: 1995, *Ap.S.S.*, **229**, 105.
- Herrera L. & Falcon N.: 1995, *Ap.S.S.*, **234**, 139.
- Joseph D. & Preziosi L.: 1989, *Rev. Mod. Phys.*, **61**, 41.
- McGraw J.T.: 1977, *PhD Thesis. University of Texas at Austin.*
- Kippenhahn R. & Weigert A.: 1990, "*Stellar Structure and Evolution*", Springer-Verlag, Berlin.
- Vath H., Koester K., Kepler S.O. & Robinson E.L.: 2001, [http : //www.astrophysik.uni - kiel.de/pershome/supas097/reprints/proc_wd96/proc_wd96.html](http://www.astrophysik.uni-kiel.de/pershome/supas097/reprints/proc_wd96/proc_wd96.html).

CEPHEIDS AS DISTANCE INDICATORS: SOME CURRENT PROBLEMS

M. Feast

Astronomy Department, University of Cape Town, Rondebosch, 7701,
South Africa. *mwf@artemisia.ast.uct.ac.za*

ABSTRACT. A general review is given of the calibration of the Cepheid distance scale, with particular reference to its use in the determination of H_0 . Emphasis is placed on the advantage of using a galactic calibration of the Cepheid scale, rather than relying on an adopted distance to the LMC. It is then possible to use LMC data to test for possible metallicity effects on this scale.

Key words: Cepheids, Distance Scales, Magellanic Clouds, H_0 .

1. Introduction

Cepheid variables are at the present time of key importance for establishing distances within our own Galaxy and to nearby galaxies and as the basis for the determination of cosmological parameters. As is well known, the determination of H_0 by groups working with the Hubble Space Telescope (e.g. Saha et al. 1999, Freedman et al. 2001 = F2001) rests on Cepheid observations in relatively nearby galaxies which are then used as calibrators of more general distance indicators (e.g. SNIa, the Tully-Fisher relation, surface brightness fluctuations etc.) It is therefore important that every effort should be made to understand these stars and their luminosities, and particularly to determine where present uncertainties lie.

The requirements of a primary distance indicator are easily stated. They must be bright, so that they can be seen and measured at large distances. They must also be recognizable for what they are. That is, they must not be confused with other types of objects. Their absolute magnitudes must be accurately known. This means that the intrinsic scatter in the absolute magnitudes must be small and that these absolute magnitudes can be accurately calibrated locally. There are two other considerations which are of equal importance to these. Firstly, the reddenings must be measurable. This is a crucial requirement. Secondly if there are effects due, or likely to be due, to differing metallicities or ages between the calibrators and the programme stars, these effects must be known and measurable. In addition to all this, it is highly desirable that the calibration and use of a primary distance indicator should be as free as possible from theoretical derivations or assumptions. Unless we can establish distance scales

empirically we have no way of testing theory.

Very few objects, if any, can match the classical Cepheids in fulfilling the requirements just set out. The main reason for this is that they have been extensively studied both locally and in the Magellanic Clouds for many years by a large number of investigators. It can thus be fairly claimed that they are the best understood of all pulsating variables. Other distance indicators will be mentioned below, but it can also be claimed with justification that Cepheids are the best understood of all the distance indicators.

The importance of Cepheids for distance determinations rests of course on the period-luminosity (PL) relation. The existence of this relation is well established, particularly in the Magellanic Clouds. The PL relation has relatively small scatter and the period-luminosity-colour relation seems to have negligible intrinsic scatter. A detailed discussion of some of these issues is given in Feast (1999). Furthermore it will be shown below that a reliable calibration of the Cepheid scale can now be obtained locally.

Whilst therefore we can have some confidence in the Cepheids as indicators of distance we should not be complacent. As will be indicated later there are a number of areas where an improvement of our knowledge of Cepheids is very desirable in order to further strengthen their use as distance indicators.

2. The HST Key Project Procedure

In order to focus the discussion, the present paper is limited to a discussion of factors relevant to the use which is made of Cepheids in the HST programmes for the determination of H_0 . These depend on V and I photometry. In their "final results" paper (F2001) the HST Key Project workers adopt period-luminosity relations at V and I (PL(V) and PL(I)) of the following forms;

$$M_V = -2.760 \log P - 1.458, \quad (1)$$

and

$$M_I = -2.962 \log P - 1.942. \quad (2)$$

These relations are derived from the observations of LMC Cepheids by Udalski et al. (1999, table 1), assuming the distance modulus of the LMC is 18.50. For a Cepheid in a programme galaxy the observed (intensity weighted) mean V and I are used with these

equations to derive apparent moduli. The difference between these is $E_{(V-I)}$ and multiplying this by 2.45 gives A_V and hence the true modulus.

The large number of Cepheids in the Udalski et al. work on the LMC obviously makes this data-set attractive to use as a basis. It has, however, the drawback that individual reddenings of the Cepheids themselves could not be determined (as can be done from multi-colour photometry). The reddenings were derived by dividing the LMC into a number of areas and estimating mean reddenings from the colours of giant-branch-clump stars. The mean reddening of the Cepheids used by Udalski et al. to derive equations 1 and 2 was $E_{(B-V)} = 0.147$ (not 0.10, as implied by F2001, section 3.1). The method used by F2001 only requires the relative reddenings of the LMC and their programme Cepheids. The absolute value of the LMC reddening is not required. However, F2001 have not discussed whether the Udalski et al. reddenings (which are considerably larger than have been used in the past) are consistent with their adopted true modulus of the LMC. It would also be useful in the future to have individual reddenings from multi-colour photometry (see e.g. Caldwell and Coulson 1985) for many more LMC Cepheids than are presently available. This could be used to check whether equations 1 and 2 are affected by a dependence of mean reddening on period which would affect the slope of the relations. In addition relations 1 and 2 depend heavily on short period Cepheids ($\log P \sim 0.5$) (see Udalski et al. 1999 figs 2 and 3) with very few at the long period end because of saturation of the detector used by Udalski et al. A derivation of the PL relation based on long period Cepheids would be important since the weighted mean $\log P$ of the F2001 programme Cepheids is 1.42. In addition to this there is some evidence that Cepheid moduli derived from V,I photometry require a metallicity dependent correction. This will be discussed in detail below, where it will be noted that the LMC Cepheids are metal-weak compared with the mean of the HST Key Project sample which has a mean metallicity near solar. Thus if Cepheid absolute magnitudes are based on the LMC, a metallicity dependent uncertainty will enter.

3. A Galactic Calibration of Cepheids

A calibration of Cepheid luminosities and colours based on observations in the general solar neighbourhood seems very desirable. It would avoid basing distance scales on the metal-poor LMC Cepheids. It would also be free of estimates of the LMC distance based on non-Cepheid estimators, most of which are less well understood than Cepheids themselves. However, as discussed below these non-Cepheid LMC estimates can be used together with a Galactic Cepheid calibration, to place some limits on metallicity effects on Cepheid luminosities. Such a Galactic Cepheid calibration is now possible.

Individual reddenings of many Galactic Cepheids have been derived (Caldwell and Coulson 1987) based on the BVI system. These lead to the relation;

$$\langle V \rangle_0 - \langle I \rangle_0 = 0.297 \log P + 0.427 \quad (3)$$

(see Feast 1999 where a slightly more exact procedure is given). In this equation angle brackets denote intensity mean values. Using a relation of this kind to obtain reddenings, together with a PL(V) relation is equivalent to the HST Key Project procedure.

The PL(V) relation can be written;

$$M_V = \alpha \log P + \gamma. \quad (4)$$

Various estimates have been made for the slope α of this relation. Caldwell and Laney (1991) derived -2.63 ± 0.08 from SMC Cepheids; The OGLE results for the LMC discussed in the previous section gave -2.76 ± 0.03 . The uncertainty is bracketed since much of the weight is in very short period Cepheids. Caldwell and Laney (1991) derived -2.81 ± 0.06 for the LMC. For Cepheids in the general solar neighbourhood Gieren et al. (1998) obtained -3.04 ± 0.14 from Baade-Wesselink luminosities. There is a slight hint here that there may be a trend of slope with metallicity since this changes in the sequence, SMC, LMC, Galaxy. It would be valuable to study this further, but at present there is no strong evidence of a significant trend of slope with metallicity. In the following we adopt for the Galaxy the result of Caldwell and Laney for the LMC, -2.81 ± 0.06 . This is the only result taken from the LMC in the present calibration.

It is of interest to see how the Cepheid distance scale would be affected by a change of slope from the adopted value, -2.81 , to the Galactic value of Gieren et al., -3.04 . The mean $\log P$ of the Cepheids used in F2001, weighted according to their contributions to the final value of H_0 , is 1.42. Most of the Cepheids used as calibrators in the discussion below are of shorter period. The weighted mean $\log P$ of the parallax calibrators is 0.8 whilst for the clusters it is 1.1. Changing the PL(V) slope from -2.81 to -3.04 would result in an increase in the parallax scale when applied to the F2001 results of 0.14 mag (a seven percent increase in distance scale) over that actually adopted. Thus if a variation in slope with metallicity in the sense tentatively suggested by the possible SMC/LMC/Galaxy trend is actually confirmed it would result in a decrease in the revised value of H_0 discussed in section 7.

A change of slope from the value adopted here (-2.81) to the LMC OGLE value (-2.76), would result in a negligibly small increase in H_0 .

There are four principal ways of obtaining a value of the PL(V) zero-point γ for galactic Cepheids (see Feast 2001).

1. A bias free analysis of the Hipparcos parallaxes of Cepheids leads to $\gamma = -1.43 \pm 0.12$ (Feast and Catch-

pole 1997, Feast 1999). This result and its bias free nature has been confirmed both directly and with Monte Carlo simulations (Pont 1999, Lanoix et al. 1999, Groenewegen and Oudmaijer 2000).

2. Hipparcos proper motions can be combined with radial velocities in a statistical-parallax type solution. This requires a model. The dominant effect in the case of Cepheids is that of differential galactic rotation which is clearly seen in the radial velocities and the proper motions separately. The model therefore is rather firmly based. Using this method Feast, Pont and Whitelock (1998) obtained $\gamma = -1.47 \pm 0.13$.

One can attempt a solution using the solar motion obtained from a combined discussion of solar motion and differential galactic rotation using proper motions and radial velocities. In this way the solar motion has a value which is averaged out over the whole large region covered by the Hipparcos and radial velocity Cepheids and is not confined to a small region near the Sun. The results of Feast and Whitelock (1997) imply a scale which is 0.04 ± 0.26 mag larger than that just given (Feast 2000). However, the uncertainty is too large for this solution to make any significant contribution to a final value.

The above discussion refers to the use of the systematic motions of the Cepheids. Because the velocity dispersion of Cepheids is small, any comparison of radial velocity and proper motion residuals will be sensitive to the treatment of observational scatter and probably also to group motions.

3. Pulsation parallaxes (the Baade-Wesselink method in its various forms) requires a number of assumptions to be made regarding such things as limb darkening, the colour-surface brightness relation etc. Thus whilst the internal consistency of the method is good, the external uncertainty is difficult to estimate. Feast (1999) derived, $\gamma = -1.32 \pm 0.04$ (internal) from the discussion of Laney (1998). The angular diameters of a few Cepheids have recently been determined interferometrically (Kervella et al. 2001; Nordgren et al. 2000; Armstrong et al. 2001) and the change in angular diameter of ζ Gem due to pulsation has been detected (Lane et al. 2000). When more measurements along these lines are made it should be possible to refine the pulsation parallax method further.

4. Young open clusters containing Cepheids can be used to derive γ provided the cluster scale is known. Feast (2001) shows how this scale can be rather firmly based on the well-determined Hipparcos parallax of the Hyades. This leads to $\gamma = -1.43 \pm 0.05$ (internal).

Because some of the error estimates are internal only, it is not safe to use these errors to weight the four estimates of γ given above. A straight mean gives -1.41 . The uncertainty in this value is probably somewhat less than 0.10. It should be noted that methods 1 and 2 for determining γ lead to distance scales which do not depend on the zero-point of the reddening scale adopted,

so long as consistent reddenings are applied to both calibrating and programme Cepheids. This is not the case for the other two methods. This is particularly so in the case of the clusters where the main sequence fitting depends sensitively on the adopted reddening in a way which does not cancel out in application to programme Cepheids.

4. Tests for Metallicity Effects. I

It has long been believed from observations of metal-poor Cepheids in the Magellanic Clouds that there is a metallicity effect at least in the (B-V) colours of Cepheids. Laney (quoted by Feast 1991) showed that the BVI colours of SMC Cepheids could not be brought into agreement with those in the LMC unless such an effect was assumed to exist due to the SMC Cepheids being more metal-poor than those in the LMC (a result which is known spectroscopically).

There are at least three effects attributable to metallicity differences which could affect the PL relation at a given wavelength.

1. Laney and Stobie (1986) showed from infrared photometry of galactic and Magellanic Cloud Cepheids that metallicity changes lead to a change in surface temperature at a given pulsation period.

2. There must be some effect (especially at the shorter wavelengths) due to a change of blanketing with metallicity at a given surface temperature.

Both the above have the effect of changing the bolometric corrections applicable at different wavelengths.

3. Although it is generally assumed that the bolometric PL relation is insensitive to metallicity changes, not all theorists agree on this issue.

Laney (1999) showed that the radii of Magellanic Cloud Cepheids as derived from Baade-Wesselink analyses fitted the galactic period-radius relation. Infrared photometry (Laney and Stobie 1986) shows that at a given period the metal-poor Cepheids in the Clouds are slightly hotter than the galactic ones. The evidence thus suggests that the bolometric luminosities of Cepheids of a given period increases with decreasing metallicity. However, the effect is small and within the uncertainties of the measurements.

Evidently in the case of the HST work we require to estimate the effects of metallicity changes on equations 3 and 4 above (or equivalently, equations 1 and 2). There has been some confusion in the literature since the effect on the derived distance moduli due to a metallicity change is found to be in opposite directions for the equations 3 and 4. It is thus essential to discuss the combined effect on these two equations of a change in metallicity.

The most direct empirical test of the effect of metallicity in determining distance moduli from V,I photometry is that carried out by Kennicutt et al. (1998). They observed Cepheids in the galaxy M101 at different distances from the centre. At these different posi-

tions they could estimate abundances ($[O/H]$) from HII region observations. Their results lead to a metallicity effect on Cepheid distance modulus determinations of $0.24 \pm 0.16 [O/H]^{-1}$ in the sense that without the correction the distance of a metal-poor Cepheid would be overestimated. This result suggests that a metallicity effect in the V,I method exists, but the uncertainty is evidently still large. (For a more detailed discussion of metallicity effects, see Feast (1999)).

5. Tests for Metallicity Effects. II. The LMC.

It has often been suggested that the Cepheid distance scale can (and should) be determined by deriving the distance to the LMC in some non-Cepheid way and then using this as the standard. However, quite apart from possible metallicity effects on the Cepheid scale, it must be born in mind that all non-Cepheid distance indicators so far used to estimate the distance of the LMC have their own problems and uncertainties. These problems include the calibration of these other indicators, their possible metallicity dependence, and, their reddenings relative to the Cepheids. Nevertheless, these non-Cepheid indicators can give a useful indication of a probable metallicity effect on Cepheid moduli.

Non-Cepheid moduli of the LMC were discussed by Feast (2001). The following is a slightly updated summary of that discussion which should be consulted for details.

1. RR Lyraes. The absolute magnitudes of RR Lyrae stars can be derived from; parallaxes (Koen and Laney 1998), parallaxes of horizontal branch stars (Gratton 1998), globular clusters with distances derived from sub-dwarf fitting (Carretta et al. 2000), δ Sct parallaxes (McNamara 1997) and statistical parallaxes (Gould and Popowski 1998). These can be combined with the data on LMC field RR Lyraes (Clementini et al. 2000) to obtain an LMC true distance modulus of 18.54.

2. Mira Variables. The infrared (K) period-luminosity relation for Miras can be calibrated using Hipparcos parallaxes (Whitelock and Feast 2000) and also using Miras in globular clusters with cluster distances on the subdwarf scale of Carretta et al. (2000). Using these calibrations with the LMC Mira data (Feast et al. 1989) gives (Feast, Whitelock and Menzies, to be published) an LMC modulus of 18.60.

3. The ring round SN1987A. The best estimate of the LMC modulus from this is probably that of Panagia (1998) which is 18.58.

4. LMC globular clusters. Main-sequence fitting (Johnson et al. 1999) of LMC clusters can be used to derive a modulus of 18.52.

5. The red giant clump. The use of the red giant clump as an LMC distance indicator is complicated by age and metallicity effects and by reddening uncertainties. The best estimate is probably that of Girardi and

Salaris (2001) who find a modulus of 18.55.

6. Eclipsing Variables. Although the use of eclipsing variables as distance indicators seems rather straight forward in theory, its application to the LMC requires at present a number of assumptions. The best current estimated of the modulus by this method is probably that of Groenewegen and Salaris (2001) who obtain 18.42.

The real uncertainties of the above estimates are probably about 0.1mag. The first three estimates seem likely to be the most secure and a straight mean of them is 18.57. A straight mean of all six estimates is 18.54. The V,I distance modulus of the LMC using equations 3 and 4 and $\gamma = -1.41$ is 18.66, uncorrected for metallicity effects. If we adopt a metallicity effect of 0.2 mag $[O/H]^{-1}$ and $[O/H]_{LMC} = -0.4$ as is done by F2001 following Kennicutt et al. (1998), we obtain a corrected Cepheid modulus of 18.58. The close agreement of this value with the mean non-Cepheid estimate is no doubt partly fortuitous since the uncertainties in both estimates are probably of order 0.1. However, the results do suggest that a metallicity correction of the approximate amount suggested by Kennicutt et al. is present in V,I estimates.

6. A Cepheid test using NGC4258

A distance to the galaxy NGC4258 has been derived from the motion of H_2O masers in the central region and a simple model (Herrnstein et al. 1999). Newman et al. (2001) have recently published HST V,I observations of Cepheids in this galaxy which can thus also be used to derive a distance. The metallicity adopted by Newman et al. (from HII region measurements by Zaritsky et al. 1994) is slightly below solar ($[O/H] = -0.05$). Thus any reasonable metallicity correction to a galactic calibration will be very small. Adopting the galactic calibration given above and a metallicity effect of 0.20 mag $[O/H]^{-1}$ one obtains a true distance modulus of 29.53 ± 0.17 , where the standard error is taken from the discussion of Newman et al. together with an estimated error of the galactic zero-point of ~ 0.10 . In deriving this value we have followed the procedure of Newman et al. and used template-fitted DoPHOT mean magnitudes kindly supplied by Dr Newman. These magnitudes differ slightly from the values given in Table 2 of Newman et al. A metallicity correction of -0.01 mag has been applied. The Cepheid distance is therefore greater than the maser one by 0.24 ± 0.21 mag. This difference is not significant.

7. Key Project Value of H_0 based on a Galactic Calibration

F2001 have summarized the HST Cepheid Key Project data together with related HST data by other groups (especially the SNIa group). As indicated in the Introduction they use an adopted LMC modulus as the ba-

sis of their analysis. They also introduce a metallicity correction for the first time in their series of papers. They derive a value of $H_0 = 72 \pm 8 \text{ km s}^{-1} \text{ Mpc}^{-1}$. Using their data and with the same metallicity term ($0.2 \text{ mag } [O/H]^{-1}$) but with the galactic calibration derived above, one obtains $H_0 = 67 \pm 8$ where the standard error is taken from F2001. These two estimates of H_0 are gratifyingly close. Amongst the reasons for preferring a scale based on the galactic calibration is that it is practically immune to the uncertain metallicity correction. This follows since the mean metallicity of the F2001 Cepheid galaxies, weighted according to their contribution to the final value of H_0 is close to solar ($[O/H] = -0.08$). It has been hypothesized that the metallicity correction could be as high as $0.6 \text{ mag } [O/H]^{-1}$. Whilst it seems unlikely that it could be as large as this, even such a large value will have only a very small effect on H_0 derived using the galactic calibration. On the other hand, since $[O/H]_{\text{LMC}} = -0.4$, such a large correction coefficient would have a significant effect (a six percent decrease in H_0) on a calibration based on an adopted LMC modulus.

It should be made clear that the above discussion is given to illustrate how the galactic calibration affects the conclusions of F2001. There appears still to be considerable differences in the interpretation of the HST data by different groups, unrelated to the adopted basic Cepheid distance scale (see for instance Saha et al. 1999). Full agreement on these matter is required before the value of H_0 can be considered properly established.

8. Conclusions

The calibration of the Cepheid zero-point is now quite well established from galactic observations. The present uncertainty is about 0.10 mag. It is obviously desirable to improve this accuracy, though it is not clear that this can be achieved without further astrometry from space (GAIA etc.). It is evident that further work is needed on the PL(V) and PL(V-I) slopes at long periods and it would be very desirable to determine empirically if these slopes depend on metallicity. In doing this it would be essential to derive individual reddenings for the Cepheids from multicolour photometry. It would also be of considerable interest to measure the metallicities of many more galactic Cepheids. In particular it would be useful to know more precisely the spread in metallicities amongst local Cepheids.

Acknowledgements.

I am grateful to Patricia Whitelock and John Menzies for allowing me to refer to work in progress.

References

- Armstrong J.T. et al.: 2001, *A.J.*, **121**, 476.
 Caldwell J.A.R., Coulson I.M.: 1985, *M.N.R.A.S.*,

- 212**, 879, (erratum **214**, 639).
 Caldwell J.A.R., Coulson I.M.: 1987, *A.J.*, **93**, 1090.
 Caldwell J.A.R., Laney C.D.: 1991, in *The Magellanic Clouds*, Proc. IAU Symp. 148, 249.
 Carretta E., Gratton R.G., Clementini G., Fusi Pecci F.: 2000, *Ap.J.*, **533**, 215.
 Clementini G., Gratton R., Bragaglia A., Carretta E., Di Fabrizio L.: 2000, astro-ph/0007471.
 Feast M.W.: 1991, in *Observational Tests of Cosmological Inflation*, Kluwer, Dordrecht, p.147.
 Feast M.W.: 1999, *P.A.S.P.*, **111**, 775.
 Feast M.W.: 2000, *M.N.R.A.S.*, **313**, 596.
 Feast M.W.: 2001, in *New Cosmological Data and the Values of the Fundamental Parameters*, Proc. IAU Symp. 201, 17.
 Feast M.W., Catchpole R.M.: 1997, *M.N.R.A.S.*, **286**, L1.
 Feast M.W., Glass I.S., Whitelock P.A., Catchpole R.M.: 1989, *M.N.R.A.S.*, **241**, 375.
 Feast M.W., Pont F., Whitelock P.A.: 1998, *M.N.R.A.S.*, **298**, L43.
 Feast M.W., Whitelock P.A.: 1997, *M.N.R.A.S.*, **291**, 683.
 Freedman W.L. et al.: 2001, *Ap.J.*, **553**, 47. (F2001)
 Gieren W.P, Fouqué P., Gómez M.: 1998, *Ap.J.*, **496**, 17.
 Giradi L., Salaris M.: 2001, *M.N.R.A.S.*, **323**, 109.
 Gould A., Popowski P.: 1998, *Ap.J.*, **508**, 844.
 Gratton R.G.: 1998, *M.N.R.A.S.*, **296**, 739.
 Groenewegen M.A.T., Oudmaijer R.D.: 2000, *As.Ap.*, **356**, 849.
 Groenewegen M.A.T., Salaris M.: 2001, *As.Ap.*, **366**, 752.
 Herrnstein J.R. et al.: 1999, *Nature*, **400**, 539.
 Johnson J.A., Bolte M., Stetson P.B., Hesser J.E., Somerville R.S.: 1999, *Ap.J.*, **527**, 199.
 Kennicutt R.C. et al.: 1998, *Ap.J.*, **498**, 181.
 Kervella P. et al.: 2001, *As.Ap.*, **367**, 876.
 Koen C., Laney.: 1998, *M.N.R.A.S.*, **301**, 582.
 Lane B.F., Kuchner M.J., Boden A.F., Creech-Eakman M., Kulkarni S.R.: 2000, *Nature*, **407**, 485.
 Laney C.D.: 1998 in *A Half-Century of Stellar Pulsation Interpretations*, ASP. Conf. Ser., **135**, 180.
 Laney C.D.: 1999 in *The Stellar Content of Local Group Galaxies*, IAU Symp. 192, 459.
 Laney C.D., Stobie.: 1986, *M.N.R.A.S.*, **222**, 449.
 Lanoix P., Paturel G., Garnier R.: 1999, *M.N.R.A.S.*, **308**, 969.
 McNamara D.H.: 1997, *P.A.S.P.*, **109**, 1232.
 Newman J.A. et al.: 2001, *Ap. J.*, **553**, 562.
 Nordgren T.E. et al.: 2000, *Ap. J.*, **543**, 972.
 Panagia N.: 1998, *Mem. Soc. Astron. Italiana*, **69**, 225.
 Pont F.: 1999 in *Harmonizing the Cosmic Distance Scale in the Post-Hipparcos Era*, ASP. Conf. Ser., **167**, 113.
 Saha A. et al.: 1999, *Ap. J.*, **522**, 802.
 Udalski A., et al.: 1999, *Acta Astr.*, **49**, 201.
 Whitelock P.A., Feast M.W.: 2000, *M.N.R.A.S.*, **319**, 759.
 Zaritsky D., Kennicutt R.C., Huchra J.P.: 1994, *Ap.J.*, **420**, 87.

CEPHEID PULSATIONS FROM RADIAL VELOCITY MEASUREMENTS

N.A. Gorynya¹, N.N. Samus^{1,2}

¹ Institute of Astronomy, Russian Academy of Sciences

48 Pyatnitskaya Str., Moscow 109017 Russia, *gorynya@sai.msu.ru*, *samus@sai.msu.ru*

² Sternberg Astronomical Institute, Moscow University

13 University Ave., Moscow 119899 Russia

ABSTRACT. We discuss the results of our many-year program of Cepheid radial velocities concerning the Hertzsprung sequence in radial-velocity curves, double-mode Cepheids, the period–radius relation, binary Cepheids.

Key words: Variable stars: Cepheids.

1. Introduction

In this contribution, we present some results of our program based upon observations of Galactic Cepheids with a CORAVEL-type correlation spectrometer. The program uses the principal advantage of small-telescope programs, namely, the possibility to have plenty of observing time in the course of many years, combined with special advantages of the particular radial velocity spectrometer, namely, its outstanding effectiveness combined with quite modest requirements to the size of the telescope used and with the possibility to carry the spectrometer from one observing site to another, according to availability of telescopes and to weather conditions.

The spectrometer, ILS, was designed and built by Tokovinin (1987) in 1986. It uses the ideas first suggested by Felgett (1953) and by Griffin (1967) and then implemented for echelle spectrometers in the CORAVEL machine (Baranne et al., 1979). The general idea of a CORAVEL-type spectrometer is the following. An echelle spectrograph forms an image of a star's spectrum. In the focal plane, a physical mask is placed. It is actually an image of the spectrum of a "standard" star, in our case, of Arcturus; the positions of the mask corresponding to spectral lines are transparent, those between them are not. A special plane mirror added into the optical scheme oscillates at a frequency about 10 Hz so that the observed spectrum moves back and forth along the mask. The flux passing through the mask is minimal when the lines of the observed spectrum coincide with the "lines" of the mask. The light passing through the mask is then col-

lected and measured with a photomultiplier. A special controller (in the earlier configuration of the instrument) or a computer (currently) serves to collect the measurements of light separately for 50 time intervals of each oscillation cycle of the plane mirror. Thus, we obtain a "generalized spectral line", actually corresponding, in our case, to 1500 lines in the spectrum of the program star or of Arcturus. The registered "line" covers the range of approximately ± 25 km/s; but we can search for the radial velocity in a much wider interval, about ± 300 to 500 km/s, using calibrated rotation of the diffraction grating of the spectrometer. The generalized line is then fitted to a relevant profile (usually, but not exclusively, Gaussian), and the position of its minimum determines the radial velocity. Preliminary reductions are performed already during observations, but more sophisticated software can be used off-line to improve accuracy. The reductions take into account all necessary corrections for the motion of the observer; the zero point correction, characteristic of similar instruments, is determined using observations of radial velocity standards acquired each night. The profile shape gives additional information about abundances or rotation.

The main technical characteristics of the ILS machine are the following. It can measure radial velocities of main-sequence stars with "normal" chemical abundances in the spectral type range approximately from F5 to M5; somewhat earlier giants can also be measured. The characteristic accuracy for sufficiently bright stars in the middle of the spectral type range is ± 0.3 to 0.5 km/s. The limiting magnitude for telescopes of the 1-m class is about $12^m.5$; in record cases, stars as faint as 14^m could be measured. The typical exposure time for brighter stars is about 5 min; for faint stars, it seldom exceeds 30 min.

Several instruments of CORAVEL-type design were built in the 1980ies or early 1990ies in different countries. By now, ILS seems to be one of very few survivors. Surely there are advantages in registering the complete spectrum with a CCD and then determining

the radial velocity (and numerous other parameters) by means of purely digital reductions. However, instruments like the ILS have proved to be excellent machines for “the poor”, the reductions are very simple, almost no additional technical support is needed, and you can bring your instrument to an isolated observatory and start observing the next night. We are going to continue the use of the ILS for several more years.

During 15 years of active exploitation of the ILS, it was used by several groups for rather many scientific programs, among them:

- orbits of binary and multiple stars;
- kinematics of the Galaxy;
- kinematics of stars in open and globular clusters;
- pulsations of stars (Cepheids and some others).

Here we’ll discuss only the latter program.

2. Observations

Table 1: Telescopes and Observations of Cepheids.

No	Telescope	Years	No. of observ.
1	70 cm, Moscow, Russia	1987–2000	867
2	60 cm, Nauchny, Crimea, Ukraine	1987–1990	47
3	200 cm, Shemakha, Azerbaijan	1988	2
4	122 cm, Abastumani, Georgia	1988	8
5	125 cm, Nauchny, Crimea, Ukraine	1989–1990	64
6	100 cm, Mt.Maidanak, Uzbekistan	1989–1993	283
7	100 cm, Simeiz, Crimea, Ukraine	1990–2000	3792
8	60 cm, Simeiz, Crimea, Ukraine	1990–1998	1902
9	200 cm, Mt.Rozhen, Bulgaria	1990	16
10	60 cm, Mt.Maidanak, Uzbekistan	1991	212
11	60 cm, Zvenigorod, Russia	1997	18

Grand total: 14 years, 1341 nights, 7211 observations of 144 Cepheids

In 1987–2000, we acquired more than 7000 observations of 144 Cepheids using 11 telescopes in 6 countries (Russia, Ukraine, Georgia, Azerbaijan, Uzbekistan, Bulgaria), from 60 cm to 2 m aperture. Table 1 shows some additional information on the telescopes. Mainly, telescopes of the 1-m class were used. Probably we may call our main instrument the 1 m telescope of the Simeiz Observatory (Crimea, Ukraine). The observatory is now a department of the Crimean Astrophys-

ical Observatory, but, despite the disintegration of the Soviet Union, the telescope still belongs to the Institute of Astronomy, Moscow. Note also that we use, rather effectively, the 70 cm telescope of the Sternberg Astronomical Institute, installed in Moscow, in less than 10 km from the Kremlin! The observations have been continued in 2001, but the reductions have not been completed yet.

The specific feature of our program is that we try to obtain a good coverage of the pulsation velocity curve for each Cepheid during each year season. Our data base of original accurate radial velocity measurements for Cepheids currently appears to be the world-richest.

3. Results

Figure 1 shows characteristic radial velocity curves for Cepheids, folded with their pulsation periods. Note that the scatter of data points in the upper panel is very low, and the velocity curve looks not worse than good photoelectric light curves of Cepheids. Thus, if applying the Baade–Wesselink technique to determine Cepheid radii, the factor crucially limiting the accuracy is no longer the uncertainty in radial velocities. The two lower panels show examples looking not so nice. If the period of the Cepheid is correct and does not vary strongly, there can be two reasons for the increased scatter. The first of them is double-mode pulsation (middle panel).

We have observed several double-mode Cepheids and were able to separate the two pulsation modes in their radial velocities. EW Sct is a well-known double-mode Cepheid; its amplitude of radial velocity variations corresponding to the fundamental mode exceeds that corresponding to the first overtone. V458 Sct (Fig. 2) is a new double-mode Cepheid discovered by Antipin (1997). (Less than 20 double-mode Cepheids are currently known in the Galaxy, two of them recently discovered in Sternberg Institute by S.V. Antipin.) We have already accumulated enough observations of V458 Sct to separate its two modes in radial-velocity variations (Antipin *et al.*, 1999). For this star, the first overtone amplitude is larger; the same effect is revealed by the star’s light curve, but the interpretation of the radial velocity curve in terms of energy is more straightforward, and coexistence of two oscillations, the first-overtone one with higher energy, poses a problem in front of the theory of stellar pulsations.

The second reason for the higher scatter is Cepheid binarity (bottom panel of Fig. 1). TX Del is an extreme case (it is not definite if the star is a classical Cepheid or a Population II Cepheid). We independently discovered the binarity of this star, first noted by Harris and Welch (1989). Its pulsation period is 6^d.17; its orbital period is only 133^d, a very low value for binary Cepheids (remember that classical Cepheids

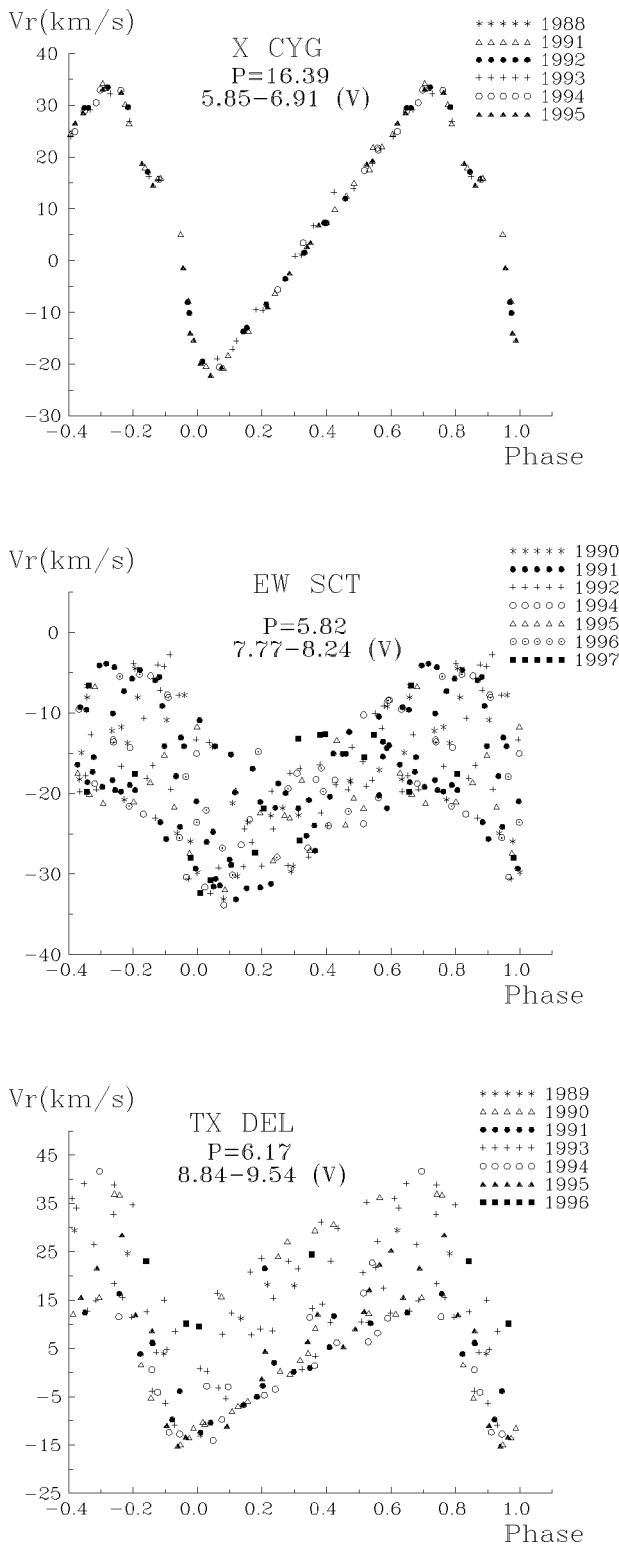


Figure 1: Radial velocity curves for three Cepheid, folded with their pulsation periods. See text for explanations.

are supergiants). Its separated pulsational and orbital velocity curves show comparable amplitudes. The star is rather unusual for binary Cepheids, even its velocity curve based on observations of a single year reveals quite obvious signatures of binarity.

We discovered the binarity of the classical Cepheids V496 Aql, BY Cas, VY Cyg, VZ Cyg, MW Cyg. A number of stars have been suspected in binarity from our data. Figure 3 is the velocity curve of the newly-discovered binary Cepheid V496 Aql (Samus and Gorynya, 2001). Table 2 presents a summary of our results on spectroscopic binary Cepheids. Our observations show that at least 22% Cepheids are binaries (Gorynya *et al.*, 1996); however, we consider much higher estimates of some other authors, like 50% or more, to be too high.

As noted above, our data are very advantageous for determinations of Cepheid radii using the Baade–Wesselink technique. Here we make extensive use of the detailed data base on Cepheid photometry compiled and supported in Moscow by Berdnikov (1995). From our original radii of 62 Cepheids, we derived the period–radius relation in the form (Sachkov *et al.*, 1998):

$$\log R = 1.23(\pm 0.03) + 0.62(\pm 0.03) \log P.$$

The radii derived with the Baade–Wesselink technique are very important as a tool to distinguish between different pulsation modes for Cepheids.

From our observations, we also have studied the Hertzsprung sequence, a relation quite well known for Cepheids as a dependence of their light curve shapes upon the period value but here revealed, for the first time, in their radial velocity curves rather than in their light curves (Gorynya, 1998).

4. Some prospects

In the recent years, we have entered a most fruitful collaboration with Dr. Pawel Moskalik (Warsaw) who uses our data for Fourier decomposition of radial velocity curves. This sensitive tool of research also makes it possible to study the Hertzsprung sequence as well as to reveal resonances between different pulsation modes. Currently, Dr. Moskalik studies our most recent observations and gives us advice on our program of observations, indicating insufficient coverage of velocity curves for stars of interest, hints to binarity, etc. In the nearest future, we are planning to continue this cooperation. Also, we try to apply our instrument to different variability type, but this is already outside the scope of this presentation.

Acknowledgements. Our study was financially supported, in part, by grants from the Russian Foundation for Basic Research, Program of Support for Leading Scientific Schools of Russia, and the Russian

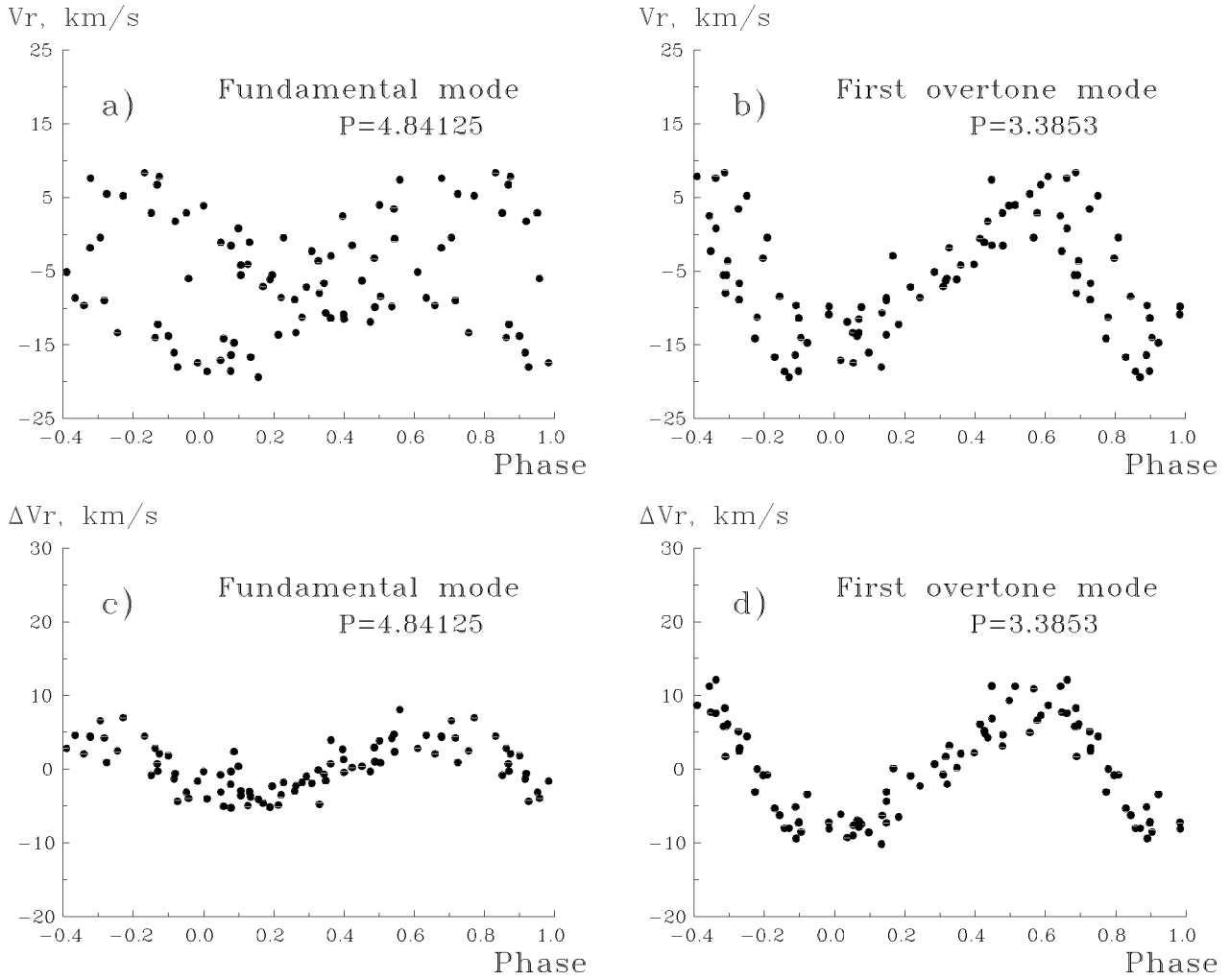


Figure 2: The radial velocity curves for the double-mode Cepheid V456 Sct: (a) folded with the period of the fundamental mode; (b) folded with the period of the first overtone; (c) same as for panel (a), but with the first overtone pulsations removed; (d) same as for panel (b), but with the fundamental mode pulsations removed.

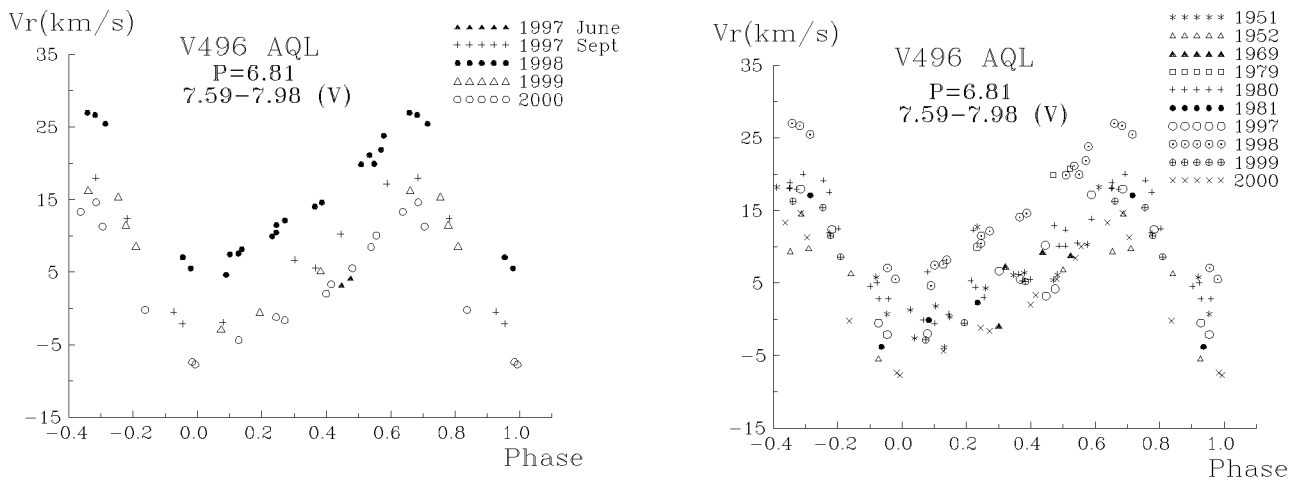


Figure 3: The radial velocity curves for the binary Cepheid V496 Aql, folded with its pulsation period. Top: from our observations only; bottom: with data from the literature added.

Table 2: Results for binary Cepheids.

Cepheid	P_{puls} , d	P_{orb} , d	$a \sin i$, AU	$f(m)$, M_{\odot}	M_1 , M_{\odot}	M_2 , M_{\odot}
FF Aql	4.4709	1432.2	0.67	0.02	5.5	$\geq 1 \pm 0.2$
V496 Aql	6.8072	1447(573)	–	–	–	–
RX Cam	7.9122	1116	1.2	0.19	6.5	$\geq 2.5 \pm 0.2$
SU Cas	1.9495	407.2	0.13	0.002	4	–
BY Cas	3.2223	563	–	0.04	–	–
DL Cas	8.0007	684.4	–	0.2784	–	–
SU Cyg	3.8456	549.25	1.42	1.27	5.0	≥ 5
VY Cyg	7.8570	941	–	–	–	–
VZ Cyg	4.8644	1483	1.39	0.16	5.5	$\geq 2 \pm 1.5$
MW Cyg	5.9547	437.3	0.25	0.011	6	$\geq 0.8 \pm 0.05$
V532 Cyg	3.2838	388?	–	0.0001?	–	–
V1334 Cyg	3.3325	1947(1463)	–	–	–	–
TX Del	6.1659	133.3	0.17	0.037	6	$\geq 1.25 \pm 0.15$
Z Lac	10.8860	376.9	0.54	0.14	6	$\geq 0.8 \pm 0.1$
T Mon	27.0333	25000	–	–	–	–
AU Peg	2.4115	53.34	0.22	0.49	4	$\geq 2.7 \pm 0.2$
AW Per	6.4636	1911?	–	0.016?	–	–
S Sge	8.3823	675.75	0.93	0.23	$\cong 6.5$	$\geq 1.1 \pm 0.05$
V350 Sgr	5.1539	1481.8	1.34	0.15	$\cong 5.5$	$\geq 2.1 \pm 0.2$
BQ Ser	4.2712	136 or 1009	–	0.005	–	–
SZ Tau	3.1489	1244?, 240?	–	–	–	–
EU Tau	2.1025	980?	–	–	–	–

Remarks to Table 2.**SU Cyg:** A triple system.**TX Del:** 1) If considered a classical Cepheid:

$$M_1 = 6.0M_{\odot}; M_2 \geq 1.25 \pm 0.15M_{\odot}$$

2) If considered a Population II Cepheid:

$$M_1 \cong 0.7M_{\odot}; M_2 \geq 0.35 \pm 0.05M_{\odot}$$

AU Peg: 1) If considered a classical Cepheid:

$$M_1 = 4M_{\odot}; M_2 \geq 2.7 \pm 0.2M_{\odot}$$

2) If considered a Population II Cepheid:

$$M_1 \cong 0.7M_{\odot}; M_2 \geq 1.2 \pm 0.1M_{\odot}$$

AW Per: The first known SB2 Cepheid.**BQ Ser:** CEP(B) with $P_0 = 4^d.27073$ and $P_1 = 3^d.012$.

Federal Scientific and Technological Program "Astronomy". Thanks are due to many observers who participated in our program. We wish to thank S.V. Antipin for his help during preparation of the manuscript.

References

- Antipin S.V.: 1997, *Comm. 27 and 42 IAU Inform. Bull. Var. Stars*, No. **4485**.
- Antipin S.V., Gorynya N.A., Sachkov M.E. et al.: 1999, *Comm. 27 and 42 IAU Inform. Bull. Var. Stars*, No. **4718**.
- Baranne A., Mayor M., Poncet J.L.: 1979, *Vistas in Astronomy*, **23**, 279.
- Berdnikov L.N.: 1995, *ASP Conference Series*, **83**, 349.
- Felgett P.B.: 1953, *Optica Acta*, **2**, 9.
- Gorynya N.A., Rastorguev A.S., Samus N.N.: 1996, *Astronomy Letters*, **22**, 33.
- Gorynya N.A.: 1998, *Comm. 27 and 42 IAU Inform. Bull. Var. Stars*, No. **4636**.
- Griffin R.F.: 1967, *Ap.J.*, **148**, 465.
- Harris H.C., Welch D.L.: 1989, *A.J.*, **98**, 981.
- Sachkov M.E., Rastorguev A.S., Samus N.N., Gorynya N.A.: 1998, *Astronomy Letters*, **24**, 377.
- Samus N.N., Gorynya N.A.: 2001, in: *Proceedings of the IAU Colloquium No. 183* held in Kenting, Taiwan (in press).
- Tokovinin A.A.: 1987, *Soviet Astronomy*, **31**, 98.

NUMERICAL CRITERIA OF THE VARIABILITY OF THE INDIVIDUAL PULSATING CYCLES IN THE LPVs

V.I. Marsakova

Astronomical Observatory, Odessa National University
T.G.Shevchenko Park, Odessa 65014 Ukraine, *vlada@mail.od.ua*

ABSTRACT. Some numerical parameters of long term changes of light curves in LPVs are obtained. Results of analysis of the sample of 53 LPVs and classification of these stars are discussed.

Key words: Stars: long-periodic variables, Mira-type stars, semi-regular variables.

1. Introduction

The long period variables (LPVs) is characterized by significant changes of their light curves from cycle to cycle. So the parameters of light curves are unstable and can not be used as reliable classification criteria. One of the way is to use types long term changes of light curves as criteria for classification.

The sample of 53 LPVs, which are actively observed by amateur astronomers, has been studied. Most of them (43) are Mira-type stars, according to GCVS (Kholopov et al., 1985), others are semiregular (SR) variables.

2. Data analysis

To study cycle-to-cycle changes in these variables, the dense series of data during long time interval are needed. We use the AFOEV and VSOLJ data-bases for this research. We have obtained the following characteristics of each individual cycle: moments and magnitudes of extrema and hump at the ascending branch, periods between maxima and minima, amplitudes of both branches, asymmetry, slopes of the ascending and descending branches, mean brightness of the branches. Analysis of variations of these characteristics with time and correlation analysis of them have been made. We also applied the periodogram, Fourier and wavelet analysis to study the periodicities and its stability. Parameters of the mean light curves such as period, amplitude, asymmetry has been obtained by using the trigonometrical polynomial fit. (Below these characteristics are mentioned as "mean period", "mean amplitude", etc.) The example of our analysis has been described by Marsakova and Andronov (1998).

3. Results

Also we have analyzed the relations between numerical characteristics of the cycle-to-cycle changes and the parameters of the mean light curves (including the degree of trigonometrical polynomial fit) and the spectral class. For spectral class we have used conditional scale from -5 (spectral class K5) to 29 (C9), where interval 0-9 corresponds to spectral classes M0-M9, 10-19 corresponds to S0-S9, 20-29 corresponds to C0-C9. For the cycle-to-cycle changes we have used the following characteristics:

- relative quantity of humps at the ascending branch;
- scatter the of mean brightness;
- scatter the of amplitudes;
- scatter the of asymmetry;
- scatter of the individual periods between maxima;
- scatter of the individual periods between minima.

Four last characteristics also have been used as arbitrary to mean light curves characteristics.

We have obtained a sequence of diagrams, such as spectral class – arbitrary amplitude scatter, spectral class – arbitrary mean brightness scatter, arbitrary period scatter – arbitrary amplitude scatter, etc.

Several diagrams show that all values differ for different spectral classes in sequence C–M–S. They show no changes between Miras and semiregular variables in the sample. But diagram spectral class – arbitrary scatter the of amplitudes shows that three stars (RU Cyg, V Boo, V CVn, all of them were classified as semiregular in GCVS) significantly differ by the value of arbitrary scatter the of amplitudes from other stars in group of spectral class M. Y Per (classified as Mira, but with significant irregularity in last decade) also differ from other stars in group of spectral class C.

Almost all stars of spectral class C have amplitudes smaller than 2 magnitudes mentioned in GCVS as the limit for discerning Miras and SR variables. And there is a subgroup of stars where Mira-type and semiregular variability exchange each other in the different time intervals. Diagram mean amplitude – scatter of the individual periods between maxima shows that the transition between small amplitude and large amplitude

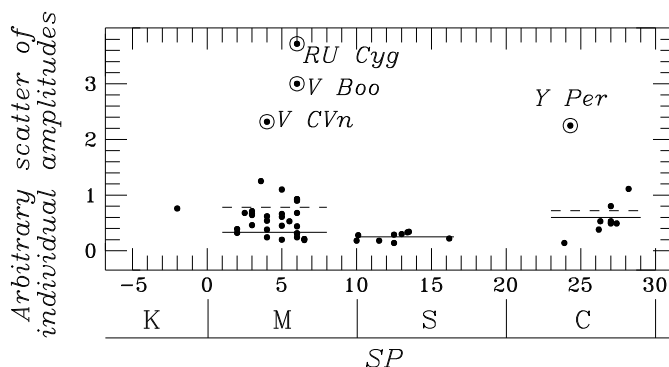


Figure 1: Dependence of arbitrary scatter the of amplitudes on spectral class. Horizontal lines show mean values for spectral classes M, C, S. Solid lines correspond to mean value of scatter the of amplitudes for spectral classes M and C without the stars marked by double circles. Dashed lines – with these stars.

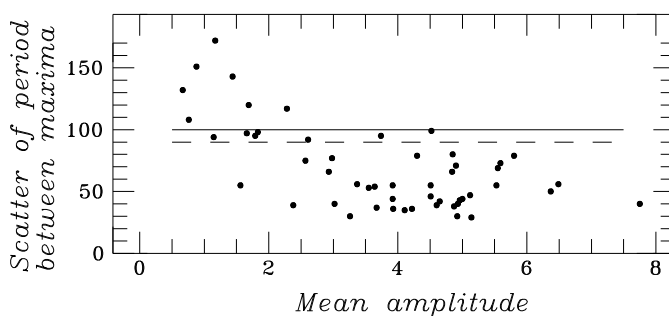


Figure 2: Dependence of period between maxima on mean amplitude. Solid line corresponds to 100^d.

stars is very fluent. So the majority of stars in our sample of spectral class C may be classified as periodic carbon LPVs. There are no significant differences between Miras and SR variables.

Other diagrams also show that limited quantity of stars (both SR and Miras) differ from majority by values of characteristics of the cycle-to-cycle changes.

Stars RU Cyg, V Boo, V CVn lie separately at the majority of diagrams. So these stars may be classified as semiregular variables confidently.

In stars wit progressive period changes were pointed out two types of light curve transformation: in R Aql and R Hya period decrease is followed by very strong amplitude decreasing, in T UMi fast period decreasing is followed by significant changes of curve sharpness. In some papers (Wood and Zarro, 1980; Gal and Szatmary, 1995) it is suggested, that T UMi is in the beginning of helium shall flash, but R Aql and R Hya are in the more later stages of it.

The secular amplitude increase or decrease (except the stars on the stage of helium shell flash) probably also may serve to classification. Also for 5 stars (4 Miras and SS Vir which was classified as SR in GCVS) the amplitude increase has been obtained. For V Boo, RU Cyg we have obtain amplitude decrease.

In three Miras: R LMi, R Dra and V CrB we also have found the decrease of mean brightness.

In some Miras were found period and amplitude changes which like cyclic ones in the observational interval. But there are some difficulties: characteristic times of this cyclicity is about 15000-23000 days, so we can't study more than 2-3 long cycles.

The group of periodic carbon LPVs shows different types of amplitude variations (cyclic, irregular, parabolic trend).

So analysis of the long-term light curve changes allows to introduce the new criteria of the classification of LPVs into Miras and semiregular variables.

Acknowledgements. For our time series analysis, we have used the observations published in the AFOEV (<http://cdsarc.u-strasbg.fr/aftev>) and VSOLJ (<http://www.kusastro.kyoto-u.ac.jp/vsnet>) international databases. The author is thankful to I.L.Andronov for supervision of current research.

References

- Gal J., Szatmary K., 1995: *Ap.J.*, **297**, 461.
 Khopolov P.N. et al.: 1985, *General Catalogue of Variable Stars*, 4-th ed., Moscow, Nauka.
 Marsakova V.I., Andronov I.L.: 1998, *Ap. Space Sci.*, **257**, 49.
 Wood P.R., Zarro D.M., 1981: *Ap. J.*, **247**, 247.

FALSE ALARM PROBABILITY IN THE MULTIPERIODICITY SEARCH

J. Molenda-Żakowicz¹

¹ Institute of Astronomy, Wrocław University
ul. Kopernika 11, 51-622 Wrocław, Poland, *molenda@astro.uni.wroc.pl*

ABSTRACT. We apply the False Alarm Probability analysis, (FAP), to the multiperiodicity search. Then we show the necessity of using the FAP method in the analysis of the astronomical time-series. We present the results obtained for 153 stars supposed or known to be pulsating variables. We examine the statistical properties of the excited frequencies and find a relation between the parameters of the fitted sine-curves and the FAP. Finally we show the application of our results to the individual stars and large samples of stars.

Key words: Stars: variables; statistics: numerical methods.

1. Introduction

Testing significance of periodogram peaks is very important. Identifying a frequency we should be sure that we do not take stochastic fluctuations of noise as an intrinsic variability. In our analysis we examined the *Hp* magnitudes of 153 stars observed by the *Hipparcos* satellite (ESA 1997). All of the stars are situated in the domain of instability of Slowly Pulsating B stars. We computed the least-squares power spectra as described in Jerzykiewicz & Pamyatnykh (2000), using the Lomb (1976) method modified by adding a floating mean and weights calculated for each *Hp* magnitude. Then we prewhitened data fitting simultaneously all frequencies found so far. The False Alarm Probability method described by Cumming et al. 1999 was used by us to test significance of periodogram peaks. We generated hundreds sets of gaussian noise and compared the height of the highest peaks produced by the noise with the height of the highest peak, z_{\max} , obtained for the stellar data.

Having derived all excited frequencies, we examined the distributions of A_i/σ_{A_i} obtained for all the stars. We analysed the statistical properties of the distributions and compared the results obtained for the *Hipparcos* observations with the results obtained for pure gaussian noise and for gaussian noise with the sinusoidal signal added.

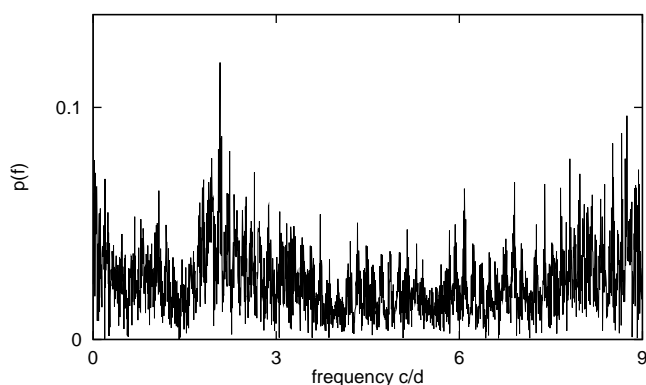


Figure 1: A periodogram of pure gaussian noise.

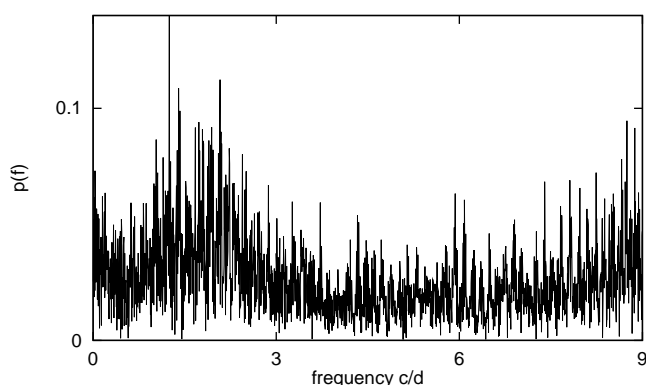


Figure 2: A periodogram of the pure gaussian noise from Fig 1 with a sine-curve added. The highest peak indicates the hidden periodicity.

2. Testing significance of periodogram peaks.

It is well-known that noise can give rise to high periodogram peaks and fluctuations of noise can mimic periodic variations. To show how high such noise-originated peaks can be, we show two periodograms in Figs 1 and 2. In Fig 1 we can see a periodogram of pure gaussian noise while in Fig 2 we can see a periodogram of the same noise with a sine-curve added. In both figures the highest peaks, z_{\max} , have comparable height. When we analyse data which consists of little number of observations scattered over hundreds of days, as in the case of *Hipparcos* observations, we often face situation when fluctuations of noise are comparable with the supposed variability. Therefore for stars with small-amplitude variations it is easy to miss a hidden periodicity taking it as fluctuations of the noise.

Most of the statistical tests are not applicable in astronomy. The majority of the tests are devised for equally spaced observations containing noise or noise with a *known* number of periodic signal present. While the stellar observations are usually unequally spaced and contain huge gaps. The False Alarm Probability (FAP) method used by us gives the probability that the highest periodogram peak, z_{\max} , is due to the noise-fluctuations. The advantage of the FAP method is that FAP does not require equally-spaced observations and can be applied to all data with the know distribution.

In case of gaussian distribution, which is the most common in astronomy, we are able to generate sets of gaussian noise with the same mean and variance as the original observations. Computing the power-spectra we can compare the height of peaks computed for the noise, with the height of z_{\max} computed for the original observations. When we express in percents the number of peaks which are higher than z_{\max} , we obtain the probability (FAP) that we deal with pure noise. Using the FAP method we obtain information of presence of not periodic variations which produce more power than the pure noise could do. We can also know whether the high peaks in the low frequency region indicate a changing mean of the time-series or are rather due to fluctuations of the noise.

3. Analysis of individual stars.

As the FAP method requires knowledge of the distribution of observations we used the Liliefors-Kolmogorov and the Shapiro-Wilk statistical tests to find stars with gaussian distribution of observations. We used the STATISTICA software package which provides both tests. We found that over 50% of the distributions were accepted by both tests as gaussian at the $\alpha = 0.05$ level, where α is the probability that we incorrectly classify a distribution as non-gaussian. For these stars we performed the periodogram analysis

and, having found the frequency of the hidden periodicity, we fitted the data with a sine-curve and obtained the amplitude of the variation, $A_1 \pm \sigma_{A_1}$. Then we performed the FAP analysis accepting a periodicity as real only if the FAP was less than 1%. Seeking for the next frequencies we repeated all the described procedure.

Then we found that FAP is strongly correlated to the value of A_i/σ_{A_i} , where i is the number of a derived frequency (Molenda-Żakowicz 2000) and found this correlation as a useful tool for testing significance peaks for stars with non-gaussian distribution of data. We show this correlation in Fig. 3 where we denoted A_1/σ_{A_1} with dots, A_2/σ_{A_2} with squares, A_3/σ_{A_3} with triangles and A_4/σ_{A_4} with crosses. One can see that for each next frequency the threshold where FAP becomes greater than 1% is higher. We list in Table 1 the thresholds accepted by us for the first four periodicities detectable in the *Hipparcos* data.

Table 1: The accepted thresholds for A_i/σ_{A_i} .

number of frequency, i	threshold for A_i/σ_{A_i}
1	5.8
2	6.2
3	7.0
4	7.8

When dealing with stars with non-gaussian distribution of observations, we assume that the general population of the observations was gaussian and the observed irregularities were due to sampling. Then we performed the periodogram analysis and accepted only these frequencies for which the values of A_i/σ_{A_i} were greater than the accepted thresholds. Because there was some scatter present around each threshold, we set the thresholds high enough to protect us from considering fluctuations of noise as a hidden periodicity.

2. Analysis of large samples of stars

In this section we pay attention to large samples of stars. We defined a sample as large when the number of stars exceeds 30 and analysed the distribution of the values of A_i/σ_{A_i} of constant, mono- and multiperiodic stars in order to examine the statistical properties of these distributions.

We studied samples of stars denoted as constant in the *Hipparcos Catalogue* and mono- and multiperiodic stars extracted from the 153 stars examined by us. In all cases we obtained skewed distributions of A_i/σ_{A_i} (in case of constant stars we analysed distribution of A_i/σ_{A_i} obtained by fitting data with a sine-curve with the frequency indicated by the highest peak of the periodogram). This result is in a full agreement with the theoretically predicted distribution of extreme values (Sachs 1984 and references therein). The new result

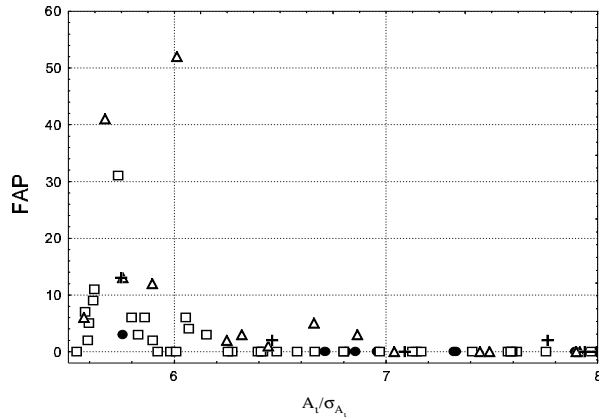


Figure 3: The correlation of A_i/σ_{A_i} and FAP for the first four frequencies detectable in the *Hipparcos* observations. We denoted $i = 1$ with asterisks, $i = 2$ with triangles, $i = 3$ with squares and $i = 4$ with dots.

is a dependence of the skewness coefficient, γ , on the amount of multiperiodic stars in the sample. The skewness coefficient, γ , is defined as

$$\gamma = \frac{\mu_3}{\sigma^3},$$

with

$$\mu_3 = \frac{1}{n} \sum_{i=1}^n (x_i - \bar{x})^3$$

where μ_3 is the third central moment, x_i is the observed magnitude, \bar{x} is the mean magnitude derived from the data, n is the number of observations, and σ is the standard deviation of the analysed time-series.

We found that the distribution of A/σ_A obtained for constant stars was steep on the left and flat to the right as we expected. For all the other distributions we observed cutting of the left tail. This cutting arises because of the observational selection: the histograms obtained for variable stars were limited from the left side to these values of A_i/σ_{A_i} for which FAP was less than 1%. This result is an important indication that we still miss many low-amplitude periodicities looking for multiperiodic stars.

Analysing the dependence of γ on the amount of multiperiodic stars in the sample we found that the higher is the value of γ , the higher is the amount of multiperiodic stars. For samples containing only constant

stars we obtained values of γ from the range 0.6–0.9 while for samples containing a mixture of mono- and multiperiodic stars, γ was much higher. We performed the same analysis for pure gaussian noise and noise with sinusoidal signal added and obtained a full agreement with the results for *Hipparcos* observations. In this way we showed that not only the cutting of the distribution of A_i/σ_{A_i} but also its skewness gives information of the non-detected periodicities hidden in data.

3. Conclusions

Basing on our results we recommend the FAP analysis as a tool that should be used to testing periodogram peaks of mono- and multiperiodic stars. Our work gave two important results. The first was the relation of A_i/σ_{A_i} –FAP which should be used for testing significance of periodogram peaks when it is not possible to compute FAP directly. The second result was the relation between γ and the amount of multiperiodic stars in the sample. This relation, however not so strict as the first one, can be used for estimating the number of not-detected variables present in large data-bases.

Acknowledgements. We thank Prof. M. Jerzykiewicz and Dr R. Getko for their help. We acknowledge the the KBN grant 5 P03D 014 20.

References

- Cumming A., Marcy G.W., Butler R.P.: 1999, *ApJ*, **526**, 890
- ESA 1997 The *Hipparcos* and *Tycho* Catalogues ESA SP-1200, Nordwijk: ESA
- Jerzykiewicz M., Pamyatnykh A.A.: 2000, *PASP*, **112**, 1341
- Koen C.: 1990, *Ap.J.*, **348**, 700
- Lomb N.R.: 1976, *Ap.Space Sci.*, **39**, 447
- Molenda-Żakowicz J.: 2000, *Hipparcos and the Luminosity Calibration of the Nearer Stars*, XXIV IAU Symp., Manchester, England
- Sachs L.: 1984, *Applied Statistics. A Handbook of Techniques. Sec. Ed.*, Springer-Verlag, New York Inc.
- STATISTICA For Windows 95/98/2000 Version 5.5, 1984-2000 StatSoft Inc.

STRÖMGREN PHOTOMETRY AND SEARCH FOR SHORT PERIOD VARIABLES IN THE OPEN CLUSTERS NGC 6910 AND NGC 6913

J. H. Peña¹, R. Peniche^{1†}, A. García Cole², J. C. Plascencia³,
L. Parrao¹, R. Peña³

¹ Instituto de Astronomía, UNAM; Apdo. Postal 70 264, México, D. F., 04510;
jhpena@astroscu.unam.mx, laura@astroscu.unam.mx

² CCH-Sur, UNAM; *cole@astroscu.unam.mx*

³ Facultad de Ciencias, UNAM; *placenci@astroscu.unam.mx, rafael@correo.unam.mx*

ABSTRACT. Analysis of the absolute $uvby - \beta$ photometry of the Open Clusters *NGC 6910* and *NGC 6913* show well-defined peaks that clearly define the accumulation of stars. Differential photometry of five stars in the direction of each cluster determines that at least two stars in each cluster are variables. For *NGC 6910* both belong to the cluster and are δ Scuti stars and for *NGC 6913* two short period variables one does not belong to the cluster and it might be a δ Scuti star. The other one is a B type star and it belongs to the cluster.

Key words: δ Scuti, variable stars, open clusters, photometry; stars: individual: H01, H05, H09, H10.

1. Introduction

Since Strömgren $uvby - \beta$ photometry provides unique opportunities for determining both cluster membership and physical characteristics of observed stars, several bright stars in the direction of the clusters, as well as several standard stars, were observed in order to transform their photometric values into the standard system. Simultaneously, differential photometry of a few stars within the instability strip limits was carried out for detection of new short period variables.

2. The Open Cluster NCG 6910.

Due to its youth, this cluster has been a subject of numerous studies, the last one of which, Delgado & Alfaro (2000), provides us with an excellent review. They report the following values for this cluster:

$$\begin{aligned} E(B - V) &= 1.02 \pm 0.13, \\ V_0 - M_V &= 11.2 \pm 0.2 \text{ and} \\ \text{age} &= (6.53) \times 10^6 \text{ yr.} \end{aligned}$$

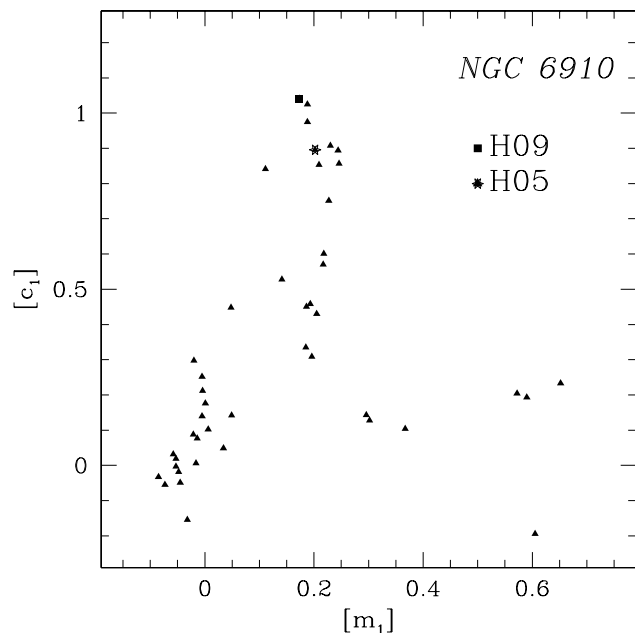


Figure 1: Diagram $[m_1]vs[c_1]$

We carried out observations of a few stars in the $uvby - \beta$ system that complemented those of Crawford, Barnes and Hill (1977) in 35 stars, 10 of which were in common with CBH and 13 were observed by them but not by us, constituting a total sample of 48 stars. Their unreddened indexes $[m_1] - [c_1]$ which establish their spectral class as early *A* are also shown in Fig. 1.

3. The Open Cluster NCG 6913

This cluster (M29, 20h, 23m; +38.32 (2000), is located in the *Cygnus OB1* Association. A fine recent com-

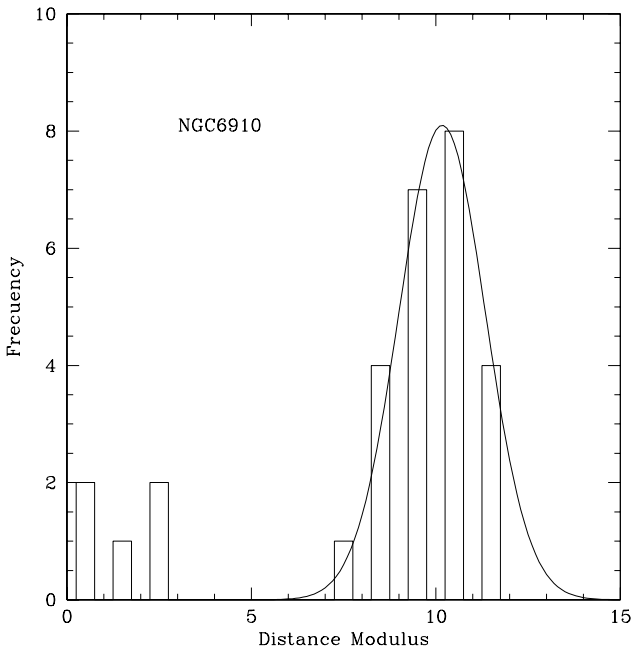


Figure 2: Distances modulus at 10.02 ± 1.17 of NGC 6910.

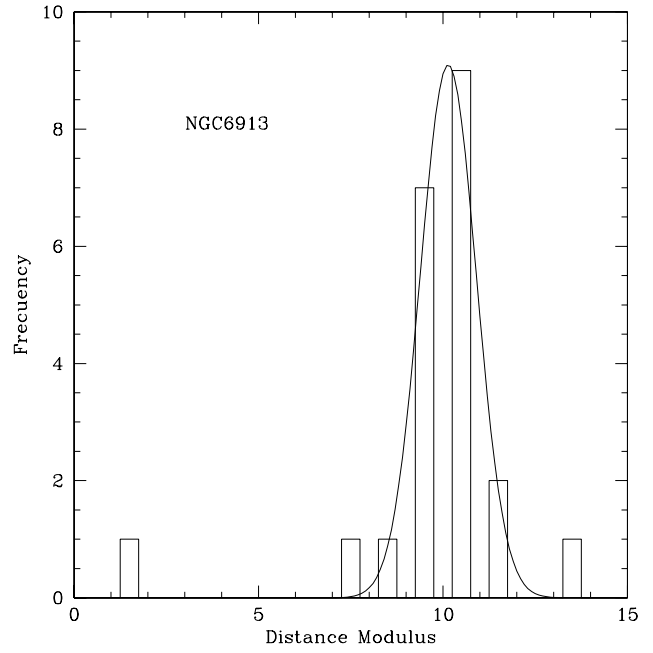


Figure 4: Distances modulus at 10.14 ± 0.76 of NGC 6913.

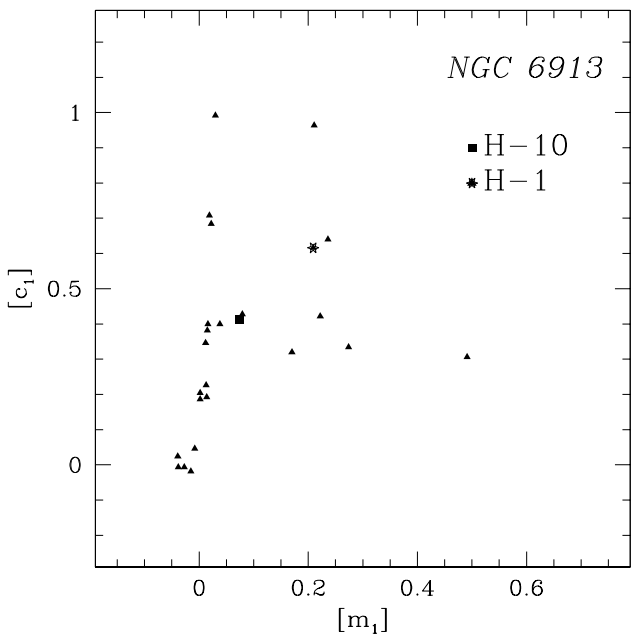


Figure 3: Diagram $[m_1]$ vs $[c_1]$.

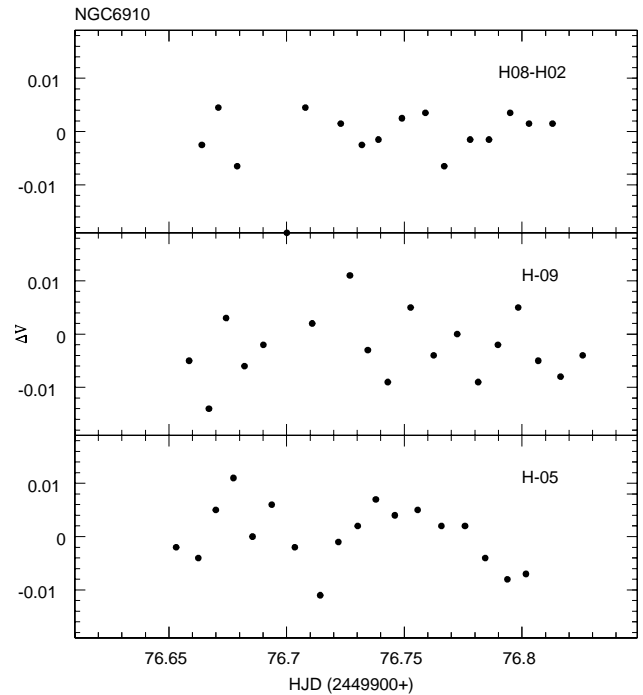


Figure 5: Light Curves of variable stars in NGC 6910.

pilation of the cluster can be found in Wang & Hu (2000). In summary: it is considered to be a very young cluster. Its estimated age vary between 0.3 to 1.75 Myr. Since it is so young, it should have stars in the pre-main-sequence phase; a mean distance modulus

of 10.17 ± 0.14 mag (dist = 1.08 kpc) is determined; extinction in the cluster center is relatively homogeneous, but very large; out of 100 spectroscopically classified stars they found: 2 O type stars, 4 O B type stars, 33 A type stars, 15 F, 6 G, and 4 K.

3.1 Absolute photometry

We carried out *uvby* - β absolute photometry at the San Pedro Mártir Observatory, México, in two seasons: October 1989 and June 2000 with 40 stars, 21 in common with Crawford et al. (1977) and 6 more observed only by them, constituting a whole sample of 46 stars. Their $[m_1] - [c_1]$ diagram shown in Fig. 3.

3.2 Differential photometry

The stars were observed in September 1995 at the 84cm telescope. Five stars within the instability strip limits were chosen: (Hoag number 01, 07, 09, 10 and 11; Sanders number 135, 174, 146, 182, and 178, respectively) Two were constants (07 and 09) whereas two, (01 and 10) were found to be variables.

In a parallel run in the V filter in 1995, five stars (Hoag's number: 02, 04, 05, 08 and 09) were monitored for variability. Of these two had constant behaviour (02 and 08), two are clearly variables (05 and 09) and one (04) marginally variable. The corresponding light curves are shown in the Figure 5.

From the $[m_1] - [c_1]$ diagram, (Fig. 1), it is evident that both variable stars belong to early stars class A and from their distances they belong to the cluster.

The star (11) most likely is variable, but its light curve is too noisy to unambiguously establish the variability. Of the two short period variables, one, H01 does not belong to the cluster and might be a δ Scuti star. The other star, H10, is a B type star and it belongs to the cluster.

4. Conclusions.

Although this study is preliminary, at this stage we can conclude the following: From the photometric analysis carried out on the *uvby* - β data, both clusters, NGC 6910 and NGC 6913 show well-defined peaks that clearly define the accumulation of stars (Figures 2 and 4). Differential photoelectric photometry of five stars in each cluster was carried out and in each cluster, at least two short period variables were found in the direction of each of the clusters. For NGC 6910, two variable stars H05 and H09 that belong to the cluster were found; for NGC 6913, of the two short period variables one, H01, does not belong to the cluster and it might be a δ Scuti star. The other one, H10 is a B type star and it belongs to the cluster.

Acknowledgements. Special thanks to the staff of the SPM Observatory who made the observations possible. We would like to thank the funds provided by Papiit IN100199 and Conacyt CNRS through grants E130.1636/2000 and E130.706. Proofreading was done by J. Miller; C. Guzmán and A. Díaz assisted with the computing. AGC and JCP thank the Instituto de Astronomía, UNAM for the observing seasons. This research made use of the Simbad databases operated at CDS, Strasbourg, France.

References

- Delgado A.J., Alfaro E.J.: 2000, *A.J.*, **119**, 1848.
- Crawford, Barnes, Hill: 1977, *A.J.*, **82**, 606
- Wang J.J., Hu J.Y.: 2000, *As.Ap.*, **356**, 118

THE INVESTIGATION OF SEMI-REGULAR VARIABLE UV BOO

A.I.Pikhun¹, L.S.Kudashkina¹, I.S.Brukhanov²

¹ Astronomical Observatory, Odessa National University,
T.G.Shevchenko Park, Odessa 65014 Ukraine, *astro@paco.odessa.ua*

² Republic Center of Technical Art Schoollars, Minsk, Belarus,
betelgeuze_astro@mail.ru

ABSTRACT Periodogram analysis of the photographic observations of UV Boo based on Hipparcos data has showed two photometric periods: $596^d \pm 47^d$ and $11^d.74 \pm 0^d.01$ and the same high peak on the value $10^d.60 \pm 0^d.02$. On Odessa plates data have showed three periods: $351^d.10 \pm 1^d.50$, $196^d.14 \pm 0^d.41$, $10^d.442 \pm 0^d.002$.

Key words: Stars: semi-regular; stars: individual: UV Boo

The variable star UV Boo = BD+26°2559 = HD 126030 = SAO 083315 has been discovered in 1929 and had variations of the light $7^m.4 - 8^m.6$. In further, the different limits of light oscillations were showed: $8^m.17 - 9^m.01$ (Kukarkin, 1930), $7^m.8 - 8^m.4$ (Kopal, 1931, 1933), $8^m.36 - 8^m.886$, $8^m.5 - 9^m.2$ PG (Ahnert, 1947), $7^m.95 - 8^m.25$ (Beyer, 1950), $7^m.46 - 8^m.30$ Vis, $7^m.1 - 8^m.0$, $8^m.11 - 8^m.16$ V, $8^m.1 - 8^m.5$ etc.

The star was classified different variable types: δ Cep, Irr, Is (Kopal 1931, 1933, Kholopov, 1959), δ Cep (Beyer, 1950), RW. The star has classified as constant by Zajtseva (1967) and other observers. Wenzel (1965) observed small oscillations about $0^m.03$. In Albireo (N25, 1973), were noted the sharp fluctuations $7^m.6 - 7^m.9$. In MVS (B.2, H.1, 4, 1963), the spectrum F5 V and slow 100 – 1000^d oscillations with amplitude $0^m.45$ are reported. Kholopov et al. (1985) report that the star is constant.

In our work, we have used the Hipparcos data and Odessa Plate Patrol Collection data. We have used the finding chart of variable star presented by Taylor (1987). Moreover, our systematic patrol observations since 1988 show the doubtless variation of this star.

The magnitudes of the comparison stars were determined in the BV-system (Kudashkina et al., 1989).

The periodogram analysis of the photographic observations of UV Boo based on Hipparcos data has showed two photometric periods: $596^d \pm 47^d$ and $11^d.74 \pm 0^d.01$. The peak on the value $10^d.60 \pm 0^d.02$ is also presented. The both peaks have the identical ratio signal/noise (more 5) and the imilar value of the test function $S(x)$. The periodograms for the Odessa data

have shown three peaks corresponding to the periods: $351^d.10 \pm 1^d.50$, $196^d.14 \pm 0^d.41$, $10^d.442 \pm 0^d.002$.

The value of test-function in every case is: (1) for $196^d.14$, $S(x) = 0.12$; (2) for $351^d.10$, $S(x) = 0.08$; (3) for $10^d.442$, $S(x) = 0.03$. The period $10^d.442$ is similar to the value corresponding to the Hipparcos' values. This period is the most interesting because this peak presents on all periodograms. However, it is necessary to assume the most certain the value of 196 days.

The periodograms of UV Boo are shown below. $S(x)$ is the test-function (Andronov, 1994). The value of the period corresponding to a highest peak is shown at the vertical axis.

For the analysis, the programm FO.EXE by Andronov (1994) has been used.

Undoubtedly, the star UV Boo is a variable star. It is possible that UV Boo belongs to the type SRd, but for all that shows the multi-periodicity.

References

- Ahnert P.: 1947, *Mitt. Ver. Sterne*, **109**.
 Andronov I.L.: 1994, *Odessa Astron. Publ.* **7**, 49.
 Beyer M.: 1950, *Erg. Astron. Nachr.* **12**, 2.
 Kazanasmas M.S., Zavershneva L.A., Tomak L.F.: 1981, *Atlas and catalogue of the stellar magnitudes of the photoelectric standards*; Kiev, Naukova Dumka.
 Kholopov P.N., Samus N.N., Frolov M.S., Goransky V.P., Gorynya N.A., Kireeva N.N., Kukarkina N.P., Kurochkin N.E., Medvedeva G.I., Perova N.B., Shugarov S.Yu.: 1985, *General catalogue of variable stars 1-3*; Moscow, Nauka.
 Kopal Z.: 1931, *Beob.Zirk.*, **13**, 11.
 Kopal Z.: 1933, *Astron.Nachr.*, **248**, 9.
 Kudashkina L.S., Rössiger S., Shugarov S.Yu.: 1989, *Astron. Tsirk.*, 1539, 18.
 Kukarkin B.V.: 1930, *NNVS* **3**, 19.
 Taylor M.D.: 1987, *Journal of the British Astron. Association* August, **97**, No 5, p. 277.
 Wenzel W.: 1965, *KVB* Nr 40, 246.
 Zajtseva G.V.: 1967, *Astron. Tsirk.*, 440.

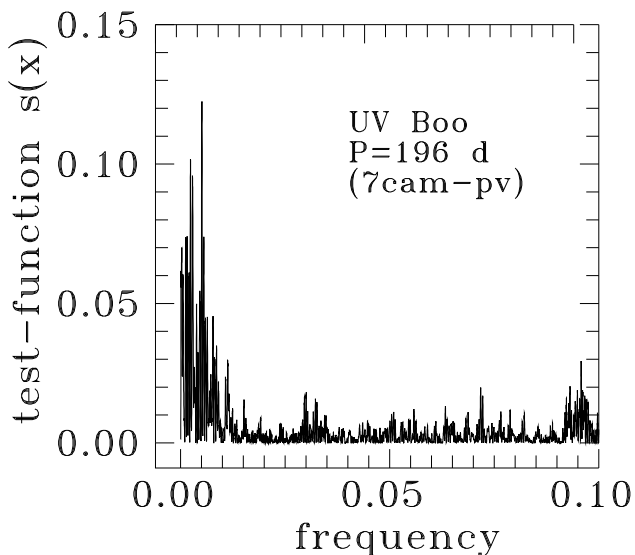


Figure 1: The periodogram of the UV Boo according to Odessa collection. The right peak corresponds to the period of about 10.442 days.

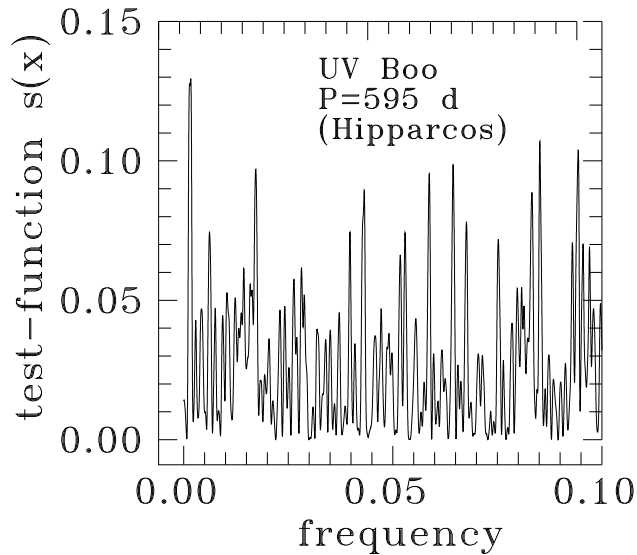


Figure 3: The periodogram of the UV Boo according to Hipparcos data. The right peaks correspond to the periods 11.74 and 10.60 days.

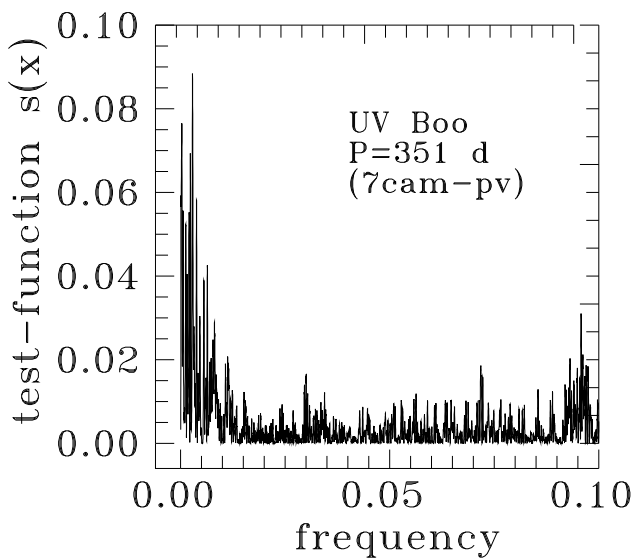


Figure 2: The periodogram of the UV Boo according to Odessa collection after subtraction of the value 196^d

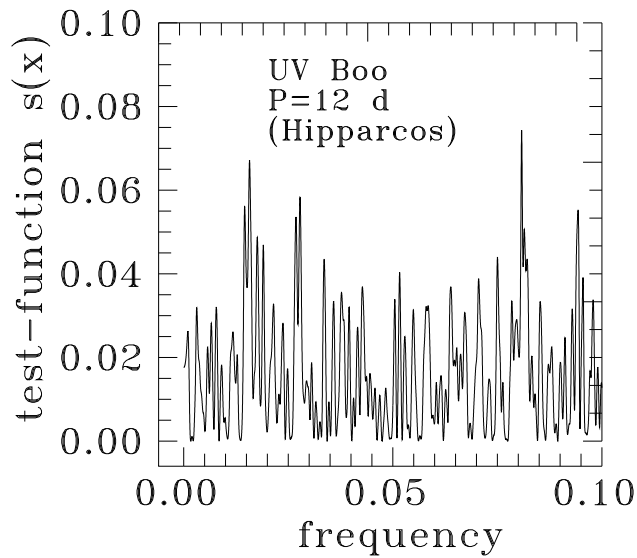


Figure 4: The periodogram of the UV Boo according to Hipparcos data after subtraction of the value 596^d

FG SGE: THE R CORONAE BOREALIS – TYPE ACTIVITY AND PULSATIONS

A. Rosenbush¹, M. Reszelski², E. Muylaert³

¹ Main Astronomical Observatory

Golosiiv, Kyiv-127, 03680, Ukraine, *mijush@mao.kiev.ua*

² Astronomical Observatory of A.Mickiewicz University

ul. Sloneczna 36, PL-60-286 Poznan, Poland

³ VVS Belgium Werkgroep Veranderlijke Sterren

Eksterstraat 6, 8400 Oostende, Belgium

ABSTRACT. Using the known connection between pulsations and the deep light decline in stars of the R Coronae Borealis – type variability, the pulsation period of FG Sge is determined, which is now equal to 103 days.

Key words: Stars: variable; stars: individual: FG Sge.

Two types of variability are observed in stars with the R Coronae Borealis (RCB) type variability: deep light declines by several magnitudes with a duration up to hundreds of days and pulsations with periods of 30–50 and more days and an amplitude up to 0.4^m . In RY Sgr, the most stable pulsating star with such variability, the declines are found to be triggered by a pulsation after its light maximum (Pugach 1977). The most deeper part of a light minimum falls at a pulsation minimum, i.e., the RCB minimum resembles a giant pulsation (Feast 1996). Similar properties were found to a different extent in other stars with the variability of this type: V854 Cen (Lawson et al. 1992) and FG Sge (Arhipova 1996). In FG Sge Gonzalez et al. (1998) found a deviation from the ephemeris of Arhipova (1996) and ascribed this to a possible change of pulsation period of the star.

The 6th RCB minimum of FG Sge which started recently manifested both these properties, and this allows us the possibility to follow the change of the pulsation period of this unique star. In addition this minimum also displays quasi-periodicity in the succession of the RCB minima.

The present research is based on visual estimations from the VSOLJ and the AFOEV databases and from the VSNET.

The definition of a light minimum and light maximum is important for our study. We propose and use such ones. A maximum is a state with the brightness close to the maximal one documented for the full

history of observations of a star. It is typical for the maximum when a star is weakened up to 0.5^m but without a stable trend to the increasing of brightness. A minimum is a state of weakening star between two successive maxima with a typical shape of light curve and a duration more than one pulsation period. The typical light curve is with a sharp light decline and a slower recovering to normal brightness.

For FG Sge this means that the state of brightness during JD 2449870–...2450100 was the giant pulsation according the definition of Feast (1996) and Menzies and Feast (1997). A relatively short-term duration of maximum state becomes typical in the behavior of FG Sge. It is so short that the star shows no more than 1–3 pulsations. The pulsation period P , according to Arhipova (1996), is nearly 114 days, and it decreases.

From the full light curve since 1992 it is obvious that the typical RCB minima follow at 530–780-day intervals (Table 1). For a more unambiguous determination of the initial moment of the RCB minimum we took into consideration that observed light curves in a minimum are described sufficiently well by the simple analytic expression as the sum of several shallower declines (Rosenbush 1996)

$$m(t) = m_{max} + \sum_{i=1}^n \Delta m_i \cdot (\tau_i + 1)^{2.7} \cdot \exp(-2.7\tau_i), \quad (1)$$

where $m(t)$ is the star brightness at the current time t , m_{max} is the star brightness in the quiet state, Σ is the sum over i from 1 to n "elementary" minima shaping the observed light curve, Δm_i is the depth of the i -th light decline, $\tau_i = (t - T_i')/T_{oi}$ is a time parameter, T_i' is the moment of minimal brightness in the i -th decline, T_{oi} is the duration of light drop in the i -th decline. Therefore the beginning of light decline was obtained by us with an accuracy of ten days and correspondingly the accuracy of determination of pulsation period was higher then two days. Here we assumed that a light

Table 1: Parameters of the RCB minima of FG Sge

Minimum number	Moment of minimum beginning, JD-2400000	Time interval between minima, day	Number of pulsations	Pulsation period, day
1	48860			
2	49430	570	5	114
3	50110	680	6	113
4	50890	780	7	111
5	51420	530	5	106
6	52030	610	6	102

Table 2: Parameters of the RCB minima of FG Sge.

Minimum number	Moment of minimum beginning, JD-2400000	Time interval between minima, day	Number of pulsations	Pulsation period, day
1	48860			
2	49430	570	5	114
3	50110	680	6	113
4	50890	780	7	111
5	51420	530	5	106
6	52030	610	6	102

minimum always begins since the same pulsation phase (at least within $0.1P$), and we oriented on the known pulsation period $P=114$ days.

As a result we derive the equation for the FG Sge pulsation period in 1992-2001:

$$P = 113.95 + 0.000361 \cdot (JD - 2448800) - 1.5285 \cdot 10^{-6} \cdot (JD - 2448800)^2. \quad (2)$$

A comparison with Arkhipova's ephemeris shows a distinction. According to our ephemeris, the pulsation period decreases faster and now the distinction reaches ten days. We cannot answer, at which pulsation phase a RCB minimum begins, as the pulsation period is very unstable and the star has two pulsation periods (see below). Thus we confirm the well-known property (Pugach 1977) that the RCB minimum begins after the light maximum in a pulsation.

As a result we can say that the RCB minima in FG Sge follow after 5-7 pulsations and, correspondingly, we can expect the 7th minimum.

The light curve of FG Sge has only two intervals of maximal light with the duration more than $2P$. In the last of these intervals, before the 6th RCB minimum, the pulsation, which was more or less well observed, had the period P_1 , which is nearly $1.4P$. Two periods with the similar ratio were noted by Arkhipova (1996),

but she suggested that the second period was false. As it seems to us in this connection, it should be noted that the time intervals between the 3th and 4th, and the 5th and the 6th RCB minima are multiples of P_1 , and $P_1=155$ days. But the data are deficient for certain conclusions. It is necessary to expect the following RCB minima. It is not improbable that the RCB type variability is operated by the interplay of pulsations with these two periods.

Acknowledgements. This research has made on the AFOEV database, operated at CDS, France, and the VSOLJ database, Japan, and the data of many observers from the VSNET, and we are grateful for that.

References

- Arkhipova V.P.: 1996, *Pis'ma Astron.Zh.*, **22**, 828.
 Feast M.W.: 1996, *ASP Conf.Ser.*, **96**, 3.
 Gonzalez G., Lambert D.L., Wallerstein G., et al.: 1998, *Ap.J.Suppl.*, **114**, 133.
 Lawson W.A., Cottrell P.L., Gilmore A.C., Kilmartin P.M.: 1992, *M.N.R.A.S.*, **256**, 339.
 Menzies J.W., Feast M.W.: 1997, *M.N.R.A.S.*, **285**, 358.
 Pugach A.F.: 1977, *Inf.Bull.Var.Stars*, No 1277.
 Rosenbush A.E.: 1996, *Astrophysics*, **39**, 78.

A NEW MAPPING OF THE CEPHEID INSTABILITY STRIP

David G. Turner¹

¹ Department of Astronomy and Physics, Saint Mary's University,
Halifax, Nova Scotia B3H 3C3, Canada, *turner@ap.stmarys.ca*

ABSTRACT. Results are presented for a new mapping of the instability strip for Milky Way Cepheids based upon field reddenings for 40 stars (mainly members of open clusters and associations), color excesses for 53 stars obtained from reddening-independent systems, and photometric reddenings for 200 additional Cepheids tied to the new system. The data provide new insights into features of the Cepheid instability strip and indicate that photometric reddenings for Cepheids are generally not of high accuracy.

Key words: Stars: variable: pulsating: Cepheids.

1. Introduction

Two unresolved issues raise concerns about the use of Cepheids as extragalactic distance indicators: “How important are metallicity differences between stars?” and “How well is interstellar (or intergalactic) reddening established?” Distances to galaxies derived from Cepheids, for example, are normally tied to a subset of Magellanic Cloud Cepheids for which reddenings are uncertain and the chemical compositions differ from those of Cepheids in the spiral galaxies targeted by the *Hubble Space Telescope* (HST) Key Project. Both features could affect the calibration of the Cepheid period-luminosity (*PL*) and period-luminosity-color (*PLC*) relations, which would affect distance estimates in a systematic fashion.

The question of Cepheid reddenings has been addressed many times in the literature. At present most adopted color excesses for Milky Way Cepheids are taken from a compilation by Fernie (1990a) based upon a scale of reddenings (Fernie 1987) linked to Strömrgren system photometry by Feltz & McNamara (1980). Turner et al. (1987) discussed problems with some of the Strömrgren system data of Feltz & McNamara, and Turner (1995) noted sizable differences between the resulting reddenings of Fernie (1990a) and well-established space reddenings for the same objects.

Presented here are the results of an empirical study of the instability strip for classical Cepheids in the Galaxy tied to a separate scale of interstellar reddening for such objects. The new system is defined

by space reddenings (E_{B-V}) for 40 Cepheids (mainly members of clusters and stellar groups) and color excesses for 53 Cepheids obtained from reddening-independent indices. Photometric reddenings for an additional 200 Cepheids have been tied to the new system by regression techniques using published data on the *UVBGRI* (six-color), *BVRI*, Walraven, DDO, Geneva, Strömrgren, Washington, and *VHK* systems, often involving recalibration of the system reddenings. The basic premise behind such a step is examined here in light of the fact that one expects a natural spread in colors for stars populating the instability strip.

2. Details of the Reddening System

The 40 Cepheids for which field reddenings are available originate from photometric studies of the surrounding fields (by Turner and collaborators) in which the exact form of the reddening law was established beforehand. It is an important caveat given that no single relationship accurately describes the reddening in all regions of the Galaxy (e.g., Turner 1989). Many published studies of Cepheids in clusters followed the more traditional use of fixed reddening relations to analyze the photometric data; they were excluded from the resulting sample. An added concern in some studies is the question of potential uncertainties in the standardization of the photometry (Turner 1990).

Full details of the study will be presented elsewhere, but it can be noted that all field reddenings obtained from early-type stars in the Cepheid fields were adjusted to values appropriate for the Cepheids themselves. The 53 color excesses obtained from reddening-free indices (Kraft 1960; Turner et al. 1987; Spencer Jones 1989; Sasselov & Lester 1980; Krockenberger et al. 1998) were adjusted, where necessary, to the system defined by Cepheids with field reddenings. A final step was to add photometric color excesses to the data base, after such values were normalized to the present system using the 93 Cepheids above as standards.

Fernie (1990b) has argued that $\langle B - V \rangle_0$ is better correlated with effective temperature for Cepheids than $(\langle B \rangle - \langle V \rangle)_0$, the latter being designated as the better

temperature index by older stellar atmosphere studies (e.g. Karp 1975). The problem was tested using the sample of 93 Cepheids of well-established reddening. The results are presented in Fig. 1, which plots unreddened color as a function of Cepheid pulsation period. The scatter in the $(\langle B \rangle - \langle V \rangle)_0$ data is similar to that in the $\langle B - V \rangle_0$ data, but is about 5% larger for the latter. If small scatter is taken as a positive test for a correlation with effective temperature of stars in the Cepheid instability strip, then it appears that older model atmosphere studies of Cepheids are correct in asserting that the optimum temperature indicator is $(\langle B \rangle - \langle V \rangle)_0$.

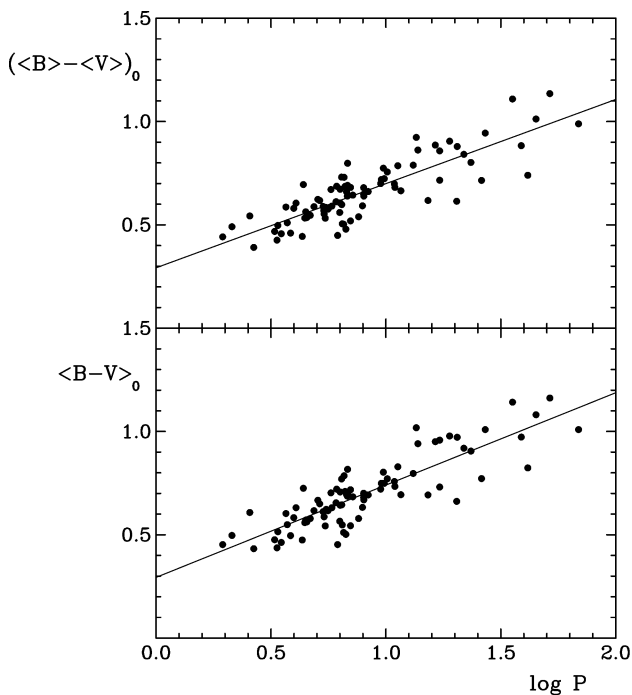


Figure 1: Derived intrinsic colors for $(\langle B \rangle - \langle V \rangle)_0$ (upper) and $\langle B - V \rangle_0$ (lower). The dispersion for the latter is about 5% larger than that for the former.

The final period-color relation is depicted in Fig. 2, in which the best-fitting relation is given by:

$$(\langle B \rangle - \langle V \rangle)_0 = 0.330(\pm 0.132) + 0.369(\pm 0.140) \log P.$$

The intrinsic dispersion in the data is ± 0.076 , although the full color width of the strip is more like 0.25, comparable to what was found by Fernie (1990b).

3. Radii and Effective Temperatures

An empirical map of the instability strip for Milky Way Cepheids can be made once a system of reddening is established, but an important step involves the derivation of effective temperatures and absolute bolometric magnitudes for individual objects. The transformation of $(\langle B \rangle - \langle V \rangle)_0$ to effective temperature was

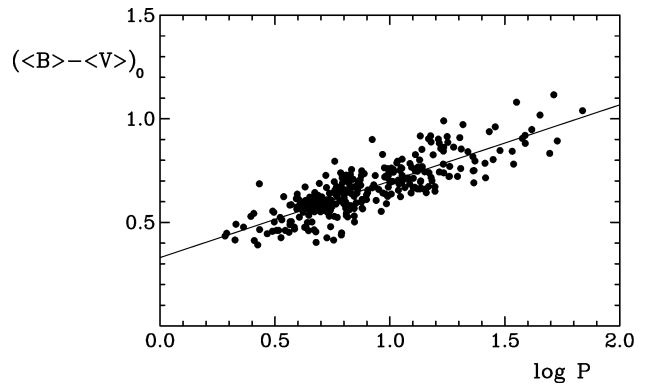


Figure 2: Derived intrinsic colors for the full sample of Cepheids, with the best-fitting relation depicted.

made here using the sixth order polynomial given by Gray (1992, eqn. 15.14), which provides an excellent fit to stars of all luminosity classes for which good model atmosphere data are available. An examination was made of the various alternative linear relationships established for Cepheids in the literature, but none were any better than Gray's relationship, and most provided poor fits to Cepheids of very red color.

Rather than depend upon an uncertain PLC relation for Cepheids, we estimated absolute bolometric magnitudes for Cepheids in our sample from their derived luminosities, through a combination of the inferred mean effective temperature of the variable (from its mean dereddened color) with a value calculated for its average radius, in other words from:

$$\langle L \rangle = 4\pi \langle R \rangle^2 \sigma \langle T_{\text{eff}} \rangle^4.$$

Such an approach does not properly account for abundance differences between stars, which presumably affect their $(\langle B \rangle - \langle V \rangle)_0$ colors, but such effects are difficult to include in any event.

Mean radii were established in simple fashion from each star's pulsation period using the period-radius relation established below. That step entailed knowledge of whether an individual star was pulsating in the fundamental mode or first overtone, but suitable tests are available to establish that characteristic.

The most reliable radii for Cepheids are generally those established from variants of the Baade-Wesselink (BW) method, although one must be wary of subtle assumptions in some versions of the BW method that may invalidate a feature of the approach adopted. Perhaps the best BW radii published for Cepheids are those of Laney & Stobie (1995) and Laney (1995) based upon *VJK* observations in conjunction with published radial velocity data.

A variant of the BW method developed by Turner (1988) uses published narrow-band *KHG* spectrophotometry from Feltz & MaNamara (1980) to isolate phases of identical effective temperature in Cepheid

light cycles. The method employs an empirical correction factor to adjust for systematic effects on the V magnitudes and $B-V$ colors during the cycles, and has some similarities to the inverted BW method of Ivanov (1984). An advantage of the *KHG* version is that the main assumptions of the BW method appear from tests to be fully satisfied in practice, while the external uncertainties in the results seem to be no larger than about 2–4%, compared with 5–8% in most other variants.

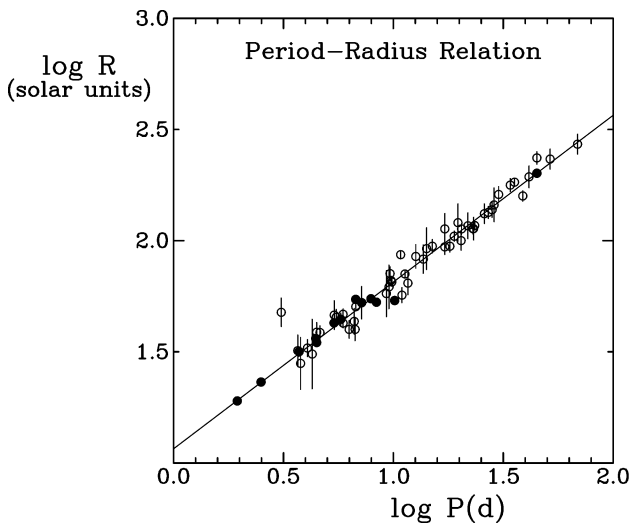


Figure 3: Derived BW radii from the *KHG* method (solid circles) and from Laney (1995) and Laney & Stobie (1995) (open circles), with the best-fitting relation depicted.

The original application of the *KHG* variant of the BW method provided a radius only for δ Cep, but unpublished results are available for ten additional Cepheids, the only objects for which good *KHG* data are available and the technique yields reliable results. The full set of BW radii for those stars, along with the independent BW radii published by Laney & Stobie (1995) and Laney (1995), are plotted in Fig. 3. The best-fitting relation, established by means of regression and non-parametric techniques, is:

$$\log(R/R_{\odot}) = 1.064(\pm 0.006) + 0.750(\pm 0.006)\log P_0.$$

Such a simple relationship between radius and pulsation period ($R \propto P^{3/4}$) appears to be valid for δ Scuti variables as well (Ferne 1992).

A survey of the data for main-sequence companions of Cepheids in open clusters (Turner 1996) noted that Cepheid mass correlates with pulsation period, namely $M \propto P^{1/2}$. From the discussion above it follows that the average surface gravity for Cepheids should also vary with period, i.e., $\langle g \rangle \propto P^{-1}$, and, from the period-density relation, that the pulsation constant $Q \propto P^{1/8}$.

4. Results

The resulting data for all Milky Way Cepheids in the complete sample are illustrated in Fig. 4, which plots the derived average bolometric magnitude for each variable as a function of inferred effective temperature, with symbol size increasing in direct proportion to observed blue light amplitude. Hidden in the scatter of Fig. 4 are a variety of features. The width of the strip, for example, appears to widen with decreasing temperature, although not to the extent indicated by Ferne (1990b). In fact, the temperature width of the strip remains essentially constant (~ 870 K) as a function of Cepheid pulsation period. There is one isolated point in Fig. 4 lying well outside the instability strip boundaries at $(\log T_{\text{eff}}, M_{\text{bol}}) = (3.784, -8.94)$. That is V810 Cen, which is clearly a Cepheid-like supergiant rather than a true Cepheid.

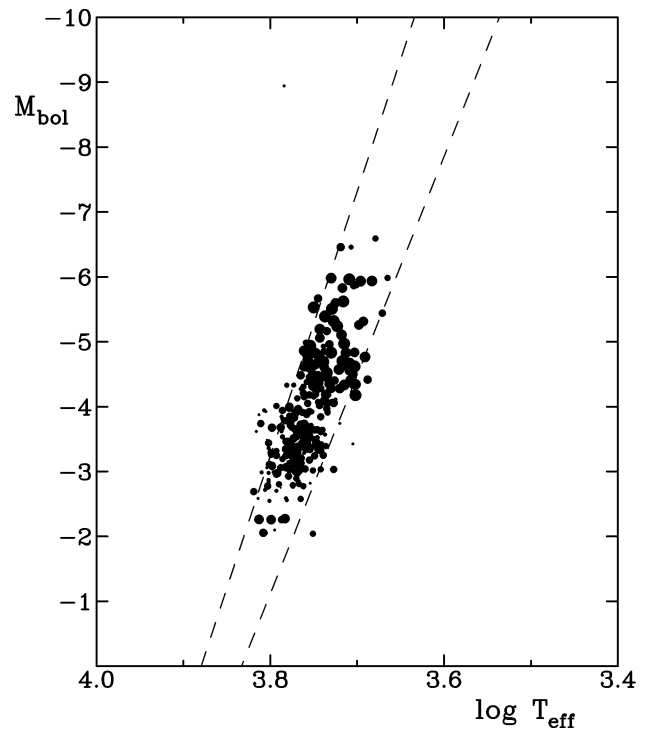


Figure 4: The new empirical map of the instability strip tied to the system of Cepheid reddenings described here. Symbol size increases in direct proportion to observed blue light amplitude.

Close examination of the data in Fig. 4 also reveals that the location of a Cepheid in the strip correlates with light amplitude, as argued previously by Pel & Lub (1978). The evidence for that is illustrated in Fig. 5, which plots blue light amplitude versus inferred effective temperature for individual Cepheids at specific pulsation periods, $P = 15^{\text{d}} \pm 1^{\text{d}}$, $8^{\text{d}} \pm 0^{\text{d}}.5$, $6^{\text{d}} \pm 0^{\text{d}}.5$, and $3^{\text{d}}.5 \pm 0^{\text{d}}.5$.

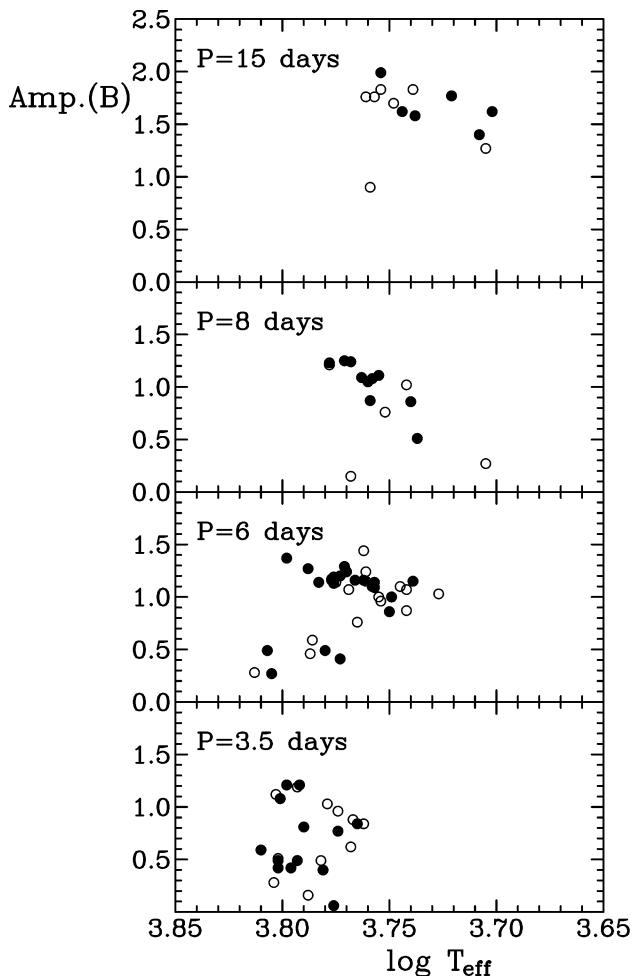


Figure 5: Plots of Cepheid light amplitude as a function of temperature for isolated cuts through the instability strip at $P = 15^d, 8^d, 6^d,$ and $3^d.5$. High weight points are represented by filled circles, low weight points by open circles.

It seems clear from Fig. 5 that there is a tendency for light amplitude to increase dramatically on the blueward (hot) side of the Cepheid instability strip and to fall off gradually toward the redward (cool) side, where surface convective layers presumably become more efficient at damping out pulsation. The evidence is strongest for the longer period Cepheids; for shorter period pulsators there is increasing contamination by small-amplitude Cepheids lying near the middle of the strip. The contamination is mostly illusory, however, and arises in large part from Cepheids for which only photometric reddenings are available. Since most photometric color excesses are derived from period-color relations, there is a natural tendency for the values to cluster objects towards the center of the instability strip, independent of light amplitude. The same systematic effect can account for the fact that Fernie

(1990b) was unable to find any evidence for a temperature dependence of light amplitude in his system of photometric reddenings, and argues that purely photometric reddenings should not be used where high accuracy is required.

There are a few high-weight points in Fig. 5 that also contribute to the low-amplitude contamination for Cepheids with periods of $3^d.5$ and 6^d . In some cases they represent objects of intermediate weight that have several independent photometric reddening sources. The systematic effect identified above probably applies to those stars as well. Stars for which the color excesses originate from the 93 standards are interesting cases. Two of them in the $P = 3^d.5$ group are Polaris (α UMi) and EV Sct, both of which are suspected overtone pulsators. The problem disappears if the stars are overtone Cepheids. The last object is V367 Sct, a double-mode pulsator in the heavily reddened cluster NGC 6649. It is conceivable that the space reddening for this Cepheid is in error, given the large and often patchy extinction that is present along the line of sight to cluster stars. NGC 6649 is a difficult cluster to observe photometrically, however, so an immediate resolution to the problem for V367 Sct is not envisaged.

References

- Feltz K.A., Jr., McNamara D.H.: 1980, *Pub.A.S.P.*, **92**, 609.
 Fernie J.D.: 1987, *A.J.*, **94**, 1003.
 Fernie J.D.: 1990a, *Ap.J.Suppl.*, **70**, 153.
 Fernie J.D.: 1990b, *Ap.J.*, **354**, 295.
 Fernie J.D.: 1992, *A.J.*, **103**, 1647.
 Gray D.F.: 1992, *The Observation and Analysis of Stellar Photospheres* (Cambridge U. Press: Cambridge).
 Ivanov G.R.: 1984, *Ap.Sp.Sci.*, **105**, 369.
 Karp A.H.: 1975, *Ap.J.*, **201**, 641.
 Kraft R.P.: 1960, *Ap.J.*, **131**, 330.
 Krockenberger M., Sasselov D., Noyes R., Korzennik S., Nisenson P., Kennelly T., Horner S.: 1998, *A.S.P. Conf. Series*, **154**, 791.
 Laney C.D.: 1995, *A.S.P. Conf. Series*, **83**, 367.
 Laney C.D., Stobie R.S.: 1995, *M.N.R.A.S.*, **274**, 337.
 Pel J.W., Lub J.: 1978, *I.A.U. Symp.*, **80**, 229.
 Sasselov D.D., Lester J.B.: 1990, *Ap.J.*, **360**, 227.
 Spencer Jones J.H.: 1989, *M.N.R.A.S.*, **238**, 269.
 Turner D.G.: 1988, *A.J.*, **96**, 1565.
 Turner D.G.: 1989, *A.J.*, **98**, 2300.
 Turner D.G.: 1990, *Pub. A.S.P.*, **102**, 1331.
 Turner D.G.: 1995, *A.S.P. Conf. Series*, **83**, 256.
 Turner D.G.: 1996, *J.R.A.S. Canada*, **90**, 82.
 Turner D.G., Leonard P.J.T., English D.A.: 1987, *A.J.*, **93**, 368.

THE STABILITY OF CEPHEID PULSATIONS

D.G. Turner¹, L.N. Berdnikov²

¹ Department of Astronomy and Physics, Saint Mary's University,
Halifax, Nova Scotia B3H 3C3, Canada, *turner@ap.stmarys.ca*

² Sternberg Astronomical Institute and Isaac Newton Institute of Chile, Moscow Branch,
13 Universitetskij prosp., Moscow 119899, Russia, *berdnik@sai.msu.ru*

ABSTRACT. Analyses of Cepheid period changes using $O-C$ diagrams are used to establish the direction of evolution of individual stars through the instability strip. The superposition of random fluctuations in period on $O-C$ data is less easy to interpret. Such chaotic behavior is a standard feature of Mira and RV Tauri variables according to the work of Percy, but has not been examined in detail for Cepheids. Unlike the situation for cooler classes of pulsators, most Cepheids do not exhibit random fluctuations in period. Binarity plays only a minor role in the scatter in $O-C$ data.

Key words: Stars: variable: pulsating: Cepheids.

1. Introduction

Stellar evolutionary tracks associate classical Cepheids with stars in a variety of instability strip crossing modes during advanced stages of nuclear fuel consumption. In the very rapid first crossing of the strip the energy originates from hydrogen burning in a thin shell surrounding a helium-rich core. In the slower second and third crossings energy is generated primarily from helium burning in the core, while during somewhat faster fourth and fifth crossings energy is generated from helium burning in a thin shell surrounding the core. During intermediate evolutionary stages as a red supergiant, large scale convection is capable of dredging up processed material from the core with abundance patterns reflecting previous stages of nuclear processing that have taken place in the core: depleted C and O abundance and enhanced N abundance reflecting prior stages of core hydrogen burning through CNO processing, and enhanced C and O abundance reflecting prior stages of helium burning (e.g. Luck & Lambert 1981). The neon-sodium cycle is responsible for enhanced Na abundances in such stars (Sasselov 1986; Luck 1994; Denissenkov 1994). Careful abundance analyses of Cepheids can therefore be used to establish likely evolutionary status on the basis of such patterns.

Alternatively, each instability strip crossing for a Cepheid is accompanied by gradual changes in overall dimensions and pulsation periods, P , as they evolve: increasing mean radius and P during evolution towards the cool side of the HR diagram (first, third, and fifth crossings), and decreasing mean radius and P during evolution towards the hot side of the HR diagram (second and fourth crossings). Since each crossing occurs at a different pace and at a different luminosity, the rate of period change is closely related to strip crossing mode, within possible constraints imposed by variations in chemical composition and pulsation mode (Berdnikov et al. 1997; Turner et al. 1999). The changes are revealed by parabolic trends in $O-C$ data, where each datum represents the difference between Observed and Computed times of light maximum calculated from a linear ephemeris. The changes amount to mere seconds or minutes per year in pulsation periods of days to months, but the effects are cumulative. The observed offsets from established ephemerides are therefore significant and measurable as differences from the predicted epochs of light maximum amounting to several hours or more — in some cases as offsets of several days.

Two other mechanisms can generate systematic trends in $O-C$ data. One is binarity, which produces light travel time differences in times of light maximum resembling cyclical changes in pulsation period as a Cepheid orbits the system's center of mass. The other is a meandering trend observed for some Cepheids that apparently originates from random changes in the period of pulsation. Of the three effects, evolution, light travel time effects, and chaotic fluctuations, evolution is the most obvious over long time baselines, while light travel time effects are usually marginally detectable at best. Chaotic period fluctuations are conspicuous relative to evolutionary trends and observational scatter for some Cepheids, but their origin is unexplained. Such behaviour is obvious in Cepheids such as S Vul, SV Vul and SZ Tau for example (Berdnikov 1994; Berdnikov & Pastukhova 1995), but is not observed in many

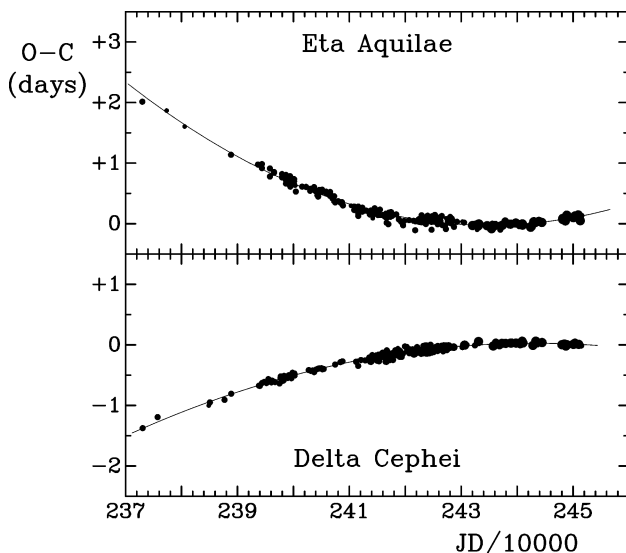


Figure 1: $O-C$ data and calculated trends for the Cepheids η Aql (upper) and δ Cep (lower).

others, such as TX Cyg, CD Cyg, and V1726 Cyg (Turner et al. 2001).

2. Evolutionary Effects

Figs. 1 and 2 illustrate evolutionary effects in the $O-C$ data for four Population I Cepheids: η Aql and δ Cep (Fig. 1), and T Ant and SV Vul (Fig. 2). The time baselines of $O-C$ data for η Aql and δ Cep span more than two centuries and the evolutionary trends are very well established: period increase for η Aql and period decrease for δ Cep. The same is true for T Ant and SV Vul (period increase for T Ant and period decrease for SV Vul), although the data for the two stars span only a century. Turner et al. (2001) recently demonstrated that evolutionary trends are detectable even in V1726 Cyg, a Cepheid discovered only two decades ago. Archival data from the Harvard Observatory plate collection were essential for augmenting the small amount of $O-C$ data for the star.

Least squares fitting of a parabola to $O-C$ data provides a rate of period change (in seconds per annum) that can be compared directly with predictions from stellar evolutionary models. In most instances the observed rates of period change agree closely with predictions and empirical expectations for different instability strip crossings (Fig. 3), although some ambiguous cases may warrant additional $O-C$ data or more careful analyses of existing data. The $O-C$ trends for the Cepheids in Figs. 1 and 2 indicate a third crossing for η Aql, a second crossing for δ Cep, a third crossing for T Ant, and either a second or fourth crossing for SV Vul (the rates of negative period change are about the same for Cepheids with periods of 40–80 days).

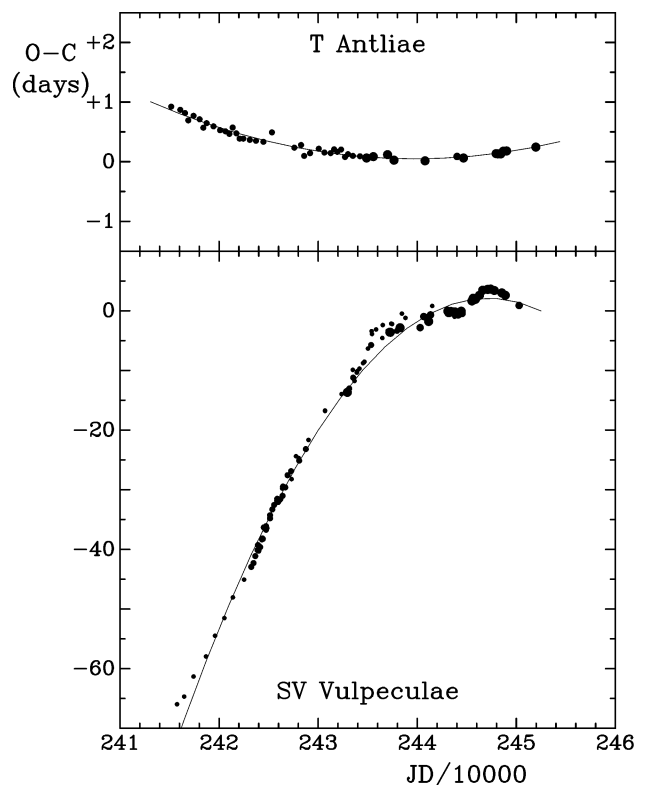


Figure 2: $O-C$ data and calculated trends for the Cepheids T Ant (upper) and SV Vul (lower).

3. Random Fluctuations in Period

Random fluctuations in period are a standard feature of long-period pulsators, as revealed by the work of Percy and his collaborators (Percy et al. 1997; Percy & Hale 1998; Percy & Colivas 1999). They have examined the $O-C$ data for Mira variables and RV Tauri stars using a test devised by Eddington & Plakidis (1929), in which one calculates the average accumulated delays between light maxima separated by x cycles, $\langle u(x) \rangle$, without regard to sign. The data should follow a trend line represented by the relation:

$$\langle u(x) \rangle^2 = 2a^2 + xe^2,$$

where a represents the magnitude of the random errors in measured times of light maximum and e represents the magnitude of any random fluctuations in period.

The “ e ” parameter, as a measure of randomness in pulsating stars, appears to increase roughly linearly with period (Percy et al. 1997; Percy & Hale 1998; Percy & Colivas 1999; Percy 2001). The available data, plotted in Fig. 4, when analyzed by non-parametric techniques (to avoid undue influence from outliers), are described by:

$$e = -0.421(\pm 0.146) + 0.015(\pm 0.001)P.$$

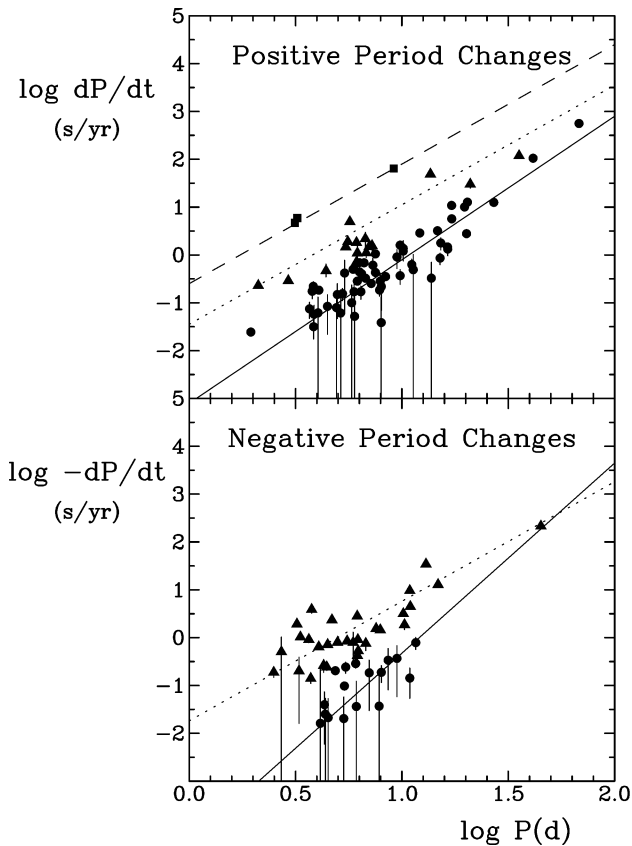


Figure 3: Observed rates of period change (with calculated uncertainties) are compared with predictions from stellar evolutionary models and empirical calculations (from top to bottom, the lines indicate first, fifth, and third crossings, upper; fourth and second crossings, lower). Different symbols indicate the assessment of likely crossing mode to individual Cepheids.

The possibility arises that the scatter in Fig. 4 originates largely from chemical composition differences between stars, but only stellar atmosphere studies can test that properly.

The situation for Cepheids is relatively unstudied, which is where $O-C$ data are useful, once evolutionary trends are removed. The situation is less straightforward than for Miras and RV Tauri stars, since very few light maxima are ever observed directly, except possibly for a few long period Cepheids. An $O-C$ datum usually represents a value obtained from fitting a light curve derived from observations over several adjacent cycles to a standard light curve. Eddington & Plakidis tests for the four Cepheids of §2 are illustrated in Fig. 5, and reveal no signature of random fluctuations in period for η Aql, δ Cep, and T Ant, but a strong positive signature for SV Vul. The case for V1726 Cyg is described by Turner et al. (2001). According to the results of Fig. 4, chaotic fluctuations in period should be relatively uncommon in Cepheids, except possibly

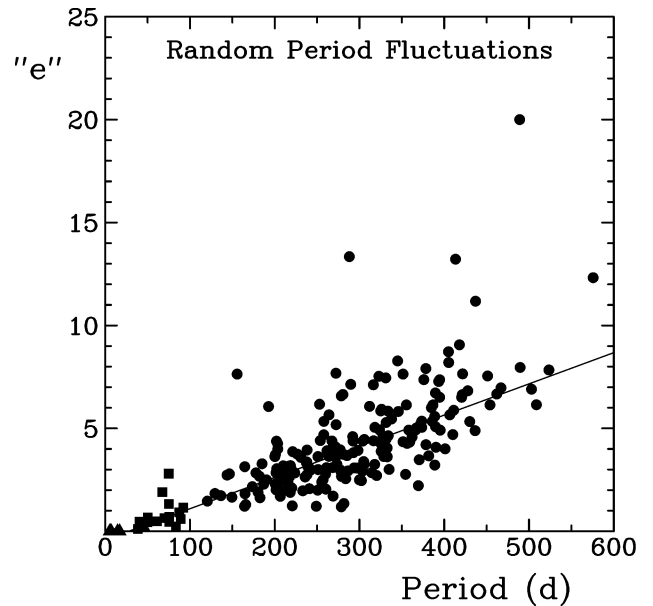


Figure 4: The dependence of the parameter e as a function of pulsation period for Cepheids (triangles), RV Tauri variables (squares), and Miras (circles).

for those of long period.

The cases for T Ant and SV Vul are rather curious, given that the residuals for both stars appear to display similar signatures (Fig. 6). The alternative possibility to random fluctuations in period is to consider light travel time effects in a binary system. Such an alternative fails for SV Vul since it produces unreasonable parameters for the system ($P \simeq 57.5$ yrs, $a_1 \sin i \simeq 329$ A.U., $M_1 \geq 10^4 M_\odot$). It is a possibility for T Ant, where the derived parameters are more reasonable ($P \simeq 42.4$ yrs, $a_1 \sin i \simeq 10.8$ A.U., $M_1 \geq 0.7 M_\odot$).

4. Discussion

Few correlations exist between deductions about instability strip crossing mode for Cepheids made from atmospheric abundance analyses and the modes inferred from rates of period change. Sometimes the latter are ignored entirely, as was the case for SV Vul in the recent study by Luck et al. (2001). Luck et al. argue that SV Vul seems likely to be in the first crossing of the instability strip on the basis of C, O, and Na abundances that appear to be representative of its original composition. As demonstrated in §2, however, SV Vul is crossing the instability strip for the second or fourth time. The possible discrepancy with the abundance data is now rather interesting. In order to resolve the two seemingly discordant results, it is necessary to consider other possibilities, such as (i) SV Vul is in the fourth crossing of the instability strip and its abundance pattern reflects a partial second dredge-up,

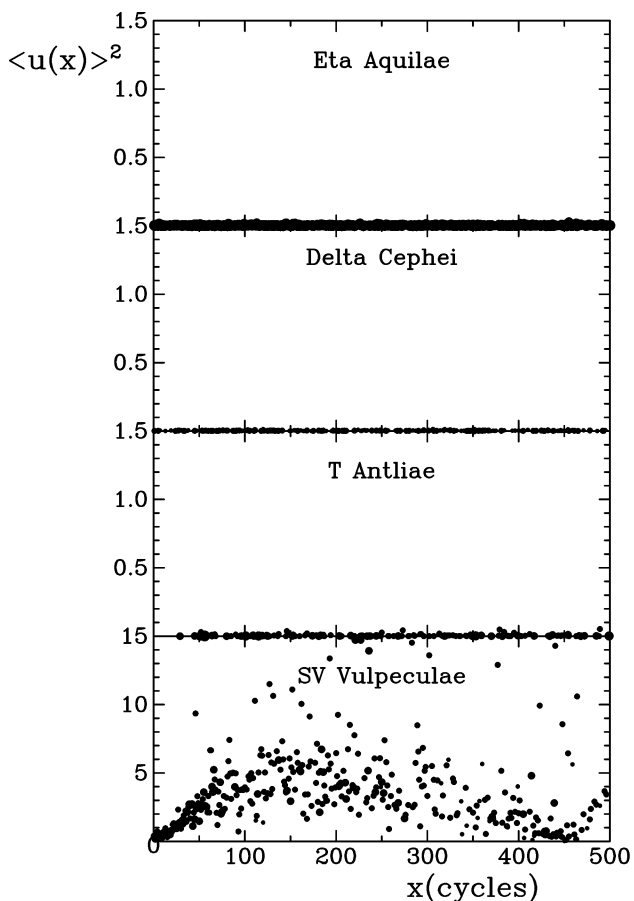


Figure 5: Randomness diagrams (plots of $\langle u(x) \rangle^2$ versus cycle count difference x) derived from residuals in the $O-C$ data for η Aql (upper), δ Cep (upper middle), T Ant (lower middle), and SV Vul (lower). Symbol size increases with increasing weight for the data.

or (ii) SV Vul merged with a close companion prior to reaching the first dredge-up and is presently in a second crossing of the strip without displaying the abundance anomalies of other second crossing Cepheids.

Examination of abundance patterns in the Cepheids studied by Luck & Lambert (1981) suggests that the second scenario proposed above is unnecessary. All Cepheids in the fourth crossing of the strip (DT Cyg, RT Aur, and ζ Gem) or fifth crossing (X Sgr) share similar abundance anomalies to SV Vul, namely solar or mildly underabundant C and O and overabundant N. If the analogy extends to Cepheids with long periods like SV Vul, one can conclude that the second dredge-up is not as efficient as the first in bringing core-processed material to the stellar surface.

Of the other Cepheids studied by Luck & Lambert (1981) which have derived rates of period change, five (SU Cas, η Aql, X Cyg, T Mon, and RS Pup) are in-

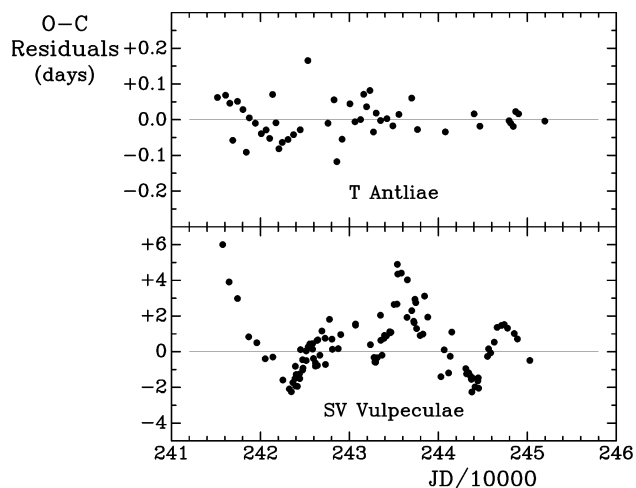


Figure 6: The residuals from evolutionary trends for T Ant (upper) and SV Vul (lower) plotted as a function of Julian date.

dicated to be in the third crossing of the strip and two (T Vul and δ Cep) are indicated to be in the second crossing. They exhibit the underabundance of C and O and overabundance of N expected for such stars.

References

- Berdnikov L.N.: 1994, *Astron. Lett.*, **20**, 232.
 Berdnikov L.N., Pastukhova E.N.: 1995, *Astron. Lett.*, **21**, 369.
 Berdnikov L.N., Ignatova V.V., Pastukhova, E. N., Turner, D. G.: 1997, *Astron. Lett.*, **23**, 177.
 Berdnikov, L. N., Ignatova, V. V., Caldwell, J. A. R., Koen, C.: 2000, *New Astronomy*, **4**, 625.
 Denissenkov, P. A.: 1994, *Astron. Astrophys.*, **287**, 113.
 Eddington, A. S., Plakidis, S.: 1929, *M.N.R.A.S.*, **90**, 65.
 Luck, R. E.: 1994, *Ap. J. Suppl.*, **91**, 309.
 Luck, R. E., Lambert, D. L.: 1981, *Ap. J.*, **245**, 1018.
 Luck, R. E., Kovtyukh, V. V., Andrievsky, S. M.: 2001, *Astron. Astrophys.*, **373**, 589.
 Percy, J. R.: 2001, private communication.
 Percy, J. R., Hale, J.: 1998, *Pub. A.S.P.*, **110**, 1428.
 Percy, J. R., Colivas, T.: 1999, *Pub. A.S.P.*, **111**, 94.
 Percy, J. R., Bezuhly, M., Milanowski, M., Zsoldos, E.: 1997, *Pub. A.S.P.*, **109**, 264.
 Sasselov, D. D.: 1986, *Pub. A.S.P.*, **98**, 561.
 Turner, D. G., Horsford, A. J., MacMillan, J. D.: 1999, *J.A.A.V.S.O.*, **27**, 5.
 Turner, D. G., Billings, G. W., Berdnikov, L. N.: 2001, *Pub. A.S.P.*, **113**, 715.

THREE CEPHEIDS IN GALACTIC OPEN CLUSTERS: CHEMICAL COMPOSITION AND EVOLUTION

I.A. Usenko, V.V. Kovtyukh

Astronomical Observatory, Odessa National University
T.G.Shevchenko Park, Odessa 65014 Ukraine, *igus@deneb.odessa.ua*

21 August 2001

ABSTRACT. Three classical Cepheids in galactic open clusters (CF Cas, DL Cas and WZ Sgr) were investigated, using high-resolution CCD spectra. Their T_{eff} and E_{B-V} estimations have a good agreement with photometrically determined ones. CF Cas and DL Cas have metallicity values, close to those of the Sun, whereas WZ Sgr has overabundant metallicity content with $Z=0.029$. Chemical abundance data show that they are the post first dredge-up stars. C and O content and ages have a good agreement with the theoretically predicted values. All these objects have a good fit with the PL relation for galactic Cepheids.

Key words: Stars: abundances ; stars: Cepheids in open clusters; stars: individual: CF Cas, DL Cas, WZ Sgr.

1. Introduction

Since until now classical Cepheids in galactic open clusters are the calibration objects for "period – luminosity" relation, it would be important to determine spectroscopically their atmospheric parameters and metallicity. It is very appreciable for the faint Cepheids, for which T_{eff} and metallicity values estimated till recently using multicolour photometries data. In our work we represent the results of investigations for three Cepheids in galactic open clusters: CF Cas (NGC 7790), DL Cas (NGC 129) and WZ Sgr (C1814-191). Thus, there was set the problems:

- 1) To obtain the high-resolution CCD – spectra in different phases of light curve for each Cepheid.
- 2) Using the new method of effective temperature determination, based on the ratio of the spectral line depths (Kovtyukh & Gorlova 2000), to obtain the T_{eff} estimates for these stars.
- 3) To compare our mean T_{eff} estimations with ones, obtained from UBV– photometry and to specify the colour excess values.
- 4) On the base of equivalent widths data of Fe I and Fe II lines to determine the gravities and turbulent velocities for these Cepheids, using the atmosphere

Table 1: Program stars spectra

Star	Period (days)	V (mag)	(B-V) (mag)	Number of spectra	Region (Å)
CF Cas	4.88	11.126	1.232	6	5500–7200
DL Cas	8.00	8.964	1.206	12	5500–7200
WZ Sgr	21.85	8.030	1.485	10	5500–7200

V and (B-V) data from Berdnikov (1987)

models from Kurucz (1992) grid and WIDTH 9 code.

5) To calculate the elemental abundance for these Cepheids, drawing the main attention for carbon and oxygen content.

6) To compare our C and O abundance results with theoretically predicted ones from Schaller et al.(1992) evolutionary models grid.

7) To estimate the evolutionary masses and ages for these Cepheids and to determine their evolutionary status.

2. The observations and analysis

All spectra was obtained using échelle spectrograph Sandiford, fed by 2.1–m Struve reflector, McDonald Observatory. The resolving power $R = 60000$, $S/N \approx 100$. The information concerning the program stars and their CCD spectra is given in Table 1.

Using the IRAF procedure we extracted échelle orders from CCD frames, made dark and cosmic ray hit subtraction, and wavelength calibration. The continuum level drawing, wavelength calibration, equivalent width measurements, – were made using the IBM/PC compatible DECH 20 package (Galazutdinov, 1992).

The atmospheric parameters:

- 1) T_{eff} were found using the ratio of the depths of spectral lines by the method of Kovtyukh & Gorlova (2000) with an accuracy of ± 10 –30 K.
- 2) The surface gravities were determined by forcing the Fe I and Fe II to produce the same abundance (within an accuracy of about ± 0.20 dex).
- 3) V_t were obtained by forcing the abundances from the Fe II lines to be independent of the equivalent widths (with an accuracy of about ± 0.30 km s⁻¹).

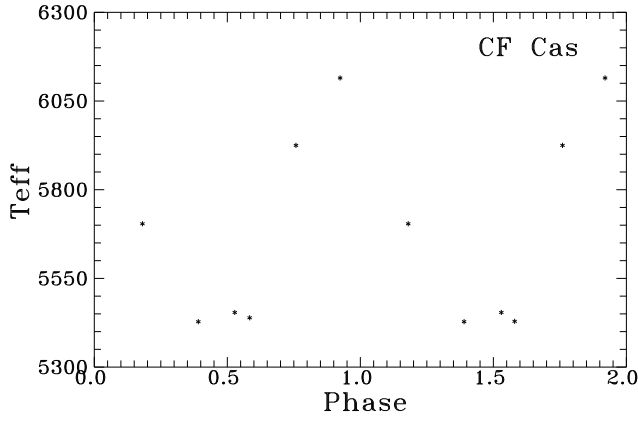


Figure 1: CF Cas effective temperature variation through the pulsation cycle.

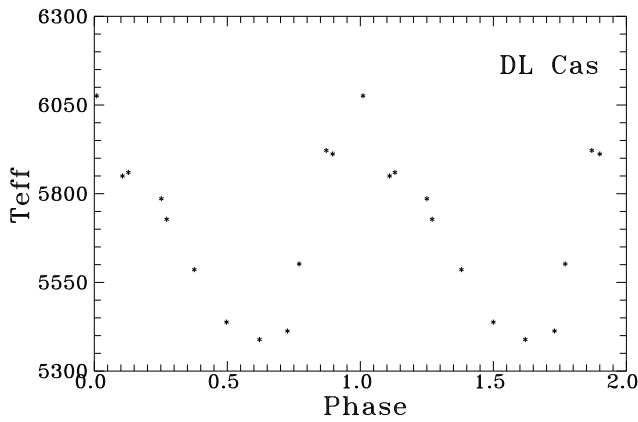


Figure 2: DL Cas effective temperature variation through the pulsation cycle.

Moreover, we have estimated the corresponding T_{eff} values for this Cepheids using $BVRI$ photometry data, Bessel, Castelli & Plez (1998) (BCP) calibrations and Grey (1992) relationship:

$$\log T_{eff} = 3.988 - 0.881(B - V) + 2.142(B - V)^2 - 3.614(B - V)^3 + 3.2637(B - V)^4 - 1.4727(B - V)^5 + 0.2600(B - V)^6 \quad (1)$$

All these data and colour-excesses estimates, determined by us and another authors are given in Table 2. In the Figures 1, 2 and 3 we displays the T_{eff} variations through the pulsation cycles for the investigated Cepheids.

The analysis of chemical composition was carried out using of Kurucz's WIDTH 9 code. Atmosphere models were interpolated from the Kurucz (1992) grid. All the oscillator strengths were so-called "solar" $\log gf$ values (Kovtyukh & Andrievsky 1999), derived using unblended solar lines. All the data of Cepheids chemical composition are given in Table 3.

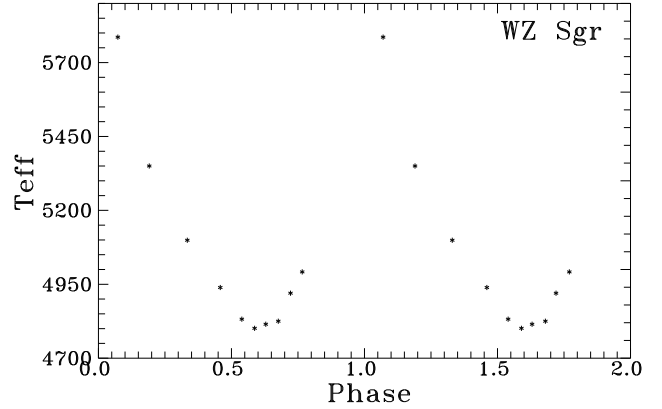


Figure 3: WZ Sgr effective temperature variation through the pulsation cycle.

Table 3: Average abundances for Cepheids.

Element	CF Cas		DL Cas		WZ Sgr	
	[El/H]	σ	[El/H]	σ	[El/H]	σ
C I	-0.19	0.09	-0.31	0.12	+0.03	0.12
O I	+0.06	0.32	-0.01	0.12	+0.13	0.25
Na I	+0.09	0.08	+0.11	0.04	+0.39	0.09
Mg I	-0.21	0.12	+0.11	0.08	+0.01	-
Al I	+0.10	0.00	+0.14	0.16	+0.28	0.17
Si I	+0.01	0.10	+0.02	0.09	+0.28	0.17
Si II	+0.12	0.18	+0.09	0.16	-	-
S I	+0.10	0.19	+0.21	0.29	+0.51	0.24
Ca I	-0.01	0.19	+0.01	0.16	+0.19	0.25
Sc I	+0.16	0.18	-	-	+0.24	-
Sc II	-0.18	0.19	-0.16	0.28	-0.00	-
Ti I	+0.00	0.15	+0.06	0.14	+0.24	0.18
Ti II	-0.02	0.05	-0.22	0.13	+0.16	0.17
V I	-0.04	0.13	+0.02	0.09	+0.20	0.09
V II	-0.19	0.10	-0.19	0.13	+0.04	0.09
Cr I	+0.04	0.16	+0.05	0.08	+0.19	0.21
Cr II	+0.22	0.12	+0.23	0.14	+0.20	-
Mn I	-0.01	0.06	-0.14	0.11	+0.15	0.05
Fe I	-0.01	0.09	-0.01	0.15	+0.17	0.09
Fe II	+0.01	0.10	-0.01	0.14	+0.19	0.08
Co I	-0.15	0.10	-0.04	0.21	+0.12	0.09
Ni I	-0.03	0.10	+0.00	0.11	+0.21	0.09
Cu I	-0.11	0.16	-0.19	-	+0.13	0.18
Zn I	+0.25	0.19	+0.47	0.28	+0.35	-
Y I	-	-	-	-	+0.56	-
Y II	+0.11	0.07	+0.21	0.23	+0.30	0.08
Zr II	-0.19	0.11	+0.16	0.35	-0.08	0.05
La II	+0.14	0.09	+0.16	0.35	+0.24	0.04
Ce II	-0.17	0.13	+0.09	0.26	-0.08	0.08
Nd II	+0.04	0.20	+0.12	0.17	+0.18	0.20
Eu II	+0.06	0.06	+0.11	0.15	+0.15	0.15
Gd II	-0.02	0.15	-0.05	-	+0.08	0.08

Table 2: Atmosphere parameters, colour indices and colour excesses

Star	Our estimations			E_{B-V}		Gray		BCP	
	T_{eff}	$\log g$	V_t	E_{B-V}	Other authors	$(B-V)_0$	T_{eff}	$(B-V)_0$	T_{eff}
CF Cas	5636	1.7	3.8	0.55	0.55 (1)	0.682	5650	0.685	5635
DL Cas	5715	1.7	4.4	0.55	0.50 (2)	0.656	5702	0.660	5725
WZ Sgr	5036	0.7	4.2	0.57	0.56 (3)	0.920	5023	1.030	5025

(1) – Matthews et al. (1995); (2) – Gieren et al. (1994); (3) – Turner et al. (1993)

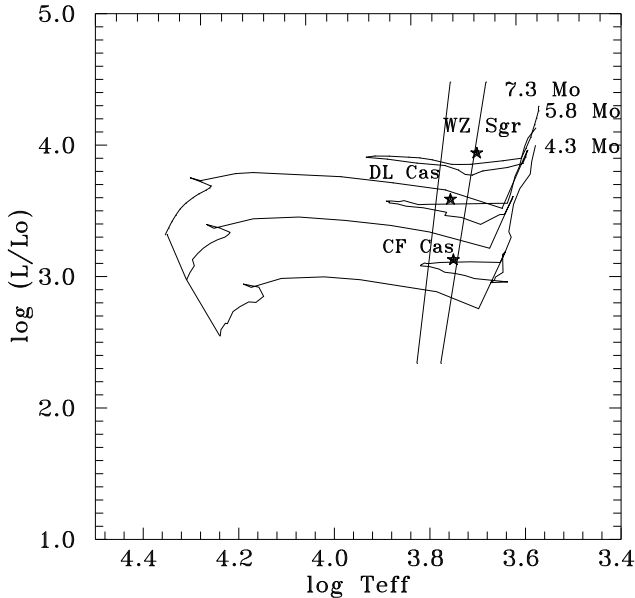


Figure 4: The HR diagram for CF Cas, DL Cas and WZ Sgr. The instability strip edges for fundamental mode pulsation were derived using relations from Chiosi et al. (1992)

Since carbon and oxygen are the best indicators of the evolutionary state of yellow supergiants, it would be interesting to compare our observational data with the theoretically predicted ones from Schaller et al. (1992) evolutionary models grid. All these results are given in Table 4.

As seen from Tables 3 and 4, all these Cepheids are the post first dredge-up yellow supergiants. Therefore their evolutionary masses can be determined from the mass–luminosity relation with overshooting (Antonello & Morelli 1996):

$$\log(L/L_{\odot}) = 3.52\log(M/M_{\odot}) + 0.9; \quad (2)$$

The final results, including our ages estimation from Schaller et al. (1992) evolutionary models grid, are given in Table 5.

In the Figures 4 and 5 we represent the positions of our investigated Cepheids on the HR and PL diagrams, respectively.

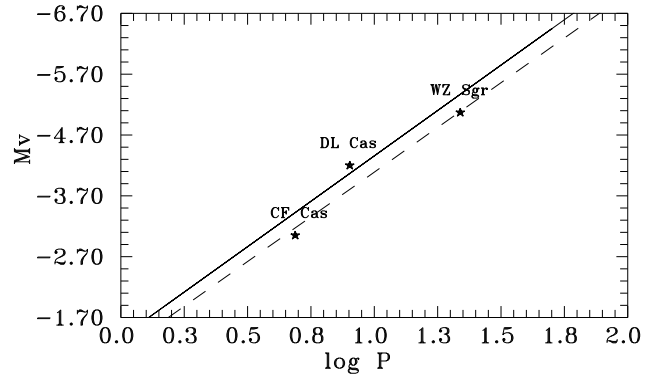


Figure 5: Positions of CF Cas, DL Cas and WZ Sgr on PL diagram. Solid line, – PL relation from Gieren, Barnes & Moffit (1993), dashed, – the same from Turner (1992)

3. Conclusions

1) The mean effective temperatures of CF Cas, DL Cas and WZ Sgr, obtained by using of the spectroscopical criterion have a good agreement with ones, determined photometrically.

2) Our colour excesses for CF Cas and WZ Sgr are in good agreement with the estimates of other authors, while for DL Cas it has a slightly more value.

3) CF Cas and DL Cas have metallicity values, close to those of the Sun, whereas WZ Sgr has overabundant metallicity content with $Z = 0.029$.

4) Chemical abundance data for all these Cepheids show that they are the post first dredge-up stars. Their carbon and oxygen content have a good agreement with the theoretically predicted ones.

5) Both positions of CF Cas and DL Cas on the HR diagram corresponds to their third crossing of Cepheids instability strip. Position of WZ Sgr is not clear and it might be connected with uncertainty in the distance determination. Moreover, WZ Sgr located near the red edge of the instability strip.

6) The ages of these Cepheids have a good agreement with ones, determined for their open clusters. Their positions on the PL diagram have a good fit with the "period–luminosity" relation for galactic Cepheids.

Table 4: Metallicities and C and O abundances

Star	[Fe/H]	Z	Carbon				Oxygen	
			Carbon		Oxygen			
			Predicted	Observed	Predicted	Observed		
CF Cas	0.00	0.020	-0.175	-0.19±0.09	-0.030	+0.06±0.32		
DL Cas	-0.01	0.020	-0.174	-0.31±0.12	-0.032	-0.01±0.12		
WZ Sgr	+0.18	0.029	-0.181	+0.03±0.12	-0.036	+0.13±0.25		
WZ Sgr ([El/Fe])			-0.181	-0.15±0.12	-0.036	-0.05±0.25		

Table 5: Luminosities, distances, radii, evolutionary masses and ages

Star	M_V	d (pc)	$\log(L/L_\odot)$	R/R_\odot	M_{ev}	$\log t$	$\log t$ (Other authors)
CF Cas	-3.05	3130	3.13	40.6	4.3	8.14	8.0 – 8.1 (1)
DL Cas	-4.20	2034	3.59	66.0	5.8	7.78	7.6 (2)
WZ Sgr	-5.07	1787	3.94	122.9	7.3	7.66	7.3 (3)

(1) – Matthews et al. (1995); (2) – Gieren et al. (1994); (3) – Turner et al. (1993)

References

- Antonello E., Morelli P.L.: 1996, *As.Ap.*, **314**, 541
 Berdnikov L.N.: 1987, *Perem. Zvezdy*, **22**, 530
 Bessel M.S., Castelli F., Plez B.: 1998, *As.Ap.*, **333**, 231
 Chiosi C., Wood P.R., Bertelli G., Bressan A., Mateo M.: 1992, *Ap.J.*, **385**, 205
 Galazutdinov G.A.: 1992, *Preprint SAO RAS* No. **92**
 Gieren W.P., Barnes T.G., Moffit T.J.: 1993, *Ap.J.*, **418**, 135
 Gieren W.P., Welch D.L., Mermillod J.C., Matthews J.M., Hertling G.: 1994, *A.J.*, **107**, 2093
 Gray D.: 1992, *Observation and Analysis of Stellar Photospheres*, Cambridge Univ. Press, *2nd Edition*.
 Kovtyukh V.V., Andrievsky S.M.: 1999, *As.Ap.*, **351**, 597
 Kovtyukh V.V., Gorlova N.I.: 2000, *As.Ap.*, **358**, 587
 Kurucz R.L.: 1992, *The Stellar Populations of Galaxies*, B. Barbuy, A. Renzini (eds.), *IAU Symp.*, **149**, 225.
 Matthews J.M., Gieren W.P., Mermillod J.C., Welch D.L.: 1995, *A.J.*, **110**, 2280
 Schaller G., Schaere D., Meynet G., Maeder A.: 1992, *As.Ap.Suppl.*, **96**, 269
 Turner D.G.: 1992, *A.J.*, **104**, 1865
 Turner D.G., van den Bergh S., Younger P.F., Danks T.A., Forbes D.: 1993, *Ap.J.S.*, **85**, 119

FREQUENCY ANALYSIS OF RADIAL VELOCITIES VARIATIONS OF XZ CYG

S.V. Vasilyeva

Astronomical Observatory, Odessa National University
T.G.Shevchenko Park, Odessa 65014 Ukraine, *astro@paco.odessa.ua*

ABSTRACT. The observation of RR Lyr type star XZ Cyg were carried out at 50" telescope of Crimean Astrophysical observatory and covered the time interval of JD 2441483 - 2441579. For radial velocities measuring were used H, CaII and other metals line of low dispersion spectrograms. The frequency analysis was carried out using computer code FOUR-1 (Andronov I.L., Odessa Astron. Publ., 1994, 7, 49). Radial velocities variations are sufficiently fitted by sinusoid. The variations of radial velocities with the phase of curve lights and of Blazko effect was investigated.

Key words: Stars: RR Lyr-type; Stars: individual: XZ Cyg.

1. Introduction

The spectral observations of the variable star of RR Lyra type-stars XZ Cyg were carried out at 50" telescope of the Crimean Astrophysical observatory with the new to investigate of the changes of radial velocities v_r . The spectrograms XZ Cyg were obtained in the minimum of its brilliancy with the maximal possible resolution of the lines were converted into radial velocities v_r considering the corrections of the orbital motion and axial rotations of the Earth. The radial velocities were mainly determined with the help of lines of absorption H_γ , H_δ , H_8 and H_9 .

In certain cases the radial velocities were determined with the help of H_β orthother hydrogen lines till H_{14} homeliness in the region of the ascending branch of the curve of brightness certain lines of absorption bifurcate. Due to the phenomenon two radial velocities were determined with the aid of the bifurcated lines.

The phases of the basic period ϕ and of the period of the Blazhko effect ψ were calculated the elements Kynchev (1974):

$$\text{JD Max hel} = 2440445.789 + 0.466497 E$$

$$\text{JD Max A} = 2441571.50 + 57.52 N$$

In the atmospheres of stars of this type occur stormy, rapid processes, which are accompanied by impact wave and by the appearance of the excessive radiation. May be that's why calcium atoms which are easily ionized can be in the higher grade of ionization, and their

lines of absorption's can be located beyond the visible of the spectrum. It might be the reason for the weakening of the intensity of lines of absorption K CaII in comparison with stationary stars. Though the measuring of the H and K lines CaII was difficult, we radial velocities v_r for ψ phases of the Blazko effect. In certain spectrograms we managed to measure separate lines of iron, magnesium, and titanium and their v_r .

The radial velocities XZ Cyg were determined with the help of the spectra with prolonged exposition without taking into account the influence of the changes of brilliance and velocity.

Using the multi-frequency changes of the parameters of the stars, which was worked out at the Odessa Astronomical Observatory by Andronov I. L.

$$x_t = C_1 + C_2 \sin \omega t + C_3 \cos \omega t, \text{ where } f_1(t_k) = 1, \\ f_2 = \sin(\omega t_k), f_3 = \cos(\omega t_k).$$

Here $\omega = 2\pi f$, where f is trial frequency.

The changes of the radial velocities may be represented by trigonometric polynomial of the first degree $v(\varphi) = C_1 + C_2 \cos 2\pi(\varphi - C_3)$,

C_1 - is the mean value of the radial velocity i.e. γ - velocity.

C_2 - the semi-amplitude of the radius variations of the layer of formation of spectral lines H, H and K Ca II and Me.

C_3 - the phases ϕ_{max} of maximum (the approximation after iterating).

The results obtained are represented in table 1.

The table also represents the number of lines n , which were included in the determination of the mean radial velocity.

σ_γ - error estimate of γ - velocity and σ_r - error estimate of r and σ_φ - error estimate of φ .

Acknowledgements. Special thanks to I.L. Andronov for his kind help in making necessary modification to his computer code.

References

- Andronov I.L.: 1994, *Odessa Astron. Publ.*, **7**, 49.
Andronov I.L.: 1997, *As. Ap. Suppl.*, **125**, 207.
Kynchev P.Z.: 1974, *VS*, **19**, 447.

Table 1: Radial velocities of XZ Cyg

Elements	n	γ km/s	σ_γ	R	σ_R	φ_{max}	σ_φ
$\psi = 0.135 - 0.275$							
H	11	-157.52	16.8	58.15	11.5	0.87	0.072
CaII	8	-130.73	14.2	31.66	25.1	0.76	0.073
$\psi = 0.465 - 0.570$							
H	18	-175.25	6.7	31.93	9.2	0.99	0.061
CaII	13	-159.08	10.28	17.60	9.26	0.870	0.183
Me	6	-185.71	78.01	94.24	105.65	0.073	0.089
$\psi = 0.570 - 0.670$							
H	18	-172.88	5.95	39.45	11.14	0.044	0.038
CaII	8	-131.73	21.00	49.02	51.09	0.601	0.076
$\psi = 0.990 - 0.130$							
H	21	-169.18	5.50	61.39	10.54	0.065	0.026
CaII	17	-156.26	5.77	37.58	8.05	0.965	0.047
Me	9	-139.85	13.71	55.53	49.25	0.169	0.083

ASYMPTOTIC GIANT BRANCH VARIABLES

P.A. Whitelock

SAAO, P.O. Box 9, Observatory, 7935,
South Africa. paw@saa.ac.za

ABSTRACT. Asymptotic Giant Branch variables are the brightest and most distinctive individual stars to be found in the resolved, old and intermediate age, stellar populations of galaxies in the Local Group and beyond. The characteristics of these stars are reviewed here with particular emphasis on the luminous AGB stars in the LMC. Most large amplitude variables, both carbon- and oxygen-rich, fall close to a linear extrapolation of the period luminosity relation determined for shorter period Miras. The few such stars which are more luminous than predicted appear to be experiencing extra energy production via hot bottom burning.

Key words: AGB stars, Mira variables, carbon stars, OH/IR stars, hot bottom burning.

1. Introduction

The very first pulsating star on record is Mira itself, now known as α Ceti (e.g. Hoffleit 1997). The discovery of Mira as a variable is usually attributed to the Netherlands astronomer, David Fabricius, who noted extreme changes of brightness in 1596, although there are hints that it might have been recognized at even earlier times. Some while later the star was named *Stellar Mira* meaning *the Wonderful Star*, when it was appreciated that its extreme changes in brightness, from visible to invisible, were actually periodic on a time scale of 11 months. We now know Mira Ceti as the prototypical Asymptotic Giant Branch (AGB) variable. Given their long history it is perhaps surprising that the AGB variables have remained such an enigma; they are the most poorly understood of all the recognized classes of variable star - to the extent that even their pulsation modes remains a source of controversy. A visual light curve for Mira Ceti, from amateur observations, is reproduced in AAVSO Report 38 (note that amateur observations remain important in characterizing the behaviour of these very large amplitude variables). The peak-to-peak amplitude, which is typical of these variables, is about 3 mag and the period is 332 days. The behaviour is somewhat erratic with different maxima from one cycle to another; this is quite typical of Mira variables.

Studies of extragalactic resolved populations are be-

coming both practical and important as we develop not only telescopes in space, but also large telescopes with adaptive optics on the ground. At the same time, advancements in the appropriate array technology is pushing near-infrared observations onto the critical path for understanding of individual stars in these resolved populations. When we examine old or intermediate age populations what we see most clearly are the very brightest individual stars at the very top of the Asymptotic Giant Branch and those are typically the AGB, or Mira, variables. The fact that we are still far from a detailed understanding of these stars, even in our own galaxy, is bound to hinder our attempts to characterize populations in and beyond the Local-Group galaxies.

With this in mind I briefly review below our current understanding of AGB evolution, mentioning dredge-up and hot bottom burning, before looking in more detail at recent observations of AGB variables in the LMC, which provide our first step to more distant populations. *AGB variable* is a term that means different things to different people, but the stars covered here include the Mira variables, mentioned above, OH/IR stars and dusty carbon stars. Where appropriate the lower amplitude, semi-regular variables are also referred to.

The classical defining characteristics of Mira variables are: a large amplitude, emission line spectra (Me, Se or Ce), and periods in excess of 100 days. The OH/IR- and dusty carbon-stars are assumed to be similar to the Miras although they are often too faint at visual wavelengths to determine amplitudes or measure spectra. Their periods are generally long, up to 1000 days for the carbon stars and up to about 2000 days for the OH/IR stars.

2. AGB Evolution

The AGB evolution of low and intermediate mass stars was described by Iben and Renzini (1983); the salient features are outlined below. Stars leave the horizontal branch when they run out of helium in the core; they ascend the AGB burning hydrogen in a shell around an inert C/O core. As the hydrogen burning

proceeds a helium shell gradually builds up and will eventually ignite explosively producing a helium shell-flash and starting the phase of evolution known as thermal pulsing; successive shell flashes will occur on time scales of the order of 10^5 years. At the very top of the thermally pulsing AGB the outer atmosphere of the star becomes unstable to pulsations and the Mira variable is born. The Mira pulsations drive mass-loss from the outer atmosphere and most of the hydrogen envelope is eventually lost. Our star then leaves the AGB to cross the HR diagram, becoming first a planetary nebula and then cooling to oblivion as a white dwarf.

The internal structure of an AGB star at the time its atmosphere starts to pulsate is that of an inert C/O white dwarf surrounded by helium and hydrogen burning shells. This core is surrounded by the huge convective hydrogen atmosphere of the red giant and that in turn is surrounded by material of the circumstellar shell. This shell is dominated by dust and molecular effects - showing perhaps Maser emission from SiO, H₂O and/or OH molecules. One of the consequences of thermal pulsing is to allow carbon-rich material from the core to be dredged up into the convective envelope from which it can reach the surface. In this way some stars dredge up sufficient carbon to overwhelm the oxygen and they become carbon stars. At this stage carbon chemistry and carbon dust dominate the stars' observed characteristics.

It is perhaps worth emphasizing that there is no connection between the atmospheric pulsations that give us the AGB variables and the thermal pulsing of the core. The AGB variations occur in the outer atmosphere of the red giant on a time scale of about one year, while thermal pulsing occurs in the core on a time scale of 10^5 years.

To a first approximation the larger the initial mass of a star the higher the luminosity at which its AGB will terminate. Thus the metal-rich Globular Clusters have AGB tips only slightly brighter than the tip of the first giant branch ($M_{bol} \sim -3.7$ mag), while the brightest AGB variables in the LMC, which probably have progenitors of about $M_i \sim 8M_{\odot}$, are found at about $M_{bol} \sim -7.2$ mag.

For the most part the luminosities of AGB stars are a function of their core mass (Paczynski 1970). However, towards the end of AGB-evolution, for stars with an initial mass in excess of 4 or 5 M_{\odot} , the base of the convective envelope can dip into the hydrogen-burning shell, resulting in hot bottom burning (HBB), with far reaching consequences for the evolution of the star. The transition from oxygen-rich to carbon-rich is affected; exactly how seems to depend on the specific model and in particular on how mass loss is treated. HBB may prevent carbon stars happening at all, or prevent them from happening until the envelope mass is depleted (Frost et al. 1998). In some models carbon stars do form and then HBB turns them back into

oxygen-rich stars (Marigo et al. 1999). Another consequence, for stars in a rather narrow mass range, is the formation of lithium via beryllium (Sackmann and Boothroyd 1992). One of the most important results in the present context is a rapid increase in luminosity (Blöcker and Schönberner 1991); again the details depend on mass loss which will tend to decrease the effect of HBB. This is obviously very important in terms of the behaviour of the most luminous AGB stars and the apparent observational consequences of HBB are discussed in more detail below.

3. AGB Stars in the LMC

The following discussion and Fig. 1 assume a distance modulus for the LMC of 18.5 mag, for convenience; the best current estimate of the distance modulus is actually 18.58 ± 0.1 mag (Feast 2001). Until relatively recently our knowledge of AGB variables in the LMC was very heavily biased towards large amplitude variables and stars with only thin dust shells. The results of the microlensing surveys and the follow-up work from the IRAS survey has changed the picture considerably during the last decade.

Period luminosity (PL) relations were established by Feast et al. (1989) for carbon- and oxygen-rich Miras in the LMC. They were derived from large amplitude variables monitored over their light cycles to derive mean luminosities. At K ($2.2 \mu\text{m}$) the carbon- and oxygen-rich stars obey the same PL relation, with a scatter of < 0.18 mag, up to periods of around 420 days. Bolometric luminosities were determined by fitting blackbodies to JHK photometry - a reasonable approximation for those stars which have only very thin dust shells. The bolometric PL relations appeared to be different for the oxygen- and carbon-rich Miras, although it was never clear if this was really so, or an artifact of the way the bolometric luminosities were derived.

Groenewegen and Whitelock (1996) derived a bolometric PL relation for LMC carbon Miras using all the spectroscopically confirmed carbon stars, although there were only single epoch observations for many of them. Their PL relation was essentially indistinguishable from that for oxygen-rich stars. At the time this work was done no LMC carbon Miras were known at periods significantly longer than 500 days, and the optically visible longer period oxygen-rich stars lay clearly above an extrapolation of the PL relationship for short period stars. As discussed below this is quite possibly because they are experiencing extra energy production via HBB.

Smith et al. (1995) performed a survey for lithium among AGB stars in the SMC and LMC. They found that a very large fraction of those with bolometric magnitudes in the range $-6 \lesssim M_{bol} \lesssim -7$ were lithium rich, as were a much smaller number of lower luminosity

stars. Our present understanding of lithium enhancements in AGB stars is that most of them occur as a result of HBB as described in section 2 above.

According to Sackmann and Boothroyd (1992) lithium enhancements are to be expected in stars with initial masses around 4 or 5 M_{\odot} , the exact value depending on metallicity. In view of this it is interesting to note that a very large fraction of the stars which fall above the PL relation must be undergoing HBB, as their high lithium abundance indicates. Note that in fig 6 of Smith et al. (1995) the PL relation runs through the low luminosity ridge line of the points. A few of the brighter star will be SR variables which we would expect to lie above the Mira PL relation and some others almost certainly have erroneous periods. Furthermore, the luminosities of all these stars require more detailed investigation, most are based on single observation of large amplitude variable.

As we would expect to detect enhanced lithium only from a fraction of the stars actually experiencing HBB it is possible to speculate that all of the stars with luminosities above the PL are there because of HBB. It is perhaps important to remember that the stars investigated by Smith et al. are not representative of AGB stars generally; they are the brightest ones with the thinnest dust shells, as it was only practical to obtain spectra, with sufficient resolution to measure the lithium lines, of that subgroup.

A group of people with whom I have been working (see, e.g. van Loon et al. 1999b) have, over the last few years, obtained ground-based and ISO data of about 50 thick-shelled LMC sources originally selected from the IRAS data-base. We have also been able to derive periods for many of them. By combining ground-based, *JHKL*, photometry with ISOCAM and ISOPHOT photometry and spectroscopy it has been possible to derive luminosities by fitting models to the combined dataset. Because the ISO observations do not cover the light cycle and most of the energy is emitted longward of $5\mu\text{m}$ we should expect a lot of scatter in the results. Carbon- and oxygen-rich stars were distinguished on the presence or absence of the $3\mu\text{m}$, $\text{C}_2\text{H}_2 + \text{HCN}$, feature which is a very clear diagnostic of carbon-rich chemistry (van Loon et al. 1999b and references therein). A PL diagram of the results is shown in Fig. 1.

Seven of the stars in Fig. 1 are common with the sample discussed by Wood (1998), and some of the long-period oxygen rich stars are OH/IR stars. Although our periods agree very well with those derived by Wood, the luminosities (van Loon et al. 1999b) do not, and five of the six carbon stars we find to be considerably brighter than he did (Whitelock and Feast 2000a). The Groenewegen and Whitelock (1996) relation for carbon stars extrapolates between the two lines shown in Fig. 1. In interpreting this figure it is crucial to remember that the luminosities illustrated

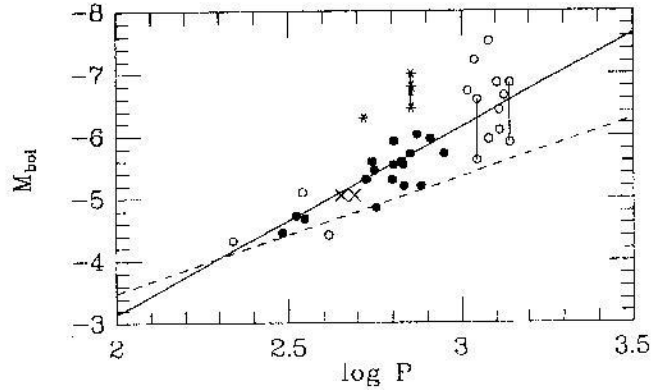


Figure 1: The PL relation for long period AGB stars in the LMC. The luminosities are from van Loon et al. (1999b) and are single phase measurements. The periods are from Whitelock et al. (in preparation). The solid and broken lines are extrapolations of the PL relations, determined by Feast et al. (1989), for oxygen- and carbon-rich stars, respectively. Solid symbols represent carbon stars and open ones oxygen-rich stars. The stars marked as asterisks are IRAS 04496-6958 and SHV F4488 which are both carbon-rich (but see text). Connected points represent measurements of the same star at different epochs. The crosses represents carbon stars in LMC clusters and their luminosities and periods are from Nishida et al. (2000).

here are one-off measurements of large amplitude variables, because we have, in general, only single epoch ISO observations. Where points are joined together they represent separate observations of the same star at different phases. It has to be clear from this that a good deal of the scatter in this diagram is due to variability. It is also clear that the bulk of these stars, both oxygen- and carbon-rich, fall close to the extrapolated PL relation for oxygen-rich variables.

4. Some Interesting Individual Stars

Figures 2 and 3 illustrate *K* light curves for two of the LMC carbon stars. These particular examples combine SAAO data with Wood's published observations to give very good light curve coverage - over a time interval of 5 to 6 years. With an 830 day period TRM 4 is one the longest period carbon stars in our sample, and indeed one of the longest period carbon stars known. The peak-to-peak amplitude is almost 2 mag at *K*. The other star, TRM 88, has a somewhat shorter period and lower amplitude, although it has a very marked secular or long period variations on top of the pulsation. The net result of this is an effective peak-to-peak amplitude of about 2 mag. This type of erratic behaviour is quite common among mass-losing carbon stars both in the LMC and in the Galaxy. It is

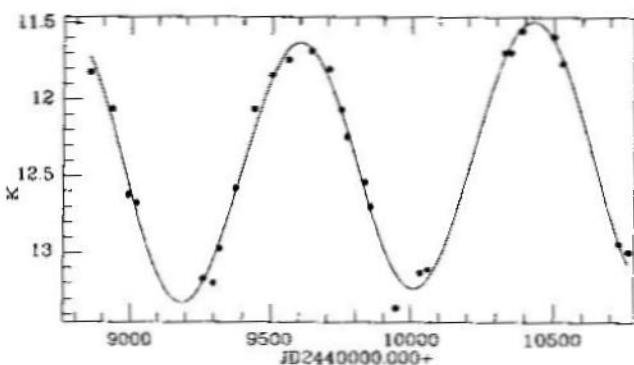


Figure 2: The light curve of carbon star TRM 4, using data from Wood (1998) and Whitelock et al. (in preparation). The curve is a sinusoid of period 830 days together with a long-term trend.

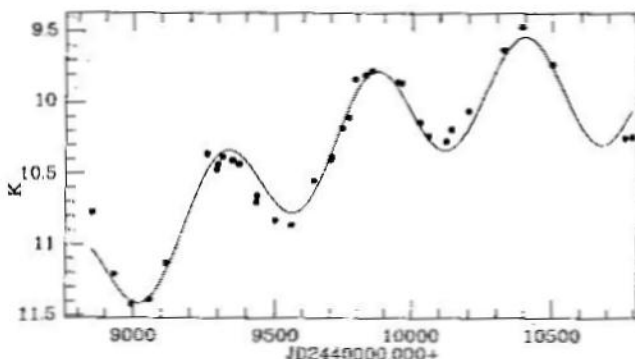


Figure 3: The light curve of carbon star TRM 88, using data from Wood (1998) and Whitelock et al. (in preparation). The curve is a sinusoid of period 543 days together with a long-term trend.

probably caused by variations in the mass-loss rates.

It is difficult to put an accurate figure on the bolometric amplitudes of these stars as very little monitoring has been done at wavelengths beyond $4\mu\text{m}$. The best we can do (see van Loon et al. 1998) is look at the individual ISO measures we have for these LMC sources together with $10\mu\text{m}$ repeated measures of Galactic sources by Le Bertre (1992) and by Harvey et al. (1974). This leads to an estimate of a bolometric amplitude for the carbon stars of a little under 1.0 mag peak-to-peak and for the oxygen-rich stars with periods over 1000 days between 1.0 and 1.5 mag.

Returning again to the PL plot in Fig. 1, The asterisks represent luminous carbon-stars at which we will take a closer look. For IRAS 04496-6958 there are four independent measures of the luminosity (from van Loon et al. 1998, 1999a, 1999b) as indicated in the figure. Its $3\mu\text{m}$ spectrum shows the clear signature of the $\text{C}_2\text{H}_2 + \text{HCN}$ carbon-star feature, but its $10\mu\text{m}$ ISO spectrum (Trams et al. 1999) is very unusual - showing a feature which indicates the presence of both silicates, which suggest an oxygen-rich shell, and silicon carbide, which suggests a carbon-rich shell. It is therefore the first extragalactic example of a carbon star with silicate emission. There are several Galactic stars which show a similar combination of oxygen- and carbon-rich features. They are generally understood to be binary systems in which silicate dust surrounds the binary of which one component is a carbon star (Lloyd Evans 1990). It may be that the same explanation applies here, although in view of its high luminosity Trams et al. offered an alternative explanation - that it was, until recently, a star undergoing HBB - hence the silicate dust. It would thus be an example of a star in which HBB terminated, perhaps due to mass-loss, and which then underwent a thermal pulse and dredge-up, turning it into a carbon star.

The other high luminosity carbon star in Fig. 1, SHV F4488, was noted by Smith et al. (1995) as lithium rich.

Our luminosity is considerably higher than that used by Smith et al. ($M_{\text{bol}} = -6.3$ mag compared to -5.7). This might be due either to variability or possibly to the flux used by Smith et al. being underestimated, as they had no information on the contribution from mid-infrared wavelengths. In any case we can presume the star is undergoing HBB and it is interesting to see that lithium and carbon enrichment can coincide at these high luminosities. So it would appear that even among the carbon-stars the most luminous examples show signs of HBB.

There have also been some recent discoveries of obscured carbon stars in Magellanic Cloud star clusters, which are particularly interesting because we know something about their ages and metallicities. Nishida et al. (2000) have published periods for three such stars, two of which are in LMC clusters. These are marked as crosses on the PL diagram of Fig. 1. They seem to be quite comparable to the obscured field-carbon-stars. These two clusters have turn-off masses of around $1.5 M_{\odot}$. This initial mass for 500 day carbon Miras is very similar to that found in a recent study of obscured AGB variables in the solar neighbourhood, by Olivier et al. (2001). They estimate that both the carbon- and oxygen-rich stars, with periods in the 400 to 800 day range have masses between 1 and $2 M_{\odot}$. They also estimate the initial masses of OH/IR stars with periods over 1000 days at around $4 M_{\odot}$. The same may be true of the obscured LMC stars under discussion, although it is difficult to say with certainty.

5. Other AGB Variables

Wood (2000) discusses the PL relationship (his fig. 1) for LMC variables found from the Macho data-base. He assumes, probably reasonably, that those stars with redder $J-K$ colours are carbon-rich. Most of the stars he describes are more luminous than the tip of the giant

branch and are therefore clearly on the AGB. What he finds are four (perhaps five) PL relations running approximately parallel to each other. The luminosities are derived from single observations and therefore show a certain amount of scatter.

The large amplitude variables fall close to the Mira sequence, which is identical to the one discussed above, but so do some of the smaller amplitude variables. Two sequences at shorter periods contain variables with smaller amplitudes and another sequence is seen at longer periods. Wood interprets this diagram as demonstrating that fundamental pulsators lie on the Mira sequence, while the shorter period sequences mark the positions of overtone pulsators. Of course we know nothing about the relationship of the stars in the various sequences to each other and it is possible that their differences are in more than pulsation mode. The origin of the fourth, long period, sequence is unclear, although Wood discusses various possibilities.

If Miras pulsate in the fundamental mode, which seems possible, we must still explain why their diameters, which have many optical and near-IR measurements, imply that they are overtone pulsators (e.g. Whitelock and Feast 2000b).

6. Conclusions

Observations of AGB variables in the LMC show the following:

1. Those which are close to the end of their AGB lifetimes fall close to the Mira PL relation.
2. Carbon- and oxygen-rich Miras obey the same PL as well as we can establish with the available data.
3. Many, perhaps all, of the *large amplitude* variables which lie above the PL relation are undergoing hot bottom burning.
4. The sequences of variables identified from the Macho data show pulsation in a variety of modes, and indicate that we are far from fully understanding AGB variables even in our nearest galaxy.

Acknowledgements. My thanks to my colleagues, particularly Jacco van Loon, Albert Zijlstra and Michael Feast, for allowing me to use the data on LMC variables in advance of publication and to Michael Feast for constructive comments on a draft manuscript.

References

- Blöcker T., Schönberner D.: 1991, *Astron. Astrophys.*, **244**, L43.
- Feast M.W.: 2001, in *New Cosmological Data and the Values of the Fundamental Parameters*, Proc. IAU Symp. 201, 17.
- Feast M.W., Glass I.S., Whitelock P.A., Catchpole R.M.: 1989, *Mon. Not. R. Astr. Soc.*, **241**, 375.
- Frost C.A., Cannon R.C., Lattanzio J.C., Wood P.R., Forestini M.: 1998, *Astrophys. Lett.*, **332**, 17.
- Groenewegen M.A.T., Whitelock P.A.: 1996, *Mon. Not. R. Astr. Soc.*, **281**, 1347.
- Harvey P.M., Bechis K.P., Wilson W.J., Ball J.S.: 1974, *Ap. J. Suppl.*, **27**, 331.
- Hoffleit D.: 1997, *J. A. A. V. S. O.*, **25**, 115.
- Iben I., Renzini A.: 1983, *Ann. Rev. Astron. Astrophys.*, **21**, 271.
- Le Bertre T.: 1992, *Astron. Astrophys. Suppl.*, **94**, 377.
- Lloyd Evans T.: 1990, *Mon. Not. R. Astr. Soc.*, **243**, 336.
- Marigo P., Girardi L., Bressan A.: 1999, *Astron. Astrophys.*, **344**, 123.
- Nishida S., Tanabé T., Nakada Y., Matsumoto S., Sekiguchi K., Glass I.S.: 2000, *Mon. Not. R. Astr. Soc.*, **313**, 136.
- Olivier R., Whitelock P.A., Marang F.: 2001, *Mon. Not. R. Astr. Soc.*, in press.
- Paczynski B.: 1970, *Acta Astron.*, **20**, 47, 287.
- Sackmann I.-J., Boothroyd A.: 1992, *Ap. J.*, **392**, L71.
- Smith V.V., Plez B., Lambert D.L., Lubowich D.A.: 1995, *Ap. J.*, **441**, 735.
- Trams N.R., van Loon J.Th., Zijlstra A.A., Loup C., Groenewegen M.A.T., Waters L.B.F.M., Whitelock P.A., Blommaert J.A.D.L., Siebenmorgen R., Hesse A.: 1999, *Astron. Astrophys.*, **344**, L17.
- van Loon J.Th., Zijlstra A.A., Whitelock P.A., te Lintel Hekkert P., Chapman J.M., Loup C., Groenewegen M.A.T., Waters L.B.F.M., Trams N.R.: 1998, *Astron. Astrophys.*, **329**, 169.
- van Loon J.Th., Zijlstra A.A., Groenewegen M.A.T.: 1999a, *Astron. Astrophys.*, **346**, 805.
- van Loon J.Th., Groenewegen M.A.T., de Koter A., Trams N.R., Waters L.B.F.M., Zijlstra A.A., Whitelock P.A., Loup C.: 1999b, *Astron. Astrophys.*, **351**, 559.
- Whitelock P., Feast M.: 2000a, *Mem. Soc. Astr. Italy*, **71**, 601.
- Whitelock P., Feast M.: 2000b, *Mon. Not. R. Astr. Soc.*, **319**, 759.
- Wood P.R.: 1998, *Astron. Astrophys.*, **338**, 592.
- Wood P.R.: 2000, *Publ. Astr. Soc. Australia*, **17**, 18.

ROTATION PERIODS AND ACTIVITY ON RED DWARFS

N.I. Bondar'

Crimean Astrophysical Observatory
Nauchny, Crimea 98409 Ukraine, *bondar@crao.cromea.ua*

ABSTRACT. Relation between duration of cycles of photospheric activity and stellar rotation are considered here for samples of dKe–dMe stars and compared with similar ones for solar-like stars. Fast and slowly rotating stars shown two sequences on the diagram. Cycle length of slowly rotating stars is close to solar and not depend on rotation, but red dwarfs with $P_{rot} < 5^d$ show tendency to increasing of cycle time with faster rotation. Activity of fast rotating K and M dwarfs are more higher as well on photospheric level as coronal region.

Key words: Stars: stellar activity, magnetic cycle on red dwarfs.

1. Introduction

Magnetic activity on late-type dwarfs are manifested in different atmosphere layers through photospheric spots, chromospheric Ca II H and K emission lines and coronal X-ray fluxes. This type of activity reflects the processes of interaction between magnetic field, rotation and convective motions in subsurface convective zone and described for solar-like stars due to action of dynamo mechanism (Parker 1955). Studying of active processes on the bright F–K dwarfs are based on the long-term monitoring chromospheric Ca II H and K emission lines (Baliunas and Vaughan 1985). Research of these stars allow to find the relation between cyclical changes in H and K fluxes, rotational velocities and stellar ages. Rotational velocity of the main-sequence stars (MSS) with $B - V < 1$ is fitted well as $t^{-1/2}$ (Skumanich 1972, Rengarajan 1984).

2. Rotation and activity properties of red dwarfs

To study of magnetic activity nature on dKe–dMe stars we obtained long-term light curves using photographic archives and photometric data and found slow changes, suspected cyclical, in photospheric spottedness. Rotation–activity relation for late dwarfs with $0.4 < B - V < 1.9$ are represented on fig. 1. Data includes chromospheric active stars taken from so-called

H–K project (Baliunas et al. 1995, Bruevich et al. 2001) and active red dwarfs (Bondar' 1996, 2001; Alekseev 2000).

According to the diagram P_{rot} vs. $B - V$, the rotation period of the MSS increases steady towards the later spectral classes. Most of dKe–dMe stars and few F–G dwarfs are the fast rotating objects with $P_{rot} < 10^d$. This stellar group contains young stars and independently of spectral classes they have the similar rotation periods before they reach the main sequence (NS) stage. Then rotational velocity drops in many times, especially for late-type stars, and P_{rot} increases smoothly along the MS as a function of stellar age.

The plot $\log L_{bol}$ vs. P_{rot} shows the obvious relation between total luminosity and rotation for F–K MSS. According this diagram the upper value of rotation period for MSS is 2 days. The lower luminosity dKe–dMe stars show any relation between the considered values. Most of red dwarfs have $P_{rot} < 6^d$. Surface spottedness of red dwarfs is changed with time and that has produced their long-term light variations. Typical time of such variations is about one or some decades and comparable at present with their observational spans. In this sense P_{cyc} is uncertain value for K–M dwarfs and should be considered as suggested. Diagrams P_{cyc} vs P_{rot} and A_{cyc} vs. $\log P_{cyc}$ show that fast rotating stars have more strength and long spot cycles than it defined for stars with $P_{rot} > 10^d$, which cycles are not exceed of 18 years. Both fast rotation and large cycle length represent observational evidences that magnetic activity on the lower luminosity red dwarfs and on solar-like stars are different and produced by different dynamo mechanism. It seems that period of 5 or 6 days is the critical for existence of cyclical stellar activity. According diagram $\log L_x/l_{bol} - P_{rot}$ stars with chaotic chromospheric activity are located in region, where rotation period is less than 6^d and they absent at all when $P_{rot} > 20^d$.

The photospheric activity level of fast rotating dKe stars is higher than dMe stars. These stars show large amplitude of long-term variations and long cycles. They are the most active among late-type dwarfs. The same conclusion follows from the plot $\log L_x/L_{bol} - P_{rot}$. The fast rotation of K dwarfs leads to their high coronal fluxes. The other observational fact is

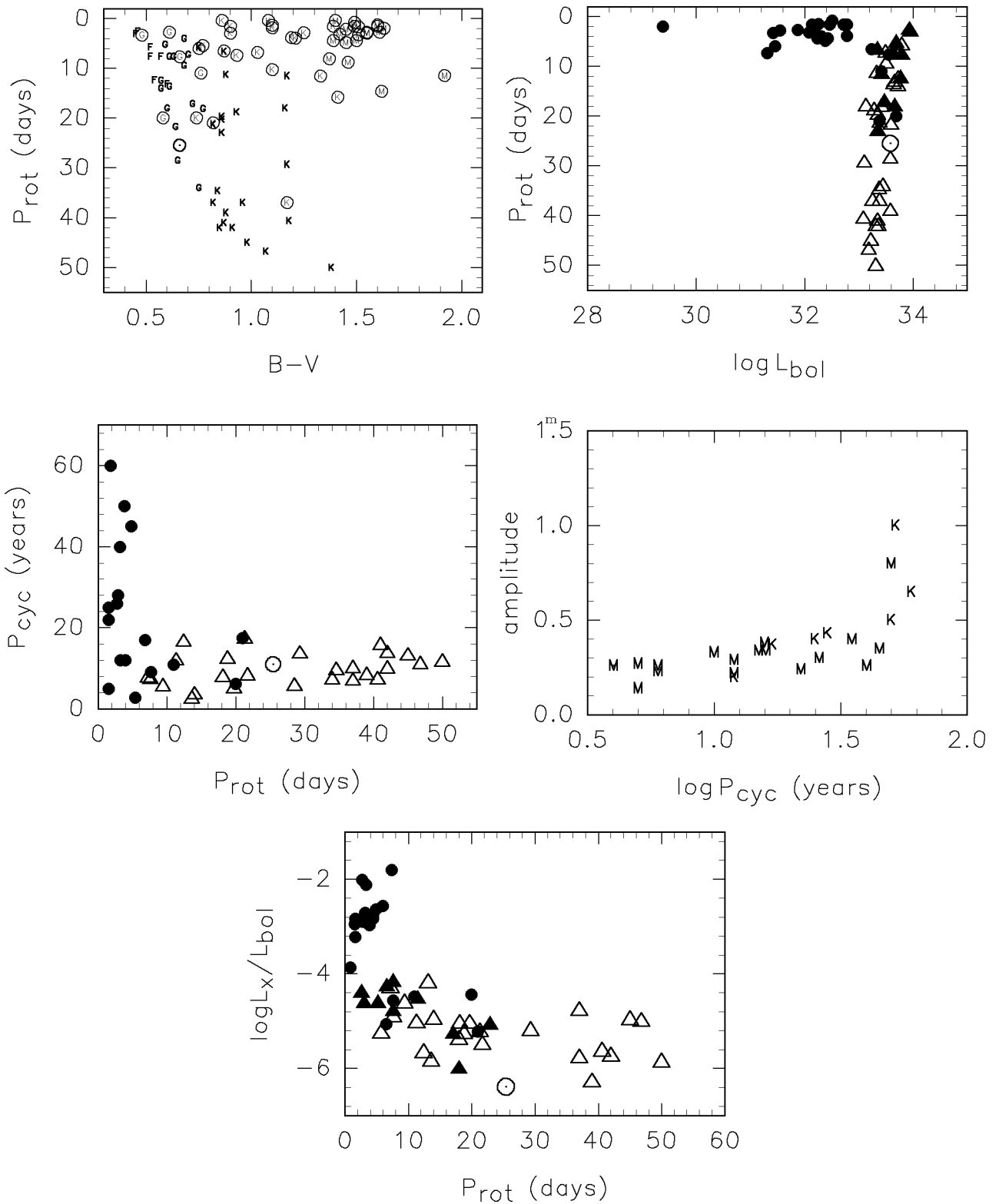


Figure 1: Rotation-activity relations for F-M dwarfs. The filled circles indicate spotted dKe-dMe stars. Chromospheric active F-K dwarfs are represented by open triangles (cyclical changes) and by filled triangles (chaotic changes). Special symbol signs the Sun.

that some chromospheric active stars with $P_{rot} < 20^d$ and chaotic changes in H and K fluxes have the higher ratio L_x/L_{bol} than slow rotating stars.

3. Summary

Rotation period is not one but a dominant factor responsible for a development of cyclical stellar activity and its level. Fast and slowly rotating stars are separated on two sequences on the rotation-activity diagrams when $P_{rot} < 6^d$. This value appears the critical to occur the different activity properties in low and fast rotating late-type dwarfs and may be a different dynamo mechanism. Cycle length of slow rotating stars with $P_{rot} > 20^d$ is not longer than 18 years that are close to the solar cycle. Chaotic chromospheric activity starts occur on several stars when $6^d < P_{rot} < 20^d$. When rotation period of chromospheric active stars drops to 6^d then activity character becomes chaotic only. If the spotted activity of fast rotating K and M dwarfs is cyclical these stars show tendency to insce-

asing cycle length twith rotation period. Among active F–M dwarfs the fast rotating dKe stars appear the highest activity level as well on photosphere as in a coronal region.

References

- Alekseev I.Yu.: 2000, *Astron. Reports*, **77**, 784.
Baliunas S.L., Vaughan A.H.: 1983, *Ann.Rev.Astron. Astrophys.*, **23**, 379.
Baliunas S.L., Donahue R.A., Soon W.H., et al.: 1995, *Astrophys.J.*, **438**, 269.
Bondar' N.I.: 1996, *Bull.Crimean Astrophys.Obs.*, **93**, 111.
Bondar' N.I.: 2001, *Bull.Crimean Astrophys.Obs.*, **97**, 17.
Bruevich E.A., Katzova M.M., Sokoloff D.D.: 2001, *Astron. Reports*, **78**, 1.
Parker E.N.: 1955, *Astrophys.J.*, **122**, 293.
Rengarajan T.N.: 1984, *Astrophys.J.*, **283**, L63.
Skumanich A.: 1972, *Astrophys.J.*, **171**, 565.

ON THE SPECTRAL AND PHOTOMETRIC ACTIVITY IN YOUNG STARS

N.Z. Ismailov

Shemakha astrophysical observatory NAS of Azerbaijan
373243 pos.Y.Mamedalieva, Shemakha, Azerbaijan,
box1955n@yahoo.com

ABSTRACT. Results of long time homogenous medium resolution spectral observations of classic T Tauri type stars DI Cep, T Tau and GW Ori obtained during 1972-1990 are analyzed. Weak correlation with on metallic absorption lines of optical spectrum spectral types and equivalent widths of hydrogen lines is discovered. It is showed that spectral types of these stars are varying during observation seasons in different ranges. More wide range of variations of spectral types, is observed in DI Cep - F4-K5V, are of all 21 subtypes, in GW Ori - F3-G5V, are of all 13 subtypes and T Tau - G1-K5V, are in all 9.5 subtypes. Observational photometric and spectral properties of these stars may be explained by formation of hot (in case of DI Cep) and cool (in case of GW Ori and T Tau) spots on these stars. We are suggesting that simultaneously a presence of variable circumstellar dust may also be a cause of variability of following two stars.

Key words: stars: pre-main-sequence - stars: spectral types - photometry- variability.

1. Introduction

Studies of photosphere absorption spectrum of T Tauri type stars (TTS) are much confused. Observations by modern detectors shows that the optical absorption spectrums of TTS, consist of a star absorption line spectrum, stellar continuum, superimposed non-photosphere continuum and linear emission spectrum (e.g. Appenzeller 1986; Finkenzeller and Basri 1987; Hartigan et al. 1989; Franchini et al. 1989). Because of superimposed nonphotospheric emission continuum, all the photosphere absorption lines look generally wide than in the standard stars with comparable effective temperature. In some strong-emission TTS this veiling absorption spectrum is so strong that the photosphere absorption lines are not detectable on low-resolution spectrograms. Spectral classification on the visual blue range of absorption spectrum gives more high effective temperature in TTS than on spectral lines in red range (Herbig 1977; Walker 1980; Appenzeller 1986). Non-

photospheric continuum is free on spectral lines and superimposed to star continuum especially in blue side of spectrum (see, e.g., Hartigan et al. 1989).

More early spectral observations of TTS evidence on short time (see, e.g. Mundt 1979, 1984; Aiad et al. 1984; Hartigan et al. 1986; Ismailov 1987, 1988) and long time (see, e.g. Krasnobabtsev 1982; Grinin et al. 1985; Guliev 1994) variations of Balmer lines of hydrogen, H, K CaII, FeII, etc. Investigators more often studied weak absorption components of shell spectrum (see, e.g. Holtsman et al. 1986, Hartigan et al. 1986, Petrov et al. 1996). However photosphere absorption spectrum investigations in visual range were provided poorly.

The aim of our work is to study a time variability of absorption spectrum of some T Tauri type stars and to search its possible connection with emission lines and in whole with star activity for these objects.

2. Observations and results

All the observations of program stars were carried out in Cassegrain focus of 2 m Karl Zeiss telescope of ShAO AS of Azerbaijan with 2X2 prism "Kanberra" spectrograph. Spectral range is $\lambda\lambda 3600-5100 \text{ \AA}$, dispersion 93 \AA/mm at H_γ and 60 \AA/mm at H, K CaII. All spectrograms were processed in standard conditions, identical methods and homogenous equipment. In our previous works a method of processing this spectrograms was described in detail (Ismailov, 1992, Rustamov, 1987).

For this work we were chosen of all 46 spectrograms for DI Cep, obtained in 1978-1988 (Ismailov, 1987, 1988), 13 spectrograms for GW Ori - 1972-1988 (Ismailov, 1993), 88 spectrograms for T Tau, obtained in 1972-1985 (Guliev, 1991, 1994, Rustamov, 1999).

For investigation of relation with emission and absorption spectrum in this TTS we used definition equivalent widths of emission lines H_β , H_γ , H_δ , H, K CaII (Ismailov, 1987, 1988, 1993; Guliyev, 1991, 1994; Rustamov, 1999).

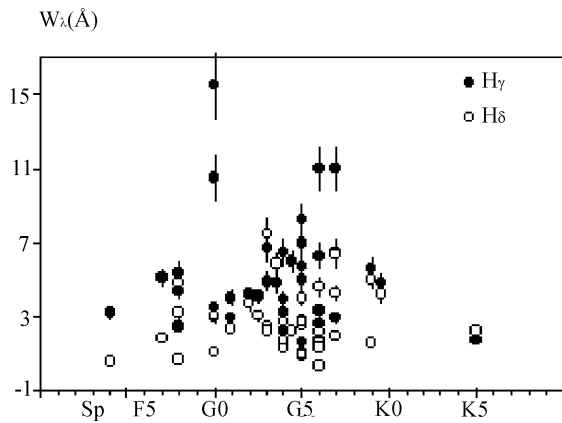


Figure 1: Relation of equivalent width W_λ of emission lines H_γ (black circles) and H_δ (light circles) with spectral types.

DI Cep. In fig. 1 was showed equivalent width of emission lines of H_γ and H_δ and spectral types for DI Cep. As demonstrated in this figure, weak correlation between W_λ and spectral type till spectral range of spectral types G5-G7 was observed. For all range of observed spectral types variability quantity of coefficient of correlation R for this lines is equal to 10.6% and 13%, correspondingly.

In fig. 2 was given histograms on frequency distribution of spectral types of star DI Cep in all observation time. In ordinate were given the relation of spectral types in given observed subrange N_i to all observed spectral types N . Every subranges include 2.5 spectral subtypes. On the abscissa spectral subranges are presented. For DI Cep were observed of all 9 subranges where including number of spectral types varied from 1 to 14. Limits of spectral types of each subrange were given in fig. 2.

Thus, a range of variability of spectral types for DI Cep is corresponding 21 subtypes, from F4V to K5V. A maximum in diagram is G5-7.5V. As shown in this diagram spectral condition after maximum was observed rarely (of all 4 spectrum from 40), while till maximum 11 subtypes were observed (of all 22 spectra ~55%) in the range F4-G5V, where a number of spectral types is increasing monotonic till maximum.

As shown in fig. 2 after maximum (G5-7V) of spectral types frequency distribution we observed highly rare condition, while till maximum of diagram spectral types shows smooth distribution. From side of later spectral types is destroyed normal distribution of random values, which we conditionally will call as "cool break".

In a fig. 3 (a, b, c) were displayed diagrams of light distribution of DI Cep in UBV photometric bands. For analysis UBV photometric characteristics of this star we used literature data from Kardopolov and Filipyev (1985), Grinin et al. (1980), Keleman (1985)

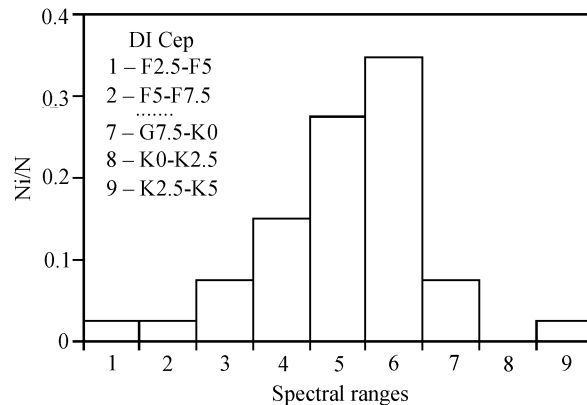


Figure 2: A diagram of spectral distribution of DI Cep. Of all 8 subranges, include 2.5 subtypes of each. A maximum is corresponding G5-7V. In ordinate relative number of spectra in subrange was given.

and proper observations of Ismailov (1988, 1999) (of all ~500 measure in each bands). In these diagrams each column from left to right decreased with step 0.^m1. Light variations of star occur in range 11.^m5 (1 band) -12.^m8 (13 band) in U, 11.^m9 (1 band) -12.^m9 (10 band) in B, 11.^m1 (1 band) - 11.^m8 (7 band) in V with amplitudes $\Delta U=1.^m3$, $\Delta B=1.^m0$, $\Delta V=0.^m7$. It is shown that distributions of lights in U and V bands have similar kind with spectral distribution diagram. Thus, in U and V bands we see, more frequently a star being in more wide light range, i.e. "cool break" are observed in light distribution diagram. Consequently, small quantity of equivalent width of absorption lines (t.i. more early spectral type) of photosphere absorption more frequently correspond more bright condition of star.

GW Ori. In fig. 4 dependence of equivalent width of emission line of H_β (filled circles) and H_γ (open circles) and spectral types for GW Ori. As demonstrated here, till range G2.5-G5V, with increasing W_λ emission lines, spectral type becomes more lately. In whole coefficient of correlation R for W lines of H_β and H_γ is equally to 25% and 19%, correspondingly.

In fig. 5 was demonstrated diagram of spectral distribution for spectral conditions of GW Ori. We obtained variation of spectral types in ranges F3-G5, of all 13 subtypes. Maximal number of spectral types was placed in ranges G2.5-G5, of all 5 (38.5%) were observed. A diagram maximum unlike of DI Cep placed nearly in lately condition of spectral types. In this diagram as in case of DI Cep we also observed "cool break" effect.

A diagram of light distribution on the UBV photometry data for GW Ori was presented in Ismailov's work (1993). In this work it was shown that for GW Ori in all photometry bands light distribution diagram without exception had a maximum corresponding to more bright condition of star. We also observed break in

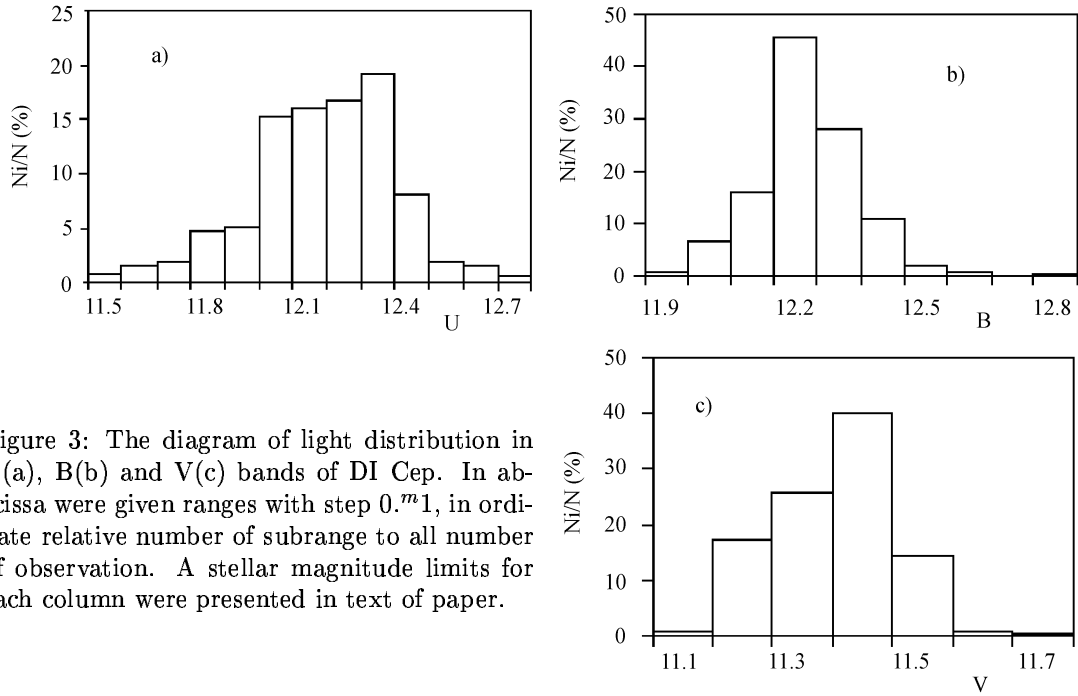


Figure 3: The diagram of light distribution in U(a), B(b) and V(c) bands of DI Cep. In abscissa were given ranges with step $0.^m1$, in ordinate relative number of subrange to all number of observation. A stellar magnitude limits for each column were presented in text of paper.

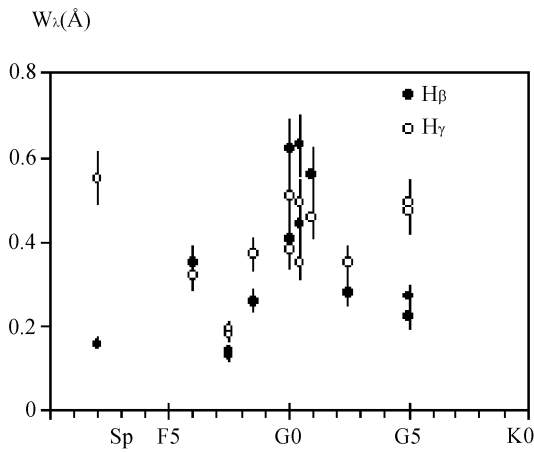


Figure 4: Dependence of equivalent width of emission lines of H_{β} (filled circles) and H_{γ} (open circles) for spectral types of GW Ori.

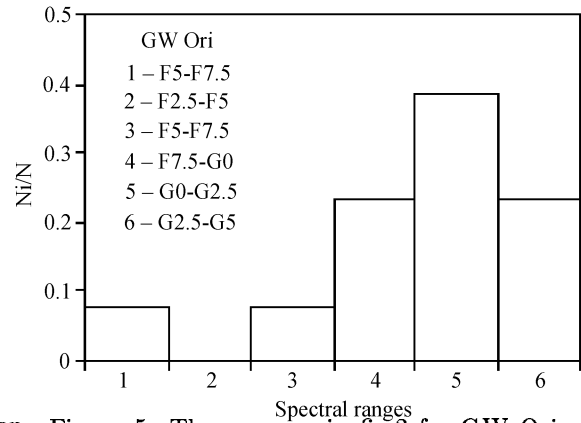


Figure 5: The same as in fig.2 for GW Ori. A maximum of diagram corresponds G2.5-G5V.

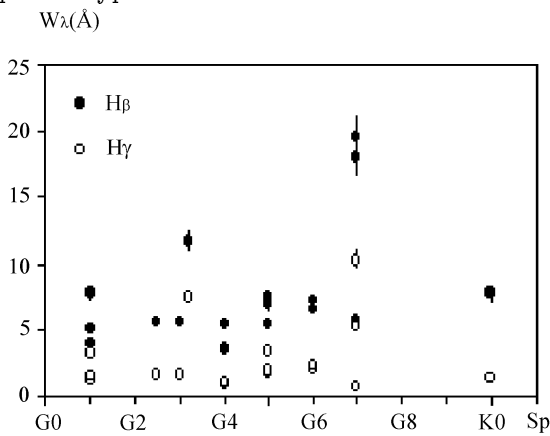


Figure 6: Dependence of equivalent width of emission lines of H_{β} (filled circles) and H_{γ} (open circles) for spectral types of T Tau.

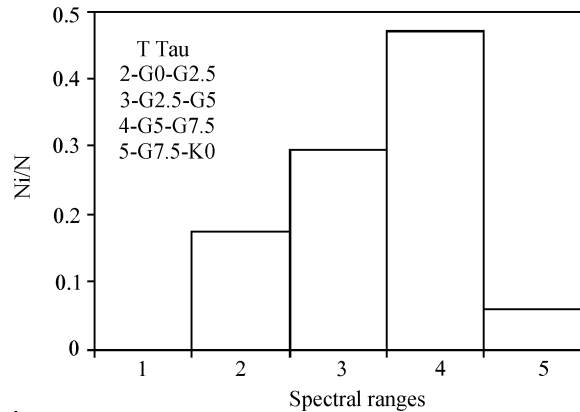


Figure 7: The same as in fig. 2 for T Tau. A maximum of diagram corresponds G5-G7.5V.

distributions of light in direction of increase of magnitudes. Thus, if suppose that maximums in spectra and light diagrams are more stable conditions of the star, then we must accept that more early spectral types are observed in more weak brightness. Consequently decrease of equivalent widths of absorption photosphere lines must be observed in case of decrease of brightness of star.

T Tau. Of all 87 spectrograms of T Tau during 17 separate nights were obtained. In fig. 6, was demonstrated relation of mean for each night equivalent widths of emission spectral lines H_β and H_γ W_λ and obtained mean for night spectral types for T Tau. A number of spectrogram differs in different nights from 1 to 12, often 5-6. Therefore, statistical weight of each point in fig. 6 considerable larger than in case of DI Cep and GW Ori. As showed in this figure, there is a weak correlation between W_λ of this emission lines and spectral types. For lines H_β and H_γ correlation coefficient is 40% and 18%, correspondingly. We must note that unlike analogy diagrams for previous stars in T Tau some maximum W_λ of emission lines do not distinguish here.

In diagram of spectral type distribution demonstrated in fig. 7 for T Tau we obtained similarity with previous stars. So, spectral types varied in range G1-K0.5V, of all 9.5 subtypes. A maximum of spectral types distribution was obtained at G5-G7.5V, in lately spectral types. At maximum of diagram we observed 47% of all observations, and in latter column 6% (of all 1 case). From this diagram we may confirm that, a) later than G5-G7.5V spectral types was not observed or observed rarely, b) more possible condition of spectral types of star is G5-7.5V and with a time spectrum crosses to more early spectral types fluently.

3. Conclusions

Thus, spectral and photometry results obtained in long time period for some TTS allowed doing following conclusions: 1. More stable condition of spectral types of DI Cep is determined as G5-G7.5V, and maximal variable ranges of spectral types is 21 subtypes. Spectral types more often vary to more early types, *cool break effect* is observed. Taking into account photometric characteristics, variability of star can be explained with formation of hot spots on the star surface.

2. More stable spectral type condition of GW Ori determined as G2.5-G5V, maximal observable range of spectrum variability -13 subtypes. A spectral type more often varied to more early types, which have cool break. With take account photometry characteristics a variability of star may be explained dust obscuration of star with circumstellar matter. Moreover one cannot accept cool spot origin effect.

3. More stable spectral condition of spectral types of T Tau is determined as G5-G7.7V, maximal range

of variation is -9.5 subtypes. Is observed cool break at more probable condition of spectrum. Taking into account photometric observations variability of star may be explained with cool spots on star surface. One mustn't except dust obscuration by circumstellar matter.

4. More often observed spectral types on our data are more stable and near to real mean spectral types of stars. Simultaneously, cause of variation of real physical conditions is observed in different spectral types for a time in TTS, which were obtained, perhaps, by same authors.

5. Emission line equivalent widths variability, which weakly correlated with spectral types in all three stars, only in part may be described by variable total luminosity of central star. It shows that main causes of variability of emission lines in TTS are other unclear processes.

References

- Aiad A., Appenzeller I., Bertout C. et. al.: 1984, *As.Ap.*, **130**, 67.
 Appenzeller I.: 1986, *Physica Scripta*, **11**, 76.
 Cabrit S., Edwards S., Strom S.E., Strom K.M.: 1989, *Ap.J.*, **354**, 687.
 Finkenzeller U., Basri G.: 1987, *Ap.J.*, **318**, 823.
 Franchini M., Ferluga S., Stalio R.: 1989, *An Atlas of CASPEC Spectra of T Tauri Stars, Department of Astronomy, University of Trieste*.
 Grinin V.P., Petrov P.P., Shakhovskaya N.I.: 1985, *Izv. Krim. A.O.*, **71**, 109.
 Grinin V.P., Yefimov Y.S., Krasnobabtsev V.I., et al.: 1980, *Peremennie zvezdi*, **21**, 247.
 Guliyev N.Kh.: 1994, *Peremennie zvezdi*, **23**, 241.
 Guliyev N.Kh.: 1991, *Kinem. fiz. nebes. tel.*, **7**, 51.
 Hartigan P., Hartmann L., Kenyon S., Hewett R., Stauffer J.: 1989, *Ap.J.Suppl.*, **70**, 899.
 Hartigan P., Mundt R., Stocke J.: 1986, *A.J.*, **91**, 1357.
 Herbig G.H.: 1977, *Ap.J.*, **214**, 747.
 Holtsman J.A., Herbst W., Booth J.: 1986, *A.J.*, **92**, 1387.
 Ismailov N.Z.: 1988, *Peremennie zvezdi*, **22**, 892.
 Ismailov N.Z.: 1992, *Peremennie zvezdi*, **23**, 11.
 Ismailov N.Z.: 1987, *Peremennie zvezdi*, **22**, 489.
 Ismailov N.Z.: 1993, *Kinem. fiz. nebes. tel.*, **N 3**, 65.
 Ismailov N.Z.: 1998, *Inform. Bull. Var. Stars*, 4470.
 Kardopolv V.I., Filipev G.F.: 1985, *Peremennie zvezdi*, **22**, 103.
 Keleman J.: 1985, *Inform. Bull. Var. Stars*, 2744.
 Krasnobabtsev V.I.: 1982, *Izv.Krim.A.O.*, **65**, 100.
 Mundt R.: 1979, *As.Ap.*, **74**, 21.
 Mundt R.: 1984, *Ap.J.*, **280**, 747.
 Petrov P.P., Gullbring E., Ilyin I., et al.: 1996, *As.Ap.*, **314**, 821.
 Rustamov B.N.: 1999, *Circular ShAO*, **N 97**.
 Rustamov B.N.: 1987, *Kinem. fiz. nebes. tel.*, **3**, 15.
 Walker M.F.: 1980, *P.A.S.P.*, **92**, 66.

ULTRA FAST EVOLUTION OF SAKURAI'S OBJECT

Ya. Pavlenko

Main Astronomical Observatory, National Academy of Sciences of the Ukraine
Golosiiv woods, Kyiv-127, 03680, Ukraine

ABSTRACT. We model theoretical spectral energy distributions of the "born-again" V4334 Sgr for our grid of hydrogen-deficient model atmospheres with a range of $T_{\text{eff}} = 4000\text{-}5000$ K and $\log g = 1.0 - 0.0$. These SED's are compared with the observed in 1997-1998 spectra of V4334 Sgr. In that way we determine T_{eff} of Sakurai's object for the years, and parameters of interstellar + circumstellar reddening in the frame of self-consistent approach.

Key words: post-AGB stars: V4334 Sgr: stellar evolution: model atmospheres: SED

In many ways, the existence of irregular hydrogen-deficient (Hd) variables remains puzzling. R CrB is the most well-known member of the post-AGB group. Sakurai's object (SO, V4334 Sgr) provides another, extreme case of stellar evolution.

It has been firmly established that the most abundant elements in atmosphere of V4334 Sgr are helium and carbon (see table 1).

Opacities.

In the photosphere of V4334 before 1997 ($T_{\text{eff}} > 7000$ K), the continuum opacity was governed mainly by a bound-free absorption of C atoms. There the situation was quite different from the case of solar-like atmospheres. Later opacity above the photosphere of V4334 Sgr with $T_{\text{eff}} < 6500$ K was determined, to a large extent, by absorption of molecules consisting of C, N and O (Pavlenko, Yakovina & Duerbeck 2000).

Table 1: Abundances of H, He, C, N, O (scaled to $\sum N_i = 1$) in atmospheres of R CrB and, V4334 Sgr (Asplund et al. 1998) and the Sun (Anders & Grevesse 1979).

	R CrB	Sakurai	the Sun
H	-4.03	-2.42	-0.4
He	-0.01	-0.020	-1.05
C	-2.01	-1.62	-3.48
N	-2.13	-2.52	-3.99
O	-2.73	-2.02	-3.11

Model atmospheres and SEDs of Sakurai's object.

We computed a grid of model atmospheres of R CrB-like stars and Sakurai's object of $T_{\text{eff}} = 7000\text{-}4000$ K, $\log g = 0 - 1$ (Pavlenko & Yakovina 1994, 2000, Pavlenko, Yakovina & Duerbeck 2000). Opacity sampling treatment was used to take into account atomic and molecular absorption. We used JOLA as a model of absorption by electronic band systems of diatomic molecules.

Fits of theoretical SEDs to observations in 1997 - 1998 ones allow us to determine T_{eff} and E_{B-V} of Sakurai's object at the latest stages of its evolution (Pavlenko & Duerbeck 2001). In 1996-1999 T_{eff} of SO was reduced from 7000 K (Asplund et al. 1998) down to 5200 K (Pavlenko & Duerbeck 2000). Due to the high sensitivity of molecular densities of C_2 and CN to temperature in the atmosphere of SO its molecular bands intensities were changed drastically both in IR and optical regions (Fig. 1). Identification of the main molecular features in SO spectrum is given in Fig. 2a. Fig. 2b shows a fit to observed spectrum of SO in August 1998. For the time the photosphere of SO was engulfed by a dusty envelope ($E_{B-V} = 1.3!$). Later SO was completely covered by the dust (Duerbeck 2001).

Acknowledgements. I thank Drs. Hilmar Duerbeck and Larisa Yakovina for collaboration. Partial financial support of the work was provided by SRG of AAS.

References

- Anders E., Grevesse N.: 1989, *Geochimica et Cosmochimica Acta.*, **53**, 197.
 Asplund M., Gustafsson B., Kameswara Rao N., Lambert D.L.: 1998, *As. Ap.*, **332**, 651.
 Duerbeck H.: 2001, *Ap. Space Sci.*, in press.
 Pavlenko Ya.: 1999, *Astr. Reports*, **43**, 94
 Pavlenko Ya., Yakovina L., Duerbeck H.W.: 2000, *As. Ap.*, **354**, 229
 Pavlenko Ya., Yakovina L.: 2000, *Astr. Reports*, **44**, 209
 Pavlenko Ya., Duerbeck H.W.: 2001. *As. Ap.*, **367**, 933.

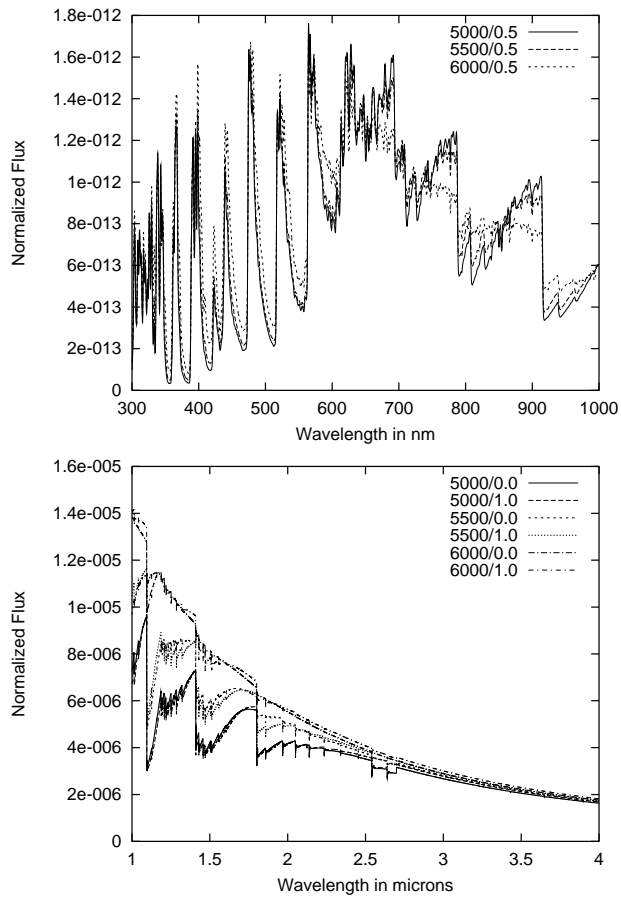


Figure 1: Dependence of optical and IR SEDs of V4334 Sgr on T_{eff} .

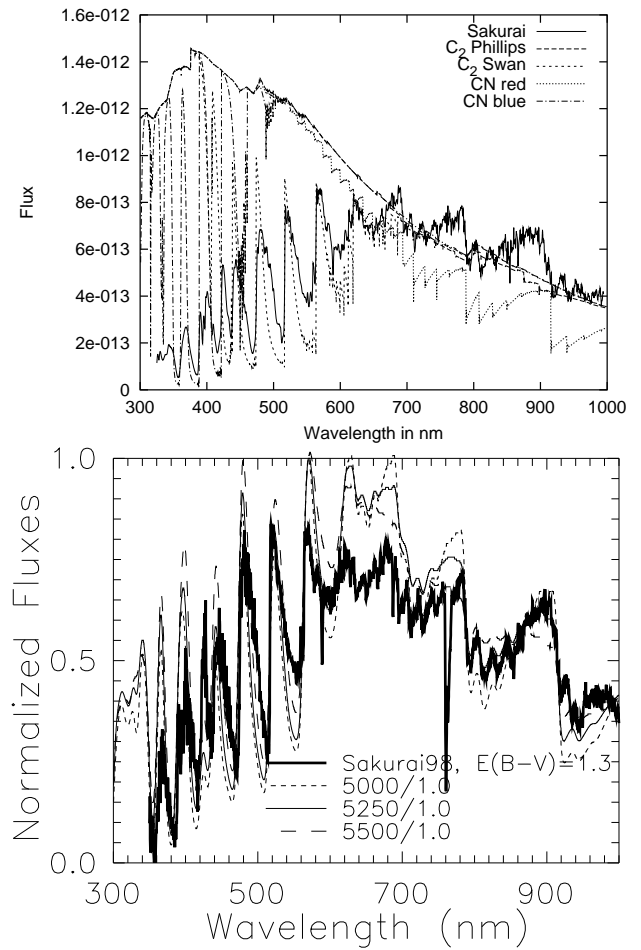


Figure 2: Identification of the molecular band systems that govern the SED of V4334 Sgr in 1997 (top). Fits to the SED of V4334 Sgr in August, 1998 (from Pavlenko & Duerbeck 2000) (bottom).

MAGNETOSPHERIC ACCRETION IN T TAURI STARS: OBSERVATIONAL TEST

P.P. Petrov

Crimean Astrophysical Observatory
p/o Nauchny, Crimea 98409 Ukraine, *petrov@crao.crimea.ua*

ABSTRACT. In the classical T Tauri stars (CTTS) the magnetic field plays an important role in the interaction between the star and the accretion disk. In 1996-2000 we have carried out an extensive spectroscopic and photometric monitoring of the extremely active CTTS RW Aur A in order to check for predictions of the magnetospheric accretion model. We find periodic rotational modulations in many spectral features, which may be explained as due to non-axisymmetric accretion, well in accordance with the model. The stable period ($2^d.64$) was also found in the variations of the blue colours. Nevertheless, some of the important predictions of the model were not found in the star.

Key words: Stars: individual: RW Aur A—stars: pre-main sequence—stars: variables

1. Introduction

The young pre-main sequence objects of solar mass are known as irregularly variable T Tauri type stars. The classical T Tauri stars (CTTS) with strong emission spectrum, veiling and IR excess, are believed to possess accretion disk (Berout et al. 1988). The stellar magnetic field plays an important role in the interaction between the star and the disc. The concept of magnetically channeled accretion has been a guiding idea in the recent decade. The magnetospheric accretion model (Königl 1991, see also Calvet 1998 and references therein) predicts existence of accretion shocks at the footpoints of magnetic accretion channels. The hot spots at the stellar surface, associated with the accretion shocks, are believed to be responsible for the veiling and brightness variations.

In order to study the expected correlation between the veiling and brightness, we selected the most active CTTS RW Aur A, which varies in brightness in a wide range and shows clear evidences of accretion. Simultaneous spectroscopic and photometric observations were carried out during 32 nights in three seasons of 1996, 1998 and 1999, at the Nordic Optical Telescope (La Palma, Spain), with additional photometry at the Swedish telescope at the same site (for details see

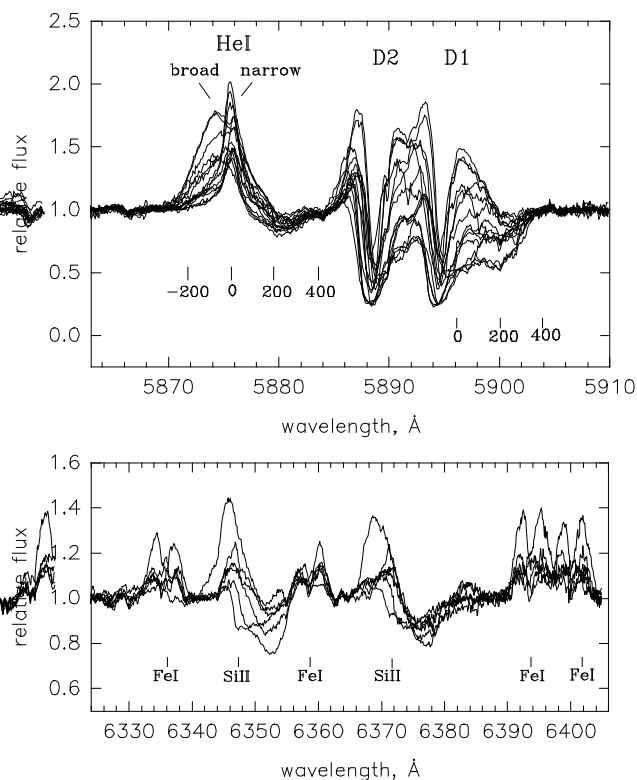


Figure 1: Two fragments of the spectrum of RW Aur A, showing the range of variability in the line profiles with accretion components. The wavelength scale is in the stellar rest frame. The radial velocity scales (in km s^{-1}) are shown for the HeI and the NaI D1 lines.

Petrov et al., 2001a, hereafter referred to as Paper I). During our observations the star varied in brightness within $V=9^m.8-11^m.0$, which is the most typical range of its variability.

2. Spectral variability

The spectrum of RW Aur A shows different components, among those are: a) highly veiled photospheric spectrum of K1-K4 star, a) broad emission lines of H, HeI, neutral and ionized metals, b) narrow emission

lines of HeI and HeII, 3) red-shifted absorption components in many lines. An example of the night-to-night variability is shown on Figs. 1. The red-shifted absorptions, hereafter called the "accretion components", are present in most of the spectra. As a parameter of the accretion component we will use the equivalent width of the NaI D1 absorption within the interval of radial velocities from +200 to +400 km s⁻¹. The HeI emission consists of the broad and narrow components (which is also observed in some other CTTS). The two components can be decomposed and the equivalent width and radial velocity of each one can be measured. The equivalent width of emission can be converted into flux using the simultaneous photometry.

From analysis of the spectra collected during the three seasons, we discovered periodic variations in many spectral features, the most pronounced are those in radial velocity and equivalent width of the narrow HeI emissions, and in the equivalent widths of the accretion components, with a period within 2.6–2.8 days. More exact value of the period, $P = 2^d641$, was found from the long time series of the photometrical data (see next Section). The phase diagrams are shown in Fig. 2. Note that the D1 accretion component vary in phase with the HeI narrow emission, while there is a phase shift, about 1/4 period, between the radial velocity and the flux of the HeI narrow emission. The period within 2.6–2.8 days is also present in radial velocity of the photospheric lines, which may be an indication that a low-mass invisible companion is orbiting the star (Gahm et al. 1999).

The veiling of the photospheric spectrum was derived in several spectral regions relatively free from the emission lines, within 5550–6050 Å, by means of cross-correlation technique using the template spectra of K-stars. The veiling factor varied irregularly within 1–10, with the average value about 3. One unexpected result is that *no correlation between the veiling and the brightness* was found, although both parameters varied in wide ranges. This is illustrated in Fig. 3, where two spectra shows very different levels of veiling at the same brightness of the star. Analysis of the variations in other spectral features is given in the Paper I.

3. Photometric variability

The photometry made simultaneously with our spectroscopic observations was used to convert the equivalent widths of emission lines into fluxes, and to study the correlations between spectral and photometric variability. In order to search for the periodicity in the photometrical data, we combined our data with much more extended time series available from the electronic catalogue compiled by Herbst (1994), which covers a time span over 30 years. For RW Aur A, the catalogue contains 575 observations in V and B–V and some-

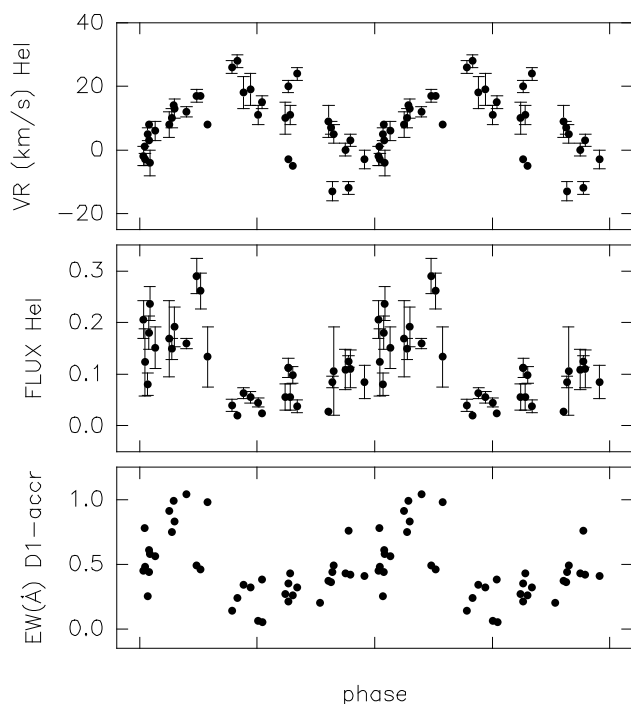


Figure 2: Phase diagrams for the period 2.641 days. Upper: radial velocity of the HeI narrow emission. Middle: flux (in 10^{-12} erg cm⁻² s⁻¹) in the HeI narrow emission. Lower: equivalent width of the D1 accretion component.

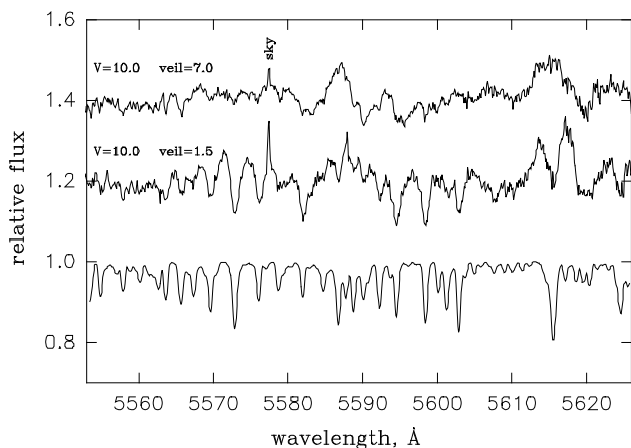


Figure 3: Two spectra with very different veiling, but with the same brightness of the star. Lower: the spectrum of γ Cep artificially veiled by factor 2

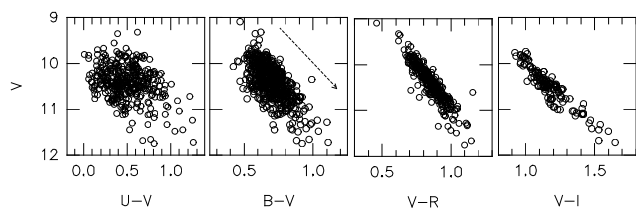


Figure 4: Colour-magnitude diagrams. The direction of the mean interstellar reddening law is shown on V versus $B-V$ diagram. The UBVRI bands are in the Johnson system, the I band is in the Cousins system.

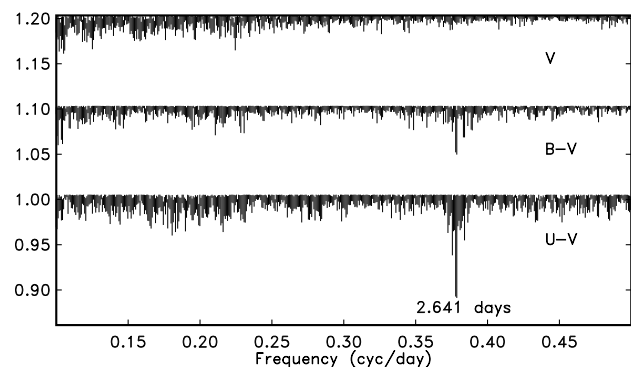


Figure 5: LS spectra for the brightness and colours in the range of periods from 2 to 10 days.

what less in other colours. The major part of the data are from the Majdanak Observatory (the ROTOR program by V.S.Shevchenko's group) and from Van Vleck Observatory (unpublished).

There is a good correlation between V and the colours $B-V$, $V-R$ and $R-I$, with the slopes roughly corresponding to the mean law of interstellar extinction (Fig. 4). It looks very much like the result of variable circumstellar extinction. Note, however, that for the spectral type of RW Aur A (K1-K4 V) the normal photospheric colour $B-V$ should be 0^m86-1^m05 . With $A_V = 0^m3$ (Paper I) the observed photospheric colour $B-V$ is expected to be within 0^m95-1^m14 . Most of the observed $B-V$ colours are much bluer. This effect is also known for other CTTS: the stars typically have closest to normal photospheric colours when they are at minimum brightness, while becoming overly blue at maximum light (Vrba et al., 1993). This is believed to be due to an additional, variable non-photospheric hot continuum which also accounts for the veiling of the photospheric line spectrum. The contribution of the emission lines to the photometric bands also accounts for a part of the excessively blue colours. From the spectra with the strongest emission lines we estimate the maximal contribution to the $B-V$ colour as 0^m2 .

The search for periods in the brightness and colours variations was made using the LS-statistic (Pelt 1992): variance of the least square fit residual divided by orig-

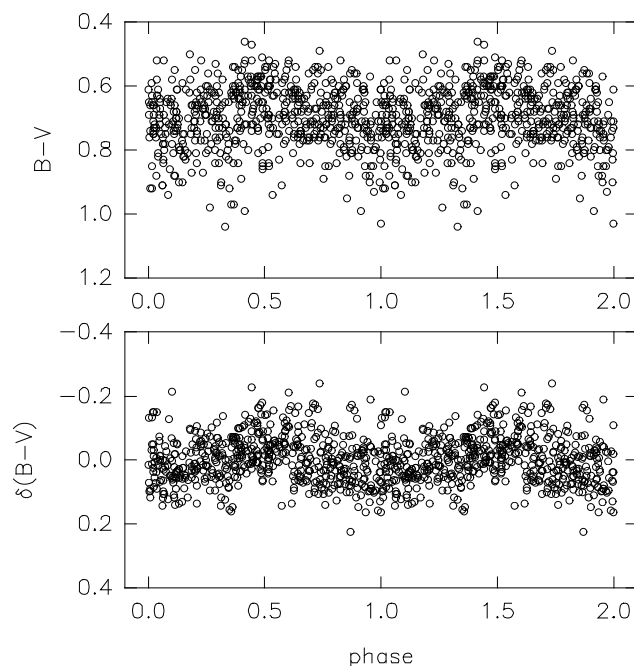


Figure 6: Phase diagram for the period 2.641 days. Upper panel: variations in the observed colour. Lower panel: variations in the residual colour (see text).

inal variance of the data. As a model to be fitted we used a single harmonic curve. No periodicity was found in the V -magnitude within a region of periods from 1 to 100 days, while the blue colours reveal a significant period around 2.64 days, in accordance with that found from the spectral analysis. The LS spectra are shown in Fig. 5.

From the colour-magnitude diagrams (Fig. 4) we can conclude that the total variability of RW Aur consists of at least two components: a large-scale variability in all the colours within about 0^m5 , and a scatter around the linear trend on the diagrams. This scatter is very small in the red colours but steeply increasing towards the UV, which indicates the presence of a hot variable source of radiation. We can eliminate the linear trend in the colour-magnitude diagrams and investigate the time variations in the *residual* colours, which can be defined as $\delta(B-V) = (B-V) - C \cdot V + const$ for $B-V$ and in a similar way for other colours. The period 2.641 days is better seen in the residual colours (see Fig. 6). When the whole data set is used, the full amplitude of the sinusoidal variations is: 0^m21 in $U-V$, 0^m07 in $B-V$, and about 0^m02 in $V-R$ and $V-I$. More detailed analysis of this periodicity is given in Petrov et al. (2001b).

4. Discussion

The correlated periodic variations in the HeI narrow emission and the D1-accretion components (Fig. 2) is the most important finding of our research. The vari-

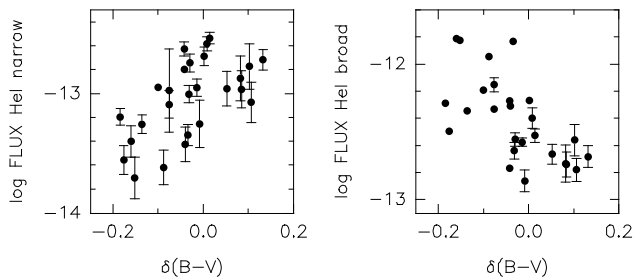


Figure 7: Correlation between the residual B-V colour and the fluxes in the HeI narrow and broad emission lines.

ations are most probably caused by rotational modulation of the non-axisymmetric accretion, as it is described below.

The quarter-period phase-shift between the radial velocity and the flux variations is a clear indication to the spot-like region of the HeI narrow emission: the radial velocity is minimal when the spot is face on to the observer, and maximal when the spot is at the limb (all the velocities discussed here are in the stellar rest frame). Note, that the average radial velocity of the HeI narrow emission is not zero, but positive: $+10 \text{ km s}^{-1}$. This emission may arise from the post-shock region at the footpoint of the accretion column (Calvet & Gullbring 1998). The accretion components of NaI D and many other lines indicate the inflow velocity up to $+450 \text{ km/s}$, which is consistent with the free-fall velocity to the star. The broad emission lines may originate from the global magnetosphere of the star threaded by streams of gas flowing towards the star (Calvet 1998). At the moments when the star is seen through the accretion column, both the strength of the accretion components and the flux in the HeI narrow emission are enhanced. The rotational modulation arise due to the presence of one or two dominating columns of accretion, that is accretion is non-axisymmetric. The asymmetry may arise due to a misalignment of the magnetic and rotational axes (Königl 1991). An alternative hypothesis (a binary star) is discussed in Paper I.

So far, the results of our research seem to support the magnetically channeled accretion model. Since the model predicts the existence of a hot photospheric spot below the accretion shock, we should expect periodic modulations in brightness and colours as well. The amplitudes of the periodic colour variations (Section 3) rising steeply towards the UV indicate the presence of a hot source of radiation, which might be identified with the expected hot spot. Using black body approximations for the fluxes from the photosphere and the hot spot, one can estimate the temperature of the hot spot and the fraction of the visible stellar disc covered by the spot. With $T_{\text{phot}}=4800 \text{ K}$, and the amplitudes given in Section 3, we get $T_{\text{spot}}=15000 \text{ K}$ and the covering fraction 0.1%. Such a small spot gives only a

0^m05 amplitude in the V magnitude. Then, we should expect the bluer colour when the HeI narrow emission is stronger. However, quite the opposite is observed: when the residual colours are bluer, the flux in the narrow HeI emission is lower (Fig. 7). The "normal" correlation exists between the colour and the *broad line* flux: the larger the broad line flux, the bluer the colour.

Hence, the residual blue colours vary in "anti-phase" to the strength of the accretion components and to the flux in the narrow HeI emission, in the sense that the star is redder when the shock region is facing the observer. There is no doubt that magnetospheric accretion is going on in RW Aur A, and that the accretion column(s) exists, but the expected hot spot at the base of the accretion column does not reveal itself in our series of data. The small hot spot, discussed above, may belong to the non-uniformly distributed hot gas, which also radiates in the broad emission lines.

In the case of RW Aur A we met with the following contradiction. On the one hand, the large level of the veiling of the photospheric spectrum and the large amplitude of the irregular light variations suggest the presence of strong accretion shocks. On the other hand, the strong spectroscopic evidences of accretion do not show any relation to the brightness of the star. In addition, no correlation between the veiling and brightness was found, when both parameters varied in a wide range.

The apparent absence of the hot spot related to the accretion column is really puzzling. Either the accretion shock is absent indeed, i.e. all the kinetic energy of the infalling gas dissipates before it reaches the stellar surface, or the complicated geometry of the flows and possible extinction of light within the gas streams makes the observed variations so complicated.

References

- Bertout C., Basri G., Bouvier J.: 1988, *Ap.J*, **330**, 350.
 Calvet N., 1998, in: *Accretion processes in Astrophysical Systems: Some Like it Hot!* (eds.: Holt & Kallman), American Institute of Physics.
 Calvet N., Gullbring E.: 1998, *Ap.J*, **509**, 802.
 Gahm G.F., Petrov P.P., Duemmler R., et al.: 1999, *As.Ap.*, **352**, L95.
 Herbst W., Herbst D.K., Grossman E.J., et al.: 1994, *A.J*, **108**, 1906.
 Königl A.: 1991, *Ap.J*, **370**, L3.
 Pelt J.: 1992, *Irregularly Spaced Data Analysis. User Manual*, University of Helsinki
 Petrov P.P., Gahm G.F., Gameiro G.F., et al.: 2001a, *As.Ap.*, in press.
 Petrov P.P., Pelt J., Tuominen I.: 2001b, *As.Ap.*, submitted.
 Vrba F.J., Chugainov P.F., Weaver W.B., Stauffer J.S.: 1993, *A.J*, **106**, 1608.

A STUDY OF IONOSPHERIC REFRACTION OF RADIO WAVES FROM OBSERVATIONS OF COSMIC RADIO SOURCES USING THE RADIO TELESCOPE URAN-4

V.V. Galanin¹, Ya.V. Derevyagin², V.G. Derevyagin¹

¹ URAN-4 Observatory, Institute of Radioastronomy NASU
Pushkinskaya str. 37, Odessa 65011 Ukraine, *uran@paco.net*

² Radiotechnical department, Odessa National Polytechnic University
Shevchenko av. 1, Odessa 65044 Ukraine, *rtu@rtf.ospu.odessa.ua*

ABSTRACT. The questions of the ionosphere refraction account at radiosources observation on the radiotelescope URAN-4 at 20-25 MHz are considered. The experimental data are received which will be coordinated to results of ionosphere refraction modeling.

Key words: Radiosource, refraction, ionosphere

The radiotelescope, RT, URAN-4 (Galanin et al., 1989) is one of elements of the radio interferometer long baseline system. The operating frequency range of system is 10-30 MHz. The antenna of the instrument consists of 128 crossed dipoles forming the phased array with dimensions of 232.5 x 22.5 m. The hardware of telescope provides receiving of the radio signals with two linear polarizations. The instrument as part of the radio interferometer with a very long baseline (radiotelescopes UTR-2 and URAN-4) and to perform research in a single regime as well is used. The instrument antenna pattern HPBW at frequency 25 MHz is $2.7^\circ \times 22^\circ$.

Simultaneously at two frequencies 20 and 25 MHz the space radiosources observations carry out by modulation radiometers. The computer saves received information on the disk and operates orientation of directional pattern in the space. The information about sources and the current time synchronized by digital clock standard in the computer are entered.

The ionosphere provides the essential influence on the space radiosources radiowave propagation in the HF band. The variations of its electronic density create heterogeneities, which cause refraction as shift of a seen location of the radiosource.

It is known, that there are a right ascension refraction Δt and a declination refraction $\Delta \delta$. Refraction carries regular and not regular character. Usually its value depends from a ionosphere condition, Sun zenithal corner, time of day.

The given work is devoted to an opportunity of an experimental research of the refraction with using of

the radiotelescope URAN-4.

The technique of measurement of the refraction value is known. It is based on measurement of the refraction angle, using comparison of a radiosource location to its true calculated coordinates. For an illustration of this method figure 1 is given. In this figure the record of a source 3C-144, received at June 20 in 1998 year in day time on the frequency 25 MHz is represented. In the experimental directional pattern, DP, is entered calculated DP with determined width. The measured and calculated DP position value is marked and the shift Δt by right ascension is determined. Also seen, that the source passes through DP before calculated time and the refraction carries positive character.

It is necessary to notice the RT URAN-4 have wide directional pattern by declination. The signal value change for the account influence of the refraction will be less than 0.5% at the shift value 20 angular minutes. Therefore the experimental investigation was carried out only on a right ascension.

The regular refraction dependences from time of day were given by Megn and Antonov (1973). From this work follows, that the refraction by right ascension Δt is minimal at night, and at forenoon and in the afternoon is maximal. Its character varies from negative to positive. Its minimal value makes units of angular minutes at night, and in the day time comes nearer 20 angular minutes.

Therefore the most suitable time for measurement of the refraction on RT URAN-4 is first and second half of day, when the refraction is maximal.

For refraction researches the source 3C-144 with the flux of radiation in 3300 jans was chosen. The measurements were carried out during Mays – Junes, when the source had the culmination in middle of day. The record 3C-144 was carried out by scans of 20th minutes in the hour angles range from -160 to +160 minutes on two frequencies 20 and 25 MHz simultaneously. It is necessary to note, that the character of record was

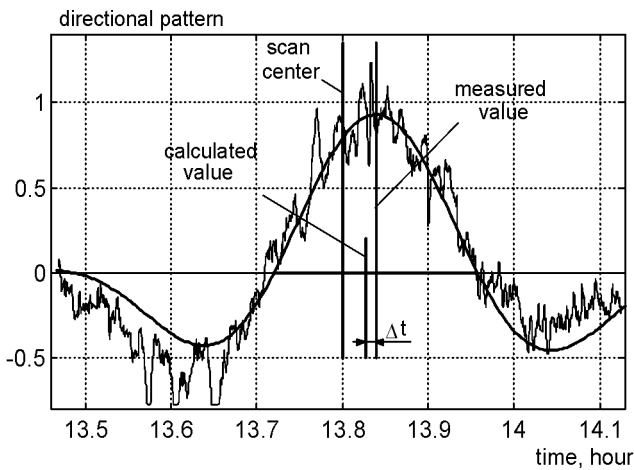


Figure 1: The refraction size definition by directional pattern displacement.

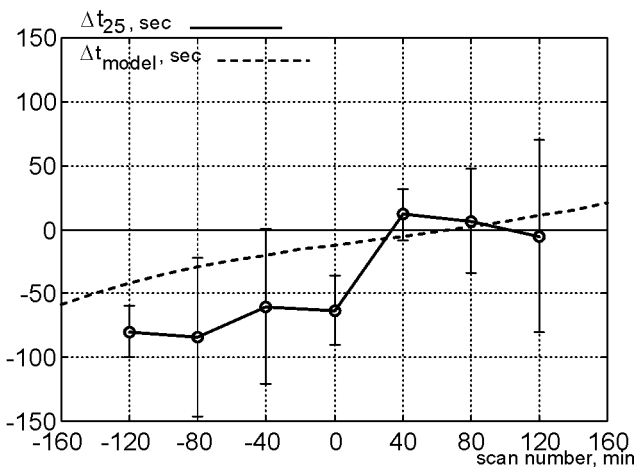


Figure 2: Comparison of the measured and calculated values of the refraction on the 25 MHz.

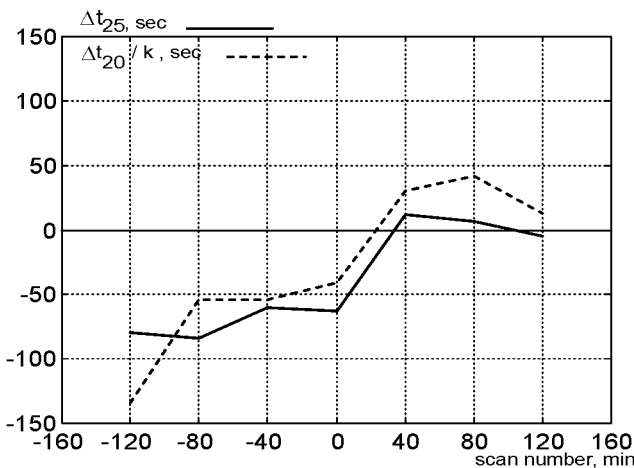


Figure 3: Comparison of the refraction average values $\Delta t_{20}/k$ and Δt_{25} .

affected by radiohandicaps and sporadic solar flares. Therefore the observation not subject to influence of handicaps were selected for processing. The processing included the described above standard procedure. Finally information was averaged and was analyzed.

In figure 2 the diagram of the dependence refraction value from a hour angle is submitted. It contain calculated and measured refraction values for frequency 25 MHz. The measured and average data received for the mentioned above period, are put on figure with confidential intervals. The calculated values of the refraction are received from ionosphere model which was described by Davies (1973) and Antonov (1973). It is submitted by a electronic concentration gradient which appears in consequence of Sun zenithal distance change. The refraction calculation was carried out for ionosphere model received at the square-law equation of recombination. The character of two curves basically is identical also calculated curve is in the field of confidential intervals.

The frequency dependence is important parameter which characterizes the refraction. It is known, that it should be square-law.

The average refraction values Δt obtained at the frequencies 20 and 25 MHz are shown in figure 3. The curve $\Delta t_{20\text{MHz}}$ was drew as $\Delta t_{20\text{MHz}}/k$, where k is a square ratio of 20 and 25 MHz. The curve character on 20 MHz basically repeats measurements on 25 MHz. Their divergence is caused of the insufficient statistics of measurements.

From told above it is possible to make conclusions. The wide directional pattern and limited sensitivity of the radiotelescope URAN-4 allow to carry out by the specified technique of regular refraction measurement only on a right ascension and in a light time of day. As the directional pattern value of instrument by declination is 22° , its refraction displacement does not render an appreciable influence on measurements.

Acknowledgements. The authors express deep gratitude to O.A. Litvinenko for the valuable remarks and offers at discussion of results of the research.

References

Antonov A.V., *Ph.D. thesis*, Kharkov, 1973.
 Davies K., *Ionospheric radio waves*, Moscow: Mir, 1973. (In Russian).
 Galanin V.V., Inyutin G.A., Kvasha I.M., et al.: 1989, *Kinemat. Fiz. Nebesnykh Tel*, 5, 5, 87.
 Megn A.V., Antonov A.V.: 1973, *Radiofizika*, 16, 9, 1434.

VARIABLE RADIO SOURCES AND TAKING INTO ACCOUNT OF IONOSPHERIC EFFECTS

O.A. Litvinenko, S.K. Panishko

URAN-4 Observatory, Institute of Radioastronomy NASU
Pushkinskaya street, 37, Odessa 65011 Ukraine, *uran@paco.net*

ABSTRACT. Histograms and mean value of scintillations indexes are obtained for power cosmic radio sources on observations during 1998-2001. Using simulations it is showed that scintillations with periods more than 10 minutes give the error of measuring of amplitude of radio telescope response pattern within the limits from 5 into 50 per cent in dependence of strength of the scintillations.

Key words: Cosmic radio sources: ionospheric scintillations; radio telescope: response pattern: amplitude.

The preliminary analysis of the ionospheric scintillations on the cosmic radio sources observation data obtained with the radio telescope URAN-4 during 1998-2001 at the frequency 25 MHz is presented. Long time on the radio telescope URAN-4 observations of the power cosmic radio sources 3C144, 3C274, 3C405, 3C461 carried out to study the behaviour of their flux densities (Ryabov et.al.1987). Method of measurements consist that for each source 4 - 6 records of passing through the radio telescope array direction pattern registered every day. Amplitude of the direction pattern response for the signal from radio source is the measuring value. Most regular data were received as analog records on the paper tape of recorder in 1987-1989 and in 1998-2001 when data were stored to the computer memory.

Such phenomenon as scintillations of the radio source flux densities on the ionospheric irregularities (Crane 1977, Yeh and Liu) is ordinary for decametric range that is really display all records obtained on the URAN-4. It would be useful to estimate the effect of radio source signal fluctuations on the accuracy measurement of record amplitude. For this purpose it is necessary know characteristics of the ionospheric scintillations. In the previous paper (Litvinenko and Panishko 2000) we analyzed scintillation analog data for 1987-1989. Similar results obtained in 1998-2001. As the characteristic of fluctuations the index of scintillations was used. It was determined as follows: the computational direction pattern was fitted in a source record by selection of parameters, then for processing

the part of record of length 15 minutes near to maximum counting was selected and from it the appropriate part of the fitting response pattern was subtracted. The square root of standard deviation of this realisation divided on amplitude of record, gives an index of scintillations. In a figure 1 it is possible to see, that the values of indexes vary within the limits from 0.25 up to 0.41. The characteristic times T of scintillations constitute from 64 up to 148 seconds.

The effect of scintillations to measuring accuracy of amplitude of record can be estimated with simulating calculations. For this purpose the theoretical response pattern F with known amplitude A was multiplied on a function, which sets scintillations with two parameters: AF/A - ratio of amplitudes of fluctuations and response pattern and P/PF - ratio of periods of the response pattern and fluctuations. In the results we receive a function FS , which is the simulation of real record. Further is used a fitting procedure of a function of the response pattern FA and is computed its amplitude. The comparison with initial value gives error of measuring. The changes of amplitudes of fluctuations were set in limits from 0.1 up to 1.0, and ratio of periods - in limits from 2 up to 20. In general it is possible to select two characteristic cases: 1) at change of ratio of periods from 4 up to 20 and amplitudes of scintillations from 0.1 up to 1.0 functions F and FA coincide; 2) for ratio of periods 2 and 3 and at change of amplitudes of fluctuations from 0.1 up to 1.0 measurement errors of amplitude varies within the limits from 5 up to 50 per cent (Figure 2).

From the received calculations, it is possible to make a conclusion, that in case of simulating scintillations with ratio of periods from 4 up to 20 it is possible to apply a fitting procedure to measure of amplitude of record. If the scintillations have characteristic periods more than 10 minutes, depending on amplitude of fluctuations the error can considerably effect outcome of measurements. The observational data show, that the records with large-scale scintillations constitute about 1/10 part of all observable. Thus, measuring characteristic time of fluctuations on record of a radio source and having the dependence of measuring error on scintillation parameters, it is possible to estimate an error

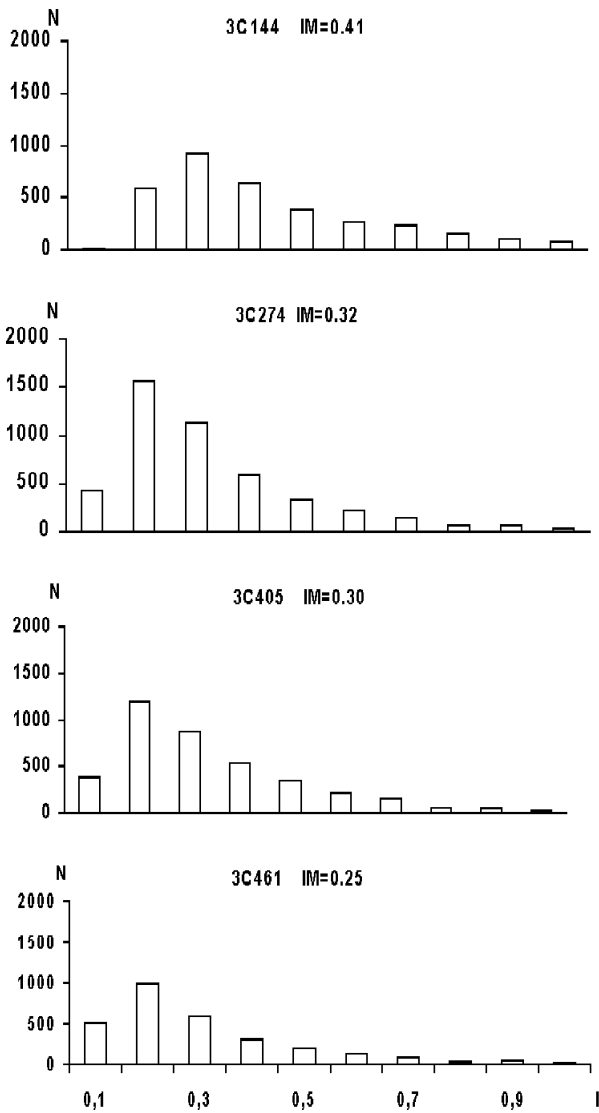


Figure 1: Histograms and mean values of scintillation indexes for cosmic sources were observed on RT URAN-4 in 1998-2000.

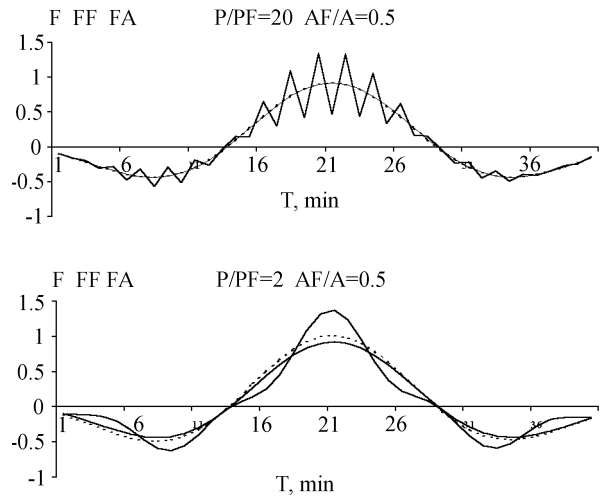


Figure 2: Examples of calculations of functions F, FS (solid line), FA (dotted line) for two case

of obtaining of amplitude of record at fitting of the computational response pattern.

References

Crane R.K: 1977, *Proc. IEEE.*, **65**,180.
 Litvinenko O.A., Panishko S.K.: 2000, *Geomagnetizm i aeronomiya*, **40** , 116
 Ryabov M.I. et.al.: 1987, *Galactic and extra galactic radioastronomy. Abstracts*, 30.
 Yeh K.C., Liu C.-H.,*Proc. IEEE.*,**70**,324.

RADIATION FROM VICINITY OF SUPERMASSIVE OBJECT WITHOUT EVENTS HORIZON

E. Yu. Bannikova

Kharkov National University, Svobody Sq.4, 61077, Ukraine, *bannikova@astron.kharkov.ua*

ABSTRACT. Spectra of the radiation arising at interaction of the spherically symmetric accreting flow with the matter of the atmosphere of the supermassive compact object without events horizon are found.

Key words: Galactic center, Sgr A*.

1. Introduction

The observations of the Galactic center give evidences that a supermassive compact object can be identified with the nonthermal radiosource Sgr A* (Eskart A. and Genzel R., 1996), (Eskart A. and Genzel R., 1997), (Ghez A.M., et al., 1998). The mass of this object is equal to $(2.6 \pm 0.2) \cdot 10^6 M_{\odot}$. It is supposed that similar supermassive compact objects exist also in the nuclei of other galaxies (Ferrarese F., et al., 1996), (Iyomoto N., et al., 2001), (Miyoshi M., et al., 1995). These objects are usually identified with a supermassive black hole, but there are also other attempts to explain the observation data (Tsiklauri D. and Violler R.D., 1998), (Torres D., et al., 2001). In the paper (Verozub L.V., 1996) another possibility was proposed, which is based on bimetric gravitation equations (Verozub L.V., 1991), the spherically symmetric solution of which has no a physical singularity in flat space-time from the viewpoint of a remote observer. The physical consequences from the equations coincide with the consequences from the Einstein equations at the distances, much larger than the Schwarzschild radius $r_g = 2GM/c^2$, however the ones essentially differ from them at $r \leq r_g$. According to the equations the events horizon is absent in the spherically symmetric solution. The radial component of the gravity force F affecting a test particle with mass m in the spherical coordinates system in flat space-time is given by

$$F = -m [c^2 B_{00}^1 + (2B_{01}^0 - B_{11}^1)v^2]. \quad (1)$$

Here B_{00}^1 , B_{01}^0 and B_{11}^1 are nonzero components of the strength tensor $B_{\alpha\beta}^{\gamma}$ of gravity field in flat space-time:

$$B_{00}^1 = \frac{C'}{2A}, \quad B_{01}^0 = \frac{C'}{2C}, \quad B_{11}^1 = \frac{A'}{2A},$$

$f = (r_g^3 + r^3)^{1/3}$, v is the radial component of the

particle velocity, the prime is the derivative on r ,

$$C = 1 - \frac{r_g}{f}; \quad A = \frac{r^4}{f^4 C}.$$

It follows from these equations that there can exist

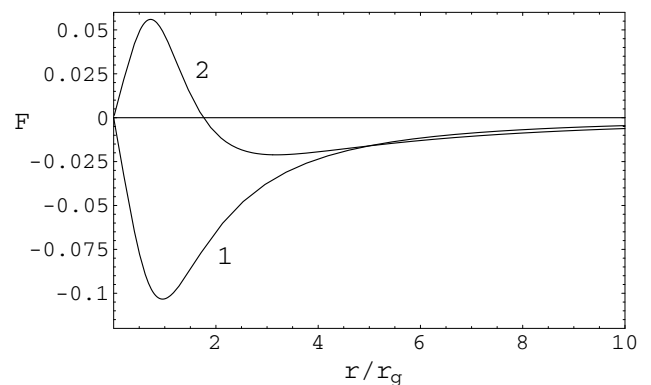


Figure 1: The gravitational force F (in arbitrary units) as the function of r/r_g affecting a particles at rest (the curve 1) and free falling particles (the curve 2).

the equilibrium stable configurations of the degenerated electronic gas with masses up to $10^9 M_{\odot}$ or more than that and with the radius less than Schwarzschild radius (Verozub and Kochetov, 2001). Such objects are an alternative to black holes.

The object without events horizon, unlike the black hole has a surface and atmosphere, a radiation from which at an accretion can be essential. In this paper a simplified model of the radiation arising at interaction of the spherically symmetric accreting flow with the matter of the atmosphere of such an object is considered without taking into account the magnetic field.

2. The radiation from the vicinity of the object

To find a spectrum of the radiation arising from the atmosphere, we find the profiles of temperature and matter density near to the surface using a method by Zeldovich and Shakura (1969).

Let's introduce parameter $y = \int_{R_0}^{\infty} \rho dR$, where ρ is

the matter density, R is the radial coordinate. This parameter characterizes a quantity of the matter which was decelerated. The quantity of the matter of the atmosphere needed to the complete stop, we shall designate through y_0 . Similarly (Zeldovich and Shakura, 1969) we will assume that $5 < y_0 < 20$.

The transfer of the radiation in the atmosphere is governed by the equation for the radiation energy density U which, in spherically symmetry and using the Eddington approximation, can be written as:

$$\frac{1}{3} \frac{dU}{dy} = k_1 \frac{L}{4\pi R_*^2 c}, \quad (2)$$

where $L = L_\infty(y_0 - y)/y$, L_∞ is the total radiative luminosity at outer edge of the atmosphere, R_* is the radius of the object. It follows from the solution of the equations of the hydrostatic balance that to the given value of the mass of the central object $M_* = 2.6 \cdot 10^6 M_\odot$ corresponds radius $R_* = 0.04 r_g$ (Verozub and Kochetov, 2001). Taking into account the scattering and bremsstrahlung, the mean opacity it is possible to write down: $k_1 = k_{es} + k_p$, where $k_{es} = 0.4 \text{ cm}^2/\text{g}$ is the coefficient of the scattering on free electrons, $k_p = 6.4 \cdot 10^{22} \rho T^{-7/2} \text{ cm}^2/\text{g}$ is the Planck mean opacity, T is the gas temperature.

The equation of the hydrostatic balance and radiative energy equilibrium is

$$\frac{dP}{dy} = \frac{GM_*}{R_*^2} \left(1 - \frac{r_g}{(r_g^3 + R_*^3)^{1/3}} \right), \quad (3)$$

$$\frac{W}{c} = k_p(aT^4 - U) + 4k_{es}U \frac{kT}{m_e c^2} \left(1 - \frac{T_\gamma}{T} \right), \quad (4)$$

where $W \approx L_\infty/(4\pi R_*^2 y_0)$ is the energy, that release on 1g. of the matter at $y \leq y_0$. At $y > y_0$, $W = 0$.

We neglect pressure in a layer y_0 , which is created by the falling particles since it is much lower than the pressure due to the matter of the atmosphere, and also we use the perfect gas equation of state assuming that the matter is the completely ionized hydrogen. The radiation temperature T_γ is related to U as $U = aT_\gamma^4$, where $a = 7.56 \cdot 10^{-15} \text{ erg}/(\text{cm}^3 \text{ grad}^4)$. Thus, we have received the system of differential equations (2), (3), (4), the solutions of which are U , T , ρ as the functions of y . The boundary condition at the outer edge is $U(0) = L_\infty/(4\pi(R_* + H)^2 c) \approx L_\infty/(4\pi R_*^2 c)$, where H is the height of the atmosphere; $\rho(0) = 10^{-12} \text{ g}/\text{cm}^3$ corresponds to the solution of the equations of the spherically symmetric accretion near the surface (Verozub L.V. and Bannikova E.Yu., 1999); $T(0) = 10^5 \text{ K}$ (the solution there exists only for $T(0) < 4 \cdot 10^5 \text{ K}$). L_∞ end y_0 are the parameters. The thermal properties of the atmosphere are illustrated in fig.2 for different luminosities at outer edge of the atmosphere in the case $y_0 = 20 \text{ g}/\text{cm}^2$. The solution slightly depends on the boundary conditions. Near the surface

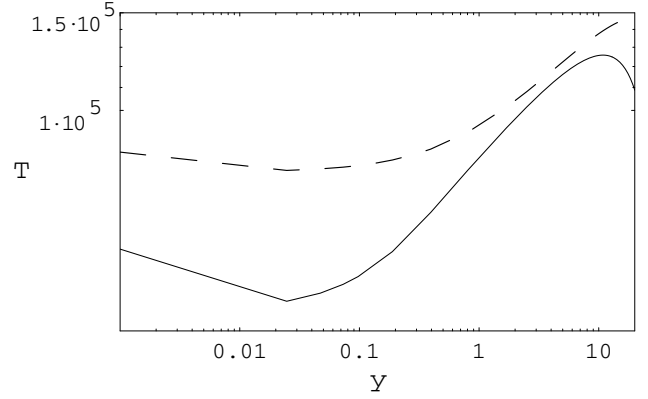


Figure 2: The temperature T as the function of y for $L_\infty = 10^{38} \text{ erg/s}$ (dashed line) and $L_\infty = 10^{37} \text{ erg/s}$ (solid line).

$\rho(y_0) \approx 5 \cdot 10^{-6} \text{ g}/\text{cm}^3$. The height of the homogeneous atmosphere is

$$H = \frac{kTR_*^2}{\mu m_p GM_*} \left[1 - \frac{r_g}{(r_g^3 + R_*^3)^{1/3}} \right]^{-1} \quad (5)$$

and for the maximum temperature $H \approx 10^6 \text{ cm}$.

To find the spectrum of the radiation, it is necessary to take into account the gravitational redshift and gravitational capture of the radiation by the central object, as in the case for a black hole (Shapiro and Teukolsky, 1985). The light frequency ν measured close the object is related to the light frequency ν_0 as measured at infinity:

$$\nu = \left(1 - \frac{r_g}{(r_g^3 + r^3)} \right)^{-1/2} \nu_0. \quad (6)$$

At $r = R_*$ obtain $\nu = 216.5\nu_0$. The equations of motion of a test particle in the spherically symmetric field is

$$\left(\frac{dr}{dt} \right)^2 = \frac{c^2 C}{A} \cdot \left[1 - \frac{C}{E^2} \left(1 + \frac{r_g^2 \bar{J}^2}{B} \right) \right], \quad (7)$$

$$\frac{d\varphi}{dt} = \frac{c \bar{J} r_g}{B \bar{E}}, \quad (8)$$

where (r, φ, θ) are the spherical coordinates, $B = f^2$, $\bar{E} = E/(mc^2)$, $\bar{J} = J/(r_g mc)$, E is the particle energy, J is the angular momentum. If we through ψ denote the angle between a direction of motion of the photon and the radius, taking into account the equations of motion (7) and (8) we receive

$$\text{tg } \psi = \frac{b_{\max} r^2}{f^3} \left(1 - \frac{C b_{\max}^2}{f^2} \right), \quad (9)$$

where $b_{\max} = 3\sqrt{3}/2$. Fig.3 shows $|\cos \psi|$ as the function r/r_g . Take into account to scattering and gravi-

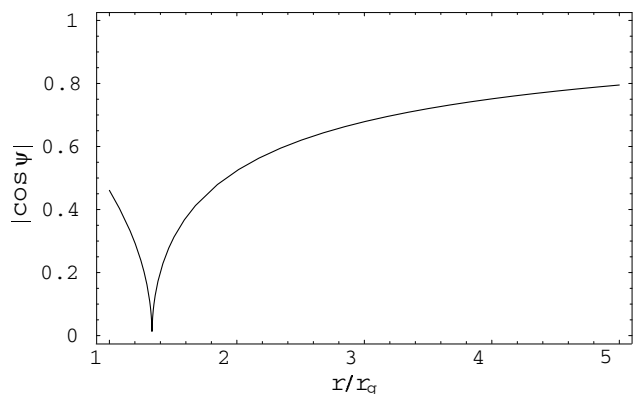


Figure 3: The plot $|\cos \psi|$ versus r/r_g .

tational effects we found that the flow of the radiation is

$$F_{\nu_0} \approx (1 - \cos \psi(R_*)) \pi B_{\nu_0} \sqrt{\frac{\chi}{k_{es} + \chi}}, \quad (10)$$

where $\chi = 1.14 \cdot 10^{56} T^{-1/2} \nu^{-3} (1 - \exp(-h\nu/(kT))) \rho$, ν is determined by expression (6) at $r = R_*$. The values of T and ρ correspond to the solution of the system (2), (3), (4) at $y = y_0$. Thus we obtain the following results.

a) Let $L_\infty = 10^{37}$ erg/s. Thus $k_{es} < \chi$ at the frequency interval $\nu_0 < 10^{14}$ Hz and the atmosphere radiates as a black body; at $\nu_0 > 10^{14}$ Hz ($k_{es} > \chi$) and taking into account that the atmosphere of the object is not homogeneous (density grows very quickly with depth), the flow of the radiation (Zeldovich and Shakura, 1969)

$$F_{\nu_0} \approx (1 - \cos \psi(R_*)) \left(\frac{3\chi}{\rho k_{es}^2 H} \right)^{1/2} \pi B_{\nu_0}, \quad (11)$$

where B_{ν_0} is the Planck function. The maximum of the frequency spectrum is at $\nu_0 \approx 5 \cdot 10^{13}$ Hz and corresponds the luminosity $L_{\nu_0} \approx 10^{19}$ erg/(s·Hz).

b) For $L_\infty = 10^{38}$ erg/s the radiation is a black body at the frequency interval $\nu_0 < 3 \cdot 10^{13}$ ($k_{es} < \chi$); at $\nu_0 > 3 \cdot 10^{13}$ Hz the flow of the radiation is according to (11). Here the maximum of the frequency spectrum is at $\nu_0 \approx 10^{13}$ Hz with the appropriate value of the luminosity $L_{\nu_0} \approx 10^{22}$ erg/(s·Hz). In figures 4 and 5 the frequency spectra in the vicinity of the maximums for the various luminosities is shown. Both cases are considered at $y_0 = 20$ g/cm². Thus the spectrum 5) are in accordance with the observation data of the Galactic center.

3. Conclusion

It follows from the above results that the our hypothesis that Sgr A* is a supermassive compact object without events horizon does not contradict the observation results and required further deeper investigation.

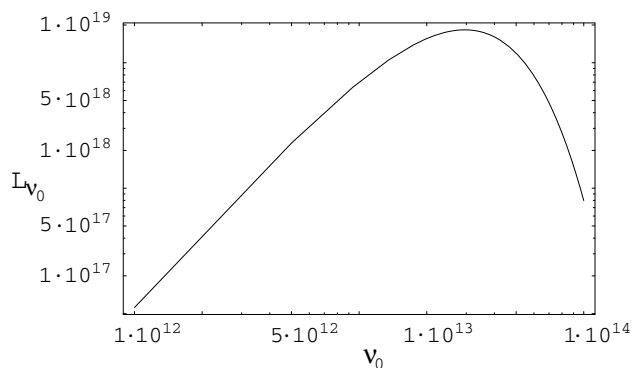


Figure 4: The frequency spectrum for $L_\infty = 10^{37}$ erg/s.

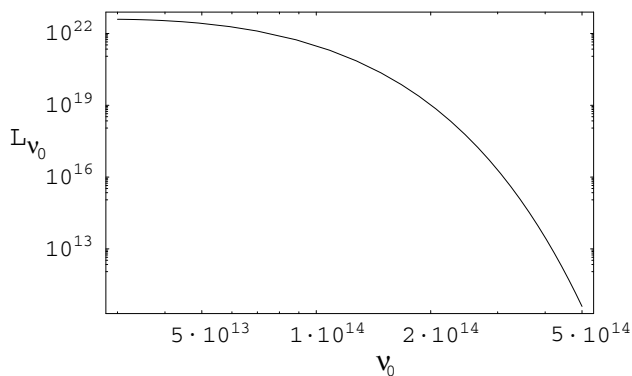


Figure 5: The spectrum for $L_\infty = 10^{38}$ erg/s.

References

- Eskart A., Genzel R.: 1996, *Nature*, **383**, 415.
 Eskart A., Genzel R.: 1997, *MNRAS*, **284**, 576.
 Ferrarese F., Ford H.C., Jaffe W.: 1996, *ApJ*, **470**, 678.
 Ghez A.M., Klein B.I., Morris M., et al.: 1998, *ApJ*, **509**, 678.
 Iyomoto N., Makishima K.: 2001, *MNRAS*, **321**, 767.
 Miyoshi M., Moran J., Herrnstein J., et al.: 1995, *Nature*, **373**, 127.
 Shapiro S., Teukolsky S.: 1985, *Black Holes, White Dwarfs and Neutron Stars*, v.2, 656p.
 Torres D., Capozziello S., Lambiase G.: 2001, *Phys. Rev.D*, **62**, 104012.
 Tsiklauri D., Violler R.D.: 1998, *ApJ*, **500**, 591.
 Verozub L.V.: 1991, *Phys. Lett. A*, **156**, 404.
 Verozub L.V.: 1996, in: "Galactic center", ed. G.Greder, *ASP Conf. Ser.*, **102**, 357.
 Verozub L.V., Bannikova E.Yu.: 1999, preprint astro-ph/9805299.
 Verozub L.V., Kochetov A.Y.: 2001, *Astron. Nachr.*, **322**, 3, 143.
 Zeldovich Ya.B., Shakura N.I.: 1969, *Astron. Zh.*, **46**, 2, 225.

PLANETARY SYSTEMS OF THE GALAXY

N.N. Evsukov, V.A. Zakhzhaj, V.A. Psaryov

Kharkov National University, Svobody Sq.4, Kharkov 61077, Ukraine,
zkh@astron.kharkov.ua, pva@astron.kharkov.ua

ABSTRACT. Definition of planets, relative contents of planetary systems in Galaxy, and main results of searching for them are adduced. It is supposed to distinguish four types of planets accordingly their inner substance composition: hydrogenous-helium (H_2 , He, Ne), ice (H_2O , CH_4 , NH_3 and their cluster tree, also N_2 and Ar), silicate, or metallic (alligations of Fe with Ni, Co, Cr) ones. Hydrogenous-helium compositions of planets are the most possible. But existence of two metallic (or metallic and silicate) and one ice planet in pulsar systems are suspected.

Key words: planetary system, types of planets.

1. Definitions

Planets are generated in circumstellar disks with a residual of angular momentum, where exist conditions for forming space bodies with mass of about some Jupiter masses (Ruzmaykina, 1981, Dole, 1970).

Evolution of planets is bond with gravitational differentiation that defines the lowest values of planetary masses of about $10^{-10}m_{\odot}$ with a diameter of about 500 km) (Alexandrov and Zakhzhaj, 1980).

Depending on medium elemental composition values of planet masses and can deflect from the mentioned above (mass at a tenth, and size at 100 less).

Space bodies with masses less then stellar, which are possible to be formed, as well as stars, by means of autogravitation, are defined as substars (Alexandrov and Zakhzhaj V.A., 1980), or brown dwarfs (Tarter, 1975). As the highest possible mass of planet is accepted the least mass of substar.

So, in accordance to Rees (1976), if temperature of the coldest interstellar clouds is about 10 K, then the highest valuation of planet mass makes up $(0.003 - 0.007)m_{\odot}$.

In the article under 'planetary system' we understand a space bodies system, in which at least one planet is present (Alexandrov and Zakhzhaj, 1983ab, 1986). Other components of the system can be planets, substars, stars, or their remnants (white dwarfs or pulsars).

2. Desired relative composition of planetary system

Hohlfeld and Terzian (1977), using results of Heppenheimer (1974) about influence of secondary components on protoplanetary nebula evolution, and using mass function of secondary components, inputed by Abt and Lavy (1970), proposed method for estimation of relative composition in double stellar systems. Alexandrov and Zakhzhaj (1983a) have generalized the results on different multiplicity stars with taking into account Branch's (1976) remarks about propriety of reduced power dependency of mass function for secondary components after Abt and Lavy (1970). Using mainly statistic characteristics of the nearest stars, they have determined value of relative contents of planetary systems in Galaxy as $0.2 \div 0.3$. Another authors appraisals are about 0.1 (Problema CETI, 1975, Problema Poiska vnezemnich Tzivilizatsiy, 1981, Problema Poiska Zhizni vo Vselenny, 1986).

3. Results of searching for planetary systems

The most effective methods of searching for planetary systems are the astrometrical one, radial velocities, direct images of protoplanetary formations, coverings, analyses of pulsars emission (Alexandrov and Zakhzhaj, 1983b, 1986, Gold, 1975, Zakhzhaj and Aleksandrov, 1981, Zakhzhaj and Ruzmaykina, 1986, Moroz V.I., 1981, Black, 1980, Greenstein, 1977). It is known already, that masses of invisible (obscure) satellites of Proxima (Niedzielski, 2001), Barnard's star (till three planets) (van de Kamp, 1974, 1975), and Laland 21185 (Gatewood, 1996) correspond to planets. It is suspected existence of planets or substars in systems of ϵ Eridanus (Lippincott, 1974, van de Kamp, 1974, 1975b) and $DM + 59^{\circ}1915$ (Shaht, 1984), and double star 61 of Cygnus (two satellites near A component and one - near B) (Deych, 1978, 1977, Niedzielski A., 2001). Till April, 2001, 53 solitary obscured satellites and three components near ν And were detected by means of radial velocities' variations measures (Burrows, Hubbard, Lunine, Liebert, 2001). For the objects $m \cdot \sin i < 38m_J$, where m_J -Jupiter mass, i - declination of planet orbit to viewing plane. For 37 satellites

among mentioned ones $m \cdot \sin i = 0.15 \div 3m_J$. As the method gives masses of satellites with accuracy up to $\sin i$, it is too early to assert, that all the objects are planets. And only for system HD 209458, that is found as shadowing variable (Charbonneau et al., 2000), it succeeded determine angle i . Mass of component as it was shown was planetary one $m \approx 0.69m_J$.

Measurements of pulsar emission frequency variations allowed to detect two and suspect one planetary systems. Till four planets are disclosed near pulsar PSR B1257+12 (Wolszcan and Frail, 1992, Wolszcan, 1994, 1997). One planet is found near pulsar PSR B0329+54 (Demianski and Proszynski, 1979). A planet, or substar is revealed near double pulsar PSR B1620-26, which is located in spherical cluster N1 (Arzoumanian et al., 1996).

The orbital telescope IRAS has permitted to reveal protoplanetary formations near Vega and β Pic (Robinson, 1984, Smith and Terrile, 1984). Later it has succeeded to receive protoplanetary disk image β Pic (Fizika za Rubezhom, 1986) with using of special eclipse coronagraph. In the inner vicinity of the disk (to 30 A.U.) area without gas and dust was detected. It can't be excluded presence there some formed planets. In nearstellar disk of HD 141569 (radius of the disk - 400 A.U.) there is a slit at 250 A.U. from the central star, where a planet with mass $m \approx 1.3m_J$ is prospected (Perryman, 2000, Weinberger et al., 1999). Now altogether about a hundred of protoplanetary disks are revealed around young stars of the main sequence with ages $10^6 \div 10^7$ years, including T Tauri stars (Kalas, 1998). Typical disk size is about 10^3 A.U. (Beckwith and Sargent, 1996, Perryman, 2000).

4. The main types of hypothetical planets

Depending on physical conditions (temperatures and pressures) in planets formation zones of protoplanetary clouds, and if chemical elements prevalence there likes to the solar one, so it is proposed to separate planet composition substances in four groups (Flirenskiy et al., 1981, Cameron and Pine, 1973). To *group I* actually volatile elements (H_2 , He and Ne), which can't be condensed under temperatures higher then 10 K, are related. Substances, that can be condensed into ices under temperatures $10 \text{ K} \leq T \leq 200 \text{ K}$ (H_2O , CH_4 , NH_3 and their clutrat tree, also N_2 and Ar). *Group III* consists of silicates (can be condensed under temperatures less 1700 K and pressure about 0.1 bar). Alligations of Fe with Ni, Co, Cr are included to *group IV*. Under pressure less 10^{-5} bar and temperatures less 1350K iron can be condensed after wide spread silicates of enstatite and forsterite. Under the higher pressures condensation of iron surpasses silicates condensation. Under pressure 0.1bar iron condensation temperature ($T \approx 1700 \text{ K}$) is higher by 80 K than forsterite. con-

densation temperature. With increasing of pressure the tendency keeps. If temperature is below 700 K, then begins FeS, which stands apart in the cores of planets jointly with iron alloies.

H_2 and He, as gases, can be captured by enough massive planets (masses more 10^{29} g) under temperatures below 200 K (Zharkov, 1980). Such planets are hydrogenous-helium ones. In less massive planets of low-temperature vicinity will predominate ices (ice planets). In middle-temperature zone of protoplanetary disk ($T > 200 \text{ K}$) ices can't be condensed. They disappear like hydrogen and helium. Under temperatures $T < 350 \text{ K}$ will be appeared hydrated silicates, which under heating educe water and can form hydrosphere, or cryolitesphere. In range of temperatures less $1500 \div 1700 \text{ K}$ (depending on pressure) are to be formed *silicate planets*. Higher by 200 K is a zone, where silicate substance is lost but exist conditions for forming of *metallic planets*.

Zone of metallic planets has too narrow temperature interval ($T = 1700 \div 1900 \text{ K}$) under pressure $P = 1$ bar and $T = 1600 \div 1700 \text{ K}$ under $P = 0.1$ bar. In Solar system this vicinity spreads from 0.1A.U. till 0.4A.U. Correspondingly, silicate planets zone has upper temperature limit about 200 K and spreads up approximately to 3 A.U.

Increasing of protoplanetary disk density by k times causes the same growth of optical thickness at arbitrary distance r . To restore optical thickness to previous meaning it is necessary decrease the distance r by k times. But, as result, right away it causes insolation increasing and upgrowth of temperature by \sqrt{k} times. So, dimensions of temperature zones are to decrease by \sqrt{k} times correspondingly. If star like Sun has a protoplanetary disk 10-ly denser, than Sun's one, so dimensions of metallic and silicate planets zones are to be less 3, i.e. $0.03 \div 0.1A.U.$ and $0.1 \div 1A.U.$

Extension of temperature zone boundaries is possible as result of star luminosity (L) increasing, because dust particles temperature in nonabsorbing interstellar medium $\propto L^{1/4}/r^{1/2}$. When increasing of star luminosity is 10 arm (A5V spectrum), boundaries dimensions rise by 3 times, i.e. reach $0,3 \div 1 \text{ A.U.}$ for metallic planets and $1 \div 10 \text{ A.U.}$ for silicate ones. In model of protoplanetary cluster after Cameron and Pine (1973) masses of silicate planets reach $20m_{\oplus}$ and faintly depend on density of cluster substance. For metallic planets zone mass of planet is limited by $0.2m_{\oplus}$, that corresponds to Earth core. Thus the largest radius of metallic planets is finite by 3000 km, and upper limit for silicate planets masses is, probably, equal some tens of m_{\oplus} .

For low-luminosity stars (M0V spectrum) and for density of near-Sun protoplanetary disk situation becomes reverse - magnitudes of temperature zones decrease by 3 times $0.03 \div 0.1 \text{ A.U.}$ for metallic planets and $0.1 \div 1 \text{ A.U.}$ for silicate planets). Masses of the

planets decrease by order too. Hydrogen-helium planets could be formed at orbits like orbit of the Earth.

5. Desired physical properties of extrasolar planets

Masses of invisible (obscure) satellites of main sequence stars correspond to hydrogen-helium giant planets. Their parameters (0.38 g/cm^{-3} - medium density of planet in system HD 209458, mentioned before) are in good coincidence with models of hydrogen-helium planets, located near stars.

Masses of planets near pulsar PSR B1257+12 equal to $2.8m_{\oplus}$ and $3.1m_{\oplus}$, their big orbit semi-axes amount to 0.17 A.U. and 0.36 A.U. Most probably, the planets are silicate or metallic. The third desired planet with period 25.34 days is metallic. The fourth planet with period 170 years is hydrogen-helium one.

There is a planet with mass more than $2m_{\oplus}$ and big orbit semi-axis $a = 7.3$ A.U. near pulsar PSRB 0329+54. Most probably the planet is icy or hydrogen-helium.

Temperatures of hydrogen-helium planets in range $200 \div 1500$ K increase thickness of their atmospheres and can't provide dissipation of atmosphere hydrogen. As result, there is a wide variety in optical properties of their atmospheres.

Sudarsky et. al. (2000) have proposed to segregate giant planets into four types, or classes. 'Jupiter' class ($T_{eff} \sim 150\text{K}$) planets have ammoniac clouds, for 'water' class ($T_{eff} \sim 250$ K) is specify predominance of condensed water. For planets 'without clouds' $T_{eff} \geq 350$ K. In fourth, 'high temperature' class ($T_{eff} \geq 900$ K) predominance of absorption by alkaline metals and by iron is specify.

References

- Abt H.A., Lavy S.G.: 1970, *Ap.J.Suppl.*, **30**, 273.
 Alexandrov Yu.V., Zakhozaj V.A.: 1980, *Astron. vestn.* **14**, 129.
 Alexandrov Yu.V., Zakhozaj V.A.: 1983a, *Astron. vestn.*, **17**, N2, 82.
 Alexandrov Yu.V., Zakhozaj V.A.: 1983b, *Astron. vestn.*, **17**, N3, 131.
 Alexandrov Yu.V., Zakhozaj V.A.: 1986, in: *Problemy poiska gizny vo Vselennoy*.-M. Nauka, 201p.
 Arzoumanian A., et al.: 1996, *A.S.P. Conf.Series*, **105**, 525.
 Beckwith S.V.W., Sargent A.I.: 1996, *Nature*, **383**, 139.
 Black D.C.:1980, *Space Science Rev.*, **25**, N1, 35.
 Branch D.:1976, *Ap.J.*, **210**, 392.
 Burrows A., Hubbard W.B., Lunine J.I., Liebert J.: 2001, preprint astro-ph/0103383.
 Cameron A.G.W., Pine M.R.: 1973, *Icarus*, **18**, 377.
 Charbonneau D., et al.: 2000, *Ap.J.*, **529**, 45.
 Demianski M., Proszynski M.: 1979, *Nature*, **282**, N 5737, 383.
 Deych A.N., Orlova O.N.: 1977, *A.Zh.*, **54**, 327.
 Deych A.N.: 1978, *Pis'ma v A.Zh.*, **4**, 95.
 Dole S.: 1970, *Icarus*, **13**, 500.
 Flirenskiy K.P. et al.: 1981, *Ocherki sravnitel'noy planetologii*.-M. Nauka, 328s.
 Gatewood G.D.: 1996, *B.A.A.S.*, **188**, 40.11.
 Gold T.:1975, in: "*Problema CETI*", ed. S.A.Kaplan. - M., Mir, 15.
 Greenstein J.L., Black D.: 1977, *NASA*, **SP-419**, 53.
 Heppenheimer T.A.: 1974, *Icarus*, **22**, 436.
 Hohlfeld R.G., Terzian Y.: 1977 *Icarus*, **30**, 598.
 Izobrazhenie s vysokim razresheniem protoplanetnogo diska, obrashayushegosya vokrug zvezdy, in: "*Fizika za Rubezhom*", ed. Danilov Yu.A.: 1986, Ser. A. -M., Mir, 240pp.
 Kalas P.: 1998, *Earth, Moon, Planets*, **81**, 27.
 Lippincott S.L.:1974, *Coll. Astron. Europ.*, Coimbra, Pino Torinese, Oct., 131.
 Moroz V.I.:1981, in: "*Problemy Poiska vnezemnich Tzivilizatsiy*". -M., Nauka 171.
 Niedzielski A.: 2001, *Urania*, **4**, 156.
 Perryman M.A.C.: 2000, *Preprint Rep. Prog. Phys.*, **31** May, 1.
Problema CETI (Svyaz' s vnezemnimy Tzivilizatsiyami), ed. Kaplan S.A.): 1975.- M, Mir, 352pp.
Problema Poiska vnezemnich Tzivilizatsiy: 1981.- M., Nauka, 264pp.
Problema Poiska Zhizni vo Vselennoy: 1986.- M., Nauka, 256pp.
 Rees M.J.: 1976, *M.N.R.A.S.*, **176**, N3, 483.
 Robinson L.J.: 1984, *Sky, Tel.*, Jan., 4.
 Ruzmaykina T.V.: 1981, *Pis'ma v A.Zh.*, **7**, 188.
 Shaht N.A.: 1984, *Pis'ma v A.Zh.*, **10**, 765.
 Shabanova T.: 1995, *Ap.J.*, **453**, 779.
 Sl'uta E.H., Voropaev S.A.: 1993, *Astron. vestn.*, **27**, N1, 71.
 Smith B., Terrile R.J.: 1984, *Science*, **226**, 1421.
 Sudarsky D., Burrows A., Pinto P.: 2000, *Ap.J.*, **538**, 885.
 Tarter J.: 1975, *Ph.D. thesis, Univ. Calif.*, Berkeley.
 van de Kamp P.: 1974, *A.J.*, **79**, N4, 491.
 van de Kamp P.: 1975, *A.J.*, **80**, N8, 658.
 van de Kamp P.: 1975, *A.R.A.A.*, **13**, 295.
 van de Kamp P.: 1982, *Vistas in Astron.*, **26**, 141.
 Weinberger A.J., et. al.: 1999, *Ap.J.*, **525**, 53.
 Wolszcan A.: 1994a, *Science*, **264**, 538.
 Wolszcan A.: 1994b, *As.Sp.Sci.*, **212**, 67.
 Wolszcan A.: 1997, *A.S.P. Conf.Ser.*, **119**, 135.
 Wolszcan A., Frail D.A.: 1992, *Nature*, **355**, 145.
 Zakhozaj V.A., Aleksandrov Yu.V.: 1981, *Tezisy vsesoyuzn. Symp SETI, Tallin"81"*.-Tallin, 27.
 Zakhozaj V.A., Ruzmaykina T.V.: 1986, *Astron. vestn.*, **20**, N2, 128.
 Zharkov B.N., Trubitzin B.P.: 1980, *Fizika planetnih Nedr.*- M., Nauka, 448pp.

PERIODICITY OF LUMINOSITY OF QUASARS AND GALAXIES AT COSMOLOGICAL SCALE

A.P. Miroshnichenko

Institute of Radio Astronomy of National Academy of Sciences,
Chervonopraporna St., 4, Kharkov, 61002, Ukraine,
mir@ira.kharkov.ua

ABSTRACT. We found the cosmological luminosity periodicity in decametric and optical ranges on basis of spectral analysis of luminosity distribution in quasar and galaxy samples. Comparison with known redshift periodicity for quasars and galaxies is made. Characteristic scales of luminosity periodicity are conformable to cell structure of the Universe and to activity recurrence of object nuclei.

Key words: quasar, galaxy, luminosity distribution, decametric range, cosmological luminosity periodicity, cell Universe structure, activity recurrence, synchrotron mechanism of radiation.

1. Introduction

G. Burbidge (1968) revealed the periodicity in redshift distribution of quasars. In following years number of authors confirmed the redshift periodicity of quasars, for example (Cowan 1969, Karlsson 1977). The periodicity of galaxy redshifts was found in 1990 (Broadhurst et al. 1990). Then the conclusion about connection of peaks in redshift distribution with cell Universe structure was made (Cohen et al. 1996).

In this paper the periodicity of luminosity distribution of quasars and galaxies is determined in decametric and optical ranges. The calculations are carried out within the framework of Friedmann world model with parameters $q_0 = 0.25$, $H_0 = 100 \text{ km/sMpc}$. We assume the synchrotron mechanism of radiation of object active nuclei in decametric and in optical ranges. Obtained estimations of characteristic parameters suppose connection of the cosmological luminosity periodicity both with cell large-scale structure of the Universe, and with recurrence of activity of galaxy nuclei and quasars.

2. Periodicity peaks of luminosity in decametric and optical ranges

During the lifetime of cosmic object an activity of its

nucleus may display the cyclic changes (activity recurrence). In this case the cosmological periodicity in the object luminosity distribution should be observed. For examination of our assumption we used the statistically complete samples of 114 galaxies and 69 quasars from the UTR-2 catalogue at 25 MHz with corresponding optical data (Miroshnichenko 1994). We considered luminosity distribution of quasars and galaxies upon the redshift, which indicated on possible periodicities both in decametric and in optical ranges. The subsample of powerful radiogalaxies (FRII-type) was examined separately.

We derived power spectra (periodograms) of sample luminosity distribution at 25 MHz and in optics for quasars and galaxies. Significant luminosity peaks, connected with certain values of redshifts, were revealed in this power spectra (significance levels are from 90% to 99%), as shown in Table 1.

Four from six peak values z_p , found by us for luminosity distributions in decametric and optical ranges, agree with results by other authors for object redshift distribution (Karlsson 1977, Broadhurst et al. 1990, Duari et al. 1992, Gwyn and Hartwick 1996). Moreover, positions of three peaks in the luminosity distribution in decametric range coincide with analogous values in optical range (see Table 1). Conformity of obtained values of z_p may be caused by the cell Universe structure.

3. Space and time scales of cosmological periodicity of quasar and galaxy luminosities

As follows from our data, the redshift values z_p , corresponding to periodicity peaks in luminosity distributions of quasars and galaxies in decametric and optical ranges, are from $z_p = 0.0125$ to $z_p = 2.222$. We assume, that revealed values z_p are multiple to the least from these, and determine space and time scales of the cosmological periodicity in object luminosity distribution.

The characteristic size r_p in object space distribu-

tion, associated with luminosity periodicity, is found at Friedmann Universe model with parameter $q_0 = 0.25$ and Hubble constant $H_0 = 100 \text{ km/sMpc}$ for $z_p = 0.0125$ as distance (Zeldovich and Novikov 1975) in comoving volume:

$$r_p = c \frac{q_0 z_p + (q_0 - 1)[(1 + 2q_0 z_p)^{1/2} - 1]}{H_0 q_0^2 (1 + z_p)} \quad (1)$$

It is received from (1), that $r_p = 40$ Mpc. This value of r_p is close to the characteristic size of galaxy supercluster. As we know, chains of these superclusters form the cell large-scale Universe structure, so the size of large-scale inhomogeneities in object distribution may be multiple to supercluster size. It should be noted, that galaxy clustering is described well by fractal distribution with dimension $D = 2$ at scale 20-30 Mpc (Amendola and Palladino 1999, Joyce et al. 1999). So, the estimation of value r_p conforms with data of other authors, concerning characteristic scale in space object distribution.

Let us consider, that quasar and galaxy distribution is inhomogeneous, that is fractal at the scale $r_p = 40$ Mpc, with the fractal dimension $D = 2$. Then we determine "correlation length" r_0 - the scale, at which the correlation function of object space distribution (in sphere by radius r) must be $\xi(r_0) = 1$ (Sylos Labini and Amendola 1996):

$$r_0 = [(3 - \gamma)/6]^{1/\gamma} r, \quad (2)$$

where $\gamma = 3 - D$. Hence, at $\gamma = 1$ and $r = r_p$ it is received, that $r_0 = 13.3$ Mpc. It is known, that values of "correlation length" for space distribution of objects are next: $r_0 = 6-10$ Mpc for galaxies and quasars, and $r_0 = 18$ Mpc for galaxy clusters (Peebles 1980). So, our estimation of value r_0 by value r_p is conformed with literature data.

We define the time scale, connected with obtained cosmological periodicity of luminosity from expression:

$$t_p = t - t_0 = -\frac{1}{H_0} [z - (1.5 + 0.5q_0)z^2], \quad (3)$$

where t, t_0 - is the cosmological time for epochs z and $z_0 = 0$ (our epoch), respectively (Zeldovich and Novikov 1975). At parameters $q_0 = 0.25$ and $H_0 = 100 \text{ km/sMpc}$ for $z = z_p = 0.0125$ it is obtained, that characteristic time of the cosmological periodicity of luminosity is equal $t_p = 1.2 \cdot 10^8$ years. This time scale allows an existense of the activity recurrence of galactic nuclei and quasars. The value t_p is close to period of galaxy rotation ($\simeq 2 \cdot 10^8$ years).

Also, the value t_p is conformed with estimations of the quasar stage duration ($10^7 - 10^8$ years) (Martini and Weinberg 2001, Haiman and Hui 2001). Besides, the obtained value t_p corresponds to the estimation of

time variation in relationship of dust and gas masses for spiral galaxies ($10^7 - 10^8$ years) (Hirashita 2000). This fact may be significant evidence of the activity recurrence of objects.

According to synchrotron mechanism of the object radiation (Kardashev 1962), positions of periodicity peaks of luminosity distributions in optical and decametric ranges may not coincide due to decrease of the time of synchrotron radiation decay t_d with increase of frequency:

$$t_d \simeq 340 B^{-3/2} \nu^{-1/2}, \quad (4)$$

where B - is magnetic field strength in source of radiation, that is, in object (μG), ν - is frequency (MHz), t_d - is in units 10^9 years. Let us estimate difference of the times of synchrotron radiation decay for the same relativistic electron ensemble in source in decametric and optical ranges. If the strength of magnetic field in the source is supposed be equal $B = 10^{-5}$ G, then the difference of corresponding times of synchrotron radiation decay (by formulae (4)) is: $\Delta t_d = 1.18 \cdot 10^8$ years at considered frequencies 25 MHz (decametric range) and $5.45 \cdot 10^8$ MHz (optical range). With assistance of expression (3) for Friedmann world model at $q_0 = 0.25$ and $H_0 = 100 \text{ km/sMpc}$, we found that given difference of times of synchrotron radiation decay corresponds to the redshift difference $\Delta z_d = 0.013$. Everybody can see, the analogous difference of radiation decay times is $\Delta t_d = 3.69 \cdot 10^9$ years at strength of magnetic field $B = 10^{-6}$ G, so the corresponding redshift difference is $\Delta z_d = 0.264$.

Thus, the difference in positions of corresponding luminosity peaks upon redshift may change from $\Delta z_d \simeq 0.01$ to $\Delta z_d \simeq 0.3$ in decametric and optical ranges. Inhomogeneities of magnetic field in sources, and different values of magnetic field strength in different objects of our sample may cause additional variations of the value Δz_d , that is incoincidence of corresponding luminosity peak positions observed in two frequency ranges.

4. Conclusion

Results of our examination for luminosity distribution of quasars and galaxies in decametric and optical ranges indicate on cosmological periodicity of luminosity of these objects with the time scale $\simeq 10^8$ years and the space scale $\simeq 40$ Mpc. We note the conformity in positions of peaks of luminosity periodicity and known redshift periodicity of quasars and galaxies. The accomplished analysis of luminosity periodicity in decametric and optical ranges allows to consider the cosmological periodicity of luminosity as evidence on cell Universe structure and on activity recurrence of objects.

Table 1: Values of redshifts z_p , corresponding to significant peaks in power spectra for luminosity distributions of galaxies and quasars.

Objects of samples	Decametric(25MHz) range	Optical range
Galaxies	0.200	0.0125
Galaxies FR II	0.192	0.048
Quasars	1.124	1.124
	2.222	2.222
		0.448
		0.224

References

- Amendola L., Palladino E.: 1999, *Astrophys. J.(Lett.)*, **514**, L1.
 Broadhurst T., Ellis R., Koo D., Szalay A.: 1990, *Nature*, **343**, 726.
 Burbidge G.: 1968, *Astrophys. J.(Lett.)*, **154**, L41.
 Cohen J., Cowie L., Hogg D. et al.: 1996, *Astrophys. J.(Lett.)*, **471**, L5.
 Cowan C.: 1969, *Nature*, **224**, 655.
 Duari D., Gupta P., Narlikar J.: 1992, *Astrophys. J.*, **384**, 35.
 Gwyn S., Hartwick F.: 1996, *Astrophys. J.(Lett.)*, **468**, L77.
 Haiman Z., Hui L.: 2001, *Astrophys. J.*, **547**, 27.
 Hirashita H.: 2000, *Astrophys. J.*, **531**, 693.
 Joyce M., Montuori M., Sylos Labini F.: 1999, *Astrophys. J.(Lett.)*, **514**, L5.
 Kardashev N.S.: 1962, *Astron. J.(Sov.)*, **39**, 393.
 Karlsson K.: 1977, *Astron. and Astrophys.*, **58**, 237.
 Martini P., Weinberg D.: 2001, *Astrophys. J.*, **547**, 12.
 Miroshnichenko A.P.: 1994, *Cinematics and Physics of Celestial Bodies*, **10**, 52.
 Peebles P.: 1980, *The large-scale structure of the Universe*, Princeton, Princeton University Press
 Sylos Labini F., Amendola L.: 1996, *Astrophys. J.(Lett.)*, **468**, L1.
 Zeldovich Ya. B., Novikov I.D.: 1975, *The structure and evolution of the Universe*, M., Nauka

GRAVITATIONAL LENSING BY GLOBULAR CLUSTERS. INFLUENCE OF MICROLENSING

A.V. Yushchenko¹, P.G. Niarchos², S. Terpan³, V. Manimanis²

¹Astronomical observatory, Odessa National University, Ukraine

65014, park Shevchenko, Odessa, Ukraine, *e-mail*: *yua@lens.tenet.odessa.ua*

²Department of Astrophysics, Astronomy and Mechanics, University of Athens, Greece

³Department of astronomy, Odessa National University, Ukraine

ABSTRACT. Quasar-galaxy associations can be explained as gravitational lensing by globular clusters, located in the halos of foreground galaxies. We propose new observational test for checking this hypothesis. We used SUPERCOSMOS sky survey to find overdensities of star-like sources with zero proper motions in the vicinities of foreground galaxies from CfA3 catalog. Preliminary results show that our hypothesis is true. We discuss the influence of microlensing on the results of observations. We made CCD VRI photometry on 1.22 meter telescope of Kryonerium observatory (Greece) to select extremely lensed objects around 6 galaxies.

Key words: quasi-stellar objects; galaxies: halos, gravitational lensing

1. Introduction

Quasar-galaxy associations is one of the most intriguing puzzles of modern astronomy. Arp (1968) was the first, who noticed it. There were a lot of papers, with possible explanations of Arp's objects. We must mention a series of Schneider's articles (from Schneider, 1988 to Bartelmann, Schneider, 1993). In these papers it had been shown that the gravitational lensing can be a good hypothesis for explanation of this phenomena. But the nature of objects which can act as gravitational lenses in this case was unknown.

In our previous papers (Baryshev et al., 1993, Yushchenko et al. 1998, Yushchenko & Raikov 1998) we proposed, that gravitational lensing by cores of globular clusters, dwarf galaxies or other middle mass objects (MMO) in the halos of foreground galaxies can be the reason of quasar-galaxy associations. We used Yakovlev et al. (1983) formulae for calculation of amplification of background objects by foreground objects with King's mass distribution, for example by globular clusters. Yushchenko et al. (1998) developed the software which permit to use these formulae for calculations of amplifications of extended sources. The ampli-

fication can reach 5-10 magnitudes for typical cases and QSO-galaxy associations can be explained by this effect. Baryshev & Ezova (1997) and Yushchenko (1999) proposed the observational tests for validation of this hypothesis.

Yushchenko (1999, 2000) showed that simple calculations of surface density of star-like sources around galaxies can be a good test. In these papers author predicted that surface density of star-like sources around foreground galaxies must be increased. Why?

Let us imagine, that Arp's objects are produced by gravitational amplification of distant sources by objects in the halos of foreground galaxies. It is well known that gravitational lensing can not strongly influence on the spectral properties of the sources. That is why spectral properties of distant sources must be similar to that of quasars. We must find the class of objects whose spectral properties are quit close to properties of QSO. Seyfert galaxies can be this type of objects. If Seyfert nuclei, amplified by globular clusters in the halos of foreground galaxies, are responsible for quasar-galaxy association, we must to point, that (usually) there are not only one globular cluster in the halo of the ordinary galaxy. There are near 10^2 or more globular clusters in the halo. And every cluster can amplify the background source by 5-10 magnitudes. If there are sufficient number of sources at high redshifts, the globular clusters will amplify these source. The result will be the increasing of surface density of star-like sources around foreground galaxies.

Star-like? Baryshev & Ezova (1997) and Yushchenko (1998) showed, that the angular size of extremely amplified images are equal to angular size of the core of the globular cluster. The angular size of the core of the globular cluster at redshift near 0.01 is near 0.05 arcseconds - it is a point-like source for optical telescope. The extremely high level of amplification will help us to detect the high redshift objects, but the structure of the images of these objects will be broke by gravitational lensing. That is why (in the first approach) we can receive only spectral and coordinate informa-

tion about extremely lensed objects (ELO). It will be very difficult to investigate internal structure of these objects.

Galaxies with z higher than 5 can be discovered now. For example Hu et al. (1999) found the galaxy with $z=5.74$, Yahata et al. (2000) identified near 4000 galaxies over the range in redshifts from 0 to 10 and beyond. That is why the big number of sources can exist, and they can be amplified due to gravitational lensing by globular clusters. The number of Seyfert galaxies is near 1% of the total number of galaxies. We must expect, that the surface density of extremely lensed objects must be two orders higher than the surface density of QSOs. The spectral properties of ELOs will be similar to that of ordinary galaxies with correction for redshift and evolution.

We wrote ordinary galaxies. But we have very little knowledge about the properties of objects at high redshifts. That is why it will be better to write that the spectral properties of ELOs will be the same as the spectral properties of unknown objects at high redshifts. The investigations of ELOs, will help us to learn more about the nature of the Universe at high redshifts.

Yushchenko (1999, 2000) showed that the expected overdensity exist. The USNOA2.0 catalog (Monet D. et al. 1998) was used as a catalog of star-like sources. The vicinities of 35862 galaxies with redshifts more than 3000 km/s from CfA3 catalog (Huchra et al., 1995) were investigated to find or reject overdensities. The well pronounced effect was found.

But one can point, that USNOA2.0 catalog contain only coordinate and magnitude information. There is no objects classification information in this catalog. That is why usual clustering of galaxies can strongly influence on surface densities, calculated with these data. To avoid contamination of the results by galaxy clustering we must use catalog with stellar/galaxy classification of the objects.

2. SUPERCOSMOS sky survey

SUPERCOSMOS sky survey (Hambly et al., 2001) is a digitization of photographic survey of the southern hemisphere obtained with 1-meter class Schmidt telescopes at two different epochs. It is full up to 21 magnitude. For each object this catalog contains classification of the object (star/galaxy), coordinates, magnitudes in three filters, proper motions and other information.

For testing of our hypothesis we used SUPERCOSMOS catalog as a catalog of star-like images. We selected from the catalog only star-like images with zero proper motions as a background images. We investigated the expected overdensity in the vicinities of more than 19 thousands galaxies from CfA3 catalog. We calculated the number densities of selected objects in

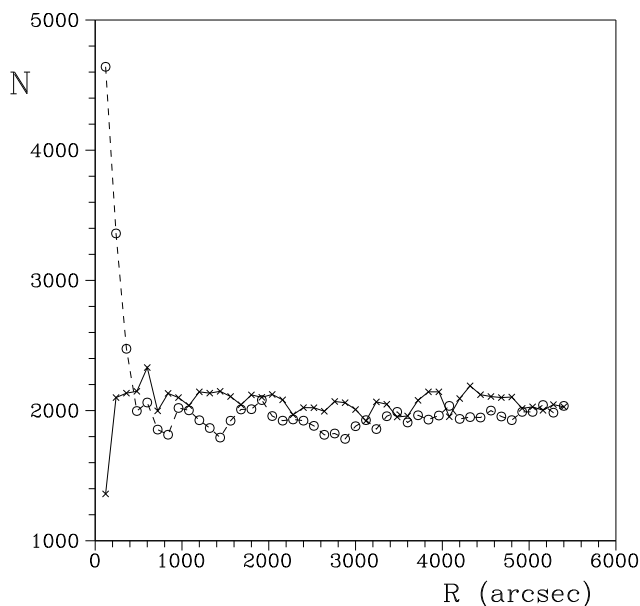


Figure 1: Surface density of star-like sources with zero proper motions in the vicinities of two groups of galaxies. The axes are the distance from the galaxy center in arcseconds and the surface density of investigated objects per square degree. Circles and dashed line - mean of 5 regions around galaxies with redshifts from 60,000 to 65,000 km/s. Crosses and solid line - mean of 5 regions around galaxies with redshifts from 5,000 to 6,000 km/s.

the concentric rings (the widths of the rings are 120 arcseconds) around each galaxy. The similar calculations were made for random centers. Random centers showed the zero overdensity.

Results for the regions with the galaxies in their centers are more interesting. As we have wrote, we expected to find overdensity of star-like sources with zero proper motions around galaxies. But it appeared, that the results are quit different for different groups of galaxies. We are able to show only preliminary results in this article. On the fig. 1 one can see mean results for two different groups of galaxies. The first group consist of 5 galaxies with redshifts from 60,000 to 65,000 km/s. The second group consist of 5 galaxies with redshifts from 5,000 to 6,000 km/s.

The expected overdensity is well detected for the first group of galaxies - for the galaxies with higher redshifts. The overdensity begins from the distance near 300 arcseconds from the galaxy centers. It corresponds to the linear distance near 1 Mpc from the galaxy centers. Globular clusters and dwarf galaxies can concentrate around host galaxy in the radii less than 1 Mpc and produce amplification of distant sources due to gravitational lensing. We expected to find this effect and we found it.

Now we discuss the second group of galaxies - the

galaxies with redshifts from 5 to 6 thousands km/s. We see no overdensity for these galaxies. We can see underdensity of the star-like objects with zero proper motions in the vicinities of these galaxies. We have wrote that these data are preliminary. But we can write that for all distant galaxies with redshifts less than, say, 20 thousands km/s we can observe underdensity, not overdensity. That is why we must point the reason of this underdensity.

We must also explain the reason of zero overdensity for foreground galaxies with redshifts more than 300,000 km/s. The results are also preliminary, but big number of galaxies permit us to claim that the final result will be changed insignificantly.

In all our previously cited papers we considered the properties of the globular clusters as gravitational lenses neglecting microlensing effects. Let us consider the influence of microlensing on amplification properties of globular clusters.

3. Microlensing?

Microlensing is the lensing by individual stars or planets. Now we will try to estimate the importance of this effect for our observations. The extremely high level of amplification of the MMO can be explained in the following way. All light rays from the source to the solid angle of the core of MMO will be focused near the observer. That is why the amplification can be estimated as the ratio of angular squares of the MMO's core and of the source. The typical diameter of the core of MMO is 10-50 pc, the size of emitting region of QSO can be of the order of 1 pc or less. The square ratio of these quantities give us the amplification coefficient from 10^2 to 10^4 or from 5 to 10 magnitudes. If we observe not overdensity, but underdensity of the objects, it means that above described effect is destroyed. How it can be destroyed?

Individual star in the core of MMO must produce its own Einstein ring. In the first approach all light beams from Einstein ring of the star will reach the observer. All light beams from the area inside the Einstein ring must be strongly declined and will not rich the observer. If the total square of Einstein rings of individual stars will be of the order of the square of the core of MMO, then all light beams from the source will be strongly declined and will pass beside the observer. That is why the amplification coefficient will be not very large. In this case it can be less than 1.0.

Let the typical radii of the core of MMO is 10 pc, the typical number of 0.2 solar mass stars within this radii is of the order of 10^5 . Let the sources distance is near 3000 Mpc.

For the first group of galaxies with z near 60,000 km/s we can estimate the linear radii of Einstein ring to be near 10^{-2} pc. The total square (the optical depth)

of 10^5 circles is near 10 pc^2 or near one tenth of the total square of the core of MMO.

For the second group of galaxies with z near 5,000 km/s we can estimate the linear radii of Einstein ring to be near $2 \cdot 10^{-3}$ pc. The total square of 10^5 circles is near 0.4 pc^2 or less than 10^{-2} of the total square of the core of MMO.

In both cases low massive stars can not strongly influence on the lensing properties of MMO. The optical depth due to microlensing by stars is small and we can neglect microlensing produced by stars if the redshift of MMO is less than 100,000 km/s. For foreground galaxies with higher redshifts the influence of microlensing by stars must be significant, The effect of overdensity of star-like objects around these galaxies can disappear.

We can see, that microlensing by stars can explain the zero overdensity of ELOs in the regions around foreground galaxies with redshifts more than 300,000 km/s.

We must to mention, that recently Sahu et al. (2001) pointed that the number of planets in globular cluster M22 can be 3 orders higher than the number of stars. Let us suppose that all globular clusters contain the similar number of planets. If we repeat previous calculations with 0.0002 solar mass objects and the number of these objects will be 10^8 we can obtain that the optical depth of the cluster will be increased by factor near 2.

That is why the optical depth of globular cluster with redshift higher than 60,000 km/s will be increased and it will be impossible to have a high level of amplification for clusters with significantly higher redshift.

It should be noted that de la Fuente Marcos and C. de la Fuente Marcos (2001) performed detailed numerical simulations and showed that the existence of a big number of the planets in the globular clusters is impossible.

In any case we can not neglect the microlensing produced by planets. Now we are preparing the software for direct calculation of influence of microlensing on the lensing properties of globular clusters.

4. How we can find ELOs?

For final testing of our hypothesis we must find several ELOs and measure their redshifts. Results, obtained from digitized photographic sky surveys can help us to find individual ELOs. ELOs are star-like objects with zero proper motions and with high redshifts. The spectra of ELOs must be similar to that of normal galaxies. We can not expect to observe emission lines in their spectra. We must search for ELOs in the vicinities of bright foreground galaxies. Usual two-color diagrams permit us to find objects with unusual colors. Spectra of these objects can be measured with big telescopes. With high probability objects with un-

usual colors can show cosmological redshifts in their spectra.

We observed the vicinities of six galaxies, namely A2046+1925, A2021+6127, A0051-0038, A2153+0109, A0008-0001 from CfA3 catalog. The 1.22 meter telescope at Kryonerion observatory, Greece, was used for VRI CCD photometry of regions around these galaxies. The redshifts of the galaxies are from 55000 to 78000 km/s. The full list of selected objects will be published later.

4. Conclusion

We predicted and found the overdensity of star-like images with zero proper motions (ELOs) around foreground galaxies. But it appears that this overdensity exist only for intermediate-redshift groups of galaxies. For galaxies with highest redshifts we observed the zero overdensity. For nearest galaxies we observe the negative overdensity - underdensity.

We are able to explain the observations for intermediate and high-redshift groups of galaxies. We have some difficulties with the nearest groups of galaxies. Now we are preparing software for direct calculation of imaging by globular clusters with full inclusion of all stars (planets?). The first results obtained with this software show, that it is possible that central image produced by globular cluster can be high amplified at intermediate redshifts, but degenerated at low redshifts. It can be a good explanation of observational data.

In the previous section of this paper we show a way for selection the individual ELOs. Spectral observations of preselected objects will be performed in the nearest time. We hope that at least part of these objects will show cosmological redshifts. It will be direct spectral confirmation of our hypothesis.

References

- Arp H. 1968, *ApJ*, **153**, L33
 Bartelmann M., Schneider P., 1993, *Astron. Astrophys.*, **271**, 421
 Baryshev Yu.V., Raikov A.A., Yushchenko A.V., 1993, in: Proc. of 31 Liege Astrophys. Coll. Gravitational lenses in the Universe, ed. J. Surdej (Liege, Belgium), 307
 Baryshev Yu.V., Ezova Yu.L., 1997, *AZh*, **41**, 436
 de la Fuente Marcos R., de la Fuente Marcos C., 2001, *Astron. Astrophys.*, **379**, 872
 Hu E.M., McMahon R.G., Cowie L.L., 1999, *ApJ*, **522**, L9
 Hambly N.C., MacGulliver H.T., Read M.A. et al., 2001, *MNRAS*, **326**, 1295
 Huchra J.P., Geller M.J., Clemens C.M., Tokarz S.P., Michel A., 1995, ADC CD ROM, Vol. 3
 Monet D. et al., 1998, USNOA2.0. A catalog of astrometric standards (CD edition)
 Sahu K.C., Kasertano S., Livio M., Gilliland R., Panagia N., Albrow M.D., Potter M., *Nature*, 2001, **411**, 1022
 Schneider P., 1987, *Astron. Astrophys.*, **179**, 71
 Yahata N., Lanzetta K.M., Fernandez-Soto A., Pascarella S.M., Chen H.-W., 2000, *American Astron. Soc. meeting*, **197**, 117.04
 Yakovlev D.G., Mitrofanov I.G., Levshakov S.A., Varshalovich D.A., 1983, *Astrophys. and Space Sci.*, **91**, 133
 Yushchenko A.V., Baryshev Yu.V., Raikov A.A., 1998, *Astron. Astrophys. Transactions*, **17**, 9
 Yushchenko A.V., Raikov A.A., 1998, in: Proc. of the II conf. Selected problems of astronomy and astrophysics, ed. I. Vakarchuk (Lviv, Ukraine), 204
 Yushchenko A.V., 1999, *Odessa Astron. Publ.*, **12**, 85
 Yushchenko A.V., 2000, *Kinematics and Physics of Selectial Bodies Suppl. Ser.*, **3**, 174

A STATISTICAL APPROACH TO THE INVESTIGATION OF MAGNETIC PROPERTIES OF MAIN SEQUENCE STARS

D.N. Monin, S.N. Fabrika, G.G. Valyavin

Special Astrophysical Observatory of the Russian AS
Nizhnij Arkhyz 369167, Russia, *mosha@sao.ru*

ABSTRACT. The results of a systematic magnetic survey of the brightest northern MS stars are presented. A homogeneous and representative sample of 30 upper MS stars was observed. Both fast and slow rotating normal and CP stars have been investigated by the same technique. A limit in accuracy of magnetic field measurements at a level of 10 G was reached for the stars with sharp lines in spectra. A statistical analysis of the magnetic field strength distribution of MS stars have been made. In the surface magnetic field range, $B_S = 0.1 \div 100$ kG, the distribution cannot be represented by a single power relation. There is a real break at $B_S \approx 3 - 5$ kG earlier suspected, and which cannot be explained by observational selections only. We discuss a possible mechanism of the break. The distribution of highly magnetic stars is represented by a power law. It was shown that normalization of the high-field part of the distribution could be obtained in the study of the low-field part where the probabilities of finding are much higher. The distribution of weakly magnetic stars is flat. It is very similar to that of magnetic white dwarfs. It has been determined that there are $7.2 \div 8.7$ % of MS stars with surface magnetic fields higher than 1 kG among MS stars of B8 \div F9 spectral classes.

Key words: Stars: Magnetic fields: Magnetic survey: Surface field strength distribution; stars: individual: χ Dra, α Aql.

1. Introduction

Magnetic fields can be found everywhere in the universe. The existence of a field was discovered in many types of stars having different evolutionary status: pre-main sequence stars, main sequence (MS) stars, subdwarfs and degenerate objects such as white dwarfs and neutron stars.

There is evidence that magnetic fields evolve during star's life (Glagolevskij 2001, Hubrig et al. 2000, Valyavin & Fabrika 1999). In studying general mag-

netic properties of stars which are at different stages one may hope to follow the magnetic fields evolution from protostar to degenerate object. It is believed that when MS star becomes a white dwarf, the field of degenerate remnant are thought to form from the field of its progenitor, MS star, by simple flux conservation. But it is not clear how the field is preserved during the convective giant phase. It can in principle be newly generated by dynamo processes or these processes can amplify initial field. To understand the ways of magnetic fields evolution after MS the general magnetic properties of both MS stars and white dwarfs should be analyzed and compared.

First statistical investigation of white dwarfs has been done by Angel et al. (1981). And latter their methods have been strongly improved by Fabrika et al. (1997) and Fabrika & Valyavin (1999).

Progenitors of white dwarfs, upper MS stars, show the presence of global magnetic fields. They has been definitely and repeatedly detected in two hundred MS stars, mainly chemically peculiar (CP) stars (Romanjuk 2000). Their longitudinal field strength are from a few 10^2 G to 10^4 G. But most of upper MS stars do not seem to have a magnetic field. For a few brightest stars with narrow spectral lines very high precision of measurements was obtained. Example of such data are field measurements of Procyon (Landstreet 1982), for which an uncertainty of 7 G was achieved. Only about 10 upper MS stars have been measured so far with error of less than 50 G (Wade et al. 2000). But for all that stars no field has been detected. Are they distinguished group of stars or their fields simply less than limit of measurements? Or may be they have complex field structure? How frequent are the magnetic stars? How many of stars are weakly magnetic? What is the limit of global field strength that may occur in MS stars? To answer all this questions one should analyse the distribution of magnetic fields of a sample of MS stars.

Based on all available longitudinal magnetic field measurements of upper MS stars Bychkov et al. (1997)

constructed such distribution. It reflects the ratio of stars having surface magnetic field in interval $B_S, B_S + \Delta B$ to the total number of stars. In logarithmic coordinates $\log(P_B) = \alpha \log(B_S) + const$ the distribution has been found to be almost linear in the range of surface fields $\approx 3 \cdot 10^3 - 3 \cdot 10^4$ G, the spectral index is $\alpha \approx -1.9$. Bychkov et al. (1997) pointed out that constant term *const* cannot be determined correctly. It means that the total number of stars in the sample is indefinite and the percentage of magnetic stars is unknown. The magnetic field measurements have so far been made basically in stars which are very likely to possess magnetic fields, sharp lined CP stars. These measurements are not homogeneous both in methods, accuracies and selection criteria. Authors do not always publish null results. Thus the sample cannot be considered as unbiased.

Bychkov et al. (1997) have also noted that the distribution can have a different behavior in the low-field part, where the surface field is less than a couple of kG.

2. The magnetic survey: uncertainties of measurements and promising candidates

We have started systematic magnetic survey of an unbiased sample of upper MS stars with high accuracy of measurements (Monin et al. 2000). The criteria for stars to be included in the sample are as follows:

- stellar magnitude $V \leq 4^m0$,
- luminosity class V,
- declination $\delta \geq 0^\circ$.

Our sample of 57 stars represents well MS stars in spectral classes B3 ÷ F9. Chemically peculiar stars are included in the list.

The magnetic survey is carried out on the coude echelle spectrograph CEGS of the 1 m telescope of the Special Astrophysical Observatory. The spectra were taken between March 1996 and June 2000. The total number of observed stars is 30. The uncertainty of B_l is varied from star to star and is mainly determined by signal-to-noise ratio, line contrast, and the number of simultaneously measured lines. We used weighted values of B_l . The weighting is made over the signal-to-noise ratio and central depth of lines. It improves the precision of field estimates up to factor 2. The measurements of slow rotating stars with a great number of measurable lines tend to be more precise. It appears that the smallest error which can be reached is 10 ÷ 15 G. The remnant instrumental effects which cannot be removed even by differential measurements lead to the precision limitation at the level of 10 G.

Except for 4 well known magnetic stars, ϵ UMa, θ Aur, α^2 CVn, β CrB, only two stars out of 30, χ Dra (F7V) and α Aql (A7V), have shown a global magnetic

field, which is slightly above the 3σ level. Simultaneous analysis of more than 500 metallic lines in the spectra of χ Dra gives $B_l = -45 \div -55 \pm 10 \div 15$ G. The field of the same strength is detected from the Zeeman broadening of the spectral lines. A search for magnetic field in the fast rotating stars is more difficult task. The accuracy is dependant on radial velocity. As compared with slow rotating stars having the same brightness, one needs to get better spectra quality (signal-to-noise ratio) to have similar accuracies. Among fast rotating stars being included in our list α Aql is the brightest one. The most accurate measurement of its field gives $B_l = 122 \pm 35$ G. It has been made using hydrogen lines only. The field is detected at 3.5σ level. Further time resolved spectropolarimetric observations are necessary to ascertain if longitudinal magnetic field variation is occur with a period of rotation. But the detailed study of any star in the list is beyond the scope of the present work. We conclude that χ Dra and α Aql are likely to possess a magnetic field. And they must be considered as promising candidates.

3. The magnetic field function

Using the results of the magnetic survey, all published high-accuracy observations of the brightest MS stars and the published data on highly magnetic stars, the magnetic field strength distribution of MS stars (the magnetic field function) have been constructed (Fig. ??).

The magnetic field function (MFF) is the probability of finding a star with a surface magnetic field in the interval $B_S, B_S + \Delta B$ per one G. Where measurements give B_l rather than surface fields, we take the limit on surface field to be three times of B_l (Angel et al. 1981). The probability can be evaluated as the ratio of the number of magnetic stars to the total number of stars observed with an accuracy which allows a magnetic field to be detected in the interval. And it is supposed to be constant within that interval. That intervals are arbitrary chosen. We propose they should be two-fold.

There is a probability of null detection of a longitudinal field because of the star rotation (Schmidt & Smith 1995; Fabrika & Valyavin 1999). We can miss magnetic star in isolated observation. The probability is independent of the rotational period because an observation falls within a random phase of rotation. It is determined by the accuracy of measurements and the field strength. We take into account the probability of null detection for each star. It reduces the probability of finding a star.

The sample of 57 stars was used to get the MFF in the range 60 G–8 kG. We obtained a field strength in 30 upper MS stars through our survey program. Let recall that two of them are supposed to be magnetic. 27 additional stars were studied by other authors, mainly

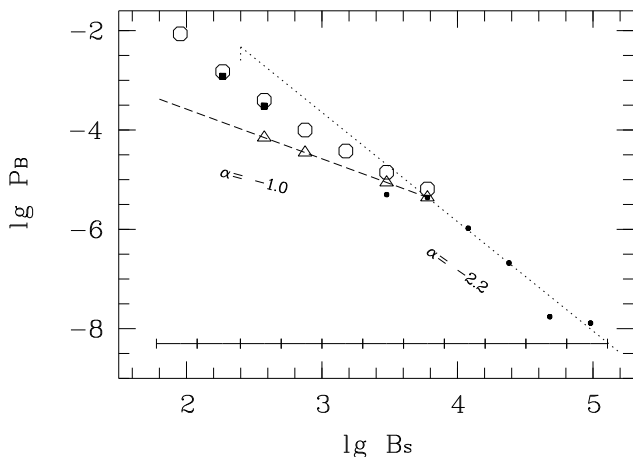


Figure 1: The MFF of the upper MS stars derived in 11 intervals of the surface magnetic fields. Horizontal bars below show the interval boundaries. *Open circles* and *open triangles* represent the upper and lower limits respectively. *Filled circles* correspond to stars whose a mean magnetic field modulus has been derived. The *dotted line* is the best fit power relation to the filled circles with index -2.2 . The line bends downwards where the total probability becomes equal to 1 (see text). The *dashed line* is the fit to the lower limits. The index is -1.0 . The *Filled squares* represent the probability in the 2nd and 3rd intervals supposing χ Dra and α Aql to be magnetic.

by Landstreet (1982). For the sample we can set the upper limits in the 6 low-field intervals (60 G–4 kG). Not all of stars from the target list of the survey have been studied so far. It may happen that some of them are magnetic. An upper limit value is proportional to $1 - \sqrt[n]{1 - Q}$, where n is a number of stars in the interval and Q is a significance level. Q was chosen to be 0.75. Such significance level is strong enough. There are 4 stars with well established magnetic fields in the list. They were used to derive the lower limits. The lower and upper limits in intervals 6 and 7 (2–8 kG) are close to each other and, obviously, to the true probability values. It is hardly probable that there are other strongly magnetic stars among brightest MS stars.

Measurements of mean magnetic field modulus of 49 stars with spectral lines resolved into magnetically split components form the high-field part of the distribution (B_S more than two kG). This data was taken from Mathys et al. (1997) and Romanyuk (2000) (filled circles in Fig. ??). We have a poor knowledge of the normalization factor in the high-field part because the way in which the magnetic stars are discovered is far from being systematic. The high and low-field parts are intersected in both the 6th and 7th intervals. Below a few kG the sensitivity of measurements of mean

magnetic field modulus is greatly reduced. So, in the 6th interval the frequency of magnetic stars is underestimated. We shifted the high-field part to bring it into coincidence with low-field one in the 7th interval. Thus, normalization factor of the high-field part of the distribution is obtained in the study of the low-field part where the probabilities of finding a magnetic star are much higher. Indeed, below 8 kG the star frequency exceeds 1/50. Therefore, it is necessary to observe a few tens stars to find a magnetic one. In high-field part the probabilities are lesser by two orders. So, one should observe about 1000 stars to discover one with a strong magnetic field. The precise measurements of weak fields in unbiased sample of stars give a possibility to analyse general magnetic properties in a wide range of surface fields.

In the surface magnetic field range, $B_S = 0.1 - 100$ kG, the magnetic field function cannot be represented by a single power relation. The distribution of highly magnetic stars is represented by a power law with index -2.2 ± 0.2 . We confirm the steep slope obtained previously by Bychkov et al. (1997). The distribution of weakly magnetic stars is flat, with index $-1.0 \div -1.3$. It is very similar to that of white dwarfs (Fabrika & Valyavin 1999). There is a real break at 3–5 kG earlier suspected by Preston (1971) and Mathys et al. (1997), and which cannot be explained by observational selections only. Behavior of the MFF in the low- and high-field parts is clearly different. Below a surface field 1 kG the density of motions energy of matter and the density of the thermal energy in the atmosphere of MS stars become higher than the density of energy of magnetic field. The global field configuration can become unstable. And a field can organize more complex structures. Such fields do not detect through Zeeman measurements. As a result the probability of finding a star decreases.

The total probability in whole range must equal to 1. It is not so if the index is -1. We suggest that the incidence of magnetism in the low-field part is somewhat large. In fact, if χ Dra and α Aql are magnetic, the probabilities in 2nd and 3rd intervals are significantly higher (see Fig. ??). With the index -1.3 the limiting field strength (where the total probability becomes 1) is approximately 1 G.

The total probability of finding a star with a field $B_S > 1$ kG among MS stars of B8 through F9 spectral classes is $7.2 \div 8.7\%$. There are about 205 MS stars brighter than 5^m0 on the northern sky. So, one may expect about 18 highly magnetic stars among them. 14 such stars are in the latest catalogue of magnetic chemically peculiar stars by Romanyuk (2000). One may hope to discover some others. Considering the incidence of the weak magnetic fields in MS stars, we find that every 5–6th star is expected to have a magnetic field in the range $B_S = 120 - 4000$ G.

4. Conclusion

The MFF is a powerful tool to diagnose general properties of stellar magnetism. A principal advantage of this method is a possibility to derive statistics of the data obtained in not systematic manner using measurements (which include null ones) of unbiased sample of stars. The distribution can be compared with those of other type stars, for example, white dwarfs to follow the magnetic field evolution. The essential result is the presence of the break in the MFF of upper MS stars. To understand its nature it is important to continue an extensive study of stars having a weak surface magnetic field. Do most of them really have complex magnetic field geometry?

In the future, we aim at completing the survey of bright upper MS stars of luminosity class V and do the same analysis for a sample of stars of luminosity class IV.

Acknowledgments. D.N. Monin and G.G. Valyavin thank for the travel support from the organizing committee of International Conference "VARIABLE STARS - 2001", Odessa, Ukraine. The work was supported by a grant of the Russian AS for young researchers (project N 8) and partly by the RFBR grant N 98-02-16554.

References

- Angel J.R.P., Borra E.F., Landstreet J.D.: 1981, *ApJS*, **45**, 457.
- Bychkov B.D., Monin D.N., Fabrika S.N., Valyavin G.G.: 1997, in: *Stellar magnetic fields*, eds. Yu.V. Glagolevskij, I.I. Romanyuk, Moskow, 124.
- Fabrika S.N., Shtol' V.G., Valyavin G.G., Bychkov V.D.: 1997, *Astronomy Letters*, **23**, 43.
- Fabrika S.N., Valyavin G.G.: 1999, in: *11th European Workshop on White Dwarfs, ASP Conference Series*, eds. J.-E. Solheim and E.G. Meistas, **169**, 214.
- Glagolevskij Yu.V., Chountonov G.A.: 2001, *Bull. Spec. Astrophys. Obs.*, **51**, 88.
- Hubrig S., North P., Mathys G.: 2000, *ApJ*, **539**, 352.
- Landstreet J.D.: 1982, *ApJ*, **258**, 639.
- Mathys G., Hubrig S., Landstreet J.D., Lanz T., Manfroid J.: 1997, *A&AS*, **123**, 353.
- Monin D.N., Fabrika S.N., Valyavin G.G., Barsukova E.A.: 2000, in: *Magnetic fields of chemically peculiar and related stars*, eds. Yu.V. Glagolevskij, I.I. Romanyuk, Moskow, 89.
- Preston G.W.: 1971, *ApJ*, **164**, 309.
- Romanyuk I.I.: 2000, in: *Magnetic fields of chemically peculiar and related stars*, eds. Yu.V. Glagolevskij, I.I. Romanyuk, Moskow, 18.
- Schmidt G.D., Smith P.S.: 1995, *ApJ*, **448**, 305.
- Valyavin G.G., Fabrika S.N.: 1999, in: *11th European Workshop on White Dwarfs, ASP Conference Series*, eds. S.-E. Solheim and E.G. Meistas, **169**, 206.
- Wade G.A., Donati J.-F., Landstreet J.D., Mathys G.: 2000, *MNRAS*, **313**, 823.

DIRECT MEASUREMENTS OF THE GENERAL MAGNETIC FIELD ON THE SOLAR-LIKE STARS

S.I. Plachinda¹, C.M. Johns-Krull², T.N. Tarasova³

¹ Crimean Astrophysical Observatory and Isaac Newton Institute of Chile, Crimean Branch Nauchny, 98409 Crimea, Ukraine, *plach@crao.crimea.ua*

² Space Sciences Laboratory, University of California Berkeley, CA 94720-7450 USA

³ Crimean Astrophysical Observatory and Isaac Newton Institute of Chile, Crimean Branch Nauchny, 98409 Crimea, Ukraine

ABSTRACT. We report the high-precision spectropolarimetric measurements of the general magnetic field (GMF) on a solar-like star 61 Cyg A. The magnetic field shows periodic variations due to stellar rotation with a period of $P_{mf} = 36.59 \pm 0.18$ days. The net longitudinal magnetic field of 61 Cyg A varied from -13 G to $+4$ G. The conclusion was made that the non-axisymmetric large-scale magnetic field (original magnetic field - OMF) on the surface of the Sun and solar-like stars ξ Boo A and 61 Cyg A is present in addition to toroidal and axisymmetric poloidal fields, which are produced by dynamo. The characteristics of the OMF point to a presence of a global magnetic field in the star radiative interior and reflect internal field properties on the surface. The birth and formation of magnetic active regions (ARs) on the surface of the solar-like star 61 Cyg A has been registered. The numerical simulations were compared with magnetic measurements, and lead us to the conclusion about the presence on 61 Cyg A of more strong magnetic fluxes of ARs ($\sim 10^{23} - 10^{24}$ Mx) than on the Sun. These ARs can be formed at the same latitudes as on the Sun.

Key words: Stars: late-type; stars: individual: 61 Cyg A, ξ Boo A, Sun; stars: magnetic fields.

1. Introduction

1.1. SUN

The Sun is the only star for which detailed observations with very high spatial and temporal resolution are available. The general magnetic field on the Sun, seen as a star (GMFS), is the surface-averaged value of the longitudinal component of small- and large-scale magnetic structures (Severny 1969; Scherrer et al. 1977; Kotov et al. 1998). Small-scale magnetic structures

are one manifestation of the large-scale, organized magnetic field on the Sun.

As we believed, there are two main components of the large-scale magnetic field on the Sun in terms of standard α - ω dynamo:

1). The magnetic field at the base of the convection zone of approximately toroidal geometry with a field strength in the range $(3-10) \times 10^4$ G and manifests itself when magnetic loops emerge on the surface in bipolar active regions. The latitude distribution of the toroidal field is mirrored by the observed active latitudes. In the northern and southern hemispheres of the Sun the directions of the azimuthal field components are reversed and the direction of these fields changes cyclically with a period of about 22 yr.

2). The second component of the large-scale field is an axisymmetric poloidal field (essentially a dipole) that also changes its polarity with a period of about 22 yr. The poloidal dipole reaches peak values of about 2-3 G on the surface of the Sun during minima of spot activity (see, for example, Zhang, Zirin, and Marquette 1997).

Variability of the GMFS with the synodic rotation period of 26.92 days is shown in Figure 1 (see Plachinda and Tarasova 2000). The average daily values of the GMFS from 1968 to 1997 ($N = 10838$ measurements) were kindly provided by Kotov V.A. and Haneychuk V.I. (1999, private communication). Results of GMFS observations obtained at three observatories (Crimean Astrophysical Observatory, 1968 – 1976; Mount Wilson Observatory, 1970 – 1982; Wilcox Solar Observatory of the Center for Space Science and Astrophysics of Stanford University, 1975 – 1997) were used as the basic data. The full rotation period is plotted twice on the X-axis. Filled circles are measured data binned into 16 bins, and error bars are rms errors above the binned means. One can see that during 29 years of observation of GMF of the Sun as a star, the excess of

the positive magnetic flux dominated on one side of the Sun, the excess of the negative flux dominated on the opposite side, and GMFS does not reverse its polarity with the 22 yr solar cycle period.

1.2. ξ Boo

The first observational study of the general magnetic field (GMF) as a function of rotation on a solar-like star other than the Sun was carried out for ξ Boo A (Sp G8 V) by Plachinda and Tarasova (2000). The magnetic field variations on ξ Boo A phased with the rotation period of 6.1455 days are represented in Figure 2 (see Plachinda and Tarasova 2000). Magnetic field measurements are in gauss and the total period is shown twice. The "X" shows the single measurement by Brown and Landstreet (1981), obtained with multislit magnetometer. Measurements obtained by Borra et al. (1984) using the multislit magnetometer are shown by filled triangles and by small open triangles as well. Measurements obtained with Stokesmeter by Hubrig et al. (1994) are shown by filled circles and by small open circles. Results of observations presented by Plachinda and Tarasova (2000) are shown by filled squares. Small open circles and triangles represent data that lie out of the supposed curve of magnetic field variations with rotational period. Bars are mean values of rms errors of every type of measurements. The GMF of the ξ Boo A varies from -10 G up to +30 G as a function of stellar rotation phase and the phase of the polarities has remained constant for about 16 yr. ξ Boo A is more young and more active solar-like dwarf than the Sun with variability of the Ca II emission but without clearly expressed solar-like periodicity of the activity (Baliunas et al. 1995).

1.3. 61 Cyg A

Cyg A were made at the Crimean Astrophysical Observatory and at the McDonald Observatory. This star has the same level of activity as the Sun and clearly expressed solar-like Ca II emission periodicity 7.3 yr (Baliunas et al. 1995). We find significant power in the magnetic field variations with a period equal to $P_{mf} = 36.59 \pm 0.18$ days. The rotational period P_{mf} , which determined using magnetic field measurements is smaller than the rotational period P_s determined using the variability of Ca II H and K line index S both for ξ Boo A ($P_s = 6.2$ and $P_{mf} = 6.1455$ days) and 61 Cyg A ($P_s = 37.9$ and $P_{mf} = 36.59$ days). Furthermore, for ξ Boo A Toner and Gray (1988) determined the period of 6.45 days from the variations in line asymmetries and temperature. We supposed that observed discrepancy in the values of the rotational periods for ξ Boo A and 61 Cyg A can be caused by differential rotation

of these stars. The magnetic field variations on 61 Cyg A phased with the rotation period are represented in Figure 3. Magnetic field measurements are in gauss and the total period is shown twice. Phases are calculated with a zero epoch at the positive extremum of the magnetic field: $HJD_{(max)} = 2,450,989.20 + 36.59 \pm 0.18$, where HJD is the Julian Date in the heliocentric coordinate system. Measurements obtained using 2.6-m Shajn telescope are shown by filled and open circles, and measurements obtained using 2.7-m Harlan J. Smith telescope are shown by filled and open squares. The filled down triangle shows the single measurement by Borra et al. (1984), obtained with multislit magnetometer. Single measurement obtained by Brown and Landstreet (1981) using the multislit magnetometer is shown by open up triangle. The measurements, which lie out of the fitting curve more than 3σ were single out by open signs. If deviations of the measurements from a curve in following night or in one-two nights exceeded 2σ they also were designated by open symbols. Dashed arrows connect progression of the observations in time for lie out points. The solid curve was obtained by least squares fitting numerical simulations for the filled signs. We used magnetic configuration that was produced by two centered magnetic dipoles: the axis of the first dipole coincides with rotation axis of the star (axisymmetric dipole) and axis of the second dipole lies in the plane of rotation equator of the star (nonaxisymmetric dipole). We do not know geometrical structure of a global magnetic field of this star therefore the values of both formal magnetic churches of the dipoles were taken equal each other (by analogy to the Sun, where magnitudes of the axisymmetric dipole and general magnetic field of the Sun as a star are close on values and varies in the range 0.2 - 3 G). For the case of such approximation conditions there is a unique solution for the angle between the rotation axis and the line of sight, $i = 52^\circ$, and for the polar strength of the field of both dipoles, $B_p = \pm 34$ G. The error in standard deviation of the magnetic field measurements (filled signs) concerning the fitting curve $\sigma = 1.9$ G. The best fitting curve in the case of modeling by one dipole is practically coincides with the found curve for two dipoles, but in the latter case $i = 33^\circ$, $B_p = \pm 60$ G and $\sigma = 1.9$ G.

These abovementioned high-precision spectropolarimetric measurements open up the question: *Whether GMF contains the third large-scale component of the common magnetic field on the Sun and solar-like stars or it is the surface-averaged value of the longitudinal component produced by presence of the toroidal and axisymmetric fields only?* In particularly, Plachinda and Tarasova (2000) hypothesized that the GMF is observed as a bicomponent magnetic field composed of a large-scale axisymmetric magnetic field and a large-scale nonaxisymmetric magnetic field. A possible contribution to the GMF by strong local magnetic fields

(manifestation on the star surface of the toroidal large-scale component) similar to solar active regions was not considered, because authors assumed the mutual cancellation of opposite polarities typically found in active regions.

2. General Magnetic Field

According to theoretical researches executed by Mestel (1967), Alfvén (1981), Rudiger and Kitchatinov (1977), Gough and McIntyre (1998), MacGregor and Charbonneau (1999), Schussler (1975), Parker (1981), Dudorov et al. (1989), and Kitchatinov, Jardine, and Cameron (2001) we can build following scenario:

1) a magnetic flux (primordial magnetic field) is captured from a protostellar cloud by the forming star;

2) pre-main sequence rotating fully convective star (Hayashi-phase) can drive hydromagnetic dynamos;

3) the dynamo-generating field is incorporating into the growing radiative core;

4) magnetic field of the radiative core is largest for an orientation normal to the rotation axis of the star (non-axisymmetric field); 5) Gough and McIntyre (1998): "...it seems unlikely that the rapidly oscillating field associated with the solar cycle would contribute significantly to the dynamics in the radiative zone, particularly in view of the 10^6 yr tachocline ventilation time" (stability of the internal magnetic field).

On the other hand, today we have measurements of the GMF for three solar-like star: Sun (observations average about 30 yr), ξ Boo A (observations average about 16 yr), and 61 Cyg A (observations average 2 yr). In all three cases nonaxisymmetric large-scale component of the field is present. For the Sun the reverse of the nonaxisymmetric field sign with activity cycle is absent. For ξ Boo A phases of GMF field variability also remained to be a constant without the reverse of the sign in contradiction to a non-periodic long-time variability of the Ca II emission. These coincidences on the one hand of abovementioned theoretical conclusions of different authors as well as results of their numerical simulations and on the other hand the observed data (the presence of the nonaxisymmetric large-scale field component and the absence of the sign reverse with periodicity of the activity (Sun) or with non-periodic time of the activity (ξ Boo A) allows us to make the assumption that the nonaxisymmetric large-scale component of GMF is really present and its characteristics point to a presence of a global magnetic field in the solar-like radiative interior and reflect internal field properties on the surface as well. We define the nonaxisymmetric large-scale component of GMF as the "origin magnetic field" (OMF), meaning that this field point to a presence of a global magnetic field in the solar-like star's radiative interior beneath the tachocline, reflect its properties on the surface of the star, and this field

can be initial magnetic field for hydromagnetic dynamo of solar-like stars. If nonaxisymmetric field is really a large-scale component then it is necessary for taking into account OMF both at modelling a dynamo and at an explanation of phenomena of activity. Kitchatinov, Jardine and Cameron (2001) assume that the presence of the nonaxisymmetric field rooted in the core may be the reason why the solar activity statistics lack axial symmetry. Besides, a superposition of the nonaxisymmetric field of internal origin with the toroidal field of the axisymmetric dynamo makes an enhanced field on the longitude region where both fields coincide in sign and it makes a decreased field where both ones have opposite signs (phenomenon of the active longitudes observed in solar and stellar activity (in the last case see Berdyugina and Tuominen (1998) and Korhonen et al. (1999)). Also the observed alteration of high and low activity cycles on the Sun is explained in terms of a weak internal magnetic field (Pudovkin and Benevolenskaya 1984).

3. Local Active Regions on the Surface of the 61 Cyg A

The greatest duration of observable magnetic disbalance on 61 Cyg A (see Figure 3) is only four days, while the period of rotation $P_{rot} = 36.59 \pm 0.18$ days. What is nature of these events? We have rejected the hypothesis of short-time variations of the GMF because we have not found real arguments for the benefit of such assumption. After numerical simulations, using the spots of the round form with dipole geometry of the magnetic field, we have rejected also the hypothesis about unipolar very big spot, which crossing the visible hemisphere of the star near the limb. It is not possible to approximate the observed behaviour of the longitudinal field component without rapid changing in time of dipole parameters. Additionally, the strength of such spot field must be 60,000-70,000 G. It not seems real, because for more active M dwarfs Saar and Linsky (1985), Saar (1994), and Johns-Krull and Valenti (1996) detected spot magnetic fields not exceeding 5 kG. Furthermore, Savanov and Savelyeva (1996) using Stenflo-Lindergen method detected spot magnetic fields for 61 Cyg A $B_f = 1300 \pm 250$ G, but f , filling factor, is unknown value.

Owing to the above we have assumed the following. Open circles and squares indicate the process of emergence in the atmosphere of a first "preceding" part of the active region (complex of the magnetic flux tubes of one sign), and after that, with a time lag, a second "following" part of the active region with opposite sign of flux that compensates registered disbalance of the observed magnetic field emerge on the surface. In other words, it is supposed that the birth (stage of the disbalance growth) and formation (stage of the disbalance

compensation) of magnetic active regions on the surface of the solar-like star 61 Cyg A has been registered. It does not seem impossible that the occurrence on the surface of one magnetic polarity outstrip another, and, in result, a balance of total magnetic flux on the surface can be broken for a short time. As we know for the Sun, first manifestation of a new bipolar active region in the solar atmosphere is the appearance of a small, compact and bright bipolar plages (Sheeley 1969). In different terms, an emerging flux region is caused by the emergence of the top of a loop bundle, shaped as a peaked arch, consisting of many magnetic flux tubes. It is meaning that areas of strong magnetic field of one sign are paired with strong, adjacent fields of the opposite sign during first manifestation of magnetic flux of new active region (AR) on the surface. In this case we can not register the disbalance of the magnetic flux because occur the mutual cancellation of opposite polarities, and therefore the GMF is registered only. What is necessary for receiving the observed short-time magnetic disbalance? One can supposed follow most simple scenario: 1) the rising magnetic loop (as complex of the magnetic flux tubes) must be broken off by motions of the matter and after that 2) the passage outside on a surface both arms of the magnetic loop with opposite signs should not be synchronous. Owing to the above the magnetohydrodynamic computation of the process of the magnetic flux tubes capture and avulsion by convective motions of the matter, as well as more detailed observations, are needed to build an actual picture of the observed disbalance events on the 61 Cyg A.

What parameters of AR on the surface of the 61 Cyg A are necessary to describe observed events of the disbalance? One can see there is no unambiguous solution because excessive number of free parameters: coordinates, magnetic flux, and size of area. Therefore the question needs to be restated: Whether there are solutions which would be relative to parameters (flux, size, and latitude) of ARs on the Sun? Such type question based on the general ideas today about analogies of processes of activity on the Sun and late-type stars, because we have a wealth of evidences for such analogies. Alekseev and Gershberg (1997) have successfully applied models of a zonal spottedness of G - K - M dwarfs in order to study the photometric rotational variability of these stars. The our numerical simulations were compared with magnetic measurements, and lead us to the conclusion about the presence on 61 Cyg A of more strong magnetic fluxes of ARs ($\sim 10^{23} - 10^{24}$ Mx) than on the Sun ($\sim 5 \times 10^{22}$ Mx). These ARs can be formed at the same latitudes as on the Sun.

4. Summary

1) The magnetic field on a solar-like star 61 Cyg A shows periodic variations due to stellar rotation with a

period of 36.59 days and varies from - 13 G to + 4 G.

2) The supposition that observed discrepancy in the values of the rotational periods for ξ Boo A and 61 Cyg A can be caused by differential rotation of these stars was made.

3) The conclusion was made that the nonaxisymmetric large-scale component on the surface of the Sun and solar-like stars ξ Boo A, and 61 Cyg A is present, in addition to toroidal and axisymmetric poloidal fields, which produced by dynamo. The characteristics of the OMF point to a presence of a global magnetic field in the stars radiative interior and reflect internal field properties on the surface.

4) The birth (stage of the magnetic disbalance growth) and formation (stage of the magnetic disbalance compensation) of magnetic active regions on the surface of the solar-like star 61 Cyg A has been registered. The occurrence on the surface of one magnetic polarity outstrips another, and, in result, a balance of total magnetic flux on the surface is broken for a time of the AR formation.

5) The conclusion about the opportunity of the presence on 61 Cyg A of more strong magnetic fluxes of active regions ($\sim 10^{23} - 10^{24}$ Mx) than on the Sun ($\sim 5 \times 10^{22}$ Mx), which can be formed at the same latitudes as on the Sun, was made.

Acknowledgements.

This research was supported in part of P.S.I. and T.T.N. by Ukraine State Fundamental Investigation Foundation grant 02.07/00300.

References

- Alekseev I.Yu., Gershberg R.E.: 1997, *Astron. Rep.*, **41**, 207
 Alfven H.: 1981, *Cosmic plasma*, Dordrecht et al., Reidel
 Baliunas S.L., et al.: 1995, *ApJ*, **438**, 269
 Berdyugina S.V., Tuominen I.: 1998, *As.Ap.*, **336**, 25
 Borra E.F., Edwards G., Mayor M.: 1984, *ApJ*, **284**, 211
 Brown D.N., Landstreet J.D.: 1981, *ApJ*, **246**, 899
 Dudorov A.E., Krivodubskij V.N., Ruzmaikina T.V., Ruzmaikin A.A.: 1989, *SvA*, **33**, 420
 Gough D.O., McIntyre M.E.: 1998, *Nature*, **394**, 755
 Hubrig S., Plachinda S.I., Hunsch M., Schroder K.-P.: 1994, *As.Ap.*, **291**, 890
 Johns-Krull C.M. and Valenti, J. A. 1996: *ApJ*, **459**, L95
 Kitchatinov L.L., Jardine M., Cameron A.C.: 2001, *As.Ap.*, **374**, 250
 Korhonen H., Berdyugina S.V., Hackman T., Duemmer R., Ilyin I.V., Tuominen I.: 1999, *As.Ap.*, **346**, 101

- Kotov V.A., Scherrer P.H., Howard R.F., Haneychuk V.I.: 1998, *ApJS*, **116**, 103
- McGregor K.B., Charbonneau P.: 1999, *ApJ*, **519**, 911
- Mestel L.: 1967, in *The magnetic and related stars*, Ed. R.C.Cameron, (Baltimore: Mono Book Corp.), 101
- Parker E.N.: 1981, *Geophys. Astrophys. Fluid Dyn.*, **18**, 175
- Plachinda S.I., Tarasova T.N.: 2000, *ApJ*, **533**, 1016
- Pudovkin M.I., Benevolenskaya E.E.: 1984, *SvA*, **28**, 458
- Rudiger G., Kitchatinov L.L.: 1977, *Astron. Nachr.*, **318**, 273
- Saar S.H.: 1994, IAU Symp. 154, *Infrared Solar Physics*, ed. D.M. Rabin et al., Dordrecht, Kluwer, 493
- Saar S.H., Linsky J.L.: 1985, *ApJ*, **299**, L47
- Savanov I.S. Savelyeva Y.Y.: 1996, *Astrofizika*, **39**, 5
- Scherrer P.H., Wilcox J.M., Svalgaard L., Duvall T.L., Dittmer P.H., Gustafson E.K.: 1977, *Sol. Phys.*, **54**, 353
- Schussler M.: 1975, *As.Ap.*, **38**, 263
- Severny A. B.: 1969, *Nature*, **224**, 53.
- Sheeley N.R.: 1969, *Sol.Phys.*, **9**, 347
- Zhang L.D., Zirin H., Marquette W.H.: 1997, *Sol. Phys.*, **175**, 59

MAGNETIC FIELDS OF ISOLATED NEUTRON STARS: EVIDENCE FOR DECAY

S.B. Popov, M.E. Prokhorov

Sternberg Astronomical Institute, Moscow State University,
Universitetskii pr. 13, Moscow 119899 Russia,
polar@sai.msu.ru; mystery@sai.msu.ru

ABSTRACT. We show, that different types of isolated neutron stars (INSs) show evidence in favor of magnetic field decay in these objects and discuss how observations of INSs can help to constrain models of field decay.

Key words: Stars: neutron, magnetic fields.

1. Introduction

Evolution of isolated stars of any type is much more simple in comparison with the case when the object is a member of a close binary system, where mass transfer takes place. That is why looking for some undetected process it is much better to search for it in a more simple isolated case.

In this short note we will speak about magnetic field decay (MFD) in neutron stars (NSs), see the paper by Kononkov and Geppert (2001) for recent calculations of MFD. Of course it is much more convenient to discuss this process in INSs, where there is no influence of strong accretion from the second companion.

In some details we will discuss anomalous X-ray pulsars (AXPs), soft gamma repeaters (SGR) and ROSAT INSs (RINSs). See for recent reviews on SGRs (Hurley 2000), AXPs — (Mereghetti 1999), RINSs — (Treves et al. 1999, Popov 2001). In the final section we briefly review indications of MFD in other types of INSs.

2. Soft gamma repeaters and anomalous X-ray pulsars: period clustering for magnetars

Most probably AXP and SGR are ultramagnetized INSs, so called *magnetars* (Duncan, Thompson 1992). The alternative hypothesis that these objects are young INSs accreting from a remnant (fall-back) disk meets difficulties (see Kaplan et al. 2001 and Duncan 2001 for a recent discussion on difficulties of both models).

The main feature of SGR and AXP which we are going to discuss here is period clustering: periods of all this objects are situated in a very narrow range 5–

12 s (see the table). This phenomenon can be easily explained by MFD. We follow here Colpi et al. (2000).

The authors discuss three main mechanisms of the MFD in magnetars (in normal NSs mechanisms can be different): ambipolar diffusion in the irrotational and solenoidal modes and the Hall cascade. For all three cases Colpi et al. calculate $p-\dot{p}$ diagrams.

They obtain that if the Hall cascade is the main working mechanism and if typical decaying time scale is $\sim 10^4$ years, then it is possible to explain the observed data. For these parameters INSs reach asymptotic periods, i.e. their spin rate is not changing significantly during their subsequent evolution. The period "remembers" the value it had before the magnetic field significantly decrease as far as spin-down rate is strongly dependent on the value of the magnetic field.

Note, that as far as during MFD the NS's crust is heated, this phenomenon is necessary to explain relatively strong thermal radiation of these sources.

3. Seven ROSAT INSs: old accretors or/and young coolers

Now we know seven RINSs (Treves et al. 1999, Zampieri et al. 2001). Their nature is not clear. They can be young cooling or old accreting INSs. For three of them spin periods are determined (see the table). In this section we will try to show, that in both alternative hypothesis it is necessary to introduce MFD.

3.1. Old accretors

Old low velocity INSs can reach accretion stage (see a recent review in Treves et al. 2000). In (Popov et al. 2000a,b) we calculated evolution of populations of INSs in order to explore relative numbers of INSs at different stages. One of the result is that without MFD it is impossible to explain the observed population of RINSs by old accretors.

Fitting parameters of decay it is possible to obtain necessary number of accretors. It is unexplored yet

Table 1: Periods of INs (from Mereghetti 1999, Hurley 2000, Treves et al. 2000, Zampieri et al. 2001)

Source	Type	Period, s
1E 1048-59.37	AXP	6.44
AX J1845-0258	AXP	6.97
1E 2259+586	AXP	6.98
4U 0142+61.5	AXP	8.69
RX J1708.49-400.90	AXP	11.00
1E 1841-045	AXP	11.77
SGR 1900+14	SGR	5.16
SGR 1627-41	SGR	6.41
SGR 1806-20	SGR	7.48
SGR 0526-66	SGR	8.1
1RXS J130848.6+212708	RINS	5.15
RX J0720.4-3125	RINS	8.37
RX J0420.0-5022	RINS	22.7

if it is possible to explain the observed $\log N - \log S$ distribution.

After the first period determination for RINS was announced (Haberl et al. 1996) two papers appeared, in which authors explained this period as a result of MFD in old accreting INS, (Wang 1997, Konenkov, Popov 1997).

The idea is the following. For such short periods and typical parameters of INs and interstellar medium accretion is not aloud. The only possibility is that the magnetic field is very low, $\sim 10^8$ G. If the NS was born with such field and typical period of a young NS (about 20 ms), then it is impossible to decrease spin period up to 8.4 s even in 10^{10} years! So, the INS should be born with "normal" pulsar parameters, and then magnetic field decays and the period again "remembers" the value, when the field was strong.

3.1.1 Constraints on magnetic field decay

If we assume, that accreting INS are really observed, then we can put limitations onto the models of MFD.

MFD can both increase and decrease number of accretors (Colpi et al. 1998, Livio et al. 1998, Popov et al. 2000a). In (Popov, Prokhorov 2000) we tried to estimate these limitations for exponential decay, $\mu = \mu_o \exp -t/t_d$, $\mu > \mu_b$. In this case we can discuss two parameters: time scale, t_d , and bottom magnetic moment, μ_b . The later is the value, when decay stops.

For typical "pulsar" parameters of NSs we find out that intermediate values of the bottom magnetic moment, $10^{28} \text{ Gcm}^3 < \mu_b < 10^{29.5} \text{ Gcm}^3$, and time scale, $10^7 \text{ yrs} < t_d < 10^8 \text{ yrs}$, are forbidden.

3.2. Young coolers

If we try to explain all observed RINSs as young cooling NSs, then we come to a conclusion, that $\log N - \log S$ distribution can not be explained without an assumption that the total number of INs is higher than the one derived from radiopulsar statistics at least locally in time ($< 10^7$ years) and space (< 300 pc around the Sun) or that the time, when an INS is still hot, is longer than it is assumed in standard models of NS cooling (Neuhauser, Trümper 1999, Popov et al. 2000b).

Such high rate of recent supernova explosions in the solar vicinity is in wonderful correspondence with recent results of computer simulations of the Local Bubble formation (Smith, Cox 2000, Maíz-Apellániz 2001). These authors argue, that it is necessary to have at least 3-6 recent ($< 10^7$ yrs) bursts in the region close to the Sun and the youngest explosion should appeared less than $< 10^6$ years ago. Other data (even geophysical!) also supports recent and close supernova explosions.

As far as it is necessary to introduce magnetars in order to explain periods of RINSs, we can also ask why relative fraction of ultramagnetized NS is so high among RINSs. The answer can be the following: due to MFD the crust of the INS is heated, and it can stay hot for a longer time. This effect is especially important for magnetars, that is why their fraction is so high.

3.3. ROSAT INs: mixed population?

As the nature of RINSs in unclear they can be not a one-type population, but a mixture of coolers and accretors.

It is very difficult to distinguish between cooling and accreting INs. The only case, about which most of scientists are sure that it is a cooler, is RX J185635-3754. For this object parallax, proper motion and many other characteristics are known (see Pons et al. 2001 for the latest information about this object).

$\log N - \log S$ calculations (Popov et al. 2000b) show, that it is nearly impossible to explain significant part of RINSs by accretors with constant field. Nobody made careful population synthesis for isolated accretors with MFD. Most probably it is possible to find parameters for which we can explain $\log N - \log S$ distribution with accretors with decayed magnetic field, but the exact answer should come from observations. Future observations of \dot{p} of RX J0720.4-3125, RBS1223 (1RXS J130848.6+212708) and RX J0420.0-5022 can provide direct evidence for field decay in INs and help to distinguish between two interpretations.

4. Discussion

Here we briefly discuss types of objects which are not described in details in previous sections.

Pfahl and Rappaport (2001) suggested, that some of dim X-ray sources in globular clusters can be old accreting INSs. In our paper (Popov, Prokhorov 2001a) we checked this possibility with a simple population synthesis model, and found, that results of calculations were not in contradiction with observations.

As far as no spin periods are observed for these objects one can suggest two hypothesis: very long spin periods (see for example Popov, Prokhorov 2001b for discussion about spin periods of old accreting INSs) or accretion onto significant part of the NS's surface due to small magnetic field (Popov, Prokhorov 2001a). Relatively low temperatures of dim X-ray sources suggest, that accretion proceeds not onto small polar caps, corresponding to fields $< 10^9$ G (such values of magnetic field can be reached in these extremely old objects due to MFD). It can be an indication, that between two hypothesis the second one is closer to reality.

It was suggested (Popov 1998), that a compact X-ray source inside the supernova remnant RCW 103 can be a relatively old accreting INS, and the remnant itself was produced by an explosion of the secondary component of a binary system. The object does not show any modulation of radiation on short time scales (which can correspond to spin period), but demonstrates flux variability on long time scale (years). It can be an indication of accretion onto very large polar caps, corresponding to low magnetic field ($< 10^9$ G). As far as such values are not typical for most part of known young NSs (i.e. radiopulsars), one can suggest, that magnetic field significantly decayed during the lifetime of the NS.

We conclude that different types of INSs show evidence for magnetic field decay.

Acknowledgments. We thank Monica Colpi, Roberto Turolla Aldo Treves and Denis Konenkov for discussions and Universities of Como, Padova and Milan for hospitality.

SP thanks University of Como for financial support.

MP also thanks the organizing committee for support of his participation in the conference.

This work was supported by grants of the RFBR 01-02-06265 and 01-15(02)-99310.

References

- Colpi M., Geppert U., Page D.: 2000, *Ap.J.*, **529**, L29.
 Colpi M., Turolla R., Zane S., Treves A.: 1998, *Ap.J.*, **501**, 252.
 Colpi M., Possenti A., Popov S.B., Pizzolato F.: 2001, in "Physics of Neutron Star Interiors", Eds.

- D. Blaschke, N.K. Glendenning, & A. Sedrakian (Springer-Verlag, Berlin), (astro-ph/0012394).
 Duncan R.C.: 2001, astro-ph/0106041.
 Duncan R.C., Thompson C.: 1992, *Ap.J.*, **392**, L9
 Haberl F., Pietsch W., Motch C., Buckley D.A.H.: 1996, *Circ. IAU*, no. 6445.
 Hurley K.: 2000, in "Gamma-ray Bursts", 5th Huntsville Symposium, Eds. R.M.Kippen, R.S.Malozzi, G.J.Fishman, published by American Institute of Physics, Melville, New York, p.763, astro-ph/9912061.
 Kaplan D.L., Kulkarni S.R., van Kerkwijk M.H., Rothschild R.E., Lingenfelter R.L.; Marsden D., Danner R., Murakami T.: 2001, *Ap. J.*, **556**, 399.
 Konenkov D.Yu., Popov S.B.: 1997, *Pisma Astron. Zh.*, **23**, 569.
 Konenkov D.Yu., Geppert U.: 2001, *MNRAS*, **325**, 426.
 Livio M., Xu C., Frank J.: 1998, *Ap.J.*, **492**, 298.
 Maíz-Apellániz J.: 2001, astro-ph/0108472.
 Mereghetti S.: 1999, astro-ph/9911252.
 Neuhäuser R., Trümper J.E.: 1999, *As. Ap.*, **343**, 151.
 Pfahl E., Rappaport S.: 2000, *Ap.J.*, **550**, 172, astro-ph/0009212.
 Pons J.A., Walter F.M., Lattimer J.M., Prakash M., Neuhäuser R., Penghui An: 2001, astro-ph/0107404.
 Popov S.B.: 1998, *As. Ap. Trans.*, **17**, 35, astro-ph/9708044.
 Popov S.B., Colpi M., Treves A., Turolla R., Lipunov V.M., Prokhorov M.E.: 2000a, *Ap.J.*, **530**, 896.
 Popov S.B., Colpi M., Prokhorov M.E., Treves A., Turolla R.: 2000b, *Ap.J.*, **544**, L53.
 Popov S.B., Prokhorov M.E.: 2000, *As. Ap.*, **357**, 164.
 Popov S.B., Prokhorov M.E.: 2001a, *As. Ap. Trans.* (accepted), astro-ph/0102201.
 Popov S.B., Prokhorov M.E.: 2001b, astro-ph/0108503.
 Popov S.B.: 2001, astro-ph/0101031.
 Smith R.K., Cox D.: 2000, *Ap. J. Supp.*, **134**, 283.
 Treves A., Turolla R., Zane S., Colpi M.: 2000, *Publ. Astron. Soc. Pac.*, **112**, 297.
 Wang J.C.L.: 1997, *Ap.J.* **486**, L119.
 Zampieri, L., Campana S., Turolla R., Chierigato M., Falomo R., Fugazza D., Moretti A., Treves A.: 2000, *As.Ap.* (accepted), astro-ph/0108456.

THE SYSTEM OF SECONDARY PERIODICITIES AND RESONANCES BASED ON β LYRAE MAGNETIC FIELD

M. Yu. Skulsky

Lviv Polytechnic National University, 12 Bandera st., Lviv 79013, Ukraine,
mysky@polynet.lviv.ua

ABSTRACT. Original integral interconsistent and interconnected magnetohydrodynamical system of periodicities and resonances over their long-time variabilities is developed. The study is based upon three different observed secondary periods in β Lyrae system and taking into account geometrical features of the non-standard magnetic field in a losing star, as well as due to the asynchronism of the orbital and rotational periods.

Key words: Stars: binary: cataclysmic; stars: individual: AM Her, TT Ari, BZ Cam.

1. Introduction

It should be recognized that after twenty years of magnetic field research of the β Lyrae system (Skulsky 1985, 1986, 1990; Skulsky and Plachinda, 1993) our comprehension of the subject appears to be insufficient. Existence of the losing star (hereafter, loser) as the magnetic rotator in an interacting close binary system should produce complex causal relationships and their detection could occur unexpectedly. Recently we have shown this with the example of the first stage of nature studies of the three mostly observable secondary periods in their detected relationship with the magnetic field geometry of the loser (Skulsky, 2000). To develop our ideas we present here certain results of further studies of nature of this phenomenon. Firstly, we will characterize these secondary periods and elaborate the matter of the issue.

2. To physics of observational second periods.

The first of these periods has a century-old prehistory of researching the long-term changes of the light curve. However, similar and reliable data concerning such changes in the shape of the light curve between its two extremes, namely with the duration of 240d and (275 \pm 20)d respectively, were presented in relatively recent studies by Alduseva and Kovalenko (1976) and Guinan, (1989). Yet, Van Hamme et al., 1995 found

the period of (283.39 \pm 0.26)d due to the deviations from 150 years-averaged light curves; and Harmanec et al., 1996 found the period of (282.425 \pm 0.070)d with the amplitude of $A=0.^m0326 \pm 0.^m0008$ with the similar procedure for the averaged light curve using the most accurate observations available over the last 36 years. Only then, was the secondary period of (283 \pm 1)d considered a fact. It was unclear why such a considerable difference (much more than 3σ) in 0.965d for the value of this period was obtained by the two groups of scientists, as well as the reasons of existence of this period itself and its physical nature.

The second of these periods, a much shorter one of 4.74d was given in Harmanec's et al. (1996) as well. This period is detected by the deviations from averaged curves of radial velocities of strong emission lines (which were obtained with the use of the most accurate available measurements along with our CCD-observations at the 2.6 m telescope - Skulsky and Malkov, 1992; Skulsky, 1993). They have assumed certain causal relationships between long- and short-term periods (let us denote them as T and T_1 respectively) and orbital period P, which is more conveniently to express analytically as:

$$T_1^{-1} = 3(P^{-1} - 2T^{-1}) \quad (1)$$

Trying to understand the nature of secondary periodicity, we have noticed (Skulsky, 2000) that the period T_1 in the scale of orbital cycle is almost in phase agreement with the first extremum of magnetic field of the loser. This was considered rather strange, since the third independently observed 1.85d secondary period (which is the seventh part of the orbital period) with high amplitude of variable parameter, which we had discovered earlier while performing the absolute spectrophotometry in the H_α a line (Burnashev and Skulsky, 1980), was also clearly revealed during observations of magnetic field strength at the loser surface (Skulsky, 1990; Kosovichev and Skulsky, 1990; Burnashev and Skulsky, 1991). Therefore, we had sufficient background to assume, that there could exist a certain causal relationships between these three observable secondary periods. This is more so if we take into

consideration the existing, already clear correlations of magnetic field strength curves with change curve the flux of radiation with phase in H_α a line, with the radial velocity curves of emission lines (Burnashev and Skulsky, 1991; Skulsky and Malkov, 1992; Skulsky, 1993).

Having analyzed the relationship between T_1 and T_2 , we presumed (Skulsky, 2000) that: there should exist yet another secondary period with the duration of $T_2 \cong T_1 + T/2$ in the β Lyrae system, which is physically similar to T_1 (it means period T_2 should be in phase coincidence with the second extremum of magnetic field of the loser, and periods T_1 and T_2 should reflect the magnetic field axis orientation); period T_2 should be determined by an equation similar to the (1) equation; long-term period T could arise as (analogue) the particular case of beating period for two much shorter paired periods T_1 and T_2 . This equation was found to be expressed as follows:

$$T_2^{-1} = P^{-1} + 4T^{-1} \quad (2)$$

Solving the system of equations (1) and (2) brings forth in the simple relationships

$$P = \frac{9T_1T_2}{3T_1 + 2T_2} \quad \text{and}$$

$$T = \frac{18T_1T_2}{3T_1 - 2T_2} = \frac{2T_1T_2P}{4T_1T_2 - P(T_1 + T_2)}, \quad (3)$$

which remind us of classical formulas for the resulting period and beating period of the oscillations with close periods:

$$T_{res} = \frac{2T_1T_2}{T_1 + T_2} \quad \text{and} \quad T_{bt} = \frac{T_1T_2}{T_2 - T_1}. \quad (4)$$

These relationships have confirmed our assumptions and their studies have led to the detection of several other periods. For example, more fully set of periods associated with the season of 1980, taking into account the variability of the orbital period (corresponding corrections were made in the equation (1) by Harmanec et al., 1996), is expressed as follows (Skulsky, 2000):

$$\begin{aligned} P &= 12.9355d, \\ T_1 &= 4.746634d, \\ T_2 &= 10.932617d, \\ T &= 282.42524d, \\ P_{bt} &= 2T = 564.85158d, \\ T_{res} &= 6.619338d, \\ P_{rot} &= P_{mag} = 2T_{res} = 13.238675d \end{aligned} \quad (5)$$

Finally, this has allowed us to make certain conclusions, most of them also presented in the paper of Skulsky, 2000:

1. Secondary periods of T_1 , T_2 and T are in the causal resonance interaction between each other and the orbital period.

2. When expressing T_1 and T_2 periods as the phase fractions of the orbital period their determinations is preset by the structure and geometry of magnetic field of the loser, and they are almost projections of magnetic field dipole axis to the orbital plane.

3. When rotational and magnetic periods of the loser rotation are equal, their values are $P_{rot} = P_{mag} = 2T_{res}$ (due to (4) formula T_{res} is resulting for periods T_1 and T_2 , which are strictly connected with the geometry of magnetic field of the loser), which exceed the orbital period by several percents, but then the beating period of the orbital and rotational periods of the loser is equal to $P_{bt} = 2T$ and is the fundamental one, and observations-based period T being its first harmonics, by its physical nature is a running tidal wave at the loser surface.

4. Difference in $\Delta T = 0.965d$ between T values, obtained by the deviations from averaged light curves by two groups of scientists Van Hamme et al., 1995 and Harmanec et al., 1996, is the consequence of variability of the orbital period and is caused by the observation sampling which were used for formation of these independent light curves (time difference of the efficient formation is equal to 60 years, and increment of the orbital period over these years is $\Delta P = 0.0131d$, which caused corresponding changes of related periods T_1 , T_2 and T ; in this case period $T = (282.425 \pm 0.070)d$ concerns the averaged light curve with the center in the season of 1980, and the period $T = (283.39 \pm 0.26)d$ – in the season of 1920 respectively.

3. Interconnected magnetohydrodynamical system of periodicities.

Therefore, yet before starting the present study, we already had the unconventional concepts about the nature of the observed secondary periods and even discovered three new periods T_2 , P_{rot} , P_{bt} , thus reaching a certain level of confirmation of the asynchronism of the loser. To the aggregate, conclusions made and the new set of periods claim also that there exists certain group of interconsistent periods in the β Lyrae system, with the pair of adjusted periods T_1 and T_2 being the basic one. This fact convinced us to perform a deeper study of the nature of secondary periodicity in the β Lyrae system, which was based on the following statements and predictions: there are two axes in the β Lyrae system (gravitational axis, passing through the centers of the both components, and magnetic axis of the loser),

which spatial location is considerably different along the phase of the orbital period, and this effects on the passing of physical processes in the system; the real magnetic field of the loser has a complex configuration and its magnetic axis could not be the straight line of the classic dipole, in particular, presented above set of the secondary periods could be considered as the result of about $\pm 0.01P$ discrepancy of T_1 and T_2 periods (as phase fractions of the orbital period), with the values of phase angles of the averaged axis of magnetic field dipole (due to the observations at the 6 m telescope and solution of averaged magnetic field strength curve, the field maximum and minimum are equal to $0.355P$ and $0.855P$ – Skulsky, 1990; Burnashev and Skulsky, 1991).

In other words, our predictions are based on the statement of non-standard magnetic field structure (one may predict its noticeable quadrupole component, loser asynchronism should be important here as well). This reinforces our assumption that the straight line passing through the loser center and phases of $0.355P$ and $0.855P$ of field maximum and minimum of the averaged magnetic field strength curve, is only an imaginary dipole axis, and the real magnetic field dipole is either a little curved or has some other deviations from a line (let us call it "broken dipole") and appears at the loser surface in another phases of the orbital cycle. However, it corresponds to the phase angles of the periods $T_1=4.746634d=0.366946P$ and $T_2=10.932617d=0.845164P$ (by the calculations for the light curve, presented by Harmanec et al., 1996, which we have centered for the season of 1980). In this case one may predict that the pair of adjusted periods T_1 and T_2 is not unique as well, and the group of already discovered periods should be the fragment of yet more full system of periods, which are in a causal relationship between each other. One of them should be the period of 1.85d which we had discovered earlier. It is also observed at the magnetic field strength curve of the loser.

These ideas are presented at the figure, where the loser and gainer are defined with the cross-section of their Roshe surface in the orbital plane. The magnetic field dipole axis of the loser (according to the solution of averaged magnetic field strength curve it passes along the phases of $0.355P$ and $0.855P$) is designated by the thin straight line H_α . Phase angles $0.367P$ and $0.845P$, which correspond to the periods T_1 and T_2 of the "broken dipole", are given with the thicker lines. Assuming that the direction of these lines corresponds to the direction of real magnetic field axis, which spatial location does not depend on the gravitational axis of the binary system, we see that the determination of T_1 and T_2 periods as the phase angles in relation to the gravitational axis is arbitrary. Such angles for example could be counted from the $0.5P$ phase also; one of them could be counted from the $0.0P$ phase and the

other one from the $0.5P$ phase or, vice versa. There are eight such variants of adjusted pairs of periods. We will present here only the results of the interaction of four of them. Let us denote as $T_{1,I}$ and $T_{2,I}$ the first variant of adjusted and paired periods which corresponds the set of periods (5). Another three variant II-IV are given in the table, and these pairs of adjusted periods according to the figure above are defined as follows: $T_{1,II}=0.5P-T_{1,I}$ and $T_{2,II}=P-T_{2,I}$; $T_{1,III}=T_{1,I}$ and $T_{2,III}=T_{2,I}-0.5P$; $T_{1,IV}=T_{2,I}$ and $T_{2,IV}=T_{1,I}+0.5P$. Values of three corresponding resulting periods $T_{res,I}$ are also given in the table, which are calculated from the formula (4) as well as the value of $T_{res,I}$.

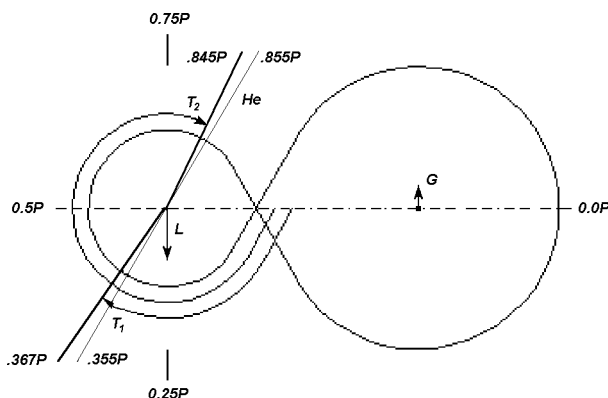


Figure 1: Sketch of the β Lyrae system.

II variant

$$\begin{aligned} T_{1,II} &= 1.721116d = 0.133054P \\ T_{2,II} &= 2.002883d = 0.154836P \\ T_{res,II} &= 1.851340d = 0.143121P \\ P/T_{res,II} &= 6.9871 \cong 7 \end{aligned}$$

III variant

$$\begin{aligned} T_{1,III} &= 4.74663d = 0.366946P \\ T_{2,III} &= 4.464867d = 0.345164P \\ T_{res,III} &= 4.601441d = 0.355722P \\ P/T_{res,III} &= 2.8111 \cong 14/5 \end{aligned}$$

IV variant

$$\begin{aligned} T_{1,IV} &= 10.932617d = 0.845164P \\ T_{2,IV} &= 11.214384d = 0.866946P \\ T_{res,IV} &= 11.071707d = 0.855916P \\ P/T_{res,IV} &= 1.1683 \cong 7/6 \end{aligned}$$

Looking at this table let us emphasize, firstly, interadjustment of resulting periods which are multiple with high accuracy to $(1/14)P$: $T_{res,II}/P=2/14$; $T_{res,III}/P=5/14$; $T_{res,IV}/P=12/14$. There are also very accurate resonance relationships: $3P_{bt} = 131P_{orb}$

$= 128P_{rot}$ or $11P = 30T_{1,I} = 13T_{2,I}$, and they are satisfied for the data of Van Hamme et al., 1995 as well as for the data of Harmanec et al., 1996, which averaged light curves are separated with the interval of 60 years. However, the next two results are much more important from the physical point of view. The first states the fact of coincidence of $T_{res,II}$ with the accuracy of 0.001d with the secondary period of 1.85d, which was firstly detected with high amplitude of variable parameter in absolute spectrophotometry of β Lyrae in H_{α} line (Burnashev and Skulsky, 1980) and was also clearly revealed during observations of magnetic field strength at the loser surface Skulsky, 1990. We can now state that all three observable secondary periods with the duration of 1.85d, 4.74d and 282.425d are causally interconnected. The second result fixes the coincidence of $T_{res,III}$ and $T_{res,IV}$ with the accuracy of 0.001P with the values of 0.355P and 0.855P of magnetic field extrema, obtained on the base of solution of averaged magnetic field strength curve, formed by the observations of 1980-1988 at the 6 m telescope – Skulsky, 1990; Burnashev and Skulsky, 1991. We can also state now that observed values of magnetic field extrema are averaged, but could be simply calculated if configuration of real magnetic field of the loser reminds the "broken dipole", i.e. it is not the field structure with classic dipole.

3. Conclusion

Main conclusion is that the loser as the component, which is at the final stage of intensive matter loss in the close binary system and at the same time as magnetic rotator of complicated configuration of magnetic field, produces a self-adjusted magnetohydrodynamic system of periods and resonances part of which has already been discovered from methodically different observa-

tions of β Lyrae. We see the theoretical background for this new phenomenon in the concepts of parametric resonance when the losing mass of magnetic rotator is a variable parameter. At the stage of active mass transfer to more massive satellite it leads to the observable increase of the orbital period and to the observable changes in the whole magnetohydrodynamic system of the secondary periods.

References

- Alduseva V.Ya., Kovalenko V.M.: 1976, In "Close binary systems and their evolution", *Publ. Moscow Univ.*, 195.
- Burnashev V.I. Skulsky M.Yu.: 1980, *Pis'ma in Astron. Zhurn.*, **6**, 587.
- Burnashev V.I., Skulsky M.Yu.: 1991, *Bull. Crim. Astrophys. Obs.*, **83**, 108.
- Guinan E.F.: 1989, *Space Sci. Rev.*, **50**, 35.
- Harmanec P. et al.: 1996, *As.Ap.* **312**, 879.
- Kosovichev A.G., Skulsky M.Yu.: 1990, *Pis'ma in Astron. Zhurn.*, **16**, 240.
- Skulsky M.Yu.: 1985, *Sov. Astron. Lett.*, **11**, 21.
- Skulsky M.Yu.: 1986, In "Upper Main Sequence Stars with Anomalous Abundances", *Utrecht, Coll. IAU N 90*, 365.
- Skulsky M.Yu.: 1990, *Mittelungen KSO Tautenberg*, **125**, 146.
- Skulsky M.Yu.: 1993, *Astron. Lett.*, **19**, 45.
- Skulsky M.Yu.: 2000, *Kinemat. and Phys. of Celestial Bodies, Suppl. Ser.*, **3**, 425.
- Skulsky M.Yu., Malkov Yu.F.: 1992, *Astron. Zhurn.*, **69**, 291.
- Skulsky M.Yu., Plachinda S.I.: 1993, *Astron. Lett.*, **19**, 203.
- Van Hamme W., Wilson R.E., Guinan E.F.: 1995, *Astron. J.*, **110**, 1350.

DETERMINATION of THE FUNDAMENTAL CHARACTERISTICS of COLD STARS

S.I.Belik, N.S.Komarov, A.V.Dragunova

Astronomical Observatory, Odessa National University
T.G.Shevchenko Park, Odessa 65014 Ukraine, *astro@paco.odessa.ua*

ABSTRACT. The effective temperatures, logarithms of surface gravities and parameters of metallicities $[Fe/H]$ for stars of spectral classes G and K from the list of the Odessa catalogue of energy distributions in spectra of stars 555 are received. The different grids of Kurucz models of atmospheres are used. The comparison of the received results is carried out.

Key words: Stars: cold stars: fundamental characteristics

Plenty of the catalogues of energy distributions in spectra of stars now are saved; the mechanisms of accounts of theoretical spectra of stars are developed on the basis of models of star atmospheres. All this represents an opportunity to lead search of fundamental parameters of atmospheres of stars, directly comparing theoretical flows with observable. We carried out the work in this direction in some stages.

Using the models of atmospheres (Kurucz, 1979, 1988, 1993) and the program for computation of the synthetic spectra of stars (Tsymbal, 1996), we have calculated synthetic flows for comparison with distributions of energy in spectra of cold stars. The observed flux distribution was taken from the catalogue by Komarov et al. (1995). The random errors of results of the catalogue are nearly equal to 2-3(to 5%) in the visual range of a spectrum and 5-10% at the edges of the spectral bands - near ultraviolet and near infrared regions. For reduction of time of accounts firstly we carried out calculations not on all observable area of a spectrum, but only in sites of width 10 nm in 7 characteristic points - in the "windows of a transparency" (Dragunova, 1996). Selecting model giving the best concurrence of a theoretical spectrum with observable, we received thus the values of T_{eff} , $\lg g$ and the metallicity parameter $[Fe/H]$. As a criterion of best agreement, the achievement of the minimal value of sum of modules of differences of compared sizes was considered.

Later, with occurrence of the calculated synthetic spectra (Kurucz, 1994) for a wide set of T_{eff} , $\lg g$ and $[Fe/H]$ values, we began to compare the theoretical flows with the observable spectra on all area, i.e. in 103 points (Belik, 1997; Komarov, 1999). We estimate

the accuracy of reception of temperature in 50, and $\lg g$ in 0.5, that is conditioned by a step of a grid of set parameters in theoretical spectra. The parameter of metallicity has appeared for the majority of stars close -1. For an exit from this situation we have carried out search of sites in spectra of stars sensitive to change $\lg g$ and $[Fe/H]$.

For the further work two wavelengths areas were chosen: 365 - 415 nm and 480 - 530 nm. The following stage of our searches of fundamental parameters became calculations under the following circuit: effective temperature is determined by comparison of distributions of energy in spectra of stars with the calculated spectra and selection of the most suitable theoretical spectrum with its values of T_{eff} , $\lg g$ and $[Fe/H]$; then with fixed T_{eff} also $[Fe/H]$ the closest theoretical spectrum is selected by a variation $\lg g$, but the comparison will be carried out in a narrow site of a spectrum from 480 to 530 nm; then with the already found and fixed values of T_{eff} and $\lg g$ the search of the most suitable theoretical flow on parameter $[Fe/H]$ is made in the range 365 - 415 nm. Control search $\lg g$ with new value of $[Fe/H]$ further will be carried out, and, if the meaning which is distinct from already turns out received the new cycle of searches is carried out.

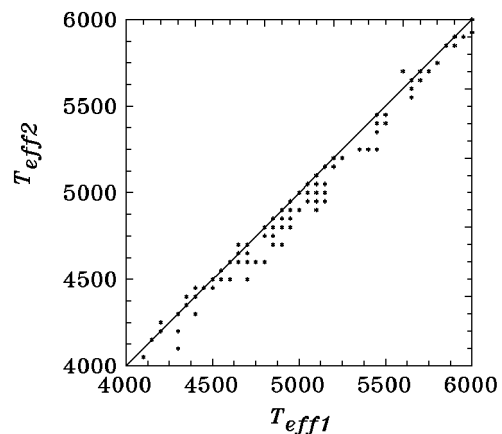


Figure 1: Comparison of temperatures, received on different model grids: T_{eff1} (old), T_{eff2} (new).

Table 1. The fundamental characteristics of stars.

HD	Sp	T_{eff}	$\lg g$	Fe/H	T_{eff}	$\lg g$	Fe/H	T_{eff}	$\lg g$	Fe/H	T_{eff}	$\lg g$	Fe/H
1	2	3	4	5	6	7	8	9	10	11	12	13	14
74	K2III				4670	2.1	0.09	4550	1.5	-0.5	4550	1	-0.5
163	G5III	4843	2.58	-0.67				5050	2.5	-0.5	5050	2.5	-0.5
		4950*	2.1*	-0.63*									
188	K0III				4995	2.6	0.01	4800	2.5	-0.5	4800	2	-0.5
219	G0V	5920	4.37	-0.3				5650	2.5	-0.5	5650	3.5	-0.5
265	G8-IV	4785	2.55	-0.75	4810	2.6	-0.49	4850	3	-0.5	4700	2.5	-0.5
		4800*	2.5*	-0.19*									
285	K2III				4600	2.1	0.07	4550	1.5	-1	4500	1	-1
456	G8II-III							4900	0	-1	4800	1	-1
489	K3III	4070	1.41	-0.27	4150	1.7	-0.13	4350	0.5	-1	4350	0.5	-1
509	G8V							5450	2	0	5400	3	-0.5
		5270*	4.2*	-0.56*									
510	K0III				4960	2.6	-0.22	5000	0	-0.5	4900	2	-0.5
660	G0V	5594						5700	4	-1	5650	5	-1
788	F9V							5950	4	-0.5	5900	5	-0.5
937	G4V	5944	4.08	0.03				5650	3	-0.5	5600	3	-0.5
941	K0III	5958	4.4	-2.01	5040	2.6	-0.03	5050	2.5	-0.5	5000	2.5	-0.5
1017	F5Ia							6000	1	-1	6000	1	-0.5
1030	G8III				5075	2.85	-0.23	5150	0	-1	5050	2.5	-0.5
1052	K3III				4130	1.7	-0.16	4300	1	-1	4300	1	-1
1136	K0IV							5100	4	-0.5	5050	3.5	-0.5
1311	G5III							5200	1.5	-0.5	5150	2	-0.5
1325	K0V							5250	4	-0.5	5200	4	-0.5
1346	K0III				5050	2.6	-0.03	4850	2.5	-0.5	4800	2.5	-0.5
1373	K0III				5070	2.65	0	5100	2.5	0	5100	2.5	-0.5
1409	G9III				5050	2.6	0.05	4950	3	-0.5	4950	3	-0.5
1454	G8II							4350	0.5	-1	4400	1	-1
1580	K2III				4515	2.15	-0.26	4650	2.5	-0.5	4600	2.5	-0.5
1601	K2II							4600	0.5	-0.5	4500	1	-1
1729	G0V	5840	4.16	0				5850	3.5	0	5850	4	0
1995	G8III				4960	2.7	-0.3	5100	0	-0.5	5100	0	-1
2012	K0III	4597	2.17	-0.1	4725	2.35	-0.06	4650	2	-0.5	4600	2.5	-1
2035	G8III				4725	2.55	-0.7	4800	3	-0.5	4800	2	-0.5
2047	G0V	5913	4.38	-0.02				5800	3.5	-0.5	5750	3	-1
2134	G5III							5000	3	-1	5000	2.5	-1
2473	G8Ib							4350	0.5	-1	4350	0.5	-1
2693	F8Ia							5650	0	-1	5650	0	-1
2985	G8III	4950	2.78	-0.08	5030	2.75	-0.17	5100	1	-0.5	4950	1	-0.5
2990	K0III	4850	2.71	-0.02	4950	2.6	-0.1	4950	0	-0.5	4850	1	-0.5
3323	G5III							5350	2	0	5250	2	-0.5
3547	K0III	4870	2.49	-0.01	4910	2.6	-0.18	4950	2.5	-0.5	4900	2.5	-0.5
3748	K3III				4185	1.7	0.02	4200	1.5	-1	4250	1.5	-1
3771	G2IV							5450	3.5	0	5250	3.5	-0.5
3873	G0II							5250	0	-1	5200	0	-1
3905	K2III	4511	2.32	0.3	4775	2	0.32	4350	1.5	-0.5	4350	2	-0.5
4166	G2II							5200	2	-0.5	5200	1.5	-0.5
4301	K0III				4945	2.6	-0.05	4700	1.5	-1	4700	1	-1
4418	G8II-III							4900	1	-0.5	4900	0.5	-0.5
4471	G9III				4845	2.6	-0.36	5050	0	0	5000	0	-0.5
4518	K0III	4360	1.62	-0.44	4430	2.2	-0.36	4600	1.5	-0.5	4500	2	-1
4527	G5III-IV							5650	0.5	-1	5550	0	-1

Table 1 (continued)

HD	Sp	T_{eff}	$\lg g$	Fe/H	T_{eff}	$\lg g$	Fe/H	T_{eff}	$\lg g$	Fe/H	T_{eff}	$\lg g$	Fe/H
1	2	3	4	5	6	7	8	9	10	11	12	13	14
4785	G0V	5887	4.39	-0.14				5750	2	-0.5	5700	2.5	-0.5
4932	G9III	5028	2.81	0.12	5105	2.75	-0.08	5200	0.5	-1	5200	3	0
4983	G0V	5979	4.34	0.01				5900	1.5	0	5900	2	0
5235	G0IV				6100	3.5		6000	3.5	0	5925	3.5	0
5315	K3III				4155	1.8	-0.3	4150	1	-1	4150	1	-1
5340	K2III				4250	2		4400	2.5	-1	4300	2	-1
5544	G8V							5200	4	-0.5	5200	4	-0.5
5601	K0III				4765	2.5	-0.26	4650	1	-1	4700	0.5	-1
5602	G8III				4950	2.7	-0.24	5150	3	-0.5	4950	2.5	-1
5616	K2III				4475	2.1	-0.13	4500	1.5	-0.5	4450	2	-1
5681	G8III				4835	2.6	-0.5	5000	0	-1	4900	0	-1
5787	G8-IV				4805	2.55	-0.42	4800	1.5	-0.5	4600	1.5	-1
5868	G0V							5900	3.5	0	5850	4	0
5889	G5-IV				5130	2.95	-0.5	5500	2	-0.5	5450	3	-0.5
5968	G2V							5500	4	-1	5400	3.5	-1
6075	G8III				4855	2.65	-0.34	4900	1.5	-0.5	4850	2	-1
6148	G8III	4967	2.62	-0.27	5000	2.8	-0.26	5150	0	-1	5000	0	-1
6212	G0IV	5793	3.77	0.03				5700	3.5	0	5700	4	0
6526	K4III				4120	1.6	-0.04	4300	2	-1	4200	1.5	-1
6623	G5IV	5518	3.87	0.19				5500	3	0	5400	3	-0.5
6695	K1III				4300	0.75		4600	0	-1	4600	0	-1
6698	K0III				4940	2.5	-0.08	4900	2.5	-0.5	4800	2.5	-0.5
6703	K0III	5011	2.71	0.09	5040	2.7	-0.17	5150	1.5	-0.5	5050	1.25	-1
6752	K0V	5094	5	-0.25				5100	4	-0.5	4900	4	-0.5
6770	G8-IV				4975	2.65	-0.18	5050	0	-1	5050	0	-1
6895	K2III				4580	2.1	-0.14	4700	2.5	-1	4500	2.5	-1
7063	G5II							4750	0	-1	4600	0	-1
7150	K1III				4820	2.4	-0.03	4700	2.5	-1	4600	2	-1
7176	K2III				4945	2.35	0.08	4850	2.5	-0.5	4750	2.5	-0.5
7193	K1III				4715	2.3	-0.14	4650	2	-1	4650	2	-1
7310	G9III	4818	2.54	-0.14	4835	2.6	-0.29	4950	0.5	-0.5	4800	1	-1
7314	K0II							4350	1.5	-1	4400	1.5	-1
7352	K3III				4480	2		4450	3	-1	4450	3	-1
7417	K3II							4400	2.5	-1	4400	2.5	-1
7478	G8III				5000	2.65	-0.1	5050	1	-0.5	4950	0	-1p
7479	G0II							5400	1.5	-0.5	5250	2.5	-0.5
7488	G8II				4800	2.7		4850	2	-1	4850	2	-1
7576	K3III				4350	2.25		4400	2.5	-1	4400	2.5	-1
7602	G8IV	5120	3.14	-0.08				5050	2	-0.5	5050	2.25	-0.5
7660	K1Ib							4700	1.5	-1	4600	1.25	-1
7685	K3III							4400	2.5	-1	4450	2.5	-1
7744	K3III				4210	1.7	-0.37	4100	1	-1	4050	1	-1
7747	G3Ib							4900	0	-1	4700	1	-1
7754	G9III				5005	2.65	-0.2	5100	3	-0.5	5000	3	-0.5
7796	F8Ib							5600	0.5	-0.5	5700	1	-0.5
7806	K3III				4275	1.75	-0.04	4150	1	-1	4150	1	-1
7896	G5IV	5513	3.54	-0.08				5450	3	-0.5	5450	3	-0.5
7949	K0III	4780	2.52	-0.12	4750	2.45	-0.32	4900	0.5	-0.5	4900	0	-0.5
8008	K4III				4110	1.5	0.02	4300	2	-1	4100	0.5	-1
8115	G8II	4945	2.49	0				5150	0	-1	5050	0	-1
8167	G8III	5129	2.74	-0.05	5045	2.8	-0.28	5150	2	-1	5050	1	-1
8232	G0Ib	5452	1.38	-0.04				5450	2.5	0	5350	0	-1
8308	K2Ib	4290	0.96	-0.07				4200	0	-1	4200	0.5	-1
8321	K0Ib							4400	0.5	-1	4450	0.5	-1

Table 1 (continued)

HD	Sp	T_{eff}	$\lg g$	Fe/H	T_{eff}	$\lg g$	Fe/H	T_{eff}	$\lg g$	Fe/H	T_{eff}	$\lg g$	Fe/H
1	2	3	4	5	6	7	8	9	10	11	12	13	14
8308	K2Ib	4290	0.96	-0.07				4200	0	-1	4200	0.5	-1
8321	K0Ib							4400	0.5	-1	4450	0.5	-1
8414	G2Ib	5246	1.32	0.18				5150	0	-0.5	5150	0	-0.5
8465	K1Ib							4150	1	-1	4150	1	-1
8538	G9III				4760	2.5	-0.4	4700	1.5	-1	4650	1.5	-1
8667	G8II-III	4775	2.47	-0.09				4850	0.5	-1	4850	0.25	-1
8684	K0III	4991	2.78	-0.09	4960	2.7	-0.31	5100	2.5	-0.5	4900	3	-1
8694	K1III	4748	2.35	0.01	4820	2.5	-0.12	4800	2.5	-1	4750	2	-1
8796	K0II							4500	2.5	-1	4500	2	-1
8812	K0III				4870	2.4	0.09	4500	2.5	-1	4500	2	-1
8852	G7III	4861	2.54	-0.44	4910	2.75	-0.52	4950	0.5	-0.5	4800	1.5	-1
8916	K1III				4815	2.4	-0.08	4800	3	-1	4800	3.5	-1
8923	G8III				5080	2.7	-0.1	4900	3	-1	4900	2.5	-1
8974	K1IV	4833	2.99	-0.01	4810	3		4900	3	0	4800	3.5	-0.5
9003	G5Ib							4600	2	-1	4600	2	-1

Later F.Castelli found out the mistakes in ATLAS9, and R.Kurucz has amended to the program and has presented the new convective models and flows (Kurucz, 1996) we have lead repeated definitions of parameters on new flows. The received results differ from former (Fig. 1) a little.

In the Table 1 the characteristics of stars found by various methods from different sources are given: in columns 3-5 from Cayrel de Strobel (2001), Mishenina (2001); in columns 6-8 from Korotina (1998); and also our old (columns 9-11) and new (columns 12-14) data . The undertaken attempt to improve accuracy of definition [Fe/H] has not resulted in success. Apparently, the technique, developed by us, can be applied to definition of temperature and tentative estimation $\lg g$ and [Fe/H]. The accuracy of definition can be increased if to use distributions of energy with a smaller step, at least, about 10 A, i.e. - with higher spectral resolution.

References

- Belik S.I., Dragunova A.V., Komarov N.S.: 1997, *Odessa Astron. Publ.*, **10**, 50.
- Cayrel de Strobel G., Soubiran C., Ralite N.: 2001, *As.Ap.*, (in press).
- Dragunova A.V., Belik S.I.: 1996, *Odessa Astron. Publ.*, **9**, 64.
- Komarov N.S., Belik S.I., Dragunova A.V.: 1999, *Kinematika i fizika nebesnykh tel*, **15**, N3, 215.
- Komarov N.S., Dragunova A.V., Belik S.I., Karamysh V.F., Zakozhurnikova N.N., Orlova L.F., Kantsen L.E., Cherkass A.G., Depenchuk E.A., Shevchuk T.V., Golubovskiy V.V.: 1995, *Odessa Astron. Publ.*, **8**, 115pp.
- Korotina L.V., Dragunova A.V., Komarov N.C.: 1989, *Astrofizika*, **31**, No.3, 539.
- Kurucz R.L.: 1979, *Ap. J. Suppl.*, **40**, 1.
- Kurucz R.L.: 1988, *Smithsonian Astrophys. Obs.*, Tape list.
- Kurucz R.L.: 1993, *CD-ROM SAO (Smithsonian Astrophys. Obs.)*, **13**, 18.
- Kurucz R.L.: 1994, *CD-ROM*, **19**.
- Kurucz R.L.: 1996, *CD-ROM*, **25**.
- Mishenina T.V., Kovtyukh V.V.: 2001, *As.Ap.*, **370**, 951.
- Tsymbal V.V.: 1996, *ASP Conf. Ser.*, **108**, 198.

THE ABUNDENCES OF NUCLIDES MAGNESIUM IN THE ATMOSPHERES OF ARCTURUS AND ALDEBARAN

T.I. Gorbanjeva, L.E. Kantzen, N.S. Komarov

SII "Astronomical observatory" Odessa National University
T.G. Shevchenko Park, Odessa 270014 Ukraine,
astro@paco.odessa.ua

ABSTRACT. The abundances of nuclides magnesium in the atmospheres of Arcturus and Aldebaran thick and thin disks of Galaxy have been studied. The stars have various chromospheric activity. We used the new data on molecular constants of radiation for every electrically-vibrationally-rotating line of molecular system $A^2\Pi-X^2\Sigma$ for MgH. The synthetic spectra were calculated. The values determined are generally close, but not equal, to the solar ratios.

Key words: Cool stars: abundances isotopes: individual: α Boo, α Tau.

1. Introduction

The determination of the contents of nuclides both with small, and with large nuclear numbers, is necessary for testing the processes of nuclear fusion and radioactive decay and theories of the stellar evolution. The contents of nuclides in the atmospheres of giant stars should vary during their own evolution and the chemical evolution of interstellar medium as a result: of Supernova and Nova outbursts, of the matter outflow from the outer layers of stars at various stages of their evolution. The nuclides

H/D, $^3\text{He}/^4\text{He}$, $^6\text{Li}/^7\text{Li}$, $^{12}\text{C}/^{13}\text{C}$
 $^{14}\text{N}/^{15}\text{N}$, $^{16}\text{O}/^{17}\text{O}/^{18}\text{O}$, $^{24}\text{Mg}/^{25}\text{Mg}/^{26}\text{Mg}$,
 $^{28}\text{Si}/^{29}\text{Si}/^{30}\text{Si}$, $^{35}\text{Cl}/^{37}\text{Cl}$,
 $^{40}\text{Ca}/^{42}\text{Ca}/^{43}\text{Ca}/^{44}\text{Ca}/^{46}\text{Ca}$,
 $^{46}\text{Ti}/^{47}\text{Ti}/^{48}\text{Ti}/^{49}\text{Ti}/^{50}\text{Ti}$,
 $^{90}\text{Zr}/^{91}\text{Zr}/^{92}\text{Zr}/^{94}\text{Zr}/^{96}\text{Zr}$

would be originated as a result of those or other nuclear processes (s and r-processes of neutron capture, processes of burning of hydrogen and helium in the cores of stars and in higher layers of stars, proton capture etc.), and, therefore, their ratios of their abundance can differ from the ones in the Solar system, including the terrestrial crust and the atmosphere of the Sun. The determination of the contents of these nuclides in the atmospheres of stars at different stages of evolution will help to test processes of nuclear fusion for transitions from the branch of dwarfs (main sequence -MS) to the red

giants branch (RGB), and, consequently, to the asymptotic giant branch (AGB). It is important for stars belonging to thin and thick disks of the Galaxy, which originated, a-priori, in different conditions. So the nuclides Mg could arise as a result of burning of carbon, or sequential caption of the α -particles, i.e. burning of helium. Tomkin and Lambert (1976, 1980) have shown, that ^{25}Mg and ^{26}Mg will be found as a result of burning of helium in the core of AGB stars and an outburst during a thermal pulsing, and ^{24}Mg - during carbon burning at the advanced stage of AGB. All three stable nuclides of Mg can arise during explosive burning of carbon. The MgAl and NeNa - cycles operate in the interior of MS stars. Their products are brought to the stellar atmospheres by convection after the transition to the RGB phase. The relations $^{24}\text{Mg}/^{25}\text{Mg}/^{26}\text{Mg}$ are 78.99/10.00/11.01 (de Bièvre and Barnes, 1985) for the Solar system or for the terrestrial crust and for the solar corona 76/12/12 (Wallace et al., 1999), respectively. The star Gumbridge 1840 (very old subdwarf with a small mass) has the contents of isotopes Mg within limits $^{24}\text{Mg}/^{25}\text{Mg}/^{26}\text{Mg} = (0.88-0.94) / (0.07-0.03) / (0.05-0.03)$ (Tomkin and Lambert, 1980). The contents ^{24}Mg for this star is possible can reach even 100 % (Mewaldt and Lambert, 1989). These relations of isotopes essentially differ from the relations in the Solar system and in the terrestrial crust. The role of those or other nuclear processes can be changed during evolution of galaxies. The content of nuclides of a magnesium in the atmospheres of Arcturus (thick disk) and of Aldebaran (thin disk) have been investigated.

2. The synthetic spectra

Komarov and Shevchuk (1995) have shown for a branch of the giants, that the partial pressure of molecules - hydrides does not vary almost along this branch from $T_{\text{eff}}=5000\text{K}$, $\log g = 3.0$ to $T_{\text{eff}}= 3500\text{K}$, $\log g = 0.75$ dex. The determination of the contents of isotopes of a magnesium on electronic - vibration - rotation lines of the molecule MgH will depend on

fundamental parameters of atmospheres of researched stars very weakly, and will depend on an accurate of molecular constants and on blending by other atomic and molecular absorption lines.

For a research of the contents of nuclides of a magnesium, the Atlases of spectra of Arcturus and Aldebaran with the resolutions 0.02 and 0.08 Å have been used, respectively. The synthetic spectra have been calculated using the programs by Tsymbal (1995), kindly given to our operation. The models of atmospheres were selected from the grid by Kurucz (1992, 1993) interpolated on fundamental parameters of stars. The fundamental parameters were taken from Komarov (1999) and are given in the Table 1.

Table 1: The characteristics of stars and abundances isotopes Mg.

*	T_{eff}	$\log g$	A_{Fe}	$^{24}\text{Mg}/^{25}\text{Mg}/^{26}\text{Mg}$
α Tau	3800	1.67	7.65	88:5:7
α Boo	4350	1.73	7.05	80:10:10

For two investigated stars of the input data, were took identical sets of absorption lines.

The relative content of the nuclides Mg was determined using the synthetic spectra. The oscillator strength were changed (analog change of contents of nuclides Mg) to get best agreement of observational and theoretical spectra. The comparison with theoretical spectra was made after convolution with the apparatus function. The apparatus function is assumed to be a Gaussian with a half-width equal to the spectral resolution of the spectrographs, using which the spectra of Arctur and Aldebaran were received. The check was conducted using the method of comparison of the observational and calculated contours of absorption lines of iron.

3. Conclusion

In Table 1, the main result is given. The differences in the relative contents of nuclides of a magnesium for cold giant stars of thin and thick disks of the Galaxy are within the limits of errors of their determination. For final conclusions, the study of the relative contents of nuclides of the magnesium, and nuclides of other elements, and for the greater number of stars - giants of thick and thin disks of a Galaxy, is necessary. As have been shown earlier, the processes of enrichment of atmospheres of stars by products of nuclear fusion (s-process) can happen at the stage of transition from the Main Sequence on the branch of the Giants.

References

- de Bierre P., Barnes I.L.: 1985, *Int. J. Mass Spectrum Ion Processes*, **65**, 211.
- Komarov N.S., Shevchuk T.V.: 1995, *Vienna, IAU Symposium N176: Stellar Surface Structure*, 223.
- Komarov N.S.: 1999, The cool giant stars. *Odessa, Astroprint*, 213p. (Rus.)
- Kurucz R.L.: 1992, *Rev.Mex.Astron.Astrofis.*, **23**, 181.
- Kurucz R.L.: 1993 CD-ROMs I-23 *Smithsonian Astrophys. Obs.*
- Mewaldt R.A., Lambert D.L.: 1989, *Astrophys. J.*, **337**, 959.
- Tomkin J., Lambert D.L.: 1976, *Astrophys. J.*, **208**, 436.
- Tomkin J., Lambert D.L.: 1980, *Astrophys. J.*, **235**, 436.
- Tsymbal V.V.: 1995, *ASP Conf. Ser.*, **108**, 198.
- Wallace L., Hinkle K., Li G., Bernath P.: 1999, *Astrophys. J.*, **524**, 454.

ABOUT THE HEAVY ELEMENTS ABUNDANCES IN THE ATMOSPHERES OF STARS WITH LOW METALLICITY

V.F. Gopka, A.V. Yushchenko, T.V. Mishenina, V.V. Kovtyukh

Astronomical Observatory, Odessa National University, Ukraine
Shevchenko Park, Odessa, 65014, Ukraine, *gopka@lens.tenet.odessa.ua*

ABSTRACT. We present results of preliminary determinations of abundances of heavy elements in three metal-poor stars: HD37828, HD44008, HD221170. Careful comparison of observed and synthetic spectra permit us to increase the number of lines heavy elements identified in observed spectra. Results will be used for determinations of the abundances of these elements with the spectrum synthesis method in these and other metal-poor stars.

Key words: nucleosynthesis; stars: abundances; stars: poor-metal; stars: individual: Arcturus, HD37828, HD44008, HD221170.

1. Introduction

The elements heavier than the iron peak are mainly produced through neutron capture reactions. Two main mechanisms are generally distinguished: the s-process (slow) and r-process (rapid), depending on the magnitude of the neutron flux available. Other mechanisms are p-process and α -process (Woosley, Hofman, 1992). The site of the r-process is explosive situations, such as those encountered in Type II supernovae seem to be required. The most popular site for the operation of the s-process is the thermally pulsing shell in intermediate mass asymptotic giant branch (AGB) stars.

Investigation of abundances of heavy elements in the atmospheres of old stars with low metal content is the direct method for detection of AGB stars, for testing the theories of stellar evolution and nucleosynthesis.

Table 1: Parameters of atmosphere models for Arcturus and program stars

Star	T_{eff} (K)	lg g	V_{micro} (km s ⁻¹)
Arcturus	4350	1.60	1.6
HD37828	4350	1.00	1.5
HD44007	4950	2.25	1.5
HD221170	4500	1.00	1.5

The comparison of chemical composition of stars of different populations is very interesting because of the

information about the process of chemical enrichment during early stages of Galaxy formation.

2. Observations

In this work we report the preliminary results of determination of chemical composition of Arcturus-like red-giants stars with low metallicity: HD37828, HD44008 and HD221170. Spectra of these stars were selected from a library of high-resolution stellar spectra (Soubiran et al., 1998). The spectra of the library were obtained with the echelle spectrograph ELODIE attached to the 1.93 m telescope at the Haute-Provence, France. The spectra cover the spectral range 4400–6800 Å, resolving power was $R=42000$, signal to noise ratio was about $S/N=100$ and higher. Wavelength calibration, continuum fitting and other preliminary data reduction were made by Mishenina & Kovtyukh (2001).

Griffin (1968) Atlas of Arcturus spectrum and Delbouille et al. (1973) Atlas of the spectrum of the center of solar disk were used as a spectra of comparison stars. The resolving power of these Atlases are $R=150000$ and $R=500000$, signal to noise ratio are $R=100$ and more than one thousand respectively.

3. Methodics

The abundance analysis needs little description. It is based on technique of synthetic spectra and comparison of synthetic spectrum with observed one. We calculated the synthetic spectra of Arcturus, Sun and program stars in the wavelength region covered by observed spectra using Kurucz (1995) SYNTHE program. Synthesis was performed taking into account all possible blending by atomic and molecular lines with measured wavelengths and oscillator strengths from Kurucz (1995) database (CD-ROMs 1, 15, 18, 23). We used also new data from VALD database (Piskunov et al., 1995) and recently published Morton (2000) data.

The values of abundances of elements were adopted from previous investigations of the stars (see Mishenina

Table 2: Abundances of heavy elements in Arcturus and three metal-poor stars

Z	Element	Arcturus (Griffin)		Arcturus (ELODIE)		HD37828		HD44007		HD221070	
		$\Delta\lg A$	N	$\Delta\lg A$	N	$\Delta\lg A$	N	$\Delta\lg A$	N	$\Delta\lg A$	N
30	Zn I	-0.83	3	-0.92	1	-1.33	4	-1.45	3	-1.97	3
38	Sr I	-0.63	4	-0.83	1	-1.35	2	-1.61	1	-1.62	3
39	Y I	-0.79	3			-1.43	2	-1.26	1		
	Y II	-0.72	15	-0.64	6	-1.47	7	-1.46	12	-2.22	7
40	Zr I	-0.65	17	-0.63	9	-1.21	9			-1.80	3
	Zr II					-1.33	3			-1.84	3
41	Nb I									-2.02	1
42	Mo I	-0.45	2	-0.51	1	-1.04	1	-1.10	1		
44	Ru I	-0.62	1	-0.65	1	-1.20	1				
56	Ba II	-0.72	2			-1.40	2				
57	La II	-0.68	11	-0.71	9	-1.44	10	-1.46	7	-1.99	8
58	Ce II	-0.69	22	-0.68	14	-1.32	15	-1.52	7	-1.83	11
59	Pr II			-0.83	2	-1.63	3	-1.34	1	-1.86	1
60	Nd II	-0.49	25	-0.50	19	-1.20	20	-1.20	12	-1.74	10
62	Sm II	-0.51	20	-0.52	9	-1.27	9	-1.25	23	-1.82	9
63	Eu II	-0.41	2	-0.41	1	-1.50	2	-0.99	1	-1.40	1
64	Gd II	-0.62	2	-0.31	1	-1.57	2	-1.21	1		
66	Dy II	-0.37	1							-1.46	1
68	Er II	-0.36	1							-1.25	1
74	W I	-0.82	1							-2.29	1

& Kovtyukh (2001) and references there in). Careful comparison of calculated and observed spectra permit us to identify the lines of heavy elements. URAN software (Yushchenko, 1998) was used for screening the observing and synthetic spectra of program and comparison stars simultaneously in any desired scale. This methodics permit us to minimize the number of errors in the identifications of faint spectral lines and to find new lines of heavy elements in the spectra of program stars.

Determination of equivalent widths was made with URAN software (Yushchenko, 1998). Fig. 1 show the comparison of equivalent widths of heavy elements obtained from the two spectra of Arcturus - Griffin's atlas and ELODIE spectrum.

The overabundance of lanthanides (with respect to iron) in the atmosphere of HD221170 was detected without difficulties. As an example on Fig. 2 we show an example of the spectra of Arcturus and HD221170 in the vicinity of Nd II λ 5291.815 Å and Fe I λ 5320.039 Å lines. The Fe line can be detected only in the spectrum of Arcturus, while the Nd line is well detected in both spectra.

The used parameters of atmosphere models were determined by Mishenina & Kovtyukh (2001) and can be found in Table 1. Abundances of selected heavy elements were derived using WIDTH9 code (Kurucz, 1995).

4. Results

The mean values of abundances of heavy elements derived for Arcturus and program stars can be found in Tab. 2. In this table one can found the relative abundances with respect to the solar values and number of lines, used for determination of abundance of investigated heavy elements.

The difference in abundances of heavy elements in the atmosphere of Arcturus, obtained from spectra with different resolving power (Griffin's atlas and ELODIE spectrum) is quite little. The are no big systematic trends in determinations of equivalent widths (see Fig. 1) and, respectively, in calculated abundances.

The abundance patterns for HD37828 and HD44007 are similar to that of Arcturus, shifted approximately by -0.9 dex (see Fig. 3). The abundances of heavy elements in HD221170 is different from scaled Arcturus and solar patterns. The abundances of heavy lanthanides in the atmosphere of this star show large overabundance with respect to iron (see Fig. 4). The overabundance reach 0.8 dex for erbium.

5. Conclusion

We made a detailed analysis of abundance of heavy elements in the atmospheres of three stars with low metal

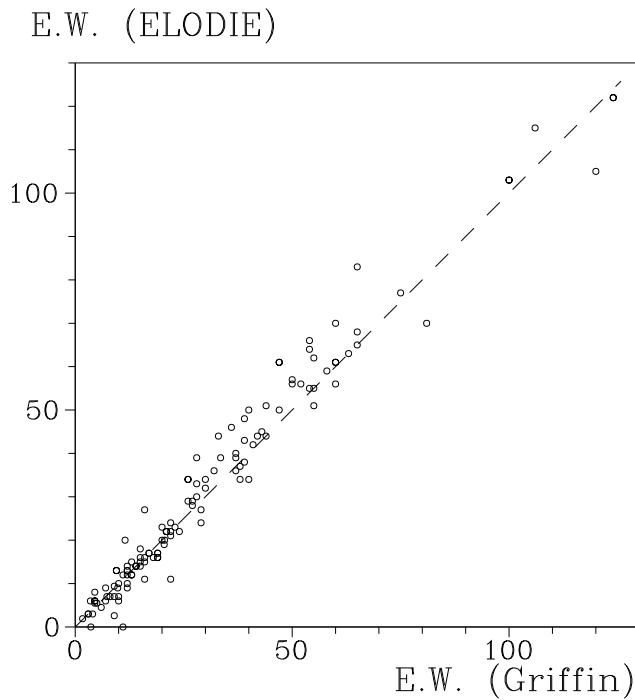


Figure 1: The comparison of equivalent widths of heavy elements measured in the Atlas of the spectrum of Arcturus (Griffin, 1968) and in the ELODIE spectrum of the Arcturus.

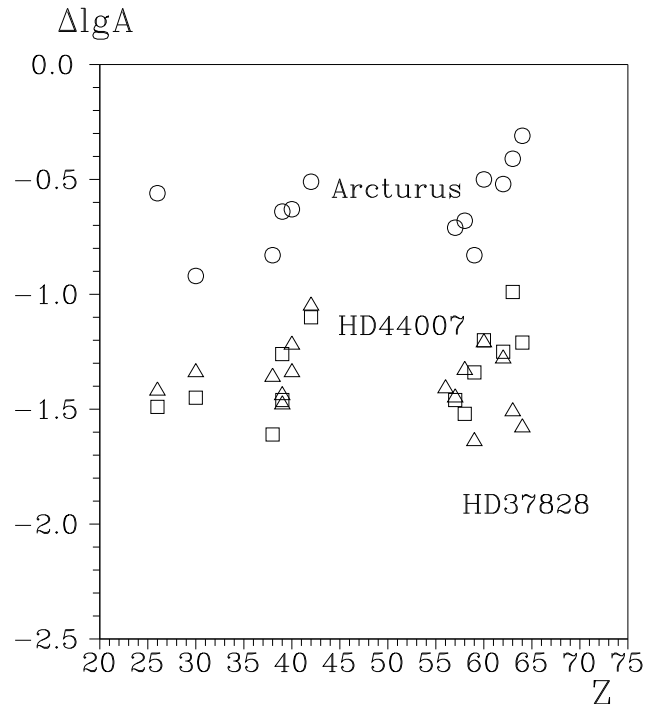


Figure 3: Relative abundances (with respect to the Sun) of iron and heavy elements in the atmospheres of Arcturus (circles), HD37828 (triangles), HD44007 (squares) obtained from ELODIE spectra. The abundances of iron were determined by Mishenina and Kovtyukh (2001).

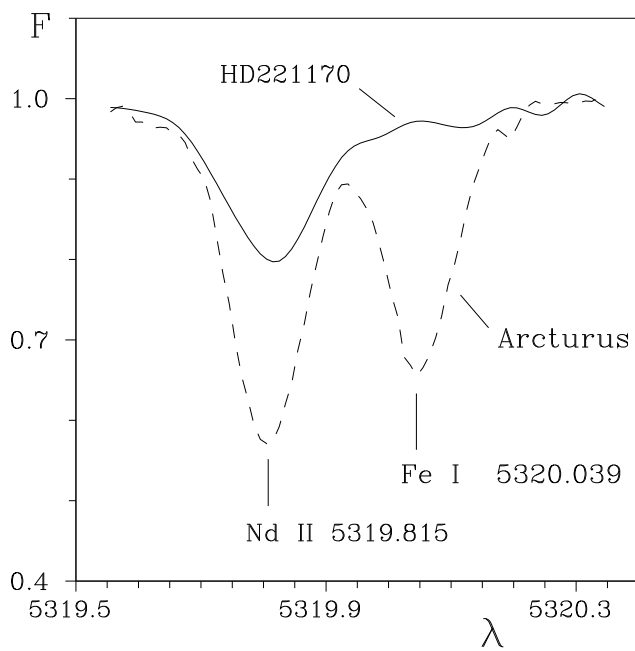


Figure 2: Spectra of HD221170 and Arcturus in the vicinity of Nd II line λ 5291.815 Å. Fe I line λ 5320.039 is well detected in Arcturus spectrum but disappears in the spectrum of HD221170. The decrease of strength of Nd II λ 5291.815 Å line is significantly less than the decrease of iron line. in HD221170

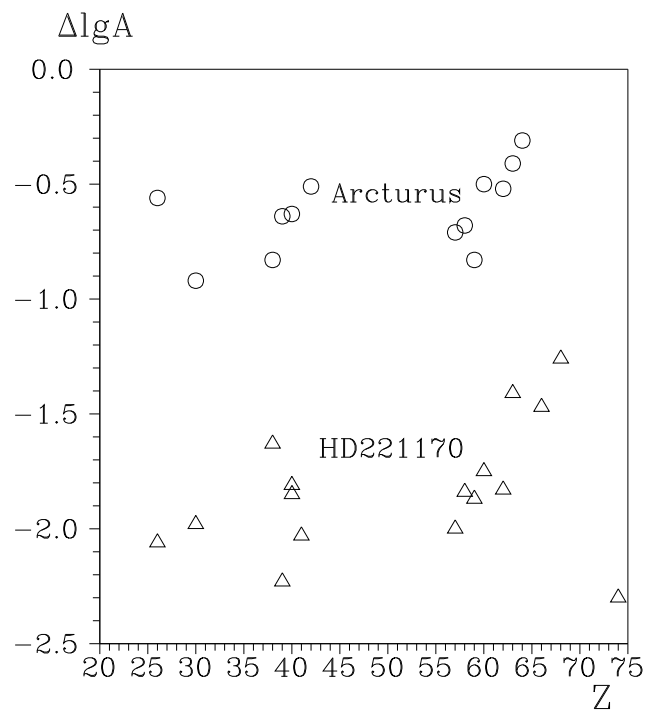


Figure 4: The same as Fig. 3 for Arcturus (circles) and HD221170 (triangles)

Table 3: The number of heavy elements investigated in program stars

Star	[Fe/H]	N
Arcturus	-0.56	13
HD37828	-1.41	14
HD44007	-1.49	11
HD221170	-2.05	14

content. Our methodics permit to identify the bigger number of lines of heavy elements in the observed spectra. In Table 3 one can find the number of heavy elements, which were investigated in the atmosphere of Arcturus and program stars. The values of [Fe/H] were determined by Mishenina & Kovtuykh (2001).

These preliminary results will be used for more detailed investigations of these and other metal-poor stars with spectrum synthesis method.

Arcturus and Arcturus-like stars with low metallicity showed abundance patterns for heavy elements:

Acknowledgements. V. Gopka, T. Mishenina, V. Kovtuykh were supported in part by National Scientific-Technical Committee of Ukraine (project 02/07/00091).

References

- Delbouille L., Rouland G., Neven L.: 1973 / Photometric atlas of the Solar spectrum from λ 3000 to λ 10000 (Liege: Institute de d'Astrophysique de l'Universitete' de Liege)
- Griffin R.: 1968 / A photometric atlas of the spectrum of Arcturus (Cambridge: Cambridge. Univ. Press)
- Kurucz R.L.: 1995, *Laboratory and Astronomical High Resolution Spectra*, Eds. Sauval A.J., Blomme R., Grevesse N., ASP Conf. Ser. 81, 595.
- Mishenina T.V., Kovtuykh V.V.: 2001, *Astron. Astrophys.*, **370**, 951.
- Morton D.C.: 2000, *Astrophys. J. Suppl. Ser.* **130**, 403.
- Piskunov N.E., Kupka F., Ryabchikova T.A., Weiss W.W., Jeffery C.S.:1995, *Astron. Astrophys. Suppl. Ser.*, **112**, 525.
- Soubiran C., Katz D., Cayrel R.: 1998, *Astron. Astrophys. Suppl. Ser.*, **133**, 221.
- Woolley S.E., Hofman R.D.: 1992, *Astrophys. J.* **395**, 202.
- Yushchenko A.V.: 1998, *Proc. of the 29th Conf. on Variable Star Research*, Eds. Dušek J., Zeida M., Brno, p. 202.

SEARCH FOR TiO-BAND VARIABILITY OF COOL GIANT

N.S. Komarov, N.I. Dorokhov, T.N. Dorokhova
 Astronomical Observatory, Odessa National University
 T.G. Shevchenko Park, Odessa 65014 Ukraine,
komarov@farlep.net

ABSTRACT. The dissipation of acoustic energy and bombardment of high energy particles of TiO molecules can be sources of temperature "inversion" and nonstability of outer layers of atmospheres of cool giants. In 1993 the trial observations on variability of outer layers of the cool giant HD73665 was made at the Mt. Dushak-Erekdag station of Odessa Astronomical Observatory. For simultaneous observations in TiO-band and Johnson V-band, a split prism in the dual-channel photometer was used. The observations show quasi-periodical variations at the time scale of 2-12 min.

Key words: Stars: cool giants, stars: individual: HD73665, stars: oscillations

Recently, the TiO spectroscopy is used for investigation of surface peculiarities of cool giants, particularly, for purposes of Doppler imaging. The speckle imaging in various TiO bands is used for determination of angular size of stars. We decided to use a narrow-band photometry instead the spectroscopy of high resolution. The two pairs of interference filters have been made in Kiev. When the 80 cm Ritchey-Chretien telescope at the Mt. Dushak-Erekdag station of Odessa Astronomical Observatory (Dorokhov et al., 1994a) was put into operation, and the high accuracy of the data was obtained (better than 2 mmag), we took a chance to test rapid variability in outer layers of cool giants. The reports of such experiments appeared in 80th (see, for example, Smith, 1983, Livi and Bergman, 1982).

We used for observations a split prism in the dual channel photometer (Dorokhov et al., 1994b). A narrow band interferometric filter with FWHM=50Å centered at the $\lambda=5500\text{\AA}$ (TiO-band) was mounted in the first channel, the Johnson V filter (the effective length of band 5450Å) was in the second channel.

This way assumes to exclude sky transparency and scintillation variations entirely because of high correlation in two channels. Therefore the normalized data showed the "clear" pattern of TiO-band processes relative to "continuum".

The set of observations of cool giant HD73665 ($m=6.39$, K0III), belonging to Praesepe, was about 100

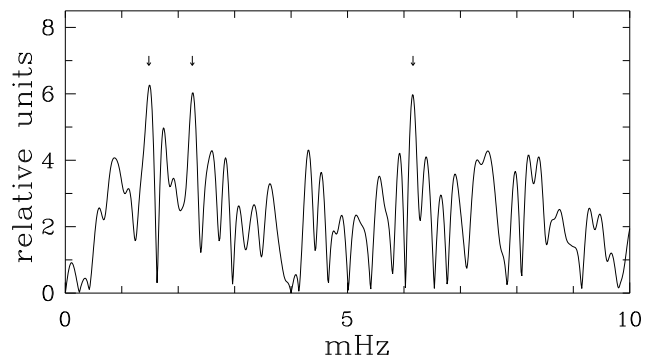


Figure 1: Amplitude Fourier-spectrum of normalized data. The arrows show peaks, for which S/N ratios exceed 2.

min. with the 10 sec. integrating time on the night October 19, 1993.

In Fig.1, an "amplitude" Fourier-spectrum of normalized data obtained by using the program PERIOD (Breger, 1989) is shown. The arrows indicate the peaks at the frequencies 1.48 mHz (11.3 min), 2.25 mHz (7.4 min), 6.16 mHz (2.7 min), where the signal/noise level exceeded 2. There were no similar features in the Fourier-spectrum of V-filter's data.

We do not expound the result, it was only a trial test for variability. Unfortunately, the work was not continued because of hard economical situation with our science.

References

- Breger M.: 1989, *Commun. Asteroseismology*, **6**, 1.
 Dorokhov N.I., Dorokhova T.N., Komarov N.S., Mukhamednazarov S.: 1994a, *Odessa Astron. Publ.*, **7**, 167.
 Dorokhov N.I., Dorokhova T.N.: 1994b, *Odessa Astron. Publ.*, **7**, 167.
 Livi S.H.B., Bergmann T.S.: 1982, *A.J.*, **87**, 1783.
 Smith M.A.: 1983, *Ap.J.*, **265**, 325.

ABUNDANCES OF Na, Ca, Mg AND Al IN THE ATMOSPHERES OF K SUPERGIANTS OF THE SMALL MAGELLANIC CLOUD

N.S. Komarov, N.S. Zgoniajko, S.V. Vasilyeva¹

¹ Department of Astronomy, Odessa State University
T.G.Shevchenko Park, Odessa 270014 Ukraine, *astro@paco.odessa.ua*

ABSTRACT. The abundances of chemical elements Na, Ca, Mg and Al of the nine K-supergiants in SMC was investigated by a method of models of atmospheres. With this goal the CCD-spectrograms with high resolution was used. It is shown that all stars have a deficit abundances of iron from -0.40 to -0.97 dex. relatively of Sun. The some differences of contents of elements Na, Ca, Mg and Al in atmospheres of stars SMC and our Galaxy relatively of content of iron was found.

Key words: Stars: K-supergiants SMC ; stars: abundances of chemical elements.

1. Introduction

The Large and Small Magellan Cloud (LMC and SMC) together with our Galaxy enter into a Local System of a cluster of galaxies and consequently the research of all objects which are included in the LMC and the SMC represents doubtless interest from testing of evolution of a Local System, including our Galaxy. The last years due to application of large telescopes and modern equipment of a radiation it was possible to receive the important data about parameters and chemical structure of a number of bright objects LMC, SMC and stars YC, in main, for supergiants. It is seem, that for these stars, as well as for stars of the population II types and thick disk of a Galaxy the common deficit of metals. The spectra were obtained in an European Southern observatory (CHILE) on a telescope equipped EMMI, and on 3.6 telescope with K spectrograph. The spectra obtained with EMMI have the resolution $R = \lambda/\Delta\lambda = 30000$. Spectra obtained on K - spectrograph $R \sim 20000$. The relation a signal-to- noise $S/N \sim 100$. A spectral interval $\Delta\lambda - (500 - 630nm)$ and $(580 - 700nm)$. Early the nine stars were investigated us of method of model of atmospheres and send in publication. In the given work the results of a research of contents Na, Ca, Mg

and Al in atmospheres of nine stars SMC (from them three stars earlier are resulted are not investigated Hill (1997) and Hill et al. (1997) by method of synthetic spectra. The spectral lines of this elements are blended of lines other elements. For stars - supergiants it is necessary to take into account deviations from LTE and an approximation of plane geometry. As have shown accounts, the effects of a deviation from LTE and spherical geometry influence in an opposite direction on intensity of lines of absorption. The grid of models Bell et al. (1976) was used. The lines were selected from the list of lines, as well as their input parameters - force of oscillators, of energy of lower layers of excitation of atom or ion (Kurucz, 1992, 1993). The synthetic spectra for stars was calculated on code Tsymbal (1996). The list of lines was made for each line of investigated elements in interval 50 Å. The average contents of chemical elements in atmosphere of the Sun were taken from work Grevesse and Sauval (1998). The parameters of atmospheres of stars PMMR 23, PMMR 27, PMMR 48, PMMR 102, PMMR 144, PMMR 145 are taken from Hill (1997). For stars PMMR 219, PMMR 390, PMMR 667 parameters of atmospheres were determined on equivalent widths of lines of iron. Effective temperature (T_{eff}) was determined from a condition of independence of the contents of neutral iron $lg(Fe/H)$ from potential of excitation. The accounts were made for an interval of temperatures from 4000 to 4500 K through 100 K. Acceleration of gravity $\log g$ was selected from ionization equilibrium for elements Fe, Ti, V. The turbulent velocity V_t was selected from a condition of absence of correlation between the contents of iron $lg(Fe/H)$ and of equivalent width (W_λ) of different lines FeI. V_t varied in an interval from 3 km/s up to 4.5 km/s. An error in definition(determination) of a turbulent velocity of ± 0.5 km/s. In Table 1 the parameters of atmospheres of stars for choice of models of atmospheres from a grid Bell et al. (1976) and for their interpolation are represented.

Table 1: Physical parameters of stars

Star	T_{eff} (K)	$\log g$	V_t (km/s)	[M/H]
PMMR23	4200	0.2	4.0	-0.8
PMMR27	4300	0.1	3.0	-0.6
PMMR48	4300	0.3	3.5	-0.6
PMMR102	4300	-0.2	3.5	-0.6
PMMR144	4100	-0.7	3.5	-0.9
PMMR145	4300	0.3	3.0	-0.6
PMMR219	4200	0.3	3.5	-0.5
PMMR390	4200	0.2	4.0	-1.0
PMMR667	4300	0.2	3.5	-0.4

2. Conclusion.

The results of determination of the contents of chemical elements of Na, Ca, Mg and Al researched stars SMC are indicated in Tab. 2. From Table 2 it is visible, that the atmospheres of all investigated of stars have a deficit in the contents of iron on a comparison with the solar ones. For all stars the same method was used. All stars have close photometric and spectral characteristics. The variations of the contents of iron [Fe/H] at selected stars SMC, on all probability, reflect differences primordial of chemical structure of an interstellar medium. The interest represents the contents of elements of α - process in our case the contents of elements Ca, Si. In our Galaxy in atmospheres of stars with a deficit of metals have the enrichment contents of these elements. At investigated stars SMC, on the contrary, the small deficit in the contents Si, Ca to relative iron are observed. The values [Si/Fe] vary from - 0.5dex up to -0.1dex. The contents Ca is more close the contents one for stars with solar content of iron. From all elements, considered by us, noticeable exceed in the contents to relation to iron show Na. It is notes, that at stars - giants of the disk of a Galaxy the enrichment in the contents Na (Komarov, 1999) is detected. This result is agreed in work (Bojarchuk et al., 2001). The magnitude of enrichment depends on a luminosity of a star. With increasing of a luminosity of a star the abundance Na is increased. It is consider, may be, that at stars - supergiants SMC on a stage of dwarfs was proceeded with convective outflow of products of nuclear processes in surface of stars.

References

- Bell R.A., Eriksson K., Gustafsson B., Nordlund G.: 1976, *As.Ap.Suppl.*, **29**, 37.
- Bojarchuk A.A., Antipova L.I., Bojarchuk M.E., Savanov I.S.: 2001, *Astron.J.*, **78**, 349.
- Grevesse N., Sauval J.: 1998, *Space Science Reviews*, **85**, 161.
- Hill V.: 1997, *As.Ap.*, **324**, 435.
- Hill V., Barbuy B., Spite M.: 1997, *As.Ap.*, **324**, 461.
- Komarov N.S.: 1999, *The cold giant stars*, Odessa, Astroprint, 213p.
- Kurucz R.L.: 1992, *Rev.Mex.Astron.Astrofis.*, **23**, 45.
- Kurucz R.L.: 1993, CD-ROMs I-23, *Smithsonian Astrophys. Obs.*
- Tsybmal V.: 1995, *ASP Conf.Ser.*, **108**, 198.

Table 2: Abundances

Star	[Na/H]	σ	N	[Na/H]
PMMR				Hill
23	-0.36	0.17	4	-0.55
27	-1.20	0.14	2	-0.88
48	-0.83	0.06	3	-0.62
102	-0.63	0.35	5	-0.62
144	-1.16	0.14	3	-0.77
145	-1.02	0.11	3	-0.91
219	-0.10	-	1	-
390	-0.50	-	1	-
667	-0.34	0.23	2	-

Star	[Mg/H]	σ	N	[Mg/H]
PMMR				Hill
23	-0.71	0.18	2	-0.75
27	-	-	-	-
48	-1.23	-	1	-
102	-0.74	0.34	4	-0.40
144	-	-	-	-
145	-0.83	0.21	2	-0.47
219	-0.39	0.14	2	-
390	-1.28	-	1	-
667	-	-	-	-

Star	[Al/H]	σ	N	[Al/H]
PMMR				Hill
23	-0.97	-	1	-0.71
27	-1.27	0.02	2	-0.85
48	-1.17	-	1	-0.79
102	-	-	-	-
144	-0.87	-	1	-0.87
145	-	-	-	-
219	-0.44	0.09	2	-
390	-	-	-	-
667	-	-	-	-

Star	[Si/H]	σ	N	[Si/H]
PMMR				Hill
23	-0.71	0.22	5	-0.72
27	-1.14	0.24	6	-0.90
48	-1.10	0.27	2	-0.92
102	-1.04	0.25	10	-0.71
144	-1.07	0.12	2	-0.86
145	-1.00	0.27	5	-0.69
219	-0.87	0.43	5	-
390	-0.90	0.49	2	-
667	-1.08	0.11	2	-

CHEMICAL ABUNDANCES IN BINARIES WITH TWIN COMPONENTS

Yu. Lyubchik¹, E. Martin², G. Basri³, Ya. Pavlenko¹

¹ Main Astronomical Observatory of NASU, Kiev 03680 Ukraine,
lyu@mao.kiev.ua, yp@mao.kiev.ua

² Institute for Astronomy, University of Hawaii at Manoa, 2680 Woodlawn Drive,
Honolulu HI, 96822, USA,
ege@ifa.hawaii.edu

³ Astronomy Department, University of California, Berkeley, CA 94720, USA,
basri@soleil.berkeley.edu

ABSTRACT. Procedure and some preliminary results of abundances determination in binaries with twin components from solar neighbourhood are discussed. Numerical analysis were carried out by fits of synthetic spectra and COG to high resolution ($R=50000$) observed data. To fit the observations we used model atmospheres of Kurucz with different metallicities and (modified) VALD line list.

Key words: Stars: binary stars: chemical abundances.

1. Introduction

Binary stars with twin components from Solar neighbourhood are interesting because they allow to test the validity of stellar evolution models. If all the properties of stars are determined by age, mass and chemical composition, twin componenys should be identical. However, King et.al.(1997) found that in binary 16 Cyg components are nearly identical ($T_{\text{eff}}=5785$ K, $\log g=4.28$; $T_{\text{eff}}=5747$, $\log g=4.35$), but lithium abundances dramatically differ from each other - for component A - $\log N(\text{Li})=1.25\pm 0.05$, but for component B - $\log N(\text{Li})<0.6$. (Lithium abundances are given in the the customary logarithmic scale with $\log N(\text{H})=12$). Thus, the systematic study of binaries may help us to establish causes of different rates of lithium depletion or any other deviations in chemical abundances in identical stars.

2. Observations.

Observable set of stars was selected from the list of common proper motion pairs compiled by Halbwachs (1986). Spectral type of chosen stars are between F8 and K0. Four stars from our list are given in Table 1.

High resolution (0.05 \AA) observations were obtained during several observing runs at Lick and Keck observatories between January 1998 and February 1999 by E.Martin et.al.

3. Analysis.

Since the photometry of our sample of binaries does not come from a single source, and there could be problems with systematic errors, we have preferred to determine the temperatures and chemical abundances of our stars using synthetic spectra fitting to the observed spectra.

We determined the continuum level in the observed echelle spectra using the DECH20 software (Galasutdinov, 1992). Preliminary determination of T_{eff} and $\log g$ of observable stars was done using the astrometrical catalogues (Hipparcos was included) from programmes and data of Kharchenko N.V. (private communication). Then, these data were compared to Simbad references.

We carried out computations using spectral synthesis program Abel8 (Pavlenko, 2002) Our computations of LTE synthetic spectra were carried out in the frame of classical approaches: a plane-parallel model atmosphere in LTE, with no energy divergence. In our computations we refer to the solar abundances given by Anders & Grevesse (1989).

Kurucz model atmospheres (Castelli et.al.,1997) were used to compute synthetic spectra. In these models convection is treated with overshooting. We compared the results of synthetic spectra computation using different approximations of convection (mixing length theory and overshooting) and concluded that differences are not very strong for temperature range $T_{\text{eff}}=5250 - 6500$ K.

We had to use metallicities in the range $[m/\text{H}]=0 \div$

Table 1: Characteristics and element abundances of program stars.

HD/BD	Sp.T.	T _{eff} (K)	[m/H]	log N(Li)	logN(Si)	logN(Al)	logN(Ca)	logN(Fe)
SUN:					7.51	6.43	6.32	7.63
HD 6872 A	F8	6250	-0.2	<1.8	7.5	6.05	6.24	7.4
HD 6872 B	F8	6250	-0.2	2.6	7.4	6.15	6.14	7.4
HD 224984	F8	6000	-0.1	2.3	7.5	6.25	6.24	7.5
HD 224994	G0	6000	-0.1	2.3	7.4	6.25	6.24	7.5

Table 2: List of identified lines and changes in *gf*'s.

Chemical element	λ , Å	<i>gf</i> , VALD	<i>gf</i> , Gurtovenko & Kostyk, 1989
Si	6696.044	1.479e-02	—
	6721.848	3.236e-02	7.079e-02
Ni	6690.770	5.620e-03	—
Al	6696.023	4.170e-02	2.630e-02
	6698.673	1.780e-02	1.259e-02
Ca	6717.681	2.535e-01	—
Fe	6696.320	2.138e-02	—
	6699.142	7.925e-03	—
	6704.481	2.188e-03	—
	6705.101	3.190e-02	6.400e-02
	6707.432	4.470e-03	—
	6713.046	3.090e-02	2.511e-02
	6713.195	2.754e-03	—
	6713.745	5.010e-02	2.951e-02
	6715.383	2.291e-02	—
	6716.237	1.202e-02	—
	6717.298	1.107e-02	—
	6724.082	3.013e-02	—

more observations are necessary to establish the fraction of binary twins that show similar lithium abundance anomalies and to establish the causes of these anomalies.

Acknowledgements. Yu.Lyubchik and Ya.Pavlenko are thankful to LOC of VS-2001 for partial financial support to participate in this conference.

References

- Anders E., Grevesse N.: 1989, *Geochim. et Cosmoch. Acta*, **53**, 197.
- Castelli F., Gratton R.G., Kurucz R.L.: 1997, *As.Ap.*, **318**, 841.
- Galazutdinov G.A.: 1992, "Stellar echelle-spectra processing system. I. Image processing. II. Spectra processing. **Prepr.92**, SAO RAN, Nizhnii Arhyz.
- Gurtovenko E.A., Kostyk R.I.: 1989, *Fraungher spectrum and solar lines oscillator strengths.*, Naukova Dumka, Kyiv.
- Halbwachs J.L.: 1986, *As.Ap.Suppl.*, **66**, 131.
- King J.R., Deliyannis C.P., Hiltgen D.D., et al.: 1997, *Astron. J.*, **113**, 1871.
- Kurucz R.L.: 1993, CD ROM No. 15.
- Martin E., Basri G., Pavlenko Ya., Lyubchik Yu.: 2001, *Astron. J.*, in preparation.
- Pavlenko Ya.V.: 2002, *Kinemat. and Physics of Celest. Bodies*, submitted.
- Pavlenko Ya.V., Magazzù A.: 1996, *As.Ap.*, **311**, 961.
- Piskunov N.E., Kupka F., Ryabchikova T.A. et.al.: 1995, *As.Ap.Suppl.*, **112**, 525.
- Ryan S.G.: 2000, *Mon. Not. of Roy. Astron. Soc.*, **316**, L35.
- Tsuji T.: 1973, *As.Ap.*, **23**, 411.

PRELIMINARY ABUNDANCE ANALYSIS OF 9 SUBDWARFS

T.V. Mishenina, T.I. Gorbaneva, L.E. Kantsen

Astronomical Observatory, Odessa National University

T.G.Shevchenko Park, Odessa 65014 Ukraine, *tamar@deneb.odessa.ua*

ABSTRACT. We provide parameter and abundance determination of 9 subwarfs including two SMR stars (HD 161797 and HD 182572). These stars show metallicity overabundance in agreement with previous results. Further we plan to carry out the detailed analysis of luminosity, evolutionary status, age and belonging of studied stars to spatial structures of the Galaxy.

Key words: Stars: abundances; stars: subdwarfs.

1. Introduction

The stars showing metal abundances far larger than solar one were found by Spinrad & Taylor (1969) and named the super metal rich (SMR) stars. Till now this rather small group of stars attracts attention of many researchers because the properties of metal-rich are important for interpretation of metal-rich stellar populations, such as the Buldge and their possible connection with extra-solar planets. Taylor (1996) made a critical appraisal of published values of the metallicity $[\text{Fe}/\text{H}]$ of stars and the status of SMR star (with 95% confidence) was confirmed only for seven dwarfs and subdwarfs including the subgiant 31 Aql (HD 182572). Malagnini et al. (2000) analyzed a sample of 91 bright stars in the solar vicinity and found that 73 stars of their sample correspond to Taylor's (1996) criterion ($[\text{Fe}/\text{H}] \geq 0.2$ dex). The goal of our work is comparative analysis of two SMR subdwarfs HD 161797 (Malagnini et al. 2000) and HD 182572 (Taylor 1996) with another subdwarfs. We study the chemical composition and physical parameters of 7 subdwarfs by using model atmosphere and spectra with a high dispersion and a high signal-to-noise ratio.

2. The observations and reduction

The investigated spectra are part of the library collected at the Haute Provence Observatory (Soubiran et al. 1998) and they were obtained with the 193 cm telescope equipped ELODIE spectrometer (R=42000). The spectral range is 4400–6800 ÅÅ, signal-to-noise ratios are more than 100. Spectra were previously reduced (Katz et al. 1998), the further processing of spectra (continuum level location, measuring of equivalent

Table 1. Basic characteristics of the program stars

HD	V	B - V	T_{eff}	log g	V_t	Sp
161797	3.42	0.75	5750	3.87	1.3	G5IV
182572	5.17	0.76	5580	4.22	1.0	G8IV
188512	3.17	0.86	5250	3.14	1.4	G8IV
191026	5.38	0.85	5300	3.49	1.4	K0IV
196755	5.07	0.70	5680	3.54	1.4	G5IV
198149	3.41	0.91	5150	3.19	1.2	K0IV
216385	5.45	0.47	6400	3.97	1.4	F7IV

widths etc.) was carried out by us using the DECH20 software (Galazutdinov 1992). Equivalent widths EWs of lines were measured by means of a Gaussian fitting.

3. Parameter determination

The basic characteristics and atmospheric parameters of studied stars are listed in Table 1.

As the first approximation for T_{eff} we took the T_{eff} derived in the paper of Soubiran et al. (1998). Then, T_{eff} were specified from the condition that the abundances obtained from individual Fe I lines must be independent of the excitation potential Elow. The gravities log g have been determined through the ionization equilibrium by forcing Fe II lines to yield the same total Fe abundances as Fe I lines. Microturbulent velocities V_t were determined by forcing the abundances determined from individual FeI lines to be independent of equivalent width. The precision of parameter determination is $\Delta T_{\text{eff}} = \pm 100$ K; $f \Delta \log g = \pm 0.3$; $\Delta V_t = \pm 0.2$ km s⁻¹, respectively.

4. Abundance determination

The abundance analyses presented in this paper were carried out using WIDTH9 code by Kurucz. Appropriate models for each star were derived by means of standard interpolation within the grid of atmosphere models by Kurucz (1993). The choice of model on metallicity was done with accuracy of $\Delta [\text{Fe}/\text{H}] \pm 0.25$. The oscillator strengths log gf were taken from Gurtovenko & Kostyk (1989). The stellar abundance derived in this study are summarized in Table 2.

Table 2. Abundance of the program stars

Element	HD 161797	HD 182572	HD 188512	HD 191026	HD 196755	HD 198149	HD 216385
OI	8.94		8.74				
NaI		6.96	6.24	6.54	6.47	6.44	6.20
MgI		8.00					
AlI	6.89	6.91	6.46	6.77	6.65	6.57	6.25
SiI	7.95	8.05	7.42	7.61	7.70	7.61	7.51
SiI I		7.58					
CaI		6.84					
ScI		3.29					
ScI I	3.45	3.43	2.82	2.97	3.10	3.10	2.99
TiI	5.41	5.42	4.96	5.17	5.06	5.11	4.96
TiI I	5.18	5.32	4.75	4.95	5.01	4.95	4.99
VI	4.41	4.32	3.96	4.19	4.11	4.13	4.03
CrI	7.44	6.10	6.52	6.33	6.15	6.35	6.13
CrI I		6.08					
MnI		6.27					
FeI	7.97	7.98	7.45	7.60	7.66	7.58	7.52
FeI I	7.83	7.90	7.26	7.44	7.62	7.48	7.54
CoI		5.36	5.27	5.56	5.04	5.52	5.14
NiI		6.65	6.01	6.16	6.26	6.17	6.12
CuI		5.27			4.68		4.59
ZnI	5.35	5.17		4.78	4.47	4.50	4.33
SrI	3.03	3.29	2.58				
YI	2.60	2.99		2.41	2.37	2.44	
YII	2.46	2.44		2.10	2.29	2.90	2.26
ZrI		3.01		2.74			
ZrI I		3.57					
RuI		3.01					
BaI I	2.33	2.32	1.91	1.91	2.20	2.20	2.4
LaI I	1.23	1.16	0.95				
CeI I	1.88	1.83	1.61				
PrI I	1.02	1.01		0.73		0.78	
NdI I		1.56	1.40	1.47	1.63	2.12	1.5
SmI I		1.80					
EuI I		3.84	0.38				

5. Discussion

HD 161797 and 182572 show slight overabundance in agreement with previous results (Taylor 1996; Mishenina 1996; Malagnini et al. 2000). Further we plan to carry out the detailed analysis of luminosity, evolutionary status, age and belonging of studied stars to spatial structures of the Galaxy.

References

- Galazutdinov G.A.: 1992, *Preprint SAO RAS*, **92**, 27
 Gurtovenko E.A., Kostyk R.I.: 1989, *Fraunhoffer spectrum and system of solar Oscillators strengths*, Naukova Dumka, Kiev, 200p.
 Katz D., Soubiran C., Cayrel R., Adda M., Cautain R.: 1998, *As.Ap.*, **338**, 151
 Kurucz R.L.: 1993, *CD ROM n13*
 Malagnini M.L., Morossi C., Buzzoni A., Chavez M.: 2000, *PASP*, **112**, 1455
 Mishenina T.V.: 1996, *As.Ap.Suppl.*, **119**, 321
 Soubiran C., Katz D., Cayrel R.: 1998, *As.Ap.Suppl.*, **133**, 221
 Spinrad H., Taylor B.J.: 1969, *Ap.J.*, **157**, 1279
 Taylor B.J. 1996, *Ap.J.Suppl.*, **102**, 105.

LITHIUM BLEND FITTING FOR roAp STAR HD101065 (PRZYBYLSKI'S STAR)

A.V. Shavrina¹, V. Khalack¹, N.S. Polosukhina², J. Zverko³, J. Žižnovský³,
V.F. Gopka⁴, P. North⁵, V.V. Tsymbal⁶, A.V. Yushchenko⁴

¹Main Astronomical Observatory of NAS of Ukraine

Golosiivo, 03650, Kyiv, Ukraine, *shavrina@mao.kiev.ua*

²Crimean Astrophysical Observatory

Nauchnyj, Crimea, Ukraine

³Astronomical Institute of the Slovak Academy of Sciences

05960 Tatranska Lomnica, the Slovak Republic

⁴Astronomical observatory, Odessa National University, Ukraine

65014, park Shevchenko, Odessa, Ukraine

⁵Inst. d'Astronomie, Univ. Lausanne, Switzerland

CH-1290 Chavannes-des-Bois, Switzerland

⁶Tavrian National University,

Simpheropol, Ukraine

ABSTRACT. We have considered the possibility for modelling of remarkable spectral feature 6708 Å for HD101065 (Przybylski's star) in two ways - as a blend of Li and REE lines and as blend of REE lines only. We show by model calculations that Li lines absorb significantly in the range 6707.72 - 6708.02 ÅÅ and resulting Li abundance 3.3 dex (in the scale $\lg N(\text{H})=12.0$) is near to the primordial value.

Key words: Stars: chemically peculiar; individual: HD101065 stars: individual: HD101065.

1. Introduction

Following to Cowley & Mathys (1998) and Cowley et al. (2000) we undertaken the new analysis of the spectrum of Przybylski's star (HD101065, V816 Cen), which has the most unusual of all stellar spectra (Wegner et al., 1983). As was first noted by its discoverer, A. Przybylski (1961, 1977), in the spectrum of HD101065 the strongest spectral lines generally belong to lanthanides. For this star the relative abundances of elements depend critically on the assumed stellar temperature and applied line identification method (Cowley et al., 2000).

The strong complicated spectral feature at λ 6708 Å in the observable spectra creates the problem of correct line identification in this region. The comprehensive analysis of REE lines was performed and the main contribution of lithium was shown for this blend.

Table 1: List of observations for HD101065.

#	Date	UT	Exp.	HJD	Range
	d.m.y	h m	[m]	2450000+	
04	11.3.96	5 11	20	153.726	6675-6735 Å
26	10.3.96	4 41	20	152.705	6120-6180 Å

2. The observations and their reductions

The observations were made by PN with the ESO Coudé Auxiliary Telescope. The Coudé Échelle Spectrograph was used with resolving power $R=100000$ and the S/N ratio for an individual spectrogram was better than 100 at the 1σ level. The detector was ESO CCD 34 with 2048 pixels along the dispersion. A thorium-argon lamp was used for the wavelength calibrations with an accuracy better than 0.3 km s^{-1} . Primary data reduction was done by PN during the observing run, using the old IHAP system of ESO. In Table 1 the date, exposure time and wavelength coverage are given.

3. Atmosphere model

The values of $T_{\text{eff}} = 6750$, $\log g = 4.0$ and $v \sin i = 3.5 \pm 0.5 \text{ km s}^{-1}$, that are close to the model parameters of Cowley et al. (2000) $T_{\text{eff}} = 6600$, $\log g = 4.0$

Table 2: Abundances of the elements ($\log N/N_{tot}$) for HD101065 as compared with data of Cowley et al. (2000) for this star, for the HD166473 (Gelbmann et al., 2000) and for the Sun (Grevesse & Sauval, 1998).

El	HD101065	n	HD101065	HD166473	Sun
Li I	-8.70 ± 0.10	2	-	-	-10.88?
C I	-4.10 ± 0.10	3	-3.97 ± 0.01	-4.24 ± 0.11	-3.52
O I	-4.40 ± 0.10	3	-3.72 ± 0.25	-4.76 ± 0.21	-3.21
Na I	-5.50 ± 0.10	3	-5.81 ± 0.23	-5.84 ± 0.37	-5.72
Al I	-6.10 ± 0.10	1	-	-4.78 ± 0.37	-5.57
Si I	-4.60 ± 0.10	9	-4.38 ± 0.24	-4.10 ± 0.26	-4.48
Ca I	-6.35 ± 0.10	4	-6.67 ± 0.34	-5.34 ± 0.29	-5.69
Ti I	-7.05 ± 0.20	3	-7.08 ± 0.29	-6.70 :	-7.10
Cr I	-4.70 ± 0.20	6	-6.19 ± 0.21	-5.50 ± 0.45	-6.35
Fe I	-5.10 ± 0.20	6	-5.41 ± 0.26	-4.34 ± 0.22	-4.54
Co I	-6.20 ± 0.20	1	-5.67 ± 0.20	-6.03 ± 0.12	-7.13
Y I	-6.60 ± 0.20	3	-7.67 :	-	-9.81
Ba II	-9.10 ± 0.25	1	-7.69 ± 0.01	-10.37 ± 0.06	-9.82
La II	-7.82 ± 0.20	6	-7.75 ± 0.35	-8.30 ± 0.25	-10.82
Ce II	-7.35 ± 0.25	4	-7.19 ± 0.33	-7.55 ± 0.41	-10.41
Pr II	-9.16 ± 0.20	5	-8.63 ± 0.31	-8.81 ± 0.22	-11.24
Pr III	-8.00 ± 0.25	6	-7.05 ± 0.36	-7.60 ± 0.38	-11.24
Nd II	-7.55 ± 0.20	11	-6.91 ± 0.34	-7.97 ± 0.28	-10.55
Nd III	-6.10 ± 0.20	2	-6.52 ± 0.40	-6.43 ± 0.37	-10.55
Sm II	-7.60 ± 0.15	16	-7.12 ± 0.39	-8.25 ± 0.23	-11.06
Eu II	-7.53 ± 0.20	1	-8.03 ± 0.41	-8.43 ± 0.20	-11.49
Gd II	-7.52 ± 0.25	7	-7.14 ± 0.38	-7.87 ± 0.20	-10.95
Tb II	-8.90 ± 0.25	1	-	-	-12.10
Dy II	-7.64 ± 0.20	1	-7.52 ± 0.27	-7.79 ± 0.37	-10.87
Er II	-7.81 ± 0.20	1	-7.82 ± 0.28	-8.22 ± 0.17	-11.07
Yb II	-7.96 ± 0.20	2	-8.92 ± 0.34	-8.93 ± 0.32	-11.08
Lu II	-7.28 ± 0.25	1	-8.31 ± 0.28	-8.82 ± 0.27	-11.91
Os I	-7.59 ± 0.25	1	-	-	-11.55
Ir I	-7.95 ± 0.25	1	-	-	-11.65

and $v \sin i = 3.5 \pm 0.5 \text{ km s}^{-1}$ were used by us for analysis. Model with $[M/H]=0.0$ was applied. In order to take into account the magnetic broadening of spectral lines for the surface magnetic field 2.3 kG Cowley et al. (2000) value of microturbulent velocity $V_{micro} = 2 \text{ km s}^{-1}$ was applied.

4. Rotation and magnetic field

The high-speed photometric observations reveal that HD101065 pulsates with at least three frequencies near 1.37 mHz (Kurtz, 1978). But the detected frequencies are not equally spaced and hence cannot be straightforwardly interpreted in terms of the oblique pulsator model (Martinez & Kurtz, 1990). Therefore these authors can not obtain the value of stellar rotation velocity from the analysis of photometric data variability.

The first magnetic field observations for HD101065 were carried out by Wolff & Hagen (1976), that obtained the three evaluations of the mean longitudinal

field ranging from -2100 to -2500 G , with estimated error of 450G. Such large uncertainties could be due to the severe blending (Cowley, 2000), that is usual as for the Przybylski's star. Another estimates of the mean longitudinal magnetic field ($-1408 \pm 50 \text{ G}$) as well as of the crossover ($-2670 \pm 980 \text{ km s}^{-1} \text{ G}$) and the mean quadratic field, with a 3σ upper limit of 8.7 kG , (the analysed spectrum of HD101065 was obtained in June 1992) were performed by Cowley & Mathys (1998) in the same way as described by Mathys & Hubrig (1997). The last derived value for the mean longitudinal field is marginally smaller (in absolute value) than previous ones. But in order to make a final conclusion about the reality of mean longitudinal magnetic field variation during the time interval of about 20 years, that separates these two determination moments, the new additional observations (Mathys, 2001) should be carried out. At the recent paper of Cowley et al. (2000) authors have relatively well represented the observed line profiles of HD101065 (obtained at

Table 4: The shares of main absorption contributors.

Line (λ_0 , Å)	El	λ (Å)	Share (%)	El	λ (Å)	Share (%)
6707.72	⁷ Li I	6707.756	11	⁷ Li I	6707.768	16
	*Sm II	6707.779	1			
6707.82	⁷ Li I	6707.756	9	⁷ Li I	6707.768	17
	*Sm II	6707.779	1	⁷ Li I	6707.907	2
	⁷ Li I	6707.908	1	⁶ Li I	6707.916	2
	⁷ Li I	6707.919	3	⁷ Li I	6707.920	2
	⁶ Li I	6707.928	2			
6707.92	⁷ Li I	6707.756	1	⁷ Li I	6707.768	2
	⁷ Li I	6707.907	4	⁷ Li I	6707.908	2
	⁶ Li I	6707.916	4	⁷ Li I	6707.919	6
	⁷ Li I	6707.920	4	⁶ Li I	6707.928	6
6708.02	⁷ Li I	6707.907	1	⁷ Li I	6707.908	1
	⁶ Li I	6707.916	1	⁷ Li I	6707.919	2
	⁷ Li I	6707.920	1	⁶ Li I	6707.928	3
	⁶ Li I	6708.067	1	⁶ Li I	6708.068	1
	⁶ Li I	6708.079	1	⁶ Li I	6708.080	1
	*Ce II	6708.099	6			

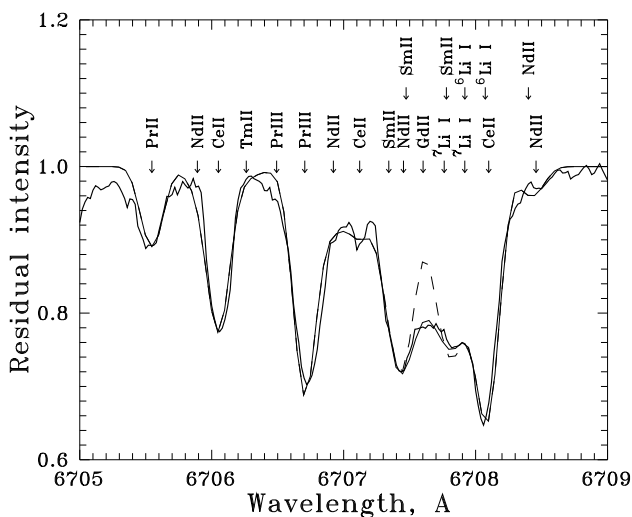


Figure 1: The observed (thick line) and simulated with Gd II 6707.462 Å line (dashed thin line) spectra for HD101065. Thin line - calculated spectrum with shifted Gd II line 6707.602 Å.

February 1998) by synthetic profiles calculated with a mean surface magnetic field $B_s = 2300 \pm 350$ G and $v \sin i = 3.5 \pm 0.5$ km s⁻¹.

5. Abundance analysis

All the available spectra have been analysed with the help of "STARSP" and "ROTATE" code developed by V. Tsybmal (1996). The last code was modified by A. Yushchenko. "URAN" (Yushchenko, 1998) and "SYN-

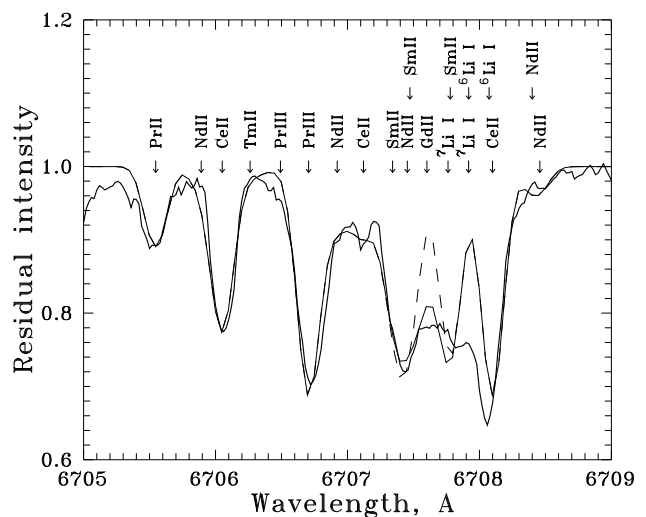


Figure 2: The same as at the Fig.1, but without the lithium lines (only REE lines).

THE" (Kurucz, 1995) codes were also used.

The chemical element abundances used in synthetic spectra simulations are given in Table 2. Table 3 contains the line list used in model calculations. The wavelengths of lines marked by asterisk were calculated on the base of NIST energy levels. Corresponding gf -values were estimated by us using the abundances of each element determined on the base of other lines with known gf -values (from VALD and Kurucz lists) in two spectral regions, 6113-6173 Å and 6675-6735 Å.

The line Sm II λ 6707.779 Å coincides almost with the centre of lithium blend λ 6707.844 Å. We tried to

Table 3: Line list used in synthetic spectra.

El	λ (Å)	E_{low} (eV)	$\log gf$
*Pr II	6705.5470	0.000	-2.985
Ce II	6706.0510	1.840	-1.253
*Tm II	6706.2620	3.955	-1.253
*Pr III	6706.4920	3.104	-1.285
Pr III	6706.7050	0.550	-1.285
*Nd II	6706.9220	3.211	-2.179
*Ce II	6707.1210	1.255	-2.303
*Sm II	6707.3420	0.885	-2.579
*Nd II	6707.4530	2.880	-2.179
Sm II	6707.4730	0.930	-2.679
*Gd II	6707.6021	3.270	-0.679
⁷ Li I	6707.7560	0.000	-0.427
⁷ Li I	6707.7680	0.000	-0.206
*Sm II	6707.7790	2.037	-2.679
⁷ Li I	6707.9070	0.000	-0.931
⁷ Li I	6707.9080	0.000	-1.161
⁶ Li I	6707.9160	0.000	-0.927
⁷ Li I	6707.9190	0.000	-0.712
⁷ Li I	6707.9200	0.000	-0.931
⁶ Li I	6707.9280	0.000	-0.706
⁶ Li I	6708.0670	0.000	-1.431
⁶ Li I	6708.0680	0.000	-1.661
⁶ Li I	6708.0790	0.000	-1.212
⁶ Li I	6708.0800	0.000	-1.431
*Ce II	6708.0990	0.700	-1.950
*Nd II	6708.4580	3.536	-2.579

* gf -values were estimated by us (see text).

calculate this blend without lithium lines with shifted Sm II line on λ 6707.844 Å. Result fitting was bad (see Fig. 2). Only the including of ⁷Li and ⁶Li doublets with ratio ${}^6\text{Li}/{}^7\text{Li} = 0.3$ permitted us to well represent the observed profile of blend (see Fig. 1). In Table 4 we show the shares in total absorption of the main contributors as ones were given by "STARSP" code in four representative wavelengths for lithium doublet range 6707.72-6708.02 Å of blend profile (for $V_{micro} = 2 \text{ km s}^{-1}$) without instrumental smoothing.

6. Discussion

We have considered the possibility for modelling of remarkable spectral feature 6708 Å for HD101065 (Przybylski's star) in two ways - as a blend of Li and REE lines and as blend of REE lines only. We show by model calculations that Li lines absorb significantly in the range 6707.72-6708.02 Å and resulting Li abundance 3.3 dex (in the scale $\lg N(\text{H})=12.0$) is near to the primordial value.

Our synthetic spectra calculations show the necessity of additional absorption at 6707.6 Å. Instead of includ-

ing of new unknown lines for better fitting to observed profile we shifted Gd II line centre at 6707.602 Å. We changed the gf -value for +0.2 dex for line Gd II 6707.462 Å, calculated by us, when shifted it at 6707.602 Å with fixed Gd abundance. In the Li absorption range (6707.72-6708.02 Å) this line does not add any noticeable contribution (see Table 4).

Acknowledgements. The data from Kurucz's CDROMs, NASA ADC, VALD2, NIST, were used and we thank the administrators of these databases, accessible through INTERNET. V. Khalack is grateful to Prof. G. Mathys for useful advices. V. Gopka were supported in part by National Scientific-Technical Committee of Ukraine (project 02/07/00091).

References

- Cowley C.R. Mathys G.: 1998, *MNRAS*, **339**, 165.
 Cowley C.R., Ryabchikova T., Kupka F., Bord J.D., Mathys G., Bidelman W.P.: 2000, *MNRAS*, **317**, 299.
 Cowley C.R.: 2000, private comm. (<http://www.astro.lsa.umich.edu/users/cowley/przyb.html>)
 Cowley C.R., Hubrig S., Ryabchikova T.A., Mathys G., Piskunov N., Mittermayer P.: 2001, *Astron. Astrophys.*, **367**, 939.
 Dupret M.E.: 2001, *Astron. Astrophys.*, **366**, 166.
 Gelbmann M., Ryabchikova T., Weiss W.W., Piskunov N.E., Kupka F., Mathys G.: 2000, *Astron. Astrophys.*, **356**, 200.
 Grevesse N., Sauval A.J.: 1998, *Space Sci. Rev.*, **85**, 161.
 Kupka F., Piskunov N.E., Ryabchikova T.A., Stempels H.C., Weiss W.W.: 1999, *Astron. Astrophys. Suppl. Ser.*, **138**, 119.
 Kurucz R.L., 1995, *Laboratory and Astronomical High Resolution Spectra*, Eds. Sauval A.J., Blomme R., Grevesse N., ASP Conf. Ser. 81, 595.
 Martinez P., Kurtz D.W.: 1990, *MNRAS*, **242**, 636
 Mathys G.: 2001, private comm.
 Mathys G., Hubrig S.: 1997, *Astron. Astrophys. Suppl. Ser.*, **124**, 475.
 Piskunov N.E., Kupka F., Ryabchikova T.A., Weiss W.W., Jeffrey C.S.: 1995, *Astron. Astrophys. Suppl.*, **112**, 525.
 Przybylski A.: 1961, *Nature*, **189**, 739.
 Przybylski A.: 1977, *MNRAS*, **178**, 71.
 Ryabchikova T.A., Piskunov N.E., Stempels H.C., Kupka F., Weiss W.W.: 1999, *Physica Scripta*, **T83**, 162.
 Tsymbal V.: 1996, *Odessa Astron. Publ.*, **7**, P. 2, 146.
 Wegner G., Petford A.D.: 1974, *MNRAS*, **168**, 557.
 Wolff S.C., Hagen W.: 1976, *PASP*, **88**, 119.
 Yushchenko A., 1998, *Proc. of the 29th Conf. on Variable Star Research*, Eds. Dušek J., Zeida M., Brno, p. 202

Li I LINE λ 460.3 nm IN SPECTRA OF SUPER LITHIUM-RICH CARBON STARS

L.Yakovina, Ya. Pavlenko

MAO NASU

Golosiiv woods, Kyiv-127, 03680, Ukraine

ABSTRACT. Subordinate Li I line λ 460.3 nm is quite strong and sensitive on lithium abundances at $\log N(\text{Li}) = 3-5$ that are typical in atmospheres of super lithium-rich AGB giants. However, this line cannot be a good indicator of lithium abundances due to severe blending, especially by line Fe I λ 460.294 nm. On the other hand, a sensitivity of calculated blend containing Li I line λ 460.3 nm on $\log N(\text{Li})$ increases for more complete system of continuum opacity sources in the blue and if use this indicator for metal-deficient stars.

Key words: AGB stars: WZ Cas: lithium abundance indicator: subordinate Li I lines.

Super lithium-rich AGB stars (SLR, $\log N(\text{Li}) \geq 4$) are of great cosmological interest, because ones belong to the main suppliers of lithium into interstellar media. Resonance Li I line λ 670.8 nm is very strong in spectra of SLR stars. Besides, there are some strong subordinate Li I lines in optical and near IR regions formed by transitions from a level 2p. Four strong lines of this series lie in $\lambda\lambda$ 450-820 nm, namely, $\lambda\lambda$ 812.6, 610.4, 497.2 and 460.3 nm. From Abia et al. (1999) and Yakovina & Pavlenko (2001) computations follow that Li I lines $\lambda\lambda$ 812.6 and 610.4 nm are saturated in spectra of SLR C-stars and therefore they are rather non sensitive on lithium abundance. Li I lines $\lambda\lambda$ 497.2 and 460.3 nm are quite sensitive on $\log N(\text{Li})$, but really only Li I line λ 497.2 nm can be good lithium abundance indicator due to severe blending of the line λ 460.3 nm. The last almost coincides in wavelengths with strong Fe I line λ 460.294 nm. Furthermore, it lies in region of strong bands $\Delta v = -2$ of CN violet system. Li I line λ 460.3 nm is blended mainly by the band 0-2 with head at $\approx \lambda$ 460.6 nm. We investigate if there are any conditions for blend at λ 460.3 nm which make one more sensitive on $\log N(\text{Li})$.

For the first time subordinate triplet Li I λ 460.3 nm was considered by Abia et al. (1999). But estimation of $\log N(\text{Li})$ was not derived due to not perfect fit of synthetic spectra to observed spectrum of C-star in this region. To improve the fit we refine line lists for region near Li I line λ 460.3 nm. Then we consider one as indicator of lithium abundance. The

Table 1: The parameters of triplet Li I λ 460.3 nm. (Kupka et al. 1999).

Wavelength[nm]	log gf	Ei[eV]	Transition(i->k)
460.2826	-0.613	1.848	2p 2P - 4d 2D
460.2894	-0.353	1.848	2p 2P - 4d 2D
460.2897	-1.313	1.848	2p 2P - 4d 2D

triplet line parameters are listed in Table 1. We use the observed spectrum of WZ Cas (C9.2J) kindly provided by C.Abia (see (Abia et al. 1999) for more details).

Synthetic spectra were computed in LTE approach by the program WITA6 (Pavlenko 2000). Continuum opacities for a case of carbon-rich atmospheres were used. Then, we implement additional continuum absorption to account of unidentified yet sources by increasing of continuum opacity by factor κ . Parameters of the used model atmosphere (see Eriksson et al. 1984) are: $T_{\text{eff}}/\log g/[\mu] = 3000/0./0.$, $C/O=1.007$. We adopt oxygen and nitrogen abundances from the atmosphere model. Carbon abundance was refined using fits to observed spectrum. Microturbulence velocity $V_t = 2.5$ km/s and isotopic ratio $^{12}\text{C}/^{13}\text{C} = 5$ were used (see Abia et al. 1999).

We compile line list using atomic lines from (Abia et al. 1999) and molecular lines from CD-ROM N18 of Kurucz (1993-1994). Molecular line list includes lines of A-X and B-X systems of CN, D-A system of C_2 , A-X and B-X systems of CH and A-X system of MgH. The list of atomic lines was verified by a fit to spectrum of the Sun (Fig.1a). Atlas of solar spectrum (Kurucz et al. 1984) and solar atmosphere model from Kurucz (1993-1994) were used. Some atomic lines were taken from Bell's tape kindly provided by T.Kipper. Fit of λ 460.3 nm region to observed spectrum of WZ Cas is quite good (Fig.1b). The differences of the observed and synthetic spectra are caused mainly by the lack of precision and completeness of used molecular line lists,

especially C_2 lists.

Sensitivity of Li I line λ 460.3 nm profile and λ 460.3 nm blend on $\log N(\text{Li})$ for different κ and $[\mu]$ and fit of this blend to the observed spectrum of WZ Cas are shown in Fig.2. Fig.2a shows the modelled Li line itself. Fig.2b illustrates the blend at λ 460.3 nm for case $\kappa=1$ (no additional opacity) and $[\mu]=0.0$ (solar metallicity). Cases of $\kappa=5$, $[\mu]=0.0$ and $\kappa=5$, $[\mu]=-1.0$ are shown in Figs. 2c and 2d, respectively. We see, that sensitivity of the blend on $\log N(\text{Li})$ is rather weak in case 2b) and essentially rises if additional opacity sources are implemented (Fig.2c). Note, $\kappa=5$ was chosen from the best fit to the observed spectrum of WZ Cas. Fig.2d shows that this Li abundance indicator is more suitable for metal-deficient stars.

We cannot use the line Li I λ 460.3 nm for $\log N(\text{Li})$ determination because the computed blend's core is too deep in comparison with the observed one (Fig. 2c). This can be explained by different reasons: a) used gf of line Fe I λ 460.294 nm is too high, b) too rough model atmosphere and adopted approaches, c) NLTE effects in Fe I line λ 460.294 nm. Note, that NLTE correction to $\log N_{\text{LTE}}(\text{Li})$ from line λ 460.3 nm is $\Delta \log N(\text{Li})=+0.1$ for used atmosphere model (cf Abia et al. 1999). Then, we use $\log gf=-2.220$ for line Fe I λ 460.294 nm from Blackwell et al. (1980) as the most exact. It is the lowest value among known gf.

Fig.2 shows, that the λ 460.3 nm blend is the most sensitive on lithium abundance at $\log N(\text{Li}) = 3-4$. It cannot be used yet for lithium abundance determination in SLR AGB stars, but a situation can be improved in the case of more precise calculations. This indicator is more suitable for metal-deficient stars.

Acknowledgements. We thank Dr. C.Abia (Granada University) for providing spectrum of WZ Cas and Dr. T.Kipper (Tartu Observatory) for providing of line lists. Our work was partially supported by Small Research Grant of AAS.

References

- Abia C., Pavlenko Y., de Laverny P.: 1999, *As.Ap.*, **351**, 273.
 Blackwell D.E. et al.: 1980, *Mon.Not.R.Astron.Soc.*, **191**, N2, 445.
 Eriksson K., Gustafsson B. et al.: 1984, *As.Ap.*, **132**, 37.
 Kipper T.A.: *private communication*.
 Kupka F., Piskunov N., et al.:1999, *As.Ap.Suppl.*, **138**, 119.
 Kurucz R.L.: 1993-1994, *Data Bank, CD-ROM NN 1-22*.
 Kurucz R.L., Furenlid I., et al.: 1984, *Solar flux atlas from 296 to 1300 nm, National Solar Observatory Atlas No.1., Cambridge: Harvard Univ.*, 239.
 Pavlenko Ya.V.: 2000, *Astron. Reports*, **77**, N4, 254.
 Yakovina L.A., Pavlenko Ya.V.: 2001, *Kinemat. and Physics of Celest. Bodies*, **17**, N5, 446.

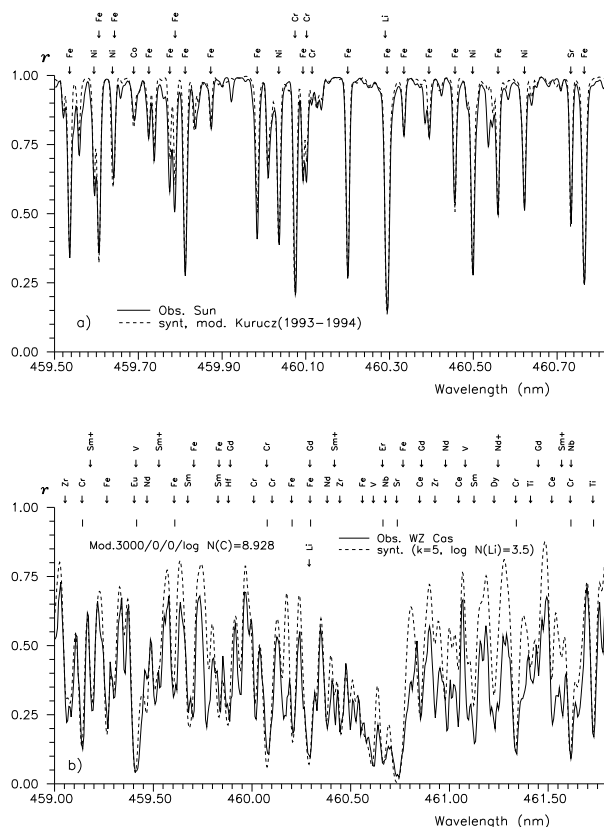


Figure 1: Fits to observed spectra (solid lines) of the Sun (a) and WZ Cas (b). The synthetic spectra are showed by dashed lines. Vertical strokes mark positions of strong atomic lines used for connection of observed and synthetic spectra.

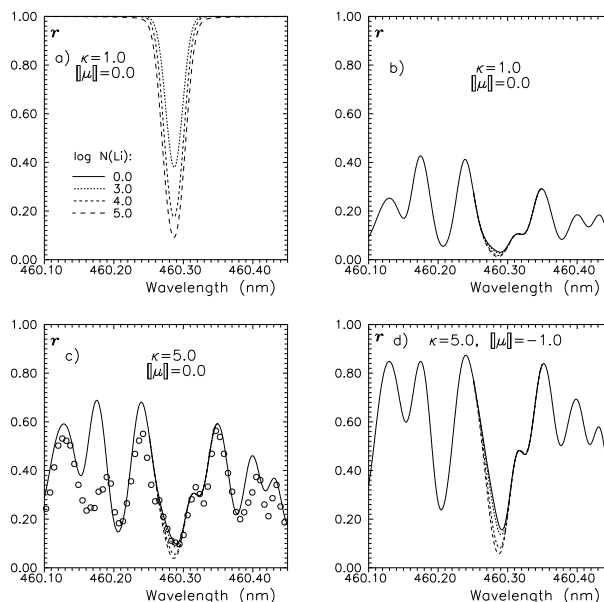


Figure 2: Sensitivity of the Li I triplet λ 460.3 nm and the blend containing one on $\log N(\text{Li})$ for different κ and metallicity. $\log N(\text{Li}) = 0.0, 3.0, 4.0, 5.0$. Observed spectrum of WZ Cas is shown by circles.

"OBSERVATION OBSCURER" - TIME SERIES VIEWER, EDITOR AND PROCESSOR

I.L. Andronov

Department of Astronomy, Odessa National University,
T.G.Shevchenko Park, Odessa 65014 Ukraine, *il-a@mail.od.ua*

ABSTRACT. The program is described, which contains a set of subroutines suitable for fast viewing and interactive filtering and processing of regularly and irregularly spaced time series. Being a 32-bit DOS application, it may be used as a default fast viewer/editor of time series in any computer shell ("commander") or in Windows. It allows to view the data in the "time" or "phase" mode, to remove ("obscure") or filter outstanding bad points; to make scale transformations and smoothing using few methods (e.g. mean with phase binning, determination of the statistically optimal number of phase bins; "running parabola" (Andronov, 1997, As.Ap. Suppl. 125, 207) fit and to make time series analysis using some methods, e.g. correlation, autocorrelation and histogram analysis; determination of extrema etc. Some features have been developed specially for variable star observers, e.g. the barycentric correction, the creation and fast analysis of "O-C" diagrams etc. The manual for "hot keys" is presented. The computer code was compiled with a 32-bit Free Pascal (www.freepascal.org).

Key words: Data reduction

1. Introduction

Despite hundreds of programs exist for various operating systems, which allow to visualize data and create graphs of different complexity, it takes time to run the program, load the data file. Many programs may draw graphs with automatically determined limits with further possibility of formatting the graph.

One of the aims of this program is fast visualizing the data, which allows the batch mode. Besides, it has additional possibilities oriented to data checking and preliminary data reduction. A part of these features is oriented to specific astronomical needs, partially connected to the variable star research. After running, the data are visualized with determining the limits automatically. The cursor marks the point, the characteristics of which are shown. This possibility allows to check the data, especially outstanding points and, if decided that this point is wrong, to delete (obscure) it. If the data are the compilation, there may be groups of

points of joint origin (same filter, telescope, observer), which should be deleted or analyzed. There is a possibility of a conversion of times to phases and vice versa, to scale and transform coordinates from linear to logarithmic and back, inverting etc.

The arrays reserved are the following: t_i - argument; x_i - signal; s_i - error estimate (sometimes may be used as a working array); e_i - working array. Contrary to electronic tables, the number of arrays is fixed. The graph always show a dependence of x_i vs t_i . Hereafter the value i will indicate a number of the current point, i_1 and i_2 are the first and last numbers of the point seen at the current screen.

The program is issued "as is", without warranty of any kind. If using, please refer to this paper.

The program is rapidly operated by "hot keys", contrary to the menu-oriented mouse control, which is usually applied in professional packages. Such an approach allows to speed up the work after learning the keys for most frequently used operations. The program can be classified as a viewer or simplified editor, complementary to that used in the shells like Norton Commander, Volkov Commander or FAR.

Running the program

The simplest way to run is just to launch "o.exe". Then the prompt for the file name occurs. The input file should contain columns of numbers separated by spaces. The commas and the tabulation symbol (#9) are not acceptable. It is possible to add one to four parameters in the fixed sequence:

[path]o.exe [[FileIn] [[Column] [[FileOut] [Skip]]],

where *[FileIn]* is the input file. Parameter *[Column]* is the column number - default is 0 for the "time" (t) axis and 1 for the "signal" (x) axis. If the column is set to zero, $t_j = j$, $j := 1..N$ where j is the trial number of observations, and N is their total number read by the program. If changing the column from within the program ("C" button, one may use negative values to use their absolute values without changing t from current values to column zero. The parameter *[FileOut]* is the name of the output file, to which one may write

results of data transformation/reduction. There is a special value "-", which will force typing to the screen the input data. This option is needed, if there are errors in the input data ("illegal real", often appears, if there are additional symbols or absence of the space separating the columns). The last parameter allows to skip [skip] lines at the beginning of the file. So large files may be viewed or processed in parts.

To exit the program, press **F10**, "Escape" or "Enter"; other "hot keys" are not duplicated;

The 16-bit "lite" version *O.EXE* is compiled with Turbo Pascal 6.0 (www.borland.com) and works with the number of data $N \leq 10\,000$, whereas the 32-bit version *OO.EXE* compiled with the Free Pascal (www.freepascal.org) has a limit $N \leq 300\,000$ and a lot of additional features.

If the number of data exceeds the limit, only a limiting value is read. To read other parts of the file, one may skip N_B lines. If the data are not sorted according to the argument, a note appears with a listing of inverse $t_{i-1} > t_i$. In the 32-bit version, it is possible to sort these data in ascending order of t_i . In the 16-bit version, the program determines the graphic resolution and automatically uses monochrome Hercules or 16-color EGA mode. The appropriate driver *herc.bgi* or *egavga.bgi* should be copied in a fixed directory *c:\Andronov*. In the 32-bit version, only EGA mode is possible.

For further designations, we use symbols @("Alt"), ^("Shift") and ^("Ctrl"). If few digits are listed after #, e.g. #123, this corresponds to a special symbol with this ASCII code. These digits should be pressed only at the numerical keyboard, after *Alt* is pressed, and releasing *Alt* after the code is entered completely. Alternatively, @6 means "Alt 6" (6 at the main, not numerical, keypad). The letters may be inserted in any case. Some "hot keys" are binary, e.g. *QR* means that the keys *Q* and *R* are pressed consequently. The number of the current point is designated as i , whereas usage of the index j means that all data points are transferred: $j := 1..N$. If the index $j - 1$ is used, then the cycle is $j := 2..N$.

The output files with fixed names corresponding to different functions, have the ".dat" extension, if they may be used as columns of data for further viewing/plotting, and have no extension, if they contain values of various nature. All these files have an underline "-" symbol as the first one in the file name.

The "hot keys" used in both versions, they are shown in the **bold** font, whereas the advanced commands, which are used in the 32-bit version only, are shown in the *slanted* font.

The first used line of the file is a control one. The program uses it for automatic definition of the format, which is used for the point and axis labels and the output. An entry likewise "-.1" is interpreted as -0.1 with adding a missing position. The data should be

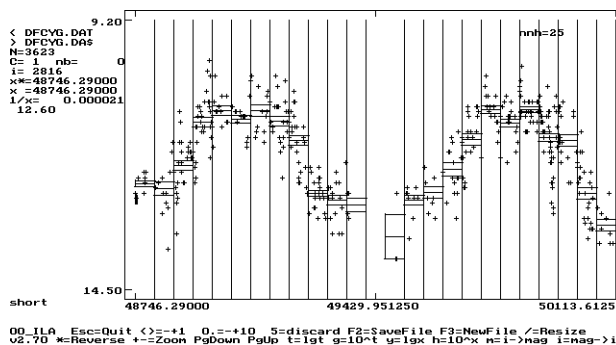


Figure 1: Interface of the program. Part of the light curve of pulsating variable star DF Cyg from the AFOEV database. The parameters listed at the left part of the figure (up to bottom):

input file (*dfcyg.dat*), output file (*dfcyg\$.dat*), number of data $N = 3623$, number of column $m = 1$, number of lines skipped $nb = 0$, number of current point marked with a vertical line $i = 3623$, current argument t_i (x^*), current argument t_i (x , not affected), inverse argument $1/t_i$, value of the signal x_i . The numbers at the borders show the limits of the argument and signal, respectively. Two bottom lines contain a short help. After pressing **F4**, the interval is splitted into $m(= 20)$ subintervals separated by vertical lines. The horizontal lines show mean values and $\pm 1\sigma$ values.

in fixed (not exponential) format in this line, whereas the rest may be in both formats. The format may be changed by pressing the "J" button - " $j1 : j2$ " ($j1$ digits, including $j2$ digits after decimal point) for t and $j3 : j4$ for x .

After reading the columns for t and x , the data are plotted with automatic determination of the limits and corresponding scaling.

Note, there is no multiple "undo", thus, using "undo" with switches, one should use them in the reverse order (likewise hierarchical loops).

To make the work with the program faster, the operation is based on the "hot keys" instead of menu. Here we present their list with a short description.

Screen changes

- + - zoom (twice pixels per argument interval);
- - unzoom (twice argument interval per pixel);
- L** - input axis limits;
- R** - restore automatic limits;
- E** - center current point at the screen;
- / - resize current window according to the signal limits;
- * - change direction of the signal axis;
- | - initial resize (set signal borders to limits for all data);
- F6** , ^left - shift window to the left by a half-width;
- F7** - make current point the left limit of the interval;

- F8** - make current point the right limit of the interval;
F9 , **^right** - shift window to the left by a half-width;
J - change output format of the argument ($j1 : j2$) and signal ($j3 : j4$);
Tab - swap $t_j \iff x_j$;
^Tab - swap $x_i \iff s_i$.
- Change the current point**
- Generally, if changing the point number i , it will be checked for (and, if needed, changed to) the range $[1, n]$, numbering neglecting skipped lines.
Home - first point of the screen;
End - last point of the screen;
^Home - first point of data;
^End - last point of data;
Down - lowest point of the screen;
Up - upper point of the screen;
Del, 5 - delete point above cursor;
- \leftarrow , **"3"** - $i:=i+1$;
 \rightarrow , **"1"** - $i:=i-1$;
0 - $i:=i-10$;
. - $i:=i+10$;
4 - $i:=i-100$;
5 - $i:=i+100$;
Z - $i:=i-1000$;
X - $i:=i+1000$;
7 - previous local extremum;
9 - next local extremum;
V - correct current point assuming regular argument spacing and cubic interpolation using 4 symmetric points, i.e. $x_i := (4 * (x_{i-1} + x_{i+1}) - x_{i-2} - x_{i+2})/6$ for $2 < i < n - 1$; this option may be used, if the point is erroneous and should be deleted, but from some reason the gap in the data is less wanted (e.g. if computing an autocorrelation function, fast Fourier transform etc.);
")) - delete all points with current signal value (remove horizontal line). This option may be used, if such a value indicates wrong value (out of detection);
- Data transformation switches**
- First click makes changes, second one on the same button - makes an inverse transformation. Please note: the inverse transformation will be made for *current* vector, so, if it was changed between pressing the buttons, the restored vector will *not coincide* with the initial one. If restoring, the rule is simple: the inverse transforms should be made in an inverse order.
- M** - the data x are transferred from intensities to magnitudes in the sense $x_j := -2.5 \lg(x_j/x_{max})$;
I - the data x are transferred from magnitudes to intensities in the sense $x_j := 10^{-0.4(x_j - x_{min})}$;
T - linear/log time scale: $t_j := \lg(t_j)$;
Y - linear/log signal scale: $x_j := \lg(x_j)$;
H - log/linear signal scale: $x_j := 10^{x_j}$;
G - exponential/linear scale: $t_j := 10^{t_j}$;
- \backslash - inverse argument $t_j := 1/t_j$ (e.g. time-frequency switch);
F - time - phase (the initial epoch T_0 , period P and quadratic term Q may be separately read into the program after pressing the buttons **O**, **P** and **Q**, respectively. By default, they are read from the file $c:\backslash Andronov \backslash c.z$.
% - add unity to signal from current point to the end (used for a diagram phase vs time);
^ (shift 6) - subtract unity from signal from current to the end;
#2 ..**#5** - divide current signal value x_i by 2.5 (this option is used e.g. when plotting time intervals between characteristic points, and few moments between them may be lost);
^Z - decrease shift u by unity and plot a map $(x_k, x_{k+u}, k = 1, n - u)$; minimal value of $u = 1$;
^X - increase shift u by unity and plot a map $(x_k, x_{k+u}, k = 1, n - u)$; maximal value of $u = n - 2$;
^R restore the arguments from a working array and show a full interval of data;
^F9 - divide: $x_i := x_i/t_i, i := 1, n$; if $t_i = 0$ then $x_i := 10^{32}$;
- Time-phase transformations are made according to the linear expression $t = T_0 + P_0 \cdot E + Q \cdot E^2$, the phase is computed as $\phi = E - E_j$, where $E_j = \text{INT}(E)$ is the integer cycle number;
- O** - input initial epoch T_0 and write to file;
P - input period P and write to file;
[- input quadratic term and write to file;
F - toggle t_i time-phase (computed for current T_0, P_0, Q);
^S - show phase curve for the next frequency listed in the file (cyclic rule: $i : ((i - 1) \bmod N) + 1$);
^A - show phase curve for the previous frequency listed in the file;
- (- compute deviations from the best linear fit and write to the file $_o-c_lin.dat$;
^P - set period value to the value last determined with a 3-point parabolic fit (with **"Ins"** button) or current argument t_i . Initial epoch T_0 and the quadratic term Q are set to zero;
^O - set initial epoch T_0 to the argument of current point t_i and save this value;
C - change column; if $C > 0$, the zero column is set to the argument t_i , and the C^{th} column as the signal x_i ; if $C = 0$, the zero column is set to the signal x_i and argument $t_i = i$; if $C < 0$, the argument t_i is not changed and the $(-C)^{th}$ column as the signal x_i ; the last possibility is used e.g. to plot nonzero column as the argument: press **C 2 Enter Tab C -3 Enter**. As a result, t_i is the second column, and x_i is the third column.
^N - the argument $t_j := j$ and the signal x_j is not changed;

- B** - skip lines till the current point inclusive;
- ^U** - evaluation of the smoothed value using the linear fit;
- A** - compute autocorrelation function for all N data: $ACF_{u+1} := R_u/R_0$, $R_u := \sum_{i=1}^{N-u} x_i x_{i+u}$, the argument is set to $t_i := i - 1$.
- @6** - remove all data outside the window and replace the data with the autocorrelation function.
- F2** - save all data
- @F2** - save data from the current window only;
- F3** - read new file;
- F4** - split current window into subintervals $l := 1..m$, compute mean \bar{x}_l , unbiased root mean square deviation of the data from the mean σ_l , error estimate of the mean σ_{xl} . Results $(l, \bar{x}_l, \sigma_l, \sigma_{xl})$ are written (appended) to the file `_f4.dat`.
- ^F4** - compute mean values from m subsequent points and append to the same file;
- @F4** - histogram of the data from current window (split into m subintervals).
- F5** - switch between "short" and "long" types of marking the intervals. In the "short" mode, the output file name is transferred from the input name by changing the last symbol to "!" ("#" in the "long" mode). The interval limits marked with **F7** and **F8** are written to the file: n_1, t_{n1}, n_2, t_{n2} . In the "long" mode, the output format is: number of points; next lines: $t_i, x_i, i := n_1..n_2$.
- Ins** - Determination of the extremum nearest to the current point by using 3 points $(i - 1, i, i + 1)$. In the left window, the information appears on the argument and signal value in this approximation. If the argument axis is transformed, the initial value is also shown. Eg., if the argument was transferred logarithmically, then one may see the value in the linear scale.
- ^2** - switch between presenting data as small/large circles; in the 32-bit version, large symbols mode also corresponds to a local cubic interpolation line

Work with phases

- '** $x_j := \text{frac}(x_j)$ - leave only fractional part of the signal;
- Q F** - $x_j := v - \text{int}(v + 0.5)$, $v := (t_i - T_0)/P_0$, $j = 1..N$; i.e. x_j is the phase corresponding to the current values of T_0 and P_0 .
- &** $x_j := t_{j+1} - t_j$, $j = 1..N - 1$; $x_i = x_i + j_i$, where an integer j_i is determined so that $j_1 := 0$ and $|x_{i+1} - x_i| \leq 0.5$. This option is used when the signal is the phase. If the phase variations are smooth, this option is usually sufficient to restore proper cycle numbering; otherwise one may use manual cycle renumbering using buttons **@5** and **@6**.
- @5** - $x_i := x_i + 1$, $i := i + 1$;
- @6** - $x_i := x_i - 1$, $i := i + 1$;

U U - Determination of the corrected values of the period P and initial epoch T_0 assuming x_i are the phases, t_i are times, and (possibly) s_i are error estimates. For such redetermination, the current values of T_0 and P_0 are used (either read from the "c.z" file or after pressing **O** or **P**).

Error column

- K** insert column number for the array s_j (e.g. with error estimates);
- ^W** effective error corresponding to the mean weight:
- $$\sigma_h = \left(\frac{1}{n} \left(\sum_{i=1}^N \sigma_i^{-2}\right)\right)^{-1/2}, \quad \sigma_a = \frac{1}{n} \sum_{i=1}^N \sigma_i,$$
- $$N_{eff} = \left(\sum_{i=1}^N \sigma_i^{-4}\right) / \sum_{i=1}^N \sigma_i^{-2}.$$

Work with data labels

While working with data obtained from different sources, sometimes it is needed to select a part of them according to the source, e.g. to the observer. For time series analysis of the AFOEV (<http://cdsarc.u-strasbg.fr/afoev>) and VSOLJ (<http://www.kusastro.kyoto-u.ac.jp>) data, we use an intermediate format (time, magnitude, 3-symbol abbreviation of the observer). These 3 last symbols are read (in the 32-bit version) as an array and are shown at the screen with the information of the current point. Few operations are available with the subset of data having the same mark:

- ^-** - put mark (observer's abbreviation) of the current point to be a selected one. All points with the same label will be drawn in another (???) color.
- ^Del** - delete all observations with the same mark;
- ^Ins** - leave only observations with the same mark, delete others;

"Non-undo" data transformation.

- ^G** - generator of the signals, including periodic (sinusoidal and asymmetric), uncorrelated random (Gauss, χ^2 , Cauchy et al. distributions) autoregressive models of the first and user-defined order and chaotic processes;
- Q 0** - $x_j := a * x_j + b * s_j$, $j = 1..N$; the coefficients a and b are requested; this option is used e.g. if computing 1σ deviations from the signal or to compute deviations $O - C(x_j - s_j)$ of the signal from the fit;
- Q S** - $x_j := \sqrt{x_j^2 - a^2}$, $j = 1..N$; the coefficient a is requested;

- Q D** - approximation of the derivative dx/dt by linear expression: $x_{j-1} := (x_j - x_{j-1})/(t_j - t_{j-1})$; $t_{j-1} := (t_j + t_{j-1})/2$.
- Q Y** - $d(x^2)/dt$. This option is used e.g. in the scalegram analysis. Computing the scalegram the test function $\sigma_{O-C}(\Delta t)$ (unbiased r.m.s. deviation of the data from the fit, Andronov, 1997), one may determine the derivative of the energy on $\lg \Delta t$ to obtain the scalegram.
- Q 1** - t_j to the integer cycle number (e.g. primary minimum in eclipsing variables);
- Q 2** - $t_j - P_0/2$ to the integer cycle number (e.g. secondary minimum);
- Q P** - $x_j := x_j \cdot P_0$, $j = 1..N$. This option is used to transfer phases to "O-C".
- Q I** - Table of interpolated data using local cubic fit using 4 nearby data points. This is a spline of power 3 and defect 2, i.e. despite the interpolation is correct for the polynomial of power up to 3, the first derivative may be discontinuous at the arguments of points. The same interpolation is used for drawing an interpolation curve (button).
- Q 6** - square: $x_j := x_j^2$, $j := 1..N$.
- Q S**, **@S** - sort data (t_i, x_i, s_i) in ascending order of t_i .
- Q ** - switch "show s_j " (used e.g. to show both data and a fit);
- Q /** - table of values smoothed using running parabolae
- Q *** - double the data using local cubic polynomial assuming regular spacing of arguments. This option is used to make graph more smooth.
- Q T** - time correction: input two times, where corrections are made. This option is used e.g., if the file contains computer times, which should be corrected using linear approximation.
- Q Q** - linear transformation: $x_j := a + b \cdot x_j + c \cdot t_j$, the coefficients a , b , c should be requested.
- Q R** - inverse computation $x_j := (x_j - a - c \cdot t_j)/b$, is made.
- Q ?** - computes the scalegram assuming a histogram-like fit (spline of power 0 and defect 1) of the data present at the current window for numbers of subintervals $m = 1..50$.

The weights of all the data are assumed to be the same. The following test functions are written to the file with fixed name *_scale.dat*: the trial number of subintervals m , number of subintervals with at least one point m_1 ; r.m.s. deviation of the smoothing value from the mean σ_C ; unbiased value of the r.m.s. deviation of the data from corresponding smoothing values σ_0 ; the "S/N" ("signal/noise") ratio σ_C/σ_{xc} ; the r.m.s. error estimate of the smoothing value σ_{xc} ; the number of points in the current window n_v . The file "_scale.dat" may be studied separately, but, after running the present command, the program determines m_{max} corresponding to the maximal value of "S/N" and uses it for showing the "histogram-like". This feature is an extension of that

available by pressing *F4*, because allows to use the optimal value of m instead of the user-defined one.

Launching external programs

@R - runs external program from the list in the file "c:\Andronov\0.mnu"; the format of the file is "Short description of the program", "full name of the file to be run"; the symbol ";" in the first line means that the line is ignored as a comment; the symbol "-" in the first line means that the line contains "minus" symbols and is used for separation of different groups of programs; likewise menu in Volkov Commander, it is possible to make submenus by making a link to a file with ".mnu" extension. The only restriction for one submenu is 20 lines, just to make them not exceeding the standard PC text screen. At the end of the command line, the file name is added, as a parameter. This option is suitable, if using an external program to proceed (edit file, make computation or preparation of the print-quality figure etc). E.g., if the file contains the line *Edit,c:\vc\e.exe*, the command executed will be: *c:\command.com /c c:\vc\e.exe filename*, where *filename* is the name of the current file being processed by the program *OO.exe*. Of course, this option may be used as a launcher of any DOS/Windows programs, neglecting the *filename* parameter. As usual, the filenames containing spaces, should be written likewise "c:\Program Files\FAR\far.exe".

@T - the same as above, but the data visible at the current screen are written to the file *tmp.dat*, and this fixed file name is used as a parameter instead of the name of the current file containing all the data. This option may be suitable if processing subintervals of the data using an external program, e.g. for determination of the extrema or other local characteristics of variability. So the commands **@T** and **@R** may be used to make possibility of using external programs instead of plugins in the Windows programs.

Q B - runs "c:\Andronov\Bary.exe", the external program, which computes barycentric correction used in the variable star research and then replaces arguments t_i by barycentric values.

Running parabola fits

For smoothing the data, we have used the method of running parabolae with a filter half-width Δt (Andronov, 1990). This free parameter Δt may be determined from the scalegram analysis (Andronov, 1997). However, the scalegrams are computed using a separate program, thus Δt should be input manually after pressing $\uparrow F6$. The commands are:

$\uparrow F6$ - input Δt and compute the smoothing values at the arguments t_i and store them as s_i instead of possible error estimates.

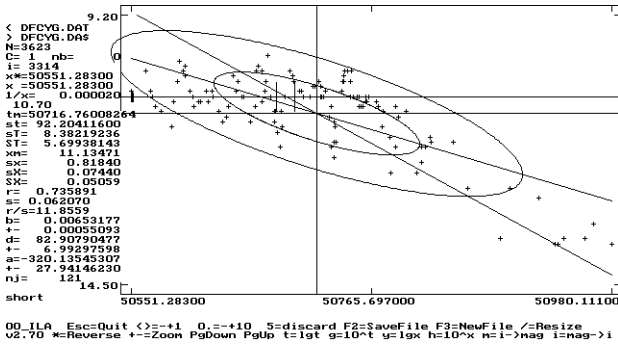


Figure 2: Results of the correlation analysis. The regression lines are $x = x_m + b(t - t_m) = a + bt$, $t = t_m + d(x - x_m) = c + dt$, the correlation coefficient r , its error estimate s , number of points n_j , mean argument tm , its r.m.s. deviation from the mean, standard error of the mean for constant sT and linear ST fits.

Evaluation of the trigonometric polynomial

This option for the data visible at the screen is available by pressing two buttons $Q8$. The fixed value of the period is used, being equal to that used for the phase computations, by default, being read from the parameter file $c.z$ or changed after pressing the P button. In the phase curve mode (switched by the F button), the period is set to unity. The test functions computed for different values of the degree of the trigonometric polynomial $s = 0..s_m$ are written both to the screen and the file $_four$ and are subject to make decision on the degree of the polynomial. The following columns are shown: s – the degree of the polynomial (starting from 0, i.e. constant); $sig_0 = \sigma_0$ – the unit weight error, $sxc = \sigma[x_C]$ – mean error estimate of the values of the smoothing function computed at the arguments of real data; S/N_a – "amplitude signal-to-noise ratio", which is equal to the r.m.s. deviation of the fit from the mean to the mean error estimate of the fit; "Degeneracy" of the matrix of normal equations being equal to 1 for diagonal matrices and 0 for degenerate ones; Lp – is the "false alarm probability" to get a signal of such an amplitude for a pure white noise of the amplitude σ_0 ; S/N_F – is the Fischer's ratio of variances with 2 and $n_j - 2s - 1$ degrees of freedom; $Ampl$ – is the amplitude of the last harmonic wave used (with a period of P/s) and $Ampl/sig$ is the ratio of this amplitude to its error estimate. To choose the optimal value of s , one may use several test functions. A classic way is to use the Lp , which shows the Fischer's probability of 10^{-Lp} , so one may use the minimum limiting value of Lp_m , e.g. 2.5 corresponding to the "3 σ " criterion and to determine a maximum value of s , for which $Lp \geq Lp_m$. We use another criterion similar to that in the method

of "running parabola" scalegrams – the maximum of S/N_a – which usually corresponds to much smaller values of s , often even $s = 1$ (single harmonic fit). In our program, the optimal value of s , corresponding to this criterion, is determined and proposed as the default one in the forthcoming dialog. However, one may use other value, e.g. corresponding to the minimum of the test function $\sigma[x_C]$. However, for noisy signals, the minimum corresponds to $s = 0$, i.e. to the mean value, neglecting variations. The formulae and the description of the more advanced specialized program $FDCN$ is described by Andronov (1994).

Further information written to the file $_four.dat$ is: the unit weight error σ_0 , then the coefficients of the fit

$$x_c(t) = c_1 + \sum_{j=1}^s (C_{2j} \cos(j\omega t) + C_{2j+1} \sin(j\omega t)) \quad (1)$$

and their error estimates. The matrix A_{ij}^{-1} , which is needed for computation of errors of the smoothing function and its characteristics (see Andronov 1994 for more details), is printed at the end of the file, and may be used by external programs. In this version, the weights are assumed to be equal for all data points.

The output file $_four.c.dat$ may be created on request to be used for creating figures. It contains argument or phase, the smoothed value x_C , its error estimate σ and then two columns $x_C - \sigma$ and $x_C + \sigma$.

The file $_four.dat$ contains 3 columns ($t_i, x_i, x_C(t_i)$) and may be used for further preparation of printer-quality graph. It should be noted, that, despite this file contains n points, the fit itself is computed for the points at the screen only. So, for "global" fit, the screen should contain all the data before processing.

Further development

In the current version, the main purpose is to include features, which need visualisation and interactive processing. The set of well-working specialised programs for the time series analysis may be run either separately or from within the program $OO.exe$. From this point of view, there is no necessity to translate these programs from other languages to FreePascal. However, some new features may be included in further releases of this program. The bugs may be reported to the author at il-a@mail.od.ua

Acknowledgements. The author is thankful to the developers of the Turbo Pascal 6.0 (www.borland.com) and Free Pascal (www.freepascal.org) for their compilers allowing to prepare these programs. For illustration, we have used the data from the AFOEV international database (cdsarc.u-strasbg.fr/afoev). Many features have been added on requests from my colleagues.

References

- Andronov I.L.: 1994, *Odessa Astron. Publ.*, **7**, 49.
Andronov I.L.: 1997, *As. Ap. Suppl.*, **125**, 207.

ELABORATION OF THE BATCH OF THE PROGRAMS FOR CELESTIAL MECHANICS FOR THE COMPUTATION OF THE ASTRONOMICAL EPHEMERIS

V.V. Mikhalchuk

Odessa State Maritime Academy
Didrikhsona 8, Odessa 65029 Ukraine, *phys@ma.odessa.ua*

ABSTRACT. The batch of the programs for celestial mechanics are elaborated in order to obtain the ephemeris of the Sun, the Moon, the planets and their satellites, the asteroids, the comets, the binary stars, the variables stars, determination of the conditions of the visibility these the celestial bodies at any point of the surface of the Earth, as well as predict the astronomical phenomena's at the celestial sphere and their circumstances.

Key words: Batch of the programs for the astronomical ephemeris.

1. Introduction

Author from 1991 elaborates the batch of the programs by celestial mechanics. The batch are created in order to obtain the ephemeris of the Sun, the Moon, the planets and their satellites, the asteroids, the comets, the binary stars, the variables stars. The programs of the batch permit determine of the conditions of the visibility these the celestial bodies in the any point of the surface of the Earth, as well as predict of the astronomical phenomena's at the celestial sphere and their circumstances as for the Earth on the whole also for given point Earth's surface.

2. Description of the batch of the programs

2.1. Possibility of the batch of the programs

When calculation of the ephemeris of the celestial bodies have primary meaning spare to informatively of the programs. The high informatively of the programs of the given batch permit comprehend the great variety of the astronomical phenomena's by ephemerid, universal, zonal and legal time of the any station.

The results of calculations take out as the form of the tables also in the form graphic. The ephemeris of the Sun, the Moon the major planets, as well as the circumstances of the astronomical phenomena's for these the celestial bodies are determine at the temporal

interval about 5000 years in the past and the future. Also have possibility determine the physical ephemeris of the Sun, the Moon, and the major planets.

The database of the batch contains the orbital elements of the 50 bright asteroids and 100 comets. The coordinates of the 1500 stars, are contains in the database of the batch, permit to get the star catalogue and the celestial map for any epoch at the temporal interval about 30000 years in the past and the future. At the celestial map show the geocentric and the topocentric positions of the Sun, the Moon and the planets on the given moment of the time, as well as the visible roads of the their motion. There are represent the phases of the Moon and the planets, the pictures of the solar and lunar eclipses. There are draw the geographic maps of the zones of the visible of the solar and lunar eclipses, the occultations of stars and planets by the Moon, the occultations of stars by the planets, the transits of planets on the disk of the Sun. There are show the pictures of the schemes of the motion of the objects for the lunar eclipses, the transits of planets on the disk of the Sun and the systems of the satellites of the planets.

All programs of the given batch are writes at the algorithmic language Quick Basic, working in the operation system MS-DOS and have the commons resources: the commons library subroutines and the commons database.

2.2 The apply methods

At the programs for determination of the position of the Sun, the Moon and the major planets, the asteroids and the comets are apply methods, are describe in the (Meeus, 1988). The position of the Pluto is determinate by the method, is describe in the (Montenbruk, Pfeleger, 1993). The main perturbations for the positions of the Sun, the Mercury, the Venus, and the Mars are complete in the (Montenbruk, Pfeleger, 1993), for the positions of the planets-giants - in the (Gaillot, 1904; 1910; 1913), for the position of the Moon - in the (Montenbruk, Pfeleger, 1993; Ed. Duboshin, 1976).

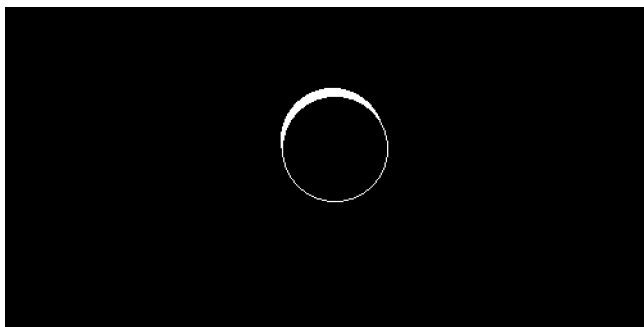


Figure 1: The solar eclipse on 11 August 1999 at 11^h12^m UT, visible in Odessa

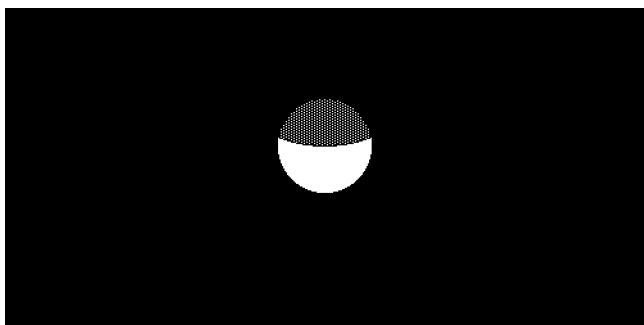


Figure 2: The lunar eclipse on 5 July 2001 at 14^h55^m UT

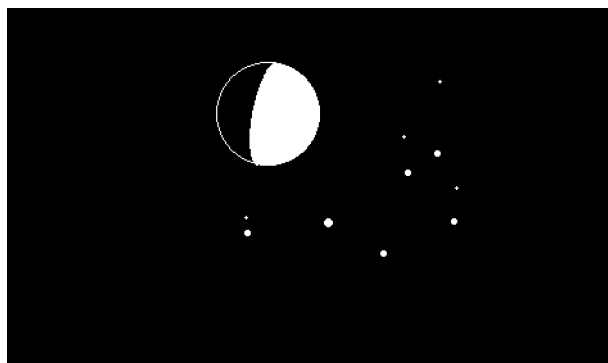


Figure 3: The Moon on 4 February 1990 at 0^h00^m UT, visible in Odessa

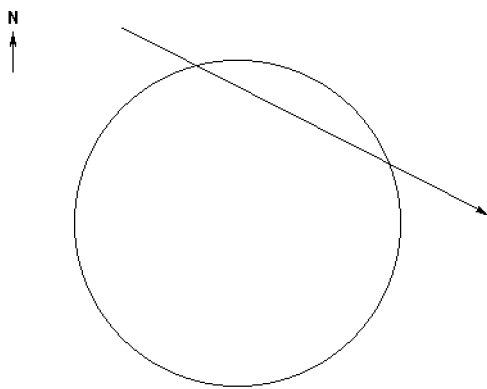


Figure 4: The transit of Mercury on the disk of the Sun on 7 May 2003

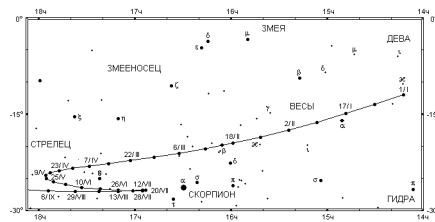


Figure 5: The visible road of the Mars from January to August 2001

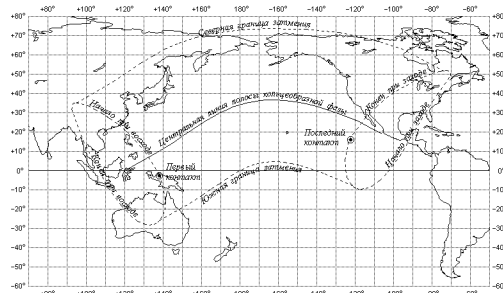


Figure 6: The map of the visible of the solar eclipse on 11 June 2002

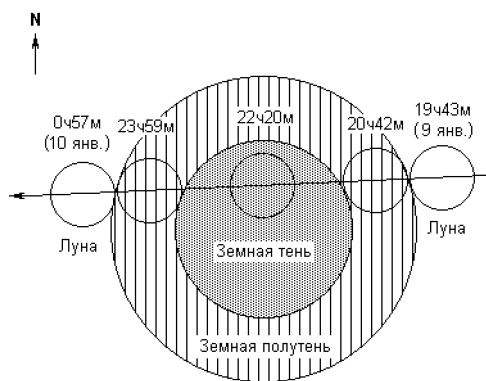


Figure 7: The visible road of the Moon on the eclipse 9 January 2001



Figure 8: The configuration of Galilean satellites of Jupiter on January 2001

Запад

Восток



Figure 9: The satellites of Saturn on 6 February 2001 at 0^h00^m UT

The physical coordinates of the Sun, the Moon and the major planets are determined by method (Abalakin, 1979; Ed. Abalakin, 1989-1997). The longitude of the central meridian of the illuminated part of the visible disks of the planets is calculated by the exact formulas (Mikhalchuk, 2001). The circumstances of the solar and lunar eclipses, occultations and the transits of planets on the disk of the Sun are determined by methods (Mikhailov, 1954). The mean and the visible places of the stars are determined by methods (Ed. Abalakin, 1989-1997). For determination of the moments of the phases of the Moon, as well as the positions of the planet's satellites and phenomena's in the systems of the planet's satellites are apply methods, are elaborated by author.

2.3 The accuracy of the output information

The accuracy of the information, which output by the programs, is equally: for the moments of the time 1 min.; for the coordinates of the points of the Earth's surface 0.1°; for the heliocentric and the geocentric ecliptic coordinates 0.1°; for the distances 0.001 AU; for the heliocentric and the geocentric equatorial coordinates of the Sun 0.1^s by the right ascension and 1'' by the declination; for the geocentric and the topocentric equatorial coordinates of the Moon, the planets, the asteroids and the comets 1^s by the right ascension and 0.1' by the declination, for the physical coordinates of the Sun, the Moon, and the planets 0.1°. Equatorial coordinates of the mean and the visible places of the stars are outputted with the accuracy to 0.1^s by the right ascension and 1'' by the declination.

All celestial coordinates of the Sun, the Moon, and the major planets are reference to the mean equinox of the date. The coordinates of the Pluto, the asteroids, the comets and the stars are can reference both to the mean equinox of the date and to any standard equinox.

2.4 The composition of the batch of the programs

In the composition of the considered batch come in the following programs:

EPHEMECL - calculation of the ephemeris of the Sun, the Moon and the major planets (the heliocentric and the geocentric ecliptic coordinates, the geocentric and the topocentric equatorial coordinates, the conditions of the visibility in the any point of the surface of the Earth (the information about the rises, the settings and the culminations of the celestial objects and about the duration their visibility), the visible diameter, the phase, the magnitude), the physical coordinates of the Sun, the Moon and the major planets, the moments of the transits of the main points of the orbits of the Earth, the Moon and the major planets, the moments of the conjunctions of planets with the Moon and with each other, the phases of the Moon, the configurations of the planets, the circumstances of the solar and lunar eclipses, occultations of planets by the Moon, the transits of planets on the disk of the Sun as for the Earth on the whole also for given point Earth's surface, the positions of the satellites of the Jupiter and the Saturn;

ASTERCOM - calculation of the ephemeris of the Sun, the Moon, the major planets, the asteroids and the comets (the heliocentric and the geocentric ecliptic coordinates, the geocentric and the topocentric equatorial coordinates, the conditions of the visibility in the any point of the surface of the Earth, the magnitudes, the visible diameters of the Sun, the Moon, the major planets and the asteroids), the moments of the beginning and the end of the twilights, the moments of the transits of the main points of the orbits of the Earth, the major planets, the asteroids and the comets, the configurations of the major planets, the asteroids and the comets;

STARS - determination of the mean and the visible places of the stars, the conditions of the visibility of the stars in the any point of the surface of the Earth, the moments of the conjunctions of the Moon and the planets with the stars, the circumstances of the occultations of stars by the Moon and the planets, the construction of the celestial maps;

SATELLIT - determination of the positions of the satellites of the planets (Galilean satellites of Jupiter and 6 the most bright satellites of Saturn), the configurations of the satellites, the phenomenon's in the systems of the satellites of the planets, as well as calculation of the ephemeris of the Sun, the Moon and the major planets;

BINSTAR - calculation of the ephemeris of the visual binary stars;

VARSTAR - determination of the moments of the maximums (minimums) of the brightness of the periodic variable stars;

MAPS - construction in the various projections of the geographic maps of the zones of the visibility of the solar and lunar eclipses, occultations of stars and planets by the Moon, occultations of stars by the planets, the transits of planets on the disk of the Sun;

ELORB - determination of the elements of the orbits

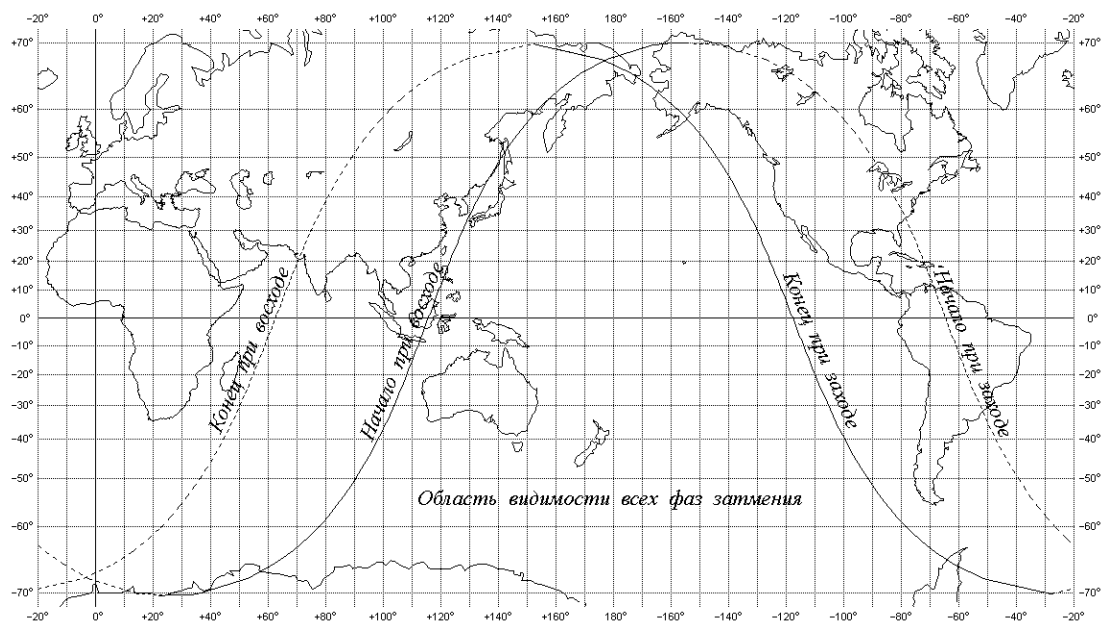


Figure 10: The map of the visible of the lunar eclipse 26 May 2002

by 3 points;

HORIZON - calculation of the correction for geographic latitude to the moments of the rising and the setting of the celestial bodies, as well as to the azimuths and the hour angles of the points of their rising and setting.

3. Conclusion

The results, are give by this batch of the programs, was permit the author do begin the annual issue of the collection of the scientific-popular articles "The Odessa Astronomical Calendar" (OAC) from 2000 in common with the Astronomical Observatory of the Odessa National University. These results are publication in the main part of the OAC and are intended for the amateurs of astronomy and the professional workers of southern locale of Ukraine.

References

- Abalakin V.K.: 1979, *Osnovy efemeridnoi astronomii (Principles of Ephemeride Astronomy)*.
- Abalakin V.K.: 1989-1997, *Ed. Astronomicheskii ezegodnik na 1991-1998 gody (Astronomical 1991-1998 Yearbook)*.
- Duboshin G.N.: 1976, *Ed. Spravochnoe rukovodstvo po nebesnoi mekhanike i astrodinamike (Reference Book for Celestial Mechanics and Astrodynamics)*.
- Gaillot M.A. *Annales de l'Observatoire de Paris, Memoires*. **V.24**, 1904; **V.28**, 1910; **V.31**, 1913.
- Meeus J.: 1988, *Astronomical Formulae for Calculators*.
- Mikhailov A.A.: 1954, *Teoria zatmenii (Theory of Eclipses)*.
- Mikhalchuk V.V.: 2001, Determination of Planetocentric Coordinates of the Center of the Illuminated Part of the Spherical Planet's Visible Disk, *Astron. Vestnik*, **35**, No.1, pp.89-96.
- Montenbruk O., Pflieger T.: 1993, *Astronomy with Personal Computer*.

ON THE ERRORS IN PRACTICE OF OBSERVATIONS AND THEIR REDUCTIONS

A.E. Rosenbush

Main Astronomical Observatory, National Academy of Sciences of Ukraine,
Golosiiv, Kyiv-127, 03680, Ukraine, *mijush@mao.kiev.ua*

ABSTRACT. Specific errors are not rare in the practice of astrophysical observations. Examples of such errors are given.

Key words: observations: errors.

1. Misidentification of object

The practice of observations on modern telescopes convince us that the accurate of telescope pointing on an object is on a level of several arcsecs. The analogic accurate may characterize the definition of observable object coordinates on the sensors. If the coordinates of objects are systematic different then this, among other things, may be caused by the distinguish of these objects, i.e., we observe two different objects.

It is presented a history of the identification of V605 Aql by the IR observations of V605 Aql, which initially lead to peculiar characteristics of this variable [Rosenbush 1999; Kimeswenger et al. 2001]. The peculiarity in the IR spectral energy distribution is disappeared after the correct identification.

As it seems to us the question of identification of this object do not be close yet. Kimeswenger et al. give the A58's coordinates which are also equal to V605 Aql: 19h 18m 20.42s (epoch 2000.0) 01° 47' 01.1". At that time the IRAS's coordinates are: 19h 18m 19.9s (epoch 2000.0) 01° 46' 49.9".

I.e., we have considerable distinguishes only in the declination which is more than the photometer's aperture size or the CCD pixel.

2. Software for the reduction of observations

The wide spreading of the software for the reduction of observations arises one more problem, connected with an re-installation of this software in other computer working with different OS.

3. On an analytical formula of the Earth's velocity

The use of high-resolution spectroscopy, in addition to others, puts in the forefront the necessity to take into consideration the nonuniform moving of the observation point. This is both the Earth's orbital velocity

and the velocity of her rotation. The latter reaches 465 m/s in the equator and it needs to take into consideration only the latitude of observatory. The taking into account of the first is more complicated by the ellipticity of the Earth's orbit, and the perturbations from the Moon and the planets. For all of these corrections exist both an analytical formulae and the analytical expressions (the latter is traditional for the computer's calculations). Comparing to one another we have the possibility to chose the best.

We made this comparison for the analytical formula for taking into account the orbital velocity of the Earth from any course of practical astrophysics beginning from Vorontsov-Velyaminov (the 30-th) and ending by Martynov (the last publication in the 80-th)

$$v = V_a \cdot \cos b \cdot \sin(l_\odot - l + i). \quad (1)$$

The ellipticity of the Earth's orbit come into the expression in two terms: the velocity V_a and the angle i . The value of the angle i varies within the limits from -57' up to 57' and the analytical formulae exists for this

$$\operatorname{tg} i = e \sin(l_\odot - \pi) / (1 + e \cos(l_\odot - \pi)). \quad (2)$$

If we make the comparison between the Earth's velocity by this formulae and by any analytical expression, for example, then we find systematic difference up to +0.6 km/s. It disappears if we change the sign of i in the common formulae. The final difference does not exceed 50 km/s. In one's turn, the comparison of the Soma et al.'s expression with the more exact ephemeris given the difference not more 1.64 m/s. I.e., the common formula has the error and it needs to change the sign of i , than the formula takes the form

$$v = V_a \cos b \sin(l_\odot - l - i). \quad (3)$$

References

- Rosenbush A.E.: 1999, *Astrophysics*, **42**, 425.
Kimeswenger S., Koller J., Schmeja S.: 2000, *As.Ap.*, **360**, 699.
Soma M., Hirayama T., Kinoshita H.: 1988, *Celest. Mech.*, **41**, 389.

GENERAL CATALOGUE OF VARIABLE STARS

N.N. Samus^{1,2}, E.V. Kazarovets¹, O.V. Durlевич²

¹ Institute of Astronomy, Russian Academy of Sciences

48 Pyatnitskaya Str., Moscow 109017 Russia, *samus@sai.msu.ru*, *elena.k@sai.msu.ru*

² Sternberg Astronomical Institute, Moscow University

13 University Ave., Moscow 119899 Russia, *gcv@sai.msu.ru*

ABSTRACT. The General Catalogue of Variable Stars (GCVS) is a large-scale project undertaken in Moscow since 1946 on behalf of the IAU. After a brief outline of its history, we discuss current problems of variable star catalogues and present our plans for the nearest future, including determination of accurate coordinates for all GCVS stars, new Name-lists, improvements of the classification scheme, *etc.*

Key words: Stars: variable; astronomical catalogues.

1. Introduction

The history of catalogues of variable stars begins as early as 1786, when Edward Pigott published his first list of 12 objects. In the early 20th century, before the 2nd World War, catalogues of variable stars were compiled at the Berlin-Babelsberg Observatory on behalf of the “Astronomische Gesellschaft”, a society competing, at that time, with the International Astronomical Union (IAU) as a coordinator of international astronomical research. These catalogues were regularly published till 1942, first by R. Prager and then, after his emigration from nazi Germany, by H. Schneller. Only after the war, the IAU assumed responsibility for variable star catalogues and commissioned this job to two groups in Moscow, the Variable Star Commission of the Academy of Sciences (now the GCVS group at the Institute of Astronomy, Russian Acad. Sci.) and the Variable Star Department of Sternberg Astronomical Institute (now the GCVS group in the Department of Galactic Studies and Variable Stars of Sternberg Astronomical Institute, Moscow University). The leaders of the project in Russia were P.P. Parenago (1906–1960), B.V. Kukarkin (1909–1977), P.N. Kholopov (1922–1988). They were among the founders of the renowned traditions of the USSR astronomers in variable star research. One of the leading representatives of this tradition was the many-year Director of the Odessa Observatory, Prof. V.P. Tsessevich. His studies of RR Lyraes and of young irregular variables, and especially his famous Atlas of Finding Charts, are still widely used by the community of astronomers studying variable stars.

B.V. Kukarkin and P.N. Kholopov initiated the work on the fourth edition of the GCVS in the second half of the 1970ies. This work was finished only comparatively recently, in mid-1990ies. The fourth edition consists of five volumes and contains more than 28000 reliable variable stars of the Galaxy, almost 11000 variable stars in external galaxies, and about 1000 reliable or suspected extragalactic supernovae. The 4th GCVS edition is complimented by the New Catalogue of Suspected Variable Stars (the NSV Catalogue; Kholopov, 1982), with 14810 objects; many of these objects have since become GCVS stars.

The Moscow GCVS team was, on behalf of the IAU, the official center of information on variable stars till 1994, when the IAU discontinued funding for the GCVS project. Nevertheless, we continue our GCVS activity and, though we do see serious problems in our work (to be discussed below), are ready to remain the world center of the variable star catalogues. Our work is supported by the IAU Commissions 27 and 42.

2. GCVS: Traditions and New Trends

The long history of the GCVS has created a number of traditions. The GCVS is intended to include only reliable variable stars that should be sufficiently well investigated, so that they could be attributed to one of numerous variability types of the existing elaborated classification system or declared “unique” variables, not attributable to any type (and maybe future prototypes of new variability types). If a star meets these criteria, it will be included in one of the Name-lists of Variable Stars where it will get its “variable star name”, like RR Lyrae (the well-known prototype of pulsating halo stars) or V1343 Aquilae (the famous SS 433). The GCVS names of prototypes and of unique objects are actively used by many astronomers, and thus we are forced to continue the use of the traditional nomenclature of variable stars (R–Z, RR–ZZ, AB–QZ, V335... in each constellation, with the letter J not used) despite its being obviously clumsy.

We have recently published the 76th Name-list of

Variable Stars (Kazarovets et al., 2001), and now the GCVS system includes 37391 "named" variables (this number does not include spurious objects, now proven to be nonexistent, but includes named variables for which further studies led to doubts in variability). Normally, the GCVS team critically evaluates published variability information; in many cases, we used to derive new light elements from published photometric data, to change published classifications according to uniform criteria, etc. Stars with doubtful variability or insufficiently studied variable stars should be included into catalogues of suspected variable stars. Recently, we published a catalogue of 11206 stars suspected in variability since the publication of the NSV catalogue (Kazarovets *et al.*, 1998).

The situation with variable stars has changed rather drastically during the recent decade. Several large-scale space-borne or ground-based projects aimed at automatic discovery of variable stars have been successfully carried out and resulted in discoveries of many thousands of new variable stars. Our traditional individual approach to each star included into the GCVS becomes very difficult to be continued. However, we cannot just drop this tradition and include new stars into the GCVS with the published information accepted "as is". Here our experience with the 74th Name-list of Variable Stars (Kazarovets *et al.*, 1999), specially devoted to new variable stars discovered by the Hipparcos mission (ESA, 1997), teaches us a number of important lessons.

The Hipparcos team initially suggested the authors of the GCVS to give GCVS names to 5665 stars, of which, only (only!) 3157 were then named by us. It may be interesting to note that the selection process, with our usual individual approach to candidate objects, was completed in one month. The majority of the stars not named were included into the Supplement to the NSV Catalog (Kazarovets *et al.*, 1998); a small number of stars were found identical with stars already having GCVS or NSV identifications (and not recognized as such by the Hipparcos team). Hipparcos variables included into the NSV Supplement (a total of 1956 objects) are mostly stars with information insufficient for even more or less reliable determination of their variability types. Of the 3157 newly named Hipparcos variables, nearly 50 percent (1464 stars) have uncertain classification. We have encountered a number of cases of spurious variability in the Hipparcos data: due to wrong identifications in the input catalogue, some stars were attributed absolutely wrong spectral types, resulting in erroneous photometric reductions.

This experience shows some drawbacks of even a very good large-scale automatic survey from the GCVS point of view:

First, observations are scheduled according to reasons far from those of variable-star research. As a

result, it is difficult to derive types for stars with certain characteristics. Interesting enough, pulsating variables dominate in the sample of the named Hipparcos variables (2027 of 3157 stars). There are practically no Cepheids among new Hipparcos variables (11 stars have been attributed to all subtypes of CEP, DCEP, or CW variables, and for 10 of them classification is uncertain). The Hipparcos team admits that it was especially difficult to derive, from their data, periods in the typical Cepheid period range. The number of RR Lyraes is also low (28 stars, only 6 of them with certain classification). Contrary, Delta Scuti and SX Phe stars are well represented (97 stars, certain classification for 68 of them). Semiregular and irregular variables give a total of 1692 stars, 54 percent of the sample. Thus, the distribution of the stars of the 74th Name-list over types is rather peculiar.

Second, insufficient attention to identifications makes it more difficult to analyse photometric data. In the Hipparcos project, extensive use was made of SIMBAD data base. This important source of astronomical information contains, however, quite a number of mistakes and incompletenesses in identifications (resulting, in particular, from the fact that, up to recently, many catalogs had very bad positional accuracy). In the process of our work on the 74th Name-list, we revealed more than 500 mistakes or imperfections in SIMBAD identifications.

It is obvious that one of the most important drawbacks of the existing catalogues of "old" variable stars, making automatic identification with "new" variable stars difficult or even impossible, is their low positional accuracy. Formally, the equatorial coordinates presented in the published 4th GCVS edition are given to 1° in right ascension and to $0'.1$ in declination. Actually, the accuracy of the GCVS coordinates, usually just taken from discovery announcements, can be very different. Till the beginning of the XXth century, many discoverers used to determine quite accurate coordinates for their newly-discovered variable stars, and these coordinates were *rounded* by GCVS compilers. Then, discoverers at Harvard and Sonneberg Observatories, who were most active in the variable star research (at each of the two observatories, more than 13000 variable stars were discovered photographically), began to present only very rough coordinates. Besides rare cases of absolutely wrong positions (errors up to 1° or even more), many *faint* variable stars have positions in error by several arcminutes. We think that drastic improvement of positional accuracy for all "old" GCVS stars is a very urgent task. Many groups in the world are now working in this field. It is now much easier to solve the problem thanks to catalogues like the US Naval Observatory A1.0/A2.0 catalogue (Monet *et al.*, 1998) containing more than 500 million stars with positional accuracy quite sufficient for automatic identifications. (Even larger catalogues begin to appear.)

For variable stars not contained in the A1.0/A2.0 catalogue, it is often possible to use A1.0/A2.0 catalogue objects as reference stars and apply simple astrometric methods to Digitized Sky Survey images. A new and very important tool is the Pixel Server of the US Naval Observatory where one can retrieve images from all existing Sky Survey Schmidt plates, often scanned with better resolution than in the Digitized Sky Survey.

Our group possesses the most complete information on “old” variable stars and is now approaching the problem of accurate coordinates systematically. We have recently prepared a version of the GCVS Volume I (constellations Andromeda–Crux) containing, whenever possible, improved positions and proper motions for variable stars. In this version, sufficiently accurate coordinates are presented for more than 8400 stars. Similar work is in progress for Volume II, improved coordinates have already been listed for about 4600 stars. For identifications, we try to use all published positions, photometric information, finding charts. Similar work on identifications and positions of variable stars is being done by several researchers in other countries, among them C. Lopez, T. Kato, B. Skiff, R. Webbink, G. Williams, and others. Comparison of results makes it possible to reveal mistakes and solve especially complicated cases.

It is to be noted that finding charts are available practically for all variable stars discovered at Sonneberg Observatory, and thus it is possible to find them despite published coordinates being very rough for many stars. On the other hand, several thousand Harvard variables have no finding charts published, and in many cases their identification is not straightforward. Fortunately, the accuracy of published coordinates is, on average, better for Harvard variables than for Sonneberg variables. Some red stars can be identified taking into account their associations with infrared objects of the IRAS catalogue. In our work on the “astrometric” version of the GCVS Volume I, we have been able to recover a number of variable stars on plates of Moscow collection of sky photographs and of the Maria Mitchell Observatory plate collection. Hundreds of variable stars were recovered in the Harvard plate stacks by Drs. M. Hazen and G. Williams, whom we are most grateful for cooperation. They are often able to use ink marks left by discoverers on the plates. Some cases remain very difficult despite serious attempts to solve them.

Another important thing to do for the GCVS team is to improve the classification scheme for variable stars. It is tempting to introduce many new types of variable stars, and we are often urged by experts on particular kinds of variables to do so. But the GCVS team must consider our catalogs as products to be used by a rather wide community of astronomers, and the existing version of the classification system already contains too many types to be easily understood by the

users. We would be grateful for suggestions aimed to a clear and *minimally* sufficient system of variable-star classification. Again, our experience with the Hipparcos Name-list teaches us some important lessons, mainly concerning the classification scheme for pulsating stars, for example:

— Among red stars, we meet probable pulsators not only among supergiants and giants but also among subgiants. For subgiants and especially for dwarfs, it is not easy to decide whether the observed variability is due to rotation or to pulsation. Already, it seems justified to introduce a type for semiregular pulsating red subgiants.

— Among red giants and supergiants, the Hipparcos team derived quite a number of short periods of variability (of the order of days). The light curves do not look very convincing. If real, such periods would cause problems for interpretation and make it necessary to revise the classification of numerous “old” SRB, SRC, LB, and LC stars for which such a behavior was even not looked for. A new type for red giant and supergiant variables with short periods (SRS), presumably overtone pulsators, has just been introduced into the GCVS scheme (Kazarovets et al., 2001).

— Among O–F stars, we meet variables, and probably pulsating ones, not quite satisfying GCVS criteria for DSCT, SXPHE, BCEP, or ACYG-type stars. The Gamma Dor stars, actively introduced as a new type of pulsating variables (*e.g.* Balona et al., 1994), are obviously a related phenomenon (the corresponding GCVS type was introduced by us in the 75th Name-list – Kazarovets et al., 2000), as are the Maia variables, suggested long ago and not understood until recent improvements of stellar opacities.

We are aware of many classification problems besides the short above list concerning only pulsating stars. Thus, most recently we have had to introduce, for the first time in many years, a new type of eclipsing variables (EP, a star eclipsed with a planet).

Having in mind future survey, to be surely expected to result in a still much higher rate of variable-star discoveries, it is important to develop a fully automated approach to preliminary classifications of variable stars on the base of photometric information. This work is now beginning in Moscow.

So far, the Hipparcos Name-list was our first experience with large surveys. Quite a number of stars of other, comparatively minor, surveys (*e.g.* Takamizawa’s program of variable star discoveries) have been included in our regular Name-lists, but new special Name-lists, dedicated to larger surveys, will follow. Here we would like to emphasize that, provided a large survey presents well-structured information on variable stars, such a survey becomes self-sufficient to a considerable degree, a variable star catalogue in itself, and delays with GCVS naming are not so worrying in such cases. Almost perfect is, for example, the pre-

sentation of data in many OGLE publications (see, for instance, Udalski *et al.*, 1994). However, the level of OGLE classification (eclipsers, short-period pulsators, miscellaneous periodic variables) is insufficient for traditions of variable star research. The same holds for the first impressive results of the ASAS project (Pojmanski *et al.*, 2000), presented as a detailed catalogue of several thousand variables, even with light curves and epoch photometry, but again with insufficiently detailed classification. On the other hand, the availability of data from some other surveys (for example, MACHO) becomes a serious problem, to be discussed at the IAU level. The MACHO team members promised, at the IAU Colloquium No. 183 (Taiwan, January 2001), to send us a list of their discoveries, with coordinates, within several weeks; this promise has not been fulfilled, despite reminders. If, in a survey project, thousands of stars are being discovered, but only a small part of them are being announced in a manner sufficient for subsequent identification, the rest of the discoveries are effectively lost.

The delays with special Name-lists for large surveys and the problem of acquiring good coordinates for “old” GCVS stars are obviously interconnected: to be able to check automatically if a newly discovered variable is really a new objects or already a GCVS star, we need good coordinates *both* for the newly discovered stars *and* for all stars of the GCVS.

It is also a problem if a comparatively small survey provides only few observations per star, like the MISAO project. The majority of stars in such surveys, good large-amplitude variables, remain objects for catalogues of suspected variables because it is not possible to classify them with the data available.

Summing up, we can say that the situation with variable stars discovered in large-scale automatic surveys is generally more or less satisfactory from the GCVS point of view, though we are somewhat slow with “special” Name-lists dedicated to such surveys: the results of many surveys are published in a self-sufficient, catalogue-like form. Variable stars discovered individually or in small surveys are regularly included into

Name-lists. Since 1999, we give GCVS designations to Novae announced in IAU Circulars within days, upon request from the IAUC editors.

For new GCVS, NSV, and NSV Supplement versions, regularly corrected and improved, with search options, see our web site at <http://www.sai.msu.su/groups/cluster/gcvs/gcvs/>

Acknowledgements. Our GCVS work is supported, in part, by grants from the Russian Foundation for Basic Research (99-02-16333), Federal Programme “Astronomy” (2.1.1.6), Council for Support to Leading Scientific Schools of Russia (00-15-96627), and American Association of Variable Star Observers.

References

- Balona L.A., Krisciunas K., Cousins A.W.J.: 1994, *M.N.R.A.S.*, **270**, 905.
- ESA: 1997, *The Hipparcos and Tycho Catalogues*, *ESA SP-1200*.
- Kazarovets E.V., Samus N.N., Durlevich O.V.: 1998, *Comm. 27 and 42 IAU Inform. Bull. Var. Stars*, No. **4655**.
- Kazarovets E.V., Samus N.N., Durlevich O.V. et al.: 1999, *Comm. 27 and 42 IAU Inform. Bull. Var. Stars*, No. **4659**.
- Kazarovets E.V., Samus N.N., Durlevich O.V.: 2000, *Comm. 27 and 42 IAU Inform. Bull. Var. Stars*, No. **4870**.
- Kazarovets E.V., Samus N.N., Durlevich O.V.: 2001, *Comm. 27 and 42 IAU Inform. Bull. Var. Stars*, No. **5135**.
- Kholopov P.N. (ed.): 1982, *New Catalogue of Suspected Variable Stars*, Moscow: Nauka.
- Monet D., Bird A., Canzian B. et al.: 1998, *USNO-A V2.0. A Catalog of Astrometric Standards, US Naval Observatory (11 CD ROMs)*.
- Pojmanski G. et al.: 2000, <http://archive.princeton.edu/~asas/>
- Udalski A., Kubiak M., Szymanski M. et al.: 1994, *Acta Astron.*, **44**, 317.

THE SYSTEM FOR QUICK MONITORING OF ASTRONOMICAL PLATE ARCHIVES. MAIN PRINCIPLES AND PURPOSES.

A.V. Sergeev¹, T.P. Sergeeva²

¹ Centre of Astronomical and Medico-Ecological Investigations

31 Akademika Zabolotnoho, Kyiv 03680 Ukraine, *sergeev@mao.kiev.ua*

² Main Astronomical Observatory, National Academy of Sciences of Ukraine,

27 Akademika Zabolotnoho, Kyiv 03680 Ukraine, *sergeev@mao.kiev.ua*

ABSTRACT. We propose to create a system for quick search and analyses of astronomical events and objects in plate archive of the Ukrainian Main astronomical observatory of NAS. The proposed idea of effective restoring of astronomic information is based on the treatment of the digitized plate archive as whole. The plates will be digitized by commercial scanner with optical resolution of 20 mkm and resolution on amplitude of 4096 grey levels. Such scanning parameters give the opportunity to receive the plate image files of the reasonable sizes suitable enough to identify the required object and to define its precise photometric characteristics. Connection of the system to Internet will allow a remote user to have access to plate images archive and to work with it. Modular structure of the system basic software and standard format of the plate image files allow future development of problem-oriented software for special astronomical researches by means of the cooperative projects.

Key words: Photographic plates: collections: data archives; photographic plate: digitization: methods; image processing: data bases.

1. Introduction

During the period when the photographic plates have been used in observational astronomy the world observatories have accumulated two, possibly up to three millions astronomical plates which have been processed only in a part accordingly to scientific task or not have been processed at all. Many of them contain the unique information about astronomical events or objects, registered at the moment of observation, but not call for till now. Among them are the variables of diverse nature, asteroids, comets and other Sun system bodies, optical sources in direction of gamma-bursts and other interesting objects. The information about this events or objects can not be obtained or restored

with the help of any modern facilities, space missions included, and so may be useful for many astronomical investigations.

The threat of astronomical plate archive loss caused by economical, technical or some other causes have put before world astronomical community a problem: the preservation of the unique information kept on those plates. The problem is solving by transformation of the information from plates to digital forms and keeping it on electronic data medium. There are two approaches to the solution. The most widespread one till some recent years is the global scanning of plates with high spatial resolution by specially designed measuring machines. The digitization of a single plate with such machines takes several hours. Volumes of the received information run up to 100 Gigabytes for one plate. Processing and storage of such data volumes are technically complicated and expensive. However, not for all astronomical investigations such image sampling is necessary.

In nineties new digitizing technology based on flat-bed commercial scanners equipped with transparency extention had appeared (see for more information the proceedings of the International Workshop "Threshure-Hunting in Astronomical Plate Archives", 1999, Sonneberg). There are a lot of scanner models from different producers on the market with rather wide range of parameters to satisfy many of astronomical scientific tasks.

2. System concept and main principles

The proposed system for quick monitoring of astronomical plate archives is intended for quick looking up and analyses of astronomical events and objects in electronic archives of plate images. For effective restoring of historical astronomic information it is necessary to work with digitized plate archive as whole. In such case

the sizes of plate image files become very crucial. But they depend significantly from the parameters of digitization. So if the plates will be digitized by commercial scanner with optical resolution of 20 mkm and resolution on amplitude of 4096 grey levels it will allow to receive file-images with sizes not exceeding hundreds and even tens Megabyte (dependently on plate size). For effective work with archive of plate images special data base for all photographic plate collection is necessary

If the exact definition of coordinates of researched object will be necessary some other digitization methods can be used among which is the measuring with precise measuring machines like an automatic measuring complex PARSEC, automated coordinatometer "Askorecord" and so on.

So the main principles of proposed system for quick monitoring of astronomical plate archives may be formulated such as:

- The system is oriented on looking up and detection of astronomical events and objects that have been registered on plates but have not been found in previous researches.

- The hardware and software of the system allow receiving file-image of the plate with spatial resolution not above 20 microns and dynamical range up to 4096 grey levels.

- The database of plates, which permits operatively receiving of the information on availability of necessary area plates and their characteristics, is employed.

- The simultaneous access to the file-images of all plates of the necessary sky region is provided.

- The three-level software is constructed on a modular approach and will be gradually developed according to problems to be solved.

- The standard formats of file-images are used.

- Extended users access to archive of the file-images, databases and software by methods of modern information technology are intended.

3. Purposes and tasks

The first step is the development of the network-accessible database of the Ukrainian Main astronomical observatory of NAS plate collection. The plate archive of MAO is accounted more than 15000 astronomical plates, obtained during last 50 years which are good for the monitoring of astronomical events and objects. When a suitable scanner will be obtained the creation of plate-images electronic archive will begin with parallel development image database and software environment creations for archive fast viewing and carrying-out researches on its basis. The next step will be the organization of access to archive and its service software for the remote user. The connection to the international integrated electronic fund of

the plate-images (incorporated virtual observatory) is assumed. The scientific programs to be solved with the system for quick monitoring of astronomical plate archives are such as:

- Opening of new and missed astronomical objects in the Universe.

- Monitoring and searching for new and missed bodies of the Solar System, near-Earth asteroids included.

- Researching of flare and other variable stars.

- Looking up and research of optical objects in directions of gamma-bursts. - Informational support of the space projects.

4. Hardware and software solutions

The minimum hardware requirements are:

- The scanner with a capability of large format (up to 300300) slides digitization with optical resolution up to 1200 dpi (20 microns image sampling) and discrediting on amplitude up to 4096 grey levels (12 bits of an analog-digital converter).

- Connected to the scanner IBM PC compatible computer with the central processing unit not lower than eleron 800Mhz, RAM 256b, hard disk not less 10Gb, and recorder for CD-ROM.

- IBM PC compatible computer with the central processing unit not lower than a Pentium - III 800Mhz, RAM 512Mb, having RAID-massive by a volume 100-200Gb for storage of digital archive and astronomical researches on its basis.

- The Internet connection based on the leased line with throughput not lower than 64Kbit/sec.

The modular software will have three levels structure:

1 level - digitization of plates, preliminary processing and storing of plate image files.

2 level - work with digital archive, image processing, search and detection of astronomical events and objects.

3 level - remote users support.

The modular and extensible basic software and standard format of the file-images allow future development of the problem-oriented software for special astronomical researches by means of the cooperative projects

5. First results

Ten plates have been scanned on small format scanners to determine the revealing abilities at various parameters and conditions of scanning, coordinate and photometric errors of scanners. The selective analysis of the MAO NAS of Ukraine plate archive have been carry out and some hundreds plate have been selected for search and rediscovery of asteroids. On plates, received in 1950 - 1970, several traces from asteroids, for

the first time discovered in 1996- 1998, were found and measured.

The photometric characteristics of the images of NGC-6913 cluster stars on two plates of the Goloseev's double wide-angle astrograph have been determined. We have found very good conformity of photometric characteristics (obtained with external accuracy of $0^m.13$ and $0^m.15$) between the plates.

The positional accuracy with the certificated test-plate has been evaluated. It was found that there is the difference between X and Y pixel size caused by the difference of mechanical and optical discretization steps sizes, and the dependence of the pixel size from the distance between a plate and CCD line. The reproducibility of distances between objects was about ± 0.5 pixel.

5. Conclusion

The development of system for quick monitoring of electronic plate- images archives based on inexpensive commercial scanner with optical resolution of 20 mkm and resolution on amplitude of 4096 grey levels give us an opportunity to extract the unique historical information from astronomical plates. Such digitization parameters will allow to receive file-images of plates with sizes not exceeding hundreds and even tens Megabyte without compression. This files allow to identify required objects and to determine their exact photometric characteristics that permit to realize various astronomical investigations.

Acknowledgements. The authors are thankful to Organizing Committee for financial support.

CCD DETECTOR IN TV STANDARD WITH SMALL EXPOSURE TIME

O.S. Shahrukhanov¹, A.V. Yushchenko¹, O. Techuk²

¹ Astronomical Observatory, Odessa National University, Ukraine
Shevchenko Park, Odessa, 65014, Ukraine, *root@lens.tenet.odessa.ua*

² Odessa National Politechnical University, Ukraine

ABSTRACT. We constructed CCD-device working in TV standard. The exposure time can be changed from 1 to 16 TV frames. We report the results of test observations with new CCD-device and discuss the possible types of observations with this device.

Key words: instrumentation: detectors;

1. Introduction

Now it is usual to use high-precision CCD-devices for photometry, spectroscopy, astrometry and other branches of astronomy. These CCD devices are of different types - from big and expensive professional CCDs with sizes up to 50-200 mm to small PC cameras, which can be used only for observations of very bright objects by amateurs.

In this work we report the results of our attempt of construction a relatively cheap device which can be used in professional astronomy for a precise measurements (guiding, search of objects, etc.). This device is working in TV standard. We show the structural scheme of this CCD and present the results of test observations.

2. The structural scheme

We constructed the device for work in TV standard. Exposition time can be selected in discrete mode (1,2,4,8,16 TV frames). The output in TV standard permit us to see images on TV-monitor, to use computer with TV-tuner for registration and digitization of images, to write images on videotapes or computer hard disk.

The device was made without cooling. It permit us to made very compact and light receiver. Our detector can be used instead of eyepiece, guide, etc. The size of CCD chip in this device is near 4.5x6 mm.

On Fig. 1 we show the structural scheme of the device. *Digital distributor* produce impulses, which are necessary for reading information from CCD in the units of amplitudes of digital electronic schemes.

Timer can block the receiving of control information. The time of the blocking can be varied by *external device*. *Voltage transformer* transform the levels of voltage of digital electronic schemes to levels, which are necessary to control CCD. After reading from CCD, the signal is amplified by an *amplifier* and transformed to TV standard by *TV pattern generator*. The next operation is output of the signal in TV standard to *external device*.

As an external device we can use TV videomonitor or computer. In the first case the exposition time can be varied with the help of digital switch. In the second case the connection with computer can be made with the help of TV-tuner. The parallel port can be used for control the exposure time. In all cases the unit of the time of exposition is one TV frame - 0.02 seconds.

2. Observations

We made test observations with photographic objective and small 15-cm refractor to find the limiting magnitude of our device with these optics. Observations were made in the center of Odessa city. The quality of the sky was quit good in both cases.

In the first case we used photographic objective with a focal length 85 mm and diameter 49 mm. We used no filters. With exposition time 16 TV frames (each frame - 0.02 sec) we detected star of 8.0 magnitude (spectral class F4). With exposition time 8 TV images we detected star of 7.5 magnitude (spectral class B9).

In the second case we used 15-cm refractor with focal length 2.8 meters. For increasing of the field of view we used simple focal reducer. The equivalent focal length of the telescope was reduced nearly twice. We observed photometric standards in Pliades. The faintest stars, that we were able to observe was 10.2 magnitude star (spectral class G0). The used exposition time was 16 TV frames.

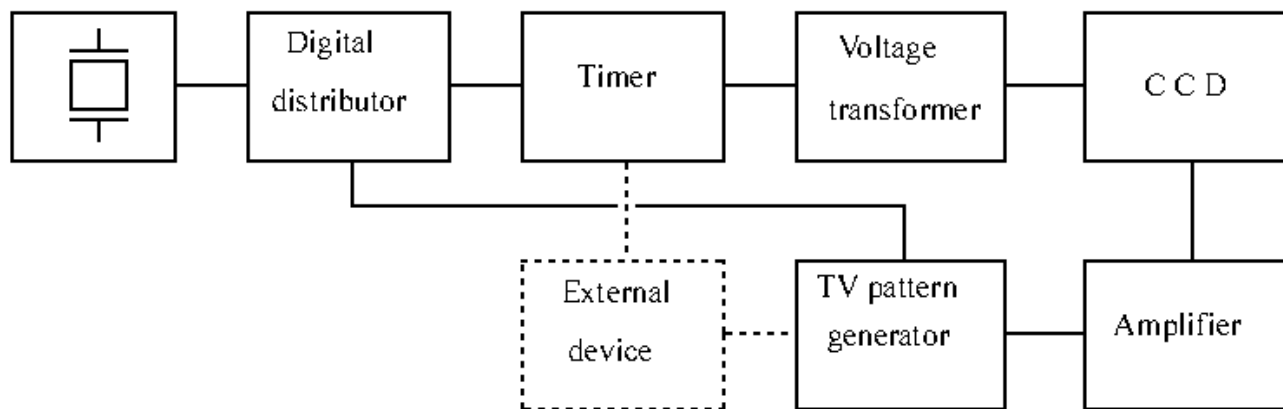


Figure 1: The structural scheme of CCD receiver in TV standard

5. Conclusion

We hope that described device will be useful for observation of artificial satellites, for guiding, for astrometry, etc. When using with the telescope with large focal length it is necessary to use focal reducer if we want to reach faint stars.

The main feature of observations in TV standard is high time resolution. This feature can be useful

in different type of observations. The digitization of image in TV standard can be made with 8-bit transformer. In many cases this precision is sufficient.

We hope that this device will be the first in the series of CCD detectors. We will use cooling in the next devices of this series. It will permit to increase limiting magnitude and exposure time.

INFRARED PHOTOMETRY OF SAKURAI'S OBJECT (V4334 Sgr) IN 1996-2000

A.M. Tatarnikov¹, V.I. Shenavrin¹, P. A. Whitelock², M.W. Feast³, B.F. Yudin¹

¹ Sternberg Astronomical Institute, Universitetskii pr. 13,
Moscow; 119899 Russia *yudin@sai.msu.ru*

² South African Astronomical Observatory, South African Republic

³ Cape Town University, Cape Town, South African Republic

ABSTRACT The results of the photometric observations of V4334 Sgr and characteristics of its evolution after outburst are presented.

Key words: Stars: variables and peculiar; stars: individual: V4334 Sgr.

On the 20, 1996, the Japanese amateur astronomer Sakurai discovered a novalike variable in Sagittarius; it was designated as V4334 Sgr and is commonly referred as Sakurai's object. It happened one year after its outburst. The observations of V4334 Sgr by Duerbeck and Benetti (1996) immediately after its discovery show that the star is similar to an F supergiant whose atmosphere is depleted of hydrogen and enriched with carbon and oxygen. They also detected an old planetary nebula of low surface brightness around the star. All these findings led them to suggest that V4334 Sgr was a star that underwent the final helium flash at the stage when it was already a planetary nebula nucleus. After the flash, the star returns to the Post AGB track, initially moving backward along it, i.e., gradually cooling down through its expansion. Such novalike stars were called born again AGB stars, which include FG Sge, V605 Aql, and V4334 Sgr.

The photometric *JHKLM* observations of V4334 Sgr are being carried out with the 1.9-m SAAO telescope (South Africa) and with the 1.25-m telescope at the Crimean Station of Sternberg Astronomical Institute.

Figure 1 shows *V*, *K* magnitude and *B* – *V*, *H* – *L* color variations in V4334 Sgr, as well as variations in its bolometric magnitude and in the optical depth of its dust shell at the wavelength of $1.25\mu\text{m}$ (Tatarnikov et al. 2001, and references therein). Before calculating m_{bol} the magnitudes were corrected for interstellar reddening with color excess $E(B - V) = 0.^m54$. In this way, the bolometric light curve differs from the remaining light curves in Fig. 1, which were not dereddened. The arrows mark the times when the bolometric flux reached its maximum and when the first profound visual fading of the star began.

After outburst V4334 Sgr has passed already through four well-defined stages as it moved backward along Post AGB track. At the first stage (1996), there was not dust in the star's shell. Its visual brightness slightly increased, as the bolometric flux, and it reddened (Fig. 1). At the second stage (1997), an optically thick dust shell condensed around the star, which, however, essentially did not manifest itself at optical wavelength ($V \approx const$, Fig.1). The bolometric flux continued to rise though an increase in the star's IR brightness alone; the rate of its rise also increased.

At the third stage (1998-March 1999), V4334 Sgr entered the R CrB phase. First two shallow minima and then two deep minima were observed in optical wavelength. Before the first deep minimum (July 1998) the bolometric flux had reached its maximum value and began to gradually fall in the second part of 1998.

At the fourth stage (since March 1999 up till now), V4334 Sgr has been at a protracted deep minimum, which is typical of the R CrB stars. The total amplitude of the bolometric flux variations was about 0.5 mag, and they did not correlate with the variations of the optical depth of the dust shell.

Until the mid-summer of 2000, the optical depth of the dust shell had increased gradually, but non-monotonically to its maximum $\tau(J) \approx 11.3$, which was reached in July. The model of a two-layer dust shell, in which each layer is formed with a constant rate of dust condensation at the inner boundary of the dust envelope, satisfactory reproduces the rate of increase in its mass, at least until the mid-summer of 2000. The second, denser layer began to form in July 1998 through an approximately fivefold increase in dust production, from $\sim 3.5 \times 10^{-8}$ to $\sim 2.0 \times 10^{-7} M_{\odot}/\text{yr}$ (Tatarnikov et al. 2001). The fraction large ($a_{gr} = 0.2 - 0.3\mu\text{m}$) grains were increasing remarkably during its formation.

References

- Duerbeck H.W., Benetti S.: 1996, *Ap. J.*, **468**, L111.
Tatarnikov A.M., Shenavrin V.I., Whitelock P.A.,
Feast M.V., Yudin B.F.: 2001, *Astron.Lett.* **27**, 534.

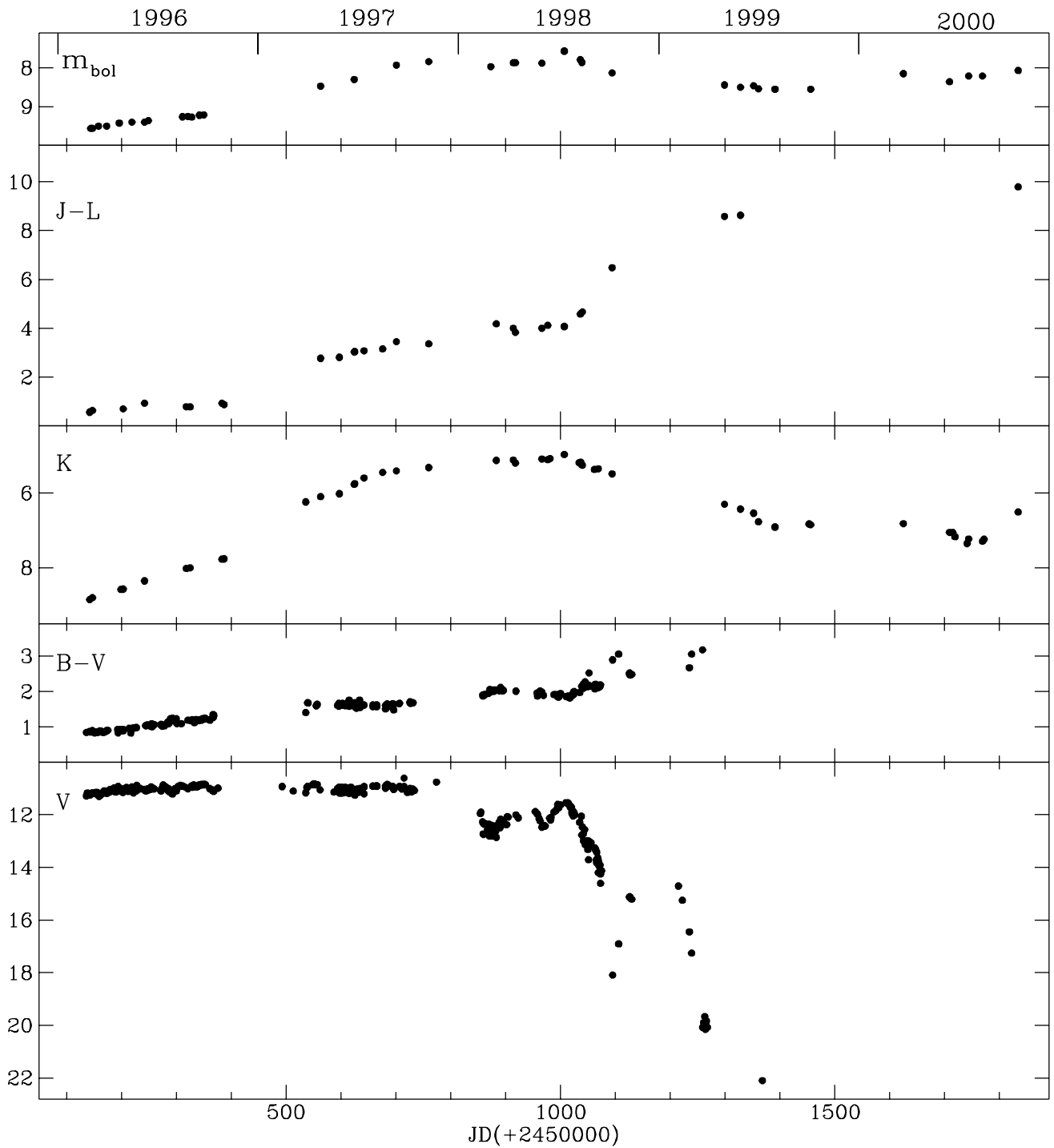


Figure 1: Variations in the V and K magnitude, $B - V$ and $H - L$ color, and bolometric magnitude m_{bol} of the V4334 Sgr and in the optical depth $\tau(J)$ of the dust envelope during 1996-2000.

PHOTOMETRIC AND SPECTROPHOTOMETRIC OBSERVATIONS OF THE CLASSICAL SYMBIOTIC STAR YY Her

A.A. Tatarnikova¹, E.A. Kolotilov¹, U. Munari², B.F. Yudin¹

¹ Sternberg Astronomical Institute, Universitetskij pr. 13,
Moscow, 119899 Russia *aat@sai.msu.ru*

² Padua Astronomical Observatory (Asiago Station), Italy

ABSTRACT The spectrophotometric and photometric observations of the classical symbiotic star YY Her both during its quiescent state and during a strong outburst in 1993 are presented.

Key words: Stars: binary: symbiotic; stars: individual: YY Her.

We carried out *UBV*-photometric, spectrophotometric and high-dispersion spectral observations of classical symbiotic star YY Her using 0.6-m and 1.25-m telescopes of the Crimean Laboratory of the Sternberg Astronomical Institute, and 1.8-m telescope of the Padua Observatory in Asiago (Italy). The results of the observations were published by Tatarnikova et al. (2001) (and references therein).

Figure 1 shows the *UBV* light curves of the classical symbiotic star YY Her both during its quiescent state and during a strong outburst in 1993.

The variability of the *U*-brightness in the quiescent state is due to eclipse of most part of the nebula by cool component and the great amplitude of the primary minimum ($\Delta U \approx 1^m6$) is indirect evidence that the line of sight is close to the binary orbital plane. The minimum in 1997 (third from the beginning of the outburst) is characterized by long-time phase ($\sim 0.17P$, where $P = 586^d$ is the orbital period) of constant lowest brightness. If we consider this minimum in the framework of classical model of eclipse of hot component and circumstellar envelope, the main contributor to the filter *U*, this would mean that cool component of YY Her fills its Roche lobe for anything real relation M_{hot}/M_{giant} .

In the quiescent state the red giant's radiation dominates in visual lights even at phases near photometric maxima. Therefore, at this time, the visual light curve characterize the variability of the cool component of YY Her. The existence of the shallow ($\leq 0^m2$) secondary minimum in the visual lights may be connected with the ellipsoidal shape of the red giant. This would mean that the cool component of YY Her fills essential

part of its tidal volume.

Figure 2 presents UV+optical spectrum of YY Her, which was obtained near maximum of brightness during strong outburst in 1993. In the quiescent state the energy distribution of YY Her in UV and optical diaspans may be represented in terms of three-component spherical model (hot subdwarf + gaseous nebula + red giant). But in the active phase the essential excess of near-UV radiation was observed. The energy distribution in the spectrum of this additional warm component (may be accretion disk) may be represented with sufficient precision by means of Planck's curve for black body radiation with $T_{warm} \approx 13000$ K. The luminosity of the warm component was near $\sim 10\%$ from the luminosity of the hot component.

On the Figure 2 the thin line indicate dereddened total UV+optical spectrum of YY Her during outburst (color excess $E(B - V) = 0^m2$); the thick line - calculated continuum energy distribution of the star in the "spherical + warm component" model; dashed lines - contributions of the radiation sources forming the total emergent flux: hot subdwarf, warm component, cool component (M3.5III) and the nebula, which absorb all Lc-photons of the hot component. The energy distribution in the spectra of first two components are black body curves with $T_{hot} = 82000$ K and $T_{warm} = 13000$ K.

In the maximum of the outburst the bolometric flux from the hot component increased by a factor of ~ 10 and its temperature decreased from $\sim 10^5 K$ to $\sim 6 \times 10^4 K$. The active period of YY Her lasted about 7 years and finished in 2000.

The main features of YY Her are:

1. The great amplitude of luminosity's growth for active hot component. Among all well-studied classical symbiotic stars (with prototype Z And) YY Her has the maximum amplitude of luminosity's change during outburst of the hot component.

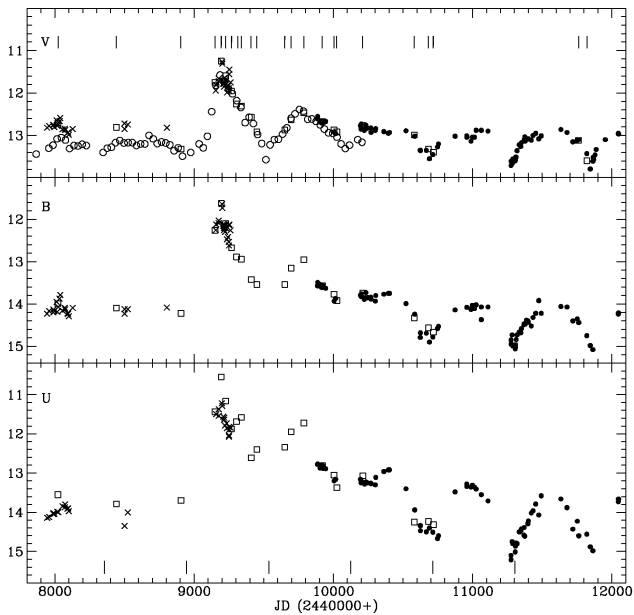


Figure 1: Light curves of YY Her in the U , B and V bands. Open circles and crosses are, respectively, visual and photoelectric brightness estimates from Munari et al. (1997), filled circles are our data. Open squares are brightness estimates obtained by convolving the spectra with the transmission curves of the corresponding filters. The vertical ticks near the horizontal axes (bottom) indicate the dates of minima in the visual light curve, calculated using the ephemeris from Tatarnikova et al. (2001). For the visual light curve, the vertical ticks indicate dates of spectrophotometric observations.

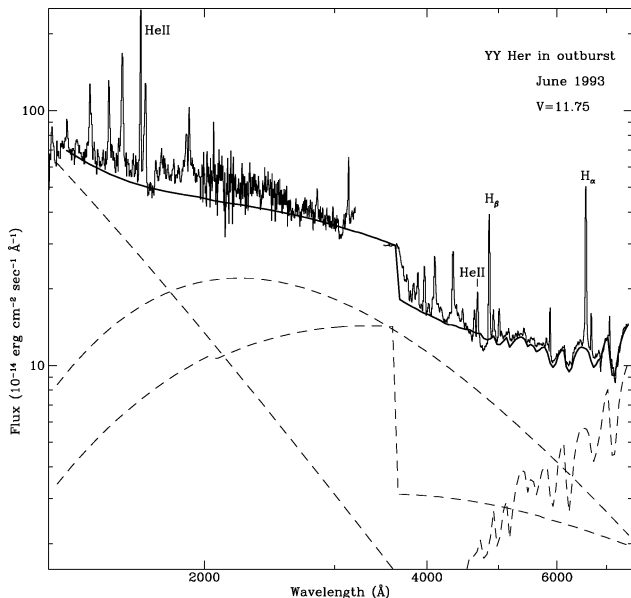


Figure 2: The UV+optical spectrum of YY Her. The solid thick line indicates the calculated continuum energy distribution of the star. The energy distribution in the spectra of the radiation sources forming the total emergent flux (hot component + warm component + M3.5 red giant + gaseous nebula) are shown by dashed lines.

2. The existence of bright HeII-lines in the maximum of outburst. But these lines totally disappeared from the typical spectrum of the active classical symbiotic star and its hot component's energy distribution is similar to A-F supergiants.
3. The appearance of the new structure element (warm component) during outburst.

The first feature doesn't allow to describe the active state of YY Her in the framework of thermonuclear runaway model because, according to theoretical calculations the growth of the hot component's luminosity must be ≤ 3 times.

The appearance of the warm radiation source is the strong argument for standard model of disk accretion. However this model could not explain the decrease of the hot component's temperature during transition from quiescent to active state.

The decrease of the temperature is connected with intensification of mass loss rate of the hot component during outburst, which, as one suppose, directly depend on the luminosity of the star. In this case the effective temperature of the hot component of YY Her in the maximum of outburst must be one of the lowest values among temperatures, characterized for hot components of classical symbiotic stars. But we have another picture.

References

- Tatarnikova A.A., Esipov V.F., Kolotilov E.A., et al.: 2001, *Pis'ma Astron. Zh.*, **27**, 825.
 Munari U., Rejkuba M., Hazen M., et al.: 1997, *As.Ap.*, **323**, 113.

INVESTIGATION OF THE DAMPING CONSTANT OF FRAUNHOFER'S LINES IN SOLAR ATMOSPHERE

L. Yankiv-Vitkovska

Department of Astrophysics, Ivan Franko National University
K. and Methodia, Lviv 79005 Ukraine,
vita@astro.franko.lviv.ua

ABSTRACT. To define chemical contents of elements in stars' atmospheres we need reliable data on their damping in spectral lines. We have found distinct expressions for damping constant with consideration of several mechanisms that influence the expansion of spectral lines. We have calculated parameter of damping for some spectral lines under different temperatures with consideration of inelastic collisions by means of these expressions. Using the most correct and empirically tested method of investigation of spectral lines we have calculated parameter of damping for spectral lines of iron group in Solar atmosphere. Calculation of Damping Constant of Fraunhofer's Lines in Solar Atmosphere.

Key words: Solar atmosphere: Fraunhofer's Lines; damping constant; inelastic collisions.

The problem of damping constant emanates from deficiency of reliable theoretical results, which according to opinion of many authors is related to computational complications. Theoretical value of damping constant does not always coincide with the value determined from observed spectra profiles. This is the case even for Solar atmosphere. Furthermore, for the conditions close to Solar atmosphere the damping constant is calculated theoretically only for several lines. The corresponding value lays within the interval $(1.1...1.9) \gamma_6$, where γ_6 is the classical (Unsold) approximation for van der Waals interaction. Results of laboratory measurements appear to be even more inconsiderable in number and unreliable since it is practically impossible to reproduce in laboratory the conditions prevailing in Solar atmosphere. Specifically, it is difficult to carry out an experiment with hydrogen as a basic agent of van der Waals collisions in conditions of Solar atmosphere. However, the results of laboratory investigations yield a correction factor for γ_6 only a bit greater than 1. Many attempts of empirical studies of Fraunhofer's lines damping constant were made in order to verify and improve theoretical and laboratory results.

Recently, modern devices have allowed improvement

of precision of observed data; there appeared more accurate laboratory measurements of atomic parameters and interaction constants and more adequate models of Solar atmosphere have been devised. However, no convenient formulae have been introduced so far which provide theoretical estimation of damping constant by account of all mechanisms bringing about the extension of spectral lines profiles. A problem of explicit calculation of a whole profile when only a few mechanisms act is apparently not simple, and also calls for separate researches. The misarranged empirical methods and inconsistency of observed data with theoretical calculations are considered as inability of theory to provide quantitative description of profiles of Fraunhofer's lines, or as unreliability of damping constant theoretical computations.

Starting from first principles for expressions for damping constant, a series of mechanisms is found which lead to its increase in comparison with Weisskopf-Lindholm damping for van der Waals interatomic interactions (Vakarchuk et al., 1998). As it's known, in order to obtain trustworthy conclusions about nature and structure of space objects, the analysis of star radiation requires detailed study of mechanisms of interaction between radiation and atomic systems. Atmospheres of majority of stars consist preliminary of hydrogen and helium, while the quantity of atoms of other elements is of few orders less. Certain amount of atoms and molecules are on various ionisation levels according to interactions with radiation and among themselves. The full description of star atmospheres needs a simultaneous solution of the transfer equation and the equations determining occupations of atoms quantum states. Within the approach of one-photon transitions a central role in the description is played by light absorption coefficient.

The profile of the so-called absorption coefficient in a line, that is its dependence on light frequency, as well as the profile of atom spectral line is formed by a series of mechanisms. The full profile is a fold of profiles which are caused by various mechanisms. Among these, the

colliding mechanism is determinative for the spectral line wing and leads to the formation of Lorentz profile.

Lorentz profile is characterised mainly by the damping constant γ , which determines the profile width. The value and temperature dependence of the constant are of particular importance for star spectra analysis. To adjust the observed profiles of Fraunhofer's lines with theoretically calculated profiles, the damping constant obtained from Weisskopf-Lindholm theory is often increased artificially. In some cases the magnification is unnaturally large, which is interpreted as theory inability to give quantitative description of profiles of Fraunhofer's lines. In our opinion this is incorrect point; it is necessary to carry out a detailed investigation of quantities, obtained from first principles and characterising profiles of atomic spectral lines.

The damping constant γ and the frequency shift Δ of radiation of an atom interacting with other particles according to mechanisms, which form Lorentz constituent of spectral line:

$$I(\omega) = \frac{\gamma}{2\pi} \frac{1}{(\omega - \omega_0 - \Delta)^2 + (\gamma/2)^2} \quad (1)$$

are connected with scattering cross-section σ by the following equation:

$$\gamma/2 - i\Delta = \frac{N}{V} \langle v\sigma \rangle, \quad (2)$$

where

$$\sigma = \int_0^\infty (1 - e^{i\delta}) 2\pi \rho d\rho \quad (3)$$

In the above formula ρ denotes aiming distance, while complex phase reads

$$\delta = \eta + i\Gamma, \quad (4)$$

where real part η is equal to the difference between shifts of atomic phases, among which the transitions of frequency ω_0 occur. This phases shift is caused by the shift of atomic energy levels as a result of interaction among atoms and perturbing particles. Let us consider for simplicity of records N particles of one sort embedded in volume V . Moreover, this is just the case which occurs in star atmospheres, since basically atoms of hydrogen are the perturbing particles there. The value of 2Γ is equal to total probability of atom transition from states, between which transition of frequency ω_0 takes place, to all other states. The quantity Γ causes additional extension of spectral lines, the so-called extension caused by elastic collisions. Natural or radiation width of atomic spectral line is not taken into account. The quantity v means atom velocity relatively to perturbing particle; brackets in Eq.(2) stay for averaging over velocities.

The computations are performed in assumption that quasi - classical approximation is fulfilled, when real

part of the phase reads:

$$\eta = -\frac{1}{\hbar} \int_{-\infty}^{\infty} \Delta E(t) dt \quad (5)$$

Here ΔE is the correction to atom energy, caused by its interaction with perturbing particle, t denotes time. We consider a rare particles system similar to star atmosphere. In this case the contribution to η will be determined mainly by interactions between particles in large distances. Then the potential energy $U(R)$ consists of interactions between their multipole momenta and decreases with the distance R according to a power law:

$$U(R) = -\hbar \sum_{l \geq 0} \frac{C_{n+2l}}{R^{n+2l}}, \quad (6)$$

where n determines the type of interaction, \hbar is Planck constant.

Considering the Maxwell distribution over velocities, the dependence of damping constant on temperature is obtained within Weisskopf-Lindholm approximation. The corresponding expression reads:

$$\begin{aligned} \gamma_0 = \frac{N}{V} 4\sqrt{\pi} \left(\frac{2T}{M} \right)^{\frac{n-3}{2(n-1)}} \Gamma \left(\frac{2n-3}{n-1} \right) \times \\ \times \Gamma \left(\frac{n-3}{n-1} \right) \left[\frac{\Gamma(1/2)\Gamma(\frac{n-1}{2})}{\Gamma(n/2)} C_n \right]^{\frac{2}{n-1}} (1+p^2)^{\frac{1}{n-1}} \times \\ \times \cos \left[\frac{2}{n-1} \arctg \frac{1}{p} \right], \quad (7) \end{aligned}$$

where M is reduced atom mass, T is temperature in atomic units, $\Gamma(x)$ is Euler's gamma-function. In the case $n=6$, $p=0$, the van der Waals damping constant is obtained within Weisskopf-Lindholm approximation:

$$\gamma_{WL} = 7.901 \frac{N}{V} C_6^{215} \left(\frac{8T}{\pi M} \right)^{3/10}, \quad (8)$$

where p is a parameter of inelastic collisions, $0 \leq p \leq 1$.

The value of γ_0 for $p \neq 0$ and $p = 0$, in particular, reads:

$$\gamma_0/\gamma_{WL} = (1+p^2)^{\frac{1}{n-1}} \frac{\cos \left(\frac{2}{n-1} \arctg \frac{1}{p} \right)}{\cos \frac{\pi}{n-1}}. \quad (9)$$

The ratio is greater than 1. Therefore, account of inelastic collisions increases the damping constant and the increase is considerable.

In order to estimate the contribution of post van der Waals interactions, let us write the expansion of the Eq. (9) in powers of temperature:

$$\gamma/\gamma_0 = 1 + \sum_{k \geq 1} A_k (T/T_0)^{\frac{k}{n-1}}, \quad (10)$$

where coefficients A_k are determined from constants of post van der Waals interactions.

The repulsion forces are also found to contribute into damping constant. The contribution is estimated approximately as follows: $\gamma > N\pi\alpha_0^2\langle v \rangle/V = N2\pi \cdot \alpha_0^2(8T/\pi M)^{1/2}/V$, where α_0 denotes a scattering length which is of atomic diameter order.

Let us make a quantitative estimate of inelastic collisions contribution to γ . In the case of van der Waals interactions ($n = 6$) for the maximal contribution of inelastic collisions ($p = 1$), elementary calculations yield: $\gamma_0(p = 1)/\gamma_{WL} = 13504$. This estimate of inelastic collisions contribution can partially improve mentioned above artificial increase of damping constant which is common in analysis of star spectra.

Let us estimate numerically the values of A_k . Consider an example of sodium atom in Solar atmosphere, where hydrogen atoms at the temperature of $T = 1000$ K serve as perturbing particles. Thus, for a Na-H system we find: $A_1 = 0.452$, $A_2 = 0.295$, $\gamma/\gamma_0 > 1.2$. Even such not so high temperature in the star atmosphere scale causes significant increase of γ . For $T = 6420^\circ\text{K}$, $\gamma/\gamma_0 > 1.32$.

The contribution of repulsion forces for the discussed above system Na-H for $\alpha > 2.6\text{\AA}$ yields $\Delta A_1 > 0.595$,

which results $\gamma/\gamma_{WL} > 1.92$ for $T = 1000$ K. For $T = 6420^\circ\text{K}$, $\gamma/\gamma_{WL} = 2.206$.

By means of the proposed explicit expressions for the damping constant, one can make numerical estimation of the constant for various temperatures in Solar photosphere attached to various values of inelastic collisions parameter. Computations, performed by us on the base of different methods of the damping constant investigations (Yankiv-Vitkovska, 1999) are well-consistent with our theoretical computations.

Thus, our newly obtained results are consistent with the data of other authors. They can be used for explanation of experimental studies of Fraunhofer's lines, in particular, for determination of chemical elements content in Solar atmosphere. The proposed theoretical method for damping constant calculations can be generalised for the case of star atmospheres.

References

- Vakarchuk I.O., Rykalyuk R.E., Yankiv-Vitkovska L.M.: 1998, *J. Phys. Stud.*, **2**, N 1, 41.
 Yankiv-Vitkovska L.M.: 1999, *Visnyk of Lviv Univ. Physical Series.* **32**, 67.

Author index

- Aliev S. G. 110
 Andronov I. L. 7, 15, 17, 113, 255
 Baktanov A. V. 21, 23, 24
 Bannikova E. Yu. 202
 Basri G. 244
 Beletsky Yu. V. 116
 Belik S. I. 231
 Berdnikov L. N. 170
 Bezdenezhnyi V. P. 118, 122
 Bjorkman K. S. 47
 Bondar' N. I. 185
 Bondarenko I. I. 25
 Brukhanov I. S. 124, 125, 162
 Chinarova L. L. 113
 Chochol D. 26, 61, 69
 Cugier H. 126
 Daszynski J. 126
 Derevyagin Ya. V. 198
 Derevyagin V. G. 198
 Dorokhov N. I. 129, 241
 Dorokhova T. N. 129, 241
 Dragunova A. V. 231
 Dudka O. I. 24
 Durlevich O. V. 266
 Efimov Yu. S. 134
 Egorova I. A. 140
 Evsakov N. N. 205
 Fabrika S. N. 215
 Falcon N. 141
 Feast M. W. 144, 275
 Friedjung M. 44
 Galanin V. V. 198
 Garcia Cole A. 159
 Gazeas K. 17
 Glazunova L. V. 48
 Gonzalez Perez M. J. 129
 Gopka V. F. 237, 249
 Garbanjeva T. I. 235, 247
 Gorynya N. A. 149
 Halevin A. V. 116
 Ismailov N. Z. 110, 188
 Johns-Krull C. M. 219
 Kulimeris T. 33
 Kanzen L. E. 235, 247
 Karetnikov V. G. 48
 Kazamovets E. V. 266
 Khalack V. 249
 Kilpio A. A. 38
 Kilpio E. Y. 41
 Kolesnikov S. V. 15
 Kolotikov F. A. 277
 Komarov N. S. 231, 235, 241, 242
 Komik-Karuzza D. 44
 Kovryukh V. V. 140, 174, 237
 Krugov V. D. 47
 Kubat J. 87
 Kudashkina L. S. 116, 134, 162
 Labrador J. 141
 Livinenko O. A. 200
 Lyubchik Yu. P. 244
 Manimzhis V. 211
 Marsakova V. I. 154
 Martin F. 244
 Mikhalchuk V. V. 261
 Miroshnichenko A. P. 308
 Miroshnichenko A. S. 47
 Mshemina T. V. 237, 247
 Molenda Zakowicz J. 156
 Monin D. N. 215
 Munari U. 277
 Myyllaeri E. 164
 Nasser M. R. 98
 Nazarenko V. V. 48
 Niarchos P. G. 15, 17, 53, 211
 North P. 249
 Ostrava N. I. 97
 Panishko S. K. 200
 Parrao L. 159
 Parimucha S. 67, 69
 Pavlenko E. P. 21, 23, 24
 Pavlenko Ya. V. 192, 244, 253
 Pena J. H. 159
 Pena R. 159
 Peniche R. 159
 Perevozkina E. L. 25
 Petrov P. P. 194
 Pikhun A. I. 162
 Plachinda S. I. 219
 Plascencia J. C. 159
 Polosukhina N. S. 249
 Polubek G. 65
 Popov S. B. 224
 Postnov K. A. 78
 Prithulla T. 26, 61, 69, 74
 Prokhorov M. E. 78, 224
 Psaryov V. A. 205
 Pustynik I. B. 82, 87
 Pustynski V. F. 87
 Reszelski M. 164
 Rosenbush A. E. 164, 265
 Rovithis P. 69, 74
 Rovithis-Livanidou H. 33, 69, 74, 91
 Samus N. N. 149, 266
 Sergeev A. V. 270
 Sergeevu T. P. 270
 Shakhovskoy N. M. 15
 Shakhrukhanov O. Sh. 273
 Shavrina A. V. 249
 Shenavrin V. I. 275
 Shugarov S. Yu. 97
 Skulsky M. Yu. 227
 Solheim J.-E. 98, 129
 Turasova T. N. 219
 Tatarsnikov A. M. 275
 Tatarsnikova A. A. 277
 Techuk O. 273
 Terpan S. 211
 Tremko J. 69, 74
 Tsymbul V. V. 249
 Turner D. G. 166, 170
 Usenko I. A. 47, 174
 Valyavin G. G. 215
 Vanko M. 106
 Vasilyeva S. V. 178, 242
 Whitelock P. 180, 275
 Yakovina L. 253
 Yankiv-Vitkovska L. 279
 Yudin B. F. 275, 277
 Yushchenko A. V. 17, 211, 237, 249, 273
 Zakhochai V. A. 205
 Zgonjajko N. S. 242
 Zola S. 15
 Zverko J. 249
 Zhyznovsky J. 249

Наукове видання

Вісті Одеської астрономічної обсерваторії

том 14 (2001)

Англійською мовою

Технічний редактор М. І. Кошкін

Підписано до друку 15.10.2001. Формат 60x84/8.

Ум. друк. арк. 33,02. Друк офсетний. Папір офсетний. Тираж 300 прим. Зам. 849.

Видавництво «АСТРОПРИНТ»

(Свідоцтво ДК №132 від 28.07.2000 р.)

65026, м. Одеса, вул. Преображенська, 24.

Тел.: +38 (0482) 26-96-82, 26-98-82, 37-14-25.

www.astroprint.odessa.ua